R. R. Scheid M.D.

THE FERNALD DOSIMETRY RECONSTRUCTION PROJECT

Task 4

Environmental Pathways — Models and Validation

Radiological Assessments Corporation
Route 2 Box 122
Neeses, SC 29107

***RAC* Report No. CDC-3**

March 1993

Contributing Authors on the
***Radiological Assessments Corporation* Research Team**
(Names appear alphabetically, except for that of the lead author)

George G. Killough[1]
Marilyn J. Case
Kathleen R. Meyer[2]
Robert E. Moore[3]
J. Felix Rogers[4]
Susan K. Rope[5]
Duane W. Schmidt[6]
Bernard Shleien[7]
John E. Till[8]
Paul G. Voillequé[9]

DRAFT REPORT FOR COMMENT

---

1. Hendecagon Corporation, Oak Ridge, Tennessee
2. Keystone Scientific Resources, Inc., Fort Collins, Colorado
3. Moore Technical Associates, Inc., Oak Ridge, Tennessee
4. Centers for Disease Control and Prevention, Atlanta, Georgia.
5. Environmental Perspectives, Inc., Idaho Falls, Idaho
6. Health Physics Applications, Darnestown, Maryland
7. Scinta, Inc., Silver Spring, Maryland
8. Radiological Assessments Corporation, Neeses, South Carolina
9. MJP Risk Assessment, Inc., Idaho Falls, Idaho

DRAFT

CONTENTS

EXECUTIVE SUMMARY

The purpose of the Fernald Dosimetry Reconstruction Project is to estimate radiation doses to members of the public who lived near the Feed Materials Production Center (FMPC) from radioactive materials released to the environment during the operation of the facility (1951 to 1988). The goal of Task 4 of the project is to develop a methodology that can be used to the translate release estimates (Tasks 2 and 3) into concentrations of radioactivity in the environment where people lived. Radiation dose will be calculated from the estimated concentrations as well as information and assumptions about people's day-to-day habits (such as time spent outdoors, level of activity, and sources of food). These dose estimates will be reported at the conclusion of the project (Task 6).

The methodology consists of mathematical models that describe the movement of radionuclides in the environment around the FMPC. These models use site-specific data whenever such data are available. If the study is to have credibility with scientists, government officials, and the public, the modeling methodology must achieve an acceptable balance of meeting several criteria, which include simplicity, flexibility, physical plausibility, adaptability to uncertainty analysis, acceptance, cost of implementation, and validity. Experience demonstrates that no methodology is likely to meet all of these criteria. Generally, it is necessary to seek a balance by accepting limitations of some criteria in order to emphasize others that are considered more important to the study.

This study places a premium on validation of the models used in pursuing its goals; a price that it pays for this emphasis is a rise in cost and some loss of simplicity. A preliminary SOURCE TERM (i.e., history of release rates) for uranium, which was developed for the years 1960 through 1962, was applied to the validations discussed in this report. Results of further validations will be reported in Task 6. Most validations carried out to date were applied to the air transport model; the comparisons involved air concentrations of uranium that were measured at the perimeter stations, depositions of particulate uranium that were collected on gummed film at various locations, and air concentrations of radon gas that have been monitored at numerous stations near the facility from the early 1980s to the present. Similar validation exercises were done with water concentrations of uranium downstream in the river and in Paddy's Run Creek. The results of the comparisons have generally been quite good when allowance is made for the complexity of the phenomena that influence the results. Some further refinements may be necessary before final doses are calculated.

Most routine monitoring data that are available were collected onsite or near the site boundary. The study, however, extends its scope to members of the public who lived within an eight-kilometer (five-mile) circle around the FMPC production area. This circular region is called the ASSESSMENT DOMAIN. It is probable that more than half of the particulate material that was released from the FMPC to the atmosphere was deposited within this circle, and dilution of the remaining airborne fraction by diffusion would result in concentrations at the outer boundary that are a factor of ten lower than those at the site boundary.

The environmental transport models simulate the movement of released radioactive materials through environmental PATHWAYS into exposure MEDIA where people may be affected. Table ES–1 summarizes some of the pathways and media considered in this study. The models

Table ES–1. Transport Pathways and Exposure Media

Pathway	Exposure medium or intake mode
Release to air	Direct inhalation Direct exposure to gamma radiation
Air-to-ground deposition	Contamination of food crops and animal forage Direct exposure to gamma radiation Direct ingestion of contaminated soil
Ground-to-air resuspension	Direct inhalation Direct exposure to gamma radiation
Runoff and leaching of radionuclides from soil to surface water and groundwater	Drinking water of people and animals Irrigation of crops Consumption of fish Direct gamma radiation from exposure to contaminated water
Storage of radioactive material	Direct exposure to gamma radiation

are a critical link between release estimates and doses, because environmental measurements alone are rarely sufficient. There usually are note enough measurements to cover the spatial region or the time considered by a study, and gaps in records and unknown analytical and sampling methods further interfere with efforts to use monitoring data directly. But environmental data are indispensable for setting parameter values and validation of models used in the assessment. Considerable thought and effort have been devoted to choosing the models and environmental data that are most appropriate to this study of the FMPC site.

Atmospheric pathways will likely dominate the total dose from FMPC releases. Accordingly, we have paid particular attention to these transport processes, including the local meteorology, dry deposition of particulates as a function of the particle-size distribution, wet deposition, plume rise, and the effect that buildings and other structures near the point of release have on the dispersion. To quantify these processes, the models require various parameters. We have estimated some of these parameters with site-specific measurements, and we have used values from the scientific literature for others.

The choice of a meteorological data base was of particular concern. Ideally, local data (wind speed, wind direction, atmospheric stability) should be available in monthly joint frequency tables for each month of the assessment period (1951–1988). At the FMPC, however, a recording meteorological tower has been in regular operation only since August 1986. The absence of site-specific meteorological information for earlier years of the facility's operation is a serious problem for the assessment. Data from the Cincinnati and Dayton airports (for which long-term records are available) were considered as alternatives, but comparisons of predictions using these datasets with the corresponding FMPC dataset for the period of its availability indicated an unacceptable degree of bias and scatter. We consider the FMPC dataset fundamental to the transport simulations of airborne releases, despite the short record and gaps resulting from problems with the instrumentation. The necessary approach is to make

In the second part of the validation, we used the model to predict monthly deposition at each of the 22 gummed-film locations during the period. For locations at the perimeter of the production area, the P/O ratios show general agreement with the measurements to within a factor of two to three. As one moves away from the site, the P/O ratios show a downtrend with distance, which may be an indication of possible bias in the deposition model. The simulated deposition may be less efficient in removing particles from the plume than measurements would indicate. It is also possible that the trend could also be influenced by predicted air concentrations that decrease too rapidly with distance. The correlations are low in magnitude, and about half of them are negative. The scatter indicated by these poor correlations could be due to the influence of a variety of variables, such as nonuniform weathering. These questions will be analyzed further before final calculations are made.

Uranium data in soil are less effective in validating air transport models when it is necessary to confine the analysis to a relatively brief period (1960–1962). Runoff, leaching, and other weathering processes gradually remove the deposited uranium from the soil, and any simulation must account for deposition and removal over the entire period of the FMPC's operation. Such simulations are not possible until the reconstruction of the source term is complete. We have studied soil data with an empirical deposition rate model and from a slightly different point of view, namely, that of estimating total deposition of uranium from the measurements of uranium in the soil. We obtained total deposition estimates of 2×10^5 to 9×10^5 kg U. We believe this range is likely to contain the true value of total deposition on soil within the assessment domain of uranium released to the air from the FMPC.

A significant component of the dose from FMPC releases is likely to result from the radioactive daughters of radon-222 (radon). The radon is produced by the decay of radium-226, which is a component of waste materials stored in the K-65 silos west of the production area. Radon gas and radon daughters have been released to the atmosphere since storage of the waste materials began in the 1950s, although starting in 1979 the FMPC has taken various actions to reduce the quantities of radon released.

Estimates of radon releases from the silos were first formulated as a part of the initial efforts of Tasks 2 and 3. The estimates have subsequently been refined and have been used, together with the same wake-effects air transport model that we are using for particulates, to estimate radon concentrations at locations where monitoring data are available. Such comparisons indicate a tendency toward underprediction by the model, with most estimates falling within a factor of two of the corresponding measured values.

The K-65 silos also present a potential source of direct gamma radiation exposures to people living nearby. We use models for calculating doses from these exposures, because the monitoring data are not sufficient for direct estimation of doses to individuals. Comparisons of model predictions of exposure with measurements indicate underprediction by about a factor of two. Factors contributing to the discrepancy might include inaccuracies in the measurements, the model, and parameter values chosen to describe the silos and the materials stored in them. The magnitude of the discrepancy is within the acceptable range, and dose estimates can be adjusted upward if further study of the measurements indicate the need to do so.

Episodic releases from the FMPC, which are defined as short-term events that warrant special dose assessment procedures, are considered primarily in connection with atmospheric transport. The criterion defined in an earlier report is that an episodic event must increase

the composite uranium release rate by a factor of at least 10 for a period of less than 10 days. During the 1960–1962 period, there was one such release from the Pilot Plant, in November 1960. Details of this release are discussed in the present report, and an approach to atmospheric transport in the absence of onsite meteorological data is outlined.

Surface water transport of radionuclides represents an important exposure pathway for liquid effluents released from the FMPC. Radioactive materials that are released to surface water are dispersed and diluted in the water and transported by the current. Potential routes of exposure are ingestion of fish, swimming or boating in the river, and using river water for irrigation.

There are two main points of release of radionuclides to surface water from the FMPC:

- The main effluent line to the Great Miami River
- Runoff and spills that enter Paddy's Run Creek.

Our method for estimating radionuclide concentrations in surface waters around the FMPC was chosen on the basis of simplicity and maximum use of site-specific data. The quantity of radioactivity released from the FMPC, based on measured concentrations in effluent water, was diluted in the river according to river flow parameters, which the U.S. Geological Survey has measured at several stations along the Great Miami River since 1910.

To supplement dose calculations based on this simple monthly dilution (MD) model, calculations were made with the NCRP Screening Model and the GENII model. Based on these three approaches, we concluded that the major pathways contributing to radiation dose from uranium in the surface water are from drinking water and eating fish. These calculations are conservative, because the Great Miami River is not used as a source of public drinking water between the FMPC and its confluence with the Ohio River, but some people do fish the river. The comparison of our predicted uranium concentrations in the river with actual environmental measurements shows good agreement.

For Paddy's Run Creek, the measured concentrations cover a wide range because of the erratic flow in the small stream. But the calculated uranium concentrations based on high and low flow rates for the creek encompass the range of measured concentrations.

Significant uranium contamination in groundwater south of the FMPC site, due to releases from the site, was discovered in 1981, and concentrations in this South Plume remain elevated. The well-sampling program has shown that only three private wells have been contaminated by the uranium, indicating that the number of people who have been affected during the period covered by the study is small. The concentrations of uranium in the South Plume for periods before 1981 will be based on two data sources. (1) The available measured concentrations of uranium in wells will be examined for trends, and (2) the concentrations of uranium in waters released to the outfall ditch and to Paddy's Run Creek (the primary source of uranium concentration in the South Plume) will also be evaluated and compared with the concentrations in the South Plume.

The agricultural model that will be applied to produce gardens is RAGTIME (RAdionuclides in AGricultural systems, a TIME dependent model), which will account for the contamination of crops by radionuclides deposited from the air or by irrigation with contaminated river water. The model considers the terrestrial pathways of the transfer of radioactivity to food crops, beef, and milk. The model is supported by data compiled on agricultural produc-

tion, growing periods, and usual planting and harvest times for garden crops in Butler and Hamilton Counties.

A substantial dosimetric data base has been assembled to support the conversion of concentrations in various exposure media to dose. Internal dose conversion factors (DCFs) provide either an internal dose per unit radioactivity ingested through contaminated food or water or the dose due to a unit quantity of radionuclide inhaled with contaminated air. External DCFs give dose rate per unit concentration of a radionuclide in air, water, or soil for exposure by immersion in the contaminated air or water or direct exposure to the contaminated soil. Our models of dose from radon and radon daughters are based on those of the National Council on Radiation Protection and Measurements (NCRP Report No. 78). For all other radionuclides, the internal dosimetry for this project is based principally on the methodology of the International Commission on Radiological Protection (ICRP) as described in ICRP Publication 30. Because the ICRP methodology is based on adult models of anatomy and physiology, and because age-dependent factors for uranium and thorium isotopes had not been published by the ICRP in time for use in this study, it was necessary to turn to other sources for ratios that would convert the dose factors to younger age groups.

For epidemiological purposes, it will be necessary to combine annual estimates of dose to groups with estimates of population dynamics. We developed four demographic models for the FMPC assessment domain to obtain estimates of location, number, and distribution of age and sex of individuals who resided in the domain during the period 1951–1988. Collectively, these models furnish estimates of population groups in each of the subdivisions of the assessment domain in each year of the period of FMPC operations.

In summary, models have been developed for use in the Fernald Dosimetry Reconstruction Project, which translate released quantities of radionuclides to concentrations in the environment where people lived. Predictions of the models for the 1960–1962 period were compared with measured concentrations in air and on gummed film. In general, the overall agreement of the models is good, but they vary as to temporal and spatial resolution. Some further refinements to the models may be necessary before final doses are calculated. In addition to environmental transport models, appropriate dosimetric and demographic models have been chosen which permit computation of doses to people based on age, living habits, radionuclides, and body organ. These models will provide the basis for incorporating dose estimates into a power analysis for an epidemiologic study.

transport estimates with this dataset and to apply conservative uncertainty distributions, based on the relationship between recent and past Cincinnati data, to the predictions.

The atmospheric transport of uranium particles is strongly influenced by the particle size distribution because of the dependence of deposition of the particles from the plume on particle size. Dose from inhaling the particles depends on the particle size distribution and on the chemical form of the uranium. The only measurements of particle size of stack emissions made at the FMPC were conducted by Northern Kentucky Environmental Services (NKES) during 1985 on stacks equipped with dust collectors. Particle size distributions for the stack emissions during the year 1985 are assumed to be the same as for the 1960–1962 period, because the plant operations served by the stacks did not change significantly from 1960 to 1985. The median particle diameters for outlet ducts of the dust collectors are in the range 5–9 μm.

Releases of uranium through the scrubbers of Plant 8 and Plant 2/3 present a different situation. Some particles passed through the scrubbers without being washed out of the gas stream; most of these particles are estimated to be relatively small — less than 2 μm in diameter. But a substantial fraction of the uranium released to the atmosphere from all FMPC processing plants during 1960–1962 — about 49% by our estimate — emerged from these scrubbers as large droplets of reentrained scrub liquor, which rapidly dried down into large particulate solids, with diameters in the approximate range of 30–150 μm. The consequences of this substantial component of large particles for estimates of transport and dose are potentially major:

- The large particles are rapidly deposited from the plume before they have had time to travel far downwind.
- Particles of the size and density of those resulting from the reentrainment are not considered respirable and are believed to have negligible dosimetric consequences for inhalation.
- Air-monitoring equipment used during 1960–1962 would have been inefficient in detecting the large particles. We have adjusted for this effect in carrying out model validations that involve the air-monitoring data.

If we had assumed that all released particles were in the smaller range attributed to the dust collectors, the effect would have been a higher estimate of inhalation dose to more people and an apparant overprediction of monitored air concentrations at the perimeter stations.

The choice of an air dispersion model for this site required careful consideration of many factors. The three main issues were

- **Curved-line vs. straight-line wind trajectories.** Models that treat wind flow as curvilinear are conceptually appealing, but they are expensive to implement and often require data of a resolution that is not available. For relatively small domains, straight-line models obtain comparable results at much less cost.
- **Handling of building wake effects.** For releases from rooftop stacks that do not extend much above the building height, the plume is drawn down near the ground into the turbulence of the building's wake, and the subsequent diffusion of the plume is affected. Some air transport models attempt to compensate for the resulting displacement and distortion of the plume by buildings.

- **Validation of the model against air-monitoring data.** Any model chosen for use in the study would be required to make predictions of air concentrations at the perimeter stations that compared acceptably with the monitoring data for those stations during the 1960–1962 period.

We carried out statistical studies of wind trajectories to demonstrate the adequacy of a straight-line model for this study. A subsequent comparison of several straight-line models identified a new building-wake model as slightly better than the standard Gaussian plume model, which does not account for wake effects. We expect to apply the new building-wake model to all rooftop releases from production plants and the Gaussian plume model with plume rise to two high-temperature sources (the old solid waste incinerator and the oil burner).

Uncertainties in atmospheric dispersion modeling require particular attention because of their potential magnitude and the relative importance of the air pathway. We have analyzed the interdependencies among the parameters and processes that influence the transport model, and we have developed an approach to quantifying each source of uncertainty in terms of a probability distribution. The resulting predictions of air concentrations and dose will have corresponding uncertainty distributions that we believe will be conservative (in the sense of overestimating the uncertainty).

The approach taken to validating the air transport calculations has relied primarily on two kinds of environmental data:

- Monthly-averaged uranium air concentrations measured at the four perimeter stations at the corners of the production area
- Monthly-averaged total uranium deposition on sheets of gummed film placed at 22 locations within the assessment domain.

Model predictions of air concentrations at the four perimeter stations for 1960–1962 are compared with measurements in Table ES–2. The results are presented as median predicted-to-observed (P/O) ratios and correlations of predicted and observed concentrations. The P/O ratios indicate the general level of bias in the prediction; the value 1.0 corresponds to no bias, and values greater than or less than 1.0 indicate over- or underprediction, respectively. The value 2.1, for example, indicates predictions that are about two times the corresponding measurements, on average. The correlations are an indication of scatter of the monthly P/O ratios about their median values, with values much lower than 1.0 indicating considerable scatter. The P/O ratios indicate reasonably good average agreement between model predictions and measured air concentrations. The low correlations are the result of month-to-month increases and decreases in the air-monitoring data that do not match up well with corresponding fluctuations in our reconstructed source term.

Table ES–2. Air Transport Model Comparison for FMPC Perimeter Stations

	NE	SE	SW	NW
Median P/O[a] ratio	1.72	2.10	1.50	0.70
Correlation	0.55	0.18	0.34	0.15

[a] Predicted to observed.

Task 4

ENVIRONMENTAL PATHWAY ANALYSIS — MODELS AND VALIDATION

INTRODUCTION

The Feed Materials Production Center (FMPC) near Fernald, Ohio, was a government-owned, contractor-operated facility that converted uranium ore concentrates and materials recycled from other stages of nuclear weapons production to either uranium oxides or ingots of uranium metal. These materials were machined into tubular form for reactor fuel cores and target fuel element fabrication. The FMPC operated from 1951 until 1988, when production was suspended. Figure 1 shows the location of the FMPC within the Cincinnati metropolitan area.

The Fernald Dose Reconstruction Project is being carried out by Radiological Assessments Corporation *(RAC)* under the auspices of the Centers for Disease Control and Prevention (CDC). The purpose of the project is to provide an independent analysis of types and amounts of radioactive materials released to the environment from the FMPC and to establish a methodology that will estimate doses to persons living offsite in the vicinity of the facility. The methodology, which will apply site-specific parameters to models of environmental transport and dose, can then be used to calculate retrospective estimates of individual and collective dose. The CDC will combine the estimates of collective dose over the period of the facility's operation (1951–1988) with radiological risk factors in order to estimate numbers of potential health effects. With this information, the CDC will be able to judge whether the sensitivity of epidemiological statistics, for the size of the exposed population, would likely be sufficient to detect an excess above the normal incidence of particular health effects.

The goal of Task 4 is to develop the methodology for modeling the transport of released radionuclides through environmental pathways and estimating the consequent radiation doses to exposed individuals and population. The methodology consists of mathematical models that describe the movement of radionuclides in the environment around the FMPC. These models use site-specific data whenever such data are available. If the study is to have credibility with scientists, government officials, and the public, the modeling methodology must achieve an acceptable balance of meeting several criteria:

- **Simplicity.** The models should not represent unnecessary processes and detail. Rather, they should focus on those processes that are directly relevant to the desired predictions (in this case, environmental concentrations and dose). And the models and methods should be applied in ways that are as easy as possible to follow and interpret.
- **Flexibility.** The implementation of a model should be sufficiently flexible to permit its application to a variety of situations. For example, in this study, an air transport model had to represent many release points and different particle sizes in order to permit comparisons of predictions with measurements of air concentrations at the perimeter monitoring stations.
- **Physical plausibility.** To the extent possible, the models should rely on basic principles of the applicable sciences to make their predictions. In contrast, an empirical model is

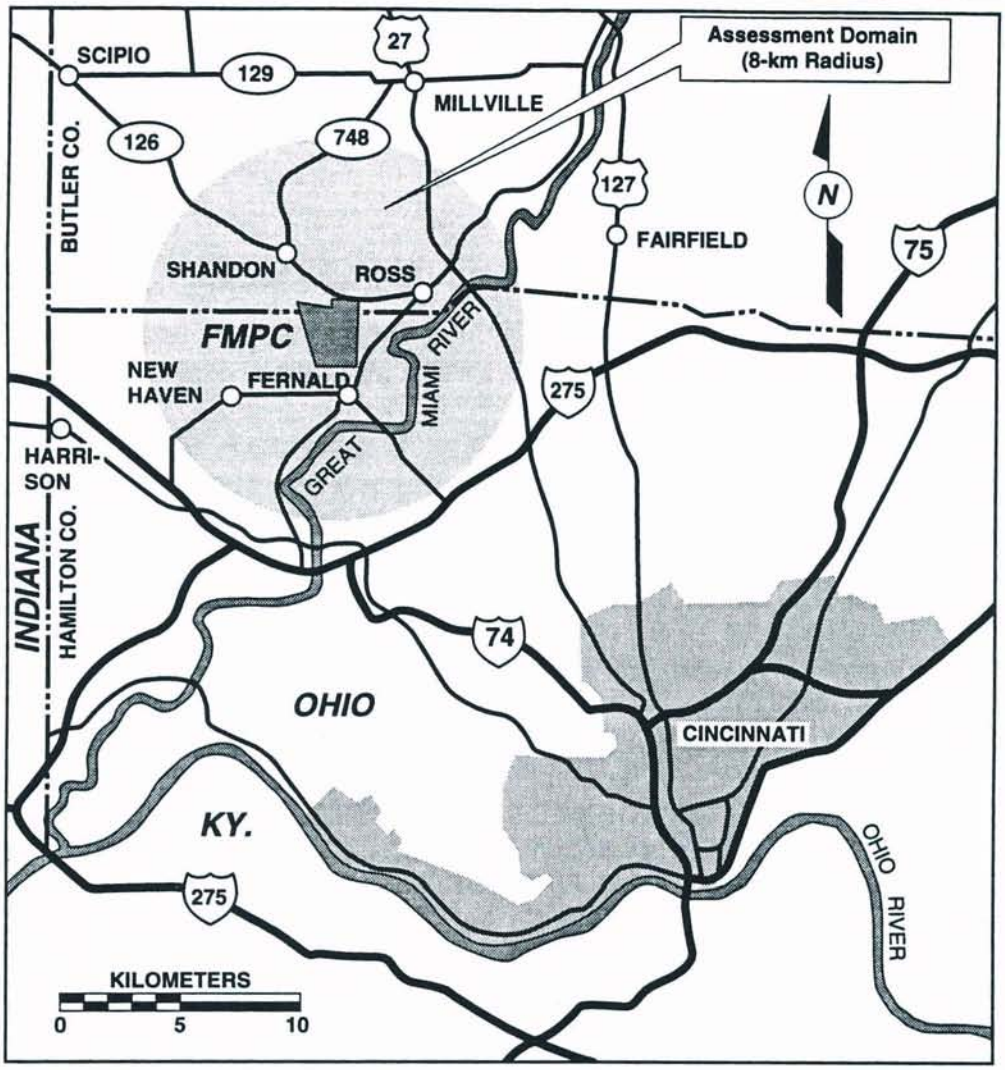

Figure 1. Location of the FMPC.

based on direct measurements that may not be applicable to anouther site or time. When the use of an empirical model is necessary, its applicability should be carefully evaluated.

- **Adaptability to uncertainty analysis.** The models should lend themselves to the process of uncertainty analysis. In particular, they should be capable of predicting ranges or distributions of results, representing uncertainty about parameters and data on which the models operate.
- **Acceptance.** It is desirable that the models and methods chosen be well known to scientists and accepted as adequate, when they are appropriately applied.
- **Cost of implementation.** It must be possible to carry out the necessary conceptualization, programming, calculation, and documentation within the financial resources and time alloted for the project.
- **Validity.** Models chosen for a particular site should be able to predict, with reasonable

accuracy, something that has been or can be measured directly. Such comparisons should be carried out to the maximum extent possible, with all relevant data, in order to increase confidence in predictions that cannot be compared with observations. The systematic process of making these comparisons is called VALIDATION of the model.

Experience demonstrates that no methodology is likely to achieve the highest marks on all of the foregoing tests in any given application. Generally, it is necessary to seek a balance by accepting limitations of some criteria in order to emphasize others that are considered more important to the study. This project is no exception to this rule: we have, of necessity, made many choices that affect the balance.

This study places a premium on model validation, which consists of comparing available measurements of the primary pollutants or other tracers in the local environment during the period of the study with corresponding predictions by the models. The degree of agreement or discrepancy of predictions with measurements, in the aggregate, will give a sense of the probable accuracy of the models in predicting the closely related quantities that pertain directly to the endpoints of the assessment. For example, internal doses due to inhalation of radioactive materials by people residing near the FMPC have never been measured; but air concentrations of radionuclides have been monitored at nearby locations, and if the models give adequate predictions of the measured air concentrations, our confidence in dose estimates calculated from these and other model-predicted air concentrations is increased.

The purpose of this report is to discuss fully the models that comprise the methodology, the anticipated application of the models to dose estimation, the validations that have been performed, and other validations that will be performed.

In the hope of making the report accessible and useful to readers with a variety of interests and backgrounds, we are arranging the presentation in a particular way. The main body of the report emphasizes presentation graphics and less-technical descriptions of pathways, models, and validation procedures. This part of the report avoids equations, complex tables, and levels of detail that may overburden the general reader. More specialized and detailed discussions, equations, tables, and graphs are given in the appendices. Also, the discussion within major sections of the main body of the report progresses from general to more specific, from overview to detail. Thus, the questions of a general reader may be adequately addressed in the earlier subsections of the major sections, or even in the executive summary.

The appendices, which contain more detail about specific models, data, and aspects of the study, are listed here for the reader's convenient reference:

A. Dosimetric Endpoints of the Study
B. The Assessment Domain
C. Radionuclides Released from the FMPC 1951–1988
D. Particle-Size Distributions for Releases of Uranium and Thorium
E. Meteorological Data for Modeling the Transport of Airborne Releases
F. The Straight-Line Gaussian Plume and Related Air Transport Models: Are they Suitable for this Study?
G. Dry Deposition and Plume Depletion
H. Wet Deposition and Plume Depletion
I. Plume Rise

J. Building Wake Effects
K. Parametric Uncertainty in the Air Transport Calculation
L. Air Monitoring Data from Stations near the FMPC
M. Gummed Film Data for Locations near the FMPC
N. Soil Data for Locations near the FMPC
O. Resuspension of Particulates
P. Radon, Radon Daughters, and Penetrating Radiation from the Waste-Storage Silos: Transport Models and Monitoring Data
Q. The RAGTIME Agricultural Model
R. Surface Water Transport
S. Groundwater Transport
T. Dose Conversion Factors
U. Demography of the Assessment Domain
V. Episodic Events

PLEASE NOTE. This report does not answer the question "How much dose did residents in the region around the FMPC receive from the facility's releases?" That is the goal of Task 6. The methodology of estimating exposure and dose is discussed, and examples are given. But the actual calculation of doses must wait for the complete estimate of releases of radionuclides from the plant during 1951–1988. This will come at the completion of Task 2/3.

ENDPOINTS OF THE STUDY

First we are going to give some background information that is necessary for understanding what the results of the study will mean. Then we are going to explain just what information the completed study will furnish to the CDC, and how that information will be broken down. Finally, we will give some indications as to why the information is sought and why it will be organized according to the plan we give.

Overall Objectives

The objectives of the Fernald Dose Reconstruction Project are twofold:

- Development of the SOURCE TERM. This expression is used in this report to mean those radionuclides released from the FMPC, broken down according to quantities released, environmental medium receiving the release (air, water), time of release, and relevant physical and chemical properties.
- Estimation of DOSE to people residing near the FMPC. Dose is a measure of the energy absorbed by an individual's organs and tissues as a result of exposure to ionizing radiation. Calculations are designed to permit relating dose to risk of radiation-induced health effects, such as some types of cancer. Units of dose used in this report are multiples of SIEVERT, abbreviated Sv (SI units), and multiples of REM (conventional units). For further details, see Appendix T.

The source term is the work of Tasks 2 and 3. A preliminary source term has been developed for the years 1960 through 1962 (Voillequé et al. 1991). Construction of this abbreviated

source term was carried out as a pilot study, with the purpose of exposing difficulties and pitfalls in the much more ambitious undertaking of developing the source term for all years of the facility's operation. Results of this pilot-study source term are available and have been used for most of the validations reported in this document.

The Role of the Data from Environmental Monitoring

One might ask why it is necessary to invest so much effort in the reconstruction of the source term if measurements of environmental levels of the radionuclides that concern us are available? The answer is, if the measurements were very complete and of high quality, they might be used for dose reconstruction in the absence of a source term. But FMPC monitoring data do not meet these conditions, for several reasons:

- Most monitoring was done near the boundary of the FMPC, with the (generally correct) assumption that concentrations of released materials would be higher at that distance than farther away. Thus doses estimated from exposures to environmental media near the boundary would represent "worst cases."
- Routine monitoring methods were not sensitive enough to give accurate measures of low levels of radioactive contaminants in the environment. Also, variable background levels of some radioactive contaminants make it difficult or impossible to distinguish low levels of materials that came from the FMPC from similar material that did not come from the FMPC. An example is the difficulty in distinguishing between uranium that was deposited on the soil following airborne releases from the FMPC and the uranium that is naturally present in the soil.
- Monitoring was done for purposes other than dose reconstruction, and the monitoring programs often did not (or could not) refine the measurements to provide information that is now needed. For example, when dose from inhaled radioactive particulates is calculated, contemporary methods require that one know (or assume) the distribution of particle sizes — or at least, a mean or median of that distribution — as well as other physical and chemical properties of the material. These measurements were not made during routine monitoring in environmental samples of airborne radionuclides released from the FMPC. Until the 1970s, the methods commonly employed for calculating dose to the lungs did not make use of particle size. In analyzing the source term, it is possible to get some sense (though far from a perfect characterization) of physical and chemical properties of releases that have not (or could not) be measured in the environment.
- It was not always clear what should be measured and at what resolution. Widespread concern for radon-222 as a contaminant with risk implications for the general public did not emerge until the late 1970s. In 1980 the FMPC undertook a radon monitoring program that became increasingly extensive throughout that decade. The principal source of radon from the site is the K-65 silos, in which a slurry of residues containing radium-226 (which produces radon-222) has been stored since the 1950s. Various actions have been taken to minimize the escape of the radon gas from these silos, but these actions are relatively recent. In addition, there was no monitoring for releases of radon and its decay products before 1980 when the release rates from the K-65 silos were higher. Thus,

we must "reconstruct" this radon source term in order to estimate exposures of nearby residents to radon before monitoring started.

- Since the early 1950s, the sensitivity and accuracy of radiation detection methods have improved, and measurements taken during the 1980s should not be casually compared with those from the 1960s. These differences, of course, affect the source term and the associated uncertainties as well as data from environmental monitoring, and efforts are being made to adjust for them.

- Even if the monitoring data were much more comprehensive than they are, an examination of the source term would still be needed to help resolve questions raised by variability and sampling times.

Monitoring data from around the FMPC — particularly before the 1980s — are, as a general rule, too limited to provide the only basis for historical dose assessment. But in the aggregate, they will be useful, together with source term reconstruction and models of environmental transport of the released radionuclides, for providing a quantitative estimate of past exposures of people living near the FMPC.

In view of these considerations, we have concluded that a thorough reconstruction and analysis of the source term is essential to a historical dose assessment. This conclusion does not discount the considerable value of the monitoring data in confirming (or disputing) transport model predictions that depend on source term estimates.

The Assessment Domain

This study is principally concerned with a circular region of radius 8 km (5 mi) with its center near the center of the FMPC production area (84° 41′ 19″ W, 39° 17′ 57″ N). We call this circular area the ASSESSMENT DOMAIN (Fig. 2). We estimate that 50% or more of the particulate material released to the atmosphere from the FMPC is likely to have been deposited within a circle of this size, and that dilution of the remaining airborne fraction would result in air concentrations at the 8-km boundary that are less by a factor of ten than those at the fenceline of the facility. This region includes the locations of almost all of the environmental samples that have been analyzed for possible contamination from the FMPC. Outside of the 8-km circle, the subject of comparison of model predictions with such sampling data becomes moot, and model predictions are difficult to validate.

The circular assessment domain of Fig. 2 will be subdivided into 16 radial lines and 8 concentric circles with radii 1 to 8 km (Appendix B, Fig. B–1). We refer to this network of lines and circles as a POLAR GRID, and the individual compartments are called CELLS. An estimate of dose will eventually be developed for each cell. We assume that most properties needed to calculate dose (such as air concentration, deposition of material on the ground, and population) are uniform within each cell.

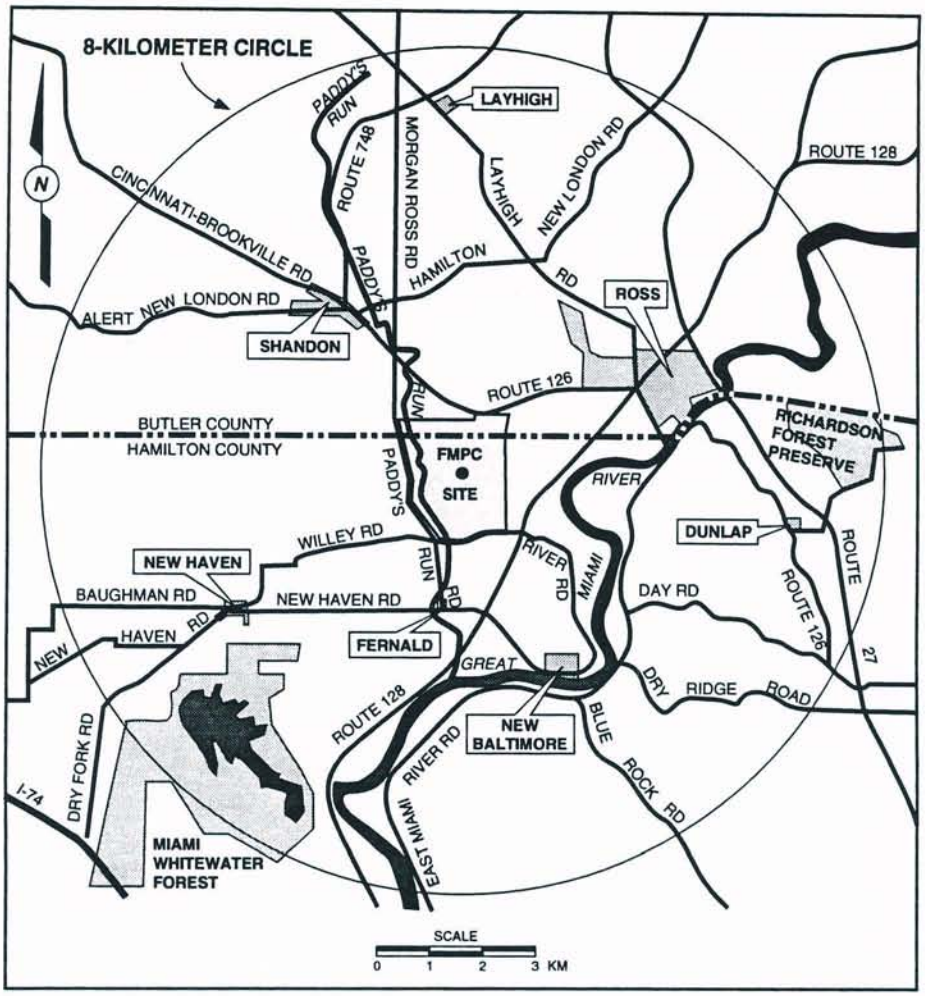

Figure 2. The FMPC site at the center of the circular assessment domain (radius 8 km). CAUTION: This map is a composite from several sources and gives an approximate representation of locations of selected roads and landmarks. It should not be used to determine whether or not a given residence, school, or other location lies within the assessment domain.

Pathways

The term PATHWAY as used in this report generally refers to the movement of radioactivity through the environment, and to the particular mechanisms of transport. An environmental or exposure MEDIUM is a reservoir for radioactivity that may affect people. The air may be considered an example of both terms. Transport by the wind and diffusion through the air constitutes a complete pathway, where inhalation of radioactivity is concerned; but atmospheric transport is only one part of a pathway when we are considering deposition of airborne material on food crops that will be eaten by people. And the ambient air is clearly an exposure medium for the inhalation of airborne radioactivity, because it is the reservoir that contains the radioactivity that is available for inhalation. A body of water, such as a stream or river, may also function as both a pathway and an exposure medium.

The radionuclide transport pathways and the associated exposure media that are considered are listed in Table 1. These pathways vary considerably in importance. Minor pathways are treated with simplifying assumptions or are eliminated from consideration.

Table 1. Transport Pathways and Exposure Media

Pathway	Exposure medium or intake mode
Release to air	Direct inhalation Direct exposure to gamma radiation
Air-to-ground deposition	Contamination of food crops and animal forage Direct exposure to gamma radiation Direct ingestion of contaminated soil
Ground-to-air resuspension	Direct inhalation Direct exposure to gamma radiation
Runoff and leaching of radionuclides from soil to surface water and groundwater	Drinking water of people and animals Irrigation of crops Consumption of fish Direct gamma radiation from exposure to contaminated water
Storage of radioactive material	Direct exposure to gamma radiation

Dosimetric Endpoints of the Study

Identification of the endpoints of an assessment study is perhaps the most important single task. By endpoints we mean what kind of dose quantities will be calculated. For this purpose, it is necessary to know how doses will be used for purposes subsequent to the immediate study.

The exact form in which the dose estimates are needed depends upon the design of the epidemiologic study being considered to relate the radiation doses and the health effects in the population. An important consideration in this process is the determination of exactly what doses will be calculated and how uncertainties will be incorporated. The dose that an individual may have received from operations at the FMPC depends upon a number of factors including the individual's residence location and history within the 8 km assessment domain (Appendix B), the time spent within the domain, the fraction of time spent outdoors, dietary habits, and age at initial exposure. Table 2 shows the different characteristics for which doses are calculated in this study. Appendix A describes a modeling approach to account for many of the variables listed in Table 2. There are two points of view that are considered. The first is concerned with tracking a particular *individual* though time and estimating the resulting dose. If one year is the increment of time considered, then we would need to know the individual's residence location, age for each year, and the other lifestyle attributes (e.g. fraction of food raised in a garden vs. commercial products consumed from outside the domain). The second point of view considers the entire *population* over time and analyzes dose in

terms of a probability distribution of dose to a randomly chosen individual. In this case, the population from which the random selection would be drawn consists of all individuals who lived in the assessment domain at any time during the specified period (1951–1988), whether or not these individuals still reside there, and whether or not the individuals are still alive.

Table 2. Breakdown of Dose Calculation in the FMPC Domain

Characteristic	Description	Appendix giving more details
Location	128 cells within an 8-km radius	B
Time	Monthly or annually	
Age	Up to 7 groups ranging from infants to adults	T
Organ	13 organs	T
Radionuclide	• 3 uranium isotopes • 4 thorium isotopes • Radon-222 and daughters • Various decay, fission, and activation products	C

RADIONUCLIDES RELEASED FROM THE FMPC

Although uranium was the primary material released to the environment from operations at the FMPC, other radionuclides were released in atmospheric or liquid releases as a result of processing of thorium and recycled uranium. Uranium and thorium decay to other radionuclides called DAUGHTERS or DECAY PRODUCTS. Most of the uranium ores processed at the FMPC had previously been separated chemically from the daughter radionuclides. In some of the early processing at the FMPC, however, these daughter radionuclides were present in the uranium ores. Wastes from that processing were placed in the K-65 storage silos, and decay of radium-226 contained in the wastes has resulted in the release of the gaseous radionuclide, radon-222. These releases are considered separately in Appendix P.

The processing of recycled uranium began in late 1961. Recycled uranium contains other radionuclides that originated in nuclear reactors. Fissioning of the uranium atom produces radionuclides, called FISSION PRODUCTS. Absorption of neutrons by uranium and other materials present in the reactor produces radioactive ACTIVATION PRODUCTS. Examples of fission products include strontium-90, technetium-99, ruthenium-106 and cesium-137. Some activation products are neptunium-237, plutonium-238 and plutonium-239,240. In addition, naturally-occurring radionuclides in uranium ores include promethium-234m, as well as the isotopes of uranium, radium and thorium. Appendix C focuses on the relative importance of these radionuclides in releases from the FMPC.

Relatively small quantities of thorium metal and thorium compounds were also produced in Plants 2/3, 4, 8, 9, and the Pilot Plant over much of the period of the FMPC operation.

It appears that thorium processing was not active during the 1960–1962 period. Most of the thorium processing equipment has been removed from the FMPC, and many production records were destroyed in the early 1970s.

Because measurements of radionuclides other than uranium were not made routinely every year, it is necessary to develop correlations between the releases of uranium and those of the other radionuclides. Ratios of releases were computed for years when measurements were made, and these ratios provide a basis for estimating releases of the these other radionuclides for years when they were not measured. The variability of the release ratios from year to year is considered in deriving the uncertainty associated with the estimated releases of other radionuclides.

A screening methodology developed by the National Council on Radiation Protection and Measurements (NCRP 1989) was used to assess the relative importance of the identified radionuclides as contributors to potential offsite radiation dose. For atmospheric releases, uranium contributes about 75% of the potential dose, followed by three thorium isotopes, which contribute about 20% of the potential dose. Each of the other radionuclides contributes less than 1% of the potential dose.

The relative importance of radionuclide releases to surface water depends upon which exposure pathways are considered. When drinking water and fish consumption are the only pathways considered, radium-228 and radium-226 isotopes contribute over 95% of the potential dose from releases to the river, while uranium contributes about 3% of the dose. When all surface water pathways are considered, radium-228 is the most important radionuclide, followed in order of importance by technetium-99, radium-226 and the uranium isotopes. Technetium-99 was of less importance when the irrigation of crops by river water was not considered. Contributions of other nuclides to the total potential dose is much smaller.

MODELS OF ENVIRONMENTAL TRANSPORT AND DOSIMETRY

The dose reconstruction will be based on simulations performed with computer programs that implement models of transport and dosimetry. The principal programs that will be applied to the assessment represent the following pathways:

- Transport through the atmosphere and deposition on the ground (Appendices E–M)
- Contamination of agricultural products by deposition, resuspension, and irrigation (the RAGTIME model; Appendix Q)
- Movement of radionuclides into surface water and groundwater (Appendices R and S).

Each of these programs incorporates one or more models of transport mechanisms. Most of the models are standard and are widely used in similar applications, but their computer implementations vary somewhat. Most of the computer programs used directly in the assessment have been specially written for this study. There are two reasons for doing this. First, most existing computer programs have been developed to meet specific requirements, and those requirements may differ from the ones that apply to this dose reconstruction. For example, general-purpose atmospheric transport programs do not explicitly take into account particle size distributions, as we are required to do in this study. Hence, any existing air transport code would need to be modified. Second, existing assessment programs often have different

outputs from those we require. For example, some can represent the result of a release of radioactivity at a constant rate for a long time (chronic release) or the result of a release of brief duration (acute release) but cannot account for a release that varies month by month for nearly 40 years. Also, some existing assessment programs give radiation doses as their outputs but do not show the corresponding environmental concentrations that we need for validation of the dose estimate.

Considerable time, effort, and thought have been given to choosing the set of models most appropriate to the FMPC site and the available data. We must distinguish between input data (that is to say, numbers that the model must have in order to calculate its results) and independent data used for comparison with those results, but on which the model does not operate directly (validation data). Although validation data are not *logically* necessary for the assessment, they are essential to the credibility of the study.

Readers who are not familiar with methods of environmental assessment may question the necessity of applying theoretical models to questions that seem directly related to what can be measured. The answer returns to some of the same ground that was covered in the previous section in pointing out why a thorough analysis of the source term is called for.

- Dose to an individual is not measured directly but must be inferred from the measurement of other quantities (or simulation of them). For example, one can infer by techniques of whole-body counting amounts of certain radionuclides that have been taken into the body; but dose (which is the part of the emitted energy that the subject's tissues absorb) must be inferred from a model.

- In general, one cannot retrospectively measure such quantities as air concentrations — which are needed to infer intake of radioactivity and then to infer the consequent dose. Models are needed to compute these quantities either from a source term or from other measured quantities.

- The monitoring results can seldom cover the spatial extent that one needs to consider. At the FMPC, air concentrations of uranium were regularly measured only onsite and at the site boundary until the 1980s. To extend these measurements, models are necessary. Indeed, at appreciable distances from the source, routine monitoring technology often lacks the sensitivity to detect the low levels of the contaminant or to distinguish those small concentrations from the natural background or worldwide fallout.

On the other hand, models must always be used with caution. Wherever possible, their results must be compared with real data, and in the absence of data for specific times or locations, the modeler must ask whether the results make physical sense and are consistent with comparable validated results. Quantitative uncertainty analyses should be carried out on the models in the context of the particular study to which they are being applied. In this report, we discuss uncertainties and sensitivity of models to input data. In Task 6 we will present model-calculated results together with estimates of uncertainty.

UNCERTAINTY

Results of scientific investigations are, by their nature, uncertain, and it is common practice for investigators to provide some estimate of uncertainties that affect their estimates. In this study, we emphasize PARAMETRIC UNCERTAINTY, by which we mean uncertainty in numbers (parameters) on which the models depend. If a parameter's uncertainty can be quantified by a probability distribution, then this uncertainty can be propagated through the model to the result, which would also take the form of a probability distribution. Various methods exist for propagating an uncertainty distribution through the model. Analytic methods are of limited use, because the equations that need to be solved are often mathematically intractable. MONTE CARLO methods are of quite general applicability and consist of repeatedly sampling the parameter distributions by computer methods with pseudorandom numbers, applying the model to each sample, and collecting all of the model results into an empirical distribution (e.g., a histogram or frequency chart). Figure 3 illustrates this process.

Much of the difficulty of parametric uncertainty analysis lies in determining the uncertainty distributions for a model's parameters. In the appendices that deal with specific models, we discuss uncertainties of model parameters and data and indicate how these uncertainties will likely be quantified for our final calculations. The distributions can be based on original site-specific measurements, on scientific literature values for conditions similar to those near the FMPC, or in the absence of alternatives, subjective judgment of experts.

There are many ramifications of the uncertainty analysis, which are brought out in some detail in the appendices. Our general approach for a dose reconstruction is to estimate target quantities (e.g., dose) as accurately as possible and to include conservatism in the uncertainties. This approach is in contrast to modeling practices for radiation protection, in which the dose itself is deliberately a conservative overestimate. Also, such exercises are often deterministic, which is to say that the quantity to be calculated is represented by a single estimate rather than a distribution.

ATMOSPHERIC TRANSPORT OF RADIONUCLIDES

Overview

Atmospheric transport involves the movement or dispersion of radionuclides from the release point at the FMPC to deposition on the ground at various locations around the site. There are many processes that affect atmospheric transport in the Fernald area. Some of these processes are better known than others. This Task 4 report covers these processes in separate appendices. The processes include the meteorology of the area (Appendix E), what model is used to predict how the material is transported downwind (Appendix F), the particle size distribution of the released material (Appendix D), the plume rise of the material, that is how far the material rises before moving downwind (Appendix I), and the effect that buildings and other structures near the point of release have on the dispersion of the material (Appendix J). Figure 4 illustrates these processes and effects.

The models initially provide estimates of air concentration at various distances from the site along with uncertainty bounds (Appendix K). With this information, other models can predict how the material is deposited on the ground in dry (Appendix G) or wet (Appendix H) conditions, and how the material may be resuspended from the ground to air (Appendix O).

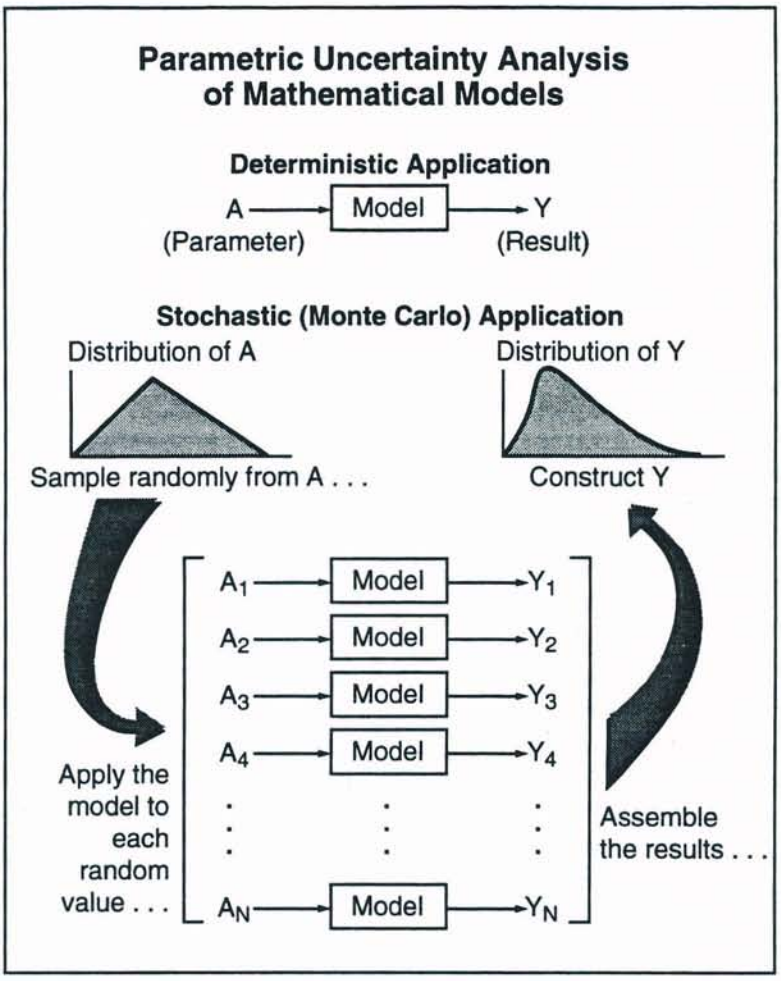

Figure 3. Schematic presentation of Monte Carlo methods for propagating a parametric uncertainty distribution through a model to its results. In this simplified illustration, A is an input parameter to the model, and Y is the result, or output, corresponding to A. For each specific input value of A, the model produces a unique output Y. Such an application of the model is DETERMINISTIC, because A determines Y. But A may not be known with certainty. If uncertainty about A is represented by a probability distribution, such as the triangular one in the figure, repeatedly sampling the distribution at random and applying the model to each of the sample input values $A_1, A_2, \ldots$ gives a set of outputs $Y_1, Y_2, \ldots$, which can be arranged into an empirical distribution for Y (grouped into class intervals for a histogram, for example). The distribution of Y is then our estimate of the uncertainty in Y that is attributable to uncertainty in A. This is a STOCHASTIC or Monte Carlo application of the model.

These processes of deposition affect the radiation doses to humans from atmospheric releases of radionuclides because the deposited materials serve as a source of contamination of the ground surface and the food-chain (Appendix Q); and this deposition reduces the amount of material in the plume that is subsequently transported downwind.

An important consideration of the atmospheric release is knowing its duration, that is,

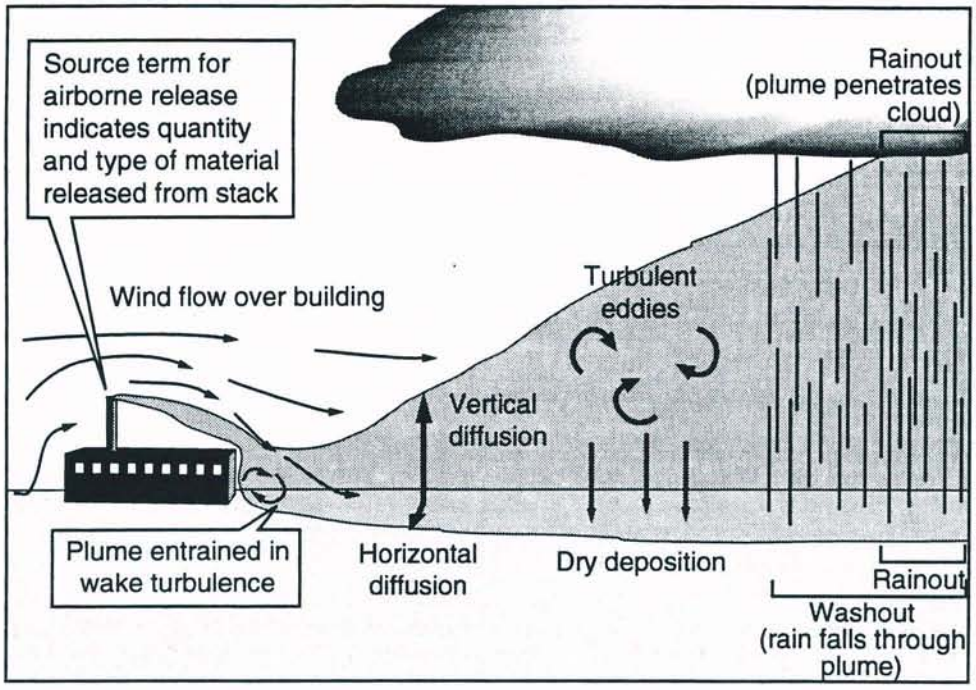

Figure 4. Physical processes associated with atmospheric dispersion. Diffusion disperses the plume horizontally and vertically, diluting its concentration as the material moves downwind. Highest diffusion rates are associated with unstable air. Wet deposition consists of washout (plume is beneath the raincloud) and rainout (plume penetrates the cloud, where the particles provide condensation nuclei for raindrops). Dry deposition is complex and consists of several stages. Turbulent eddies bring particles and gas molecules into contact with ground and vegetation surfaces. Near the ground, molecular diffusion accelerates deposition of very small particles. Gravitational fall dominates deposition for large particles.

whether the radioactive material was released over a long or short period of time. When a relatively large amount of material was released in a short time period, we refer to the occurrence as an EPISODIC RELEASE, and the transport modeling approach (Appendix V) is different from what is applied to material released over a longer period of time.

The appendices in this report describe the methods we have used to quanitfy the various transport processes. We have estimated some input parameters with site-specific measurements made at the FMPC. Estimates of others have depended on reviewing the scientific literature for similar processes at other facilities, and on mathematical models developed by others for similar processes. An important aspect of these modeling efforts is checking or validating them by comparing the model results with environmental measurements that were made at the site.

The historical records from the FMPC have provided a large amount of data that can be used to help confirm the results of model predictions. The report examines the air monitoring data (Appendix L) and gummed film data (Appendix M) available in the early sixties to compare with model predictions using atmospheric source term estimates for that same period.

In addition, soil measurement data collected at various times can be used as an approach to estimating total deposition from airborne releases for all years of operation (Appendix N). Total deposition within the assessment domain is a lower bound for the atmospheric source term.

Although we calculate the doses for radon releases from the K-65 silos separately from those for particulate releases, we use the same transport models for radon as we use for uranium, including the wake-effects model to account for the disturbance of the airstream by the K-65 silos (Appendix P).

The following subsections briefly discuss the rationale, modeling methods, uncertainty analysis, and air transport results we have calculated on the basis of the 1960–1962 source term estimates and the environmental monitoring data.

Meteorology

The atmospheric dispersion models used to reconstruct ground-level air concentrations at particular points in the assessment domain require knowledge of local meteorological data. The choice of an air dispersion model should depend, to a great extent, on the meteorological data that are available for the location and time that the model is intended to simulate. It is always better to use meteorological measurements made at the site or location of concern if suitable data are available. The types of data needed include wind speed, wind direction, temperature, precipitation, and the STABILITY CLASS, an indication of the turbulence in the atmosphere.

At the FMPC, a recording meteorological tower has been in regular operation only since August 1986, and we obtained the hourly data for the period August 1986 through December 1991. Lightning and instrumentation problems have resulted in numerous gaps of varying duration in this record (Appendix E). Many prospective assessments have based air-dispersion calculations on frequency tables that represent five years of data, also called a five-year composite dataset. For a dose reconstruction (i.e., a retrospective assessment), however, it is clearly preferable to use meteorological data for each actual year. The fact that the FMPC dataset included only five years of recent data, with gaps, posed a problem for reconstructing doses from earlier years of plant operation.

The options available to us included using the five-year composite of FMPC data for the earlier period, with a large degree of uncertainty applied to air concentration estimates, or substituting a surrogate historical dataset to use for the calculations (possibly with some bias correction or other adjustment). Accordingly, we have examined four sets of meteorological data from the Fernald area for their possible applicability to the dose reconstruction project. These datasets are summarized in Table 3. The lowest wind speed class (0–2 m s^{-1}) has a much higher relative frequency at the FMPC than at the other three sites. The mean wind speed at the FMPC site is about half of that for each of the airports. This is important information, because the downwind air concentrations of radionuclides released from the FMPC are inversely proportional to wind speed. That is, doubling the wind speed would cut the air concentration in half, if all other factors are the same. If the unadjusted Cincinnati airport data were used in place of the Fernald data, the predicted air concentrations would be lower by a factor of at least two than if the FMPC meteorological data were used (Appendix E, Fig. E–6).

Table 3. Meteorological Datasets Examined for Applicability to the Fernald Dosimetry Reconstruction Project

Dataset	Time period	Distance from FMPC	Applicability to FMPC
FMPC tower	Aug. 1986–present	Onsite	Site-specific but of short duration with numerous gaps
Cincinnati Airport	Jan. 1948–present	29 km SSE	Continuous record; underprediction of downwind concentrations, partly because of mean wind speed differences
Dayton Airport	Jan. 1987–Dec. 1990[a]	61 km NE	Continuous record; underprediction of downwind concentrations
Oxford, Ohio, (Miami U.)	Jan. 1981–Dec. 1990	30 km N	Shorter duration; some differences in wind patterns; difficult to determine stabilities

[a] A longer record is available.

Though the Cincinnati airport data may be disappointing as a surrogate for the FMPC because of bias and scatter, we examined the dataset for internal relationships between recent and past years. This was done to determine if the correspondence between the five-year composite FMPC dataset and the unknown FMPC meteorology for previous years will resemble the same correspondence for Cincinnati airport data. This information would provide information on historical trends from the longer dataset that could be applied to the limited FMPC dataset. The analysis suggested that the recent composite data for the two sites are comparable predictors of their respective past concentrations. Appendix E discusses the comparison and its possible utility.

We conclude that the FMPC onsite data are fundamental to meteorology at and about the site for the period of interest, despite the short record and gaps resulting from problems with instrumentation. Accordingly, the air dispersion predictions for the dose reconstruction study will be based on hourly wind and stability data from the FMPC meteorological tower during the years 1987 through 1991 (1986 was a partial year), with uncertainties based partly on the relationships between recent and past Cincinnati airport data.

Particle Size

The atmospheric transport of materials from the FMPC is affected greatly by the size and chemical form of the particles of materials (e.g. uranium) released. The chemical form and particle size of the material also affects the amount of material inhaled by individuals and thus affects the dose. Large particles released to the atmosphere (physical diameter greater than about 10 or 20 μm, depending on density) have high gravitational settling velocities and deposit on the ground near the point of release. Smaller airborne particles (physical diameters up to a few μm) are transported to greater distances and are of greater concern for radiation dose, because they are inhaled more deeply into the respiratory passages than large particles. Thus the size distribution of airborne particles must be considered (1) for validating

the air transport models, (2) for accounting for the distances traveled by released particulates, and (3) for estimating dose. We will return to these questions in subsequent sections. The following paragraphs summarize our approach to analyzing particle size distributions for FMPC airborne releases.

The only measurements of particle size of stack emissions made at the FMPC were conducted by Northern Kentucky Environmental Services (NKES) during 1985 (Reed 1985). The NKES study made measurements for both the inlet and outlet ducts of 15 major uranium-emitting stacks equipped with dust collectors. A dust collector is a chamber containing a parallel system of bag filters through which the effluent gas is forced. Particle sizes for the outlet ducts are representative of emissions from stacks with intact bag filters in the dust collectors. On the other hand, the values for the inlet ducts are assumed to represent emissions from the same stacks during those periods in which the bag filters failed, allowing unfiltered air from the production process to escape to the atmosphere. The filtering by the dust collector bags results in a reduction of about 25% in median particle size. Particle size distributions for the stack emissions during the year 1985 are applied to earlier periods because the plant operations served by the stacks did not change significantly.

The predominant chemical species of uranium emitted from each stack was identified from FMPC reports and engineering drawings of process equipment. Either U_3O_8 or UF_4 was emitted from all of the stacks of the NKES study, except for one stack, which emitted a mixture of UO_2 and UO_3.

The air emitted from release points not equipped with dust collectors was cleaned through SCRUBBERS. A scrubber removes particles from the exhaust gas by forcing it through a liquid mist; most of the particles are scavenged by mist droplets, which, for the most part, are collected by mist-eliminating devices and recycled to the liquid reservoir. This liquid is usually called the SCRUB LIQUOR (or SCRUBBING LIQUID), and it is changed periodically. The uranium-containing droplets accumulate on the mist-eliminators, and some of the liquid is agglomerated into larger droplets and escapes back into the exhaust gas stream (REENTRAINMENT). The large droplets are vented to the atmosphere with the exhaust gas. Figure 5 illustrates these processes. In this manner, the scrubbers of Plant 8 and Plant 2/3 emitted liquid droplets of reentrained scrub liquor of varying uranium concentration. The uranium concentration was proportional to the time elapsed since the last change of scrub liquor, but at any given time, the uranium concentration in all droplet sizes was the same. The liquid in the reentrained droplets would evaporate in the atmosphere, leaving solid particles, which are believed to have been relatively large, with physical diameters in the range 30–150 μm.

A fraction of the particles that entered the scrubbers would penetrate the mist (i.e., would not be scavenged from the air by mist droplets) and would escape to the atmosphere with the exhaust gas. The size of these particles was small; most had physical diameters less than 2 μm.

Calculations showed that 70% of the released uranium from the Plant 8 scrubbers escaped in reentrained liquid droplets with diameters in the range of 100 to 200 μm. The remaining 30% of the released uranium consisted of relatively small U_3O_8 particles with physical diameters in the range of 0–10 μm, which penetrated the scrubbers and escaped to the atmosphere. The large liquid droplets of reentrained scrub liquor contained uranates, sodium hydroxide, and dissolved sodium salts. We estimated the mean diameter of these droplets to be about

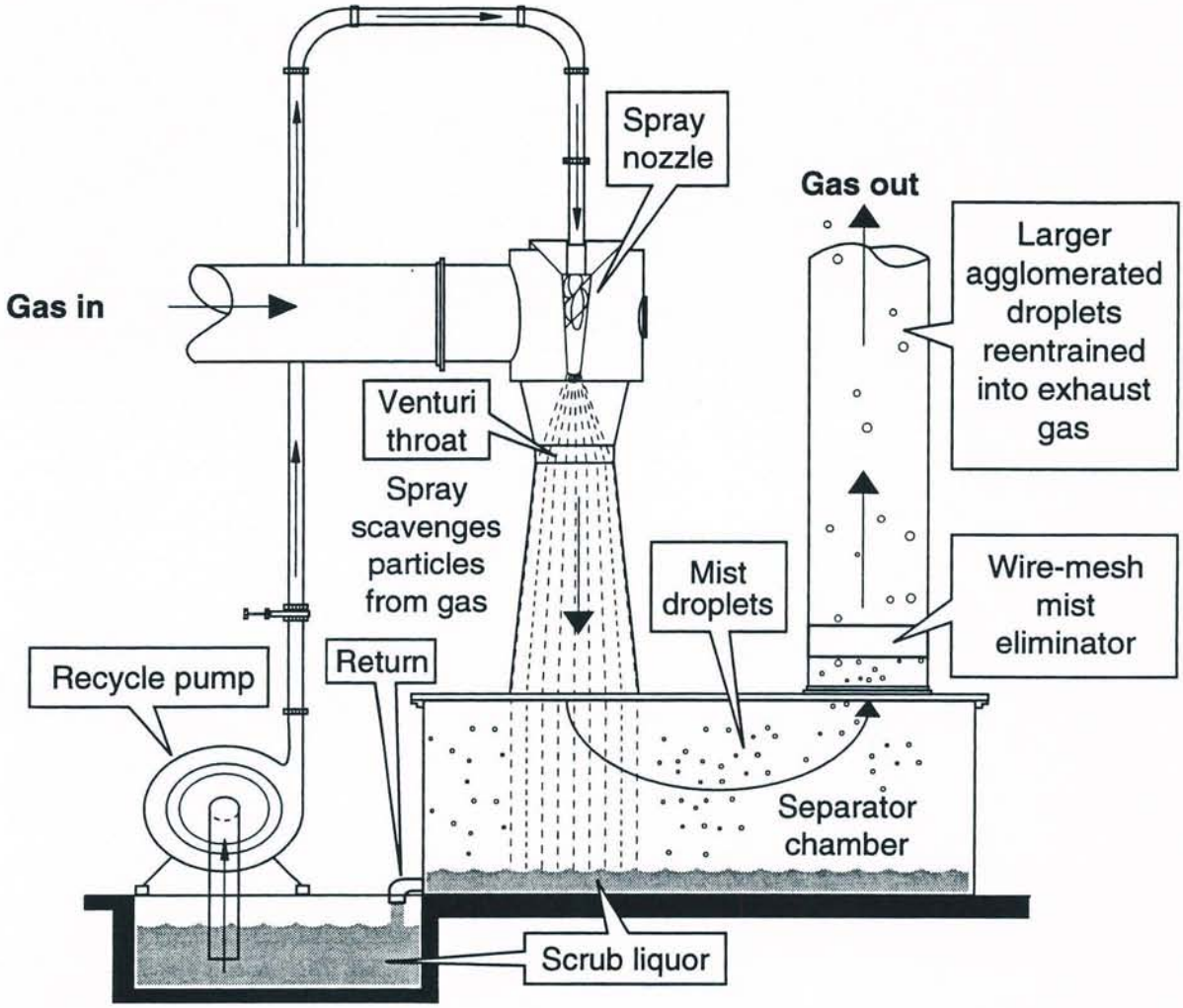

Figure 5. Scrubber schematic. Exhaust gas entering the scrubber is forced through a liquid spray into a Venturi tube. The gas then passes through a separator chamber and into the outlet duct. The spray entrains most particles into liquid droplets. Most of the liquid (or scrub liquor) is collected in the separator chamber and returns to a reservoir from which it is recycled. The scrub liquor of the Plant 2/3 and Plant 8 scrubbers was changed periodically, and uranium was recovered from it. To inhibit the escape of the uranium-containing droplets, various mist-eliminating systems were employed. The figure indicates a wire mesh mist eliminator in the outlet duct, which would trap most droplets. But some of the trapped liquid would be reentrained into the gas stream as larger agglomerates and escape to the atmosphere, where they would rapidly dry down to relatively large solids. (To keep the figure simple, we showed only one mist-eliminator. In practice, some of the FMPC scrubbers appear to have employed multiple mist-eliminators. For example, zigzag baffles were sometimes deployed in the separator chamber to take out the larger droplets, and wire-mesh systems were placed either in the separator chamber or in the outlet duct, as shown, to remove smaller droplets that penetrated the baffles.)

140 μm, and calculations indicated that they would have dried down to solid residue before reaching the perimeter of the production area (Table 4).

We verified the particle size distributions tabulated by Boback et al. (1987) by comparisons with information from the original data sheets of NKES (Appendix D). In an earlier report (Voillequé et al. 1991), we presented a series of graphs of particle size distributions of the uranium species for both the inlet and outlet ducts of each of the 15 sampled dust collectors. We carried out this procedure so that we could extend the distributions to particle sizes not covered by the measured NKES values. From these distributions, the average particle-size distributions for both the inlet ducts and the outlet ducts for stacks emitting U_3O_8 and UF_4 were calculated. Appendix D provides details of this procedure.

For some processes at the FMPC, no particle size data were available from the NKES study. In these cases, comparisons with similar operations at other facilities carrying out similar processes were used to estimate particle-size distributions.

Table 4 summarizes the key findings on particle size for stack emissions through dust collectors and scrubbers. Although the table lists only the median particle sizes for emissions from the various processing plants, distributions of particle sizes along with uncertainty estimates have been developed for these emissions. Details of these calculations are presented in Appendix D.

As we noted previously, in addition to uranium, relatively small quantities of thorium metal and thorium compounds were also produced during much of the FMPC history, although apparently not during the 1960–1962 period on which the validations in this report are based. There appears to be no particle size information available on the thorium process emissions. As a result, considerable uncertainty is introduced into the modeling of airborne thorium emissions from FMPC stacks. Because of similarities in the FMPC chemistry and processing of thorium and uranium at the FMPC, it is probable that annual uranium doses from inhalation will be incremented by an appropriate factor to account for processed thorium for those months when thorium processing was active. This factor will be varied with a suitable uncertainty commensurate with the absence of specific information.

Air Dispersion and Deposition Models

The selection of an appropriate air dispersion model for FMPC releases of uranium, fission products associated with recycled materials, and radon is important for the credibility of air pathway calculations used in this study. We considered two methods of estimating the movement of radioactive materials released from the FMPC. The first method treats each release of radioactive materials as a "puff" and follows this incremental release or puff of released material along a path that resembles the behavior of the wind recorded at hourly intervals at a station in the region at the time. The direction of the puff changes each hour according to the recorded wind direction. With this kind of model, however, the path, or TRAJECTORY, of the puff would have to be based on hourly data. This first approach requires a complex model that requires substantial computation time. It is important to determine whether this added complexity and cost would provide more defensible air concentration estimates, given the data limitations discussed previously.

The second approach makes use of air transport models related to the well-known Gaussian plume model. Models of this class assume that released materials are moved in a straight

Table 4. Particle Sizes and Chemical Forms of Airborne Releases of Uranium From the FMPC

Source of emissions	Chemical form	Basis for size estimate	Median particle diameter (μm)
Dust collectors			
Plant 1 and Plant 2/3	Mixture of U_3O_8, UO_3, UO_2 from ore handling	Similar operations at other facilities	Inlet: 7 μm Outlet: 5.3 μm
Plant 4	UF_4 (green salt) from hydrofluorination	1985 NKES measurements	Inlet: 10 μm Outlet: 7.8 μm
	U_3O_8 from foundry operations	1985 NKES measurements	Inlet: 8.6 μm Outlet: 6.0 μm
	UO_3 (orange oxide) and UO_2 (brown oxide) [a]	Unverified 1985 NKES measurement	Outlet: 8.9 μm
Plant 5	U_3O_8 from foundry operations	1985 NKES measurements	Inlet: 8.6 μm Outlet: 6.0 μm
	UF_4 (green salt) from hydrofluorination	1985 NKES measurements	Inlet: 10.0 μm Outlet: 7.8 μm
Plant 6	U_3O_8 from machining	Similar operations at other facilities	Inlet: 6.8 μm Outlet: 5.1 μm
Plant 8	U_3O_8 from foundry operations	Inferred from NKES measurements	Inlet: 8.6 μm Outlet: 6.0 μm
Plant 9	U_3O_8 from machining	Similar operations at other facilities	Inlet: 6.8 μm Outlet: 5.1 μm
Pilot Plant	UF_4 from reduction of UF_6 [b]	Derived from hydro-fluorination process	Inlet: 10.0 μm Outlet: 7.8 μm
Scrubbers			
Plant 2/3	UO_3 (orange oxide); penetrating fraction	Onsite data of gulping process, and scrubber efficiencies	Most < 2 μm
	$UO_2(NO_3)_2 \cdot 6H_2O$ (uranyl nitrate hexa-hydrate); reentrained fraction	Uranium concentrations in scrub liquor, and literature values for reentrained mist droplets	41 μm
Plant 8	U_3O_8; penetrating fraction	Calculated from particle sizes of furnace emissions, and scrubber efficiencies	Most < 2 μm
	Sodium uranates in suspension in scrub liquor; reentrained fraction	Concentrations of uranium compounds and salts in scrub liquor, and literature values for reentrained mist droplets	140 μm before evaporation; 65 μm after evaporation

[a] The median particle size for the outlet ducts of stacks releasing a UO_3–UO_2 mixture is based on measurements made from only one stack, and the data for this stack do not appear physically plausible. Accordingly, the particle sizes for these stacks will be assigned large uncertainties.

[b] No particle size information could be found for UF_4 emissions from the Pilot Plant. Composite values for the hexafluorination process will be applied to the Pilot Plant emissions, with appropriate uncertainties.

line from the source, depending upon the wind speed and direction at the time of the release. By using statistical compilations of the same hourly meteorological data as the puff model, these straight-line models greatly reduce the required computational effort. If material released from the FMPC tends to move in straight lines until it leaves the assessment domain at the 8-km boundary, a straight-line Gaussian plume model would be an appropriate and much simpler substitute for the puff model.

To test this hypothesis, we used a simulation method that we applied to the hourly wind data from the Cincinnati Airport during the years 1960–1962. We applied Monte Carlo sampling methods (Fig. 3) to the meteorological frequency tables in order to simulate trajectories of released material, and recorded the number of these trajectories that stayed within the wind sector in which they originated. This exercise strongly suggests that the straight-line models are appropriate for distances at least to the 8-km boundary (Appendix F), and therefore we base the air transport simulations on models of this type.

As airborne contaminants in the form of particles and gases are carried downwind, they are deposited on surfaces at or near ground-level through a variety of chemical, physical and biological processes. As a result of this process of deposition, particles are removed from the plume, and we refer to the loss from the plume as PLUME DEPLETION. The rate of deposition of radioactive material on the ground is related to the concentration of the material in the air by a factor called the DEPOSITION VELOCITY. We are aware of no measurements of deposition velocity in the vicinity of the FMPC during the facility's operation. Appendix G describes the theoretical and empirical approaches to estimating the deposition velocity, and Appendix H addresses wet deposition. The dry deposition velocity is a function of the particle size and density of the radioactive material (past a certain minimum point, the larger the particle size, the greater the deposition velocity), the nature of the surface (for example, snow-covered, lawn, tree-covered), and meteorological variables (for example, the higher the wind speed, the higher the deposition velocity).

Although deposition velocity was not measured directly near the FMPC, we did have some measurement data from the FMPC (uranium in air and on gummed film) that we could use to estimate deposition velocities. We could then compare these empirical values with our calculated deposition velocities based on particle size of radioactive materials released from the facility and on FMPC meteorology.

These comparisons showed that the calculated average deposition velocities (wet plus dry ≈ 0.02 m s^{-1}) were much too small to account for the magnitudes of the measured average deposition velocities of 0.08 to 0.16 m s^{-1}. Upon investigation, we deduced that a large fraction of the uranium released from the Plant 8 scrubbers and about half of the uranium released from the Plant 2/3 scrubbers was likely to be in large particle sizes, which probably contributed to high rates of dry deposition (Appendix D).

For larger particles, an important component of deposition is gravitational settling. This component becomes dominant as the physical particle diameter increases above about 10 μm. Because of this component, we needed to develop a special theory of deposition for the effluents from the Plant 8 and Plant 2/3 scrubbers.

For the uranium released from Plant 8 scrubbers we calculated a deposition velocity for the reentrained droplets of 0.37 m s^{-1}. As the droplets move downwind, they evaporate and leave the uranium salts and other residue as a solid particle. After evaporation, the

deposition velocity is estimated to be 0.28 m s^{-1}. For the 1960–1962 period, we estimated that the Plant 8 scrubbers accounted for almost 60% of the uranium released from the FMPC. A similar analysis of Plant 2/3 scrubber releases indicates that as the release moves downwind, the dry deposition velocity that is applicable to that component of the release decreases from 0.37 m s^{-1} to about 0.18 m s^{-1}. The Plant 2/3 scrubbers released about 14% of the total uranium from the FMPC during this time.

For particles that escapes scavenging by the mist and penetrated the scrubbers, we estimate average deposition velocities of 3.3×10^{-3} and 2.6×10^{-3} for Plant 8 and Plant 2/3, respectively.

For all releases of uranium from FMPC stacks equipped with dust collectors, we use a dry deposition velocity of 0.01 m s^{-1} (Appendix G). Figure 6 summarizes the calculated deposition velocities at the FMPC.

Averaged over all production sources (weighted with each source's uranium release during 1960–1962), the dry deposition velocity range is 0.18 m s^{-1} (droplets at maximum size) to 0.13 m s^{-1} (liquid evaporated) (Appendix G, Table G–7). These calculated values are comparable to the measured (empirical) deposition velocities (0.16 to 0.08 m s^{-1}) based on the air monitoring (Appendix L) and gummed film data (Appendix M).

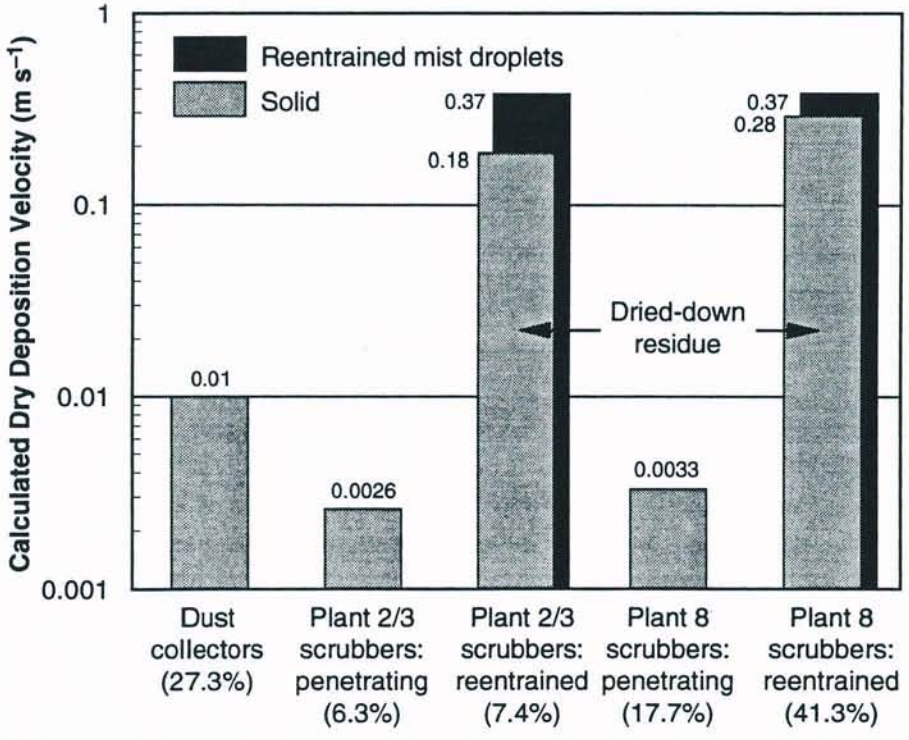

Figure 6. Dry deposition velocities (m s^{-1}), calculated for FMPC releases of uranium. High rates of deposition are believed to be associated with uranium in large liquid droplets that escape from the Plant 2/3 and Plant 8 scrubbers and quickly dry down to large-particle residues. The percentages indicate the fractions of uranium released to the atmosphere during 1960–1962 that were associated with each source.

The atmospheric plume moving from the FMPC is affected by the process of wet deposition, in which precipitation (rain, snow, sleet) removes, or washes out, radioactive material from the air. This ratio of concentrations of the material in precipitation and air is called the WASHOUT RATIO. From this ratio and the precipitation rate, a wet deposition velocity can be calculated for the area of interest (Appendix H). Field measurements of washout ratios range from 300,000 to one million with a median value of approximately 600,000. This ratio means that the concentration of radioactive materials in rain or precipitation is 600,000 times greater than its concentration in the same volume of air.

We were able to calculate a site-specific washout ratio for uranium at the FMPC based upon monthly measurements of uranium in air and precipitation for January 1961 to December 1967 (Appendix H, Table H–1). Our site-specific median washout ratio value was 290,000. A distribution for uncertainty analysis that was derived from the data is used in our model of wet deposition.

Building Wake Effects and Plume Rise

When the points of release extend only a few meters above the roof of the building as they do at the Fernald production facilities, disturbed airflow associated with the BUILDING WAKE can affect the air dispersion. Part or all of the plume is drawn down into the turbulent region near the ground in the building's wake and diffused horizontally and vertically by the turbulence. Calculations in Appendix I indicated that releases from all roof-top stacks at the FMPC would be affected by wake effects of the buildings. An entrained plume is modeled as if it came from a crosswind *area* source (such as the leeward face of the building), in contrast to an elevated release that originates from a *point* source and is not distorted by entrainment. Plume rise is not considered a factor for the entrained releases from stacks and roof vents.

Appendix J describes a comparison of several wake effects models and the Gaussian plume, which, in its usual form, does not consider wake effects. The comparison tested the models, using the uranium source term developed earlier (Voillequé et al. 1991) and the air sampling data from the four perimeter stations of the production area for the period 1960 through 1962 (Appendix L). Of the models tested that could be applied to this study, a new model of Ramsdell (1990) gave the best overall results in these tests, and this model has been adopted for use with releases from roof-top stacks at the FMPC (Appendix J). The Gaussian plume ran a close second in the comparison. Called the TIME-DEPENDENT model because of its derivation, Ramsdell's model can be regarded as a variation of the Gaussian plume.

Comparison of model predictions with measurements indicates that both models — time-dependent and Gaussian plume — overestimate the data to some degree. At least part of the overprediction of concentrations is likely due to underestimation of the removal of large particles from the plume by dry deposition (Appendix G). Agreement between measured and calculated values, however, is good, and results lie generally within a factor of two. Some of the potential sources of error are the meteorological data (Appendix E), the source term, and errors associated with air sampling and the handling and analysis of the samples (Appendix L). Overall, these results must be considered a reasonable validation of the model.

To consider uncertainty in modeling the building wake effects, we calculated a range of air concentrations assuming, at one extreme, that the wake for each building behaved as if the building were isolated, and treating the complex of buildings as a single large building,

at the other. Calculations with these two extremes gives a range, generally within a factor of ±50%, that serves as a component of uncertainty associated with building wake effects.

For release sources that are not dominated by wake effects, a parameter in the plume model is the effective height of the plume centerline. This height is the sum of the physical height of the stack or roof vent from which the materials were released and the additional height that the radioactive material moves vertically due to the buoyancy and momentum of the effluents through the stacks and vents. This additional vertical height is called the PLUME RISE.

At the FMPC, we have applied plume rise calculations only to emissions from the old solid waste incinerator, the only elevated source that is isolated from the production complex, and to those from the oil burner. Uncertainties associated with the plume rise from these facilities center on the high temperatures generated by combustion. The combined airborne releases of uranium from both facilities was a small fraction of the total, however, and relatively large ranges of uncertainty can be assigned to the parameters affecting plume rise without having a large effect on the overall uncertainty (Appendices I and K).

Resuspension of Particulates

Airborne releases of uranium from the FMPC are eventually deposited on the ground surface through gravitational settling and wet and dry deposition processes. A subsequent transport process for this deposited material is RESUSPENSION, which refers to the reentry of previously deposited particles into the air, where they are available for inhalation. For the FMPC Dose Reconstruction Project, we chose an approach called MASS LOADING for evaluating resuspension of deposited material released from the FMPC. The mass loading approach uses two main parameters to provide an estimate of the concentration of the contaminant in air. These parameters are the mass loading (concentration) of dust in the air near the ground, and the concentration of the contaminant in the surface layer of soil.

To determine the first parameter, we used weekly measurements of the total suspended particulates in air at 14 air monitoring locations surrounding the FMPC for 1989 through 1991 to characterize the variations in mass loading around the FMPC. The monthly time scale was chosen to be consistent with that being used for the source term reconstruction. These data can be used to reconstruct the probable seasonal variation in dust loading. The analysis indicated that the months May through September are relatively dustier than the annual average but are still within 30% of the annual average. The annual averages are quite consistent, and the three year-average of 34 $\mu g\ m^{-3}$ is in good agreement with the 1966 National Air Surveillance Network average for nonurban locations of 38 $\mu g\ m^{-3}$ (Healy 1980).

Several modifying factors to the basic mass loading model were considered and discussed in Appendix O. These factors include the distribution of the contaminant among different size soil particles, the fraction of airborne dust that comes from the contaminated areas, and the respirable fraction of the resuspended dust.

Uncertainties in the Air Transport Model

Appendix K describes the approaches we have developed for analyzing the uncertainties associated with meteorological joint frequency tables, wet and dry deposition, distributions of particle size, plume rise, and building wake effects. Figure 4 illustrates air transport of released material and some of the basic processes to which the uncertainty analysis is applied. We have also examined the uncertainty associated with year-to-year variability of the meteorological joint frequency tables by studying the relationship of predicted concentrations made with recent Cincinnati data (1987–1991) with estimates of past concentrations also based on Cincinnati data for particular years during 1951–1988. In addition, we have examined correlations among predictions at different receptor points in the region, but this picture is far from clear. We take a simple approach and assume that air concentrations at receptor points within the same sector are positively correlated, but that air concentrations are not correlated across sectors.

Since the dry deposition of large particles (Appendix G) dominates the deposition velocities, uncertainty in the wet deposition velocity will not contribute much to the overall uncertainty in air concentrations. The distribution of uncertainties for the dry deposition velocity will most likely cover a factor of 10 with 90% probability. For larger particles, gravitational settling is the dominant component in accounting for dry deposition, and it appears that there will be less uncertainty associated with this velocity than with deposition velocities of smaller particles.

Uncertainties associated with particle size distributions originate from the 1985 study of particle diameters of FMPC dust collector releases conducted by Northern Kentucky Environmental Services (NKES). Particles in these releases were in the respirable range (aerodynamic diameter < 20 μm) and consequently are the most important from the point of view of inhalation dosimetry. A continuous distribution was fitted to each empirical (measured) distribution for U_3O_8 and UF_4. The exact shapes, central measures, and quantiles of these distributions are the main sources of uncertainty for these small particles. Particles that penetrate the scrubbers represent about 24% of the uranium in the airborne releases from the FMPC during 1960–1962 (Fig. 5).

Reentrainment of uranium entering the scrubbers of Plant 2/3 and Plant 8 in the scrub liquor and the escape of droplets to the atmosphere has resulted in the distributions of large particles (physical diameters greater than about 30 μm). About 49% of the uranium released from the FMPC facilities to the atmosphere during 1960–1962 is believed to have been in large particles represented by these distributions. The parameters of the particle-size distributions and the fractional allocation of released uranium to each distribution will be treated as uncertain quantities.

It is possible that some observations of air concentration will be outside of the range of uncertainty estimates even after the parametric variations described in Appendix K have been incorporated into the Monte Carlo analysis. If this occurs to a significant extent, similar comparisons to those depicted in Figs. J–1 through J–4 in Appendix J will be used as a basis for adding an uncertainty factor to encompass the observed deviations of the model predictions from the measured values.

VALIDATION EXERCISES

A critical element in applications of models to environmental transport processes is the comparison of the computer estimates with site-specific environmental measurement data, if such data are available. This VALIDATION process emphasizes the importance of the historical records and original documentation from the site and stresses the value of using these historical data to assess the extent to which the models are able to predict what was observed. The exercise often uncovers problems with models and assumptions, and satisfactory comparisons of predicted and observed values build confidence in the assessment methods used in the dose reconstruction. At the FMPC, we have compiled several datasets from the historical records that can be used for model validation.

The surface water measurements of uranium concentration in the Great Miami River and in the Paddy's Run Creek are presented and discussed in Appendix R. For atmospheric transport the air monitoring data (Appendices J and L), gummed-film data (Appendix M), and soil uranium concentration measurements (Appendix N) can be used to validate our model calculations.

Air Monitoring Data

Historical air monitoring data from the FMPC are used in the dose reconstruction process to provide measurements to compare with environmental transport model predictions, to assist in choosing an appropriate building wake effects model (Appendix J), and to derive a site-specific value for the washout ratio (Appendix H).

Ambient environmental air was sampled and analyzed for uranium from the earliest years of operation. In the 1960–1962 period, samples of air were obtained weekly from four monitoring stations located at the four corners of the production area perimeter. Offsite and onsite air monitoring data for other years will be presented in the Task 5 report. It appears that the typical air sampler used during this time was a Staplex high-volume air sampler inside a louvered weather shelter. Although samples were taken about once a week, the air was not continuously sampled. A typical sampling time was 3360 minutes (56 hours), or 33% of the week. Table L–1 in Appendix L presents the individual weekly measurements of uranium in air for this time, which were transcribed directly from the original analytical data sheets. The sources of uncertainty that we considered are the determination of sample volume, the collection efficiency of filter media, isokinetic sampling and particle size considerations, flow rate fluctuation due to line voltage, loss of particulate material from the filter during collection or processing, and inadequate contamination control during collection, handling and analysis.

The collection efficiency of air samplers declines with increasing particle size. It is our judgment that the historical air monitoring data from the production area perimeter underestimate the total uranium concentrations in air primarily because of the low collection efficiency for large particles. We evaluated the collection efficiency of the high volume air samplers for the particle sizes present at the location of the samplers. Our analysis made use of information from the scientific literature on sampling effectiveness as a function of particle size and sampler orientation, combined with uranium particle size distributions at the locations of the perimeter air samplers. This calculation accounted for the source term particle size characteristics as well as the differential deposition of particles of different sizes

between the release points and the samplers. The uranium particle size distributions at the four stations were similar and bimodal with about 30% of the airborne uranium less than 5 μm (aerodynamic diameter), and 38% over 50 μm. This bimodal distribution occurs because scrubber effluents contribute to the largest size fractions and the dust collectors contribute to the relatively small size fractions (Appendix D). We performed an uncertainty analysis of sampler collection efficiency and tabulated the resulting distributions for each month of 1960 through 1962.

Deposition Measurements Using Gummed Film

At the FMPC, measurements of deposition of particles at locations within the plant boundaries and at offsite locations were performed using gummed film from 1952 until 1965. The gummed film used at the FMPC was similar to that used to measure fallout deposition at locations throughout the United States during the 1950s and 1960s. Film (exposed area of about one square foot or 0.093 m^2) was generally changed monthly, and was analyzed for uranium, gross beta, and gross alpha. The measurements of uranium deposition are of greatest interest for this project to compare with estimates of uranium deposition from model simulations of air transport.

We obtained the original analytical data sheets for gummed films from approximately 30 locations within and around the FMPC production area. Table M–2 in Appendix M lists the original monitoring results. These values have been adjusted for the GUMMED-FILM COLLECTION EFFICIENCY. This efficiency is the ratio of the fallout activity collected by the gummed film to the total amount deposited on a comparable ground surface. It can be affected by precipitation, blowoff by wind, and resuspension of material from the ground surface. In a recent study, comparisons of gummed-film data against integrated deposition results from soil samples yielded an estimated efficiency of 20% for daily measurements under dry conditions (Beck et al. 1990). The collection efficiency decreased as the daily precipitation increased. Since some gummed-film samples at the FMPC were exchanged biweekly and others monthly, it seemed inappropriate to use the collection efficiencies for one-day sampling periods for the FMPC samples.

Fortunately, daily, weekly, biweekly, and monthly gummed-film measurements of uranium deposition were made from March 1960 to March 1962. These data were analyzed to determine the gummed-film collection efficiencies for exposure periods longer than one day. To do this, we used daily precipitation measurements from a downtown Cincinnati location that were representative of the FMPC. These daily precipitation measurements were used to estimate daily collection efficiencies based on the results of Beck et al. (1990). These daily efficiencies were used to estimate the true daily deposition at the FMPC. Those estimates were then summed for weekly, biweekly and monthly periods for comparison with the total depositions measured for these time periods. Based on this procedure, the apparent mean collection efficiencies for the weekly, biweekly and monthly exposure periods are comparable. The mean collection efficiency for an exposure duration of one month is 14% with a standard deviation of 3%.

Table M–5 in Appendix M shows the revised estimates of uranium deposition on gummed-film that were derived from the reported collection efficiencies. Uncertainties of the revised estimates of uranium deposition range from 20% to 30%. These measured uranium deposition

values were then compared with air transport model predictions which had been adjusted to show the effect of loss of uranium from the plume by deposition. The time-dependent model (Appendix J) was applied to all releases from rooftop stacks, and the Gaussian plume (Appendix F) was used to predict transport from the old solid waste incinerator and the oil burner. These comparisons, shown graphically in Appendix M, indicate a tendency for the models to underpredict the gummed film estimates by about a factor of two overall. This pattern of underprediction, coupled with the factor-of-two overpredictions by the models of air concentration at the NE perimeter station (Appendix J), suggests that the deposition model is under-efficient in its prediction of the removal of the larger particles from the plume. The overall result, however, is a positive validation of the modeling approach, and the underprediction of deposition fits logically with the overprediction of air concentration. It is important to realize that the general factor-of-two accuracy is particularly good for the application of relatively simple models to atmospheric phenomena.

Soil Data for Locations Near the FMPC

Soil sampling data can be used as a measure of cumulative deposition of uranium over time in the area covered by the sampling and can possibly be used as a lower bound on the total release of uranium to the atmosphere. We investigated this approach in Appendix N, using soil sampling data gathered around the FMPC since the 1950s to estimate the total cumulative deposition over the domain up to 1988. We used six sets of soil uranium data (data bases) to obtain the information for this study. The general characteristics of each data base are outlined in Table N–1 of Appendix N. Soil samples were taken at various locations and depths, at different times from 1959 through 1991, and by several organizations, including IT Corporation, National Lead Company of Ohio, Westinghouse Materials Company, the Ohio Department of Health, EG&G, and the University of Cincinnati. Except for recent studies, the soil samples were analyzed only for total uranium. The data were identified by sector, distance from the center of the site, the year collected, the resultant value, number of samples represented by the value, and the depth of the soil layer that was sampled.

Our initial approach to estimating total uranium deposition in soils included showing the geographic distribution of uranium in the soil out to 10 km from the center of the facility (Figure N–2 in Appendix N). This figure shows evidence of uranium deposition in surface soil out to 6–7 km in the NNE and NE directions, directions toward which the prevailing winds blow. Closer to the plant itself is evidence of high uranium concentrations from 1,000 to 10,000 pCi g^{-1} in the 0–1 km sectors of E, ESE, SSE, and NNW. The average concentration of uranium in soil samples taken beyond 8 km is approximately 1 pCi g^{-1}. It is important to understand what has caused these areas of high contamination near the plant. If they are due to spills, they need to be excluded from our analysis of total soil inventory that resulted from deposition from airborne releases.

We found that the areas of highest contamination were associated with specific structures or storage areas. For example, the area immediately to the east of the production area is the site of the old solid waste incinerator (OSWI) and received localized deposition of uranium from that source (Fig. 7). The ground contamination measured in the NE direction supports this assumption. Other areas of high contamination close to the production area are most likely due to contamination from spills near the onsite storage area of Plant 1, the metal

scrap area, or the tank farm. Consequently, except for the incinerator area, we attributed levels of uranium in soil above about 100 pCi g^{-1} to spills rather than airborne deposition. However, the effect of various cutoff levels (from 20 to 1,000 pCi g^{-1}) on the estimated total cumulative deposition is negligible.

Once the levels of uranium present in the soil at specific times are characterized by measurement, a model must be developed to describe the deposition of uranium on the soil and its removal over time by leaching and runoff. The model depends upon a parameter called the SOIL-WATER PARTITION COEFFICIENT K_d (mL g^{-1}). This parameter describes the concentration ratio, at equilibrium, of uranium bound to soil and uranium in solution. With the rate of water infiltration and other soil parameters, K_d can be used to derive a rate coefficient of removal of uranium from the soil by water, or the degree to which dissolved uranium becomes bound to the soil. We estimated K_d by two methods. The first made use of observed inventories of uranium in the surface layer of the soil that had been taken at particular locations over a period of many years (time series) to estimate the rate of removal of uranium from the soil. The time-series data consisted of soil uranium concentrations from the early 1970s through 1988 that were available at the seven FMPC boundary stations. A nonlinear regression procedure was used to calculate a removal rate coefficient of deposited uranium from the surface soil compartment, based on the uranium measurements in soil over time. This analysis resulted in an average K_d value of 18 mL g^{-1} for 4 of the 7 boundary stations. Data were questionable at two of the remaining three, while the third is near the OSWI.

The second method focused on a search of the literature for values of K_d for uranium in soils similar to those near the FMPC. One set of data, the Multimedia Environmental Pollutant Assessment System (MEPAS), provided K_d values for uranium in soils of different pH and composition. We concluded that approximately 50 mL g^{-1} is an appropriate estimate of an effective uranium K_d for the soil types around the Fernald area, based on the MEPAS data.

With K_d estimates and the uranium soil data, it is possible to develop a general approach to estimating total deposition of airborne uranium throughout the region surrounding the FMPC. We describe this approach in Appendix N. The resulting estimates of total deposition of airborne uranium, adjusted for levels of non-airborne contamination associated with the OSWI, range from 1.7×10^5 kg assuming a K_d value of 50 mL g^{-1}, to 9.0×10^5 kg assuming a K_d value of 15 mL g^{-1}. The higher estimate corresponds to a value of K_d that is approximately equal to the one derived from the regression estimates (18 mL g^{-1}), which implicitly account for local conditions and weathering. We suggest that this higher estimate, even with its attendant uncertainties, carries greater weight than the lower estimate, which corresponds to values of K_d given in the literature for soils of the same type (Strenge and Peterson 1989). It is interesting to note that the lower estimate is about equal to the total release estimate for airborne uranium given in the Addendum to FMPC-2082 (Clark et al. 1989), which our current source term information indicates may too low. We believe the range 1.7×10^5 to 9.0×10^5 kg is likely to contain the true total deposition in the assessment domain of uranium released to the air from the FMPC during 1951–1988.

RADON AND RADON DAUGHTERS AND GAMMA RADIATION FROM THE K-65 SILOS

The K-65 Silos, in the waste storage area west of the production area, have been used to store K-65 materials since the early 1950s. The K-65 material was a waste product of the processing of uranium ores at both the FMPC and the Mallinckrodt Chemical Works in St. Louis. This material contains large quantities of radium-226, which decays to form radon-222, which in turn decays to form other radionuclides, called RADON DAUGHTERS. Radon gas and radon daughters have been released to the atmosphere since storage of the K-65 material began. Starting in 1979, the FMPC has taken various actions to reduce the quantities of radon released. More information about estimated releases of radon can be found in the reports for Tasks 2 and 3 of this project (Voillequé et al. 1991). There is also a potential for exposure to gamma radiation from the radium-226 decay products in the silos. To absorb gamma rays, earthen berms were constructed around the silos in 1964 and were extended in 1983. Figure 7 shows the location of the K-65 silos on a map of the FMPC site. Figure 8 summarizes exposure by inhalation to radon and radon daughters escaping from the silos and exposure to direct gamma radiation from concentrations of the two radon daughters lead-214 and bismuth-214 in the silos.

Transport and Dosimetry for Radon and Radon Daughters.

Although we calculate the environmental transport and dosimetry for radon releases separately from the particulate releases, we use the same transport models for radon as we use for uranium, including the model to account for the effects of building wakes. The radon source term includes two release components: a continuous release component, and a component that is estimated to be released only during daylight hours. The important difference for the daytime releases is the meteorology that would affect the transport of the radon. Generally, wind speeds are higher during the day than at night, and dispersion of the plume is greater. Separate meteorological data sets were developed for daylight-only releases. Appendix P can be consulted for additional information.

Several sources of environmental monitoring data for radon-222 in air have been located; however, they are relatively recent. Environmental radon monitoring around the Fernald facility was initiated in 1978 by the FMPC. We have obtained results of this preliminary radon sampling. A routine radon monitoring program was then established by the FMPC in July 1980 at locations on the site boundary. The routine monitoring program was expanded to additional locations throughout the 1980s. Summaries of the routine monitoring are provided in the annual environmental reports of the site, and we have also obtained more detailed information for some years.

Radon monitoring was also performed by Mound Laboratory (Hagee et al. 1985) and by the Ohio Department of Health (ODH) (Steva 1988). The Mound monitoring program included 17 onsite locations from September 1984 through early October 1986. The ODH monitoring occurred at 12 locations on the FMPC boundary and four control locations from June 1985 to November 1987. The Mound monitoring data were chosen for comparisons to model predictions in our study, because the locations are a greater variety of distances from the Silos. These data are evaluated in Appendix P, while the other data sets will be examined

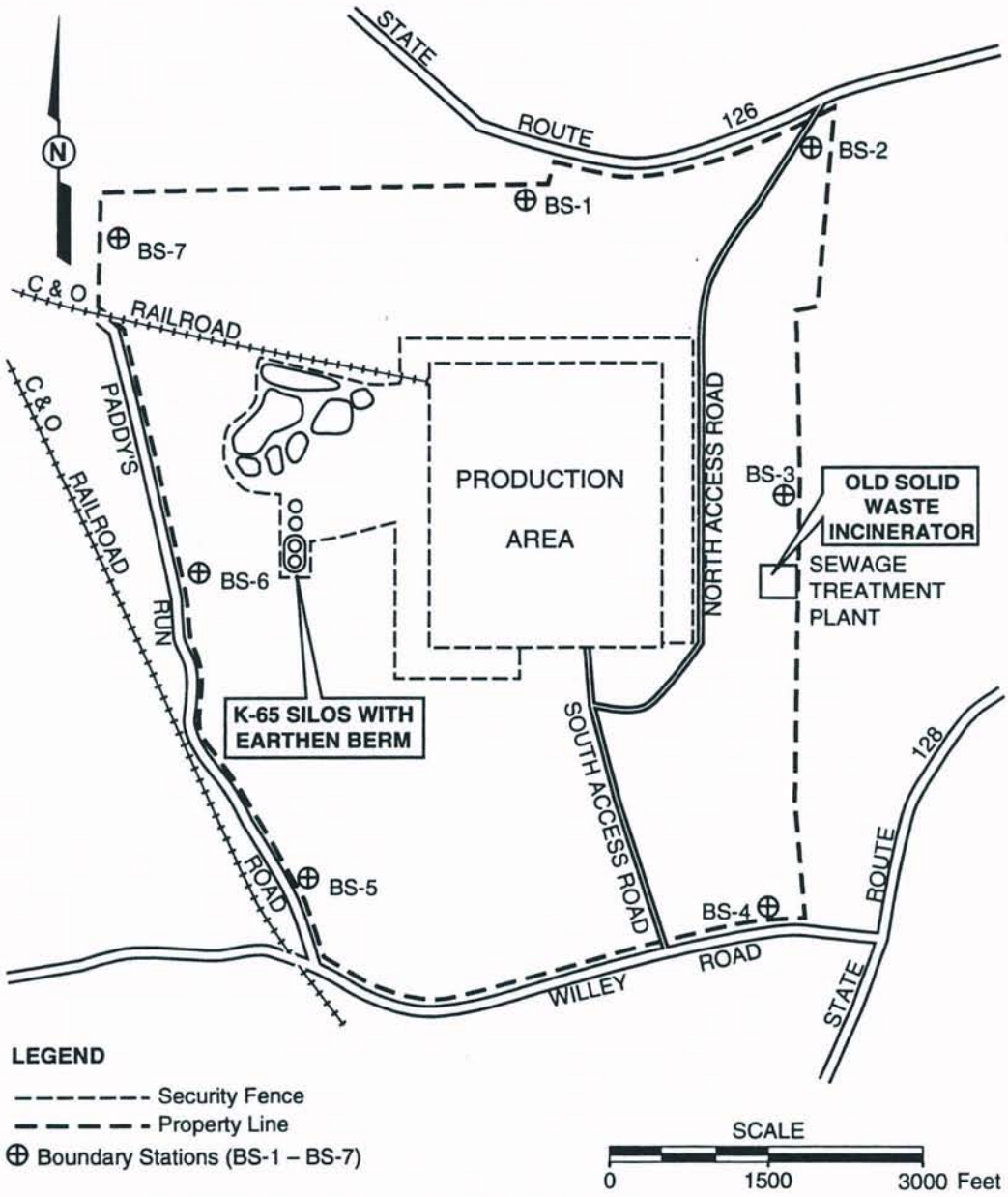

Figure 7. Layout of the FMPC site, showing the location of the K-65 silos west of the production area. Two metal-oxide storage tanks are just north of the K-65 silos. Also shown is the old solid waste incinerator (OSWI) on the east boundary.

further in the Task 5 report for this Project.

We used our transport model and estimates of radon releases to predict concentrations of radon in air at the locations of the Mound monitoring. From this comparison of predicted concentrations to the measured concentrations, it appears that our predicted concentrations are low by about a factor of two. This discrepancy could be due to inaccuracies in the atmospheric dispersion model and the associated input parameters, meteorology data, or estimated release

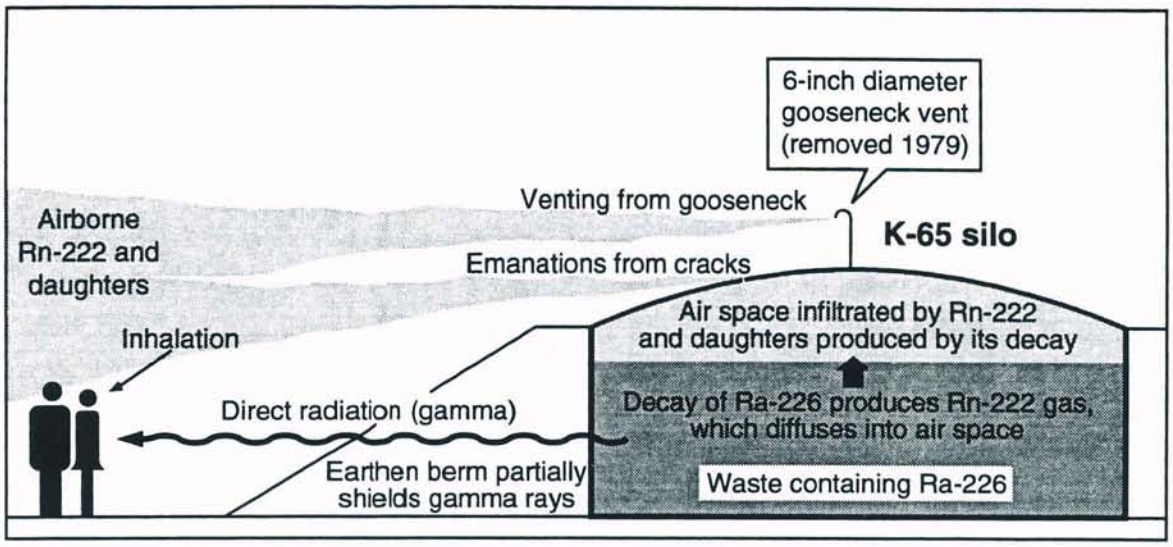

Figure 8. Potential exposure to radon-222, radon daughters, and gamma radiation from the K-65 Silos. For radon-222 and daughters that escape from the silos to the atmosphere, the principal exposure for members of the public is inhalation of the airborne material. Principal sources of direct gamma radiation from wastes in the silos are two radon-222 daughters — lead-214 and bismuth-214 — that become concentrated in the waste and the air space inside the silos. To provide shielding against the gamma rays from the silos, earthen berms were first built in 1964 and extended in 1983.

quantities. All of these possibilities will be investigated further before the final calculations are made, but the level of agreement is in the acceptable range.

Direct Exposures from Gamma Radiation Emitted from Storage Silos.

It has been recognized that the K-65 Silos (Silos 1 and 2) also present a potential source of direct radiation exposures to people living nearby. The large quantities of radium-226 in the silos decay to produce large quantities of radon and radon daughters in the K-65 material and in the silo head spaces. Two radon daughters in particular, lead-214 and bismuth-214, along with other radionuclides present, emit gamma radiations that are the source of potential exposures. The concentrations of radioactivity in Silo 3, which contains metal oxides and is just north of the K-65 Silos, are high enough that this silo may also be a significant source of direct radiation exposures.

For calculating doses to people from direct exposures from materials in the storage silos, we use models, because the monitoring data that exist are not comprehensive enough to estimate doses to individuals directly. In particular, no offsite monitoring of penetrating radiation was performed before the construction of earthen berms around the K-65 Silos in 1964. These berms provide significant shielding for gamma radiations emitted from the K-65 material, and the exposure rates to people would have changed significantly when the berms were added.

The exposure rate from gamma radiation from the storage silos decreases rapidly with increasing distance from the silos. Because of this rapid decrease, a very small number of

people, located close to the silos, would have received significant direct exposures from them. We have chosen to use a readily available computer software package, MicroShield 4, to calculate exposure rates for this pathway. Another simple model is then used to calculate doses from exposure rates. This model accounts for the fraction of time spent in the radiation field and for shielding provided by a home. The MicroShield software and the dosimetry model are discussed in detail in Appendix P. The final report of Tasks 2 and 3 will present characteristics of the K-65 and metal-oxide materials that are needed to use the models.

Only a few sources of environmental monitoring of penetrating radiation (primarily gamma radiation) have been located. Data from a survey along Paddy's Run Road were chosen for comparisons to model predictions, because the locations are at a greater variety of distances from the silos and are close enough that exposure rates were expected to be elevated above background. These data are discussed in more detail in Appendix P. The other data sets will be examined further in the report of Task 5 of this project.

The comparison of predicted and measured exposure rates indicates that our predicted values may be biased low. In general, the predicted excess exposure rates (relative to the location with the lowest exposure rate) were roughly one half the measured excess exposure rates. Factors contributing to the difference in measured and predicted exposure rates might include inaccuracies in the measurements, in the MicroShield model, or in parameter values chosen to describe the silos and the materials stored in the silos. The concurrence of this underprediction with that of radon concentrations near the silos also suggests the possibility that the quantity of radium-226 may have been underestimated as the waste was characterized. The level of agreement is acceptable, but the question will be examined further before final calculations are made.

EPISODIC RELEASES

The duration of a release of radioactivity is important in determining its air transport, deposition, and dosimetry. EPISODIC EVENTS are defined as short-term events that result in releases which warrant special dose assessment procedures. We developed the criteria and rationale for an episodic release in an earlier report (Voillequé et al. 1991): an episodic release must increase the composite uranium release rate by a factor of at least 10 for a period of less than 10 days. Episodic releases cannot be defined until the baseline source term for each year of the FMPC operations is defined. During the 1960–1962 period, there was one episodic release from the Pilot Plant, in November 1960. Appendix V describes the chronology of the accident and the methodology for treating this episodic release. Our estimate of the amount of uranium released (2,400 kg) is based upon the effluent measurements reported at the time, along with sampling bias calculations. Historical measurements of uranium in the surrounding ambient air and deposited onto gummed film were used to verify that an episodic release did occur (Appendix V).

Evaluating the airborne dispersion of the episodic releases is difficult because of the absence of local meteorological data for specific periods in the past (Appendix E). We will develop a procedure based on examining hourly weather sequences (wind speed, wind direction, stability) from the 1986–1991 Cincinnati dataset and correlating each sequence with simultaneous sequences from the Fernald dataset. The derived relationship will be assumed to hold during

the time of the accident and will be used to infer distributions of dose at verious locations in the vicinity. These distributions, which give a sense of the uncertainty in such predictions, are preferable to point estimates, which imply more certainty than is warranted.

SURFACE WATER AND GROUNDWATER TRANSPORT

Surface Water Overview

Surface water transport of radionuclides represents an important environmental exposure pathway for the dispersion of liquid effluents from the FMPC. Appendix R describes these exposure pathways and the methods that are used to determine radiation doses to individuals in the vicinity of the FMPC from these pathways. Radioactive materials that are released to surface water, such as uranium, are dispersed and diluted in the water and transported by the current. They may be deposited onto sediments on the bottom of the river, where they can enter aquatic food chains, or they may be taken up directly from the water by fish and humans. Exposure pathways are potential routes through which people may be exposed to radionuclides or radiation. For surface water transport, potential routes of exposure are ingestion of fish from the river, swimming or boating activities, and using river water for irrigation of crops or gardens near the river. The pathways are defined according to the ways that people could be exposed at certain times. Figure 9 diagrams the pathways and potential exposures.

In order to calculate radiation doses to individuals using water from the river, two primary parameters must be known. First, the source term, i.e., the quantity of material released from the site to the river, must be known. The source term can be estimated for any period of time, such as annually, monthly, or daily. Second, we must know the dilution of the material in the receiving body of water.

For the water pathways, there are two main points of release of radionuclides to surface water from the FMPC, and both are considered:

- The main effluent line to the Great Miami River
- Runoff and spills that enter Paddy's Run Creek.

The major water flow near the FMPC is the Great Miami River which enters the Ohio River approximately 18 miles (29 km) downstream from Cincinnati (Fig. 1). The river, located about a half mile east and south of the FMPC, flows in a generally southerly direction. Paddy's Run Creek is a small intermittent stream to the west of the FMPC that receives runoff from the west portion of the site during heavy rainfall (Fig. 2). The U.S. Geological Survey has measured river flow parameters, such as discharge rates and drainage areas, at several stations along the river on a daily basis since 1910, and all records are available for this project (USGS 1991). Appendix R provides flow rate data for the river, while our Task 2 and 3 report gives the data on effluent flow to the river from the site for 1960 to 1962 (Voillequé et al. 1991). The river flow rate follows a seasonal pattern with higher rates during the first half of the year and lower rates during the fall months when there is less rainfall. As the flow rate decreases, the dilution of the radioactive material decreases, and consequently, for a fixed release rate, the concentration of the radionuclides increases.

Both the source term and the flow characteristics of the river are subject to uncertainties. Some of the uncertainty is due to random variations in sampling and measurement techniques,

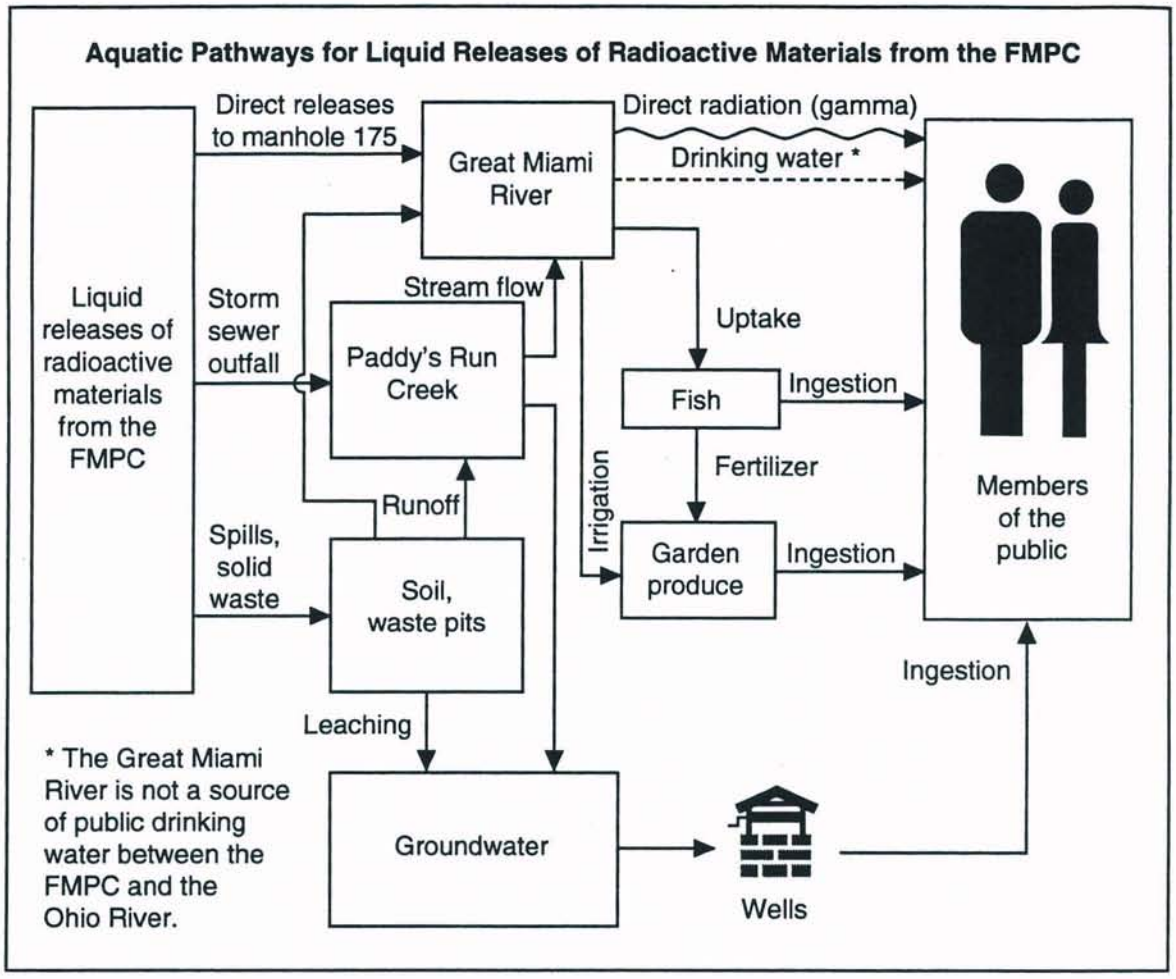

Figure 9. Aquatic pathways for liquid releases of radionuclides from the FMPC. The drinking water pathway, indicated as a dashed arrow from the Great Miami River, is hypothetical, because there has been no known use of water taken from the Great Miami River between the FMPC and the Ohio River for public drinking water. This stretch of the river is considered too turbulent for swimming, but fishing does occur there. Members of the public have reported that fish caught from the river are sometimes used for garden fertilizer.

while other types of uncertainty occur because not all processes are known exactly. In our Task 2 and 3 source term report, we emphasized the importance of estimating the uncertainty of our source term estimates. Likewise, it is important to estimate uncertainty associated with our estimates of radionuclide concentrations in the river, as well as our final radiation dose estimates.

Modeling Approach to Surface Water Transport

For this study we have evaluated the radionuclide concentrations in surface water, and ultimately the determination of radiation doses from the water pathways, in three ways. We have used two models — the NCRP Screening Model (NCRP 1989) and the GENII Model (Napier et al. 1988) — and a simplified Monthly Dilution (MD) model that we developed that combines our monthly source term estimates with uncertainty analysis. Table 5 summarizes these three methods for assessing surface water pathways. The NCRP and GENII models allowed us to do initial screening of surface water exposure pathways on annual source term estimates; however, these two models did not include uncertainty analysis (a subsequent version of GENII has incorporated this capability). The MD model is an improvement over the others because it makes use of our monthly source term estimates, relying on a statistical uncertainty analysis computer program (CrystalBall™, Decisioneering, Inc., 1727 Conestoga Street, Boulder, CO 80301) to provide bounds around our central estimates, and it provides best estimates of concentration and ultimately radiation doses.

Table 5. Methods for Assessing Surface Water Pathways

Assessment	NCRP Screening	GENII	MD Model
Source term resolution	Annual	Annual	Monthly
Exposure pathways	• External: boating, swimming, ground, and shore. • Internal: drinking water, eating fish, irrigated garden, milk, and meat	NCRP pathways plus inadvertent ingestion of soil	• Drinking river water • Consumption of fish
Type of dose estimate	Hypothetical person with maximum exposure	Hypothetical person with average or maximum exposure	Best estimate
Uncertainty analysis	No	No	Yes

From releases of radionuclides in liquid effluent, two modes of radiation exposure can occur: external and internal. External exposure can occur from ground contamination, shoreline activities or swimming. Internal exposures can occur when the radionuclides are ingested into the body, either directly in water, or indirectly through ingestion of contaminated foodstuffs or inadvertent ingestion of contaminated soil. Food crops and animal products such as milk or eggs that people ultimately consume may become contaminated with radionuclides if river or creek water used for irrigation or for watering animals. The Great Miami River is not a source of public drinking water between the FMPC and its confluence with the Ohio River. It is considered unsafe for swimming because of turbulence, but some people do fish the river.

On the basis of the information obtained from the NCRP Screening Model and the GENII code, we concluded that the major pathways contributing to radiation dose from uranium

in the surface water are from the consumption of drinking water, fish, and local garden produce. The importance of the consumption of garden produce depends greatly on the extent of irrigation with river water. Irrigation information from Butler and Hamilton Counties showed that the actual quantity of water used for irrigation is extremely small in comparison to the model assumptions.

Sediment sampling data collected since 1974 indicated that uranium has not accumulated in the sediments in the river where settling might be expected to occur. Consequently, the GENII model calculations showed that contributions from ground irradiation from shoreline deposits are not a significant contributor to radiation dose. For our MD model, we have considered the ingestion of drinking water and fish from the river as key exposure pathways from materials released from the FMPC to surface water.

Our initial approach to surface water dosimetry involved utilizing the NCRP and GENII models to provide conservative estimates of uranium concentration based on annual source term estimates for 1960–1962. Subsequently, with our MD model, using simple spreadsheet calculations, we incorporated monthly source term estimates and site-specific river flow data to provide best estimates of uranium concentration in the surface waters with uncertainty estimates. We will use our MD model to calculate radionuclide concentrations in the river and Paddy's Run Creek for all years.

Appendix R also describes the comparison of our predicted uranium concentrations with actual environmental measurements that were from the Great Miami River and Paddy's Run Creek. As discussed previously, this comparison process is called validation, and it provides a measure of proof that our models for calculating environmental concentrations, and ultimately radiation doses, are reasonable. It should be emphasized that the actual environmental measurements were not used in our model development. The sources of information for the sampling measurements are the original analytical data sheets from the Analytical Department of National Lead Company of Ohio (NLCO 1960–1962). This comparison shows good agreement between measured uranium concentrations in the river and those calculated with our MD model. For Paddy's Run Creek, the measured concentrations cover a wide range, most likely due to the erratic water flow in the small stream. However, the calculated uranium concentration based on high and low flow rates for the creek do encompass the range of concentrations measured in the creek. This agreement suggests that the methods we have developed to determine environmental concentrations of uranium and other radionuclides based on our monthly source term data are reasonable.

Groundwater Transport

Significant uranium contamination in groundwater south of the FMPC site, due to releases from the site, was discovered in late 1981, and concentrations in this South Plume remain elevated. Our earlier work on Tasks 2 and 3 of this Project indicated that the uranium contamination had not migrated outside the FMPC boundary by 1962. For an as yet undetermined length of time, uranium from the South Plume was a source of potential radiation exposures to nearby residents.

Since the discovery of the uranium contamination in the South Plume, existing private wells and additional wells have been sampled by the FMPC and others. This sampling has shown that only three of the private wells have been impacted by uranium contamination.

Thus only a small number of people could have received radiation doses from contaminated groundwater. Accordingly, we believe that detailed assessments of radionuclide transport through groundwater and resultant doses to people are not warranted. Instead, simple methods will be used to estimate likely concentrations of uranium in wells in the South Plume for times between the mid-sixties and late eighties. Additional information is provided in Appendix S.

The available measured concentrations of uranium in wells will be examined to determine if significant trends exist. Recent studies of the groundwater around the FMPC site have indicated that the primary source of the uranium contamination in the South Plume is uranium in waters released from the FMPC to Paddy's Run Creek and to the storm sewer outfall ditch (which flows into Paddy's Run Creek). The concentrations of uranium in waters released to the outfall ditch and to Paddy's Run Creek will also be evaluated, and compared with the concentrations seen in the South Plume. From these two data sources (concentrations in the South Plume since 1981 and concentrations in site releases for most years of operation), the concentrations in the South Plume for earlier time periods (prior to 1981) will be estimated. These estimated concentrations will be provided in the final report of Tasks 2 and 3 of this Project.

EXPOSURE PATHWAYS AND DOSE CALCULATIONS

To reach the endpoint of the Fernald Dosimetry Reconstruction Project, which is the calculation of radiation doses from releases of radionuclides to air and water, we analyze how the material reaches people and is taken into the human body. The potential internal exposure pathways from releases to air include inhalation, ingestion of agricultural products grown in contaminated soil, and inadvertent ingestion of radionuclides in soil. Appendix Q describes the RAGTIME model, which is used to determine how much radioactive material is ingested. To calculate doses to people of different ages, we use breathing rates specific to age and different levels of physical activity. We also derive age-specific consumption rates for various types of food.

Internal dose conversion factors (DCFs), which are also age-specific, are used to relate the amount of radionuclide taken into the body to a radiation dose. Similarly, external DCFs relate exposure to radionuclides on ground surfaces and in surrounding air to dose received by people. Finally, we need to understand how the population size and make-up, or demographics, have changed between 1950 and 1988 when the plant stopped processing (Appendix U).

Agricultural Parameters

We use a model, called RAGTIME (Radionuclides in AGricultural systems, a TIME dependent model), to quantify the transport of radionuclides through the food chain following the release of the material to the atmosphere. In the context of the FMPC assessment domain, we consider radionuclide contamination of food crops and animal forage by deposition of airborne material, and irrigation with water from contaminated sources. Through these mechanisms, radioactivity can be taken up through the plant roots from the soil or attached to plant surfaces. The radioactivity may reach people who eat the vegetables, or the products of animals that have consumed the contaminated forage or water.

The RAGTIME model was developed at Oak Ridge National Laboratory in the late 1970s (Pleasant et al. 1980). The model was later revised and reprogrammed (Killough and Hoffman 1987) for an international model validation exercise, called BIOMOVS, which focused on data from the Chernobyl reactor accident. RAGTIME was among the most successful of the BIOMOVS models in in predicting resultant concentrations of radioactivity on pasture grass, in milk, and on grain after transport through the air and deposition. Appendix Q presents the differential equations and glossary of symbols for describing these transfer processes to crops, beef, and milk. Radionuclide-specific parameters are considered. These include distribution coefficients for pasture and garden produce, and transfer coefficients for beef and other animal products and milk. Finally, we have compiled data on agricultural production, growing periods, and usual planting times for garden crops in Butler and Hamilton Counties in southwestern Ohio.

A comparison of inhalation doses with food ingestion doses in the FMPC area using RAGTIME will indicate the extent of detail that will be necessary in treating the food-chain pathway. To do this comparison, we will adopt possible agricultural scenarios for production and consumption of products by individuals living in various parts of the FMPC assessment domain. One scenario that is described in Appendix Q uses a hypothetical individual living near the FMPC boundary, who only eats beef, milk, pork, lamb, chicken, and eggs produced on his property, and who only eats vegetables produced in his own garden. This scenario represents a starting point, with assumptions that maximize the estimate of dose to the individual. If the resulting doses by ingestion are small in comparison with those for inhalation, it would seem reasonable to focus on pathways that contribute relatively more to the dose. Uncertainty estimates for plant/soil distribution coefficients and for feed-to-milk and feed-to-beef transfer coefficients are based on estimates reported in the scientific literature. These uncertainty estimates are listed in Appendix Q.

Dose Conversion Factors

To determine radiation doses to individuals from predicted exposures to radionuclides, we use quantities called DOSE CONVERSION FACTORS (DCF). Internal dose conversion factors provide either an internal dose per unit activity of a radionuclide with food or water, or the dose per unit activity inhaled. Similarly, external DCFs give an external dose rate per unit concentration in air or water from immersion in contaminated air and water or the direct exposure due to unit concentrations of radionuclides in the soil. In the case of internal exposure by inhalation of particulate matter, the dose conversion factor also depends on the distribution of particle diameters. The dosimetry for radon (^{222}Rn) and its decay or daughter products is treated separately from other internal emitters.

Dose conversion factors are dependent on the radionuclide and its physical and chemical form, exposure mode, target organ or tissue, and the age and sex of the exposed individual. Appendix T provides the details of the interpretation of DCFs for the Fernald project. At this point, it is anticipated that most risk resulting from radionuclides released from the FMPC will be associated with internal dose. Daughter products formed after radionuclides are taken into the body are implicitly considered in the internal dose conversion factors, but those formed during environmental transport must be accounted for by the transport model, and those formed while the radioactive materials are present in the production facility must

be included in the source term.

The internal dosimetry for this project is based principally on the methodology of the International Commission on Radiological Protection (ICRP) as described in ICRP Publication 30 (ICRP 1979), with some anatomical and physiological data based on data from ICRP Publication 23 (ICRP 1975). This methodology is summarized in Appendix T. Since the ICRP Publication 30 methodology is based on models for a hypothetical young adult male, we consider other sources of information for the age and sex dependence of dose conversion factors. ICRP Publication 56 Part 1 (ICRP 1990) provides dose conversion factors with dependence on age at the time of intake for six groups represented by the ages 3 months, 1, 5, 10, and 15 years, and adult. However, the factors are reported for only a limited number of radionuclides, which do not include uranium or thorium isotopes. For these latter radionuclides, we used tabulations of age-dependent factors prepared at the Oak Ridge National Laboratory for the U.S. Nuclear Regulatory Commission (Cristy et al. 1986). The factors are presented as ratios for conversion of the adult dose to that of the desired juvenile group.

For inhalation, the dose conversion factors of ICRP Publication 56 Part 1 are based on the current ICRP lung model (ICRP 1979), which is not age-specific. Although a new model based on age-specific physiology is under development, it will not be possible to incorporate the newer lung model into our methods based on the current project schedule.

The dose conversion factors for inhalation depend on the aerodynamic particle diameter (AMAD) of the inhaled material. Dose conversion factors have been computed for an AMAD of 1 μm. The DCFs are adjusted for particle sizes measured and calculated for FMPC effluents.

Dose to the lungs from the radon decay chain is handled differently than that for inhaled particulates and is based on factors summarized by the National Council on Radiation Protection and Measurements methods (NCRP 1984). These factors are given for the adult male and female and the ten-year-old child.

Dose to the embryo/fetus from radionuclides taken into the body of a pregnant woman is based on methods and data given in Regulatory Guide 8.36 of the Nuclear Regulatory Commission (USNRC 1992).

External dose from immersion in contaminated air and water is calculated from dose-rate conversion factors developed at the Oak Ridge National Laboratory and tabulated in a U.S. Department of Energy report (USDOE 1988). Age-dependent external dose-rate conversion factors are not available at this time. However, it is anticipated that external dose will constitute a minor component of the total dose to residents near the FMPC.

It is probable that an approximate method will have to be developed for adjusting the internal DCFs of Appendix T in a way that would effectively replace the 50-year integration period by a variable time. The result would be a factor that would be more appropriate for the dose estimates required for epidemiology (Appendix A).

FMPC Population Dynamics

We evaluated four sources of population data for the Fernald area for the period 1950 through 1990 to determine the best estimates of location, size, and distributions of age and sex of individuals who resided within the 8-km assessment domain centered at the FMPC site (Appendix B). Four townships within Butler and Hamilton Counties have boundaries within the domain: Ross and Morgan Townships in Butler County and Crosby and Colerain

Townships in Hamilton County. But the domain does not contain these townships in their entirety.

It was generally necessary to assume that the population changes within each township in the FMPC domain over four decades were proportional to those of the entire township. It was further assumed that the populations within the townships grew exponentially between censuses. Four demographic models based on four sources of population data are reviewed in Appendix U for their applicability to this project. Tables U–2 through U–5 in Appendix U list the population estimates derived from Models 1, 2, 3, and 4, respectively. The Model-1 population estimates are based on data prepared by Oak Ridge National Laboratory and presented in the 1989 FMPC Annual Environmental Monitoring Report. These population data within the FMPC domain are presented as a grid divided into 16 compass sectors, with each sector partitioned into cells ranging from 1 to 8 km from the center of the production area.

To verify the population estimates obtained from Model 1, a second model was developed on the basis of 1990 U.S. Census township data. Because this model assumes that the population in each township was uniformly distributed, the estimates for the Colerain township were unreasonably high since this township includes portions of greater Cincinnati. The region of the FMPC domain occupying the Colerain township is known to be sparsely populated.

The third model was developed from census-block data and census-block maps. The block data and maps provide greater spatial resolution than the census township data. However, since 1990 is the only census year for which the block data are available, we assumed that the 1990 data for Hamilton and Butler Counties would be representative of census blocks for previous decades. The population estimates from Model 3 approached the estimates of Model 1 and seemed a reasonably good model. However, although Model 3 represented an improvement in the location of the domain population over Model 2, it resulted in zero population estimates for some locations within the domain. We questioned the accuracy of the Model 3 estimates relative to the area inhabited by individuals within the Fernald domain.

To resolve this problem, we proposed a fourth model based on USGS topographical maps that are published every 30 years. These maps provide locations of highways, towns, and structures (such as residences, businesses, and farm buildings). We were able to estimate population size based on detailed locations of structures for two decades (1950 and 1980). Consequently, Model 4 was chosen as the best representation of the FMPC domain demographics for the four decades because of the resident location information provided by the USGS maps.

A comparison of the population estimates for the domain shows that Models 1, 3, and 4 are in good agreement. However, the primary advantage of Model 4 is that population size is estimated for each cell of the FMPC domain grid. Further, this model comparison provides a measure of the uncertainty of the estimated numbers of individuals living within the FMPC domain during the years 1950 to 1990 based on the four different modeling assumptions. These population estimates, combined with the uncertainty bounds, will be used for the dose calculations in Task 6.

CONCLUSIONS

The Task 4 report presents our methods for calculating radiation doses to the population in an 8-km circular assessment domain from releases of radionuclides to air and water from the FMPC. Validations that have been carried out so far inspire confidence in the models and the approaches. Validations for atmospheric dispersion of particulates have been based on the reconstructed source term and historical monitoring data for the years 1960–1962. Validation of the atmospheric transport modeling of radon and radon daughters from the K-65 silos was carried out with monitoring data from the 1980s. Relatively more attention has been given to atmospheric transport processes than to the surface water and groundwater models because the air-dependent pathways are likely to dominate the doses and because of the greater complexity of the validation for air transport models.

Particle size has proved to be an important factor in the analyses of atmospheric releases. Particles released from the stacks fitted with dust collectors, as well as those particles that pass through the scrubbers of Plant 2/3 and Plant 8 without being scavenged, are in the respirable size range and consequently are important from the point of view of inhalation dosimetry. Also, these smaller particles do not deposit rapidly from the plume and have a higher probability of being transported long distances. On the other hand, much larger particles came from the scrubbers as the result of reentrainment of droplets of scrub liquor in the exhaust gas stream. These large particles deposit rapidly from the plume and have low probability of traveling long distances. They are relatively unimportant for inhalation dosimetry. Historic air monitoring data from the production area perimeter stations underestimate the model-predicted uranium concentrations in air partly because of the low collection efficiency of the samplers for large particles. On the other hand, the model-predicted deposition underpredicts gummed film measurements at the same locations by about a factor of two. Although the models take the particle size distributions of the different release sources into account, it appears that the model's deposition mechanism may be underestimating the true deposition rate. This and related questions will be investigated further, but the general agreement of model predictions and historic monitoring data is quite acceptable and constitutes a positive confirmation of the modeling approach.

The same basic atmospheric transport models are used for radon and radon daughters released from the K-65 silos as for particulate releases from rooftop stacks of the production plants. Validation calculations indicate underprediction of measurements by about a factor of two. Comparisons of calculated gamma dose rates from the silos with measurements of the radiation field also indicate underprediction by about a factor of two. One possible reason for both underpredictions is mischaracterization of the waste in the silos with respect to the quantity of radium-226. These questions will also be examined further, but the results are in the acceptable range and provide the basis for a recalibration of the models.

Surface water calculations are in good agreement with measured uranium concentrations in the Great Miami River and Paddy's Run Creek. These results support the application of our methods of surface water analysis to all years of FMPC operation.

For the period covered by the study (1951–1988), the potential for dose from groundwater contaminated by FMPC effluents appears to be confined to three private wells. Available measurements in these and other wells will be examined for significant trends. Also, concen-

trations of uranium in waters released to the outfall ditch and directly to Paddy's Run Creek (recently shown to be the primary sources of uranium contamination in the South Plume) will be compared with the concentrations in the South Plume. The empirical relationship between these data sources and release records for recent years will be applied to earlier release records to estimate concentrations in the South Plume during earlier periods. Validations for this process are essentially foreclosed by the necessity to use the environmental data for calibrating the model. But this disadvantage is partially offset by the fact that during most of the period of maximum exposure (since 1981), the dose will be estimated directly from measured contamination in the exposure medium (i.e., the private wells).

As the reconstructed source term for the remainder of the period of FMPC operations becomes available, additional validations of the models will be undertaken. Data from the 1950s are fragmentary, however, and releases during recent years have been much lower than in the past, making validations with data during these periods more difficult and possibly less conclusive than those we have carried out for 1960–1962.

REFERENCES

Beck H.L., I.K. Helfer, A. Bouville, and M. Dreicer. 1990. "Estimates of Fallout in the Continental U.S. from Nevada Weapons Testing Based on Gummed-Film Monitoring Data." *Health Phys.* **59**: 565–576.

Boback M.W, T.A. Dugan, D.A. Fleming, R.B. Grant, R.W. Keys. 1987. *History of FMPC Radionuclide Discharges.* Rep. FMPC-2082, UC-11. Feed Materials Production Center, Westinghouse Materials Company of Ohio, Cincinnati, Ohio.

Clark T.E., L. Elikan, C.A. Hill, and B.L. Speicher. 1989. *Addendum to FMPC-2082: History of FMPC Radionuclide Discharges — Revised Estimates of Uranium and Thorium Air Emissions from 1951–1987.* Westinghouse Materials Company of Ohio, Cincinnati, Ohio.

Cristy M.W., R.W. Leggett, D.E. Dunning, Jr., and K.F. Eckerman. 1986. *Relative Age-Specific Radiation Dose Commitment Factors for Major Radionuclides Released from Nuclear Fuel Facilities.* Rep. NUREG/CR-4628, ORNL/TM-9890, Oak Ridge National Laboratory, Oak Ridge, Tennessee.

Hagee G.R., P.H. Jenkins, P.J. Gephart, and C.R. Rudy. 1985. *Radon and Radon Flux Measurements at the Feed Materials Production Center, Fernald, Ohio.* Rep. MLM-MU-85-68-0001, Mound Laboratory, Monsanto Research Corporation, Miamisburg, Ohio.

Healy J.W. 1980. "Review of Resuspension Models." In: *Transuranic Elements in the Environment,* pp. 209-235 (W.C. Hanson, Ed.). DOE/TIC-22800. National Technical Information Service, Springfield, Virginia.

International Commission on Radiological Protection (ICRP). 1990. *Age-Dependent Doses to Members of the Public from Intake of Radionuclides: Part 1.* ICRP Publication 56. *Ann. ICRP* **20**(2): 3–122. Pergamon Press, Oxford.

International Commission on Radiological Protection (ICRP). 1979. *Limits for Intakes of Radionuclides by Workers.* ICRP Publication 30 Part 1. *Ann. ICRP* **2**(3/4). Pergamon Press, Oxford.

International Commission on Radiological Protection (ICRP). 1975. *Report of the Task Group on Reference Man.* ICRP Publication 23. Pergamon Press, Oxford.

Killough G.G. and F.O. Hoffman. 1988. "Validation of the RAGTIME87 Dynamic Food-Chain Model against Fallout Data from the Chernobyl Accident." Abstract of a presentation. *J. Tenn. Academy of Sci.* **63**(2): 46.

Napier B.A., D.L. Strenge, R.A. Peloquin, and J.V. Ramsdell. 1988. *GENII — The Hanford Environmental Radiation Dosimetry Software System.* Vols. 1–3. Rep. PNL-6584, Pacific Northwest Laboratory, Richland, Washington.

NCRP. 1989. *Screening Techniques for Determining Compliance with Environmental Standards, Releases of Radionuclides to the Atmosphere.* NCRP Commentary No. 3. National Council on Radiation Protection and Measurements, Bethesda, Maryland.

NCRP. 1984. *Evaluation of Occupational and Environmental Exposures to Radon and Radon Daughters in the United States.* NCRP Report No. 78. National Council on Radiation Protection and Measurements, Bethesda, Maryland.

NLCO. 1960–1962. Analytical data sheets for three-day composite or weekly water samples taken from Paddy's Run and the Great Miami River, respectively. Analytical Department, National Lead Company of Ohio, Cincinnati, Ohio.

Pleasant J.C., L.M. McDowell-Boyer, and G.G. Killough. 1980. *RAGTIME: A FORTRAN IV Implementation of a Time-Dependent Model for Radionuclides in Agricultural Systems. First Progress Report.* Rep. NUREG/CR-1196, ORNL/NUREG/TM-371, Oak Ridge National Laboratory, Oak Ridge, Tennessee.

Ramsdell J.V., Jr. 1990. "Diffusion in Building Wakes for Ground-Level Releases." *Atmos. Env.* **24B**: 377–388.

Reed K.P. 1985. *A Study of the Emissions of the Process Stacks at NLO: Plant #9, Plant #5-260, Plant #5-261.* Unpublished report from Northern Kentucky Environmental Services (NKES) of a study commissioned by NLO.

Steva D.P. 1988. *Ohio Department of Health Study of Radioactivity in Drinking Water and Other Environmental Media in the Vicinity of the U.S. Department of Energy's Feed Materials Production Center and Portsmouth Gaseous Diffusion Plant.* Ohio Department of Health, Columbus, Ohio.

U.S. Department of Energy (USDOE). 1988. *External Dose-Rate Conversion Factors for Calculation of Dose to the Public.* Rep. DOE/EH-0070. Assistant Secretary for Environment, Safety, and Health, Office of Environmental Guidance and Compliance, Washington, D.C.

U.S. Geological Survey (USGS) 1991. *Water Resources Data Ohio Water: Year 1991. Volume 1. Ohio River Basin.* U.S. Geological Survey Water—Data Report OH-91-1. Prepared in cooperation with the Sate of Ohio and with other agencies.

U.S. Nuclear Regulatory Commission (USNRC). 1992. *Radiation Dose to the Embryo/Fetus.* Regulatory Guide 8.36, Office of Nuclear Regulatory Research, Washington, D.C.

Voillequé P.G., K.R. Meyer, D.W. Schmidt, G.G. Killough, R.E. Moore, V.I. Ichimura, S.K. Rope, B. Shleien, and J.E. Till. 1991. *The Fernald Dosimetry Reconstruction Project, Tasks 2 and 3: Radionuclide Source Terms and Uncertainties — 1960–1962.* Rep. CDC-2. Radiological Assessments Corporation, Neeses, S.C.

APPENDIX A

DOSIMETRIC ENDPOINTS OF THE STUDY

INTRODUCTION

It is the purpose of Task 4 to assemble a methodology for estimating releases of radioactive materials from the FMPC during its period of operation (1951–1988), simulating the movement of those materials through environmental pathways and into media to which people are exposed, and estimating the radiation dose to exposed individuals and population groups on the basis of individual or group-averaged exposures. The materials are uranium isotopes and several other radionuclides (either decay products of uranium, called "daughters," or other radionuclides that were introduced into feedstocks in uranium recycled from reactors); the identity and relative abundances of these radionuclides are discussed in Appendix C. They have been released, in amounts that varied over time, to the atmosphere (Appendices D through O) and to surface water (Appendix R) and groundwater (Appendix S). In addition, radon gas (^{222}Rn) and radon daughter products have been released to the atmosphere from wastes stored in the K-65 silos west of the production area (Appendix P).

Other appendices give details about the mechanisms of transport and how we model them. It is the purpose of this appendix to consider what doses will be calculated and how uncertainties will be incorporated. This question is more complicated than it may seem. First, it is constrained by the use that is to be made of the estimates of dose. The point of view of this study is that dose is calculated for the use of epidemiologists for their use in investigating the appropriateness of an epidemiological study. Such a study would have the goal of identifying any associations between exposure to radionuclides released from the FMPC and health outcomes in the local population. But the form in which dose estimates are needed depends upon the design of the study being considered and the method of calculating the power of such a study to detect an association between dose and health effects if one really exists. Second, the straightforward use of dose conversion factors for internal dose may not be sufficient for the estimates of dose that are required (Appendix T). We develop some conceptual detail of an alternative approach in this appendix. Third, the computational demands of any approach that is adopted must be considered. The Centers for Disease Control and Radiological Assessments Corporation have agreed that as a design criterion, the computations must be manageable with office computers (generally understood to be DOS machines with the Intel 80386-80387 or 80486 processors and sufficient memory). This is a practical constraint because of the anticipated need for both contractor and sponsor to be able to make repeated calculations and the substantial demand that the Monte Carlo methods used for the uncertainty analysis impose. Consequently, there are limitations on the variety of information that can be obtained from a particular implementation of the dose algorithm.

MODELING THE POPULATION OF THE ASSESSMENT DOMAIN

Dose to an individual from inhalation of airborne radioactivity, because of the direct dependence of intake on air concentration, varies with that individual's principal locations within the assessment domain over time. Dose due to ingestion is more complex to deal with because of the distribution of agricultural products that may have been contaminated by virtue of where they were produced within the region (we do not expect this component to be major for the FMPC region, but it will be considered). Intakes and doses also depend on the age of the individual at the time of exposure and on other lifestyle factors, such as fraction of time spent outdoors, level of activity, dietary habits (e.g., fraction of food raised in a garden or on a family farm vs. commercial products from outside the domain), and special exposures, such as swimming in contaminated water.

The assessment domain has been subdivided into 128 regions or CELLS, based on the 16 conventional wind sectors and eight concentric circles with radii ranging from one to eight km in increments of one km (Appendix B). It may eventually be necessary to consolidate some of these cells to reduce the total number, but for the purpose of this explanation, let keep the partitioning of the domain as we have stated. We index the cells as $i = 1, \ldots, 128$. The index i will thus represent RESIDENCE.

Age dependence will be treated by consideration of several discrete age intervals, such as newborn, infant, child, adolescent, and adult (the final breakdown may be different). For the explanations to be given below, however, it will be less confusing to pretend that we have data for age-specificity with the resolution of one year. With this assumption, we use the index j (and sometimes other symbols) to refer to an age cohort.

We choose to be a bit vague about other characteristics, which we consolidate into a single linear list indexed by k.

There are two points of view of particular interest. The first is concerned with tracking a particular individual (perhaps a hypothetical one) through time and estimating the resulting dose. If one year is the increment of time considered, then for each year we would wish to know the individual's residence cell, age for that year, and the other lifestyle attributes (which may change from year to year). The second point of view, which is associated with the power analysis of a possible epidemiological study, considers the entire population over time and seeks to treat dose in terms of a probability distribution $G(x)$, where

$$G(x) = \Pr[\text{dose to a randomly chosen individual} \leq x]. \qquad \text{(A–1)}$$

This distribution, together with specified risks of disease per unit dose, would be used in a Bayesian approach described by Lubin et al. (1988).

To be clear, we must realize that the population from which the random selection referred to in Eq. A–1 would be drawn consists of all individuals who lived in the assesssment domain at any time during the specified period (1951–1988), whether or not such individuals still reside there, and whether or not such individuals are still alive. It is the class of all exposed individuals, where "exposed" means having resided within the domain at any time during that period. The dose x in Eq. A–1 is understood to mean dose attributable to releases from the FMPC.

If all individual histories (in the sense of the first point of view) were known, and if the dose could be calculated for each, then the distribution $G(x)$ could be constructed, simply by sorting all computed doses into an array of increasing order and for any given dose x, counting the number of doses $\leq x$, and dividing that number by the total number of doses in the array (i.e., the total number of individuals).

In practice, of course, such a construction cannot be realized. The number of individuals is too large, many are no longer living in the domain, and even if it were possible to interview all of those still surviving (or a representative sample), many would likely have difficulty furnishing the kind of details that would be needed. For purposes of preliminary analyses, at least, it is necessary to use a coarser model of this population, one that combines individuals into groups according to the similarity of their exposure. This task is greatly simplified if we do not consider distribution of locally-produced agricultural products to consumers residing within the region. Rather, it is likely that we will adopt the assumption that some specified fraction of the food each individual consumes was produced in a garden or family farm, at the place of residence, with the remainder of the individual's diet coming from uncontaminated sources. Appendix Q lists types of garden produce that are typical of the region. With this assumption, interaction among the geographic cells is minimized within a given year. The dose to which an individual is committed by a particular year's exposure is determined by the cell in which the individual resided for that year, together with age and lifestyle factors.

There are individuals, of course, who reside in one cell and spend considerable amounts of time in another (or others). For example, many people commute considerable distances to and from work. If such a pattern can be quantified for the FMPC domain, it could be necessary to adjust the population of each cell, age, and lifestyle category by a full-time equivalent (FTE) factor to account implicitly for the frequent inter-cell migrations.

Once the population model has been worked out, we assume that we can partition it into subsets with (possibly FTE) numbers of individuals $n_{i,j,k,t}$, where

i = the cell of residence

j = the age group

k = the group determined by lifestyle factors

t = the year (for 1951, t = 1, and so on).

A study of population in the FMPC domain during the assessment period was undertaken by J.F. Rogers of the Centers for Disease Control, and information from his study is presented in Appendix U. This information is clearly relevant to estimating the $n_{i,j,k,t}$.

Let us summarize this section by saying that we are seeking a practical way to estimate the probability distribution $G(x)$ (Eq. A–1) for the population of the FMPC domain. The numbers $n_{i,j,k,t}$ will be used to construct an approximation to this distribution when the question of how to allocate dose to each time interval (i.e., each year) is resolved. We turn to this question in the next section.

SOME NOTATIONS FOR INTERNAL DOSE RATE AND DOSE

Dynamics of dose to an organ of the body from an external source are comparatively simple. The dose rate is given by a dose-rate conversion factor multiplied by the strength of the source (in our context, the concentration of radioactivity in the source medium; see Appendix T). There is essentially no delay in the delivery of the dose; if the organ is exposed for one hour, the dose rate from the source becomes effectively zero as soon as the source is removed.

For internal dose, the picture is quite different. When a radionuclide is taken into the body through inhalation or ingestion, dose rates to body organs vary as the material is translocated and then gradually removed from the body by metabolic processes and radioactive decay. For radionuclides of short half life, the removal is obviously rapid. But some long-lived materials are removed slowly from some organs. The result is a residual dose rate that declines slowly over time. An example is uranium in bone (Appendix T). This circumstance complicates the evaluation of dose in a dynamic population with varying distributions of age. We need some notation to help describe the dynamics.

It will help conceptually to take some fundamental period as the unit time step, and for this purpose we choose one year. The fundamental quantity that we define is

$\delta(a,t)$ = the average residual dose rate to an organ during year t after an acute (i.e., short-duration) unit intake of a radionuclide; a is the age of the individual at the time of the intake.

Figure A–1 illustrates the dose-rate curve following the intake of radioactivity at time zero and represents the residual dose rate for year t as the area under the curve (or that of an equivalent rectangle) between times $t-1$ and t. The quantity $\delta(a,t)$ could have a subscript for the organ, one for the radionuclide, and one for the mode of exposure (i.e., inhalation or ingestion), but for simplicity of explanation, we suppress these subscripts.

Suppose there is a chronic intake of the radionuclide, given by I_1 for the first year, I_2 for the second year, and so on, up to I_t for year t. To calculate the dose rate during year t, the residual dose rate for year t and those for all previous years must be added. The contribution to the total residual for material taken in during the year t is $I_t\delta(a+t-1,1)$, because year t is year 1 relative to the year of intake, and the age at the beginning of that year was $a+t-1$ (see Fig. A–1). Similarly, for the previous year's contribution, we have $I_{t-1}\delta(a+t-2,2)$, and so on. The total is

$$\begin{aligned} d(t;a,\{I_1,\ldots,I_t\}) &= I_t\delta(a+t-1,1) + I_{t-1}\delta(a+t-2,2) + \cdots + I_1\delta(a,t) \\ &= \sum_{q=1}^{t} I_{t-q+1}\delta(a+t-q,q)\,. \end{aligned} \qquad \text{(A–2)}$$

The notation $d(t;a,\{I_1,\ldots,I_t\})$ for the sum explicitly shows the intakes and their times; the time of the earliest intake is the year the individual was of age a, and the time of the latest is t, the year for which the total is being evaluated. Figure A–2 illustrates this combination schematically for the case where all of the intakes are equal.

The total dose at the year t from all of the intakes I_q is the sum of all the dose rates (each year's average dose rate is equal to the dose delivered during that year). For this total dose,

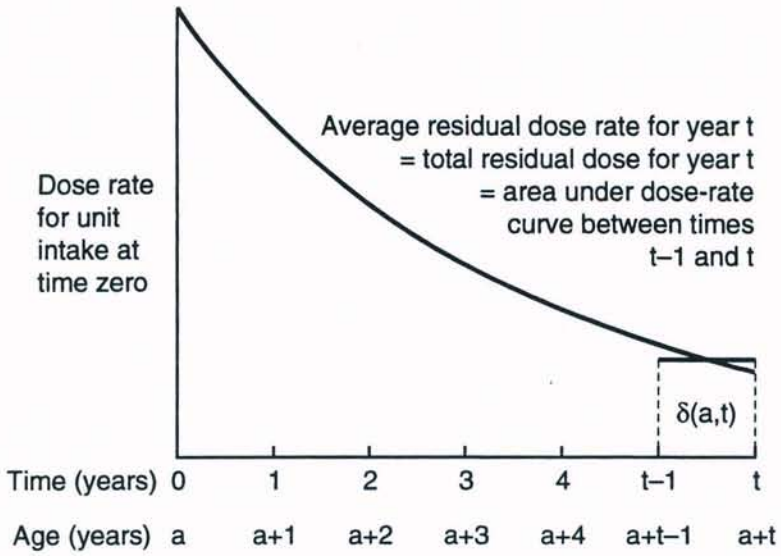

Figure A–1. Illustration of residual radiation dose rate to an internal organ after the initial acute intake of a unit quantity of a radionuclide into the body.

we invent another notation similar to the previous one:

$$D(t; a, \{I_1, \ldots, I_t\}) = d(1; a, \{I_1\}) + d(2; a, \{I_1, I_2\}) + \cdots + d(t; a, \{I_1, \ldots, I_t\}). \qquad \text{(A–3)}$$

(If you think in terms of integrals, multiply each term by Δt = 1 year. This will make the units come out right, too.)

In terms of these notations, we define a T-year dose conversion factor for age a to be

$$(\text{DCF})(a, T) = D(T; a, \{\overbrace{1, 0, \ldots, 0}^{T \text{ intakes}}\}), \qquad \text{(A–4)}$$

i.e., the dose accrued for T years due to an acute intake of the radionuclide at age a. For a = 20 and T = 50, Eq. A–4 represents 50-year adult internal dose conversion factors of the kind tabulated in Appendix T.

The notations that we have developed above will help us to explain procedures for calculating dose to individuals and population groups in the FMPC domain. We must caution the reader that there are no tables that provide the values $\delta(a, t)$ based on the most recent internal dose methodology, for a variety of radionuclides, and for age and time resolutions of one year, as our notations seem to imply. It may be necessary to approximate these quantities from 50-year age-dependent dose conversion factors, using the retention functions that presumably were used to calculate the factors (Appendix T).

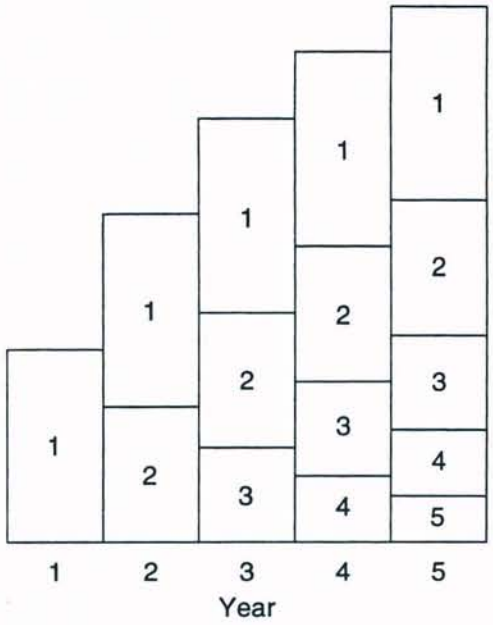

Figure A–2. Illustration of total dose rates in successive years from previous chronic intakes of a radionuclide. The scale of the figure assumes that all intakes are equal. The bottom row of boxes indicates the shape of the residual dose-rate curve. Successive curves are laid on top, each offset from the previous one by one year.

INTERNAL DOSE TO AN INDIVIDUAL BASED ON A RESIDENCE HISTORY

With the tools just developed, the formal description of internal dose to an individual who lived in the FMPC domain at some time (or times) during the operation of the FMPC is fairly simple. This may be dose to a specific organ or effective dose. We consider each year of operation and denote the years as $t = 1, \ldots, 38$ for 1951–1988, respectively. Our problem is to estimate the intake I_t for each year (obviously, $I_t = 0$ for any years in which the individual was absent from the region). In addition, we need to know the age at some time during the period, which can then be converted to an age a for $t = 1$ (zero and negative ages may be used formally for years corresponding to zero intakes, in the event that the individual was born after 1951; fetal dose will be calculated separately).

The intakes are based on such parameters as breathing rate (inhalation) and dietary assumptions (ingestion), which are dependent on age and other lifestyle factors (adults who work outdoors, for example, will average higher exposure by inhalation than those who spend most of their time indoors). For inhalation, each year's intake depends on the air concentration simulated by the air transport model for that year at the receptor point in the cell of the individual's principal location. It may be necessary to combine estimates at more than one location, if work and home are separated by cell boundaries, or in other cases of time regularly spent in widely different locations. Ingestion of radioactivity by way of food depends on dietary assumptions for the age group (or possibly specific information about a particular individual) and the agricultural model's estimate of contamination of the local garden produce.

If the individual is assumed to be still living at the end of the period of operation (1988), the residual dose commitment (i.e., the dose that will be delivered throughout the remainder of the person's life by the retained body burden of radioactivity) may be estimated by carrying the calculation forward, with zero subsequent intakes, to a year corresponding to the individual's life expectancy based on life tables. A more conservative assumption may be made if desired. There may be occasions, however, when this extension of the dose is unwarranted. We discuss this question more fully in the next section.

The calculation we have described is formally summarized by Eq. A–3, where the intakes I_t have been assembled in the manner just discussed. We point out that the process is a bit more complex than the foregoing paragraphs might suggest, involving as it does not just one component of dose, but multiple components corresponding to organ, intake mode, and radionuclide.

Once the appropriate duration of the dose integration for the individual is defined, the dose to an individual may be written in terms of the generalized dose conversion factors of Eq. A–4:

$$\text{Total dose} = \sum_{t=1}^{T} I_t\,(\text{DCF})(a+t-1, T-t+1)\,, \tag{A–5}$$

where a is the age in 1951 and T is the year marking the end of life expectancy for the individual, or if this commitment is not desired, T might be 38, corresponding to the year 1988, or any subsequent year defining the desired dose integration period.

COMBINING DOSE INFORMATION WITH POPULATION GROUPS

As we noted earlier, it is manifestly impossible to approach the estimation of the dose probability distribution $G(x)$ (Eq. A–1) by constructing individual histories for all or even a substantial sample of the population of the FMPC domain and estimating doses x by Eq. A–3 or Eq. A–5. But Eq. A–5 can conveniently be brought to bear on groups of individuals of the same age and lifestyle categories and residing in the same geographic cell.

Consider an age cohort identified by age a in 1951 (the a-cohort). For members of this cohort living in cell i with lifestyle characteristics k, we compute the COLLECTIVE DOSE

$$\begin{aligned}(\text{CD})_{i,a,k} &= \sum_{t=1}^{T_{max}} n_{i,j(a+t-1),k,t}\, I_t\,(\text{DCF})(a+t-1, T) \\ T &= \min(T_{\max},\, M(a+t-1)+t)\end{aligned} \tag{A–6}$$

where $T_{\max}$ is the time beyond which accrued dose is not to be calculated, $j(a+t-1)$ is the age index of the group aged $a+t-1$ in the year t, and $M(a+t-1)$ is the remaining life expectancy for an individual of age $a+t-1$, so that $M+t$ is the expected year of mortality relative to year t = 1 (1951); as indicated, if this year comes after $T_{\max}$, we use $T_{\max}$ instead. The symbol $I_{i,\,j(a+t-1),k,t}$ denotes the intake during year t, but now with additional subscripts to clarify its dependence on location, age, and lifestyle.

The numbers $n_{i,j,k,t}$ only tell us how many people were in the joint category indicated by the subscripts during year t, but by themselves they do not tell us the number of individuals who where exposed over time. Additional data or assumptions are required. One approach

is to recognize that the number of individuals we wish to count is the sum of the number remaining in the cell at time $t = T_{max}$ and the number who have left the cell since $t = 1$ by death or migration. The number of deaths each year can be estimated from $n_{i,j(a+t-1),k,t}$ using life tables. It is unclear whether or not reasonable estimates of migration can be made for individual cells.

Let us denote the number of individuals in cell i, age cohort a, and lifestyle category k by $N_{i,a,k}$. Then our estimate of dose to an average member of this cohort over time is

$$H_{i,a,k} = (\mathrm{CD})_{i,a,k}/N_{i,a,k}\,. \qquad \text{(A–7)}$$

The numbers $H_{i,a,k}$, together with the frequencies $N_{i,a,k}$, for all cells, cohorts, and lifestyles, are arranged into an empirical cumulative frequency distribution $\hat{G}(x)$. This empirical distribution is an estimate of the exact distribution $G(x)$ of Eq. A–1 and will be applied to the epidemiological power analysis.

UNCERTAINTIES

The source term (Voillequé et al. 1991) and environmental transport models have been developed with considerable attention to parametric uncertainties that will be propagated through the calculations to the estimates of dose. Monte Carlo methods use multiple simulations with pseudorandom sampling from distributions representing uncertain parameters to produce distributions of results (i.e., doses, in the present context).

Suppose N simulations are run in connection with the power analysis for an epidemiological study under consideration. Then we would have N distributions $\hat{G}(x)$ and consequently N estimates of the power of the study design. Such a procedure is somewhat unconventional, and its utility is still under study. Alternatively, the power analysis could be carried out in the standard way with the results of a single deterministic simulation based on central values for the uncertain parameters.

For estimation of dose to an individual, the interpretation of the uncertainty is much clearer. The several organ doses could be interpreted as a random vector from a joint distribution, but it is likely that each organ dose would be viewed in the context of its own (marginal) distribution. If lung cancer is a health effect of concern, for example, the distribution of dose to the lung could be combined with the appropriate risk factor (risk per unit dose) to provide a probabilistic upper bound on the individual's risk of contracting the disease (this illustration excludes confounding factors, such as cigarette smoking).

DISCUSSION AND CONCLUSIONS

This appendix gives a brief overview of the form that dose estimation for this study will likely take. Many considerations dictate that attention be restricted to two points of view, namely doses to individuals with specified histories of residence in the FMPC and other factors, and to certain subpopulations of cells of the 128-cell polar grid to produce a distribution of dose that will be used in the power analysis of epidemiological studies under consideration. We have given some detail of approaches to the calculation of dose for both of these points of view.

Dosimetric information of the kind presented in Appendix T will need to be adapted to the requirements that we have outlined. In particular, the age-dependent internal dose conversion factors for 50 years will likely serve as a data base for an approximate procedure that would use them to estimate the more general internal T-year dose conversion factors defined by Eq. A–4. Conventional prospective assessments for regulatory purposes have used adult 50-year dose conversion factors that were originally developed for protection of radiation workers. The result was a deliberate overestimation of dose to adults for some radionuclides, and although doses to infants and children were considered only in a few special cases, such as the dose to the thyroid from ^{131}I, the known conservatism of the adult factors usually was tacitly assumed to provide an adequate margin for children. Such an approach seems inappropriate for purposes of dose reconstruction and epidemiology. In that context, we seek to minimize bias to central estimates of dose and to place conservatism in the variances of distributions that represent uncertainty in parameters.

REFERENCES

Lubin J.H., M.H. Gail, and A.G. Ershow. 1988. "Sample Size and Power for Case-Control Studies when Exposures are Continuous." *Stat. Med.* **7**: 363–376.

Voillequé P.G., K.R. Meyer, D.W. Schmidt, G.G. Killough, R.E. Moore, V.I. Ichimura, S.K. Rope, B. Shleien, and J.E. Till. 1991. *The Fernald Dosimetry Reconstruction Project, Tasks 2 and 3: Radionuclide Source Terms and Uncertainties — 1960–1962.* Radiological Assessments Corporation Rep. No. CDC-2 (Draft interim report for comment).

APPENDIX B

THE ASSESSMENT DOMAIN

INTRODUCTION

The term ASSESSMENT DOMAIN as it is used in this report refers to a circular region with radius 8 km (approximately 5 miles) with its center near the geometric center of the FMPC production area. The coordinates of this point are 84° 41′ 19″ W and 39° 17′ 57″ N. Preliminary calculations indicate that more than half of the uranium released to the atmosphere from FMPC operations during a three-year period of special study (1960–1962) would have been deposited on the ground within this region. Air concentrations at the perimeter, as simulated by air dispersion models, are typically about a factor of ten lower than those predicted for the site boundary (about 1 km). Practically all data from monitoring of air, soil, and water for radionuclides released from the FMPC have been collected within the 8-km radius, and trends of concentrations shown by the data typically show a decline to background levels well before the boundary is reached.

For purposes of dose calculation, the assessment domain has been subdivided into 16 sectors and 8 concentric annular regions (Fig. B–1). We refer to this network of lines and circles as a POLAR GRID, and the individual compartments are called CELLS. This partitioning is an arbitrary convenience that is imposed in order to improve the resolution of the calculations without introducing an unmanageable number of receptor points. We assume that the properties we are interested in (such as air concentration, deposition of material on the ground, and population) are uniformly distributed within each cell. The number of sectors (16) is dictated by the format of the joint frequency tables that represent the local meteorology. These sectors are labeled N, NNE, NE, and so on, according to wind direction. It is necessary to distinguish carefully between the direction or sector **from** which the wind blows and the sector **into** which it is blowing. If the reference is to a RECEPTOR POINT, the sector is the one into which the wind blows. Hence, if we are concerned with the air concentration 2,000 m due north of the plant, the receptor point is in the north (N) sector, but the wind affecting it will be (primarily) from the south (in the S sector).

POPULATION MODEL FOR THE DOMAIN

A population model for this domain has been devised by J.F. Rogers of the Centers for Disease Control and Prevention (Appendix U). This model is referred to the polar grid described above and is based on various interpolations in census data. Other aspects of the study, such as production of food in gardens, will also be treated in relation to the polar grid.

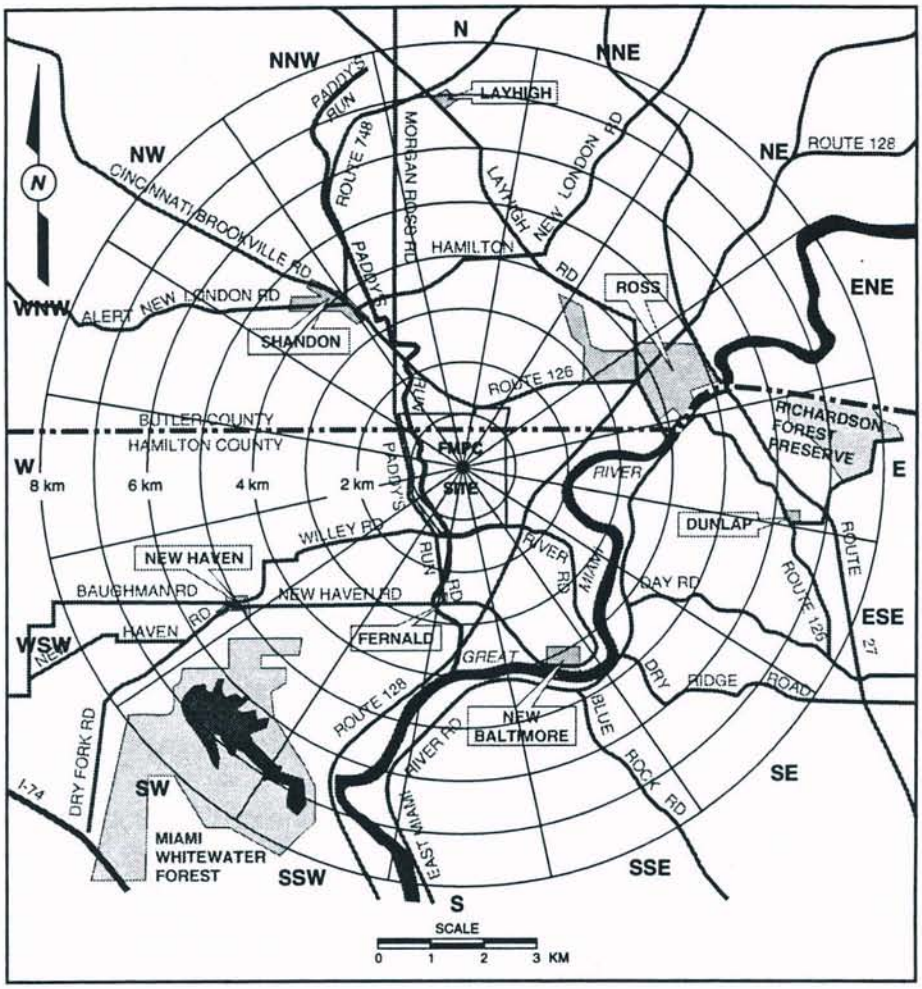

Figure B–1. The polar grid centered at the FMPC site. There are 16 circular sectors of 22.5°, each marked with a direction TOWARD which the wind would blow into the sector. The circles are at intervals of 1 km from the center of the site.

CRITERIA FOR ESTABLISHING THE BOUNDARIES OF THE DOMAIN

More formal criteria for the establishment of spatial boundaries for the study are developed in Task 5. These criteria concern such factors as (1) epidemiological need for the study, (2) radiation protection principles, and (3) application of accepted governmental standards. The choice of spatial boundaries can be evaluated against these criteria only after dose estimates are available. Computing crude dose estimates early in the study was considered and rejected for several reasons. Credibility of these preliminary results was high on the list of objections, as was the problem of resolving differences between these earlier numbers and the final more-refined estimates. Finally, there was the question of the resources that would need to be devoted to a subproject of calculating and reporting preliminary estimates that would be of sufficient quality to settle the question definitively. (We note that a number of preliminary simulations of air concentrations have been performed, but these estimates have been for

other purposes and have not been related to dose.) On the basis of these considerations and the less formal reading of data trends, the decision was made to proceed provisionally with the 8-km circular region. If final results indicated a need for extension of the domain, that question would be considered at that time.

The question of a temporal domain is also pertinent to a planned assessment. In this case, however, the contract effectively specified the entire period of plant operations (beginning in 1951 and ending with cessation of operations in 1988), and therefore all preparations have been undertaken with this temporal domain in mind.

CONCLUSIONS

We have defined the spatial assessment domain as a circular region 8-km in radius and centered at the geometric center of the FMPC production area. A polar grid has been defined for the region (Fig. B–1) to facilitate the handling of spatially distributed quantities, such as air concentrations, deposition of radioactive material on the ground, and dose. We have described relatively informal criteria that support this choice (extensiveness and trends of existing data). More formal criteria will be discussed in Task 5 of this study. This 8-km domain will be used provisionally until after final dose estimates have been calculated and evaluated. Any question of extending the domain, should that be indicated, will have to be considered at that time.

APPENDIX C

RADIONUCLIDES RELEASED FROM THE FMPC 1951–1988

INTRODUCTION

Processing of uranium was the principal function of the FMPC. Thorium processing was a secondary activity. Radioactive decay of uranium and thorium produces a series of other radionuclides that are collectively referred to as DECAY PRODUCTS. The initial decay products for the three decay series of greatest interest are shown in Fig. C–1, C–2, and C–3. The first of these illustrates the decay products of uranium-238 (^{238}U), including another important uranium isotope, uranium-234.

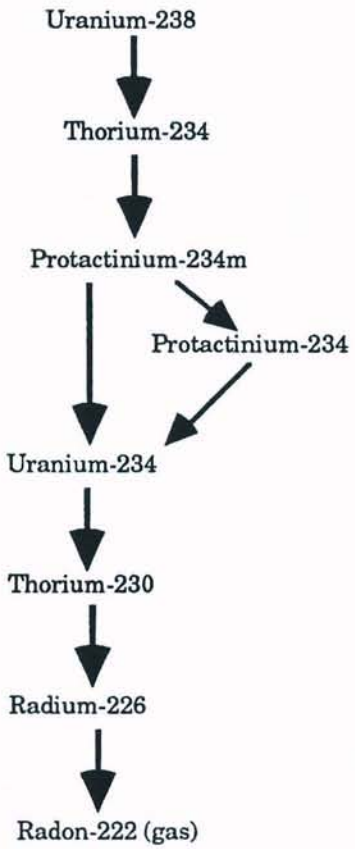

Figure C–1. Decay products of uranium-238, from thorium-234 to radon-222.

In most of the feeds received by the FMPC, the uranium had previously been separated chemically from the other decay products. As a result, the facility's effluents consisted primarily of uranium and the decay products were generally present in small quantities. Radioactive decay of uranium after the initial chemical separation from the daughter radionuclides also produced those same nuclides as trace contaminants.

However, early processing campaigns treated ores that contained near equilibrium amounts of the daughter radionuclides through radium. As shown in Fig. C–1, the decay product that follows radium is radon, a gas. The wastes from that early processing were placed in the K-65 Storage Silos (see Appendix P) and releases from the silos represent a special case of uranium decay product releases.

Some thorium was processed at the FMPC. Fig. C–2 shows a comparable sequence of the decay products of thorium-232, which includes thorium-228 and two radium isotopes. This sequence also leads to a gaseous radon isotope. Processed thorium would include both thorium isotopes and small residuals of the other solid elements. Radioactive decay after processing would also produce trace contaminants in the thorium.

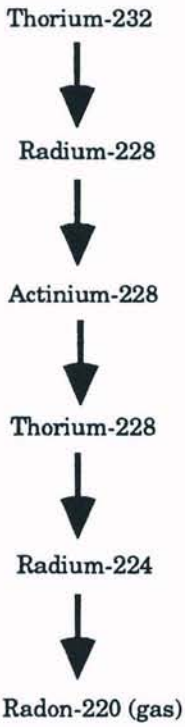

Figure C–2. Decay products of thorium-232, from radium-228 to radon-220.

The third decay chain of interest is that of uranium-235, which is present (0.72%) in natural uranium and in increased amounts (generally less than 1.5%) in enriched uranium processed at the FMPC. This decay sequence (Fig. C–3) also includes an isotope of radon.

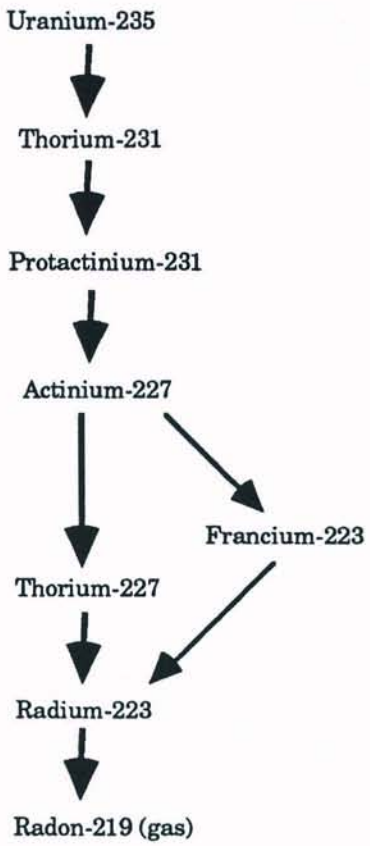

Figure C–3. Decay products of uranium-235, from thorium-231 to radon-219.

In addition to decay products, other radionuclides were released during FMPC operations. These originated in nuclear reactors, where finished uranium fuel and target elements, produced at the FMPC, were used. Fissioning of the uranium atom produces other radionuclides, called FISSION PRODUCTS. Absorption of neutrons by uranium and other materials present in the reactor produces radioactive ACTIVATION PRODUCTS. When spent fuel from the reactors was processed at fuel reprocessing plants (not at the FMPC), the uranium was not completely separated from fission and activation products. As a result, recovered uranium that was recycled (returned to the FMPC as feed material) introduced small amounts of fission and activation products into the process streams at the FMPC.

Receipts of recycled uranium began at the FMPC in fiscal year (FY) 1961. However, measurements of the amounts of these radionuclides were not performed until years later. Estimated or measured releases of radium in liquid wastes have been reported for 1957 and subsequent years; more complete assessments of the presence of fission and activation products in liquid wastes began in 1976 (Boback et al. 1987). Most of the available information on the presence of other radionuclides in dusts released to the atmosphere was collected in 1985 when about forty samples of material from dust

collectors and scrubbers were collected and analyzed (Boback et al. 1987). Most of the available data on the presence of radionuclides other than uranium in FMPC effluents was included in the draft Task 2/3 report (Voillequé et al. 1991).

The focus of this appendix is on releases of radionuclides that would be associated with particles or solutions that contain uranium. Releases of the gaseous isotopes of radon are considered separately (see Appendix P). Table C–1 lists the particulate radionuclides, other than the uranium isotopes, that have been identified in FMPC effluents (Boback et al. 1987). There are three categories of such nuclides: naturally occurring radionuclides found in uranium and thorium ores, fission products, and activation products. With the exception of ^{234m}Pa, these are all relatively long-lived radionuclides. Other fission and activation products with short half-lives would have been present in spent uranium fuel and target elements when they were removed from the reactor, but decayed prior to processing and recycle of uranium to the FMPC.

Table C–1. Particulate radionuclides identified in FMPC releases

Nuclides in uranium ores	Fission products	Activation products
^{228}Th	^{90}Sr	^{237}Np
^{230}Th	^{99}Tc	^{238}Pu
^{232}Th	^{106}Ru	^{239}Pu, ^{240}Pu
^{234}Th	^{137}Cs	
^{226}Ra		
^{228}Ra		
^{234m}Pa		

The identified activation products are all TRANSURANIC NUCLIDES; that is, they all have atomic numbers higher than that of uranium (92). The two isotopes ^{239}Pu and ^{240}Pu are grouped because they both emit alpha particles of nearly identical energies and cannot be separated by alpha spectroscopy (the common analytical technique). An important radionuclide that has not been identified, but would be expected to be present, is ^{241}Am. The energy of the alpha particle emitted by ^{241}Am is virtually the same as that emitted by ^{238}Pu. Because the special chemical separation needed to isolate ^{241}Am was apparently not performed, the results reported for ^{238}Pu no doubt include a contribution from ^{241}Am.

CORRELATIONS WITH URANIUM RELEASES

Because the measurements of other radionuclides were not made in every year, it is necessary to develop correlations between the releases of uranium and those of the other radionuclides. Ratios of releases, expressed for example as μCi ^{226}Ra per kg U, were

computed for years when measurements were made. These ratios provide a basis for estimating releases of the other radionuclides for years when they were not measured. The variability of the release ratios from year to year is considered in deriving the uncertainty associated with the estimated releases of other radionuclides.

Releases of radium and other radionuclides in liquid wastes have been determined for a longer period than for airborne effluents. Estimated radium releases were given for years back to 1957, but it appears that a definitive measurement program was not begun until about ten years later. Radium to uranium release ratios for nearly twenty years and ratios for other radionuclides for nine years were used. It was assumed that the correlations were applicable for releases to the Great Miami River and to Paddy's Run.

The concentration ratios of other radionuclides to uranium in dusts and scrub liquors that were measured in 1985 exhibit wide variations, both within a single facility and between facilities. For that reason, atmospheric releases of radionuclides were estimated on a stack by stack basis using measured ratios specific to the release point. For stacks not included in the 1985 measurements, ratios were based upon data collected for stacks that serviced comparable operations (machining of uranium metal, for example). The processes served by the various dust collectors and scrubbers are discussed in the draft Task 2/3 report (Voillequé et al. 1991).

The concentration ratios that were measured provide only a snapshot of the distributions of other radionuclides in the various facilities and there seems to be no definitive information about year to year variability. It is logical that the concentrations of transuranic nuclides in uranium would increase with time as the material was recycled. Releases of these radionuclides in previous years were probably not greater than those estimated using concentration ratios from 1985. Concentrations of fission products, which are chemically less similar to uranium, may have been relatively constant over time.

RELATIVE IMPORTANCE OF RELEASES

The relative importance of releases of radionuclides to the environment depends upon three points of comparison. These are the comparative quantities released, differences in the potential for nuclide concentration in the environment, and the relative toxicities of the radionuclides, as measured by their dose conversion factors. Differences in dispersion and dilution of uranium and the other radionuclides in the atmosphere and river are not expected to be significant.

A methodology developed by the National Council on Radiation Protection and Measurements (NCRP) (NCRP 1989) was used to assess the relative importance of the identified radionuclides as potential contributors to offsite radiation dose. The NCRP screening methodology was primarily intended to evaluate compliance with environmental standards. However, the screening factors that were developed for many radionuclides and a variety of exposure pathways can also be used to assess the relative importance of radionuclide releases to the environment. The referenced methodology has been expanded to include liquid pathways; formal publication of that work is expected later in 1993.

The screening factors for radionuclides released to the atmosphere or to fresh water address two of the three points of comparison that were listed above. The potential for

concentration in the environment is evaluated by considering environmental pathways that reflect concentration mechanisms. These are buildup of radionuclides in soils and sediments and uptake into the terrestrial and aquatic food chains by various mechanisms. The relative toxicity of each radionuclide (and any other radionuclides that may be produced by its radioactive decay) is also reflected in the NCRP screening factors. Data for the third comparison—differences in the quantities released—were available from direct measurements of releases of uranium and other radionuclides and from measurements of the relative concentrations of other radionuclides in collected dust and scrub liquors.

The relative importance of a particular radionuclide is defined as the fraction that it contributes to the total potential radiation dose from all radionuclides. This parameter was evaluated for releases to the atmosphere and for releases to water. Both surface water and groundwater were considered in the latter category. Mathematically, the relative importance of a particular nuclide (RI_j) is

$$RI_j = \frac{Q_j \ SF_j}{\sum_{j=1}^{n} Q_j \ SF_j}$$

where Q_j and SF_j are the quantity discharged and the screening factor, respectively, for releases to the atmosphere or to water. The summation in the denominator of the equation extends over all n of the radionuclides released to the medium of interest.

The releases to air and water during the years 1960–1962 were used to evaluate the relative importance of the radionuclides in FMPC discharges. In those years, relatively high releases to both air and water occurred. Measured and estimated uranium releases were used, together with data on correlations of releases of other radionuclides to releases of uranium, to develop release estimates for the radionuclides in Table C–1 for that time period. The transuranic nuclides were treated as a group, rather than individually, because all individual contributions were not defined. The environmental behavior and toxicity for the group were approximated by parameters applicable to the plutonium isotopes.

Uncertainties in the uranium releases for the period were derived as part of the source term estimates (Voillequé et al. 1991) and those uncertainty estimates were used in the present calculations. The concentration ratios obtained for airborne release locations were assumed to be medians of lognormal distributions whose geometric standard deviations were estimated to be 1.5. For the liquid releases, the observed variabilities of release ratios were used to define triangular distributions for the calculations. Because the NCRP screening factors were developed to assess compliance with standards, a cautious approach was employed that tends to overestimate potential exposures. For these calculations, it was assumed that a triangular distribution with the most probable value equal to the SF could be used to define a range of possible estimates. The upper bound of the distribution was taken to be 2 SF and the lower bound was SF/10.

Monte Carlo calculations were made of the relative importance of the released radionuclides for both atmospheric and liquid discharges during the period. The results of

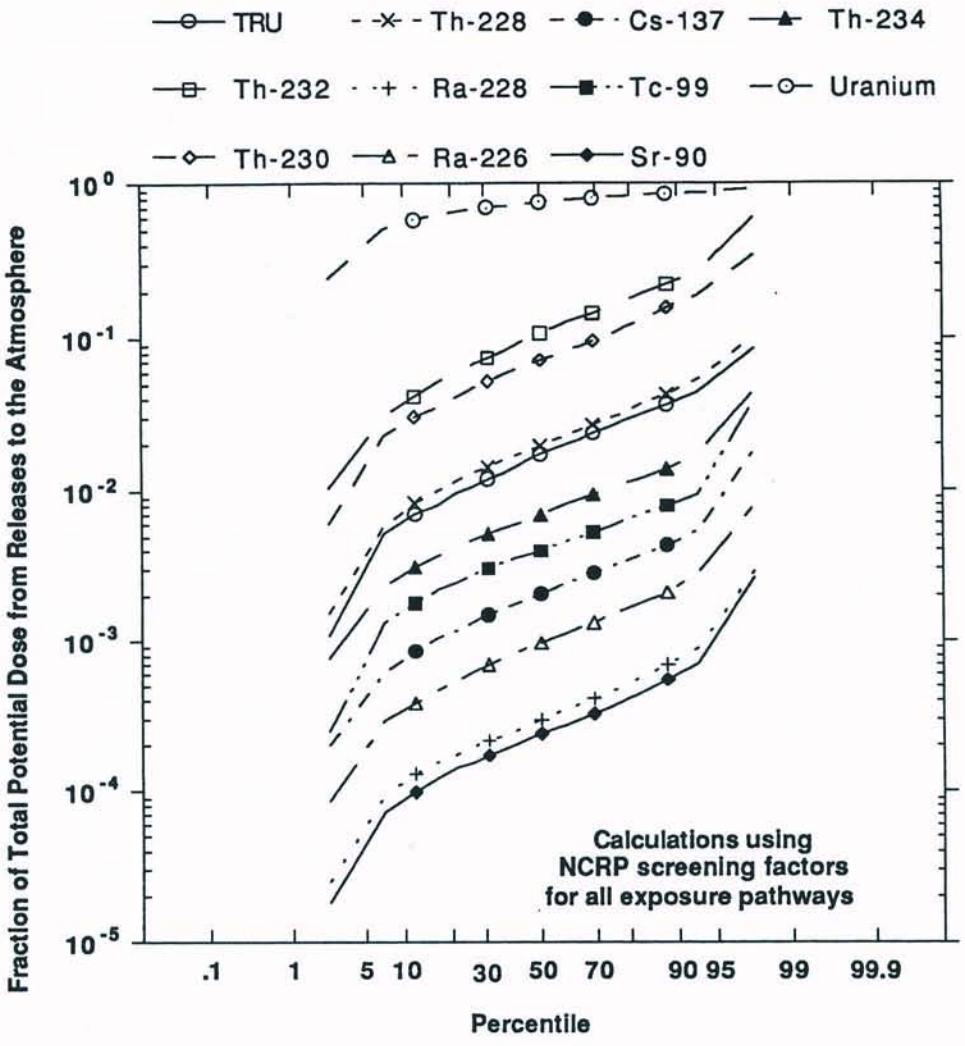

Figure C-4. Contributions of radionuclides released to the atmosphere to the potential dose.

the calculations for releases to the atmosphere are shown in Figure C–4. The most important releases are clearly those of uranium, with an estimated median *RI* of 0.76. Three thorium isotopes ^{232}Th, ^{230}Th, and ^{228}Th had median values of *RI* of 0.11, 0.072, and 0.020, respectively. The transuranic nuclide group was fifth from the top with a median *RI* of 0.0017. The figure illustrates the relative unimportance of other radionuclides and that those nuclides deserve much less attention in the dose assessment process. Inhalation was the most important exposure pathway, accounting for 86% of the potential uranium dose and about 90% of the doses from thorium isotopes. Consumption of contaminated garden vegetables was the second most important pathway, accounting for 9–12% of the total potential doses from uranium and thorium isotopes.

Three Monte Carlo calculations were performed to ascertain the relative importance of various radionuclide releases to the surface water. The first of these considered all potential exposure pathways. Because all pathways may not be realized, alternative calculations were performed. Table C–2 shows the pathways considered in each case.

Table C–2. Screening calculations performed for liquid effluents.

	Pathways considered in calculations			Most	
Case	Drinking water	Fish consumption	Irrigation water	important nuclides	Results presented in
1	yes	yes	yes	^{228}Ra, ^{99}Tc, ^{226}Ra	Fig. C–5
2	yes	yes	no	^{228}Ra, ^{226}Ra, U	Fig. C–6
3	yes	no	no	^{228}Ra, U, ^{226}Ra	Fig. C–7

For a situation when all the exposure pathways are realized, river water is used for drinking, fish from the river are used for food, and river water is used for irrigation of human food crops and plants used for feed for animals that are used in turn for human food. Under these conditions, the calculations indicate that ^{228}Ra is the most important nuclide. Next in order of importance is ^{99}Tc, followed by ^{226}Ra and the uranium isotopes. Contributions of other nuclides to the total potential dose can be seen in Fig. C–5 to be much smaller.

Fig. C–6 contains the results of calculations that address the situation when river water is not used for irrigation. For this situation, the importance of the various radionuclides is changed somewhat from Fig. C–6; however, radium isotopes are again predominant and uranium is of tertiary importance.

The third Monte Carlo calculation was performed for the situation when only drinking water is a complete pathway. Because the groundwater was contaminated by the liquid effluents from the plant, this calculation also indicates the relative importance of radionuclides that could be consumed as a result of drinking contaminated groundwater. The results are presented in Fig. C–7. For the drinking water pathway, ^{228}Ra is again the primary contributor to the dose, followed by uranium isotopes and ^{226}Ra. Two thorium isotopes and ^{99}Tc are of lesser importance for the drinking water pathway.

CONCLUSIONS

The calculations summarized in this appendix show that releases of uranium are by far the most important contributors to the potential doses from releases to the atmosphere. Of secondary importance for atmospheric releases are ^{232}Th and ^{230}Th, while ^{228}Th and the transuranic nuclides are of tertiary importance. Contributions from

other radionuclides are unlikely to contribute even one percent of the total dose from such releases.

The results of calculations for liquid releases yielded a somewhat more complex picture because not all potential pathways may be complete; that is, some pathways may not be realized. Nonetheless, the radium isotopes were found to be of primary importance. The importance of radionuclides other than ^{228}Ra and ^{226}Ra will depend upon findings regarding the reality of pathways that have been considered in these analyses.

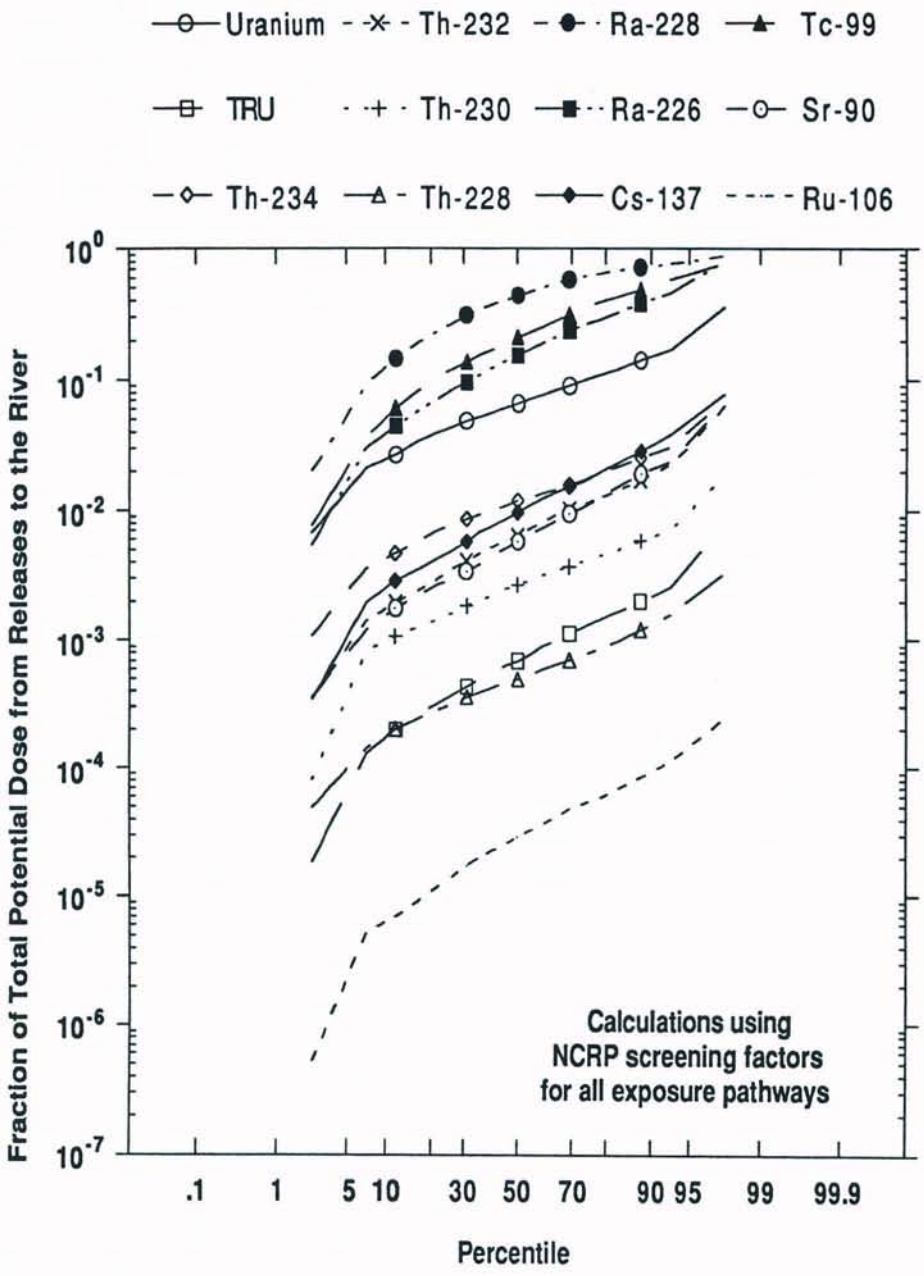

Figure C-5. Contributions of radionuclides released to water to the potential dose from all pathways.

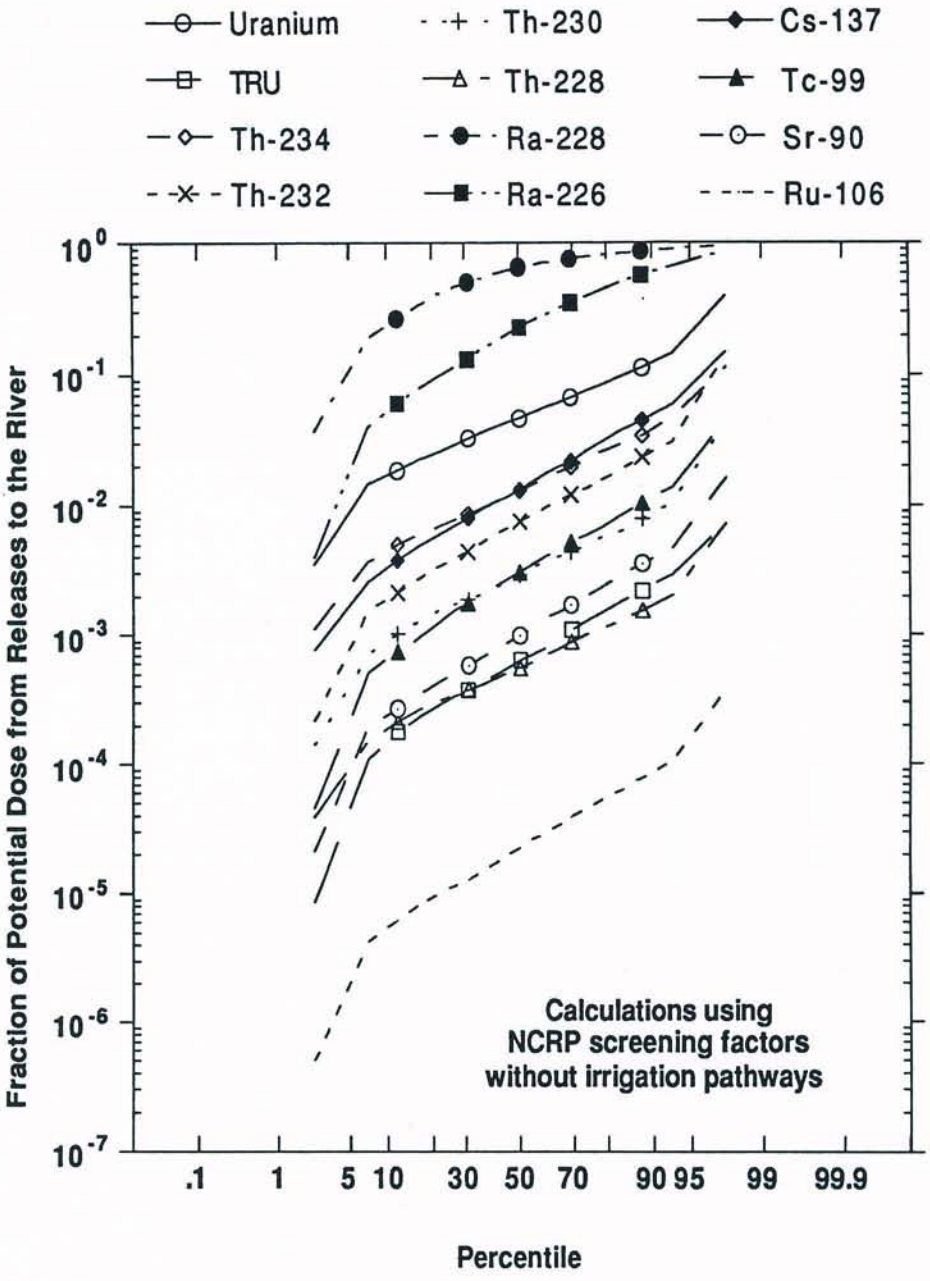

Figure C–6. Contributions of radionuclides released to water to the potential dose from drinking water and fish consumption pathways.

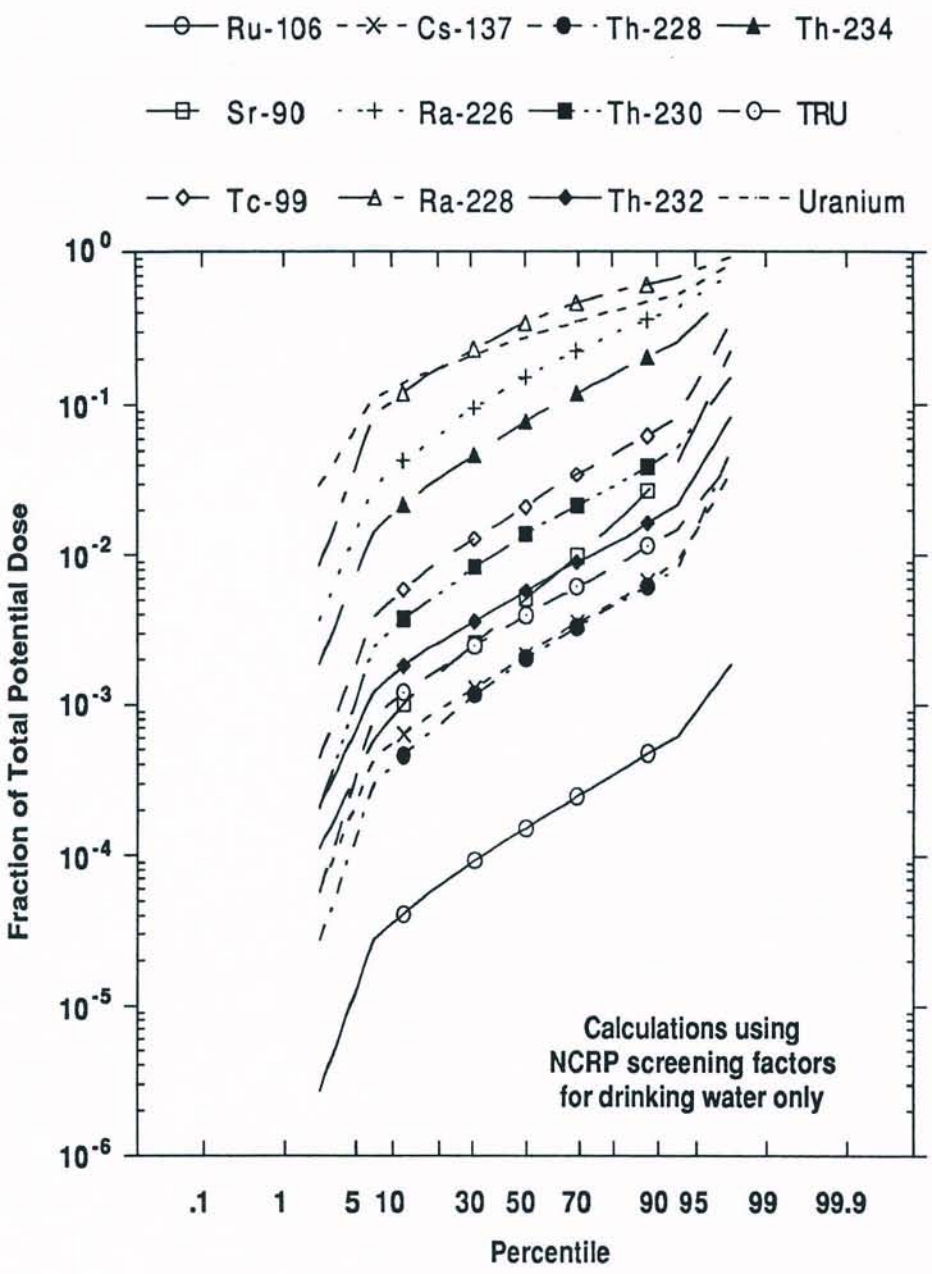

Figure C–7. Contributions of radionuclides released to water to the potential dose from drinking water from the river or contaminated groundwater.

REFERENCES

Boback, M. W., T. A. Dugan, D. A. Fleming, R. B. Grant, R. W. Keys. 1987. *History of FMPC Radionuclide Discharges*. Cincinnati, OH: Westinghouse Materials Company of Ohio; Document Number FMPC-2082 (Revision to FMPC-2058); 1987.

NCRP. 1989. *Screening Techniques for Determining Compliance with Environmental Standards, Releases of Radionuclides to the Atmosphere*. Washington, DC: National Council on Radiation Protection and Measurements, NCRP Commentary No. 3.

Voillequé, P. G., K. R. Meyer, D. W. Schmidt, G. G. Killough, R. E. Moore, V. I. Ichimura, S. K. Rope, B. Shleien, J. E. Till. December 1991. *The Fernald Dosimetry Reconstruction Project: Tasks 2 and 3: Radionuclide Source Terms and Uncertainties — 1960–1962*. RAC Report No. CDC–2. Draft interim report for comment.

APPENDIX D

PARTICLE SIZE DISTRIBUTIONS FOR RELEASES OF URANIUM

INTRODUCTION

The particle size distributions of uranium stack emissions are needed in order to permit calculation of the deposition of uranium dust from airborne plumes (Appendix G) and parameterization of the respiratory model used in calculating dose to individuals inhaling the uranium dust (Appendix T). In addition, a knowledge of the particle size distributions is necessary if corrections of uranium stack releases need to be made to account for losses through particle deposition in sampling lines. The only measurements of the particle sizes of stack emissions from the FMPC were conducted by Northern Kentucky Environmental Services (NKES) during 1985. An unpublished report on this work is available (Reed 1985). In the NKES study, measurements were made for both the inlet and outlet ducts of 15 major uranium-emitting stacks with dust collectors. The particle size distributions determined in the study are listed in an FMPC report, FMPC-2082 (Boback et al. 1987).

Appendix F of Voillequé et al. (1991) presents a series of plots of distributions of the uranium species for both the inlet and the outlet ducts of each of the 15 sampled dust collectors. The plots are based on cumulative distribution functions of continuous type fitted to the raw data for the purpose of necessary interpolation and extrapolation of the values from Boback et al. (1987). We will briefly review the functional representation of the fitted curves.

Particle sizes for the outlet ducts (or emission stacks) are representative of emissions from stacks with intact bag filters in the dust collectors. The values for the inlet ducts, however, may be assumed to represent emissions from the same stacks during those periods in which the bag filters had failed in a manner that allowed unfiltered inlet air to escape to the atmosphere.

The bag filters of the dust collectors for FMPC stacks were not all made from the same material during the 1985 NKES study. Some of the dust collectors had wool bags, but a change to Gore-Tex™ bags was in progress over a period of years that included 1985. There are too few stacks involved to draw definite conclusions about differences in the efficiencies of dust collectors made from different materials, but comparisons with the few data available to us indicated little difference.

Particle size distributions for the stack emissions during the year 1985 are included as a part of the source-term characterization for the same stacks for the 1960–1962 period because the plant operations served by the stacks did not change significantly from 1960 to 1985. The hydrofluorination process for producing UF_4 (green salt), for example, has remained basically the same over the years with respect to conditions that might affect the particle sizes of the product. The various plant operations that produce U_3O_8 particulates also have not changed in a manner that would significantly alter particle sizes.

The predominant uranium species emitted from each stack was identified from FMPC reports and engineering drawings of process equipment. In some cases, more than one uranium species was determined to be emitted from a stack. Either UF_4 or U_3O_8 was emitted from all

of the stacks of the NKES study except for one stack, which emitted a mixture of UO_2 and UO_3.

FITTING DISTRIBUTION CURVES TO THE PARTICLE SIZE DATA

Each measured particle diameter is reported as an EQUIVALENT AERODYNAMIC DIAMETER, which means the diameter of a sphere of unit density (expressed as 1 g cm^{-3}) that has the same gravitational settling velocity as the particle. Distributions of the diameters of such particles can be tabulated with respect to particle count, mass, radioactivity, or other properties. The tabulations given by Boback et al. (1987) are with respect to mass of uranium in the particle. The term EQUIVALENT refers to the spherical reference geometry and will generally be omitted. In discussions of this concept, confusion sometimes arises regarding the relationship with the familiar activity median aerodynamic diameter (AMAD) used by the International Commission on Radiological Protection (ICRP) in connection with its respiratory models. It is important to realize that AMAD refers to the median of a lognormal distribution, with respect to radioactivity, of (equivalent) aerodynamic particle diameters; moreover, the ICRP Task Group on Lung Dynamics restricted consideration to distributions with geometric standard deviation less than 4.5 (TGLD 1966, ICRP 1979). Most of the distributions of aerodynamic diameter with respect to uranium mass measured by NKES fail to be lognormal (Appendix T discusses our extension of ICRP dosimetry to nonlognormal distributions of particle size).

It is assumed with respect to emissions of uranium compounds from the FMPC that distributions of particle volumes are equivalent to distributions of uranium mass within particles. This assumption is certainly true when a single uranium compound is considered, because its uranium content would not be different for different particle sizes. Plant 4 produced only UF_4 through the hydrofluorination process, and there are no other uranium-containing products or byproducts of the reaction. Some of the dust collectors in Plant 4 serviced areas in which molten uranium derbies were solidified and in which U_3O_8 formed on the metal surface. Some of this oxide became airborne and was emitted to the atmosphere through a stack. No other uranium oxide was produced in this process, and therefore a single compound can be assumed.

Plant 5 and Plant 8 dust collector emissions of U_3O_8 came from oxidation on uranium metal surfaces in which only one oxide was involved. Thus, in these cases also, a single compound can be assumed.

Plant 8 scrubbers and Plant 2/3 scrubbers are believed to have emitted liquid droplets of reentrained scrub liquor of varying uranium concentration, which was directly proportional to the time that had elapsed since the last change in scrub liquor. At any given time in the interval between changes of the scrub liquor, the uranium concentration in all droplet sizes was the same. Therefore, the average total uranium content over time was directly proportional to particle volume.

Evaporation of water from the liquid droplets would have produced solid polycrystalline aggregates containing uranium. Since the volumes of the solids would have been directly proportional to the volumes of the liquid droplets at any given time for each scrubber, the average total uranium content of the solid spheres was also directly proportional to particle volume.

The physical diameter of a particle is its aerodynamic diameter divided by the square root of the particle density (expressed in units of g cm^{-3}) of the particular compound of uranium. This conversion is based on Stokes' law for the terminal settling velocity of a particle:

$$v_t = \frac{\rho_p d_p^2 g}{18\mu}, \tag{D–1}$$

where d_p is the physical diameter of the particle, in μm, ρ_p is the particle density, g is the gravitational acceleration constant, and μ is the dynamic viscosity of air. The quantity ρd_p^2 can be interpreted as the square of the diameter d_a of a particle of unit density that gives the same settling velocity, v_t. Thus,

$$d_p = d_a/\sqrt{\rho_p}. \tag{D–2}$$

Stokes' law is valid for particle physical diameters less than about 20 μm (Hanna et al. 1982), but we have applied the conversion of Eq. D–2 to all particles because of the practically negligible effect of particles of physical diameter greater than 20 μm on the results (Figs. D–1 through D–4).

It must be appreciated that the distributions of aerodynamic particle diameter given by Boback et al. (1987) are presented as cumulative frequency histograms represented by 8 data points each. How one chooses to manipulate such distributions in the context of the many requirements of this study is a matter of judgment and experience. But some consistent method must be adopted. We chose to represent each histogram by a fitted distribution of continuous type which would reduce to lognormal form if the data were consistent with that form. Also, the fitted distribution would permit easy inversion in order that quantiles could be calculated.

The method was devised by one of us (G.G.K.) some years ago and applied to similar situations in which distributions of unknown form were given by a small number of data points. The fitted distribution has the form

$$\Phi(x) = P(T(\ln x)) \tag{D–3}$$

where

$$P(z) = \frac{1}{\sqrt{2\pi}} \int_{-\infty}^{z} e^{-t^2/2}\, dt \tag{D–4}$$

is the standard normal cumulative distribution function, and T is a cubic polynomial of the special form

$$T(\zeta) = \alpha^2(\zeta - \beta)^3 + \gamma^2\zeta + \delta \tag{D–5}$$

where the coefficients α, β, γ, and δ are determined by nonlinear least-squares regression. But throughout this report, we invariably give the polynomial T in terms of coefficients c_0, c_1, c_2, and c_3 in the more conventional representation

$$T(\zeta) = c_0 + c_1\zeta + c_2\zeta^2 + c_3\zeta^3. \tag{D–6}$$

The transformation equations from $\alpha, \ldots, \delta$ to $c_1, \ldots c_3$ and other details are presented in Appendix F of Voillequé et al. (1991). That appendix also contains plots of the fitted curves with points from the original histograms, and in our view the representations of the scant data

are intuitively satisfying (though one can say little of how well they represent the underlying distributions of particle diameter).

PLEASE NOTE: Under no circumstances should the reader conclude that one may deduce phenomenological significance from the coefficients $c_0, \ldots, c_3$ of the polynomial $T(\zeta)$ of Eq. D–6. This representation should be treated as purely empirical, with a limited practical purpose. We know of no method for constructing a model of particle size distribution whose parameters can be mechanistically related to the FMPC operations that produced the effluent particles. Such a model would obviously be of great utility in representing changes in the distributions over time as the plant processes were modified, but we doubt that one could be developed on the basis of what is known.

VERIFICATION OF PARTICLE SIZE MEASUREMENTS

We verified the distributions that were tabulated by Boback et al. (1987) by comparisons with information from the original data sheets of NKES. Verified values reported in this appendix are those for which the original data are consistent with values listed in FMPC-2082 and which meet the test of physical plausibility. The latter test is simply answering the question of whether, as expected, the particle size distributions for the outlet ducts of specific dust collectors show less frequency of particle sizes larger than the filter mesh than do the distributions for the corresponding inlet ducts (i.e., movement of the dust through a filter should not increase the relative frequencies of the larger particles).

Most of the particle sizes listed in FMPC-2082 were verified in accordance with the criteria above, but discrepancies and omissions were found in the cases listed below.

1. The original data sheets for the inlet duct of G4-5 and the outlet duct of G4-12 were not included in the original data file, but these data sheets were later obtained from Michael W. Boback of the FMPC. Since these two data sheets appeared to contain original data taken by NKES, the particle sizes for these ducts as reported in FMPC-2082 were verified.

2. Discrepancies included outlet ducts of G5-251, G5-253, and G5-260; the particle size distributions as reported in FMPC-2082 for these cases were not consistent with the original NKES data sheets. The FMPC-2082 values for these cases had been derived from modified data sheets. Since the origin of the modifications is uncertain, the calculated particle sizes could not be verified. Also, the calculated particle sizes of the inlet duct of G5-251 were not verified because they were much smaller than those for the outlet duct and were therefore suspect.

3. It was observed that measured particle sizes for the outlet ducts of G4-7 and G43-27 were greater than those for the corresponding inlet ducts, which is physically unrealistic. No additional data sheets for these stacks could be located, so the particle sizes listed in FMPC-2082 were regarded as suspect and were not verified.

4. It was also found in the verification process that reported values for the larger particle sizes for the inlet ducts of G5-254 and G5-256 as reported in FMPC-2082 seem to contain relatively small systematic errors of 5% and 10%, respectively. These errors were

corrected, however, and the corrected values are included as a part of the verified source-term data for 1960–1962.

CALCULATION OF AVERAGES OF VERIFIED VALUES

The average particle-size distributions for both the inlet ducts and the outlet ducts for stacks emitting UF_4 and U_3O_8 were calculated from the fitted distributions shown in Appendix F of Voillequé et al. (1991). Figures D–1 through D–4 show plots of particle-size distribution data as discrete points for stack emissions of the same uranium species (UF_4 or U_3O_8) and duct type (inlet or outlet) which had been verified as described previously. The corresponding average distributions for the same size ranges are plotted as continuous curves on the same axes. The average is actually a distribution fitted by the methods outlined in Eqs. D–3 through D–6 to 51 points generated from the pointwise average of the curves fitted to the several data sets. Each caption gives the coefficients of the cubic polynomial that defines the curve fitted to the average. Tables D–1 through D–4 are based on a discrete breakdown of the fitted distributions from Appendix F of Voillequé et al. (1991) with averages of frequencies within each range of particle aerodynamic diameter. The tables are useful for certain comparisons that are discussed in subsequent sections. Small discrepancies between the tabular averages and the corresponding curves in the figures may be expected because of the different methods of derivation.

Table D–5 summarizes several percentiles, the mean, and the standard deviation for the average distributions of aerodynamic diameters shown in Figs. D–1 through D–4 and analyzed in Tables D–1 through D–4. Because these distributions are not lognormal, their medians may not be used *a priori* as AMAD values for the purpose of ICRP dosimetry. And the concept of geometric standard deviation for such distributions is not defined. The means and standard deviations were calculated numerically from the fitted distributions.

COMPARISONS OF EMISSION DISTRIBUTIONS FROM STACKS WITH DIFFERENT TYPES OF BAG FILTERS IN DUST COLLECTORS

Early in the history of FMPC operation all of the bag filters used in the dust collectors for emission stacks were made from wool felt. There was a change to bag filters made from Gore-Tex™ in later years, but the change took place gradually over a period of years. The change was taking place during 1985 when the NKES particle-size measurements were made.

The type of bag filter used during the NKES measurements was identified from plant records. Therefore, it was possible to compare any differences between wool and Gore-Tex™ bag filters in efficiency of removal of particles of different sizes. A wool bag filter was used in G4-5 while the others in Table D–1 were made from Gore-Tex™. There appears to be a higher percentage of small particles (median < 2.5 micrometers) in the outlet from this stack. The inlet particle-size distribution for this stack (Table D–2), however, was not greatly different from its outlet distribution. In Table D–3, the bag filter used for G5-261 was made from Gore-Tex™ while the other two stacks used wool bag filters in their dust collectors. Comparisons within this table indicate also that there was a higher percentage of small particles in the emissions from wool bag filters. Calculations made for efficiencies of removal of the larger

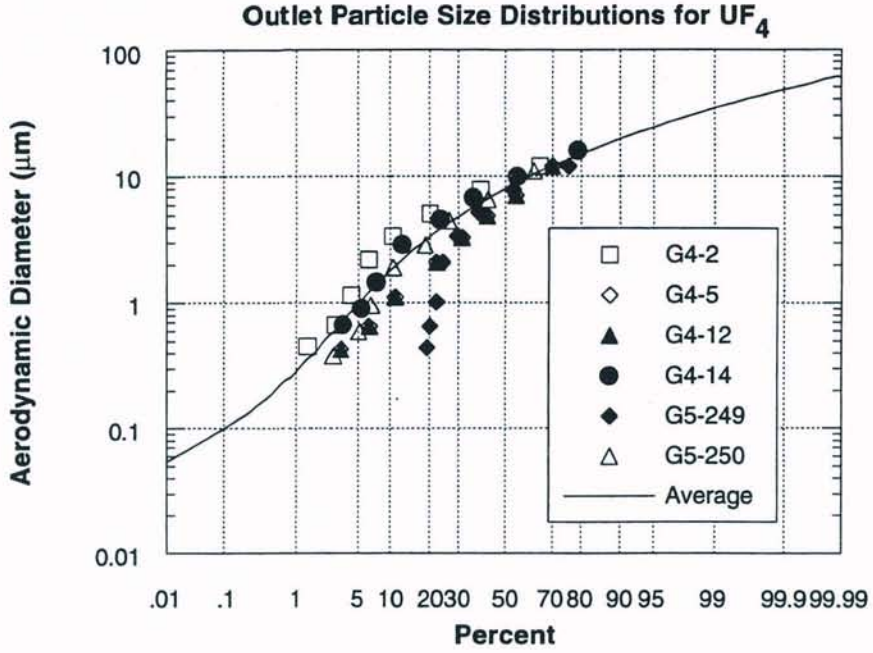

Fig. D–1. Outlet duct particle size distributions for UF_4 in FMPC dust collectors. The curve labeled "Average" has the following polynomial representation according to Eqs. D–3 through D–6: $c_0 = -1.62937$, $c_1 = 0.550176$, $c_2 = 0.041149$, $c_3 = 0.0341334$.

Table D–1. Discretized Distribution of Aerodynamic Particle Diameter (μm) For Airborne UF_4 Made by the Hydrofluorination Process in Plant 4 (Outlet Ducts)

		Percent UF_4 for Particle Diameter Range						
Plant	Stack	<2.5	2.5–5	5–7.5	7.5–10	10–15	15–20	>20
4	G4-2	8	12	15	16	29	15	5
	G4-5	25	17	14	8	13	7	16
	G4-12	5	15	22	23	25	8.5	1.5
	G4-14	11.5	13.5	15	15	21	14	10
5	G5-249	25	13	15	13	19	10.5	4.5
	G5-250	16	14	15	15	16	14	10
Average		15.1	14.1	16.0	15.0	20.5	11.5	7.8

sizes by using particle sizes in the inlet duct (Table D–4), however, do not show much difference between wool and Gore-Tex™. It was concluded on the basis of the observations above that any differences in removal efficiency between wool and Gore-Tex™ bag filters as calculated from data shown in Tables D–1 through D–4 are not significant. Examination of data from a much larger number of stacks with different types of bag filters would be required to determine whether any real differences exist.

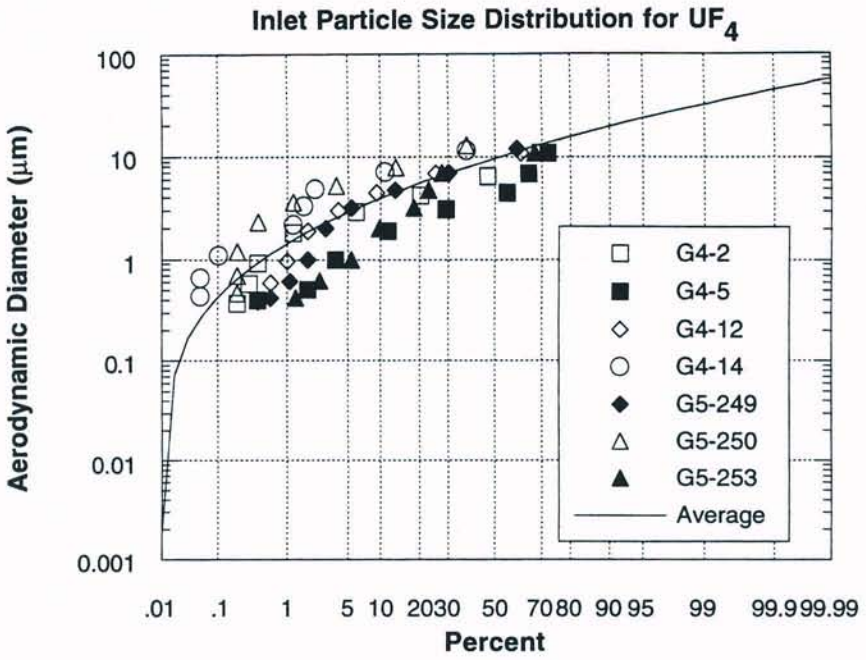

Fig. D–2. Inlet duct particle size distributions for UF_4 in FMPC dust collectors. The curve labeled "Average" has the following polynomial representation according to Eqs. D–3 through D–6: $c_0 = -2.60306$, $c_1 = 0.710504$, $c_2 = 0.162432$, $c_3 = 0.0123782$.

Table D–2. Discretized Distribution of Aerodynamic Particle Diameter (μm) For Airborne UF_4 Made by the Hydrofluorination Process in Plant 4 (Inlet Ducts)

		Percent UF_4 for Particle Diameter Range						
Plant	Stack	<2.5	2.5–5	5–7.5	7.5–10	10–15	15–20	>20
4	G4-2	5	17	26	22	22	5.5	2.5
	G4-5	23	27	14	10	11	5	10
	G4-12	3.5	8.5	18	24	29	14	3
	G4-14	0.8	3.2	8	14	34	22	18
5	G5-249	4.5	9.5	15	20	29	15	7
	G5-250	0.7	2.8	6.5	12	28	30	20
	G5-253	12	10	17	18	27	12	4
Average		7.1	11.1	14.9	17.1	25.7	14.8	9.2

HOW THE INCLUSION OF UNVERIFIED DATA WOULD AFFECT AVERAGES

If the unverified distribution listed in the FMPC-2082 report for the outlet duct of G5-253 had been included in Table D–1 for UF_4 emissions, the average values would have been skewed somewhat toward small sizes. The average percentage contribution of particles less

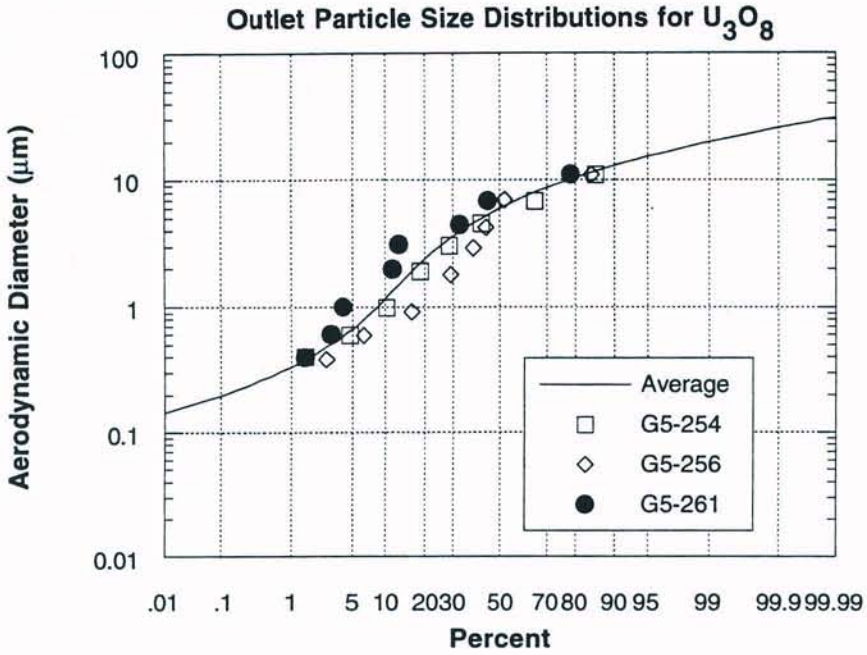

Fig. D–3. Outlet duct particle size distributions for U_3O_8 in FMPC dust collectors. The curve labeled "Average" has the following polynomial representation according to Eqs. D–3 through D–6: $c_0 = -1.36942$, $c_1 = 0.622726$, $c_2 = -0.10667$, $c_3 = 0.104758$.

Table D–3. Discretized Distribution of Aerodynamic Particle Diameter (μm) For Airborne U_3O_8 from Foundry Operations in Plant 5 (Outlet Ducts)

		Percent U_3O_8 for Particle Diameter Range						
Plant	Stack	<2.5	2.5–5	5–7.5	7.5–10	10–15	15–20	>20
5	G5-254	24	22	21	15	10	7.2	0.8
	G5-256	32	16	16	13	17	5	1
	G5-261	13	18	23	19	19	6	2
Average		23.0	18.7	20.0	15.7	15.3	6.1	1.3

than 2.5 μm would have been 25.5% instead of 15%. Contributions of the other six size-groups would have been less than the average values in Table D–1. Inclusion of the unverified distribution for U_3O_8 emitted from stack G5-260 listed in FMPC-2082 would have also resulted in a similarly skewed average for Table D–3. For particles less than 2.5 μm, the average contribution would have been 36.8% instead of 23%, and the contributions for each of the other six size-groups would have been correspondingly smaller.

If the unverified G5-251 values listed in the FMPC-2082 report had been included in Tables D–1 and D–2, the averages for these figures would not have been greatly different

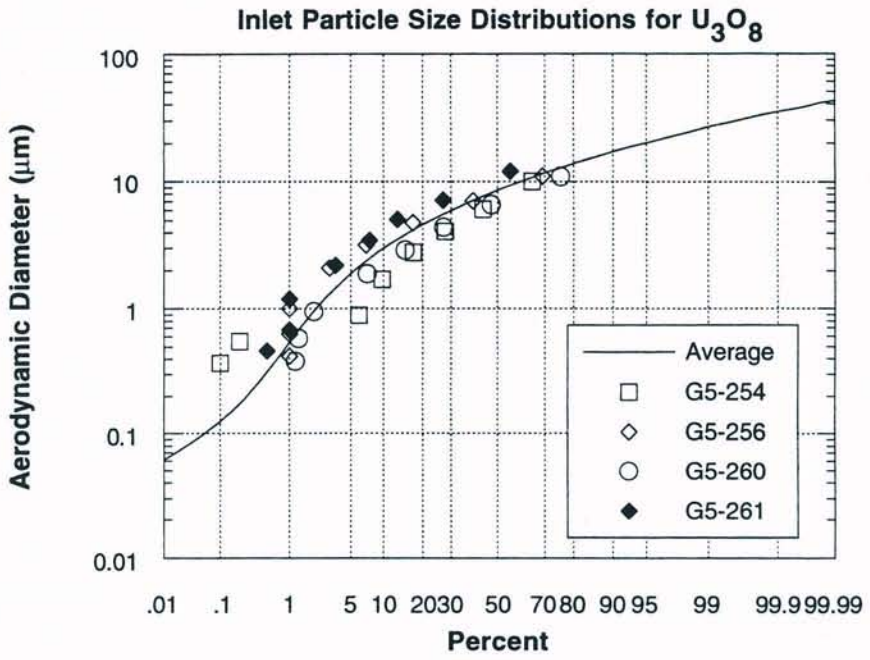

Fig. D–4. Inlet duct particle size distributions for U_3O_8 in FMPC dust collectors. The curve labeled "Average" has the following polynomial representation according to Eqs. D–3 through D–6: $c_0 = -2.03012$, $c_1 = 0.518554$, $c_2 = 0.0972778$, $c_3 = 0.0460301$.

Table D–4. Discretized Distribution of Aerodynamic Particle Diameter (μm) For Airborne U_3O_8 from Foundry Operations in Plant 5 (Inlet Ducts)

		Percent U_3O_8 for Particle Diameter Range						
Plant	Stack	<2.5	2.5–5	5–7.5	7.5–10	10–15	15–20	>20
5	G5-254	16	22	14	14	14	8	12
	G5-256	5	16	24	17	26	10	2
	G5-260	11	20	22	18	18	6.5	4.5
	G5-261	4	10	13	16	27	16	14
Average		9.0	17.0	18.3	16.3	21.3	10.1	8.1

except for the particles of aerodynamic diameter less than 2.5 μm for the inlet duct. The contribution of this size-group would have been 17.7% instead of 7.1%. Differences would have ranged between 1% and 3% for the other six size-groups for the inlet duct. There would have been differences of less than 1% for each of the seven size-groups of the outlet duct.

The averages for U_3O_8 in Tables D–3 and D–4 would not have changed greatly if the unverified particle-size distributions of the inlet and outlet ducts of G43-27 had been included. The percentage contribution of particles of aerodynamic diameter less than 2.5 μm in the outlet

Table D–5. Summary Parameters for the Averaged Particle Size Distributions

Form	Type of duct	Percentile					Mean	Standard deviation
		5	25	50	75	95		
UF_4	Inlet	2.9	6.3	9.7	14.3	23.5	11.0	6.5
UF_4	Outlet	0.97	4.1	8.0	13.4	24.2	9.7	7.5
U_3O_8	Inlet	1.9	5.3	8.6	12.7	20.1	9.5	5.7
U_3O_8	Outlet	0.67	3.0	6.0	9.4	15.2	6.6	4.6

duct would have been 19% instead of 23% with much smaller changes in contributions of the other six size-groups. The change for the inlet duct would have been less than 1% for each of the seven size-groups.

The G4-7 stack emitted a mixture of UO_3 and UO_2. This is the only stack in the group studied by NKES in which the predominant emitted species was neither UF_4 nor U_3O_8. Therefore, it was not possible to compare the unverified particle-size distribution for this stack with other distributions.

INFERRED PARTICLE SIZES FOR STACKS FOR WHICH NO MEASUREMENTS WERE MADE

The particle-size distributions for emissions during the years 1960 through 1962 from stacks for which no measurements had been made can be inferred from the results obtained from the other stacks. The particle-size distributions of the stacks which emitted UF_4 produced by the hydrofluorination process were averaged as shown in Tables D–1 and D–2, and this average distribution is assumed to apply to all stacks emitting UF_4 also produced by hydrofluorination during 1960–1962 but for which reliable measured values are not available. Airborne U_3O_8 is produced in the FMPC as a result of the oxidation of uranium metal surfaces by air. There are two general types of plant operations which can produce airborne U_3O_8 particles: (1) foundry operations such as melting and casting of uranium metal, crucible breakout of uranium derbies and ingots, and cleaning of metal surfaces, and (2) the machining of uranium derbies and ingots. The stacks which exclusively emitted U_3O_8 in the 1985 NKES study served only foundry operations in Plant 5. Hence, the average particle-size distribution for U_3O_8 emissions in this study as shown in Tables D–3 and D–4 is assumed to apply to all stacks exclusively serving foundry operations during 1960–1962 which emitted U_3O_8 and for which no measurements had been made in 1985. Surface oxidation of uranium scrap in high-temperature furnaces such as took place in Plant 8 was also assumed to be in the same category as foundry operation.

INFERRED PARTICLE SIZES FOR U_3O_8 PRODUCED DURING MACHINING

Machining operations such as cutting and milling of uranium metal ingots and derbies were conducted in Plant 6 and Plant 9 during 1960–1962. No particle-size measurements for U_3O_8 produced during machining operations were made in the 1985 NKES study, however, so comparisons with similar operations at other facilities were used to estimate particle-size distributions from machining at the FMPC.

A 1959 paper reported an average value of 2.5 micrometers for the mass median diameter of U_3O_8 particles produced in the machining of uranium at Los Alamos (Hyatt 1959). This value corresponds to a median aerodynamic diameter of 6.7 μm for an assumed density of 7.0 g cm^{-3} for the U_3O_8 particles. A mean particle size of 6.9 μm was recently reported for similar operations at AWE in the United Kingdom (Vallis 1991). An average for the two facilities (6.8 μm) may be assumed to apply to inlet ducts to dust collectors serving machining operations in Plant 6 and Plant 9 at the FMPC. An average value of about 5.1 μm is estimated to apply to the outlet ducts. This value would represent a 25% reduction in median particle size as a result of filtering, which is about the average reduction observed in measurements at the FMPC.

PARTICLE SIZES OF U_3O_8 FROM FOUNDRY OPERATIONS AT OTHER FACILITIES

Particle sizes of U_3O_8 in air during foundry operations were measured at Los Alamos and at two facilities in the United Kingdom. The results provide some confirmation of the FMPC data for similar operations. The median aerodynamic diameters are shown in Table D–6.

Table D–6. Median Aerodynamic Diameters (μm) from Foundry Operations at Other Facilities

Los Alamos (Hyatt 1959)	7.3
AWE in UK (Vallis 1991)	11
Springsfields in UK (Fishwick 1991)	8

The average value (8.8 μm) compares favorably with the average inlet value of 8.3 μm for FMPC foundry operations.

PARTICLE SIZES FOR EMISSIONS FROM PLANT 1 AND PLANT 2/3

A mixture of particles of U_3O_8, UO_3, and UO_2 is assumed to be emitted from stacks of Plant 1 and Plant 2/3 as a result of handling of ores and various other feedstocks to provide feed to digestors. Since the 1985 NKES study did not include any stacks for these plants, particle-sizes for these emissions must be inferred from measurements made for similar operations elsewhere. A study was carried out on particle sizes of uranium-containing dust from mining and milling operations in the Elliot Lake Area of Canada. (Duport and Edwardson 1985, Duport and Horvath 1989).

Median aerodynamic diameters (μm) were reported for mill atmospheres for the following processes: jaw crushing, 9.5; cone crushing, 9; screening, 7.5; grinding, 8; acid precipitation,

6; filtering, 10; concentrate drying, 8; and concentrate packing, 7.5. The corresponding geometric standard deviations (GSD) ranged between 3 and 5. The average median aerodynamic diameter for mills (possibly a weighted average) was reported to be about 7 μm. A mean particle size of 7 μm with a GSD of about 4 may be inferred for the U_3O_8 dust emitted from Plant 1 and Plant 2/3 as a result of ore handling if it may be assumed that the ore-handling processes in these plants during 1960–1962 were similar to those in the Elliot Lake Area. This inferred value would apply to inlet ducts of the dust collector stacks. A mean value of 5.3 μm would apply to the corresponding outlet ducts as a result of a reduction of 25% in the median particle size during filtration.

PARTICLE SIZES FOR UF_4 PRODUCED BY REDUCTION OF UF_6 VAPOR BY HYDROGEN GAS IN DISSOCIATED AMMONIA

One of the stacks in the FMPC Pilot Plant served a process for making UF_4 by reduction of UF_6 by hydrogen gas during the 1960–1962 period. There is no particle size information available on emissions from this process at present.

OTHER PROPERTIES OF PARTICULATES

Densities and shape factors are parameters used in calculations of the gravitational fall velocity of large or dense particles. These parameters are discussed in the following subsections.

Densities

Emitted particulates are produced rapidly during FMPC processing, and hence they would be expected to be imperfectly formed and contain voids. Therefore, their densities would be less than theoretical or "handbook" values, which would represent maximum values. The only information found in FMPC reports or other records concerning particulate density of emitted materials was a value of 6.4 g cm^{-3} for UF_4 produced at the FMPC (Freitag 1964). The "handbook" value for UF_4 is 6.7 g cm^{-3}. The value used in Los Alamos particle-size studies for U_3O_8 particulates produced by foundry operations and by machining is 7.0 g cm^{-3} (Hyatt et al. 1959). The "handbook" value listed for U_3O_8 is 8.30 g cm^{-3}.

Shape Factors

The expression for the gravitational fall velocity of a particle (Eq. D–1) should be divided by a shape factor if the particle is not spherical. Values of shape factors applicable to cyclindrical shapes are listed in Table D–7 (Chamberlain 1975).

Table D–7. Shape Factors Versus Axis Ratio

Ratio of Axes	Shape Factor
1	1.06
2	1.14
3	1.21
4	1.32

Only a few memoranda or FMPC plant reports containing photomicrographic information on plant products have been located. These reports contained photomicrographs of UF_4 produced by the Winlo Process, which was carried out in Plant 8 from 1962 to 1964. The average measured ratio of axes of this product was found to be about 1.5. Photomicrographs of U_3O_8 dust from Los Alamos foundry operations (Hyatt et al. 1959) show irregular particles with length-to-width ratios generally ranging from 1 to 2. A value of 1.5 represents an approximate average. In lieu of better information, it appears likely that the use of a shape factor of 1.1, for instance, would not lead to serious error in calculation of gravitational fall velocities.

ADDENDUM: REENTRAINMENT OF MIST DROPLETS IN SCRUBBER EMISSIONS

Recent calculations of empirical deposition velocities for uranium particles in FMPC releases have indicated a need for further scrutiny of reentrainment in the scrubbers of Plant 2/3 and Plant 8 (Appendix G). This addendum addresses this need and seeks to quantify, in a tentative way, the mass distributions of the effluent from the scrubbers, with particular attention to processes associated with reentrainment.

Plant 8 Scrubber Emissions

Ejector-venturi scrubbers were used primarily to service the furnaces emitting uranium-containing particulates from Plant 8. These scrubbers used a sodium hydroxide solution as the scrub liquor to remove U_3O_8 from the gas streams exiting the furnaces. There were five main scrubber systems that accounted for almost all of the uranium emissions from Plant 8.

The gas streams from each of the scrubbers exited downward into a hotwell containing a baffle system to remove entrained droplets of scrub liquor. Baffle systems remove large droplets in a gas stream, but they are usually inefficient at removing the smaller sizes. Three of the scrubber hotwells contained internal packed section mist eliminators near their outlets to remove the smaller particles. One of the scrubber hotwells apparently had an internal mist eliminator at its outlet which was not specifically identified as to type. The largest system, the Caustic scrubber, did not appear to have a mist eliminator at all. Unlike the Plant 2/3 scrubbers which had wire mesh mist eliminators mounted in their outlet ducts, the Plant 8 scrubbers had no mist eliminators of any kind in their outlet ducts.

There were two types of uranium emissions from the Plant 8 scrubbers: (1) fine solid particles of U_3O_8 (mostly < 2 μm) which had penetrated the venturi throats of the scrubbers and passed through baffles and mist eliminators, and (2) liquid droplets of large size (50–180 μm) containing uranium in solution or suspension which had been produced by entrainment or reentrainment. Large droplets would have been affected by gravity as the airborne plume was blown downwind of Plant 8, and they may have had a substantial gravitational fall velocity. Evaporation of water from the droplets during downwind plume travel would also have occurred. This evaporation process would have soon resulted in solid agglomerates of uranium-containing material. The high density and size of the agglomerates would have also produced a substantial gravitational fall velocity.

Very high empirical deposition velocities were reported in Appendix G for uranium particles emitted from the FMPC. These high values had been calculated from air monitoring data

and gummed film monitoring. Solid particulates emitted from dust collectors in the FMPC were not large enough to explain these high calculated deposition velocities, so the uranium releases from scrubbers in Plant 8 were analyzed in an attempt to explain the empirical data. There were no reported particle-size measurements of the emissions from the Plant 8 scrubber systems. A theoretical analysis described below is aimed at estimating what might have been the particle-size distributions of uranium-containing solid particles and droplets originating from Plant 8 scrubbers.

Estimates of Total Uranium Emitted from Each Scrubber System in Plant 8

The uranium emitted to the atmosphere from each of the five scrubber systems was estimated from scrubber efficiency studies carried out by FMPC personnel and from plant information on uranium scrubber throughput. Table D–8 lists calculated atmospheric emissions from each scrubber. The information in the table covers roughly the period 1961–1963.

Table D–8. Calculated Uranium Emissions from Plant 8 Scrubbers

Scrubber	Load (lb U month^{-1})	Efficiency (%)	Emission (lb U month^{-1})
Caustic	3700[a]	94[a]	222
Rotary kiln	1500[b]	92[b]	120
Oxid. furnace	214[c]	79[c]	45
NPR furnace	143[d]	79[d]	30
UAP furnace	460[f]	71[e]	133

[a] Starkey 1961 and numerous analytical data sheets.
[b] Starkey 1961; Bipes 1962.
[c] Calculated from an upper limit value of 45 lb U/month released to the atmosphere inferred from Chapman (1965) using an assumed efficiency of 79% for a similar scrubber (NPR furnace).
[d] Bipes 1963c.
[e] Starkey 1961; Bipes 1963a; Bipes 1963b; Bipes 1964.
[f] Starkey 1961; Bipes 1963b; Bipes 1964.

The emission estimates listed in Table D–8 may be modified later if additional information from FMPC plant records are obtained. The results of the analysis described below would accordingly be modified in that event.

Penetration of Solid U_3O_8 Particulates Through Scrubbers

The specific distribution of U_3O_8 particulates assumed to be typical of Plant 8 furnace emissions according to FMPC plant memoranda is given in Table D–9.

Venturi scrubber efficiencies as a function of particle-size ranges are given in Table D–10 (Lund 1971).

A calculated size distribution of U_3O_8 particles penetrating the venturi throat of a scrubber is given in Table D–11. The values were calculated from the inlet distribution of Table D–9

Table D–9. Distribution of U_3O_8 Particles Emitted from Plant 8 Furnaces

Diameter Range (μm)	Frequency (%)
0 – 1	4
1 – 2	11
2 – 5	34
5 – 10	30
10 – 20	14
20 – 50	7

Table D–10. Removal Efficiencies of Venturi Scrubbers

Diameter range (μm)	Efficiency (%)
0 – 1	50
1 – 2	97
2 – 5	98.8
5 – 10	99.8
>10	100

Table D–11. Calculated Distribution of Penetrating Particles of U_3O_8

Diameter range (μm)	Frequency (%)
0 – 1	71.4
1 – 2	11.8
2 – 5	14.6
5 – 10	2.1

and the efficiencies listed in Table D–10. The penetration is about 2.8% for the typical distribution of sizes listed in Table D–9.

Entrainment of Scrub Liquor at Venturi Throat

The mean droplet size (Sauter mean diameter) of the mist produced at the venturi throat of a venturi scrubber typically ranges from 100 to 200 μm in diameter (Boll et al. 1974). This range of values is characteristic only of the initial mist production within the scrubber system. Reduction of the mean droplet sizes by impingement of larger droplets on baffles within the separator chambers of the scrubber system usually occurs subsequently.

The average Sauter mean diameter is approximately 150 μm. Since the Sauter mean diameter is approximately 75% of the volume median diameter of a liquid spray distribution

(*Encyclopedia of Chemical Technology* 1984), the average volume median diameter of initial spray distributions from venturi scrubbers would be about 200 μm.

The distribution of droplet sizes emanating from a venturi scrubber system before the gas flow has passed through the baffle system and any subsequent mist eliminators may possibly be estimated by reference to a typical volume distribution of spray droplet diameters (*Encyclopedia of Chemical Technology* 1984). This distribution, which resulted from spray production of a hollow-cone (swirl-chamber) nozzle, is skewed from lognormal in the direction of small particle sizes. The median diameter is 300 μm.

Frequencies for specific diameter ranges taken from the estimated distribution curve are presented in Table D–12. The construction of the estimated curve was based on the assumption that its shape is similar to that obtained from a hollow-cone nozzle.

Table D–12. Estimated Initial Distribution of Entrained Droplet Sizes for Venturi Scrubbers

Diameter range (μm)	Frequency[a] (%)
0 – 50	3
50 – 75	4.5
75 – 100	5.5
100 – 150	17
150 – 200	20
200 – 250	17
250 – 300	13
300 – 350	10
>350	10

[a] For a volume distribution.

The typical distribution of particle sizes of liquid droplets produced at the venturi throat of a scrubber as shown in Table D–12 would be modified by preferential impingement of the larger particles on baffles in the separator chambers.

Removal of Entrained Liquid Droplets by Baffle Systems in Scrubber Hotwells

The large droplets of uranium-containing scrub liquor entrained during venturi operation were probably mostly removed in scrubber hotwells by inpingement on baffles. The scrubber hotwells for the rotary kiln, oxidation furnace #1, and the NPR furnace (oxidation furnace #2) contained vertical zigzag baffle systems according to FMPC engineering drawings (3014-S-4257 and 3014-S-4207). The gas flow was horizontal to the baffles. Specific information is not available on removal efficiencies of zigzag baffles.

The caustic scrubber served the primary calciner, the muffle furnace, and the box furnace of Plant 8. The engineering drawing for the recycle tank for the scrubber (3043-F-06-B) shows a 3/8-inch–thick vertical baffle at the tank midpoint, but no details of its internal structure are available at present. Perforations in the baffle would be required to permit a gas flow from one side of the recycle tank to other side of the tank where the exit to the outlet duct was located.

There are no engineering drawings on hand at present which show any details of liquid droplet collection systems for the UAP scrubber. A schematic drawing of the UAP system shows a section at the outlet of the hotwell that is labelled an internal demister. A vertical baffle is shown at the midpoint of the scrubber hotwell. This vertical baffle presumably operated in the same manner as the one identified as present in the Caustic scrubber hotwell.

Removal of Small Entrained Liquid Droplets by Mist Eliminators

The hotwells of scrubbers for the rotary kiln, oxidation furnace, NPR furnace, and UAP furnace had internal mist eliminators through which their gas streams pass just before exiting into outlet ducts for the stacks. The function of a mist eliminator is to remove small entrained droplets which pass through the baffle system. Various types of mist eliminators have been described (Calvert et al. 1974) including wire mesh, zigzag baffles, packed beds, and tube banks.

Packed bed mist eliminators containing Raschig rings were used in the hotwells of scrubbers for the rotary kiln, the oxidation furnace, and the NPR furnace. An unidentified type of mist eliminator is shown on a schematic diagram of the hotwell of the scrubber servicing the UAP furnace. Those engineering drawings for the Caustic scrubber which have been found do not show a mist eliminator, but there may have been one present nevertheless since all of the drawings for this scrubber system have not been located.

A cut diameter of approximately 3.5 μm for packed column mist eliminators was estimated from curves reported in the literature (Green 1984, pp. 18–20). Therefore, about half of the droplets less than 10 μm in diameter and virtually all of the larger droplets would have been removed by the packed columns.

Reentrainment of Liquid from Mist Eliminators or Baffle Systems

Reentrainment of entrained liquid which had been removed previously from a scrubber gas stream by impingement in a mist eliminator can occur at high linear gas flow rates. The exact flow rate for onset of reentrainment is not generally known because it is a complex function of a number of parameters, including type of mist eliminator, liquid-to-gas ratio, area and length of mist eliminator, and pressure drop. Reentrainment of liquid from wire screen mist eliminators in the outlet ducts of the Plant 2/3 scrubbers may have begun to occur at linear velocities as low as 400 cm sec^{-1} (Semones and Sverdrup 1988).

The linear flow rate through a mist eliminator, which is often crucial to the question of reentrainment, can be calculated by dividing the volume flow rate through the scrubber system by the cross sectional area of the mist eliminator. The cross sectional area is very nearly equal to the geometric area for some baffle types and certain wire-screen types of mist eliminators, but the cross sectional area of a packed section mist eliminator would include only open areas between packing elements. Also, random orientation of packing elements might result in localized constrictions which would result in reduced area.

Rough calculations have indicated that the scrubber gas velocities through the packed sections of the hotwells of scrubbers for the rotary kiln, the oxidation furnace, and the NPR furnace were probably high enough for reentrainment to occur. The Caustic scrubber hotwell had a 3/8-inch–thick baffle perpendicular to the direction of gas flow. The very high gas velocity through that type of baffle system might possibly have produced reentrainment even in the

absence of a mist eliminator. The UAP scrubber hotwell apparently had a mist eliminator at its outlet port, but its type is not known.

Reentrained mist droplets are reported to be generally greater than 100 μm in diameter (Black and Strauss 1981). The size distribution of reentrained droplets from the Plant 8 scrubbers is not known, but the assumption of a lognormal distribution would probably not result in serious error. An assumption of 100 μm diameter for the 15th percentile and 200 μm for the 85th percentile would result in a geometric mean of 141 μm and a geometric standard deviation of 1.42. We have adopted this distribution for subsequent calculations.

Summary of Types of Uranium Emissions from Plant 8 Scrubbers

As can be seen by reference to the discussions in the paragraphs above, different types of uranium particulates may have been emitted from the Plant 8 scrubber systems. Small solid particulates of U_3O_8 penetrating the venturi scrubber throat could have carried through the baffle and mist eliminator systems in the scrubber hotwells and entered the atmosphere. Also, reentrainment of scrub liquor as droplets could have occurred in the mist eliminators with release to the atmosphere.

The total uranium emissions from each scrubber as listed in Table D–8 minus the quantity of uranium penetrating the venturi throat (2.8% of the load for each scrubber) should represent the quantity of uranium reentrained from mist collectors exiting to the outlet ducts. Very little uranium as liquid droplets should have exited the packed bed mist eliminators except through reentrainment.

Table D–13 summarizes the calculated uranium emissions.

Table D–13. Types of Uranium Emissions from Plant 8 Scrubbers (lb U month^{-1})

Scrubber	Load	Total	Solids	Reentrained Liquid
Caustic	3700	222	104	118
Rotary kiln	1500	120	42	78
Oxid. furnace	214	45	6	39
NPR furnace	143	30	4	26
UAP furnace	460	133	13	120

According to these calculations, about 70% of the uranium emitted to the atmosphere from the Plant 8 scrubbers was in the form of droplets of reentrained scrub liquor.

Environmental Transformation of Scrubber Releases

Liquid droplets containing uranium would shrink in volume during plume travel downwind from the stack. The concentration of any dissolved material would ultimately exceed its solubility at the temperature of the droplet. In the absence of any substantial undercooling, crystalline solid material would precipitate from solution. A continuing evaporation of water would result in a polycrystalline agglomerate. Of course, any insoluble particulates initially carried in suspension by the droplets would be included within the agglomerate.

The recirculating scrub liquor used for the Plant 8 scrubbers contained sodium hydroxide which reacted with uranium compounds in the gas stream to produce a complex mixture of partially soluble uranates and other materials. The scrub liquor may also have contained insoluble uranium compounds in suspension.

A theoretical discussion of the evaporation of water droplets which may be applicable to liquid scrubber releases is given in the literature (Dickinson and Marshall 1968). The basic equation to describe evaporation of water from a droplet derives from the conceptualization that all heat transferred to the droplet from surrounding air is used to vaporize water from the surface. Equation D–7, which is an approximate relationship derived from this concept, expresses the reduction of the diameter of a droplet as a function of elapsed time.

$$d = d_0 - kt \qquad \text{(D–7)}$$

where

d = diameter (μm) of droplet at time t

d_0 = initial diameter (μm) of water droplet

t = elapsed time (s)

k = a constant for a specific temperature difference.

A value of 3.35 for k can be elicited from Figure 8 of the Dickinson-Marshall paper for a droplet with an initial diameter of 50 μm and with a temperature difference of 50°C between ambient air and the droplet. Under these conditions, a water droplet 50 μm in diameter would evaporate completely in 15 seconds. If an average air speed of 2.5 m s^{-1} is assumed, it would take a liquid droplet about 215 seconds to reach the nearest perimeter air monitoring station.

Initial temperature differences between ambient air and a droplet would vary greatly with season and time of day as well as many other factors. Evaporation of water from a droplet into surrounding air, which would occur for a relative humidity of less than 100%, would result in cooling of the droplet. If the droplet temperature was initially higher than that of surrounding air, this cooling effect would cause a rapid drop in temperature below that of surrounding air. Temperature differences between air and droplet over the wide ranges of conditions of scrubber operation are uncertain. Nevertheless, under nearly all environmental conditions, it is probable that the droplets of scrub liquor had lost all of their water content by the time they had reached the perimeter of the FMPC production area.

Calculations of Solid Sphere Diameters Resulting from Complete Water Vaporization of Emitted Liquid Droplets

When a reentrained liquid droplet was emitted from a Plant 8 stack and was blown downwind, water vaporized from the droplet, and it was converted eventually to a solid polycrystalline agglomerate. The diameter of a hypothetical sphere of this resulting solid material can be approximately calculated if composition and mass can be determined. An attempt was made to determine average values for composition and mass by employing some simplifying assumptions based on the known procedures used in the operation of the Plant 8 scrubbers.

The Plant 8 procedure called for a 10% sodium hydroxide solution to be used as the scrub liquor for most of the scrubbers. Besides U_3O_8 particles, numerous solids and acidic gases

were reported to have been removed in the Plant 8 scrubbers. The acidic gases, which react with sodium hydroxide, include hydrogen chloride, carbon dioxide, and phosphorus oxides. Quantitative information on the relative or absolute quantities of these materials removed in each scrubber system is not available. According to Plant 8 procedures, the scrub liquor was replaced with a fresh 10% sodium hydroxide solution every two weeks or whenever the sodium hydroxide concentration dropped below 1%.

The uranium in the scrub liquor was probably converted to slightly soluble sodium uranates of uncertain composition. Since the system Na_2O-UO_3-H_2O is extremely complex, containing incongruently melting phases with large ranges of solid solution (Ricci and Loprest 1955), no attempt was made to identify the uranium species involved. It is also possible that some small insoluble particulates of U_3O_8 may have been in the scrub liquor.

It was assumed that the concentration of sodium hydroxide was reduced from 10% (100 g L^{-1}) to 5% (50 g L^{-1}) on the average in the Plant 8 scrubber hotwells before it was replaced. It was also assumed that the compounds listed in Table D–14 remained in the polycrystalline agglomerates after total evaporation of water from the droplet. The densities listed are handbook values.

Table D–14. Compounds which May Have Been Present in Airborne Polycrystalline Agglomerates

Compound	Solid formula	Density (g cm^{-1})
Sodium hydroxide	NaOH	2.13
Sodium chloride	NaCl	2.165
Sodium phosphate	$Na_3PO_4 \cdot 10H_2O$	1.62
Sodium carbonate	$Na_2CO_3 \cdot 7H_2O$	1.51
Sodium uranate	Na_2UO_4	3.7

The formula listed in Table D–14 as Na_2UO_4 is only a formal representation for what may be several species of unknown composition. No density for Na_2UO_4 has been reported in the literature because a phase corresponding to this formula has probably never been obtained from the Na_2O-UO_3-H_2O system. Nevertheless, a density of 3.7 g cm^{-3} was estimated by comparisons with other uranium species with comparable uranium contents. Then a calculation was made for the quantity of "Na_2UO_4" which might have been present in a liter of the scrub liquor after the sodium hydroxide had been depleted to 5%. This calculation was based on an average concentration of 38.6 g uranium per liter, which had been estimated for the Plant 8 scrubber liquor if a total hotwell capacity of 500 cubic feet is assumed for all scrubber systems (Voillequé et al. 1991). A total of 56.4 g of "Na_2UO_4" was estimated to have been present in a liter of scrub liquor after depletion to 5% sodium hydroxide.

A total of 13 g of sodium hydroxide would have been consumed in the production of "Na_2UO_4," and a total of 50 g of sodium hydroxide would have remained in the scrub liquor. The remaining 37 g of sodium hydroxide was assumed to have reacted with acidic gases to produce equal molar quantities of the salts listed in the table. Table D–15 lists the calculated mass of each of the solids in a liter of scrub liquor and its volume as calculated from its density.

It is not intended that the mixture shown in Table D–15 should represent any specific mixture of solids resulting from a Plant 8 scrubber operation. Instead, it is intended to represent only an average mixture from all of the Plant 8 scrubber operations. Each individual scrubber services a different furnace operation which produces a different mixture of acidic gases and solids in its outlet gas stream. The specific mixture shown in Table D–15 was arbitrarily chosen as one likely composition within a range of plausible compositions.

Table D–15. Calculated Volumes of Solid Compounds in One Liter of Scrub Liquor

Compound	Solid formula	Mass (g)	Volume (cm^3)
Sodium hydroxide	NaOH	50.0	23.5
Sodium chloride	NaCl	9.0	4.2
Sodium phosphate	$Na_3PO_4 \cdot 10H_2O$	53.0	32.7
Sodium carbonate	$Na_2CO_3 \cdot 7H_2O$	35.7	23.6
Sodium uranate	Na_2UO_4	56.4	15.2

The total estimated solid volume in 1 liter of scrub liquor is 99.2 cm^3. The ratio of liquid volume to solid volume (1000/99.2) is 10.08.

The volume of a sphere is proportional to the cube of its diameter. Therefore, if the average diameter of a sphere of reentrained scrub liquor was 140 μm, the average diameter of a hypothetical solid sphere remaining after complete water evaporation would have been 65 μm. Actual densities of crystalline material produced under conditions of rapid evaporation are likely to be somewhat lower than handbook values given in Table D–14. Therefore, the diameter of the remaining sphere would probably be larger than 65 μm. Polycrystalline aggregates produced by water evaporation from droplets during downwind plume travel could possibly break apart into smaller aggregates, of course, but no information about the likelihood of this phenomenon is presently available.

Uncertainties of Plant 8 Scrubber Emissions

Penetrating Particles of U_3O_8. One type of uranium-containing emission from the Plant 8 scrubbing systems consisted of particles of U_3O_8 which had penetrated the venturi throats of the scrubbers. Table D–11 lists the distribution of particle sizes of this type of emission. Values in this table were calculated from a distribution of U_3O_8 particles emanating from Plant 8 furnaces according to FMPC plant memos and removal efficiencies of venturi scrubbers.

The sizes of the particles of this type are generally small. Only 2.1% of the particles are greater than 5 μm in physical diameter. The uncertainty in particle-size frequencies is important only for particles in this range. The removal efficiency of venturi scrubbers is reported to be about 99.8% for particles in the range 5–10 μm (Lund, 1971). Uncertainties in the frequency of particles in this range may be evaluated by reference to other distributions reported for U_3O_8 particles released during foundry operations in other facilities. These operations generally released a smaller percentage of particles with diameters greater than

5 micrometers. Typically, about half as many particles in the range 5–10 μm were released, which may be regarded as setting a lower limit to the uncertainty of −50%.

The largest mean physical diameters reported for foundry operations in other facilities was 3.8 μm. Emission of particles larger than 5 μm as assumed for the Plant 8 operations may be possible for some processes, however, but no information about this matter is currently available. An arbitrary upper limit of +50% was assumed for the percentage of particles in the pertinent 5–10-μm range to ensure that nearly all probable mean sizes were included.

Size Distribution of Reentrained Droplets. Reentrained mist droplets are reported to be generally greater than 100 μm in diameter (Black and Strauss 1981). The size distribution of reentrained droplets from the Plant 8 scrubbers is not known, but the assumption of a lognormal distribution would probably not result in serious error. An assumption of 100 μm diameter for the 15th percentile and 200 μm for the 85th percentile would result in a geometric mean of 141 μm and a geometric standard deviation of 1.42.

Equations Expressing Diameter Ratios of Solids to Liquids. Examination of the Plant 8 scrubber procedures revealed that the increase in uranium concentration would have been a linear function of time if the uranium emissions from each furnace were linear with time. Likewise, the quantity of sodium hydroxide consumed would have been a linear function of time if acidic gases had been emitted from the furnaces linearly with time. The Plant 8 procedures called for replacement of the scrub liquor with a fresh 10% solution of sodium hydroxide every two weeks or whenever the concentration of sodium hydroxide fell below 1%. No plant records could be found, however, which listed specific scrub liquor replacement times or the results of analysis of scrub liquor. Therefore, the average lower limit of sodium hydroxide concentration in the scrub liquor is not known. Nevertheless, it is certain that it is greater than 10 g L^{-1}. For purposes of estimation of particle sizes, an average lower concentration of 20 g L^{-1} was assumed.

The sodium hydroxide concentration in the scrub liquor may be considered to decrease in a linear manner from 100 g L^{-1} down to 20 g L^{-1}. The average uranium concentration was 38.6 g L^{-1} as estimated from analytical information reported by Voillequé et al. (1991) for an assumed total scrubber hotwell capacity of 500 cubic feet. If both the uranium emissions and the emissions of acidic gases from the furnaces are linear functions of time, the uranium concentration and the sodium hydroxide consumption in the scrub liquor can be related as $q = 0.965x$, where q is the uranium concentration (g L^{-1}) and x is the mass (g) of sodium hydroxide consumed.

The ratio of the diameter of a solid sphere (d_S) remaining after water evaporation from a liquid droplet to the diameter (d_L) of the droplet was evaluated for three cases described below.

Case 1. The salt mixture in solution resulting from reaction of acidic gases with sodium hydroxide was an equimolar mixture of sodium chloride, sodium phosphate, and sodium carbonate.

Case 2. The salt in solution consisted entirely of sodium chloride.

Case 3. The salt in solution consisted entirely of sodium carbonate.

Case 1 may be regarded as a most probable result of the average emission from Plant 8 scrubbers, although not typically representative of any specific scrubbing system. For exam-

ple, some furnaces may have emitted hydrogen chloride primarily, which would have resulted mainly in sodium chloride dissolved in the scrub liquor. Other furnaces may have emitted either phosphorus oxides or carbon dioxide almost exclusively. Cases 2 and 3 are representative of the extreme cases of particle diameters. Case 2 would have resulted in a small particle size, while Case 3 would have resulted in a larger size solid particle.

Equations for estimating the ratio d_S/d_L were derived. Equations D–8, D–9, and D–10 are listed below for Cases 1, 2, and 3, respectively.

$$d_S/d_L = (0.04695 + 0.0010175x)^{0.3333} \quad \text{Case 1} \qquad \text{(D–8)}$$

$$= (0.04695 + 0.0003681x)^{0.3333} \quad \text{Case 2} \qquad \text{(D–9)}$$

$$= (0.04695 + 0.0016920x)^{0.3333} \quad \text{Case 3} \qquad \text{(D–10)}$$

Calculations of d_S/d_L. The value of x, the quantity of sodium hydroxide consumed, in each of the three equations was assumed to have increased uniformly with time from 0 to 80 g. In each case, all values of d_S/d_L over the range of 0 to 80 g may be regarded as equally probable. The d_S/d_L values calculated through use of Eq. D–8 (for an equimolar mixture of three salts) varied from 0.361 to 0.504 over the range. The d_S/d_L value for the average sodium hydroxide consumption (40 g) was 0.444.

The d_S/d_L values calculated from Eq. D–9 (for sodium chloride only) varied from 0.361 to 0.424 over the applicable range of sodium hydroxide consumption. The value for average sodium hydroxide consumption was 0.395.

Calculations for Eq. D–10, which is for sodium carbonate only, gave d_S/d_L values from 0.361 to 0.567 for sodium hydroxide consumption ranging from 0 to 80 grams. The value for average sodium hydroxide consumption was 0.486.

Summary of Types of Emissions from Plant 8 Scrubbers. Two distinct types of emissions from the Plant 8 scrubbers have been identified. The first type consisted of solid particles of U_3O_8 which had penetrated the venturi throats of the scrubbers. A postulated distribution of particle sizes for this type is given in Table D–11. Approximately 30% of the total uranium released to the atmosphere from the Plant 8 scrubbers was estimated to be of this type.

The second type of emission is postulated to consist of solid spheres of polycrystalline agglomerates deriving from water vaporization of liquid droplets of reentrained scrub liquor. About 70% of the total uranium released from the Plant 8 scrubbers was estimated to come from this source. The particle-size distribution of this type of emission and associated uncertainties may be derived from the analysis above.

Plant 2/3 Scrubber Emissions

Ejector-venturi scrubbers in Plant 2/3 served gulping operations, which consisted of vacuum transfers of orange oxide (UO_3) to two cyclone separators in series. These separators removed the UO_3 product. Exhaust from the second cyclone separator entered the scrubber. Nitric acid was used as the scrub liquor to collect the UO_3 which had not been removed by the cyclone separators. The nitric acid scrub liquor reacted with UO_3 to produce soluble uranyl nitrate as per Eq. D–11 below:

$$UO_3 + 2HNO_3 \rightarrow UO_2(NO_3)_2 + H_2O. \qquad \text{(D–11)}$$

Exhaust from the scrubber, which contained dissolved uranyl nitrate in small droplets, passed through a wire screen mist eliminator in the outlet duct before it entered the atmosphere.

Quantities of uranium released from the Plant 2/3 gulping system have been estimated over the 35-year history of the plant (Semones and Sverdrup 1988). The estimates were based on uranium production records and actual measurements of entrained mist and particulates emitted from the scrubber systems. The authors have tabulated experimentally-determined mist entrainment losses of uranium and theoretically-computed particulate losses of uranium for each year from 1954 through 1988. More than half of the total uranium lost was estimated to be lost by mist entrainment. The greatest total losses of uranium occurred during the period 1958 through 1962, which was also the period of greatest UO_3 production.

The uranium lost by mist entrainment would consist of two parts. The first part would consist of small liquid droplets of entrained scrubber liquid which passed through the mist eliminator, a 10-inch–thick wire screen pad in the outlet duct. The second part of the mist entrainment would consist of large droplets (generally 100 μm or larger) reentrained from the mist eliminator as a result of excessive gas velocity.

According to the Semones-Sverdrup report, the efficiency of a mist eliminator of the type used for the Plant 2/3 scrubbers increases with increasing gas velocity up to a maximum of 99% at 3–4 m s^{-1}. Reentrainment at higher velocities drops the efficiency. Semones and Sverdrup estimated that the efficiency was only 60% for velocities of 6–12 m s^{-1}, which prevailed for the Plant 2/3 stacks. Therefore, nearly all of the mist which penetrated the mist eliminator and was emitted from the plant stacks consisted of reentrained droplets.

Solid UO_3 particulates in outlet duct. An approximate calculation was made for the particle-size distribution of solid UO_3 particles which penetrated the scrubber and exited through the plant stacks. The physical geometric mean diameter of the UO_3 aggregates transferred in the Plant 2/3 gulping operations was reported by Semones and Sverdrup to be 22 μm. By using an arbitrary value of 3 μm for the standard deviation of the distribution and by applying the efficiencies for venturi scrubbers in Table D–10, an approximate particle-size distribution was calculated for UO_3 particulates penetrating the scrubber. This particle-size distribution is listed in Table D–16.

Table D–16. Approximate Particle-Size Distribution of UO_3 in Outlet Duct

Particle-size range (μm)	Frequency (%)
0 – 2	89.0
2 – 3	5.4
3 – 4	2.2
4 – 5	2.6
5 – 6	0.7

Particle sizes of reentrained mist droplets. Reentrained mist droplets are reported to be generally greater than 100 micrometers in diameter (Black and Strauss 1981). These droplets, which contained uranyl nitrate in solution, would have shrunk during downwind

plume travel as a result of evaporation of water from their surfaces. Complete loss of water would leave solid uranyl nitrate hexahydrate (UNH) crystals in the plume. According to Eq. D–7, even the larger mist droplets would have completely lost all of their water by the time the plume had travelled a few hundred meters. The rapid crystallization of UNH from the liquid would undoubtedly result in a polycrystalline mass which may break apart during plume travel. Calculations were made as described below on the particle sizes of solid particles remaining as a result of water vaporization from mist droplets. It was assumed that the resultant UNH solids were in the form of intact polycrystalline aggregates.

For purposes of the calculations, it was assumed that the reentrained mist droplets uniformly ranged from 80 to 180 μm in diameter. The Semones-Sverdrup document states that the concentration of the scrub liquor ranged uniformly from 27.5 to 55.1 g uranium per liter. The uranium was all present in the liquor as uranyl nitrate. Using a density of 2.8 g cm^{-3} for UNH, the volume of solid UNH in a liter of solution was calculated to be about 20.7 cm^3 for a solution containing 27.5 g uranium per liter and 41.4 cm^3 for a solution containing 55.1 g uranium per liter. The ratios of the diameters of solid sphere to liquid droplet ranges from 0.275 to 0.346 for concentrations in scrub liquor ranging from 27.5 to 55.1 g uranium per liter.

Using the information above, estimates were made for the particle-size distribution of solid UNH particulates deriving from reentrained mist. The results of the calculations are listed in Table D–17.

Table D–17. Estimated Uniform Particle-Size Distribution for UNH from Reentrained Mist Droplets

Initial Droplet Diameter Range (μm)	Average Solid UNH Aggregate Diameter (μm)
80 – 100	29
100 – 120	35
120 – 140	41
140 – 160	47
160 – 180	53

Since the initial droplets were a result of rapid air flow through a wet wire screen with a distinct mesh size, there is no reason to believe that a lognormal distribution would apply. The physical constraint of the mesh size would probably be one of the most important factors in determining the size of the droplets. Hence, the assumption of a narrow droplet range with a uniform distribution of diameter sizes as shown in Table D–17 is probably as reasonable as any.

Uncertainties of Plant 2/3 Scrubber Emissions

As for Plant 8, we consider two distinct types of emissions from the Plant 2/3 scrubbers. First, small-diameter particles of UO_3 which penetrated the scrubber system were assumed to be released. The particle-size distribution of this type of emission is given in Table D–16. Second, solid particles of polycrystalline agglomerates of uranyl nitrate hexahydrate (UNH) were assumed to be produced in the downwind plume as a result of evaporation of water from reentrained droplets of scrub liquor emitted from the Plant 2/3 scrubbing systems.

Penetrating Particles of UO_3. The first type of emission consisted only of small particles. Only 0.7% of the particles, for instance, were estimated to be greater than 5 μm in diameter. Uncertainties of frequencies for smaller particle-size ranges are not important in evaluation of radiation doses.

Size Distribution of Solid Particles Resulting from Water Evaporation from Reentrained Droplets. The second type of emission, described in Table D–17, was assumed to be uniformly distributed over the diameter range of 29 to 53 μm. The average particle size is 41 μm. The uncertainty is ±50%.

Summary of Types of Emissions from Plant 2/3 Scrubbers. The report of Simones and Sverdrup (1988) calculated the percentage contributions of the two types of emissions from the Plant 2/3 scrubber systems. The first type of emission, consisting of particles of UO_3 which had penetrated the scrubbers, was about 46% of the total uranium emission. The remainder (about 54%) initially consisted of reentrained scrub liquor as droplets of mist.

SUMMARY AND CONCLUSIONS

We close this appendix with some general remarks about applications of the information that has been developed. Some applications have already been made to development and validation of the methodology discussed in other parts of this report. Others will be made when the full source term is incorporated into the final dose estimates.

Particle Sizes of Emissions from Stacks with Dust Collectors

Particle Sizes Applied to the 1960–1962 Period. The particle-size distributions measured for stack emissions in 1985 by NKES can be applied to emissions from the same stacks in the period 1960–1962 since plant operations served by those stacks have not changed over the years. Averaged distributions for UF_4 emissions and for U_3O_8 emissions as calculated from the NKES measurements can be applied for the 1960–1962 period to stacks for which there were no measurements made in 1985 for all cases in which the emitted species was produced through similar operations. Inferred values for particle sizes of U_3O_8 from machining operations in other facilities may be used for stacks serving FMPC machining operations for the 1960–1962 period. Similarly, uranium oxide particle sizes reported by other facilities may be used for similar ore-handling processes carried out in Plants 1 and 2/3 during 1960–1962.

Particle Sizes for all Years of FMPC Operation. Both the measured or inferred particle size distributions of uranium species listed in this appendix as applied to the 1960–1962 period may be used directly for all years from the beginning to the end of FMPC plant operations for all cases in which plant operations and processes were the same as in 1960–1962. An assignment of particle sizes for uranium releases over all of the years of operation

of the FMPC requires identification of both the predominant species and its generating plant process for each major emission point for each year. For the few cases for which no reliable information on particle size can be obtained, particle sizes will be assigned at midpoints of expected maximum uncertainty ranges.

Particle Sizes of Emissions from Scrubbers

Ejector-venturi scrubbers in Plant 8 and Plant 2/3 serviced furnaces and process equipment that emitted uranium compounds as small particulates. There were two types of emissions from the Plant 8 scrubbers: (1) fine solid particles of U_3O_8 (< 2 μm in diameter), which penetrated the scrubber systems, and (2) large liquid droplets of reentrained scrub liquor containing uranates, sodium hydroxide, and dissolved sodium salts. The liquid droplets (with a postulated mean diameter of about 140 μm) dried out during downwind plume travel. The polycrystalline solid agglomerates remaining after water evaporation were calculated to have had diameters of about 45% of the liquid droplet diameters. According to our calculations, about 70% of the uranium emitted to the atmosphere for Plant 8 scrubbers came from the second type above, and about 30% came from the first type.

The Plant 2/3 scrubbers were postulated to have emitted (1) solid particulates of UO_3 of small size (mostly < 2 μm in diameter), which penetrated the scrubbers, and (2) large liquid droplets of reentrained scrub liquor containing dissolved uranyl nitrate hexahydrate (UNH). Diameters of these droplets were assumed to be lognormally distributed with geometric mean 141 μm and geometric standard deviation 1.4. Average diameters of the solid UNH agglomerates resulting from water evaporation from the droplets were estimated to range from 29 to 53 μm. It was reported that the first type of emission accounted for about 46% of the total uranium emitted from the Plant 2/3 scrubbers and about 54% came from the second type.

REFERENCES

Bipes R.L. 1962. "Uranium Loss from Rotary Kiln Scrubber." FMPC Memo to H.M. Beers dated Aug. 20, 1962.

Bipes R.L. 1963. "UAP Scrubber Efficiency." FMPC Memo to K.E. Brandner dated Sept. 10, 1963.

Bipes R.L. 1963. "UAP Scrubber Loading - Plant 8." FMPC Memo to H. Mode dated Nov. 8, 1963.

Bipes R.L. 1963. "NPR Furnace Doyle Scrubber Efficiency - Plant 8." FMPC Memo to K.E. Brandner dated Nov, 27, 1963.

Bipes R.L. 1964. "UAP Scrubber Efficiency Tests." FMPC Memo to H. M. Beers dated Feb. 11, 1964.

Black G.M. and W. Strauss (Eds.). 1981. *Air Pollution Control Part IV.* John Wiley and Sons, New York.

Boback M.W., T.A. Dugan, D.A. Fleming, R.B. Grant, and R.W. Keys. 1987. *History of FMPC Radionuclide Discharges.* Rep. FMPC-2082. Westinghouse Materials Company of Ohio.

Boll R.H., L.R. Flais, P.W. Maurer, and W.L. Thompson. 1974. "Mean Drop Size in a Full Scale Venturi Scrubber via Transmissometer." *J. Amer. Air Poll. Control Assoc.* **24**: 934.

Calvert S., I.L. Yashnani, and S. Yung. 1974. "Entrainment Separators for Scrubbers." *J. Amer. Air Poll. Control Assoc.* **24**(10): 971.

Chamberlain A.C. 1975. "The Movement of Particles in Plant Communities." In: *Vegetation and the Atmosphere,* Vol. I, Chapter 5, p. 157 (J.L. Monteith, Ed.). Academic Press, London.

Chapman C.R. 1965. "Request for Feasibility Study Re: Reduction of Scrubber Losses." FMPC Memo to P. G. DeFazio dated Jan. 25, 1965.

Dickinson D.R. and W.R. Marshall, Jr. 1968. "The Rates of Evaporation of Sprays." *AIChE Journal* **14**(4): 541–552.

Duport P.J. and E. Edwardson. 1985. *Determination of the Contribution of Long-Lived Dust to the Committed Dose Equivalent Received by Uranium Mine and Mill Workers in the Elliot Lake Area.* Rep. INFO-0167-1. Atomic Energy Control Board, Canada.

Duport P. and F. Horvath. 1989. "Practical Aspects of Monitoring and Dosimetry of Long-Lived Dust in Uranium Mines and Mills — Determination of the Annual Limit on Intake for Uranium and Uran. norium Ore Dust." *Rad. Prot. Dosimetry* **26**(1/4):43–48.

Encyclopedia of Chemical Technology, 3rd Edition, Vol. 1. 1978. John Wiley and Sons, New York.

Fishwick A.H. 1991. Personal communication to P.G. Voillequé, June 19, 1991.

Freitag J.A. 1964. *Comparison of Methods for Particle Size Analysis.* Rep. NLCO-925 (Sep. 30, 1964). National Lead Company of Ohio, Cincinnati.

Green Don W. (Ed.). 1984. *Perry's Chemical Engineers' Handbook,* Sixth Edition. McGraw-Hill Book Company, New York.

Hanna S.R., G.A. Briggs, and R.P. Hosker, Jr. 1982. *Handbook on Atmospheric Diffusion.* Rep. DOE/TIC-11223. Technical Information Center, U.S. Department of Energy.

Hyatt E.C., W.C. Moss, and H.F. Schulte. 1959. "Particle Size Studies on Uranium Aerosols from Machining and Metallurgy Operations." *Amer. Ind. Hygiene Assoc. J.* **20**(1):99–107.

International Commission on Radiological Protection (ICRP). 1979. *Limits for Intakes of Radionuclides by Workers.* ICRP Publication 30. *Ann. ICRP* **2**(3/4):23–29.

Lund H.F. 1971. *Industrial Pollution Control Handbook.* McGraw-Hill Book Company, New York.

Reed K.P. 1985. "A Study of the Particle Size Distribution of the Stack Emissions at Fernald." Unpublished report by Northern Kentucky Environmental Services.

Ricci J.R. and F.R. Loprest. 1955. "Phase Relations in the System Sodium Oxide-Uranium Trioxide-Water at 50 and 75°." *J. Am. Chem. Soc.* **77**: 2119.

Semones T.R. and E.F. Sverdrup. 1988. *Uranium Emissions from Gulping of Uranium Trioxide.* Rep. FMPC/SUB-019, Westinghouse Materials Company of Ohio, Cincinnati, Ohio.

Task Group on Lung Dynamics (TGLD): D.V. Bates, B.R. Fish, T.F. Hatch, T.T. Mercer, and P.E. Morrow (Chairman). 1966. "Deposition and Retention Models for Internal Dosimetry of the Human Respiratory Tract." *Health. Phys.* **12**:173–207.

Vallis D.G. 1991. Personal communication to P.G. Voillequé. (June 20, 1991).

Voillequé P.G., K.R. Meyer, D.W. Schmidt, G.G. Killough, R.E. Moore, V.I. Ichimura, S.K. Rope, B. Shleien, and J.E. Till. 1991. *The Fernald Dosimetry Reconstruction Project, Tasks 2 and 3: Radionuclide Source Terms and Uncertainties — 1960–1962.* Rep. CDC-2. Radiological Assessments Corporation, Neeses, South Carolina 29107.

APPENDIX E

METEOROLOGICAL DATA FOR MODELING THE TRANSPORT OF AIRBORNE RELEASES

INTRODUCTION

The atmospheric dispersion models used to reconstruct ground-level air concentrations at receptor points in the assessment domain require meteorological data expressed as joint frequency tables (JFTs) of wind speed, wind direction, and atmospheric stability (Pasquill-Gifford classes A–F). Ideally, a JFT would be compiled for the FMPC region for each month of the assessment period (1951–1988), but the necessary tower and instrumentation for collecting such data at the FMPC site have been in continuous operation only since August 1986. In previous assessments, JFTs compiled from regional airports (Dayton, Ohio, and Covington, Kentucky) have been used as surrogates for the Fernald site, but our comparisons of the 1987–1991 period indicate that straightforward substitution of these data sets for JFTs based on data recorded at the Fernald tower would likely produce underestimates of air concentrations at most points of the assessment domain. If the limited FMPC dataset is applied to years preceding 1987, estimates of air concentrations for any given month are subject to considerable uncertainty.

The absence of site-specific meteorological information for earlier years of the facility's operation is a serious problem for dose reconstruction. We have investigated an hypothesis that would relate the FMPC and Cincinnati datasets in another way. By assuming that the relationship of a five-year composite of recent FMPC data to corresponding (but unknown) FMPC frequencies for past years is similar to the relationship of recent Cincinnati data to known Cincinnati data from the past, one may derive factors for adjusting estimates that are based on the recent FMPC data. If the hypothesis can be defended, it might enable us, to some extent, to take into account variations due to climatological trends over time that are recorded in the Cincinnati dataset and that are likely to have affected both sites. In this appendix, we examine this hypothesis with regard to its possible usefulness for adjusting the FMPC five-year composite data.

An alternative approach will be examined, in which uncertainty distributions are derived from ratios of predictions based on recent five-year-composite Cincinnati data to those based on Cincinnati data for earlier years. Tabulations of these distributions have been prepared for each of the twelve months and for an annual average.

We also describe the data sets that we have used to calculate the JFTs. The JFTs of the five-year composite, monthly and annual, are presented in Tables ES–1 through ES–13 ("S" for "Special") at the end of the appendix.

THE METEOROLOGICAL DATASETS

We have examined four meteorological datasets for their relevancy to the dose reconstruction. All of the datasets contain hourly records, and the versions that are in hand span different periods. These datasets are the FMPC tower data (August 1986 through December 1991), the Cincinnati Airport data (January 1948 through December 1991), the Dayton Airport data (January 1987 through December 1990; earlier records are available but have not been acquired), and data recorded at Oxford, Ohio (January 1981 through December 1990).

The FMPC Tower Data

Data transmitted to the *RAC* Team by Westinghouse Materials Company of Ohio (WMCO) for the FMPC site begin with the record of August 6, 1986, at 1200 hours and proceed in hourly intervals. Data through December 31, 1991, are in hand, providing a record that spans approximately five and one-third years. Table E–1 lists the variables that were monitored. Entries in a logbook for the data collection system covering the period May 22, 1987, through January 28, 1991, and the data files themselves indicate numerous interruptions in the record. The longest gap includes the entire month of September 1990. Table E–2 shows the percentage of valid hours for each month of the period January 1, 1987, through December 31, 1991.

> PLEASE NOTE: In their transmittal of data for the year 1991, WMCO indicated that the data had not been verified. Furthermore, there has been no indication that previously-obtained data for earlier periods had been verified by WMCO. Therefore, we caution the reader that the FMPC meteorological tower data that we have used in this study should be regarded as raw readings from the instrumentation, without interpretation or correction by WMCO personnel. We have dropped out those records for which any variable of interest to us was flagged by the computer-controlled monitoring system as invalid (code "I"; see Table E–1, footnote *b*).

Gaps in any continuously-sampled time-series data are a concern, but the primary use of the FMPC tower data in this study is to create JFTs. Accordingly, if the gaps are reasonably uniform in their distribution over time, there is less concern for the accuracy of the estimation of averages. An examination of Table E–2 indicates that aside from a few instances of low sampling efficiency in certain months — of which the worst is obviously September 1990, when no samples were recorded — most months during the period represented by the data had more than 90% of their hours recorded. We judge that the data are adequate for constructing the JFTs that will be used in this study.

We have carried out the analysis of the FMPC hourly tower data with specially-written computer programs that examine each relevant field of each record. Validity codes inserted by the computer-controlled sampling system make it possible to screen out flawed or meaningless records. We discarded those records with code "I" flagging any relevant field. In a few cases, the julian date field could not be interpreted, and such records were also discarded. The field for the stability sometimes contained an asterisk, and this condition also invalidated the record. In general, records with "Q" (Questionable) codes corresponding to one or more of the relevant fields were accepted if they had not been invalidated by one or more of the conditions enumerated above. The "Q" code generally appears in the presence of relatively rapid changes

Table E–1. File Record Format for FMPC Tower Meteorological Data

Column(s)		Field description
1–2		Year
3–5		Julian day
6–7		Hour
8–9		Minute (= 0 on hourly averages)
10–14		Wind direction (at 60 m)[a]
15–19		Wind speed (at 60 m) (miles hour^{-1})[a]
20–24		Sigma theta (at 60 m)[a]
25–29		Wind direction (at 10 m)[a]
30–34		Wind speed (at 10 m) (miles hour^{-1})[a]
35–39		Temperature (at 10 m) (°C)[a]
40–44		Dew point (°C)[a]
45–49		Delta temperature (between 10 and 60 m) (°C)[a]
50–54		Precipitation (inches)[a]
55–59		Pressure (inches of Hg)[a]
60–69		Validity codes[b]
	60	Wind direction (60 m)
	61	Wind speed (60 m)
	62	Sigma theta (60 m)
	63	Wind direction (10 m)
	64	Wind speed (10 m)
	65	Temperature (10 m)
	66	Dew point
	67	Delta temperature (10–60 m)
	68	Precipitation
	69	Pressure
70		Stability class (A–G)[c]

[a] All numerical data are given in hundredths. To get actual values, divide by 100.

[b] Validity codes: Q – Questionable data; I – Invalid data; V – Variable wind direction; C – Calm wind speed.

[c] In calculations for this study, classes F and G were consolidated. The software that prepared the data files computed the stability from the temperature gradient $\Delta T/\Delta z$ according to the following table:

Stability	$\Delta T/\Delta z$ range
A	≤ -1.9
B	-1.9 to -1.7
C	-1.7 to -1.5
D	-1.5 to -0.5
E	-0.5 to $+1.5$
F	$+1.5$ to $+4.0$
G	> 4.0

Table E–2. Percentage of Valid FMPC Tower Observations[a] by Month and Year

Month	1986	1987	1988	1989	1990	1991	1986–91	1987–91
Jan		94.8	100.0	99.3	96.0	67.7	91.6	91.6
Feb		98.5	99.9	100.0	95.7	90.5	96.9	96.9
Mar		99.7	98.5	79.3	93.4	97.0	93.6	93.6
Apr		99.3	40.3	92.5	97.8	96.8	85.3	85.3
May		79.0	97.3	93.4	95.7	83.5	89.8	89.8
Jun		67.5	90.1	99.6	99.4	94.0	90.1	90.1
Jul		38.8	87.0	98.7	94.1	93.1	82.3	82.3
Aug	69.2[b]	31.0	84.1	100.0	30.5	99.2	69.0	69.0
Sep	89.2	93.6	99.3	100.0	0.0	97.5	79.9	78.1
Oct	94.2	96.2	62.8	94.6	44.2	100.0	82.0	79.6
Nov	97.2	97.4	99.2	98.6	74.4	99.2	94.3	93.8
Dec	89.2	100.0	99.7	90.3	94.8	89.5	93.9	94.9

[a] An "observation" represents one hour.

[b] The data record begins August 6, 1986, 1200 hours.

in the variable's magnitude and would attract the attention of an examiner who was verifying the data, but it does not necessarily indicate an equipment malfunction or an invalid reading.

The 12 monthly JFTs (and one annual JFT) derived from the FMPC tower data are based on the composite hourly data for the respective months (and the annual composite) of the five years 1987–1991. These JFTs are presented in Tables ES–1 through ES–13 at the end of this appendix. Each JFT is broken down by six wind speed intervals, 0–2, 2–4, 4–6, 6–8, 8–10, and >10 m s^{-1}; 16 wind sectors; and the six Pasquill-Gifford stability classes A–F. The wind speeds and directions correspond to readings at the 10-m level. The frequencies in Tables ES–1 through ES–13 are normalized by stability, and the total frequency for the stability is given on the line preceding the breakdown by wind speed and direction of the normalized frequencies for that stability. Table E–1, footnote *c*, indicates the vertical temperature gradient scheme used by the processing software for assigning stabilities; in calculations performed for this study, classes F and G were combined. Figure E–1 is a windrose for the annual JFT derived from the FMPC composite tower data for 1987 through 1991.

The Cincinnati Airport Data

The Greater Cincinnati Airport is located near Covington, Kentucky, just south of the Ohio River and approximately 29 km south-southeast of the FMPC site. Because of its relative nearness to Fernald and the long continuous record of meteorological variables, the Cincinnati Airport dataset has been used for estimates of airborne dispersion from the FMPC site in some previous assessments. This meteorological record is available to this study from 1948 through 1991 without interruption.

The hourly data were obtained from the National Climatic Data Center (NCDC), Asheville, North Carolina, and were processed into JFTs of format similar to those for the FMPC

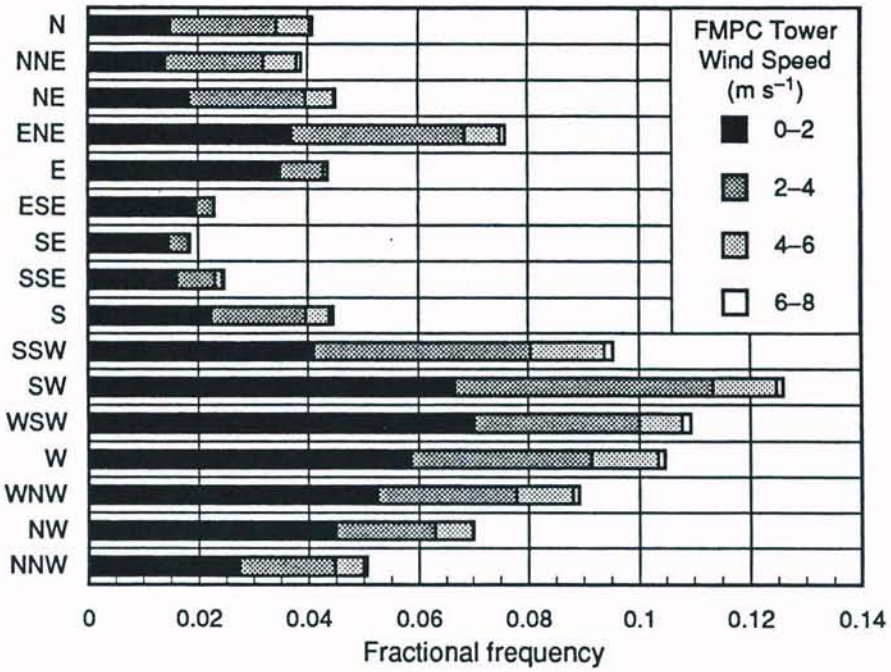

Figure E–1. Windrose diagram for the FMPC composite tower data for 1987 through 1991. Frequencies for higher wind speed classes are zero or negligible. Annual-average stability frequencies are as follows:

A	0.065	D	0.333
B	0.030	E	0.291
C	0.044	F	0.237

with the STAR program, which is available in FORTRAN source from NCDC. It is not possible to process the Cincinnati data with the same computer program that we applied to the FMPC dataset because of the different file formats and the variables that were monitored.

The character of the Cincinnati data set is different from that of the FMPC tower data in several respects. The principal structural difference is in the stability typing schemes that are supported. The airport data were taken at a level of approximately 10 m above ground, and there is no second set of temperatures measured at a higher elevation to permit the use of the vertical temperature gradient in a stability typing scheme. Instead, using a procedure of Turner (1964), the STAR program bases its assignment of stability to classes A through G on observations of wind speed, cloud cover, ceiling, and estimates of insolation computed from solar elevation angle; for nighttime, negative insolation indices are assigned. We should stress that the correspondence between the Turner stabilities and those derived from the vertical temperature gradient method used for the FMPC tower data is at best approximate, and no attempt has been made to adjust the data sets to compensate for the different stability typing methods. We judge that such an exercise would more likely be misleading than helpful.

Figure E–2 shows an annual-average windrose diagram for a 1987–1991 composite of the Cincinnati meteorological data. Note the difference in wind speed class boundaries. The

STAR program assigns frequencies to the classes 0–4, 4–7, 7–11, 11–17, 17–21, and >21 kt (i.e., knots, which are nautical miles per hour; 1 kt = 0.514 m s^{-1}). Comparison of the annual windroses for Cincinnati and the FMPC (Fig. E–1) indicate some potentially important differences in the distribution of wind speeds and stability classes between the two sites. Both figures show the dominant southwesterly wind directions, however.

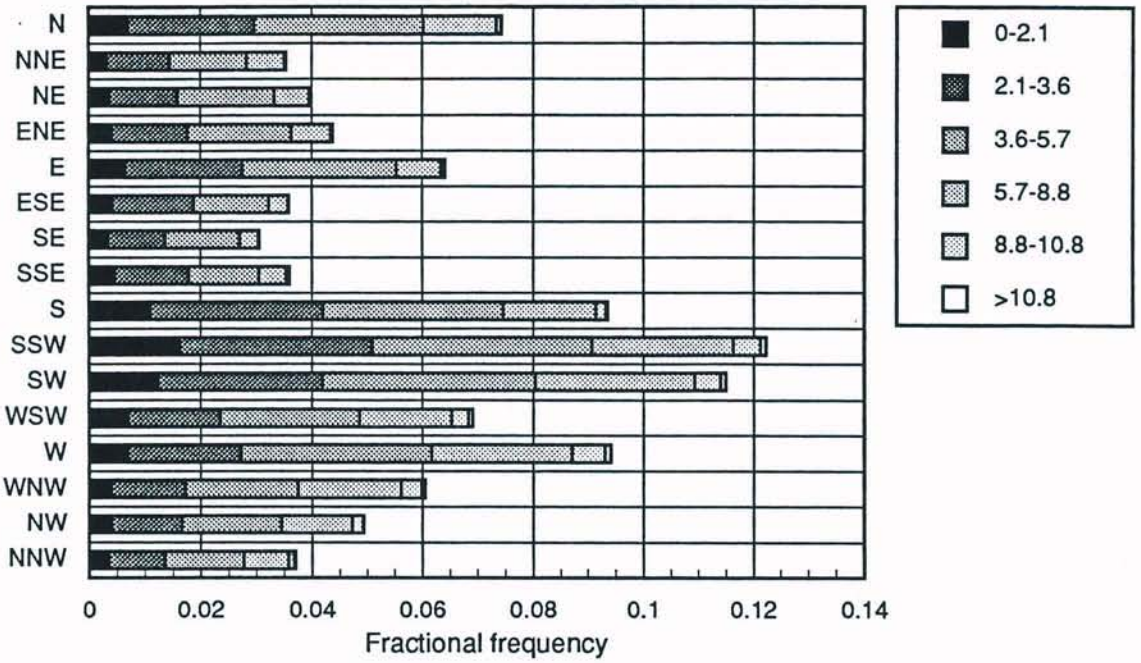

Figure E–2. Annual-average windrose diagram for 1987–1991 composite meteorological data from the Cincinnati Airport, as compiled by the STAR program. The stability frequencies are as follows:

A	0.010	D	0.525
B	0.054	E	0.133
C	0.111	F	0.167

The Dayton Airport Data

The Dayton Municipal Airport is near the city of Dayton, Ohio, about 61 km northeast of the FMPC site. Like Cincinnati, this location has previously been suggested as a meteorological surrogate for the FMPC.

The file formats for the Dayton Airport data are identical to those for Cincinnati. We have obtained Dayton data for the years 1988 through 1990; these data are available from NCDC. We converted the hourly data to JFTs with the STAR program. A composite windrose for these three years is shown in Fig. E–3. The figure shows a wind speed and directional distribution similar to that for Cincinnati (Fig. E–2).

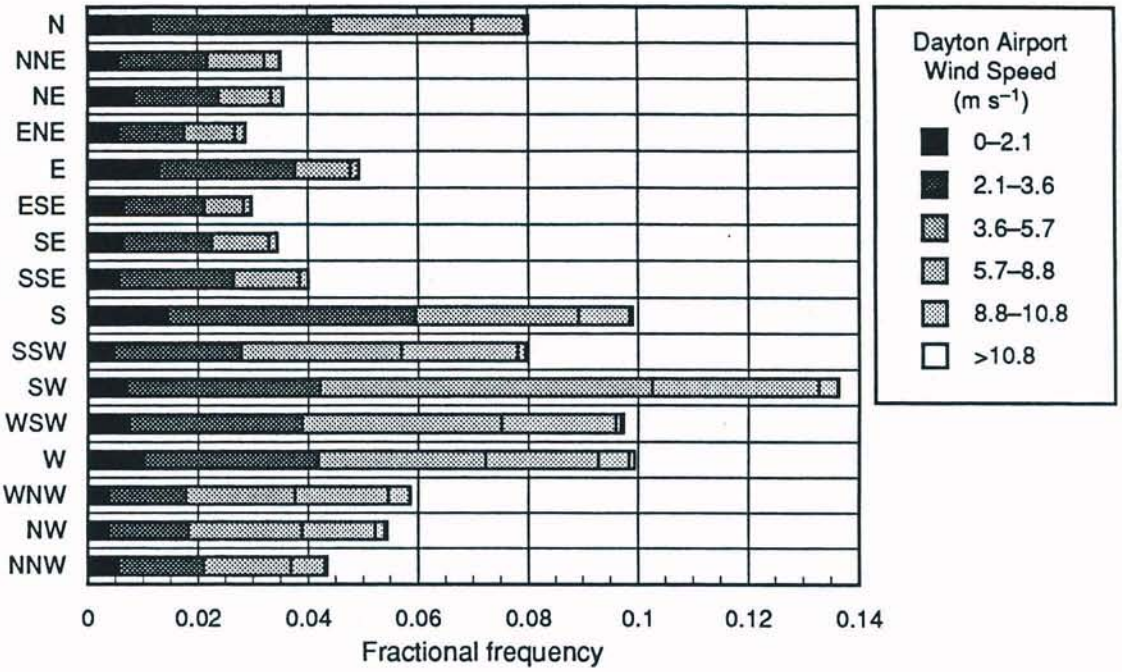

Figure E–3. Annual-average windrose diagram for 1988–1990 composite meteorological data for the Dayton Airport, as compiled by the STAR program. The stability frequencies are as follows:

A	0.011	D	0.510
B	0.055	E	0.128
C	0.114	F	0.183

The Oxford Data

The Geography Department of Miami University, Oxford, Ohio, maintains a network of eight automated weather stations, which were developed during 1980–1981 by the University in collaboration with the Ohio Agricultural Research and Development Center (Klink and Curry 1984, Curry et al. 1988). One of the nodes of the network (i.e., an observation station) is located near the Miami University Ecology Research Center at Oxford, which lies approximately 30 km north of the FMPC site. We refer to this dataset as the Oxford data.

For purposes of comparison, we obtained data from the Oxford observation station for the period from July 1, 1981, through December 31, 1990. The data present a third format, and we developed another computer program to compile windroses based on these files. Because stabilities are not readily computed from the Oxford data for nighttime, we omitted all computations of stabilities for this dataset.

Figure E–4 shows a windrose diagram based on a composite file of the Oxford data for the years 1987–1990. The figure indicates important differences between Oxford and the FMPC site in the distribution of wind speed and wind direction. Local topographies are likely influential in this difference. The Oxford instrumentation is deployed at a height of about 2 m above ground near the top a westward downslope that overlooks a stream-bed valley running

north-south. The valley floor is about 24 m below the level of the station. Channeling of wind in the valley may be responsible for the increased frequencies in the NW, NNW, N, and NE sectors.

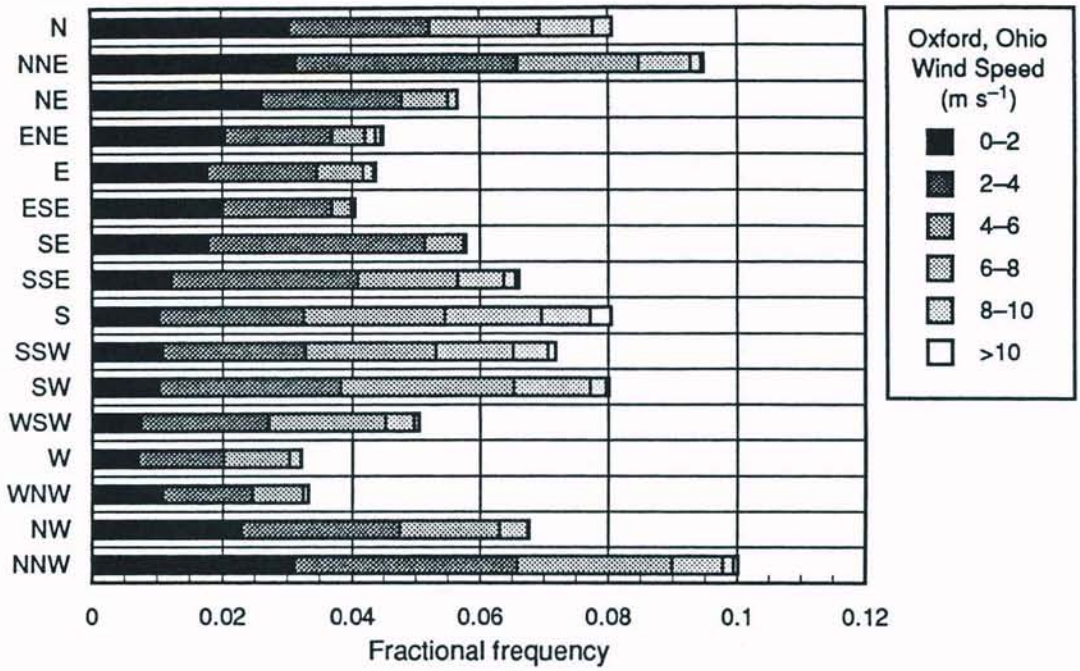

Figure E–4. Annual-average windrose diagram for 1987–1990 composite meteorological data taken at Miami University, Oxford, Ohio. Stabilities are not available.

PLEASE NOTE: The data from the Miami University station at Oxford have not been systematically verified and must be regarded as raw automated readings of the instruments. After some experimentation, we wrote our computer program to recognize clear instances of meaningless records, and such records were dropped. Using these criteria, we accepted data for 34,723 hours out of a possible total of 35,064 hours for the period 1987–1990 (99%).

The ATDD Survey

In November 1987, personnel from the National Oceanic and Atmospheric Administration's Atmospheric Turbulence and Diffusion Division (ATDD) carried out a meteorological survey of the FMPC site. The purpose of the survey was to establish siting criteria for additional meteorological towers at the site that would provide real-time data for emergency response to unplanned events. From November 2 through November 22, 14 portable meteorological towers monitored variables that characterize wind fields and turbulence near the site (Pendergrass 1989). The placement of the facility on standby status ended the survey before building wake effects could be studied and a suite of validation tests could be carried out.

The data recorded in the ATDD survey indicate possibly significant differences between the FMPC site and those of the Greater Cincinnati and Dayton Airports. The FMPC is located

at the intersection of two valley wind flows, one of which generally follows the valley of the Great Miami River northeastward, and the other of which runs south-southeastward along Paddy's Run Creek. This confluence creates wind flows on the valley floor that can differ in direction by as much as 90° from the synoptic-scale flow at the height of nearby ridgetops. Pendergrass (1989) suggests the possibility that the on-site tower may be influenced by the flow along Paddy's Run Creek. The report presents several wind-field maps, one of which (Fig. 23) shows a southward local flow along the western side of the site, whereas releases from the production area would be carried northeastward by the synoptic-scale flow.

We investigated the availability and possible usefulness of the data from the ATDD survey for this study. ATDD personnel indicated that the data could not be delivered promptly because of various difficulties, including the necessity of reformatting and transferring the information to different media. We concluded that the 21-day duration of the sampling severely limited the usefulness of the data for our purposes, and discussions with Dr. Pendergrass failed to quantify the significance of the drainage flows through Paddy's Run Creek. It is our judgment that the data from the ATDD survey are insufficient to serve as a basis for adjusting the FMPC tower data to allow for this anomalous effect, because they provide no indication of its prevalence. Accordingly, we have not made further attempts to acquire this dataset and incorporate it into the study.

DIRECT COMPARISONS OF THE METEOROLOGICAL DATASETS

The restriction of the FMPC meteorological dataset to the period since August 1986 creates a troublesome problem for reconstruction of dose related to releases from this site. The options include using a composite of recent FMPC data for the earlier period, with a large range of uncertainty applied to estimates of air concentration, or substituting a surrogate dataset to use for the calculations.

At least one previous study of the FMPC has made use of the data from the Cincinnati Airport (IT Corporation 1989). An unpublished report from the same project describes a statistical comparison of data from the Cincinnati and Dayton airports with about 11 weeks of hourly wind data recorded by the instrumentation at the 10-m level of the FMPC meteorological tower (Heron and Ubinger 1986). These investigators concluded that "wind speed and direction recorded at both Cincinnati and Dayton were adequate predictors of these parameters at Fernald, but that data recorded at Cincinnati explained a greater percentage of the variability at Fernald than did Dayton." On the basis of this report and other information then available to him, Charles W. Miller of the Oak Ridge National Laboratory (ORNL) recommended to H. Wayne Hibbitts of the DOE Oak Ridge Operations that calculations then being performed by ORNL for the Centers for Disease Control make use of the dataset from Cincinnati rather than that from Dayton, which apparently had been specified in the request to ORNL (Miller 1986). In another instance, the FMPC-2082 report (Boback et al. 1987) referred to values of temperature, humidity, wind speed, and wind direction recorded at the Cincinnati Airport at 7:00 and 10:00 a.m. in discussing a release of uranium hexafluoride (UF_6) from the Pilot Plant on February 14, 1966. For the times at which these decisions were made, they appear to have been entirely appropriate, given the lack of data for the site.

Figures E–1 through E–4 show annual windrose distributions of wind speed and direction for the respective sites, and for each of the first three figures, a table of stability frequencies is

given. This information provides some basis for comparison of the FMPC tower data with the two airport datasets and to a lesser extent with the Oxford data. It is particularly evident that the lowest wind speed class (0–2 m s^{-1}) has a much higher frequency at the FMPC than at any of the other three sites. Figure E–5 is a rough indication of the distribution of wind speed as given by the composites of recent data from the four sites. Mean wind speeds are shown in the figure's legend. The mean wind speed for the FMPC site is about half of that for each of the airports, and the mean wind speed for Oxford is intermediate. Because of the inverse proportionality of predicted concentration to wind speed in the Gaussian plume formula and other dispersion models (Appendix F), the variation of these distributions of wind speed have a direct bearing on predicted concentrations; in particular, other factors being the same, the airport data would estimate annual-average air concentrations to be lower by about a factor of 2, on average, than the corresponding estimates using the FMPC data. Variation in the distributions of wind direction and stability and adjustment of windspeed to release heights different from the measurement height complicate the interpretation. A different comparison is needed.

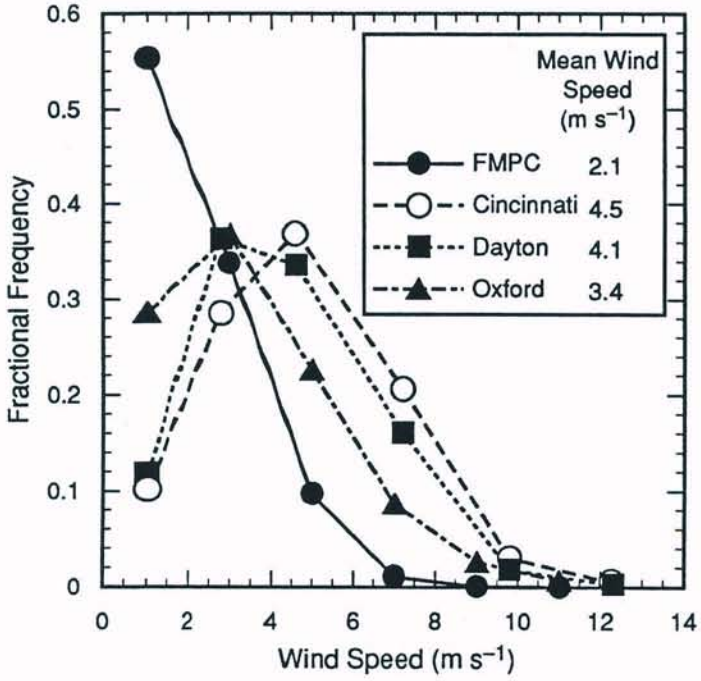

Figure E–5. Approximate distributions of wind speed, based on annual-average windrose data for the FMPC tower (1987–1991), the Cincinnati Airport (1987–1991), the Dayton Airport (1988–1990), and Miami University at Oxford, Ohio (1987–1990). Mean wind speeds are indicated in the legend.

ALTERNATIVE COMPARISON OF FMPC METEOROLOGICAL DATA WITH DATA FROM OTHER SITES

We alluded previously to unpublished statistical comparisons of the FMPC hourly wind data with the Cincinnati and Dayton datasets of Heron and Ubinger (1986). Comparisons based on regression techniques (i.e., regression of each variable of interest for one site on the corresponding variable for the other site) encounter difficulty for complex datasets such as we are considering. Successive hourly readings at the same site are not independent (autocorrelation), whereas the regression model is based on the assumption of independence. Even if adjustments for the autocorrelation were made, the interpretation of correlation coefficients and regression-line predictions for two meteorological variables (wind speed and direction) is doubtful at best and difficult to translate to the practical terms of differences in air concentrations that a dispersion model would predict on the basis of the data.

We have substituted a comparison that is more direct and more easily interpreted by nonspecialists. It is based on the quantity χ/Q (ground-level concentration per unit release rate) as predicted for a nondecaying and nondepositing tracer by the Gaussian plume model, in the form

$$\frac{\chi}{Q} = \frac{1}{\pi\sigma_y\sigma_z u}\exp\left(-\frac{h^2}{2\sigma_z^2}\right), \qquad \text{(E–1)}$$

(Hanna et al. 1982; this report, Appendix F) where u is the wind speed, adjusted from the height at which it was recorded to the release height h (for which we used 25 m in this comparison), and the dispersion coefficients σ_y and σ_z are functions of the horizontal distance from the source to the receptor point, and of the stability class (A–F). Our particular representation of the dispersion coefficients is based on Briggs' formulas (Hanna et al. 1982, p. 30, Table 4.5).

In order to connect Eq. E–1 with the meteorological datasets, we introduce the frequency f_{ijk}, where the subscripts i and j correspond to wind speed and wind direction intervals and k = A, ..., F, according to the stability class. Normalization requires that the frequencies add to unity: $\sum_{i,j,k} f_{i,j,k} = 1$. Our wind direction intervals are the conventional 22.5° sectors, and the χ/Q are evaluated at the centerlines of the sectors. The expression for the mean value of χ/Q at a receptor point (x, y) is

$$[\chi/Q](x,y) = \sum_{i,k}\frac{f_{i,j,k}}{\pi\sigma_{k,y}(r)\sigma_{k,z}(r)u_i}\exp\left(-\frac{h^2}{2\sigma_{k,z}^2(r)}\right), \qquad \text{(E–2)}$$

where (x, y) lies at a distance $r = (x^2 + y^2)^{1/2}$ from the release point and at the centerline of the sector downwind of sector j from which the wind blows (note that the direction index j in Eq. E–2 is fixed by (x, y)).

Equation E–2 is a simplified version of one of the models that we apply to estimate ground-level air concentration resulting from an elevated release. We have omitted radioactive decay and plume depletion resulting from deposition in order to confine the model to the effects of wind data on atmospheric dispersion. The procedure is to establish a polar grid of receptor points over the circular assessment domain, and for each receptor point, to evaluate Eq. E–2 twice, once for each wind dataset. One obtains two normalized concentrations, C_{FMPC} and C_{other}. The point $(C_{\text{FMPC}}, C_{\text{other}})$ is plotted relative to logarithmic axes, and the configuration of

the aggregate of such points on the plot indicates the general trend of the "other" dataset as a predictor for the FMPC dataset for use with the Gaussian plume model. In our comparisons, the grid consists of 128 points: 16 directions, with 8 points on each sector centerline at distances 1,000, 2,000, ..., 8,000 m from the source. Figure E–6 shows the results of such a comparison of annual-average wind data, where "other" is the composite Cincinnati data for 1987–1991, compared with FMPC data for the same period. Several regions have been marked off by diagonal lines to indicate the extent of over- or underprediction represented by points in the respective regions. A perfect match would occur if all points lay on the central diagonal line. In Fig. E–6, most of the points correspond to underprediction of FMPC by Cincinnati data, and for more than half of the points the underprediction is by a factor of more than 2; in a few cases, the underprediction is by a factor of more than 5.

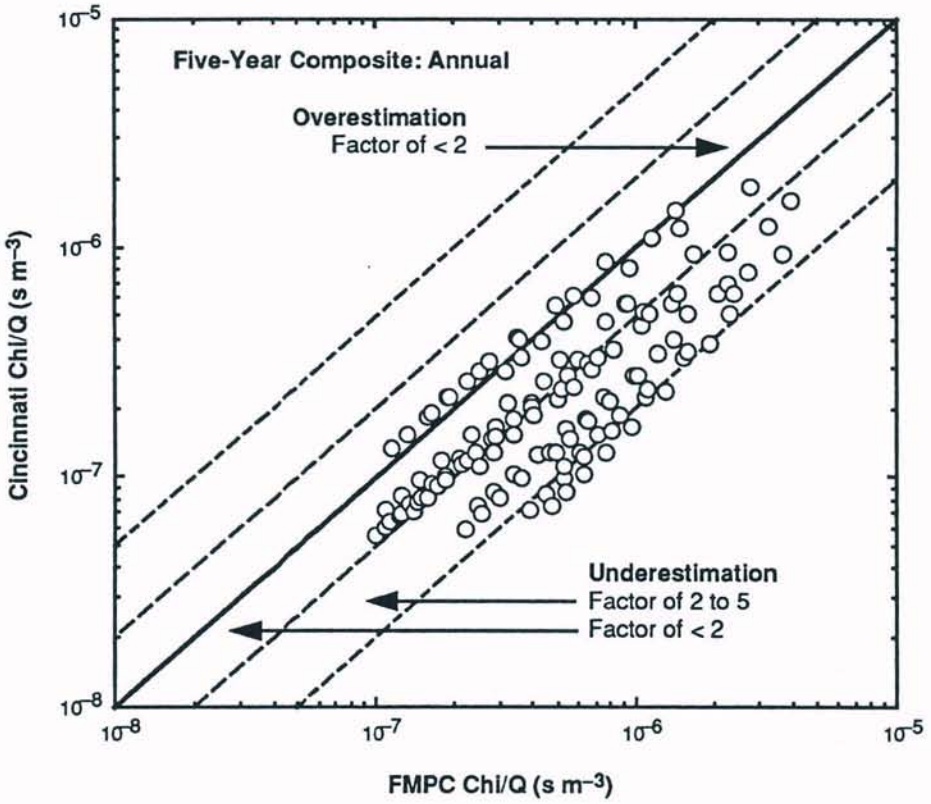

Figure E–6. A comparison of 1987–1991 composite annual-average datasets for the Cincinnati Airport and the FMPC site. Estimates of χ/Q for each dataset are plotted against each other at each of 128 points of a grid that covers the assessment domain. The regions between the lines indicate the extent of over- or underestimation of FMPC air concentrations by the Gaussian plume model using the Cincinnati data. In this comparison, most points correspond to underestimation by factors of 2 to 5.

An alternative is to work with predicted-to-observed (P/O) ratios. In our context, "predicted" corresponds to the "other" or proposed surrogate dataset; "observed" is the concentra-

tion obtained from the FMPC dataset. The ratio that we work with is

$$P/O = \frac{C_{\text{other}}}{C_{\text{FMPC}}}, \qquad \text{(E–3)}$$

where the two concentrations are calculated from Eq. E–2 at the same grid point. The array of 128 P/O ratios can then be displayed as a histogram or in tabular form. Clearly, the desired situation is to have the ratios cluster closely about $P/O = 1$.

It is of interest to extend the comparison of FMPC and Cincinnati meteorological data to the 12 monthly JFTs of the five-year composite datasets. It is not practical to present plots corresponding to Fig. E–6 for every month, but we have condensed and extended the information and put it into Table E–3. For each month, the table shows the minimum, median, and maximum of the 128 P/O ratios; then the mean and standard deviation of the log-transformed ratios are used to compute a geometric mean (GM) and geometric standard deviation (GSD); and finally, the frequency counts for several intervals are presented in order to give a more tangible sense of the distribution of the ratios.

From Table E–3, we note that the medians for all months but one (August) correspond to underprediction of the FMPC by more than a factor of 2, and for most months, 10% or more of the 128 P/O ratios correspond to underprediction by a factor of more than five. The percentage entries in the table clearly indicate substantial bias below $P/O = 1$. Overprediction is confined to factors of less than 2, except for the month of August.

Table E–3. P/O Ratios for Cincinnati as a Surrogate for FMPC Meteorological Data[a]

							Percent of ratios in interval							
Date	N	Min.	Median	Max.	GM	GSD	<.1	.1–.2	.2–.5	.5–1	1–2	2–5	5–10	>10
Ann	128	0.149	0.494	1.197	0.445	1.784	0.0	10.2	40.6	37.5	11.7	0.0	0.0	0.0
Jan	128	0.215	0.370	1.641	0.419	1.809	0.0	0.0	75.8	11.7	12.5	0.0	0.0	0.0
Feb	128	0.149	0.404	1.055	0.400	1.666	0.0	12.5	53.9	27.3	6.2	0.0	0.0	0.0
Mar	128	0.141	0.425	1.175	0.390	1.739	0.0	10.9	55.5	27.3	6.2	0.0	0.0	0.0
Apr	128	0.163	0.353	1.332	0.386	1.632	0.0	6.2	63.3	25.0	5.5	0.0	0.0	0.0
May	128	0.124	0.451	1.234	0.436	1.836	0.0	10.2	51.6	24.2	14.1	0.0	0.0	0.0
Jun	128	0.148	0.441	1.255	0.420	1.756	0.0	10.9	58.6	21.1	9.4	0.0	0.0	0.0
Jul	128	0.148	0.448	1.339	0.465	1.815	0.0	5.5	46.9	36.7	10.9	0.0	0.0	0.0
Aug	128	0.119	0.686	2.506	0.550	2.346	0.0	23.4	12.5	36.7	21.9	5.5	0.0	0.0
Sep	128	0.068	0.608	1.607	0.487	2.304	5.5	11.7	18.8	42.2	21.9	0.0	0.0	0.0
Oct	128	0.114	0.577	1.309	0.494	2.279	0.0	16.4	28.1	26.6	28.9	0.0	0.0	0.0
Nov	128	0.124	0.354	1.386	0.382	2.002	0.0	19.5	47.7	21.1	11.7	0.0	0.0	0.0
Dec	128	0.142	0.349	1.219	0.394	1.737	0.0	6.2	58.6	22.7	12.5	0.0	0.0	0.0

[a] Five-year composite.

LONG-TERM VARIATIONS IN AIR-DISPERSION PREDICTIONS

Many prospective assessments have based air-dispersion calculations on a composite of data for five years (or fewer). For a dose reconstruction (retrospective), it is preferable to apply meteorological data that are specific to the times that make up the temporal domain of the study. Though the Cincinnati dataset may be disappointing as a surrogate for the FMPC because of bias and scatter, it is worthwhile to examine the dataset for internal relationships between recent and past years. In particular, we are interested in comparing the monthly tabulations in the 5-year composite Cincinnati dataset with the corresponding tabulations for all individual years of the Cincinnati dataset during the FMPC's operation. The hypothesis that we examine is that the correspondence between the five-year composite FMPC dataset and the unknown FMPC meteorology for specific years in the past will resemble the same correspondence for Cincinnati, for which the meteorology for the same year in the past is given by data that we have in hand. Such a relationship could be exploited to introduce cycles or secular trends from the longer record into the limited FMPC dataset. The disadvantage is that the opportunity for validating such a procedure is extremely limited.

This method is based on P/O ratios between datasets, but in this case the numerator is a concentration C_0 based on the five-year composite Cincinnati dataset, and the denomiator is a concentration C_t for the same receptor point computed from the Cincinnati data for the year (or month and year) t. One can imagine a corresponding fraction for the FMPC, for which C_t exists but is unknown. We formulate our hypothesis as

$$\left[\frac{C_0}{C_t}\right]_{\text{Cinc}} \approx \left[\frac{C_0}{C_t}\right]_{\text{FMPC}} \qquad \text{(E–4)}$$

where each P/O ratio represents a central value for the 128 points of the domain. We use the geometric mean (GM). Our estimate of C_t for the FMPC is

$$\widetilde{C_t} = \frac{[C_0]_{\text{FMPC}}}{[C_0/C_t]_{\text{Cinc}}}, \qquad \text{(E–5)}$$

i.e., the desired past FMPC concentration is computed from its counterpart from the five-year composite dataset divided by the corresponding GM P/O ratio (present/past) from the Cincinnati dataset. The concentration $[C_0]_{\text{FMPC}}$ is specific to the receptor point at which the estimate is calculated. The effect, for a particular month and year, is to adjust predictions of concentrations at all receptor points in the domain up or down by the same factor.

Data for testing this procedure are scant, but there are FMPC data for five months of 1986 (August through December), and these months were not included in the five-year composite. For these five months, we analyzed both P/O ratios of Eq. E–4, and the comparison is set forth in Table E–4. We would hope for generally good agreement of the GMs for each month, although an objective criterion for the desired agreement is not obvious. The geometric means for September, November and December agree to within 15% of the smaller value. In all cases, the corresponding GMs are within a factor of two.

As a further indication of the degree of correspondence, we formed 4-year composite datasets for 1988–1991 for the FMPC site and Cincinnati, leaving the data for the year 1987 available for estimation on the basis of the reduced composite datasets. Table E–5 shows

Table E–4. Comparison of P/O Ratios[a] for Cincinnati and FMPC Aug.–Dec. 1986[a]

								Percent of ratios in interval						
	Date	N	Min.	Median	Max.	GM	GSD	<.1	.1–.2	.2–.5	.5–1	1–2	2–5	5–10	>10
FMPC	Aug-86	128	0.338	0.925	5.049	0.900	1.953	0.0	0.0	17.2	38.3	38.3	5.5	0.8	0.0
CINC	Aug-86	128	0.465	1.082	4.704	1.148	1.789	0.0	0.0	7.0	31.2	48.4	13.3	0.0	0.0
FMPC	Sep-86	128	0.561	0.939	4.345	1.029	1.587	0.0	0.0	0.0	63.3	28.9	7.8	0.0	0.0
CINC	Sep-86	128	0.494	1.069	4.644	1.144	1.668	0.0	0.0	4.7	35.9	48.4	10.9	0.0	0.0
FMPC	Oct-86	128	0.292	0.884	2.786	0.860	1.766	0.0	0.0	19.5	38.3	31.2	10.9	0.0	0.0
CINC	Oct-86	128	0.340	1.454	5.743	1.234	2.037	0.0	0.0	12.5	27.3	35.2	21.9	3.1	0.0
FMPC	Nov-86	128	0.420	0.909	2.254	0.910	1.595	0.0	0.0	13.3	49.2	32.0	5.5	0.0	0.0
CINC	Nov-86	128	0.169	0.756	2.217	0.783	2.020	0.0	6.2	25.8	21.1	43.8	3.1	0.0	0.0
FMPC	Dec-86	128	0.261	0.920	3.826	0.935	1.792	0.0	0.0	14.8	35.9	43.0	6.2	0.0	0.0
CINC	Dec-86	128	0.313	0.747	2.708	0.796	1.889	0.0	0.0	28.9	37.5	21.1	12.5	0.0	0.0

[a] P = Aug.–Dec. 1986; O = 1987–1991 composite.

the comparison; we have confined the table to the geometric means and geometric standard deviations of the P/O ratios for each month of 1987, and the ratios of the geometric means are tabulated for ease of comparison. The table indicates that the recent composite data for the two sites are comparable predictors of their respective past concentrations. The signed-rank test of Wilcoxon (Snedecor and Cochran 1967) cannot reject, at the 5% level, the null hypothesis that the two paired sets of 17 geometric means are from the same distribution. Thus the method has some promise as a means of adjusting the five-year composite FMPC data, but the appearance in Table E–5 of such divergences as the entries for October of 1986 and August and September of 1987 is worrying. Our decision is to give further consideration to this method as preparations are made for the final calculations, but at this time we are not prepared to make a commitment to its implementation.

ESTIMATION OF UNCERTAINTY WITH FMPC AND CINCINNATI DATA

The method described in the previous section aims to reduce the bias (on average) that would result from using the recent five-year composite FMPC meteorological data in estimating air concentrations during past periods to which this dataset is not strictly applicable. A more conservative approach to error management is to represent year-to-year variations in meteorological variables by uncertainty distributions applied to the estimated air concentrations at receptor points throughout the region. There are various rational approaches to constructing such uncertainty distributions. We consider two.

The first approach would utilize normalized predictions of air concentrations (χ/Q) at a particular points (say 1000 m NE) for a particular month (e.g., January) of all years of the Fernald record to obtain an estimate of variation of the January average concentration from year to year at the specified location. For January, there would be $N = 5$ estimates at location m, which we denote by X_{mi}, $i = 1, \ldots, N$. If we assume that the estimates of concentration are from a lognormal distribution, the quantities $Y_{mi} = \ln X_{mi}$ are normally distributed. The

Table E–5. Geometric Means and Standard Deviations of P/O Ratios for FMPC and Cincinnati: Prediction of 1986–1987 Concentrations by 4-Year Composite Meteorology

Date	FMPC		Cincinnati		GM ratio (Cinc./FMPC)
	GM	GSD	GM	GSD	
Aug-86	0.900	1.953	1.148	1.789	1.28
Sep-86	1.029	1.587	1.144	1.668	1.11
Oct-86	0.860	1.766	1.234	2.037	1.43
Nov-86	0.910	1.595	0.783	2.020	0.86
Dec-86	0.935	1.792	0.796	1.889	0.85
Jan-87	0.968	1.712	0.922	1.596	0.95
Feb-87	0.868	1.607	0.799	1.877	0.92
Mar-87	1.014	1.729	0.911	1.918	0.90
Apr-87	0.959	1.726	0.799	2.277	0.83
May-87	0.871	1.498	0.994	2.252	1.14
Jun-87	1.039	1.830	0.868	2.155	0.84
Jul-87	1.243	1.982	1.550	4.837	1.25
Aug-87	1.635	2.001	0.904	1.652	0.55
Sep-87	1.341	2.281	0.885	2.005	0.66
Oct-87	0.934	1.624	0.806	1.728	0.86
Nov-87	1.108	1.780	0.960	1.561	0.87
Dec-87	1.109	1.745	1.308	1.999	1.18

unbiased sample variance

$$s_m^2 = \frac{1}{N-1}\sum_{i=1}^{N}(Y_{mi} - \overline{Y})^2 \qquad \text{(E–6)}$$

can be used to estimate an upper 95% confidence limit for the true (but unknown) variance σ^2. This confidence limit is

$$\sigma^2 \leq \frac{(N-1)s_m^2}{\chi^2_{0.05}} \qquad \text{(E–7)}$$

where $\chi^2_{0.05}$ is the 5th percentile of the chi-square distribution with $N-1$ degrees of freedom (Snedecor and Cochran 1967). For $N = 5$ and $N = 6$ (d.f. 4 and 5), the chi-square 95th percentiles are 0.71 and 1.15, respectively. The limit is a random variable that will exceed the true variance 95% of the time (if one assumes that the statistic is based on a random sample of JFTs from the period of interest, which it is not). As a measure of conservatism in deriving an uncertainty distribution, one might use the upper 95% confidence limit obtained from Eq. E–7 as the basis for the variance of the normal distribution that underlies the log-normal distributions of the predicted normalized concentrations, but prudence would dictate increasing the estimate because of the limited period from which the "sample" was drawn. It is important to remind oneself that this procedure would provide only one component of uncertainty for estimates of air concentrations, namely the component that is associated with meteorological variations from year to year. Other components will be developed and applied independently.

Extended to all months and to a small set of receptor locations, the method provides distributions that would need to be generalized to all receptor locations. Such an approach has several limitations. First, it fails to consider information about secular trends contained in the Cincinnati data, which in some degree belong to wider-scale phenomena that have affected the FMPC site. Second, applied independently to successive years, it cannot take into account possible correlations between meteorology and other time series, such as the source term; for a purely hypothetical example, what if wind conditions especially favored higher-than-normal ground-level concentrations of FMPC airborne effluents during a cycle that included 1955, when the release rates are believed to have been at their highest? And finally, we have already mentioned the need for arbitrarily increasing the variance to compensate for possible sampling bias.

The second approach is similar to the one just outlined but uses the more extensive Cincinnati data set in an effort to incorporate longer-term cycles and secular trends that may have affected air concentrations. To construct the uncertainty distribution, we proceed as follows. First, we fix a receptor point and define the ratio

$$R_t = \frac{[\chi/Q]_0}{[\chi/Q]_t},$$

where the subscript 0 refers to the five-year composite dataset for Cincinnati and t denotes a year (or possibly a month and year, depending on the time resolution of the intended calculation) during the period of past plant operation. The notation χ/Q denotes the model-predicted air concentration, normalized to the release rate, at the specified receptor point, where the concentration is based on the meteorology indicated by the subscript 0 or t. We compute the ratio R_t for each period t during the history of the plant (for example, for each January, in the case of monthly resolution, or for each year in the case of annual resolution), and we form the empirical distribution of these ratios. This distribution characterizes the use of the five-year composite dataset to predict past air concentrations for Cincinnati. For the present purpose, it is reasonable to assume that the theoretical distributions is lognormal, and we have estimated the geometric means and geometric standard deviations for monthly and annual resolutions for a single receptor point 1,000 m NE of the source. Figure E–7 shows plots of the empirical distributions for the months of December, March, June, and September, and for periods of one year. Table E–6 lists the geometric means and geometric standard deviations.

To arrive at an appropriate distribution for multiplicative uncertainty factors, we normalize the empirical distributions to have geometric mean 1 and to retain the geometric standard deviations shown in Table E–6. Thus, for a random factor η drawn from the normalized distribution, the Monte Carlo estimate of χ/Q would be

$$\chi/Q = [\chi/Q]'\eta,$$

where $[\chi/Q]'$ is the deterministic predicted value (this is, of course, a simplification; other factors would be applied to account for other uncertainties). Similar tabulations to Table E–6 will be prepared for other receptor points in the region, and some consolidation will be done if appropriate (it could be, for example, that a single generic distribution would be satisfactory for the month of January for all receptor points of the region). The question of independence vs. intercorrelation of receptor points is discussed in Appendix K.

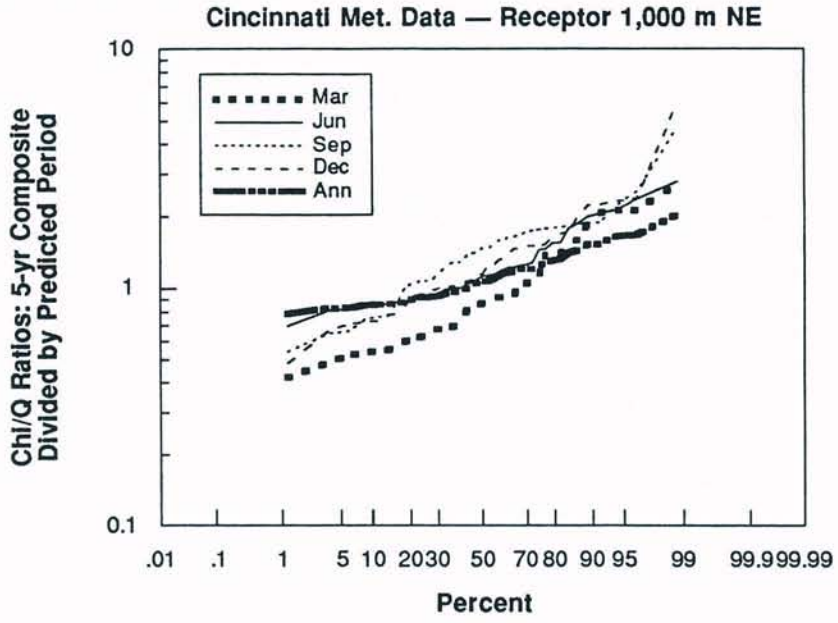

Figure E–7. Empirical distributions of χ/Q ratios computed from Cincinnati meteorological data. The ratios are $R_t = [\chi/Q]_0/[\chi/Q]_t$, where 0 refers to the five-year composite dataset and t ranges over all specified periods (e.g., all Decembers during plant operation, or all years). The plotted curves represent the distributions for all months of December, March, June, and September, and for all years (labeled "Ann"). Note that the slope of the annual curve is shallower than those of the monthly curves, indicating less variability.

METEOROLOGY AND EPISODIC EVENTS

Throughout the previous discussion, the tacit orientation has been toward estimating monthly-average air concentrations, based on the monthly resolution of the source term for routine releases. For unusual releases of high magnitude and short duration, one needs to know the local wind speed, wind direction, and stability and the variation of these quantities for the duration of the release, with at least the temporal resolution with which the episodic release is known. Lacking this specific local knowledge (which is likely to be unavailable for most if not all such incidents), it is necessary to try to limit the range of possibilities for the progression of conditions and to assign probabilities to those that remain. The procedure will depend upon the incident, its duration, and apparent uniformity of conditions in the area.

Hourly data from the Cincinnati Airport for the time of the release will be examined, with the caution implied by comparisons of the two datasets for 1986–1991 that have been discussed in this appendix. Supplementary data, such as regional weather maps for the specific times, will be employed to the extent possible. Also, efforts will be made to locate sequences of FMPC hourly data in the 1986–1991 period that occurred at nearly the same time of year and during general weather conditions (i.e., temperature, precipitation, degree of overcast) that correspond closely with those that prevailed during the event of interest. Thus, for a mid-November incident, one might select sequences from each of the Novembers from 1986 through 1991. Using each set of sequences to predict resulting air concentrations

Table E–6. Parameters of the Distributions of the Ratios R_t for Monthly and Annual Periods

Period	Geometric mean	Geometric standard deviation
Jan	1.24	1.58
Feb	1.26	1.56
Mar	0.91	1.58
Apr	0.95	1.48
May	1.10	1.53
Jun	1.19	1.39
Jul	1.12	1.50
Aug	1.11	1.58
Sep	1.37	1.50
Oct	1.39	1.65
Nov	1.20	1.55
Dec	1.24	1.56
Annual	1.10	1.25

at locations of interest, one would obtain, at each point, a "sample" of results (N = 5 or 6) that is formally similar to those discussed above in connection with deriving uncertainty distributions for monthly releases (Eqs. E–6 and E–7). But because of the shorter period spanned by the duration of the episode (hours to days, at most), additional conservatism will need to be introduced into estimating the variance of the distribution.

A variation of the foregoing approach that utilizes the Cincinnati data would require associating distributions of meteorological data points (i.e., wind speed, wind direction, and stability) for the FMPC that correspond to specific data points for Cincinnati. This would be accomplished by tabulating data points for Cincinnati (using, say, six or fewer ranges of wind speeds) for suitable periods during 1986–1991 and recording frequencies of the corresponding FMPC data points. For example, we might consider each November during 1986–1991, and corresponding to the Cincinnati data point of wind speed 0–2 m s^{-1}, wind direction from SW, and class D stability, we would have a distribution of data points for the FMPC, which occurred concurrently with each occurrence of the Cincinnati data point for those periods. The correspondence would then be applied to Cincinnati data points that occurred at the time of the event in question, and the distributions obtained for the FMPC would indicate a range of possibilities for the atmospheric transport of the release with the frequencies being interpreted as probabilities.

Although these approaches may seem crude and will necessarily involve subjective choices and decisions by the investigators, they have the virtue of focusing attention on a ranges of meteorological consequences that likely contain conditions close to those that prevailed at the FMPC at the time in question; and they emphasize the sense of uncertainty in the event, rather than leaving the impression, as point estimates inevitably do, that the resulting concentrations are better known than they can be.

Appendix V discusses a specific event and discusses these approaches in the context of

that event.

SUMMARY AND CONCLUSIONS

This appendix has described the meteorological data recorded on site at the FMPC from August 1986 through December 1991 and compared this dataset with longer records from regional airports, Cincinnati in particular, and with data from Miami University at Oxford, Ohio. Comparisons of dispersion predictions made with the FMPC dataset with predictions made with those of Cincinnati (Fig. E–6) and Dayton for the same years indicate a strong trend toward underprediction by the airport data, due in part to higher wind speeds at the airports. When annual JFTs from the five-year composite datasets are compared, the extent of the underprediction of FMPC by Cincinnati exceeds a factor of 2, and for nearly half of the test points the factor is between 2 and 5. The Oxford data show characteristics that suggest less bias overall (Figs. E–4 and E–5), but this dataset only goes back to 1981, and difficulties in stability typing it made the direct comparison impractical.

We consider the FMPC on-site data the fundamental key to meteorology at and about the site for the period of interest, despite the brevity of the record and numerous random gaps resulting from problems with the instrumentation. The direct use of the Cincinnati meteorological record as a surrogate for the FMPC, although it was considered satisfactory before sufficient FMPC tower data were available to indicate the extent of the bias, now seems quite unacceptable. For long-term estimation ("routine" releases), we have demonstrated some promise for a method of superimposing on the FMPC predictions some characteristics of the long-term secular trend that were derived from the behavior of the Cincinnati record, but a final decision on the usefulness of this adjustment technique will require further consideration. But we draw the conclusion that any method should begin by treating the five-year FMPC composite as a generic meteorology for all years, to be supplemented by adjustment factors and uncertainty distributions that may depend in part on other datasets.

Accordingly, the air dispersion predictions for the dose reconstruction study will be based on composite joint frequency tables derived from hourly wind and stability data from the FMPC meteorological tower during the years 1987 through 1991, with possible modifications as indicated above. For a specific month, the predicted ground-level concentrations are to be subjected to a stochastic uncertainty factor that is based on conservatively interpreted variability of test predictions with the meteorology for that month for each year in the composite period (Eqs. E–6 and E–7), or alternatively, the stochastic uncertainty factor based on the Cincinnati data as discussed earlier (see Table E–6 and Fig. E–7). This component of uncertainty will be combined with others associated with the source term (Voillequé et al. 1990), the dispersion model (Appendix K), and dose conversion factors (Appendix T) in arriving at predictions of dose.

REFERENCES

Boback M.W., T.A. Dugan, D.A. Fleming, R.B. Grant, and R.W. Keys. 1987. *History of FMPC Radionuclide Discharges.* Rep. FMPC-2082, Westinghouse Materials Company of Ohio, Cincinnati, Ohio.

Curry R.B., J.C. Klink, J.R. Holman, D.L. Elwell, and M.J. Sciarini. 1988. "Current Ohio Experience with an Automated Weather Station Network." *Appl. Eng. in Agriculture* 4(2):150–155.

Hanna S.R., G.A. Briggs, and R.P. Hosker, Jr. 1982. *Handbook on Atmospheric Diffusion.* Rep. DOE/TIC-11223 (DE82002045) Technical Information Center, U.S. Department of Energy.

Heron T.M. and E. Ubinger. 1986. *Comparison of Wind Speed and Direction at the Fernald Site.* Memorandum (with attached report) to J.L. Hosler, dated June 24, 1986. IT Corporation, Knoxville, Tennessee.

IT Corporation. 1989. *Assessment of Radiation Dose and Cancer Risk for Emissions for 1951 through 1984.* IT Corporation rep., Project No. 303063, Knoxville, Tennessee.

Klink J.C. and R.B. Curry. 1984. "Development of an Automated Global Solar Radiation Network in Ohio." *Solar Energy* 2:189–194.

Miller C.W. 1986. *Meteorological Data for the FMPC Historical Dose Estimates.* Letter to H. Wayne Hibbitts, dated July 18, 1986. Oak Ridge National Laboratory.

Pendergrass W.R. 1987. *Meteorological Site Survey — Feed Materials Production Center, Fernald, Ohio.* Unpublished Report, Atmospheric Turbulence and Diffusion Division, Air Resources Laboratory, National Oceanic and Atmospheric Administration, Oak Ridge, Tennessee.

Snedecor G.W. and W.G. Cochran. 1967. *Statistical Methods,* Sixth Edition. Iowa State University Press, Ames, Iowa.

Turner D.B. 1964. "A Diffusion Model for an Urban Area." *J. Appl. Meteorol.* 3:83–91.

Voillequé P.G., K.R. Meyer, D.W. Schmidt, G.G. Killough, R.E. Moore, V.I. Ichimura, S.K. Rope, B. Shleien, and J.E. Till. 1991. *The Fernald Dosimetry Reconstruction Project, Tasks 2 and 3: Radionuclide Source Terms and Uncertainties — 1960–1962.* Rep. CDC-2. Radiological Assessments Corporation, Neeses, South Carolina 29107.

Table ES–1. Composite Meteorological Frequencies for FMPC, January 1987–1991

	Wind speed range ($m\ s^{-1}$)								Wind speed range ($m\ s^{-1}$)						
	0–2	2–4	4–6	6–8	8–10	>10	Total		0–2	2–4	4–6	6–8	8–10	>10	Total
Class A frequency 0.02238								**Class B** frequency 0.01789							
N	.00000	.00000	.00000	.00000	.00000	.00000	.00000	N	.00000	.00000	.00000	.00000	.00000	.00000	.00000
NNE	.00000	.00000	.00000	.00000	.00000	.00000	.00000	NNE	.00000	.00000	.01609	.00000	.00000	.00000	.01609
NE	.00000	.00000	.00000	.00000	.00000	.00000	.00000	NE	.00000	.00000	.02156	.00000	.00000	.00000	.02156
ENE	.00000	.00000	.01723	.00000	.00000	.00000	.01723	ENE	.00000	.00000	.04492	.00000	.00000	.00000	.04492
E	.01723	.00000	.00000	.00000	.00000	.00000	.01723	E	.00000	.00000	.00000	.00000	.00000	.00000	.00000
ESE	.00000	.00000	.00000	.00000	.00000	.00000	.00000	ESE	.00000	.00000	.00000	.00000	.00000	.00000	.00000
SE	.00000	.00000	.00000	.00000	.00000	.00000	.00000	SE	.00000	.00000	.00000	.00000	.00000	.00000	.00000
SSE	.00000	.00000	.00000	.00000	.00000	.00000	.00000	SSE	.01515	.00000	.00000	.00000	.00000	.00000	.01515
S	.00000	.01723	.00000	.00000	.00000	.00000	.01723	S	.00000	.02156	.00000	.00000	.00000	.00000	.02156
SSW	.00000	.09716	.04141	.00000	.00000	.00000	.13857	SSW	.00000	.09132	.04537	.00000	.00000	.00000	.13669
SW	.00000	.12535	.12613	.02420	.00000	.00000	.27568	SW	.02156	.08319	.13577	.01512	.00000	.00000	.25564
WSW	.01723	.19276	.00000	.00000	.00000	.00000	.20999	WSW	.02156	.17499	.01566	.00000	.00000	.00000	.21221
W	.01723	.13165	.10291	.00000	.00000	.00000	.25179	W	.00000	.12151	.01609	.00000	.00000	.00000	.13760
WNW	.00000	.02932	.01286	.00000	.00000	.00000	.04218	WNW	.00000	.06243	.01609	.01512	.00000	.00000	.09364
NW	.00000	.03009	.00000	.00000	.00000	.00000	.03009	NW	.00000	.00000	.04492	.00000	.00000	.00000	.04492
NNW	.00000	.00000	.00000	.00000	.00000	.00000	.00000	NNW	.00000	.00000	.00000	.00000	.00000	.00000	.00000
Total	.05169	.62356	.30055	.02420	.00000	.00000	1.0000	Total	.05827	.55499	.35648	.03025	.00000	.00000	1.0000
Class C frequency 0.02959								**Class D** frequency 0.42969							
N	.00000	.00000	.00000	.00000	.00000	.00000	.00000	N	.00811	.01589	.00134	.00000	.00000	.00000	.02534
NNE	.00000	.00000	.00973	.00000	.00000	.00000	.00973	NNE	.00674	.01661	.00594	.00000	.00000	.00000	.02929
NE	.01304	.00000	.03250	.00000	.00000	.00000	.04554	NE	.01923	.03630	.00607	.00000	.00000	.00000	.06160
ENE	.00947	.01894	.00000	.00000	.00000	.00000	.02841	ENE	.02476	.04073	.00975	.00000	.00000	.00000	.07524
E	.01304	.00000	.00000	.00000	.00000	.00000	.01304	E	.01136	.01113	.00067	.00000	.00000	.00000	.02316
ESE	.01304	.00000	.00000	.00000	.00000	.00000	.01304	ESE	.00737	.00126	.00000	.00000	.00000	.00000	.00863
SE	.00000	.00000	.00000	.00000	.00000	.00000	.00000	SE	.00189	.00349	.00196	.00000	.00000	.00000	.00734
SSE	.00000	.00000	.00000	.00000	.00000	.00000	.00000	SSE	.00756	.00580	.00000	.00000	.00000	.00000	.01336
S	.00000	.05025	.00000	.00000	.00000	.00000	.05025	S	.00587	.01677	.00259	.00000	.00000	.00000	.02523
SSW	.00000	.09293	.00915	.00947	.00000	.00000	.11155	SSW	.01606	.04340	.01658	.00894	.00000	.00000	.08498
SW	.01889	.09667	.04576	.00000	.00000	.00000	.16132	SW	.02014	.05772	.01696	.00436	.00000	.00000	.09918
WSW	.04607	.14479	.05022	.00000	.00000	.00000	.24108	WSW	.03487	.07373	.02363	.00327	.00261	.00000	.13811
W	.02716	.07289	.00000	.00000	.00000	.00000	.10005	W	.03419	.11461	.03198	.00326	.00000	.00000	.18404
WNW	.00915	.04962	.02743	.00915	.00000	.00000	.09535	WNW	.01483	.05759	.02583	.00688	.00000	.00000	.10513
NW	.01304	.09046	.00000	.00000	.00000	.00000	.10350	NW	.01124	.04487	.01355	.00000	.00000	.00000	.06966
NNW	.00000	.02716	.00000	.00000	.00000	.00000	.02716	NNW	.01631	.02931	.00346	.00063	.00000	.00000	.04971
Total	.16289	.64371	.17479	.01862	.00000	.00000	1.0000	Total	.24053	.56923	.16030	.02733	.00261	.00000	1.0000
Class E frequency 0.35999								**Class F** frequency 0.14047							
N	.00857	.00535	.00000	.00000	.00000	.00000	.01392	N	.00655	.00000	.00000	.00000	.00000	.00000	.00655
NNE	.00587	.00540	.00000	.00000	.00000	.00000	.01127	NNE	.02339	.00000	.00000	.00000	.00000	.00000	.02339
NE	.01118	.00775	.00000	.00000	.00000	.00000	.01893	NE	.02248	.00000	.00000	.00000	.00000	.00000	.02248
ENE	.03357	.01750	.00000	.00000	.00000	.00000	.05107	ENE	.02684	.00386	.00000	.00000	.00000	.00000	.03070
E	.02071	.00564	.00080	.00000	.00000	.00000	.02715	E	.08125	.00000	.00000	.00000	.00000	.00000	.08125
ESE	.01385	.00160	.00000	.00000	.00000	.00000	.01545	ESE	.04473	.00000	.00000	.00000	.00000	.00000	.04473
SE	.01221	.00235	.00000	.00000	.00000	.00000	.01456	SE	.03464	.00000	.00000	.00000	.00000	.00000	.03464
SSE	.02748	.01235	.00153	.00000	.00000	.00000	.04136	SSE	.04029	.00000	.00000	.00000	.00000	.00000	.04029
S	.02721	.02632	.00841	.00075	.00000	.00000	.06269	S	.02546	.00193	.00000	.00000	.00000	.00000	.02739
SSW	.05007	.06948	.03553	.00226	.00000	.00000	.15734	SSW	.06536	.00393	.00000	.00000	.00000	.00000	.06929
SW	.05039	.07622	.02515	.00000	.00000	.00000	.15176	SW	.08166	.00790	.00000	.00000	.00000	.00000	.08956
WSW	.06604	.04423	.01773	.00156	.00000	.00000	.12956	WSW	.11727	.00598	.00000	.00000	.00000	.00000	.12325
W	.05453	.05108	.02088	.00233	.00000	.00000	.12882	W	.12237	.00398	.00000	.00000	.00000	.00000	.12635
WNW	.04055	.03806	.01443	.00075	.00000	.00000	.09379	WNW	.12887	.00000	.00000	.00000	.00000	.00000	.12887
NW	.03614	.01840	.00151	.00000	.00000	.00000	.05605	NW	.10804	.00000	.00000	.00000	.00000	.00000	.10804
NNW	.02067	.00491	.00075	.00000	.00000	.00000	.02633	NNW	.04323	.00000	.00000	.00000	.00000	.00000	.04323
Total	.47902	.38662	.12671	.00765	.00000	.00000	1.0000	Total	.97243	.02757	.00000	.00000	.00000	.00000	1.0000

Table ES–2. Composite Meteorological Frequencies for FMPC, February 1987–1991

	Wind speed range (m s^{-1})								Wind speed range (m s^{-1})						
	0–2	2–4	4–6	6–8	8–10	>10	Total		0–2	2–4	4–6	6–8	8–10	>10	Total
Class A frequency 0.04336								**Class B** frequency 0.02500							
N	.00000	.00000	.00668	.00000	.00000	.00000	.00668	N	.00000	.06345	.00000	.00000	.00000	.00000	.06345
NNE	.00000	.00000	.00000	.00000	.00000	.00000	.00000	NNE	.00000	.00000	.00000	.00000	.00000	.00000	.00000
NE	.00000	.00000	.00000	.00000	.00000	.00000	.00000	NE	.00000	.01278	.00000	.00000	.00000	.00000	.01278
ENE	.00000	.02272	.00000	.00000	.00000	.00000	.02272	ENE	.00000	.01278	.01278	.02451	.00000	.00000	.05007
E	.00000	.00000	.00000	.00000	.00000	.00000	.00000	E	.00000	.00000	.00000	.00000	.00000	.00000	.00000
ESE	.00000	.00000	.00000	.00000	.00000	.00000	.00000	ESE	.00000	.00000	.00000	.00000	.00000	.00000	.00000
SE	.00000	.00000	.00000	.00000	.00000	.00000	.00000	SE	.00000	.00000	.00000	.00000	.00000	.00000	.00000
SSE	.00000	.00000	.00000	.00000	.00000	.00000	.00000	SSE	.00000	.00000	.00000	.00000	.00000	.00000	.00000
S	.00000	.00000	.00737	.00000	.00000	.00000	.00737	S	.01278	.02663	.00000	.00000	.00000	.00000	.03941
SSW	.00000	.08013	.03010	.00000	.00000	.00000	.11023	SSW	.00000	.07486	.00000	.01158	.01158	.00000	.09802
SW	.00000	.13038	.07602	.00000	.00000	.00000	.20640	SW	.00000	.06293	.02352	.00000	.00000	.00000	.08645
WSW	.00000	.23952	.00688	.00000	.00000	.00000	.24640	WSW	.01194	.09541	.03857	.00000	.00000	.00000	.14592
W	.00000	.12142	.06734	.02093	.00000	.00000	.20969	W	.02472	.13415	.07194	.00000	.00000	.00000	.23081
WNW	.00000	.00737	.06693	.05005	.00000	.00000	.12435	WNW	.02472	.03857	.03682	.00000	.00000	.00000	.10011
NW	.00000	.00737	.03010	.00000	.00000	.00000	.03747	NW	.00000	.01278	.07378	.00000	.00000	.00000	.08656
NNW	.00000	.00668	.02203	.00000	.00000	.00000	.02871	NNW	.00000	.05046	.03594	.00000	.00000	.00000	.08640
Total	.00000	.61559	.31343	.07098	.00000	.00000	1.0000	Total	.07417	.58482	.29334	.03609	.01158	.00000	1.0000
Class C frequency 0.03840								**Class D** frequency 0.43837							
N	.00000	.03181	.03062	.03038	.00000	.00000	.09281	N	.01033	.06949	.01997	.00268	.00000	.00000	.10247
NNE	.00000	.02432	.00000	.00000	.00000	.00000	.02432	NNE	.00834	.05155	.01356	.00000	.00000	.00000	.07345
NE	.00000	.03173	.01554	.00798	.00000	.00000	.05525	NE	.01042	.07079	.02123	.00000	.00000	.00000	.10244
ENE	.00811	.02373	.00798	.03932	.00000	.00000	.07914	ENE	.01241	.09973	.02211	.01308	.00000	.00000	.14733
E	.00000	.03184	.00000	.00000	.00000	.00000	.03184	E	.00972	.01297	.00208	.00000	.00000	.00000	.02477
ESE	.00000	.00000	.00000	.00000	.00000	.00000	.00000	ESE	.00771	.00827	.00000	.00000	.00000	.00000	.01598
SE	.00000	.00000	.00000	.00000	.00000	.00000	.00000	SE	.00425	.00417	.00000	.00000	.00000	.00000	.00842
SSE	.00000	.00832	.00000	.00000	.00000	.00000	.00832	SSE	.00571	.00786	.00000	.00000	.00000	.00000	.01357
S	.00000	.01643	.00754	.00000	.00000	.00000	.02397	S	.00904	.01620	.00347	.00071	.00000	.00000	.02942
SSW	.00000	.04680	.02566	.00754	.00754	.00000	.08754	SSW	.01197	.03352	.01667	.00203	.00000	.00000	.06419
SW	.00000	.10626	.00832	.01621	.00000	.00000	.13079	SW	.01424	.02674	.01131	.00213	.00132	.00000	.05574
WSW	.05601	.08709	.00832	.00000	.00000	.00000	.15142	WSW	.02038	.02329	.00675	.00000	.00000	.00000	.05042
W	.02407	.06391	.01586	.00000	.00000	.00000	.10384	W	.01171	.03326	.01566	.00345	.00000	.00000	.06408
WNW	.01531	.02332	.02261	.01586	.00000	.00000	.07710	WNW	.01125	.05285	.03386	.00564	.00000	.00000	.10360
NW	.01554	.03038	.03264	.00000	.00798	.00000	.08654	NW	.01410	.04559	.01504	.00070	.00205	.00000	.07748
NNW	.00000	.03880	.00832	.00000	.00000	.00000	.04712	NNW	.01592	.03539	.01047	.00345	.00140	.00000	.06663
Total	.11904	.56475	.18341	.11729	.01551	.00000	1.0000	Total	.17749	.59169	.19220	.03386	.00476	.00000	1.0000
Class E frequency 0.32309								**Class F** frequency 0.13178							
N	.01179	.01702	.00000	.00000	.00000	.00000	.02881	N	.01837	.00000	.00000	.00000	.00000	.00000	.01837
NNE	.01048	.00565	.00000	.00000	.00000	.00000	.01613	NNE	.02112	.00000	.00000	.00000	.00000	.00000	.02112
NE	.01626	.00464	.00000	.00000	.00000	.00000	.02090	NE	.00739	.00000	.00000	.00000	.00000	.00000	.00739
ENE	.05191	.04380	.00095	.00000	.00000	.00000	.09666	ENE	.08350	.00000	.00000	.00000	.00000	.00000	.08350
E	.03323	.00473	.00000	.00000	.00000	.00000	.03796	E	.09546	.00000	.00000	.00000	.00000	.00000	.09546
ESE	.00965	.00745	.00000	.00000	.00000	.00000	.01710	ESE	.05662	.00000	.00000	.00000	.00000	.00000	.05662
SE	.01715	.00187	.00000	.00000	.00000	.00000	.01902	SE	.02338	.00000	.00000	.00000	.00000	.00000	.02338
SSE	.01434	.00944	.00000	.00000	.00000	.00000	.02378	SSE	.02404	.00000	.00000	.00000	.00000	.00000	.02404
S	.01510	.03085	.00461	.00276	.00000	.00000	.05332	S	.02416	.00243	.00000	.00000	.00000	.00000	.02659
SSW	.03167	.05071	.02149	.00269	.00000	.00000	.10656	SSW	.02772	.00000	.00000	.00000	.00000	.00000	.02772
SW	.07282	.09965	.01310	.00269	.00000	.00000	.18826	SW	.10468	.01390	.00000	.00000	.00000	.00000	.11858
WSW	.06818	.02358	.00464	.00179	.00000	.00000	.09819	WSW	.12971	.01799	.00000	.00000	.00000	.00000	.14770
W	.05342	.03955	.00940	.00193	.00000	.00000	.10430	W	.09891	.00439	.00000	.00000	.00000	.00000	.10330
WNW	.03127	.04001	.01135	.00000	.00000	.00000	.08263	WNW	.09937	.00000	.00000	.00000	.00000	.00000	.09937
NW	.04201	.01983	.00272	.00000	.00000	.00000	.06456	NW	.09874	.00000	.00000	.00000	.00000	.00000	.09874
NNW	.02005	.02085	.00095	.00000	.00000	.00000	.04185	NNW	.04814	.00000	.00000	.00000	.00000	.00000	.04814
Total	.49932	.41962	.06921	.01185	.00000	.00000	1.0000	Total	.96129	.03871	.00000	.00000	.00000	.00000	1.0000

Table ES–3. Composite Meteorological Frequencies for FMPC, March 1987–1991

	Wind speed range (m s^{-1})								Wind speed range (m s^{-1})						
	0–2	2–4	4–6	6–8	8–10	>10	Total		0–2	2–4	4–6	6–8	8–10	>10	Total
Class A frequency 0.04235								**Class B** frequency 0.03224							
N	.00000	.03283	.00000	.00000	.00000	.00000	.03283	N	.01682	.00847	.00835	.00000	.00000	.00000	.03364
NNE	.00000	.00000	.00636	.00000	.00000	.00000	.00636	NNE	.00000	.00847	.02590	.00835	.00000	.00000	.04272
NE	.00000	.02595	.00000	.00000	.00000	.00000	.02595	NE	.00000	.03587	.04163	.00000	.00000	.00000	.07750
ENE	.00000	.01324	.00000	.00000	.00000	.00000	.01324	ENE	.00000	.00835	.02481	.00000	.00000	.00000	.03316
E	.00000	.01324	.02535	.00000	.00000	.00000	.03859	E	.01739	.01739	.01695	.00000	.00000	.00000	.05173
ESE	.00000	.01959	.00000	.00000	.00000	.00000	.01959	ESE	.00000	.02481	.00000	.00000	.00000	.00000	.02481
SE	.00000	.00000	.00000	.00000	.00000	.00000	.00000	SE	.00000	.01901	.00000	.00000	.00000	.00000	.01901
SSE	.00000	.00000	.00000	.00000	.00000	.00000	.00000	SSE	.00000	.00000	.02586	.00000	.00000	.00000	.02586
S	.00000	.03964	.00636	.00000	.00000	.00000	.04600	S	.00000	.00835	.01054	.00000	.00000	.00000	.01889
SSW	.00000	.08492	.06817	.00000	.00000	.00000	.15309	SSW	.00000	.06488	.00847	.01695	.00000	.00000	.09030
SW	.00636	.07861	.06028	.01324	.00000	.00000	.15849	SW	.01888	.09750	.01901	.01901	.00000	.00000	.15440
WSW	.03269	.09911	.05786	.01316	.00000	.00000	.20282	WSW	.01682	.06290	.03440	.00000	.00000	.00000	.11412
W	.01297	.07866	.03339	.00000	.00000	.00000	.12502	W	.00835	.02682	.03402	.00000	.00000	.00000	.06919
WNW	.00000	.06045	.05904	.00000	.00000	.00000	.11949	WNW	.00894	.00000	.06782	.00000	.00000	.00000	.07676
NW	.01290	.00636	.01324	.00000	.00000	.00000	.03250	NW	.01729	.07954	.01695	.00000	.00000	.00000	.11378
NNW	.00636	.01324	.00645	.00000	.00000	.00000	.02605	NNW	.00835	.02792	.01788	.00000	.00000	.00000	.05415
Total	.07127	.56583	.33649	.02640	.00000	.00000	1.0000	Total	.11282	.49029	.35259	.04430	.00000	.00000	1.0000
Class C frequency 0.04713								**Class D** frequency 0.40801							
N	.00612	.02419	.02482	.00000	.00000	.00000	.05513	N	.00514	.02289	.02470	.00137	.00000	.00000	.05410
NNE	.00090	.02325	.01190	.00000	.00000	.00000	.03605	NNE	.00791	.05461	.03635	.01057	.00000	.00000	.10944
NE	.00134	.05320	.06451	.00580	.00000	.00000	.12485	NE	.01092	.06345	.03535	.00263	.00000	.00000	.11235
ENE	.01698	.07028	.01159	.01159	.00000	.00000	.11044	ENE	.02402	.09032	.06643	.00066	.00000	.00000	.18143
E	.01301	.01769	.00580	.00000	.00000	.00000	.03650	E	.01726	.01709	.00263	.00000	.00067	.00000	.03765
ESE	.00625	.03653	.00000	.00000	.00000	.00000	.04278	ESE	.01309	.00351	.00067	.00000	.00000	.00000	.01727
SE	.00000	.01292	.00000	.00000	.00000	.00000	.01292	SE	.00813	.01003	.00000	.00000	.00000	.00000	.01816
SSE	.00000	.00000	.00583	.00000	.00000	.00000	.00583	SSE	.00542	.01165	.00933	.00000	.00000	.00000	.02640
S	.00000	.02022	.00721	.00000	.00000	.00000	.02743	S	.00718	.01069	.00832	.00149	.00000	.00000	.02768
SSW	.00090	.04261	.03675	.00000	.00000	.00000	.08026	SSW	.01598	.02487	.01872	.00304	.00000	.00000	.06261
SW	.02445	.02486	.03688	.01159	.00000	.00000	.09778	SW	.01656	.02359	.01343	.00285	.00000	.00000	.05643
WSW	.00627	.02921	.00000	.00000	.00000	.00000	.03548	WSW	.01657	.02034	.00272	.00684	.00066	.00000	.04713
W	.01382	.03049	.02910	.00612	.00000	.00000	.07953	W	.01657	.02993	.01278	.00601	.00000	.00000	.06529
WNW	.01794	.00571	.02913	.00000	.00000	.00000	.05278	WNW	.01266	.04021	.02378	.00200	.00000	.00000	.07865
NW	.01803	.03739	.02957	.00000	.00000	.00000	.08499	NW	.01138	.02858	.01388	.00000	.00000	.00000	.05384
NNW	.01769	.06965	.02994	.00000	.00000	.00000	.11728	NNW	.01010	.02669	.01478	.00000	.00000	.00000	.05157
Total	.14369	.49819	.32302	.03510	.00000	.00000	1.0000	Total	.19889	.47845	.28386	.03747	.00133	.00000	1.0000
Class E frequency 0.28551								**Class F** frequency 0.18477							
N	.02894	.01501	.00192	.00000	.00000	.00000	.04587	N	.03449	.00148	.00000	.00000	.00000	.00000	.03597
NNE	.01535	.01162	.00191	.00000	.00000	.00000	.02888	NNE	.02288	.00000	.00000	.00000	.00000	.00000	.02288
NE	.01390	.01421	.00096	.00000	.00000	.00000	.02907	NE	.03185	.00000	.00000	.00000	.00000	.00000	.03185
ENE	.04147	.08175	.00946	.00000	.00000	.00000	.13268	ENE	.08071	.01939	.00000	.00000	.00000	.00000	.10010
E	.02669	.00750	.00000	.00000	.00000	.00000	.03419	E	.09729	.00148	.00000	.00000	.00000	.00000	.09877
ESE	.00872	.00309	.00000	.00000	.00000	.00000	.01181	ESE	.04512	.00000	.00000	.00000	.00000	.00000	.04512
SE	.01075	.00665	.00096	.00000	.00000	.00000	.01836	SE	.01944	.00000	.00000	.00000	.00000	.00000	.01944
SSE	.01438	.02690	.00571	.00096	.00000	.00000	.04795	SSE	.02186	.00000	.00000	.00000	.00000	.00000	.02186
S	.01759	.03961	.01345	.00192	.00000	.00000	.07257	S	.02821	.00156	.00000	.00000	.00000	.00000	.02977
SSW	.03438	.07918	.02671	.00769	.00000	.00000	.14796	SSW	.04002	.00880	.00000	.00000	.00000	.00000	.04882
SW	.05603	.04225	.01409	.00393	.00000	.00000	.11630	SW	.07146	.00149	.00000	.00000	.00000	.00000	.07295
WSW	.04619	.04085	.01186	.00094	.00000	.00000	.09984	WSW	.10148	.00297	.00000	.00000	.00000	.00000	.10445
W	.03436	.04262	.00573	.00000	.00000	.00000	.08271	W	.07898	.00000	.00000	.00000	.00000	.00000	.07898
WNW	.02003	.03229	.00671	.00000	.00000	.00000	.05903	WNW	.11410	.00149	.00000	.00000	.00000	.00000	.11559
NW	.02178	.01595	.00096	.00096	.00000	.00000	.03965	NW	.10082	.00149	.00000	.00000	.00000	.00000	.10231
NNW	.02000	.01026	.00192	.00096	.00000	.00000	.03314	NNW	.06636	.00477	.00000	.00000	.00000	.00000	.07113
Total	.41056	.46975	.10233	.01737	.00000	.00000	1.0000	Total	.95509	.04491	.00000	.00000	.00000	.00000	1.0000

Table ES–4. Composite Meteorological Frequencies for FMPC, April 1987–1991

	Wind speed range (m s^{-1})						
	0–2	2–4	4–6	6–8	8–10	>10	Total
Class A frequency 0.08422							
N	.00000	.00690	.01021	.00000	.00000	.00000	.01711
NNE	.02724	.00668	.00000	.00000	.00000	.00000	.03392
NE	.01330	.05829	.01155	.00000	.00000	.00000	.08314
ENE	.00331	.02048	.01021	.00690	.00000	.00000	.04090
E	.00331	.00331	.01021	.00000	.00000	.00000	.01683
ESE	.00000	.02026	.00000	.00000	.00000	.00000	.02026
SE	.00000	.00331	.00000	.00000	.00000	.00000	.00331
SSE	.00000	.00000	.00000	.00000	.00000	.00000	.00000
S	.00063	.01845	.00000	.00000	.00000	.00000	.01908
SSW	.00000	.02757	.03280	.00000	.00000	.00000	.06037
SW	.00000	.05213	.07032	.00000	.00000	.00000	.12245
WSW	.00063	.07753	.05078	.00000	.00000	.00000	.12894
W	.00507	.11385	.10318	.00331	.00000	.00000	.22541
WNW	.03801	.04748	.05433	.00000	.00000	.00000	.13982
NW	.01140	.02802	.03010	.00000	.00000	.00000	.06952
NNW	.00063	.01155	.00337	.00337	.00000	.00000	.01892
Total	.10354	.49581	.38707	.01358	.00000	.00000	1.0000
Class B frequency 0.04259							
N	.01754	.01628	.00000	.00000	.00000	.00000	.03382
NNE	.01754	.01372	.00000	.00000	.00000	.00000	.03126
NE	.00125	.05564	.00666	.00000	.00000	.00000	.06355
ENE	.00000	.02685	.00000	.00000	.00000	.00000	.02685
E	.02419	.02032	.01334	.00000	.00000	.00000	.05785
ESE	.01754	.00000	.00000	.00000	.00000	.00000	.01754
SE	.00000	.00655	.00000	.00000	.00000	.00000	.00655
SSE	.01754	.01331	.00000	.00666	.00000	.00000	.03751
S	.00000	.01364	.00000	.00000	.00000	.00000	.01364
SSW	.00000	.06151	.01323	.00000	.00000	.00000	.07474
SW	.05790	.03432	.04629	.00000	.00000	.00000	.13851
WSW	.03382	.06229	.02335	.00000	.00000	.00000	.11946
W	.01323	.04820	.06216	.00666	.00000	.00000	.13025
WNW	.01754	.03619	.01986	.00000	.00000	.00000	.07359
NW	.04048	.04069	.03578	.00000	.00000	.00000	.11695
NNW	.00125	.03000	.02001	.00668	.00000	.00000	.05794
Total	.25981	.47953	.24067	.01999	.00000	.00000	1.0000
Class C frequency 0.04897							
N	.02975	.05254	.00000	.00000	.00000	.00000	.08229
NNE	.00579	.02888	.01148	.00000	.00000	.00000	.04615
NE	.01520	.04339	.01772	.00000	.00000	.00000	.07631
ENE	.00579	.04039	.01150	.00000	.00000	.00000	.05768
E	.01743	.01766	.00579	.00570	.00000	.00000	.04658
ESE	.01743	.00614	.00000	.00000	.00000	.00000	.02357
SE	.01187	.00614	.00000	.00000	.00000	.00000	.01801
SSE	.00000	.00000	.00570	.00000	.00000	.00000	.00570
S	.00000	.03506	.01187	.00000	.00000	.00000	.04693
SSW	.00000	.07690	.01187	.00000	.00000	.00000	.08877
SW	.00000	.05319	.03773	.00000	.00000	.00000	.09092
WSW	.03830	.03829	.00614	.01158	.00000	.00000	.09431
W	.00896	.06150	.03992	.00000	.00000	.00000	.11038
WNW	.00000	.02960	.02956	.00000	.00000	.00000	.05916
NW	.00579	.04734	.01766	.00000	.00000	.00000	.07079
NNW	.02936	.03003	.01729	.00581	.00000	.00000	.08249
Total	.18566	.56703	.22422	.02308	.00000	.00000	1.0000
Class D frequency 0.35778							
N	.00612	.06414	.01642	.00000	.00000	.00000	.08668
NNE	.00551	.02898	.01097	.00079	.00000	.00000	.04625
NE	.02220	.04427	.00468	.00000	.00000	.00000	.07115
ENE	.02890	.05983	.01634	.00000	.00000	.00000	.10507
E	.01556	.02294	.00000	.00000	.00000	.00000	.03850
ESE	.02062	.00248	.00000	.00000	.00000	.00000	.02310
SE	.01075	.01085	.00000	.00000	.00000	.00000	.02160
SSE	.02321	.01619	.00548	.00158	.00000	.00000	.04646
S	.01383	.03539	.00557	.00000	.00000	.00000	.05479
SSW	.01511	.03644	.02538	.00000	.00000	.00000	.07693
SW	.01677	.04884	.01364	.00000	.00000	.00000	.07925
WSW	.02463	.03673	.01559	.00389	.00000	.00000	.08084
W	.01325	.04591	.02327	.00000	.00000	.00000	.08243
WNW	.01062	.02475	.01349	.00000	.00000	.00000	.04886
NW	.01234	.03445	.02608	.00000	.00000	.00000	.07287
NNW	.00711	.03995	.01188	.00629	.00000	.00000	.06523
Total	.24652	.55213	.18880	.01256	.00000	.00000	1.0000
Class E frequency 0.25472							
N	.01848	.01468	.00341	.00000	.00000	.00000	.03657
NNE	.00911	.01235	.00986	.00000	.00000	.00000	.03132
NE	.01650	.00775	.00223	.00000	.00000	.00000	.02648
ENE	.03631	.02564	.00472	.00000	.00000	.00000	.06667
E	.03488	.01020	.00118	.00000	.00000	.00000	.04626
ESE	.02277	.00326	.00000	.00000	.00000	.00000	.02603
SE	.03942	.00680	.00000	.00000	.00000	.00000	.04622
SSE	.03607	.01982	.00112	.00111	.00000	.00000	.05812
S	.03246	.04330	.01400	.00000	.00000	.00000	.08976
SSW	.02210	.04784	.01035	.00118	.00000	.00000	.08147
SW	.04006	.05076	.00804	.00000	.00000	.00000	.09886
WSW	.07823	.01811	.00444	.00111	.00000	.00000	.10189
W	.06238	.04223	.00223	.00000	.00000	.00000	.10684
WNW	.04127	.05364	.00558	.00000	.00000	.00000	.10049
NW	.02090	.01350	.00558	.00111	.00000	.00000	.04109
NNW	.02400	.01459	.00223	.00111	.00000	.00000	.04193
Total	.53494	.38448	.07495	.00563	.00000	.00000	1.0000
Class F frequency 0.21172							
N	.01161	.00000	.00000	.00000	.00000	.00000	.01161
NNE	.04573	.00000	.00000	.00000	.00000	.00000	.04573
NE	.01800	.00000	.00000	.00000	.00000	.00000	.01800
ENE	.03696	.00534	.00000	.00000	.00000	.00000	.04230
E	.07839	.00000	.00000	.00000	.00000	.00000	.07839
ESE	.04136	.00000	.00000	.00000	.00000	.00000	.04136
SE	.02241	.00000	.00000	.00000	.00000	.00000	.02241
SSE	.04106	.00000	.00000	.00000	.00000	.00000	.04106
S	.04908	.00000	.00000	.00000	.00000	.00000	.04908
SSW	.10168	.00000	.00000	.00000	.00000	.00000	.10168
SW	.04708	.00269	.00000	.00000	.00000	.00000	.04977
WSW	.06983	.00134	.00000	.00000	.00000	.00000	.07117
W	.12518	.00000	.00000	.00000	.00000	.00000	.12518
WNW	.11978	.00000	.00000	.00000	.00000	.00000	.11978
NW	.12781	.00000	.00000	.00000	.00000	.00000	.12781
NNW	.05467	.00000	.00000	.00000	.00000	.00000	.05467
Total	.99063	.00937	.00000	.00000	.00000	.00000	1.0000

Table ES–5. Composite Meteorological Frequencies for FMPC, May 1987–1991

	Wind speed range (m s^{-1})						
	0–2	2–4	4–6	6–8	8–10	>10	Total
Class A frequency 0.07975							
N	.00804	.02134	.00348	.00000	.00000	.00000	.03286
NNE	.00429	.02211	.02760	.00000	.00000	.00000	.05400
NE	.00794	.05534	.00865	.00000	.00000	.00000	.07193
ENE	.06863	.07680	.00865	.00000	.00000	.00000	.15408
E	.03236	.02379	.00000	.00000	.00000	.00000	.05615
ESE	.01209	.00817	.00000	.00000	.00000	.00000	.02026
SE	.00392	.00000	.00000	.00000	.00000	.00000	.00392
SSE	.00000	.00392	.00697	.00000	.00000	.00000	.01089
S	.00817	.01601	.00000	.00000	.00000	.00000	.02418
SSW	.02418	.05310	.01143	.00000	.00000	.00000	.08871
SW	.03219	.08853	.02828	.00000	.00000	.00000	.14900
WSW	.02026	.06810	.00701	.00000	.00000	.00000	.09537
W	.00392	.10147	.02767	.00000	.00000	.00000	.13306
WNW	.00392	.01893	.01045	.00000	.00000	.00000	.03330
NW	.00375	.01434	.01045	.00000	.00000	.00000	.02854
NNW	.00027	.01782	.02131	.00000	.00000	.00432	.04372
Total	.23394	.58978	.17195	.00000	.00000	.00432	1.0000
Class B frequency 0.03999							
N	.02652	.03474	.02164	.00721	.00000	.00000	.09011
NNE	.02759	.02419	.02084	.00000	.00000	.00000	.07262
NE	.00214	.04002	.05808	.00000	.00000	.00000	.10024
ENE	.01798	.01557	.00000	.00000	.00000	.00000	.03355
E	.00782	.00000	.00000	.00000	.00000	.00000	.00782
ESE	.00782	.00782	.00000	.00000	.00000	.00000	.01564
SE	.00000	.00000	.00000	.00000	.00000	.00000	.00000
SSE	.02411	.00000	.00000	.00000	.00000	.00000	.02411
S	.04041	.01629	.00000	.00000	.00000	.00000	.05670
SSW	.04041	.03115	.01443	.00000	.00000	.00000	.08599
SW	.03320	.15268	.03220	.00000	.00000	.00000	.21808
WSW	.00782	.03730	.00862	.00000	.00000	.00000	.05374
W	.01503	.00782	.03746	.00000	.00000	.00000	.06031
WNW	.02759	.02138	.01389	.00704	.00000	.00000	.06990
NW	.00374	.02111	.00721	.00000	.00000	.00000	.03206
NNW	.00802	.06386	.00721	.00000	.00000	.00000	.07909
Total	.29020	.47394	.22160	.01425	.00000	.00000	1.0000
Class C frequency 0.05383							
N	.01897	.03758	.00536	.00000	.00000	.00000	.06191
NNE	.00040	.02314	.01562	.00536	.00000	.00000	.04452
NE	.00576	.02916	.03158	.00000	.00000	.00000	.06650
ENE	.03584	.03902	.00641	.00000	.00000	.00000	.08127
E	.00536	.01177	.00000	.00000	.00000	.00000	.01713
ESE	.03643	.00581	.00000	.00000	.00000	.00000	.04224
SE	.00581	.01758	.00000	.00000	.00000	.00000	.02339
SSE	.01806	.01032	.00000	.00000	.00000	.00000	.02838
S	.01792	.00641	.00000	.00000	.00000	.00000	.02433
SSW	.00119	.07164	.02091	.00000	.00000	.00000	.09374
SW	.03167	.15263	.01163	.00000	.00000	.00000	.19593
WSW	.02308	.06916	.02078	.00000	.00000	.00000	.11302
W	.01778	.00000	.02091	.01045	.00000	.00000	.04914
WNW	.01157	.04517	.01032	.00523	.00000	.00000	.07229
NW	.00040	.01673	.03177	.00000	.00000	.00000	.04890
NNW	.00040	.01568	.02124	.00000	.00000	.00000	.03732
Total	.23063	.55180	.19653	.02104	.00000	.00000	1.0000
Class D frequency 0.31859							
N	.00787	.03039	.02618	.00000	.00000	.00000	.06444
NNE	.02005	.04698	.01501	.00178	.00000	.00000	.08382
NE	.03159	.03844	.01290	.00087	.00000	.00000	.08380
ENE	.03862	.05933	.00514	.00317	.00000	.00000	.10626
E	.04255	.01104	.00000	.00000	.00000	.00000	.05359
ESE	.02502	.00464	.00000	.00000	.00000	.00000	.02966
SE	.01738	.00444	.00000	.00000	.00000	.00000	.02182
SSE	.01765	.00796	.00360	.00000	.00000	.00000	.02921
S	.02530	.02673	.00707	.00177	.00000	.00000	.06087
SSW	.04137	.04616	.01080	.00087	.00000	.00000	.09920
SW	.04380	.05289	.00670	.00087	.00000	.00000	.10426
WSW	.03716	.01391	.00353	.00459	.00000	.00000	.05919
W	.02307	.02112	.00883	.00352	.00000	.00000	.05654
WNW	.01364	.02340	.00711	.00000	.00000	.00000	.04415
NW	.01550	.02054	.00352	.00091	.00000	.00000	.04047
NNW	.01900	.03465	.00907	.00000	.00000	.00000	.06272
Total	.41958	.44261	.11946	.01835	.00000	.00000	1.0000
Class E frequency 0.26836							
N	.02030	.02808	.00312	.00000	.00000	.00000	.05150
NNE	.01156	.03269	.00674	.00000	.00000	.00000	.05099
NE	.02308	.01813	.00466	.00000	.00000	.00000	.04587
ENE	.04842	.01264	.00000	.00000	.00000	.00000	.06106
E	.04102	.00338	.00000	.00000	.00000	.00000	.04440
ESE	.01773	.00000	.00000	.00000	.00000	.00000	.01773
SE	.02731	.00000	.00000	.00000	.00000	.00000	.02731
SSE	.03189	.01594	.00000	.00000	.00000	.00000	.04783
S	.04404	.02684	.00315	.00000	.00000	.00000	.07403
SSW	.06579	.05119	.00524	.00000	.00000	.00000	.12222
SW	.09593	.02334	.00000	.00000	.00000	.00000	.11927
WSW	.07838	.02125	.00524	.00000	.00000	.00000	.10487
W	.04627	.02555	.00629	.00000	.00000	.00000	.07811
WNW	.04549	.01397	.00000	.00000	.00000	.00000	.05946
NW	.03291	.01407	.00000	.00000	.00000	.00000	.04698
NNW	.02779	.01847	.00210	.00000	.00000	.00000	.04836
Total	.65792	.30555	.03653	.00000	.00000	.00000	1.0000
Class F frequency 0.23948							
N	.01566	.00117	.00000	.00000	.00000	.00144	.01827
NNE	.01428	.00000	.00000	.00000	.00000	.00000	.01428
NE	.01845	.00000	.00000	.00000	.00000	.00000	.01845
ENE	.03903	.00000	.00000	.00000	.00000	.00000	.03903
E	.06998	.00000	.00000	.00000	.00000	.00000	.06998
ESE	.03540	.00000	.00000	.00000	.00000	.00000	.03540
SE	.03141	.00000	.00000	.00000	.00000	.00000	.03141
SSE	.01229	.00000	.00000	.00000	.00000	.00000	.01229
S	.02904	.00238	.00000	.00000	.00000	.00000	.03142
SSW	.06658	.00379	.00000	.00000	.00000	.00000	.07037
SW	.11552	.00235	.00000	.00000	.00000	.00000	.11787
WSW	.14698	.00237	.00000	.00000	.00000	.00000	.14935
W	.12443	.00144	.00000	.00000	.00000	.00000	.12587
WNW	.12890	.00000	.00000	.00000	.00000	.00000	.12890
NW	.09457	.00144	.00000	.00000	.00000	.00000	.09601
NNW	.04110	.00000	.00000	.00000	.00000	.00000	.04110
Total	.98362	.01494	.00000	.00000	.00000	.00144	1.0000

Table ES–6. Composite Meteorological Frequencies for FMPC, June 1987–1991

	Wind speed range (m s^{-1})						
	0–2	2–4	4–6	6–8	8–10	>10	Total
Class A frequency 0.08477							
N	.00705	.00338	.01464	.00000	.00000	.00000	.02507
NNE	.01213	.03150	.06166	.01098	.00000	.00000	.11627
NE	.03833	.12241	.04987	.00366	.00000	.00000	.21427
ENE	.04513	.06932	.01437	.00000	.00000	.00000	.12882
E	.02454	.00705	.00000	.00000	.00000	.00000	.03159
ESE	.01382	.01044	.00000	.00000	.00000	.00000	.02426
SE	.01382	.01044	.00000	.00000	.00000	.00000	.02426
SSE	.02454	.01382	.00000	.00000	.00000	.00000	.03836
S	.01382	.01749	.00000	.00000	.00000	.00000	.03131
SSW	.01749	.04488	.00330	.00000	.00000	.00000	.06567
SW	.08002	.04817	.01653	.00000	.00000	.00000	.14472
WSW	.03300	.03014	.00000	.00000	.00000	.00000	.06314
W	.01916	.05228	.00000	.00000	.00000	.00000	.07144
WNW	.00000	.00705	.00000	.00000	.00000	.00000	.00705
NW	.00000	.00330	.00000	.00000	.00000	.00000	.00330
NNW	.01044	.00000	.00000	.00000	.00000	.00000	.01044
Total	.35330	.47168	.16038	.01464	.00000	.00000	1.0000
Class B frequency 0.03525							
N	.00794	.01696	.00000	.00000	.00000	.00000	.02490
NNE	.00000	.01608	.06096	.00880	.00000	.00000	.08584
NE	.03639	.08582	.01760	.00000	.00000	.00000	.13981
ENE	.03010	.04161	.00880	.00000	.00000	.00000	.08051
E	.04781	.01608	.00000	.00000	.00000	.00000	.06389
ESE	.00814	.00000	.00000	.00000	.00000	.00000	.00814
SE	.00814	.00000	.00000	.00000	.00000	.00000	.00814
SSE	.01608	.00000	.00000	.00000	.00000	.00000	.01608
S	.04206	.01184	.00000	.00000	.00000	.00000	.05390
SSW	.02489	.01608	.00000	.00000	.00000	.00000	.04097
SW	.03010	.10139	.00000	.00000	.00000	.00000	.13149
WSW	.02510	.06847	.01184	.00000	.00000	.00000	.10541
W	.03892	.03368	.00000	.00000	.00000	.00000	.07260
WNW	.05161	.03281	.02368	.00000	.00000	.00000	.10810
NW	.01967	.03260	.00000	.00000	.00000	.00000	.05227
NNW	.00000	.00000	.00793	.00000	.00000	.00000	.00793
Total	.38696	.47342	.13082	.00880	.00000	.00000	1.0000
Class C frequency 0.05504							
N	.01030	.01538	.00000	.00000	.00000	.00000	.02568
NNE	.01983	.05345	.02763	.00000	.00000	.00000	.10091
NE	.01983	.07034	.01127	.00564	.00000	.00000	.10708
ENE	.03756	.03340	.00000	.00000	.00000	.00000	.07096
E	.03877	.02742	.00000	.00000	.00000	.00000	.06619
ESE	.04076	.00508	.00000	.00000	.00000	.00000	.04584
SE	.01723	.00000	.00000	.00000	.00000	.00000	.01723
SSE	.00652	.01580	.00000	.00000	.00000	.00000	.02232
S	.00652	.02596	.00000	.00000	.00000	.00000	.03248
SSW	.01086	.02541	.00508	.00000	.00000	.00000	.04135
SW	.02233	.07232	.05270	.00000	.00000	.00000	.14735
WSW	.03639	.05296	.00758	.00000	.00000	.00000	.09693
W	.01608	.04824	.00000	.00000	.00000	.00000	.06432
WNW	.02742	.02144	.02729	.00000	.00000	.00000	.07615
NW	.01345	.04384	.00000	.00000	.00000	.00000	.05729
NNW	.00508	.01775	.00508	.00000	.00000	.00000	.02791
Total	.32893	.52879	.13664	.00564	.00000	.00000	1.0000
Class D frequency 0.27401							
N	.00681	.01900	.00000	.00000	.00000	.00000	.02581
NNE	.02175	.05751	.01217	.00226	.00000	.00000	.09369
NE	.03068	.04219	.01690	.00113	.00000	.00000	.09090
ENE	.04056	.03158	.00215	.00000	.00000	.00000	.07429
E	.03340	.00727	.00000	.00000	.00000	.00000	.04067
ESE	.02189	.00548	.00000	.00000	.00000	.00000	.02737
SE	.02457	.00878	.00000	.00000	.00000	.00000	.03335
SSE	.02188	.01071	.00000	.00000	.00000	.00000	.03259
S	.02201	.01682	.00408	.00000	.00000	.00000	.04291
SSW	.04270	.06548	.00459	.00000	.00000	.00000	.11277
SW	.05313	.08165	.01057	.00204	.00000	.00000	.14739
WSW	.05251	.02661	.00611	.00000	.00000	.00000	.08523
W	.04008	.02275	.01019	.00000	.00000	.00000	.07302
WNW	.01534	.01959	.00803	.00000	.00000	.00000	.04296
NW	.01652	.02435	.00102	.00000	.00000	.00000	.04189
NNW	.00709	.02295	.00510	.00000	.00000	.00000	.03514
Total	.45093	.46271	.08092	.00544	.00000	.00000	1.0000
Class E frequency 0.27370							
N	.02592	.00420	.00000	.00000	.00000	.00000	.03012
NNE	.01436	.01570	.00000	.00000	.00000	.00000	.03006
NE	.01239	.01833	.00000	.00000	.00000	.00000	.03072
ENE	.03195	.00719	.00000	.00000	.00000	.00000	.03914
E	.03508	.00305	.00000	.00000	.00000	.00000	.03813
ESE	.01697	.00000	.00000	.00000	.00000	.00000	.01697
SE	.01638	.00000	.00000	.00000	.00000	.00000	.01638
SSE	.01416	.00459	.00000	.00000	.00000	.00000	.01875
S	.05008	.01699	.00000	.00000	.00000	.00000	.06707
SSW	.08775	.02874	.00000	.00000	.00000	.00000	.11649
SW	.13855	.04919	.00000	.00000	.00000	.00000	.18774
WSW	.13793	.01709	.00204	.00000	.00000	.00000	.15706
W	.08191	.01530	.00000	.00000	.00000	.00000	.09721
WNW	.05558	.01826	.00102	.00000	.00000	.00000	.07486
NW	.04680	.01134	.00113	.00000	.00000	.00000	.05927
NNW	.01595	.00305	.00102	.00000	.00000	.00000	.02002
Total	.78176	.21302	.00522	.00000	.00000	.00000	1.0000
Class F frequency 0.27722							
N	.01262	.00202	.00000	.00000	.00000	.00000	.01464
NNE	.01151	.00000	.00000	.00000	.00000	.00000	.01151
NE	.01577	.00000	.00000	.00000	.00000	.00000	.01577
ENE	.02908	.00262	.00000	.00000	.00000	.00000	.03170
E	.04163	.00000	.00000	.00000	.00000	.00000	.04163
ESE	.03876	.00000	.00000	.00000	.00000	.00000	.03876
SE	.01869	.00000	.00000	.00000	.00000	.00000	.01869
SSE	.01718	.00000	.00000	.00000	.00000	.00000	.01718
S	.04857	.00000	.00000	.00000	.00000	.00000	.04857
SSW	.07637	.00112	.00000	.00000	.00000	.00000	.07749
SW	.14446	.00112	.00000	.00000	.00000	.00000	.14558
WSW	.13628	.00224	.00000	.00000	.00000	.00000	.13852
W	.13995	.00213	.00000	.00000	.00000	.00000	.14208
WNW	.11840	.00000	.00000	.00000	.00000	.00000	.11840
NW	.10112	.00000	.00000	.00000	.00000	.00000	.10112
NNW	.03738	.00101	.00000	.00000	.00000	.00000	.03839
Total	.98775	.01225	.00000	.00000	.00000	.00000	1.0000

Table ES–7. Composite Meteorological Frequencies for FMPC, July 1987–1991

	Wind speed range (m s^{-1})						
	0–2	2–4	4–6	6–8	8–10	>10	Total
Class A frequency 0.08464							
N	.00744	.04438	.00000	.00000	.00000	.00000	.05182
NNE	.01991	.03101	.00000	.00000	.00000	.00000	.05092
NE	.02787	.02705	.00000	.00000	.00000	.00000	.05492
ENE	.07378	.07482	.00000	.00000	.00000	.00000	.14860
E	.05182	.00669	.00000	.00000	.00000	.00000	.05851
ESE	.02419	.00000	.00000	.00000	.00000	.00000	.02419
SE	.00692	.00000	.00000	.00000	.00000	.00000	.00692
SSE	.00361	.00000	.00000	.00000	.00000	.00000	.00361
S	.00690	.00331	.00000	.00000	.00000	.00000	.01021
SSW	.03448	.04769	.00000	.00000	.00000	.00000	.08217
SW	.06527	.04086	.00000	.00000	.00000	.00000	.10613
WSW	.07525	.02021	.00735	.00000	.00000	.00000	.10281
W	.05491	.06288	.00000	.00000	.00000	.00000	.11779
WNW	.02764	.05437	.00000	.00000	.00000	.00000	.08201
NW	.02756	.01698	.00000	.00000	.00000	.00000	.04454
NNW	.02081	.03402	.00000	.00000	.00000	.00000	.05483
Total	.52837	.46428	.00735	.00000	.00000	.00000	1.0000
Class B frequency 0.02502							
N	.01121	.06585	.01093	.00000	.00000	.00000	.08799
NNE	.01093	.01093	.00000	.00000	.00000	.00000	.02186
NE	.03449	.03480	.00000	.00000	.00000	.00000	.06929
ENE	.05733	.04625	.00000	.00000	.00000	.00000	.10358
E	.04498	.01243	.00000	.00000	.00000	.00000	.05741
ESE	.03456	.00000	.00000	.00000	.00000	.00000	.03456
SE	.00000	.00000	.00000	.00000	.00000	.00000	.00000
SSE	.00000	.00000	.00000	.00000	.00000	.00000	.00000
S	.01121	.00000	.00000	.00000	.00000	.00000	.01121
SSW	.06083	.05967	.00000	.00000	.00000	.00000	.12050
SW	.03824	.08104	.00000	.00000	.00000	.00000	.11928
WSW	.08690	.06110	.00000	.00000	.00000	.00000	.14800
W	.05724	.09186	.00000	.00000	.00000	.00000	.14910
WNW	.00574	.02336	.00000	.00000	.00000	.00000	.02910
NW	.01121	.00000	.00000	.00000	.00000	.00000	.01121
NNW	.02570	.01121	.00000	.00000	.00000	.00000	.03691
Total	.49057	.49850	.01093	.00000	.00000	.00000	1.0000
Class C frequency 0.05561							
N	.01019	.04001	.00492	.00000	.00000	.00000	.05512
NNE	.01488	.02471	.00492	.00000	.00000	.00000	.04451
NE	.00515	.02482	.00000	.00000	.00000	.00000	.02997
ENE	.03342	.02170	.00000	.00000	.00000	.00000	.05512
E	.04332	.01821	.00000	.00000	.00000	.00000	.06153
ESE	.00504	.00492	.00000	.00000	.00000	.00000	.00996
SE	.03641	.02526	.00000	.00000	.00000	.00000	.06167
SSE	.00000	.00000	.00000	.00000	.00000	.00000	.00000
S	.01352	.01611	.00000	.00000	.00000	.00000	.02963
SSW	.01771	.01064	.00000	.00000	.00000	.00000	.02835
SW	.05898	.13809	.00000	.00000	.00000	.00000	.19707
WSW	.05862	.12452	.00000	.00000	.00000	.00000	.18314
W	.03953	.06989	.01261	.00000	.00000	.00000	.12203
WNW	.02985	.02102	.00000	.00000	.00000	.00000	.05087
NW	.02855	.01051	.00000	.00000	.00000	.00000	.03906
NNW	.01620	.01578	.00000	.00000	.00000	.00000	.03198
Total	.41137	.56618	.02245	.00000	.00000	.00000	1.0000
Class D frequency 0.26146							
N	.01880	.03253	.00000	.00000	.00000	.00000	.05133
NNE	.01889	.01388	.00000	.00000	.00000	.00000	.03277
NE	.03234	.01837	.00000	.00000	.00000	.00000	.05071
ENE	.03242	.02345	.00000	.00000	.00000	.00000	.05587
E	.03794	.00582	.00000	.00000	.00000	.00000	.04376
ESE	.01084	.00523	.00000	.00000	.00000	.00000	.01607
SE	.01398	.00435	.00000	.00000	.00000	.00000	.01833
SSE	.02460	.01088	.00000	.00000	.00000	.00000	.03548
S	.03952	.01674	.00000	.00000	.00000	.00000	.05626
SSW	.04940	.05365	.00000	.00000	.00000	.00000	.10305
SW	.10523	.08534	.00119	.00000	.00000	.00000	.19176
WSW	.07243	.05805	.00000	.00000	.00000	.00000	.13048
W	.04926	.01908	.00387	.00000	.00000	.00000	.07221
WNW	.04480	.01561	.00000	.00000	.00000	.00000	.06041
NW	.03916	.01264	.00000	.00000	.00000	.00000	.05180
NNW	.01304	.01666	.00000	.00000	.00000	.00000	.02970
Total	.60266	.39228	.00506	.00000	.00000	.00000	1.0000
Class E frequency 0.31947							
N	.06066	.00257	.00097	.00000	.00000	.00000	.06420
NNE	.01931	.00090	.00000	.00000	.00000	.00000	.02021
NE	.01897	.00086	.00000	.00000	.00000	.00000	.01983
ENE	.03583	.00000	.00000	.00000	.00000	.00000	.03583
E	.04257	.00187	.00000	.00000	.00000	.00000	.04444
ESE	.02507	.00000	.00000	.00000	.00000	.00000	.02507
SE	.02585	.00000	.00000	.00000	.00000	.00000	.02585
SSE	.02356	.00000	.00000	.00000	.00000	.00000	.02356
S	.04024	.00923	.00000	.00000	.00000	.00000	.04947
SSW	.09269	.02334	.00000	.00000	.00000	.00000	.11603
SW	.17297	.02696	.00000	.00000	.00000	.00000	.19993
WSW	.10804	.00671	.00000	.00000	.00000	.00000	.11475
W	.07893	.00456	.00000	.00000	.00000	.00000	.08349
WNW	.06401	.00402	.00000	.00000	.00000	.00000	.06803
NW	.03990	.00801	.00088	.00000	.00000	.00000	.04879
NNW	.05520	.00532	.00000	.00000	.00000	.00000	.06052
Total	.90380	.09435	.00185	.00000	.00000	.00000	1.0000
Class F frequency 0.25380							
N	.00132	.00000	.00000	.00000	.00000	.00000	.00132
NNE	.01266	.00000	.00276	.00000	.00000	.00000	.01542
NE	.00188	.00000	.00000	.00000	.00000	.00000	.00188
ENE	.00428	.00000	.00000	.00000	.00000	.00000	.00428
E	.03586	.00000	.00000	.00000	.00000	.00000	.03586
ESE	.02793	.00000	.00000	.00000	.00000	.00000	.02793
SE	.03020	.00000	.00000	.00000	.00000	.00000	.03020
SSE	.03649	.00000	.00000	.00000	.00000	.00000	.03649
S	.03527	.00122	.00000	.00000	.00000	.00000	.03649
SSW	.09276	.00276	.00122	.00000	.00000	.00000	.09674
SW	.16134	.00000	.00000	.00000	.00000	.00000	.16134
WSW	.19214	.00122	.00000	.00000	.00000	.00000	.19336
W	.12498	.00000	.00000	.00000	.00000	.00000	.12498
WNW	.11145	.00000	.00000	.00000	.00000	.00000	.11145
NW	.09663	.00000	.00000	.00000	.00000	.00000	.09663
NNW	.02560	.00000	.00000	.00000	.00000	.00000	.02560
Total	.99080	.00521	.00399	.00000	.00000	.00000	1.0000

Table ES–8. Composite Meteorological Frequencies for FMPC, August 1987–1991

	Wind speed range (m s^{-1})						
	0–2	2–4	4–6	6–8	8–10	>10	Total
Class A frequency 0.07159							
N	.00368	.01497	.01984	.00000	.00000	.00000	.03849
NNE	.00000	.00753	.00000	.00000	.00000	.00000	.00753
NE	.01502	.03591	.00000	.00000	.00000	.00000	.05093
ENE	.08344	.07932	.00000	.00000	.00000	.00000	.16276
E	.03800	.04233	.00000	.00000	.00000	.00000	.08033
ESE	.01502	.00000	.00000	.00000	.00000	.00000	.01502
SE	.00766	.00000	.00000	.00000	.00000	.00000	.00766
SSE	.02666	.00000	.00000	.00000	.00000	.00000	.02666
S	.04168	.00766	.00000	.00000	.00000	.00000	.04934
SSW	.04934	.03034	.00368	.00000	.00000	.00000	.08336
SW	.04168	.04740	.00000	.00000	.00000	.00000	.08908
WSW	.06834	.06051	.00898	.00000	.00000	.00000	.13783
W	.04934	.01193	.00000	.00000	.00000	.00000	.06127
WNW	.01900	.01121	.00000	.00000	.00000	.00000	.03021
NW	.01900	.03941	.00000	.00000	.00000	.00000	.05841
NNW	.00000	.05289	.04822	.00000	.00000	.00000	.10111
Total	.47786	.44141	.08072	.00000	.00000	.00000	1.0000
Class B frequency 0.03678							
N	.00000	.07701	.00716	.00000	.00000	.00000	.08417
NNE	.00716	.03101	.00000	.00000	.00000	.00000	.03817
NE	.00716	.09926	.00000	.00000	.00000	.00000	.10642
ENE	.03698	.09312	.00000	.00000	.00000	.00000	.13010
E	.01448	.00733	.00874	.00000	.00000	.00000	.03055
ESE	.03112	.00000	.00000	.00000	.00000	.00000	.03112
SE	.00000	.00000	.00000	.00000	.00000	.00000	.00000
SSE	.01491	.00716	.00000	.00000	.00000	.00000	.02207
S	.01491	.01465	.00000	.00000	.00000	.00000	.02956
SSW	.05342	.02224	.00000	.00000	.00000	.00000	.07566
SW	.05870	.06569	.00874	.00000	.00000	.00000	.13313
WSW	.03834	.09571	.00874	.00000	.00000	.00000	.14279
W	.02224	.03214	.00000	.00000	.00000	.00000	.05438
WNW	.00716	.00874	.00000	.00000	.00000	.00000	.01590
NW	.01448	.01590	.02396	.00000	.00000	.00000	.05434
NNW	.02940	.01491	.00733	.00000	.00000	.00000	.05164
Total	.35046	.58487	.06467	.00000	.00000	.00000	1.0000
Class C frequency 0.05328							
N	.02347	.05861	.03367	.00000	.00000	.00000	.11575
NNE	.03827	.02822	.00000	.00000	.00000	.00000	.06649
NE	.04506	.03164	.00000	.00000	.00000	.00000	.07670
ENE	.10394	.07071	.00000	.00000	.00000	.00000	.17465
E	.06365	.01713	.00603	.00000	.00000	.00000	.08681
ESE	.01576	.00000	.00000	.00000	.00000	.00000	.01576
SE	.00000	.00000	.00000	.00000	.00000	.00000	.00000
SSE	.00041	.00494	.00000	.00000	.00000	.00000	.00535
S	.00000	.01517	.00000	.00000	.00000	.00000	.01517
SSW	.01094	.03688	.00000	.00000	.00000	.00000	.04782
SW	.03700	.11640	.00603	.00000	.00000	.00000	.15943
WSW	.01012	.03360	.00000	.00000	.00000	.00000	.04372
W	.01547	.00603	.00000	.00000	.00000	.00000	.02150
WNW	.02160	.03426	.00603	.00000	.00000	.00000	.06189
NW	.00576	.02109	.03301	.00000	.00000	.00000	.05986
NNW	.00618	.04291	.00000	.00000	.00000	.00000	.04909
Total	.39762	.51759	.08478	.00000	.00000	.00000	1.0000
Class D frequency 0.28077							
N	.02463	.05261	.00428	.00000	.00000	.00000	.08152
NNE	.04829	.04137	.00114	.00000	.00000	.00000	.09080
NE	.04125	.05253	.00094	.00000	.00000	.00000	.09472
ENE	.04943	.05502	.00114	.00000	.00000	.00000	.10559
E	.02174	.01203	.00000	.00000	.00000	.00000	.03377
ESE	.01350	.00114	.00000	.00000	.00000	.00000	.01464
SE	.00625	.00094	.00000	.00000	.00000	.00000	.00719
SSE	.00891	.00096	.00000	.00000	.00000	.00000	.00987
S	.00670	.00750	.00000	.00000	.00000	.00000	.01420
SSW	.03508	.03876	.00000	.00000	.00000	.00000	.07384
SW	.07261	.04143	.01144	.00000	.00000	.00000	.12548
WSW	.07504	.02816	.00000	.00000	.00000	.00000	.10320
W	.05317	.01294	.00114	.00000	.00000	.00000	.06725
WNW	.02116	.04650	.00000	.00000	.00000	.00000	.06766
NW	.02222	.01336	.00312	.00000	.00000	.00000	.03870
NNW	.02383	.03838	.00933	.00000	.00000	.00000	.07154
Total	.52383	.44362	.03255	.00000	.00000	.00000	1.0000
Class E frequency 0.23511							
N	.03973	.00721	.00000	.00000	.00000	.00000	.04694
NNE	.03023	.00229	.00000	.00000	.00000	.00000	.03252
NE	.03389	.01171	.00000	.00000	.00000	.00000	.04560
ENE	.06750	.00995	.00000	.00000	.00000	.00000	.07745
E	.03068	.00137	.00000	.00000	.00000	.00000	.03205
ESE	.00653	.00000	.00000	.00000	.00000	.00000	.00653
SE	.01463	.00373	.00000	.00000	.00000	.00000	.01836
SSE	.02088	.00000	.00000	.00000	.00000	.00000	.02088
S	.02668	.00000	.00000	.00000	.00000	.00000	.02668
SSW	.06772	.01000	.00000	.00000	.00000	.00000	.07772
SW	.14169	.02030	.00000	.00000	.00000	.00000	.16199
WSW	.13562	.00991	.00000	.00000	.00000	.00000	.14553
W	.09749	.00873	.00000	.00000	.00000	.00000	.10622
WNW	.06757	.00115	.00000	.00000	.00000	.00000	.06872
NW	.05301	.01251	.00000	.00000	.00000	.00000	.06552
NNW	.05989	.00624	.00115	.00000	.00000	.00000	.06728
Total	.89376	.10509	.00115	.00000	.00000	.00000	1.0000
Class F frequency 0.32246							
N	.00830	.00000	.00000	.00000	.00000	.00000	.00830
NNE	.00731	.00000	.00000	.00000	.00000	.00000	.00731
NE	.00830	.00000	.00000	.00000	.00000	.00000	.00830
ENE	.02278	.00000	.00000	.00000	.00000	.00000	.02278
E	.02627	.00000	.00000	.00000	.00000	.00000	.02627
ESE	.02538	.00000	.00000	.00000	.00000	.00000	.02538
SE	.01095	.00000	.00000	.00000	.00000	.00000	.01095
SSE	.01268	.00000	.00000	.00000	.00000	.00000	.01268
S	.01401	.00000	.00000	.00000	.00000	.00000	.01401
SSW	.04797	.00272	.00000	.00000	.00000	.00000	.05069
SW	.08832	.00272	.00000	.00000	.00000	.00000	.09104
WSW	.13883	.00000	.00000	.00000	.00000	.00000	.13883
W	.14738	.00000	.00000	.00000	.00000	.00000	.14738
WNW	.20235	.00000	.00000	.00000	.00000	.00000	.20235
NW	.15909	.00000	.00000	.00000	.00000	.00000	.15909
NNW	.07190	.00272	.00000	.00000	.00000	.00000	.07462
Total	.99184	.00816	.00000	.00000	.00000	.00000	1.0000

Table ES–9. Composite Meteorological Frequencies for FMPC, September 1987–1991

	Wind speed range (m s^{-1})						
	0–2	2–4	4–6	6–8	8–10	>10	Total
Class A frequency 0.11143							
N	.01293	.00646	.01879	.00000	.00000	.00000	.03818
NNE	.00674	.02250	.00000	.00000	.00338	.00000	.03262
NE	.02978	.03833	.00000	.00000	.00000	.00000	.06811
ENE	.06440	.09554	.00313	.00000	.00000	.00000	.16307
E	.03234	.04157	.00000	.00000	.00000	.00316	.07707
ESE	.02254	.00985	.00000	.00000	.00000	.00000	.03239
SE	.01293	.00646	.00000	.00000	.00000	.00316	.02255
SSE	.02250	.00000	.00000	.00316	.00000	.00000	.02566
S	.02122	.00000	.00000	.00000	.00000	.00000	.02122
SSW	.01293	.06088	.00338	.00000	.00000	.00000	.07719
SW	.05147	.04196	.00646	.00000	.00000	.00000	.09989
WSW	.02586	.05486	.01910	.00000	.00000	.00000	.09982
W	.02588	.05208	.00000	.00000	.00000	.00000	.07796
WNW	.03233	.05799	.00000	.00000	.00000	.00000	.09032
NW	.02586	.02870	.00000	.00000	.00000	.00000	.05456
NNW	.01293	.00646	.00000	.00000	.00000	.00000	.01939
Total	.41267		.05086	.00316	.00338	.00631	1.0000
Class B frequency 0.04054							
N	.00000	.00867	.03439	.00860	.00000	.00000	.05166
NNE	.00000	.00000	.00860	.00000	.00000	.00000	.00860
NE	.01719	.01787	.00000	.00000	.00000	.00000	.03506
ENE	.02647	.15625	.00928	.00000	.00000	.00000	.19200
E	.02723	.06179	.00000	.00000	.00000	.00000	.08902
ESE	.00860	.02717	.00000	.00000	.00000	.00000	.03577
SE	.00000	.00000	.00000	.00000	.00000	.00000	.00000
SSE	.00928	.00000	.00000	.00000	.00000	.00000	.00928
S	.00928	.00860	.00000	.00000	.00000	.00000	.01788
SSW	.03356	.12316	.02663	.00000	.00000	.00000	.18335
SW	.01351	.06227	.00928	.00000	.00000	.00000	.08506
WSW	.00928	.03644	.01795	.00000	.00000	.00000	.06367
W	.03132	.04497	.00000	.00000	.00000	.00000	.07629
WNW	.00860	.02717	.00000	.00000	.00000	.00000	.03577
NW	.04572	.02717	.00928	.00000	.00000	.00000	.08217
NNW	.01719	.00867	.00860	.00000	.00000	.00000	.03446
Total	.25721	.61020	.12400	.00860	.00000	.00000	1.0000
Class C frequency 0.05188							
N	.01555	.02022	.00000	.00000	.00000	.00000	.03577
NNE	.01511	.04727	.00678	.00000	.00000	.00000	.06916
NE	.01674	.06131	.00000	.00000	.00000	.00000	.07805
ENE	.04859	.04143	.00725	.00000	.00000	.00000	.09727
E	.02746	.02080	.00000	.00000	.00000	.00000	.04826
ESE	.04148	.01449	.00000	.00000	.00000	.00000	.05597
SE	.01447	.01355	.00000	.00000	.00000	.00000	.02802
SSE	.00000	.02074	.00000	.00000	.00000	.00000	.02074
S	.00780	.01344	.00000	.00000	.00000	.00000	.02124
SSW	.02857	.06216	.00000	.00000	.00000	.00000	.09073
SW	.06985	.02741	.01449	.00000	.00000	.00000	.11175
WSW	.03479	.06178	.02080	.00000	.00000	.00000	.11737
W	.00833	.04822	.00000	.00000	.00000	.00000	.05655
WNW	.01560	.05686	.00000	.00000	.00000	.00000	.07246
NW	.00727	.02069	.02033	.00000	.00000	.00000	.04829
NNW	.01350	.02033	.01449	.00000	.00000	.00000	.04832
Total	.36513	.55072	.08415	.00000	.00000	.00000	1.0000
Class D frequency 0.23739							
N	.01994	.03673	.00589	.00734	.00000	.00000	.06990
NNE	.03719	.04408	.00000	.00000	.00000	.00000	.08127
NE	.03698	.04269	.00000	.00000	.00000	.00000	.07967
ENE	.03835	.04330	.00148	.00000	.00000	.00000	.08313
E	.02135	.01046	.00000	.00000	.00000	.00000	.03181
ESE	.02450	.00148	.00000	.00000	.00000	.00000	.02598
SE	.01658	.00444	.00000	.00000	.00000	.00000	.02102
SSE	.01869	.00148	.00148	.00000	.00000	.00000	.02165
S	.02633	.01645	.00444	.00000	.00000	.00000	.04722
SSW	.06670	.06006	.00296	.00000	.00000	.00000	.12972
SW	.06121	.02396	.00000	.00000	.00000	.00000	.08517
WSW	.03619	.02539	.00603	.00000	.00000	.00000	.06761
W	.03649	.04146	.00307	.00000	.00000	.00000	.08102
WNW	.04647	.01993	.00000	.00000	.00000	.00000	.06640
NW	.02426	.01822	.00907	.00000	.00000	.00000	.05155
NNW	.02744	.01623	.01321	.00000	.00000	.00000	.05688
Total	.53868	.40636	.04763	.00734	.00000	.00000	1.0000
Class E frequency 0.20719							
N	.03231	.01542	.00000	.00000	.00000	.00000	.04773
NNE	.02941	.01036	.00000	.00000	.00000	.00000	.03977
NE	.03103	.00871	.00000	.00000	.00000	.00000	.03974
ENE	.06642	.02079	.00000	.00000	.00000	.00000	.08721
E	.04349	.00170	.00000	.00000	.00000	.00000	.04519
ESE	.02440	.00000	.00000	.00000	.00000	.00000	.02440
SE	.03364	.00000	.00000	.00000	.00000	.00000	.03364
SSE	.02699	.00363	.00000	.00000	.00000	.00000	.03062
S	.03232	.01246	.00521	.00000	.00000	.00000	.04999
SSW	.07017	.01545	.00509	.00000	.00000	.00000	.09071
SW	.09857	.03617	.00339	.00000	.00000	.00000	.13813
WSW	.11094	.01184	.00000	.00000	.00000	.00000	.12278
W	.07191	.01727	.00000	.00000	.00000	.00000	.08918
WNW	.04340	.00673	.00000	.00000	.00000	.00000	.05013
NW	.04655	.00531	.00000	.00000	.00000	.00000	.05186
NNW	.04844	.00701	.00350	.00000	.00000	.00000	.05895
Total	.80997	.17284	.01719	.00000	.00000	.00000	1.0000
Class F frequency 0.35158							
N	.01441	.00000	.00000	.00000	.00107	.00100	.01648
NNE	.00639	.00100	.00000	.00000	.00000	.00000	.00739
NE	.02295	.00000	.00000	.00000	.00000	.00000	.02295
ENE	.02795	.00000	.00000	.00000	.00000	.00000	.02795
E	.04829	.00000	.00000	.00000	.00000	.00000	.04829
ESE	.03007	.00000	.00000	.00000	.00000	.00100	.03107
SE	.01242	.00000	.00000	.00000	.00000	.00000	.01242
SSE	.01310	.00000	.00000	.00000	.00000	.00000	.01310
S	.02960	.00000	.00000	.00000	.00000	.00000	.02960
SSW	.04922	.00000	.00000	.00000	.00000	.00000	.04922
SW	.07925	.00000	.00000	.00000	.00000	.00000	.07925
WSW	.10946	.00000	.00000	.00000	.00000	.00000	.10946
W	.13986	.00000	.00000	.00000	.00000	.00000	.13986
WNW	.19529	.00107	.00000	.00000	.00000	.00000	.19636
NW	.15318	.00098	.00000	.00000	.00000	.00000	.15416
NNW	.06245	.00000	.00000	.00000	.00000	.00000	.06245
Total	.99388	.00305	.00000	.00000	.00107	.00200	1.0000

Table ES–10. Composite Meteorological Frequencies for FMPC, October 1987–1991

	Wind speed range (m s^{-1})						
	0–2	2–4	4–6	6–8	8–10	>10	Total
Class A frequency 0.09828							
N	.00863	.01928	.03232	.00000	.00000	.00000	.06023
NNE	.02303	.00266	.00000	.00000	.00000	.00000	.02569
NE	.02037	.00554	.00000	.00000	.00000	.00000	.02591
ENE	.01484	.04118	.00554	.00000	.00000	.00000	.06156
E	.01174	.00000	.00000	.00000	.00000	.00000	.01174
ESE	.03144	.00000	.00000	.00000	.00000	.00000	.03144
SE	.01174	.00000	.00000	.00000	.00000	.00000	.01174
SSE	.01107	.01240	.00000	.00000	.00000	.00000	.02347
S	.01196	.04805	.01085	.00000	.00000	.00000	.07086
SSW	.01572	.14188	.04429	.00000	.00000	.00000	.20189
SW	.02723	.08926	.03436	.00000	.00000	.00000	.15085
WSW	.03742	.03037	.00000	.00000	.00000	.00000	.06779
W	.01240	.03277	.01396	.00000	.00000	.00000	.05913
WNW	.01178	.03166	.01950	.00000	.00000	.00000	.06294
NW	.02582	.03615	.00000	.00000	.00000	.00000	.06197
NNW	.02393	.02605	.02283	.00000	.00000	.00000	.07281
Total	.29910	.51724	.18365	.00000	.00000	.00000	1.0000
Class B frequency 0.03761							
N	.00231	.04967	.01620	.00000	.00000	.00000	.06818
NNE	.00000	.00000	.02288	.00000	.00000	.00000	.02288
NE	.01620	.00000	.00000	.00000	.00000	.00000	.01620
ENE	.01620	.00753	.00000	.00000	.00000	.00000	.02373
E	.01620	.00000	.00000	.00000	.00000	.00000	.01620
ESE	.00000	.00000	.00000	.00000	.00000	.00000	.00000
SE	.02429	.00000	.00000	.00000	.00000	.00000	.02429
SSE	.01144	.00000	.00000	.00000	.00000	.00000	.01144
S	.01967	.02140	.01620	.00000	.00000	.00000	.05727
SSW	.02823	.05722	.05220	.00000	.00000	.00000	.13765
SW	.01507	.03795	.03431	.00000	.00000	.00000	.08733
WSW	.03826	.01507	.01144	.01144	.00000	.00000	.07621
W	.03419	.03344	.01507	.00000	.00000	.00000	.08270
WNW	.00116	.03735	.02288	.00000	.00000	.00000	.06139
NW	.02017	.06978	.05329	.00000	.00000	.00000	.14324
NNW	.03354	.12327	.01448	.00000	.00000	.00000	.17129
Total	.27693	.45270	.25893	.01144	.00000	.00000	1.0000
Class C frequency 0.04527							
N	.01580	.02691	.01252	.00000	.00000	.00000	.05523
NNE	.00000	.01901	.00000	.00000	.00000	.00000	.01901
NE	.00577	.01576	.00000	.00000	.00000	.00000	.02153
ENE	.02478	.04680	.00000	.00000	.00000	.00000	.07158
E	.01203	.00000	.00000	.00000	.00000	.00000	.01203
ESE	.00950	.00000	.00000	.00000	.00000	.00000	.00950
SE	.01345	.00000	.00000	.00000	.00000	.00000	.01345
SSE	.03317	.01345	.00000	.00000	.00000	.00000	.04662
S	.04125	.02355	.00000	.00000	.00000	.00000	.06480
SSW	.01829	.09658	.02601	.00000	.00000	.00000	.14088
SW	.03662	.05924	.01576	.00950	.00000	.00000	.12112
WSW	.02202	.03718	.03317	.00950	.00000	.00000	.10187
W	.02778	.00577	.03770	.00000	.00000	.00000	.07125
WNW	.01527	.03728	.02784	.00626	.00000	.00000	.08665
NW	.02925	.03246	.04103	.00000	.00000	.00000	.10274
NNW	.03321	.02851	.00000	.00000	.00000	.00000	.06172
Total	.33819	.44251	.19403	.02527	.00000	.00000	1.0000
Class D frequency 0.24603							
N	.01753	.06999	.02206	.00000	.00000	.00000	.10958
NNE	.01981	.01786	.01555	.00000	.00000	.00000	.05322
NE	.01805	.01281	.00000	.00000	.00000	.00000	.03086
ENE	.03776	.01544	.00175	.00000	.00000	.00000	.05495
E	.02898	.00115	.00000	.00000	.00000	.00000	.03013
ESE	.01007	.00000	.00000	.00000	.00000	.00000	.01007
SE	.01242	.00348	.00000	.00000	.00000	.00000	.01590
SSE	.01531	.00685	.00000	.00000	.00000	.00000	.02216
S	.02632	.02789	.01592	.00000	.00000	.00000	.07013
SSW	.03776	.07890	.01704	.00000	.00000	.00000	.13370
SW	.04223	.05713	.00976	.00175	.00000	.00000	.11087
WSW	.03221	.03480	.00828	.00115	.00000	.00000	.07644
W	.02744	.03173	.01080	.00000	.00000	.00000	.06997
WNW	.01193	.04472	.01436	.00000	.00000	.00000	.07101
NW	.02011	.02189	.00862	.00115	.00000	.00000	.05177
NNW	.02407	.04312	.02202	.00000	.00000	.00000	.08921
Total	.38201	.46777	.14617	.00405	.00000	.00000	1.0000
Class E frequency 0.19388							
N	.01996	.02011	.00000	.00000	.00000	.00000	.04007
NNE	.01174	.00812	.00147	.00294	.00000	.00000	.02427
NE	.00708	.00222	.00000	.00000	.00000	.00000	.00930
ENE	.04039	.00281	.00000	.00000	.00000	.00000	.04320
E	.02748	.00000	.00000	.00000	.00000	.00000	.02748
ESE	.01144	.00000	.00000	.00000	.00000	.00000	.01144
SE	.00663	.00000	.00000	.00000	.00000	.00000	.00663
SSE	.01254	.00000	.00000	.00000	.00000	.00000	.01254
S	.04592	.00872	.00000	.00000	.00000	.00000	.05464
SSW	.04738	.06964	.00000	.00000	.00000	.00000	.11702
SW	.12014	.09180	.01164	.00000	.00000	.00000	.22358
WSW	.08933	.01992	.00514	.00000	.00000	.00000	.11439
W	.07042	.02896	.00314	.00000	.00000	.00000	.10252
WNW	.04570	.03972	.00293	.00000	.00000	.00000	.08835
NW	.04180	.01019	.00591	.00000	.00000	.00000	.05790
NNW	.04727	.01718	.00222	.00000	.00000	.00000	.06667
Total	.64522	.31938	.03246	.00294	.00000	.00000	1.0000
Class F frequency 0.37893							
N	.01861	.00000	.00000	.00000	.00000	.00000	.01861
NNE	.00737	.00000	.00000	.00000	.00000	.00000	.00737
NE	.00772	.00000	.00000	.00000	.00000	.00000	.00772
ENE	.02665	.00000	.00000	.00000	.00000	.00000	.02665
E	.03766	.00000	.00000	.00000	.00000	.00000	.03766
ESE	.01196	.00000	.00000	.00000	.00000	.00000	.01196
SE	.00891	.00000	.00000	.00000	.00000	.00000	.00891
SSE	.01451	.00114	.00000	.00000	.00000	.00000	.01565
S	.02990	.00114	.00000	.00000	.00000	.00000	.03104
SSW	.05600	.00227	.00000	.00000	.00000	.00000	.05827
SW	.10677	.00114	.00000	.00000	.00000	.00000	.10791
WSW	.11151	.00000	.00000	.00000	.00000	.00000	.11151
W	.13679	.00075	.00000	.00000	.00000	.00000	.13754
WNW	.16955	.00000	.00000	.00000	.00000	.00000	.16955
NW	.15014	.00000	.00000	.00000	.00000	.00000	.15014
NNW	.09679	.00274	.00000	.00000	.00000	.00000	.09953
Total	.99083	.00917	.00000	.00000	.00000	.00000	1.0000

Table ES–11. Composite Meteorological Frequencies for FMPC, November 1987–1991

	Wind speed range (m s^{-1})						
	0–2	2–4	4–6	6–8	8–10	>10	Total
Class A frequency 0.03397							
N	.00000	.00000	.00000	.00000	.00000	.00000	.00000
NNE	.00000	.03271	.00000	.00000	.00000	.00000	.03271
NE	.00801	.01669	.00000	.00000	.00000	.00000	.02470
ENE	.01100	.00801	.00000	.00000	.00000	.00000	.01901
E	.00000	.04371	.00000	.00000	.00000	.00000	.04371
ESE	.00000	.00000	.00000	.00000	.00000	.00000	.00000
SE	.00000	.00000	.00000	.00000	.00000	.00000	.00000
SSE	.00000	.00000	.00000	.00000	.00000	.00000	.00000
S	.00000	.01653	.00000	.00000	.00000	.00000	.01653
SSW	.02470	.09941	.06324	.00000	.00000	.00000	.18735
SW	.00000	.08070	.06868	.00000	.00000	.00000	.14938
WSW	.00000	.17125	.03313	.00000	.00000	.00000	.20438
W	.00000	.16515	.06349	.00000	.00000	.00000	.22864
WNW	.00801	.01659	.00832	.00000	.00000	.00000	.03292
NW	.00000	.01901	.02496	.00000	.00000	.00000	.04397
NNW	.00000	.01669	.00000	.00000	.00000	.00000	.01669
Total	.05172	.68646	.26182	.00000	.00000	.00000	1.0000
Class B frequency 0.02762							
N	.00000	.03081	.00000	.00000	.00000	.00000	.03081
NNE	.00000	.02052	.00000	.00000	.00000	.00000	.02052
NE	.00000	.00000	.00000	.00000	.00000	.00000	.00000
ENE	.00000	.00000	.00000	.00000	.00000	.00000	.00000
E	.02705	.00985	.00000	.00000	.00000	.00000	.03690
ESE	.01353	.00985	.00000	.00000	.00000	.00000	.02338
SE	.01353	.00000	.00000	.00000	.00000	.00000	.01353
SSE	.00000	.00000	.00000	.00000	.00000	.00000	.00000
S	.00000	.03053	.00000	.00000	.00000	.00000	.03053
SSW	.00000	.08873	.06422	.00000	.00000	.00000	.15295
SW	.00000	.10880	.06524	.00000	.00000	.00000	.17404
WSW	.01020	.11261	.11232	.00000	.00000	.00000	.23513
W	.00000	.08442	.04093	.00000	.00000	.00000	.12535
WNW	.00000	.02401	.02068	.00000	.00000	.00000	.04469
NW	.01048	.04058	.00000	.00000	.00000	.00000	.05106
NNW	.00000	.06110	.00000	.00000	.00000	.00000	.06110
Total	.07479	.62182	.30339	.00000	.00000	.00000	1.0000
Class C frequency 0.03252							
N	.00000	.03417	.00890	.00000	.00000	.00000	.04307
NNE	.00000	.02580	.00890	.00000	.00000	.00000	.03470
NE	.00000	.00000	.00000	.00000	.00000	.00000	.00000
ENE	.00837	.00837	.00000	.00000	.00000	.00000	.01674
E	.03165	.00837	.00000	.00000	.00000	.00000	.04002
ESE	.00000	.00867	.00000	.00000	.00000	.00000	.00867
SE	.03188	.00890	.00000	.00000	.00000	.00000	.04078
SSE	.01149	.03188	.00890	.00000	.00000	.00000	.05227
S	.00000	.04636	.01781	.00000	.00000	.00000	.06417
SSW	.00000	.03782	.03463	.00000	.00000	.00000	.07245
SW	.03490	.07521	.02634	.00000	.00000	.00000	.13645
WSW	.02876	.08928	.05242	.00000	.00000	.00000	.17046
W	.01986	.06924	.01149	.00000	.00000	.00000	.10059
WNW	.01743	.06342	.00869	.00000	.00000	.00000	.08954
NW	.01149	.05174	.01781	.00000	.00000	.00000	.08104
NNW	.01149	.03756	.00000	.00000	.00000	.00000	.04905
Total	.20732	.59679	.19589	.00000	.00000	.00000	1.0000
Class D frequency 0.32610							
N	.01126	.03574	.01046	.00000	.00000	.00000	.05746
NNE	.00979	.02630	.01486	.00178	.00000	.00000	.05273
NE	.02439	.02603	.00438	.00089	.00000	.00000	.05569
ENE	.02366	.04878	.00000	.00000	.00000	.00000	.07244
E	.01809	.01068	.00000	.00000	.00000	.00000	.02877
ESE	.00751	.00262	.00000	.00000	.00000	.00000	.01013
SE	.00600	.01116	.00000	.00000	.00000	.00000	.01716
SSE	.00704	.01977	.00520	.00000	.00000	.00000	.03201
S	.00621	.02532	.01722	.00115	.00000	.00000	.04990
SSW	.01773	.05255	.04260	.00175	.00000	.00000	.11463
SW	.02888	.06930	.02490	.00089	.00000	.00000	.12397
WSW	.02652	.04121	.02640	.00201	.00000	.00000	.09614
W	.01907	.04882	.03272	.00000	.00000	.00000	.10061
WNW	.02212	.03755	.01407	.00175	.00000	.00000	.07549
NW	.02078	.02589	.01942	.00000	.00000	.00000	.06609
NNW	.01003	.03501	.00173	.00000	.00000	.00000	.04677
Total	.25907	.51674	.21399	.01021	.00000	.00000	1.0000
Class E frequency 0.35981							
N	.00792	.00732	.00078	.00080	.00000	.00000	.01682
NNE	.00310	.00079	.00000	.00000	.00000	.00000	.00389
NE	.01031	.00237	.00000	.00000	.00000	.00000	.01268
ENE	.02859	.01561	.00000	.00000	.00000	.00000	.04420
E	.03971	.00780	.00000	.00000	.00000	.00000	.04751
ESE	.01356	.00699	.00000	.00000	.00000	.00000	.02055
SE	.01069	.00630	.00236	.00000	.00000	.00000	.01935
SSE	.01197	.01507	.00549	.00000	.00000	.00000	.03253
S	.02231	.06468	.01714	.00881	.00000	.00000	.11294
SSW	.03102	.09179	.03151	.00314	.00078	.00000	.15824
SW	.06054	.09179	.01745	.00000	.00000	.00000	.16978
WSW	.05285	.04885	.01015	.00544	.00000	.00000	.11729
W	.02959	.04169	.01646	.00000	.00000	.00000	.08774
WNW	.02879	.02667	.01046	.00236	.00000	.00000	.06828
NW	.04023	.01700	.00500	.00000	.00000	.00000	.06223
NNW	.01503	.00675	.00420	.00000	.00000	.00000	.02598
Total	.40618	.45148	.12101	.02055	.00078	.00000	1.0000
Class F frequency 0.21998							
N	.02429	.00000	.00000	.00000	.00000	.00000	.02429
NNE	.01571	.00000	.00000	.00000	.00000	.00000	.01571
NE	.02430	.00000	.00000	.00000	.00000	.00000	.02430
ENE	.06304	.00643	.00000	.00000	.00000	.00000	.06947
E	.08156	.00000	.00000	.00000	.00000	.00000	.08156
ESE	.04974	.00000	.00000	.00000	.00000	.00000	.04974
SE	.01364	.00128	.00000	.00000	.00000	.00000	.01492
SSE	.00720	.00000	.00000	.00000	.00000	.00000	.00720
S	.02420	.00000	.00000	.00000	.00000	.00000	.02420
SSW	.04700	.00129	.00000	.00000	.00000	.00000	.04829
SW	.04975	.00774	.00000	.00000	.00000	.00000	.05749
WSW	.10761	.00516	.00000	.00000	.00000	.00000	.11277
W	.13061	.00385	.00000	.00000	.00000	.00000	.13446
WNW	.13415	.00000	.00000	.00000	.00000	.00000	.13415
NW	.13776	.00000	.00000	.00000	.00000	.00000	.13776
NNW	.06369	.00000	.00000	.00000	.00000	.00000	.06369
Total	.97426	.02574	.00000	.00000	.00000	.00000	1.0000

Table ES–12. Composite Meteorological Frequencies for FMPC, December 1987–1991

	Wind speed range (m s^{-1})						
	0–2	2–4	4–6	6–8	8–10	>10	Total
Class A frequency 0.02294							
N	.00000	.00000	.00000	.00000	.00000	.00000	.00000
NNE	.00000	.00000	.00000	.00000	.00000	.00000	.00000
NE	.00000	.00000	.00000	.00000	.00000	.00000	.00000
ENE	.00000	.00000	.00000	.00000	.00000	.00000	.00000
E	.00000	.00000	.00000	.00000	.00000	.00000	.00000
ESE	.00000	.01239	.00000	.00000	.00000	.00000	.01239
SE	.00000	.01272	.00000	.00000	.00000	.00000	.01272
SSE	.00000	.00000	.00000	.00000	.00000	.00000	.00000
S	.00000	.01272	.00000	.00000	.00000	.00000	.01272
SSW	.01272	.21467	.01180	.00000	.00000	.00000	.23919
SW	.01239	.13602	.08437	.00000	.00000	.00000	.23278
WSW	.08876	.08845	.04837	.00000	.00000	.00000	.22558
W	.00000	.06459	.07672	.01272	.00000	.00000	.15403
WNW	.00000	.04812	.03830	.00000	.00000	.00000	.08642
NW	.00000	.01239	.01180	.00000	.00000	.00000	.02419
NNW	.00000	.00000	.00000	.00000	.00000	.00000	.00000
Total	.11386	.60206	.27136	.01272	.00000	.00000	1.0000
Class B frequency 0.01564							
N	.00000	.00000	.00000	.00000	.00000	.00000	.00000
NNE	.00000	.00000	.00000	.00000	.00000	.00000	.00000
NE	.00000	.00000	.00000	.00000	.00000	.00000	.00000
ENE	.00000	.00000	.00000	.00000	.00000	.00000	.00000
E	.00000	.01817	.00000	.00000	.00000	.00000	.01817
ESE	.00000	.03682	.00000	.00000	.00000	.00000	.03682
SE	.00000	.01865	.00000	.00000	.00000	.00000	.01865
SSE	.00000	.00000	.00000	.00000	.00000	.00000	.00000
S	.00000	.01865	.00000	.00000	.00000	.00000	.01865
SSW	.01817	.11153	.07095	.00000	.00000	.00000	.20065
SW	.05703	.08960	.05453	.00000	.00000	.00000	.20116
WSW	.03633	.05291	.01731	.00000	.00000	.00000	.10655
W	.01817	.05466	.11115	.00000	.00000	.00000	.18398
WNW	.00000	.07009	.05193	.00000	.00000	.00000	.12202
NW	.00000	.05450	.00000	.00000	.00000	.00000	.05450
NNW	.00000	.00000	.03886	.00000	.00000	.00000	.03886
Total	.12969	.52558	.34473	.00000	.00000	.00000	1.0000
Class C frequency 0.02580							
N	.00000	.01101	.00000	.00000	.00000	.00000	.01101
NNE	.01101	.00000	.00000	.00000	.00000	.00000	.01101
NE	.00000	.01155	.00000	.00000	.00000	.00000	.01155
ENE	.02203	.00000	.00000	.00000	.00000	.00000	.02203
E	.03334	.00000	.00000	.00000	.00000	.00000	.03334
ESE	.00000	.02232	.00000	.00000	.00000	.00000	.02232
SE	.00000	.00000	.00000	.00000	.00000	.00000	.00000
SSE	.00000	.01050	.00000	.00000	.00000	.00000	.01050
S	.00000	.02099	.00000	.00000	.00000	.00000	.02099
SSW	.00000	.10160	.04250	.00000	.00000	.00000	.14410
SW	.02232	.10938	.02099	.00000	.00000	.00000	.15269
WSW	.03388	.08917	.04205	.00000	.00000	.00000	.16510
W	.02203	.05442	.07690	.02188	.00000	.00000	.17523
WNW	.02188	.02205	.00000	.00000	.00000	.00000	.04393
NW	.01131	.05314	.01101	.00000	.00000	.00000	.07546
NNW	.04383	.02203	.03487	.00000	.00000	.00000	.10073
Total	.22163	.52817	.22832	.02188	.00000	.00000	1.0000
Class D frequency 0.41132							
N	.01100	.02701	.00952	.00000	.00000	.00000	.04753
NNE	.01219	.03568	.00264	.00000	.00000	.00000	.05051
NE	.01926	.02927	.00205	.00000	.00000	.00000	.05058
ENE	.03492	.04533	.01862	.00000	.00000	.00000	.09887
E	.01299	.01657	.00401	.00000	.00000	.00000	.03357
ESE	.01384	.00527	.00000	.00000	.00000	.00000	.01911
SE	.00771	.00201	.00000	.00000	.00000	.00000	.00972
SSE	.00360	.00533	.00000	.00000	.00000	.00000	.00893
S	.00723	.01855	.00352	.00138	.00000	.00000	.03068
SSW	.02079	.03075	.02417	.00788	.00000	.00000	.08359
SW	.02920	.05371	.01503	.00198	.00133	.00133	.10258
WSW	.02449	.02986	.01377	.00659	.00133	.00066	.07670
W	.02536	.06514	.04623	.00327	.00000	.00000	.14000
WNW	.01640	.05277	.02343	.00071	.00000	.00000	.09331
NW	.01576	.03372	.02233	.00145	.00000	.00000	.07326
NNW	.02225	.04548	.01270	.00066	.00000	.00000	.08109
Total	.27699	.49645	.19800	.02392	.00265	.00199	1.0000
Class E frequency 0.34892							
N	.00705	.00809	.00155	.00000	.00000	.00000	.01669
NNE	.00679	.00953	.00000	.00000	.00000	.00000	.01632
NE	.01113	.00563	.00000	.00000	.00000	.00000	.01676
ENE	.05755	.01434	.00000	.00000	.00000	.00000	.07189
E	.03255	.00462	.00000	.00000	.00000	.00000	.03717
ESE	.01513	.00311	.00000	.00000	.00000	.00000	.01824
SE	.01207	.00787	.00000	.00000	.00000	.00000	.01994
SSE	.01990	.00696	.00156	.00000	.00000	.00000	.02842
S	.02593	.02060	.00696	.00000	.00000	.00000	.05349
SSW	.04333	.06076	.02381	.00233	.00078	.00000	.13101
SW	.07945	.09947	.02109	.00078	.00078	.00000	.20157
WSW	.07763	.03472	.00548	.00156	.00000	.00000	.11939
W	.05145	.05679	.00962	.00000	.00000	.00000	.11786
WNW	.02938	.03538	.00813	.00000	.00000	.00000	.07289
NW	.02553	.01803	.00248	.00000	.00000	.00000	.04604
NNW	.02135	.00848	.00163	.00085	.00000	.00000	.03231
Total	.51620	.39439	.08233	.00552	.00156	.00000	1.0000
Class F frequency 0.17537							
N	.01781	.00000	.00000	.00000	.00000	.00000	.01781
NNE	.02630	.00000	.00000	.00000	.00000	.00000	.02630
NE	.02503	.00000	.00000	.00000	.00000	.00000	.02503
ENE	.04240	.00156	.00000	.00000	.00000	.00000	.04396
E	.08539	.00000	.00000	.00000	.00000	.00000	.08539
ESE	.02996	.00000	.00000	.00000	.00000	.00000	.02996
SE	.01629	.00000	.00000	.00000	.00000	.00000	.01629
SSE	.02404	.00000	.00000	.00000	.00000	.00000	.02404
S	.01394	.00000	.00000	.00000	.00000	.00000	.01394
SSW	.05056	.00155	.00000	.00000	.00000	.00000	.05211
SW	.11739	.02474	.00000	.00000	.00000	.00000	.14213
WSW	.13775	.00780	.00000	.00000	.00000	.00000	.14555
W	.11920	.00155	.00000	.00000	.00000	.00000	.12075
WNW	.12255	.00000	.00000	.00000	.00000	.00000	.12255
NW	.09125	.00000	.00000	.00000	.00000	.00000	.09125
NNW	.04142	.00155	.00000	.00000	.00000	.00000	.04297
Total	.96127	.03873	.00000	.00000	.00000	.00000	1.0000

Table ES–13. Composite Meteorological Frequencies for FMPC, Annual 1987–1991

	Wind speed range (m s^{-1})						
	0–2	2–4	4–6	6–8	8–10	>10	Total
Class A frequency 0.06374							
N	.00548	.01482	.01201	.00000	.00000	.00000	.03231
NNE	.01088	.01509	.01007	.00122	.00039	.00000	.03765
NE	.01762	.03981	.00770	.00040	.00000	.00000	.06553
ENE	.03891	.05314	.00520	.00076	.00000	.00000	.09801
E	.02178	.01596	.00253	.00000	.00000	.00037	.04064
ESE	.01375	.00688	.00000	.00000	.00000	.00000	.02063
SE	.00655	.00266	.00000	.00000	.00000	.00037	.00958
SSE	.00969	.00368	.00073	.00037	.00000	.00000	.01447
S	.01113	.01689	.00216	.00000	.00000	.00000	.03018
SSW	.01794	.07121	.02186	.00000	.00000	.00000	.11101
SW	.03382	.06934	.03479	.00144	.00000	.00000	.13939
WSW	.03371	.07260	.01689	.00076	.00000	.00000	.12396
W	.01979	.07220	.03010	.00193	.00000	.00000	.12402
WNW	.01514	.03295	.01853	.00284	.00000	.00000	.06946
NW	.01352	.02184	.00831	.00000	.00000	.00000	.04367
NNW	.00874	.01790	.01203	.00037	.00000	.00045	.03949
Total	.27846	.52697	.18289	.01010	.00039	.00119	1.0000
Class B frequency 0.03104							
N	.00805	.03271	.00926	.00152	.00000	.00000	.05154
NNE	.00641	.01174	.01408	.00155	.00000	.00000	.03378
NE	.01023	.03650	.01330	.00000	.00000	.00000	.06003
ENE	.01626	.03749	.00680	.00165	.00000	.00000	.06220
E	.02043	.01399	.00392	.00000	.00000	.00000	.03834
ESE	.01107	.00770	.00000	.00000	.00000	.00000	.01877
SE	.00447	.00318	.00000	.00000	.00000	.00000	.00765
SSE	.01028	.00223	.00224	.00076	.00000	.00000	.01551
S	.01420	.01538	.00270	.00000	.00000	.00000	.03228
SSW	.02268	.06206	.02160	.00224	.00078	.00000	.10936
SW	.02935	.08052	.03092	.00237	.00000	.00000	.14316
WSW	.02726	.06730	.02381	.00115	.00000	.00000	.11952
W	.02246	.05246	.02933	.00076	.00000	.00000	.10501
WNW	.01431	.02885	.02122	.00155	.00000	.00000	.06593
NW	.01743	.03522	.02236	.00000	.00000	.00000	.07501
NNW	.01163	.03677	.01269	.00083	.00000	.00000	.06192
Total	.24650	.52410	.21422	.01440	.00078	.00000	1.0000
Class C frequency 0.04458							
N	.01227	.03159	.01054	.00218	.00000	.00000	.05658
NNE	.00980	.02674	.00873	.00054	.00000	.00000	.04581
NE	.01186	.03378	.01465	.00166	.00000	.00000	.06195
ENE	.03285	.03767	.00390	.00384	.00000	.00000	.07826
E	.02593	.01519	.00164	.00052	.00000	.00000	.04328
ESE	.01684	.00817	.00000	.00000	.00000	.00000	.02501
SE	.01176	.00769	.00000	.00000	.00000	.00000	.01945
SSE	.00631	.00918	.00158	.00000	.00000	.00000	.01707
S	.00808	.02267	.00335	.00000	.00000	.00000	.03410
SSW	.00801	.05529	.01609	.00111	.00054	.00000	.08104
SW	.03041	.08680	.02257	.00310	.00000	.00000	.14288
WSW	.03214	.06748	.01674	.00186	.00000	.00000	.11822
W	.01979	.04125	.01882	.00279	.00000	.00000	.08265
WNW	.01738	.03271	.01579	.00275	.00000	.00000	.06863
NW	.01357	.03517	.02017	.00000	.00057	.00000	.06948
NNW	.01429	.03023	.01053	.00058	.00000	.00000	.05563
Total	.27127	.54160	.16508	.02093	.00111	.00000	1.0000
Class D frequency 0.33399							
N	.01134	.03947	.01233	.00078	.00000	.00000	.06392
NNE	.01592	.03649	.01141	.00159	.00000	.00000	.06541
NE	.02317	.04119	.00989	.00049	.00000	.00000	.07474
ENE	.03055	.05437	.01459	.00175	.00000	.00000	.10126
E	.02105	.01234	.00098	.00000	.00007	.00000	.03444
ESE	.01403	.00364	.00007	.00000	.00000	.00000	.01774
SE	.00989	.00574	.00021	.00000	.00000	.00000	.01584
SSE	.01216	.00912	.00224	.00014	.00000	.00000	.02366
S	.01447	.01962	.00607	.00065	.00000	.00000	.04081
SSW	.02734	.04451	.01655	.00255	.00000	.00000	.09095
SW	.03739	.05062	.01209	.00162	.00028	.00014	.10214
WSW	.03529	.03460	.01015	.00272	.00051	.00007	.08334
W	.02737	.04350	.01889	.00201	.00000	.00000	.09177
WNW	.01829	.03857	.01588	.00181	.00000	.00000	.07455
NW	.01753	.02915	.01249	.00037	.00022	.00000	.05976
NNW	.01588	.03314	.00946	.00108	.00015	.00000	.05971
Total	.33165	.49607	.15329	.01755	.00123	.00020	1.0000
Class E frequency 0.28810							
N	.02250	.01139	.00099	.00008	.00000	.00000	.03496
NNE	.01278	.00914	.00150	.00017	.00000	.00000	.02359
NE	.01626	.00819	.00061	.00000	.00000	.00000	.02506
ENE	.04355	.02127	.00122	.00000	.00000	.00000	.06604
E	.03378	.00459	.00017	.00000	.00000	.00000	.03854
ESE	.01528	.00240	.00000	.00000	.00000	.00000	.01768
SE	.01811	.00320	.00032	.00000	.00000	.00000	.02163
SSE	.02090	.01010	.00146	.00016	.00000	.00000	.03262
S	.03069	.02700	.00655	.00143	.00000	.00000	.06567
SSW	.05250	.05278	.01530	.00177	.00016	.00000	.12251
SW	.09163	.06151	.01053	.00067	.00008	.00000	.16442
WSW	.08408	.02649	.00617	.00123	.00000	.00000	.11797
W	.05896	.03287	.00730	.00046	.00000	.00000	.09959
WNW	.04197	.02673	.00582	.00032	.00000	.00000	.07484
NW	.03663	.01442	.00222	.00016	.00000	.00000	.05343
NNW	.02943	.01004	.00174	.00025	.00000	.00000	.04146
Total	.60905	.32212	.06189	.00670	.00024	.00000	1.0000
Class F frequency 0.23854							
N	.01479	.00042	.00000	.00000	.00011	.00022	.01554
NNE	.01584	.00010	.00024	.00000	.00000	.00000	.01618
NE	.01582	.00000	.00000	.00000	.00000	.00000	.01582
ENE	.03651	.00268	.00000	.00000	.00000	.00000	.03919
E	.05881	.00010	.00000	.00000	.00000	.00000	.05891
ESE	.03339	.00000	.00000	.00000	.00000	.00010	.03349
SE	.01867	.00010	.00000	.00000	.00000	.00000	.01877
SSE	.02029	.00015	.00000	.00000	.00000	.00000	.02044
S	.02967	.00078	.00000	.00000	.00000	.00000	.03045
SSW	.06088	.00226	.00011	.00000	.00000	.00000	.06325
SW	.09926	.00425	.00000	.00000	.00000	.00000	.10351
WSW	.12584	.00284	.00000	.00000	.00000	.00000	.12868
W	.12743	.00122	.00000	.00000	.00000	.00000	.12865
WNW	.14417	.00020	.00000	.00000	.00000	.00000	.14437
NW	.12380	.00031	.00000	.00000	.00000	.00000	.12411
NNW	.05745	.00120	.00000	.00000	.00000	.00000	.05865
Total	.98262	.01660	.00035	.00000	.00011	.00032	1.0000

APPENDIX F

THE STRAIGHT-LINE GAUSSIAN PLUME AND RELATED AIR TRANSPORT MODELS — ARE THEY SUITABLE FOR THIS STUDY?

INTRODUCTION

The selection of an appropriate air dispersion model for FMPC releases of uranium, fission products associated with recycled feedstocks, and radon is of fundamental importance for the credibility of air pathway calculations used in this study. The venerable Gaussian plume model, with origins that go back at least to the 1930s, is always a contender in such a selection, for very good reasons. Hanna et al. (1982) list several of these reasons, which we paraphrase as follows:

- Competitive parity with alternative models in its reproduction of experimental data
- Mathematical simplicity
- Conceptual appeal
- Consistency with the random nature of turbulence
- Basis in the Fickian diffusion equation (it is a solution for constant values of the parameters)
- Parity with so-called theoretical formulas, which contain considerable empiricism
- Presence in most government handbooks, giving it a "blessed" status of acceptance.

Numerous special-purpose modifications of the Gaussian plume model exist. One recent contribution of Ramsdell (1990), his so-called "time-dependent" model, was developed in an effort to give a better physical basis to the treatment of building wake effects than do existing models. The time-dependent model and the Gaussian plume are proposed as the joint basis for air transport modeling for this study.

The Work Plan for Task 4 of this project considers two approaches to the estimation of airborne dispersion of radioactive materials released from the FMPC. The first approach, which is sometimes called "Lagrangian," follows incremental releases of material along simulated wind trajectories that in general are curved paths. For long-term results, the trajectories would have to be based on hourly data for wind speed and wind direction that would be representative of the assessment domain for the period considered. The second approach assumes straight-line trajectories within each of 16 directional sectors of 22.5° and applies a Gaussian plume model to joint frequency tables based on wind speed, wind direction, and stability category. The joint frequency tables are compiled from the same hourly data, and the use of these tables greatly reduces the computational cost of the simulations.

The choice of one approach over the other must consider the question of which method affords the better representation of the spatial distribution of releases throughout the assessment domain. The Lagrangian approach is appealing because of the directness of its

interpretation: each incremental release is followed along a trajectory that is presumed to resemble the behavior of the wind recorded at a station in the region at the time, and the simulated direction changes each hour according to the recorded wind direction. But the Gaussian model superposes straight-line trajectories that are statistically based on the same data. For the long term, one would expect similar results if the real wind trajectories do not deviate too much from straight lines and tend to stay inside the directional sectors in which they originate until they leave the assessment domain.

The choice of an air dispersion model is in large degree constrained by the meteorological data that are available for the location and time that the model is intended to simulate. As was indicated in Appendix E, the FMPC site has a single meteorological tower at which a continuous record began in August of 1986. Thus there is no authentic long-term meteorological record of the type needed for the FMPC assessment domain. Moreover, comparisons in Appendix E of FMPC tower data with airport data from the Greater Cincinnati and Dayton airports indicate that (at least, with the use of a straight-line Gaussian plume model) the airport datasets would be poor surrogates for the meteorology of the FMPC assessment domain. Appendix E discusses some uses of the long-term Cincinnati record to quantify uncertainties inherent in using recent FMPC tower data for periods in the past, but the onsite data remain fundamental to air dispersion modeling for this study.

If a straight-line statistical model is inadequately supported for predictions of past years by the existing meteorological data base, it seems plain that the more data-intensive Lagrangian models suffer a proportionately greater deficiency of data. The question that remains, however, has to do with the appropriateness of the straight-line windrose. If frequent changes of the wind direction tend to turn incremental releases of material out of the wind sectors into which they are released, then the predicted distribution of material throughout the domain would likely deviate from the real distribution.

In order to gain some insight into this question, we devised a Monte Carlo experiment to test the tendency of wind trajectories to leave their sector of origin before crossing the boundary of the assessment domain. The experiment was carried out with the Cincinnati hourly data for several reasons: (1) The characteristic being tested (i.e., directional persistence of winds near the surface) is likely to be similar in all regional data sets. (2) The Cincinnati data set covered a much longer period. (3) Gaps in the FMPC data set would have made it difficult to build the necessary conditional probability tables.

The objective of the experiment was to generate trajectories that would be similar to those that would be an underlying part of a Lagrangian model, such as MESOILT2 (Ramsdell and Burk 1990), which was considered for possible use in this project. By using stochastic techniques to generate many trajectories with the wind initially blowing into a particular sector, we recorded the number of those trajectories that crossed the 8,000-meter circumference of the assessment domain within the same sector. The simulations showed that for probabilities based on hourly data from the years 1960–1962, between 80 and 90 percent of the trajectories crossed the outer boundary of the region within the sector of their origin. This range was consistent for all sectors, with one exception, which showed 77 percent. Thus, if the stochastic simulation scheme is accepted as a reasonable model of wind trajectories, and if the Cincinnati Airport hourly data set suitably represents the FMPC site with respect to the characteristic under study, these results lend support to the choice of the straight-line

Gaussian plume or related model to estimate air concentrations and deposition resulting from releases of radioactivity to the atmosphere from the FMPC.

We begin this appendix by describing the Gaussian plume and time-dependent models and their implementation in connection with the straight-line windrose. Then we give details of the stochastic trajectory simulation experiment and its results. As a general reference, we cite Hanna et al. (1983), but our notations and order of presentation differ from theirs in some respects.

THE GAUSSIAN PLUME

The Gaussian plume model is based on a diffusion function of the form

$$D(x, y, z, h) = Y(x, y)Z(x, z, h) \tag{F–1}$$

$$Y(x, y) = \frac{1}{\sqrt{2\pi}\sigma_y} \exp\left(-\frac{y^2}{2\sigma_y^2}\right) \tag{F–2}$$

$$Z(x, z, h) = \frac{1}{\sqrt{2\pi}\sigma_z} \left[\exp\left(-\frac{(z-h)^2}{2\sigma_z^2}\right) + \exp\left(-\frac{(z+h)^2}{2\sigma_z^2}\right)\right] \tag{F–3}$$

where $D(x, y, z)$ is the concentration of a unit pulse release at $x = y = 0$ and height $z = h$ after it is carried a distance x downwind. The dispersion coefficients σ_y and σ_z are empirically-determined functions of the distance x, for which several formulations have been given. The representations developed by Briggs (1973) have been chosen for this work; they are shown in Table F–1. For a constant release rate Q and a constant wind speed u, the concentration of a released radionuclide at point (x, y, z) within a plume determined by the diffusion function D is

$$\chi(x, y, z) = \frac{Q}{u} D(x, y, z, h) \exp\left(-\lambda \frac{x}{u}\right) , \tag{F–4}$$

where the factor $\exp(-\lambda x/u)$ accounts for radioactive decay during the passage of material in the plume from the release point to a distance x downwind (λ is the decay-rate coefficient and x/u is the time of passage). For a release rate in pCi s^{-1}, wind speed in m s^{-1}, λ in s^{-1}, and σ_y and σ_z in m, $\chi(x, y, z)$ has units pCi m^{-3}. Its interpretation is the steady-state air concentration that would be sustained by the (constant) continuous release Q. It is often convenient to compile concentration factors that are normalized to a unit release rate, χ/Q (and spoken of as "chi over Q"), with units such as s m^{-3}.

Table F–1. Briggs' Open-Country Formulas for Dispersion Parameters σ_y and σ_z (100 m $\leq x \leq 10^4$ m)[a]

Pasquill Category	Crosswind σ_y (m)	Vertical σ_z (m)
A	$0.22x(1 + 0.0001x)^{-1/2}$	$0.20x$
B	$0.16x(1 + 0.0001x)^{-1/2}$	$0.12x$
C	$0.11x(1 + 0.0001x)^{-1/2}$	$0.08x(1 + 0.0002x)^{-1/2}$
D	$0.08x(1 + 0.0001x)^{-1/2}$	$0.06x(1 + 0.0015x)^{-1/2}$
E	$0.06x(1 + 0.0001x)^{-1/2}$	$0.03x(1 + 0.0003x)^{-1}$
F	$0.04x(1 + 0.0001x)^{-1/2}$	$0.016x(1 + 0.0003x)^{-1}$

[a] Briggs (1973).

Wind data in a joint frequency table are usually given in terms of 16 directions (N, NNE, NE, ENE, E, etc.) representing sectors of 22.5° each. For a particular direction, wind speed, and atmospheric stability category, the x axis in Eq. F–4 would normally be oriented along the centerline of the sector and the y axis perpendicular to the centerline. But in reality the wind direction is variable, and using only the 16 discrete centerlines presents an artificial distribution of concentrations. A common practice is to average the concentration at the distance x across the sector by integrating Eq. F–1 with respect to the crosswind coordinate y from $-\infty$ to $+\infty$ (using the fact that $\int_{-\infty}^{+\infty} Y(x,y)\,dy = 1$) and dividing the result by the sector width (actually the arc length) $2\pi x/16$:

$$\bar{D}(x,z,h) = \frac{16}{2\pi x}\,\bar{\chi}(x,z,h)$$

$$= \frac{16}{(2\pi)^{3/2} x \sigma_z}\left[\exp\left(-\frac{(z-h)^2}{2\sigma_z^2}\right) + \exp\left(-\frac{(z+h)^2}{2\sigma_z^2}\right)\right] \qquad \text{(F–5)}$$

$$\bar{\chi}(x, z=0) = \frac{32\,Q}{(2\pi)^{3/2} u x \sigma_z}\exp\left(-\frac{h^2}{2\sigma_z^2}\right) \approx \frac{2.032Q}{u x \sigma_z}\exp\left(-\frac{h^2}{2\sigma_z^2}\right). \qquad \text{(F–6)}$$

In Eq. F–6 we have set $z = 0$ to correspond to the ground-level concentration that is of particular interest in this study.

The time-dependent model (Ramsdell 1990) may be interpreted as a special case of the Gaussian plume, with release height $h = 0$ and dispersion coefficients that depend not only on the distance x but also on the wind speed u and the crosswind area A of the building that creates the wake. We may characterize the model by the equations

$$\chi/Q = (\pi u \sigma_y' \sigma_z')^{-1} \qquad \text{(F–7)}$$

$$\sigma_y' = [\sigma_y^2 + K S T_s^2 F(T_s)]^{1/2}$$

$$\sigma_z' = [\sigma_z^2 + K S T_{sv}^2 F(T_{sv})]^{1/2}$$

$$F(T) = 1 - (1 + x/(uT))\exp(-x/(uT)), \quad T = T_s \text{ or } T = T_{sv}$$

where

A = characteristic crosswind area of the building creating the wake (m^2)

u = wind speed (m s^{-1}), which we adjust to the building height

x = downwind distance of the receptor from the source (m)

S = 1, 2, ..., 6 for stabilities A, B, ..., F, respectively (treated as a dimensionless parameter)

a = $0.4/\ln(z/z_0)$; z_0 is the roughness height (m), and we take z (m) to be the building height; 0.4 is the von Kármán constant

u_* = au = friction velocity (m s^{-1})

T_s = $A^{1/2}/u_*$ (s)

T_{sv} = $A^{1/2}/(Su_*)$ (s)

σ_y, σ_z = horizontal and vertical dispersion coefficients (m), expressed as functions of the downwind distance x; we used Briggs' formulas (Table F–1)

K = an adjustable parameter; Ramsdell (1990) obtained best fits with $K = 0.5$.

We should mention that the term "time-dependent" refers to the approach used in deriving the model, but the time is explicit in the final formulas only as the scaled (dimensionless) quantities T_s and T_{sv}. The version of the model shown above is interpreted as the centerline concentration χ per unit release rate Q. Sector averaging of this model in the sense of Eq. F–6 makes less sense than in the context of the Gaussian plume, which represents a point source. The time-dependent model, on the other hand, by modification of the dispersion coefficients, represents an area source (A), and consequently artificial confinement of the plume to a sector that converges to a point near the source seems contradictory and difficult to interpret. For long-term averages, however, we anticipate using a different method of angular averaging that should meet this objection.

The interpretation of Eqs. F–4, F–6, and F–7 is somewhat idealized and refers to a fixed wind speed, wind direction, and atmospheric stability category (the wind speed u is a parameter, the wind direction is implicit in the orientation of the x-axis, and the dispersion parameters, σ_y and σ_z, are functions of the distance x and the stability category, as is indicated in Table F–1). Extending the models to long-term averages is accomplished by means of a joint frequency table (JFT), which is compiled from meteorological observations for the period and location of interest. For a given receptor point (i.e., distance and direction from the source), the time-averaged concentration would be expressed as

$$\bar{\chi}_{j'}(x) = \sum_{i,k} f_{i,j,k}\chi_{i,j',k}(x) \qquad \text{(F–8)}$$

where the indices i, j, and k correspond to wind speed, wind direction, and stability category, respectively, and x is the distance of the receptor from the source. The frequency $f_{i,j,k}$ is the fraction of the time the wind blows with speed i from direction j during stability condition k. The notation j' indicates the direction that is reciprocal to direction j — the wind blows FROM j TOWARD j', where the receptor point is located relative to the source. The summation is not taken over j (i.e., j is fixed) because the receptor is assumed to experience a positive concentration only when the wind is blowing toward it. Examples of joint frequency tables for the FMPC data are given in Tables ES–1 through ES–13 of Appendix E.

Equations F–4 and F–6 represent basic forms of the Gaussian plume model for a continuous elevated point source, and Eq. F–7 applies to a continuous source in the wake of a building. As written, these models make no allowance for plume depletion due to wet or dry deposition, plume rise due to momentum or buoyancy, or confinement of the plume within the mixed layer of the atmosphere (the planetary boundary layer). These processes and factors are taken into account, where necessary, by modification of the basic models, and the modifications are discussed in separate appendices.

SIMULATIONS OF WIND TRAJECTORIES WITHIN 22.5° SECTORS

In the following subsections, we present the technical details of the Monte Carlo procedure for generating the wind trajectories and their connection with the hourly data. The same procedure can be used for any set of hourly data that specifies windspeed and wind direction in the resolution of 22.5° sectors. As noted in the introduction, however, sequential gaps in the FMPC tower data set would have created difficulties in implementing this procedure with that data set.

Probability Distributions Derived from the Hourly Data

The data consist of a sequence of hourly windspeeds u and sector angles φ from which the wind blows (as previously noted, there are 16 sectors at intervals of 22.5°). We are also concerned with the sector $\varphi+180°$ into which the wind blows and into which the trajectories move. Our coordinate system has the standard mathematical orientation, with the x-axis pointing eastward, the y-axis pointing northward, and the angles measured positively counterclockwise from the positive x-axis. This convention is contrary to the navigational orientation used by meteorologists, with directional angles being measured clockwise from north in that system. (Please note that this interpretation of x and y is different from the one used above in the definition of the Gaussian plume.)

We define a 17×17 matrix M as follows:

$$M = \begin{array}{c} \\ \text{N} \\ \text{NNE} \\ \vdots \\ \text{NNW} \\ \text{calm} \end{array} \begin{array}{c} \begin{array}{cccccc} \text{N} & \text{NNE} & \cdots & \text{NNW} & \text{calm} \end{array} \\ \begin{pmatrix} n_{11} & n_{12} & \cdots & n_{1,16} & n_{1,17} \\ n_{21} & n_{22} & \cdots & n_{2,16} & n_{2,17} \\ \vdots & \vdots & \ddots & \vdots & \vdots \\ n_{16,1} & n_{16,2} & \cdots & n_{16,16} & n_{16,17} \\ n_{17,1} & n_{17,2} & \cdots & n_{17,16} & n_{17,17} \end{pmatrix} \end{array} \tag{F–9}$$

where the bordering notations "N," "NNE," ..., "NNW," refer to directions from which the wind blows and "calm" indicates periods of calm with no specified wind direction. The notation n_{ij} counts the observed number of transitions from wind direction j to wind direction i in successive hours; i and j may be thought of as having values N, NNE, etc., but it is more convenient to think of them as integer values that correspond to the wind directions and to the category "calm."

We denote the sum of the entries of column j of M as

$$n_{\bullet j} = \sum_{i=1}^{17} n_{ij} \tag{F–10a}$$

and we note that the probability that the wind direction will be i in the next hour *given that it is j during the present hour* is

$$p_{i|j} = \frac{n_{ij}}{n_{\bullet j}} \tag{F–11a}$$

Equation F–11a defines a conditional probability that is fundamental to generating simulated wind trajectories. A second conditional probability will be necessary for generating the initial segment of each trajectory. The ith row sum of M is

$$n_{i\bullet} = \sum_{j=1}^{17} n_{ij} \tag{F–10b}$$

and the corresponding conditional probability is given by

$$p'_{i|j} = \frac{n_{ij}}{n_{i\bullet}}. \tag{F–11b}$$

Note that the conditional probability of Eq. F–11b has the interpretation of being the probability that the previous wind direction category was j given that the present direction category is i.

The foregoing sets of conditional probabilities determine discrete distributions from which we must sample in the course of generating random wind trajectories. To generate a direction i for the next hour given that the direction during the present hour is j, we must consider the discrete probability function

$$f_j(i) = \begin{cases} p_{i|j} & \text{if } \; i = 1, \ldots, 17 \\ 0 & \text{otherwise} \end{cases}$$

(based on the jth column of the matrix M), for which a standard sampling technique consists in generating a uniformly distributed random number U from the interval [0,1] and choosing direction

$$i = \begin{cases} 1 & \text{if } \; U \le f_j(1) \\ q > 1 & \text{if } \; \sum_{k=1}^{q-1} f_j(k) < U \le \sum_{k=1}^{q} f_j(k) \,. \end{cases}$$

When we are given the present hour's direction category i and wish to generate the previous hour's direction category j, as we do at the beginning of each trajectory, we form a distribution of the conditional probabilities based on the ith row of the matrix M:

$$f_i'(j) = \begin{cases} p'_{i|j} & \text{if } \; j = 1, \ldots, 17 \\ 0 & \text{otherwise} \end{cases}$$

and the sampling technique is analogous.

We must also consider windspeed distributions that depend on the transition from one wind direction to another. We assume that these distributions are of lognormal form and thus are determined by a geometric mean (GM) and a geometric standard deviation (GSD), or alternatively by the mean μ and the standard deviation σ of the underlying normal distribution of $\ln u$, where u is the windspeed. Specifically, we are interested in the distribution $F_{ij}(u)$ of the windspeed in the hour after a transition from direction j to direction i. This distribution is defined by the two parameters μ_{ij} and σ_{ij}, and we estimate them from the hourly windspeed record as follows:

$$\mu_{ij} = \frac{1}{n_{ij}} \sum_{i \leftarrow j} \ln u \,, \tag{F–12}$$

where n_{ij} is the number of wind direction transitions from j to i (Eq. F–9) and the notation $i \leftarrow j$ means that the summation is taken over the windspeeds u in the hour following the transition from j to i. Similarly,

$$\sigma_{ij} = \sqrt{\frac{1}{n_{ij} - 1} \sum_{i \leftarrow j} (\ln u - \mu_{ij})^2} \,, \quad n_{ij} \ge 2 \,. \tag{F–13}$$

Corresponding estimates of the GM and GSD are

$$\mathrm{GM}_{ij} = \exp(\mu_{ij}) \,, \quad \mathrm{GSD}_{ij} = \exp(\sigma_{ij}) \tag{F–14}$$

In those cases where $n_{ij} = 1$, we used $\mathrm{GSD}_{ij} = 1$ to correspond to zero variability in the windspeed that could not be estimated by Eqs. F–12 and F–13. Such transitions have correspondingly low probabilities of occurrence. Unobserved transitions were assigned zero probability and were not sampled in constructing the wind trajectories.

The stochastic sampling necessary in this work is from two distributions: the uniform distribution over the interval $0 \leq x \leq 1$ and the standard normal distribution (mean 0 and variance 1). The method of producing pseudo-random numbers from the uniform distribution is a linear congruence method described by Knuth (1969), adapted by Forsythe et al. (1977), and modified by one of us (G.G.K.) for personal computers using the family of Intel 80X87 coprocessors. The algorithm was recoded in the C language. The method used for sampling from the standard normal distribution is the simple expedient of generating a pseudo-random number, U, from the uniform distribution on [0,1] and solving the equation

$$U = F(X)$$

for X, where F is the cumulative distribution function (CDF) for the standard normal distribution. A rational approximation to the inverse of F from Abramowitz and Stegun (1965) was used to solve the equation for X given U. There are more complicated methods for sampling the normal distribution, which provide some improvement in efficiency, but this simply-programmed scheme was more than adequate for this exercise.

Our task involved a further step in the sampling, and that was to transform the standard normal variate into a lognormal variate from the distribution with specified geometric mean GM_{ij} and geometric standard deviation GSD_{ij}. This transformation is most conveniently expressed as

$$\xi = GM_{ij} \exp(\sigma_{ij} X) \qquad \text{(F–15)}$$

where X is the standard normal variate and ξ is the resulting lognormal variate. The relationship between GSD_{ij} and σ_{ij} is given by Eq. F–14.

These definitions and equations are sufficient background for the description of the wind trajectory simulations in the next subsection.

Construction of the Wind Trajectories

Conceptually, the construction of a wind trajectory from an initial direction is simple; describing it precisely is somewhat more difficult. The first segment is slightly more complicated than the others, and we will return to it. But after the first segment, we suppose that the previous sector index is j. We generate a random sector (index i) based on the probabilities $p_{i|j}$, $i = 1, \ldots, 17$. Within that sector, we generate a random angle ϑ. The lognormal variate ξ is generated corresponding to the transition $i \leftarrow j$ from Eq. F–15. This variate represents the windspeed (m s^{-1}), which is converted to a distance R by multiplication by the number of seconds per hour: $R = 3600\xi$. The angle ϑ and displacement R determine the segment of the trajectory.

We begin the process by specifying the initial sector and generating a random angle within that sector. Because we have no previous sector, the method of generating a windspeed that we described above will not work. Instead, if the initial sector is i, we generate a *previous* direction category according to the conditional probabilities $p'_{i|j}$, $j = 1, \ldots, 17$ (Eq. F–11b; note that this is using the ith row of the matrix M rather than one of the columns).

There is one further point in connection with the first segment of the trajectory. Our conceptual position is that of a nondispersing tracer introduced into the windflow from a specified direction at a random point in time. Thus, we should not preferentially start at the

exact beginning of an hour. Accordingly, we modify the windspeed-generated displacement R by multiplying it by a uniformly distributed random number in the interval (0,1]. This modification is performed only for the initial segment.

We end the trajectory when the "tracer" crosses the boundary of the assessment domain (the boundary is a circle with radius 8,000 m; the origin of the trajectory is at its center). We determine the point on the boundary at which the trajectory crosses, and it is the angular location of this point that determines whether the trajectory is considered to have remained within its sector or not. The trajectory could have wandered outside and returned to cross the boundary within its original sector and would still be counted as having remained.

"Calm" categories are given special treatment. The air is rarely perfectly still, and it is conventional to associate a windspeed of 0.5 m s^{-1} with nominal readings of calm (Hanna et al. 1982) for the purposes of airborne transport simulations. We chose the wind direction for each calm category at random from angles 0–360°.

The data used to construct the probability tables for our simulations were 26,304 hourly observations for the years 1960–1962. These data were obtained from the National Climatic Data Center, Asheville, N.C. Table F–2 shows the values of the entries n_{ij} in the matrix M of Eq. F–9. Note the strong diagonal dominance in this matrix, which contributes to the tendency of the trajectory to remain near their original sectors.

Two data tables are required for specifying the distribution of the windspeed following each transition. Tables F–3 and F–4 show the geometric mean and geometric standard deviation, respectively, of the windspeed for direction category i given that the previous direction category was j. Omitted entries correspond to transitions of probability zero, which are never selected in the simulations. In the calm categories, we assign a degenerate lognormal distribution with geometric mean 0.5 m s^{-1} and geometric standard deviation 1 (i.e., all of the probability is concentrated at the geometric mean, so that only the value 0.5 will be sampled from this distribution).

Results of the Simulations

We performed 1,000 simulations for each initial sector to obtain estimates of the fractions of the trajectories that crossed the 8,000-m boundary within the sector of origin. Table F–5 shows the estimates, expressed as percentages.

We also performed parallel simulations with 50 trajectories per sector to provide plots (if too many trajectories are plotted, the result becomes too tangled to give a good impression of the trajectories). The 16 plots are shown as Figs. F–1 through F–16, with captions that indicate the percentages. These percentages vary somewhat from those obtained with 1,000 trajectories per sector; we consider the latter (shown in Table F–5) our definitive results, but the plots are also instructive.

Table F–2. Counts of Wind Transitions at Hourly Intervals[a]

To \ From →	N	NNE	NE	ENE	E	ESE	SE	SSE
N	617	192	60	22	2	3	5	1
NNE	246	442	207	38	13	5	5	3
NE	83	271	678	239	64	17	12	5
ENE	28	54	286	708	180	37	16	9
E	12	11	90	246	358	108	32	16
ESE	6	11	22	61	163	273	90	48
SE	5	5	15	12	71	146	267	132
SSE	2	3	12	7	27	73	188	389
S	6	2	7	11	15	29	82	276
SSW	3	3	4	3	5	7	25	99
SW	6	1	9	2	9	5	15	30
WSW	7	2	1	2	1	4	7	9
W	9	2	5	2	1	5	2	3
WNW	11	7	2	1	2	1	0	2
NW	61	16	8	4	1	5	3	5
NNW	186	35	17	3	3	0	2	3
CALM	74	44	61	37	53	26	55	34

To \ From →	S	SSW	SW	WSW	W	WNW	NW	NNW	CALM
N	11	1	7	9	22	31	90	234	55
NNE	3	4	5	4	4	10	18	62	32
NE	9	5	3	5	8	2	9	17	57
ENE	10	4	3	0	1	2	7	5	47
E	10	11	3	0	2	0	5	3	62
ESE	21	5	6	3	3	1	5	1	25
SE	63	9	17	4	2	2	3	1	52
SSE	204	66	27	11	4	1	4	3	43
S	1027	438	118	36	15	8	3	2	90
SSW	554	1711	578	84	24	11	4	2	105
SW	114	708	1474	381	86	23	9	5	72
WSW	22	124	457	943	317	65	20	8	29
W	16	30	116	349	640	314	65	13	23
WNW	8	20	33	113	352	823	234	51	14
NW	7	12	20	38	61	283	508	177	35
NNW	4	7	10	11	20	71	219	438	26
CALM	82	67	72	27	34	27	41	33	687

[a] Total count = 26,304 hours.

CONCLUSIONS AND DISCUSSION

We have described in some detail a stochastic simulation methodology that we applied to hourly wind data for simulating wind trajectories typical of the vicinity of the Greater Cincinnati Airport during the years 1960–1962. Our purpose was to consider these trajectories as having originated at the Feed Materials Production Center (FMPC) at Fernald and to study their tendency to remain within the 22.5° sector of origin. If relatively few trajectories cross the 8,000-m circular boundary of the assessment domain outside of the sector into which they were originally released, the results of using a straight-line Gaussian plume model for predicting dispersion and deposition of released materials should not differ importantly in the longer term from corresponding results of a Lagrangian-type trajectory model that incorporates similar assumptions about plume rise, wake effects, diffusion, and deposition.

We believe that our results make a strong case for the applicability of the straight-line Gaussian model to the FMPC assessment domain for longer-term estimates such as monthly

Table F–3. Geometric Means of Windspeeds (m s^{-1}) Following Transitions

To \ From →	N	NNE	NE	ENE	E	ESE	SE	SSE
N	3.45	3.35	2.35	2.30	2.72	1.87	2.80	1.13
NNE	3.09	4.08	3.30	2.96	2.20	2.22	2.64	2.36
NE	2.52	3.10	3.35	3.13	2.05	2.06	2.04	2.36
ENE	2.04	2.81	3.33	3.95	3.34	2.75	2.40	2.56
E	2.32	1.73	2.42	3.35	3.24	3.17	2.55	2.45
ESE	2.51	2.16	2.66	3.20	3.31	3.64	3.15	2.89
SE	2.20	2.16	2.22	3.22	2.39	3.13	3.32	3.10
SSE	2.52	1.76	2.04	2.00	2.33	3.32	3.55	3.89
S	2.42	2.30	1.96	2.43	2.32	2.43	2.33	3.32
SSW	2.36	2.14	2.95	1.97	2.46	2.86	2.87	3.89
SW	1.32	0.434	1.88	9.43	2.30	2.45	2.93	2.70
WSW	2.27	2.82	1.28	3.56	0.434	3.64	2.76	3.22
W	2.56	1.99	2.29	1.26	1.28	2.36	3.78	2.39
WNW	2.91	2.73	2.57	0.434	4.08	1.41	—	3.09
NW	2.99	3.14	2.24	1.41	1.64	2.12	2.36	2.61
NNW	3.48	3.29	3.19	2.22	3.77	—	5.49	3.20
CALM	0.5	0.5	0.5	0.5	0.5	0.5	0.5	0.5

To \ From →	S	SSW	SW	WSW	W	WNW	NW	NNW	CALM
N	2.27	1.41	3.54	2.26	2.86	2.56	2.78	3.49	1.58
NNE	2.22	1.88	2.63	2.68	2.35	2.97	2.30	3.14	1.53
NE	1.66	1.77	2.01	2.01	2.02	3.41	2.47	2.07	1.58
WNE	2.68	3.92	2.67	—	0.722	2.91	2.58	2.46	1.51
E	2.39	2.42	1.07	—	2.52	—	1.67	1.76	1.53
ESE	1.91	1.60	1.96	1.94	1.48	1.13	1.54	0.722	1.62
SE	2.52	2.45	2.06	4.07	2.18	1.63	1.87	0.434	1.57
SSE	3.24	3.25	2.41	1.74	2.50	0.0285	2.41	2.36	1.51
S	3.41	3.25	2.70	2.13	2.11	2.13	2.54	2.52	1.24
SSW	3.81	4.45	3.96	2.91	2.48	2.00	1.26	3.85	1.69
SW	2.83	4.25	4.28	3.85	2.67	3.53	2.71	1.73	1.51
WSW	3.12	3.88	4.40	5.12	4.21	3.56	2.73	2.39	1.49
W	2.80	3.05	3.18	4.40	4.34	4.26	2.64	1.86	1.51
WNW	2.03	2.90	4.75	4.10	4.44	4.98	3.78	3.37	1.77
NW	3.02	3.08	2.59	3.28	3.45	4.40	3.88	3.87	1.86
NNW	3.12	5.20	3.09	3.41	2.81	3.62	4.06	4.39	2.04
CALM	0.5	0.5	0.5	0.5	0.5	0.5	0.5	0.5	0.5

averages. The argument breaks down, of course, for short-term episodic releases. If the local meteorology were known for such a release, a strong argument could be made for simulating it with a Lagrangian-type model that uses wind trajectories observed during the actual period of release. But on the basis of the results presented in Table 4, we believe that the use of a Lagrangian model for longer term estimates within this assessment domain would gain little in quality of information.

With regard to the exercise that we have described, one might reasonably ask, why not use real sequences of data from the records rather than simulated sequences based on probability tables compiled from the data. The principal consideration that led to the procedure reported here was the need to convey a sense of variability in the wind trajectories that would not be revealed directly by the data. During the period in question, wind directions were recorded only as numeric codes corresponding to the 16 22.5° direction sectors and the calm category. In order to analyze the effect on the trajectories of the variability of the wind direction within the sectors, one has to replace the "real" trajectories (which are unknown) with some model,

Table F–4. Geometric Standard Deviations of Windspeeds Following Transitions[a]

To \ From →	N	NNE	NE	ENE	E	ESE	SE	SSE
N	1.29	1.27	1.45	1.15	1.17	1.03	1.59	1
NNE	1.25	1.21	1.33	1.33	1.44	1.05	1.97	1.06
NE	1.35	1.30	1.29	1.27	1.43	1.28	1.10	1.12
ENE	1.36	1.27	1.28	1.22	1.26	1.33	1.53	1.16
E	1.22	1.06	1.22	1.21	1.24	1.21	1.25	1.13
ESE	1.23	1.15	1.17	1.18	1.23	1.19	1.27	1.19
SE	1.18	1.13	1.41	1.28	1.35	1.29	1.23	1.28
SSE	1.09	1.26	1.27	1.83	1.45	1.21	1.20	1.26
S	1.24	1.03	1.21	1.32	1.57	1.20	1.25	1.38
SSW	1.29	1.13	1.39	1.48	1.54	1.64	1.17	1.29
SW	1.09	1	1.54	1.04	1.45	1.25	1.36	1.43
WSW	1.16	1.02	1	1.04	1	1.07	1.30	1.56
W	1.59	1.14	2.71	1.09	1	1.12	4.98	1.02
WNW	1.30	1.40	1	1	1.03	1	1	1
NW	1.29	1.18	1.13	2.04	1	1.05	1.06	1.35
NNW	1.24	1.15	1.21	1.02	1.01	1	1.94	2.64
CALM	1	1	1	1	1	1	1	1

To \ From →	S	SSW	SW	WSW	W	WNW	NW	NNW	CALM
N	1.17	1	1.60	1.47	1.37	1.38	1.37	1.29	1.28
NNE	1.02	1.06	1.43	1.17	1.12	1.14	1.42	1.28	1.20
NE	1.49	2.28	1.07	2.15	1.34	1.67	1.22	1.27	1.23
ENE	1.33	1.14	1.08	1	1	1.27	1.28	1.29	1.35
E	1.08	1.21	1.50	1	1.09	1	1.65	1.26	1.34
ESE	1.26	1.08	1.25	1.17	1.13	1	1.73	1	1.41
SE	1.31	1.17	1.23	1.56	1.27	1.52	1.66	1	1.42
SSE	1.34	1.23	1.57	1.30	1.48	1	1.32	1.06	1.21
S	1.36	1.39	1.29	1.24	1.35	1.62	1.27	1.62	1.27
SSW	1.30	1.28	1.33	1.39	1.41	1.31	1.06	1.01	1.27
SW	1.37	1.30	1.31	1.33	1.29	1.20	1.09	1.30	1.27
WSW	1.42	1.42	1.29	1.19	1.22	1.26	1.27	1.21	1.37
W	2.08	1.14	1.32	1.34	1.30	1.27	1.35	1.40	1.32
WNW	2.07	1.54	1.38	1.21	1.26	1.23	1.33	1.23	1.54
NW	2.19	1.49	1.33	1.34	1.36	1.23	1.28	1.31	1.31
NNW	1.08	1.37	1.68	1.26	1.37	1.30	1.26	1.21	1.11
CALM	1	1	1	1	1	1	1	1	1

[a] The notation "1" indicates calm or too few transitions to estimate the GSD.

Table F–5. Percentage of Simulated Trajectories Remaining within the Sector of Origin

N	NNE	NE	ENE	E	ESE	SE	SSE	S	SSW	SW	WSW	W	WNW	NW	NNW
84.2	86.8	86.1	88.8	90.4	90.6	88.2	86.6	87.6	85.7	83.4	82.2	82.5	77.2	84.0	84.4

as we have done. The hourly interval between observations also presents a problem, for which no suitable refinement suggested itself to us. Given the data as they were, the Markov hypothesis appeared the most reasonable treatment of transitions at the one-hour boundaries.

REFERENCES

Abramowitz M. and I.A. Stegun. 1965. *Handbook of Mathematical Functions.* Dover Publications, Inc., New York.

Briggs G.A. 1973. *Diffusion Estimation for Small Emissions.* Rep. ATDL Contribution File No. 79. Atmospheric Turbulence and Diffusion Laboratory, Oak Ridge, Tennessee.

Forsythe G.E., M.A. Malcolm, and C.B. Moler. 1977. *Computer Methods for Mathematical Computations.* Prentice-Hall, Englewood Cliffs, N.J.

Hanna S.R., G.A. Briggs, and R.P. Hosker, Jr. 1982. *Handbook on Atmospheric Diffusion.* Rep. DOE/TIC-11223 (DE82002045) Technical Information Center, U.S. Department of Energy.

Knuth D.E. 1969. *The Art of Computer Programming: Vol. 2, Seminumerical Algorithms.* Addison-Wesley, Reading, Mass.

Ramsdell J.V., Jr. 1990. "Diffusion in Building Wakes for Ground-Level Releases." *Atmos. Env.* **24B**: 377–388.

Ramsdell J.V., Jr., and K.W. Burk. 1990. *MESOILT2, A Lagrangian Trajectory Climatological Dispersion Model.* Unpublished draft report PNL-7340 HEDR, Pacific Northwest Laboratory, Richland, Washington.

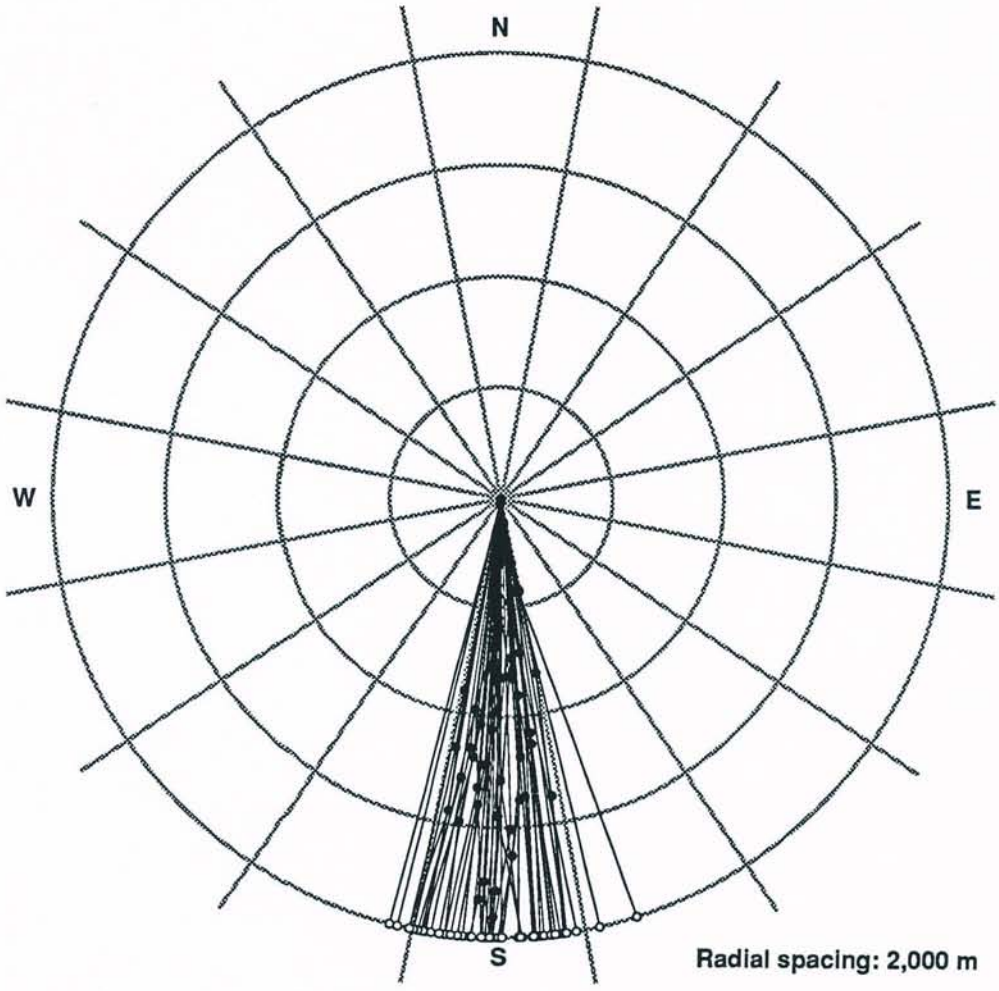

Figure F–1. Wind trajectories initially from N. The fraction remaining in sector S from the simulation shown was 88%.

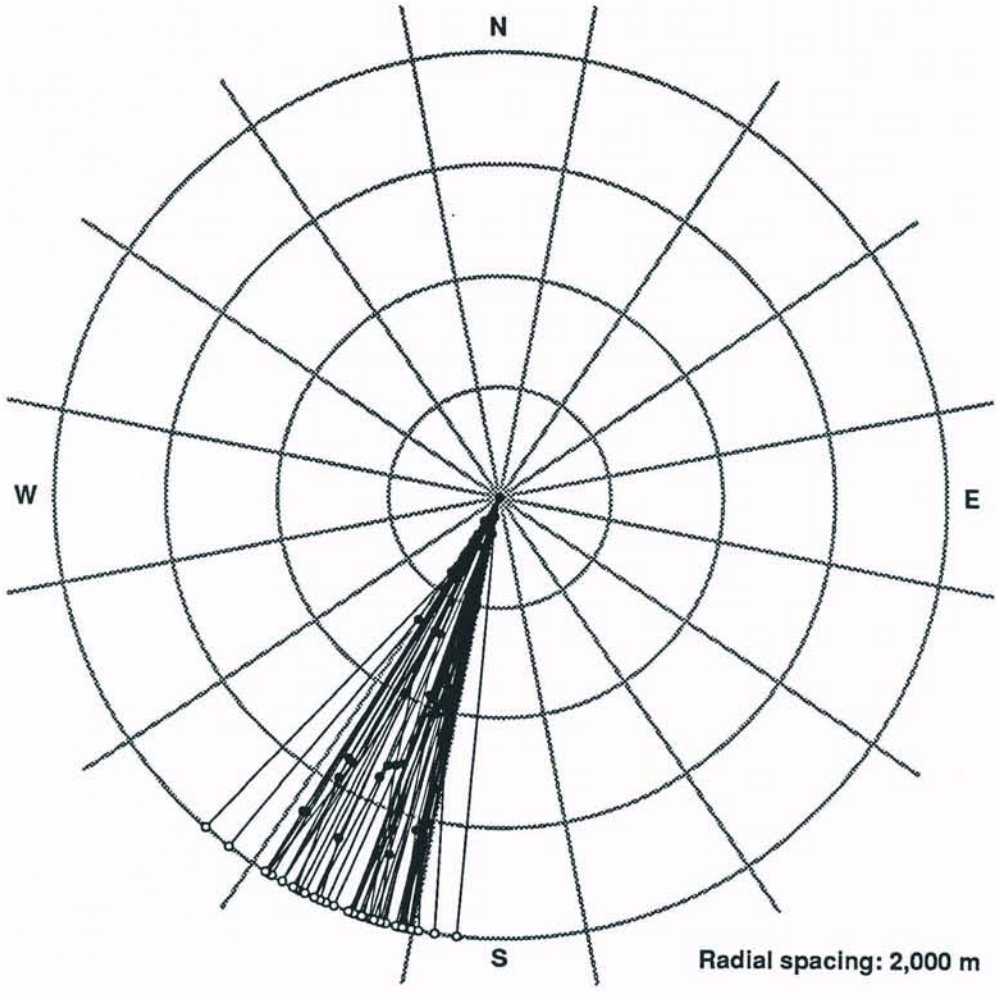

Figure F–2. Wind trajectories initially from NNE. The fraction remaining in sector SSW from the simulation shown was 90%.

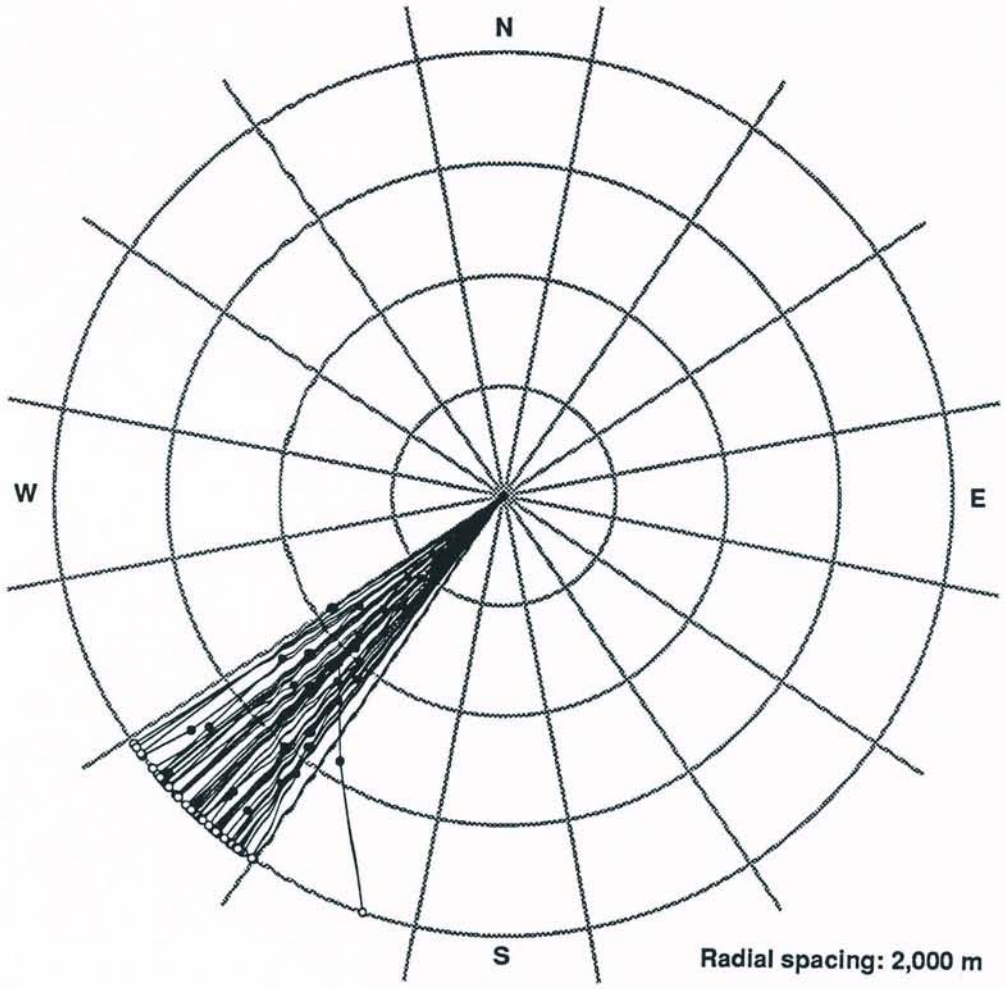

Figure F–3. Wind trajectories initially from NE. The fraction remaining in sector SW from the simulation shown was 98%.

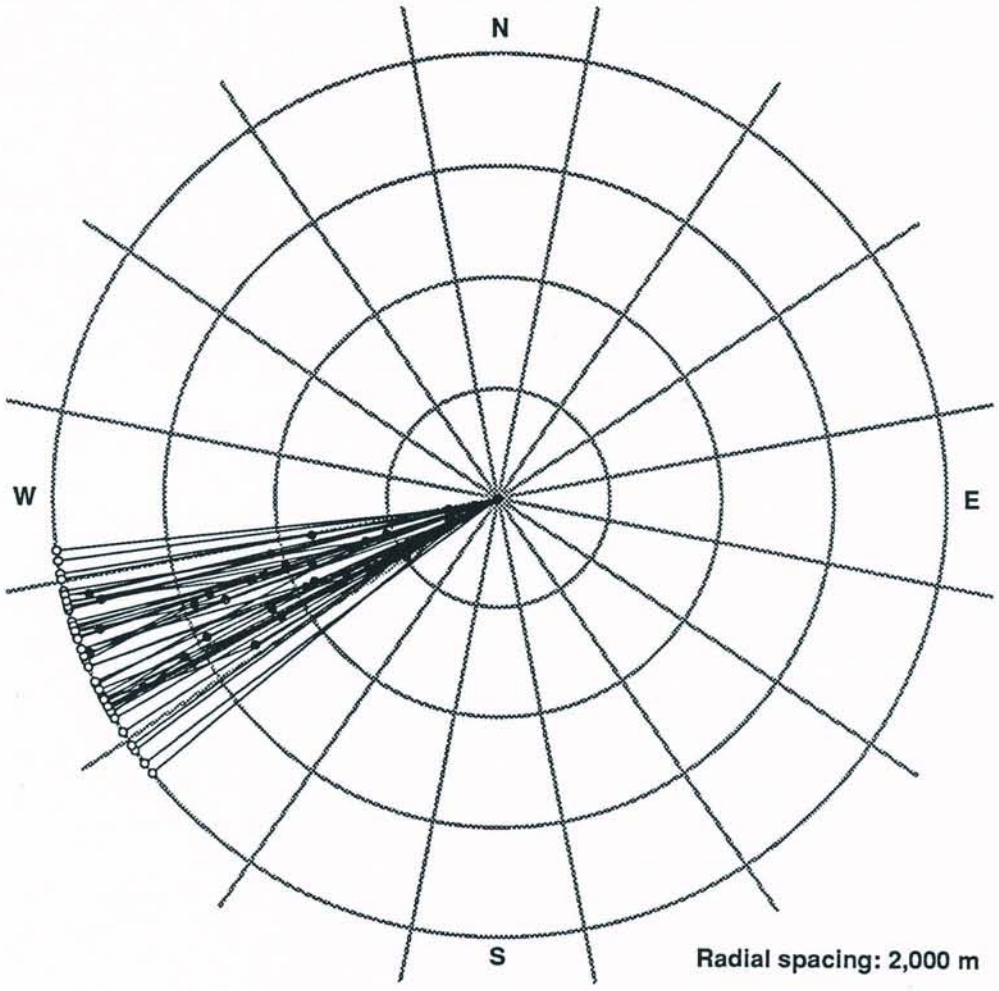

Figure F–4. Wind trajectories initially from ENE. The fraction remaining in sector WSW from the simulation shown was 84%.

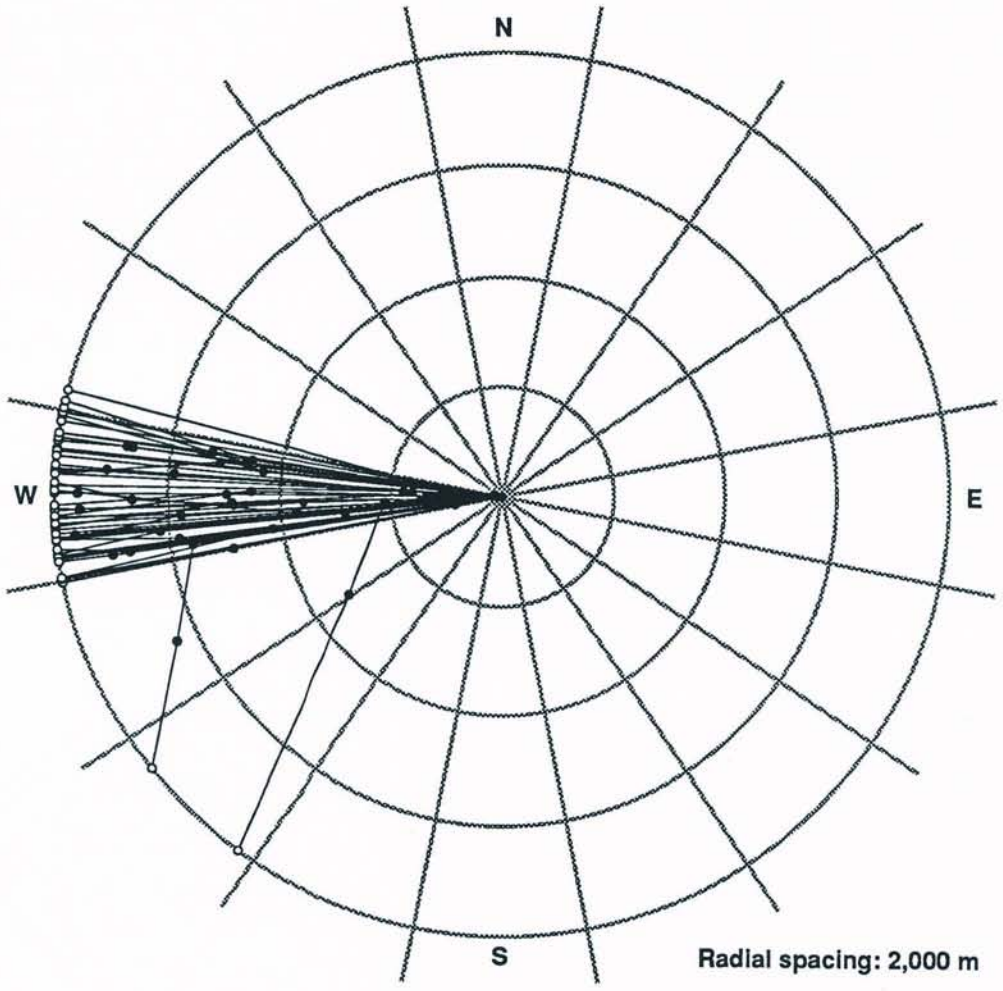

Figure F–5. Wind trajectories initially from E. The fraction remaining in sector W from the simulation shown was 88%.

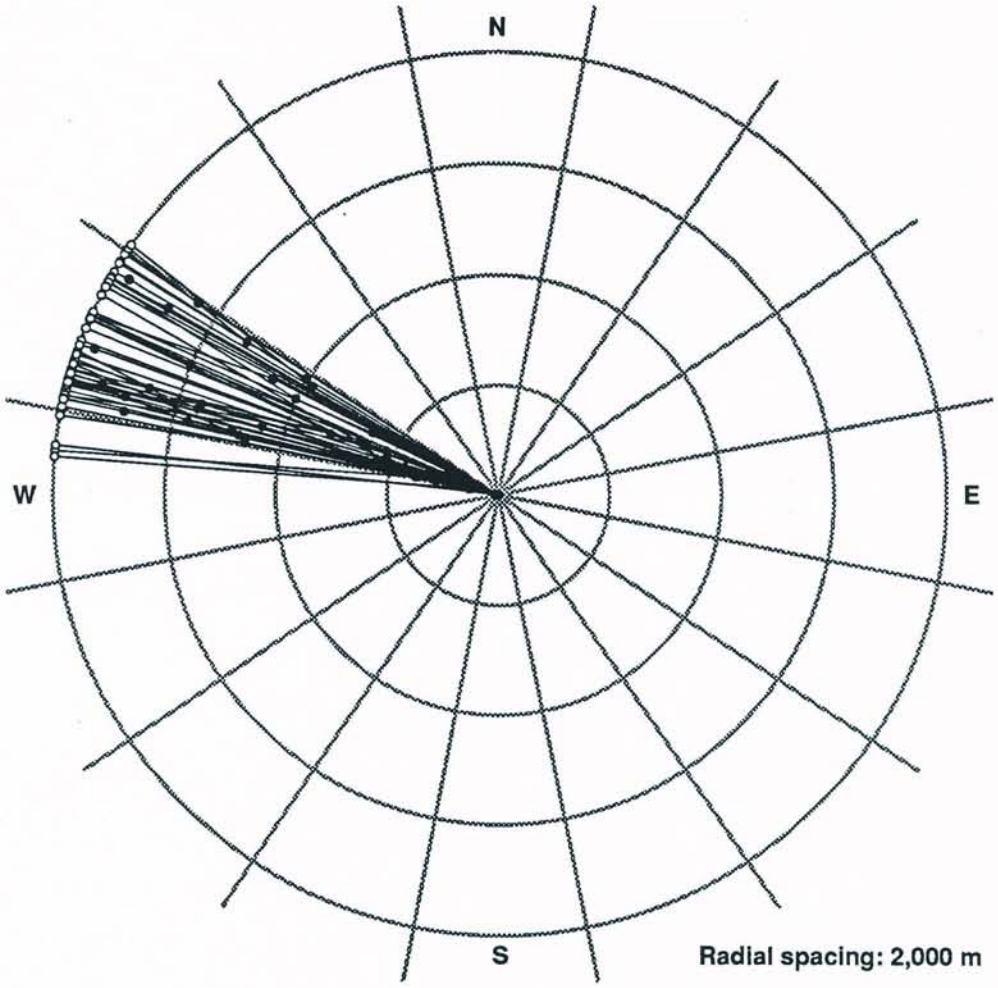

Figure F–6. Wind trajectories initially from ESE. The fraction remaining in sector WNW from the simulation shown was 88%.

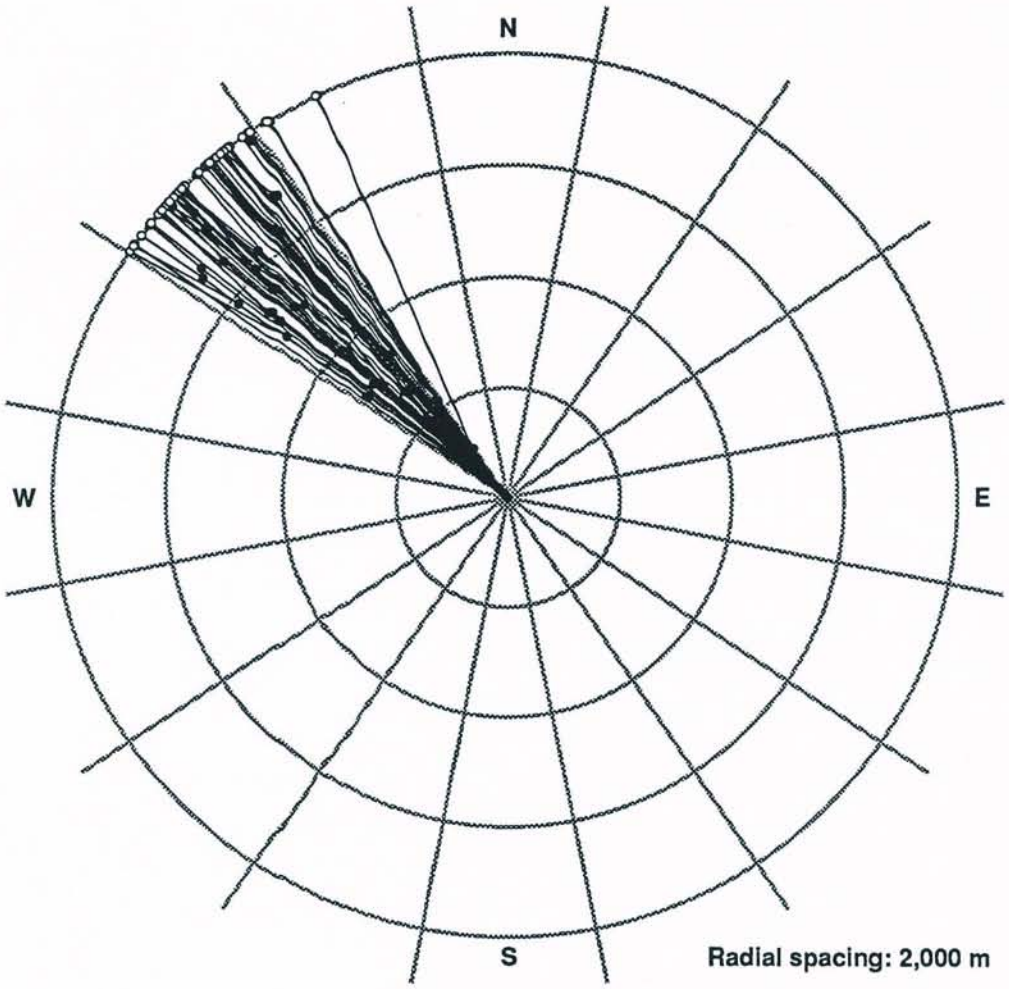

Figure F–7. Wind trajectories initially from SE. The fraction remaining in sector NW from the simulation shown was 94%.

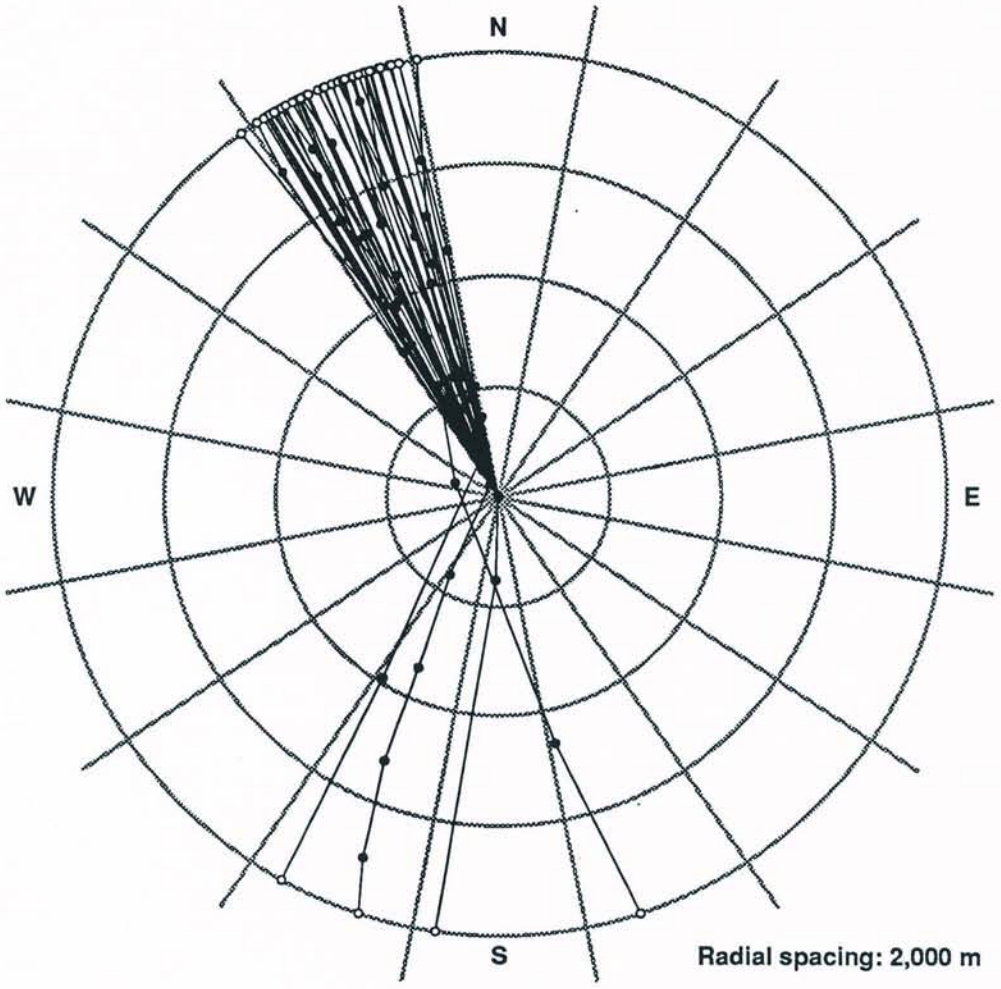

Figure F–8. Wind trajectories initially from SSE. The fraction remaining in sector NNW from the simulation shown was 88%.

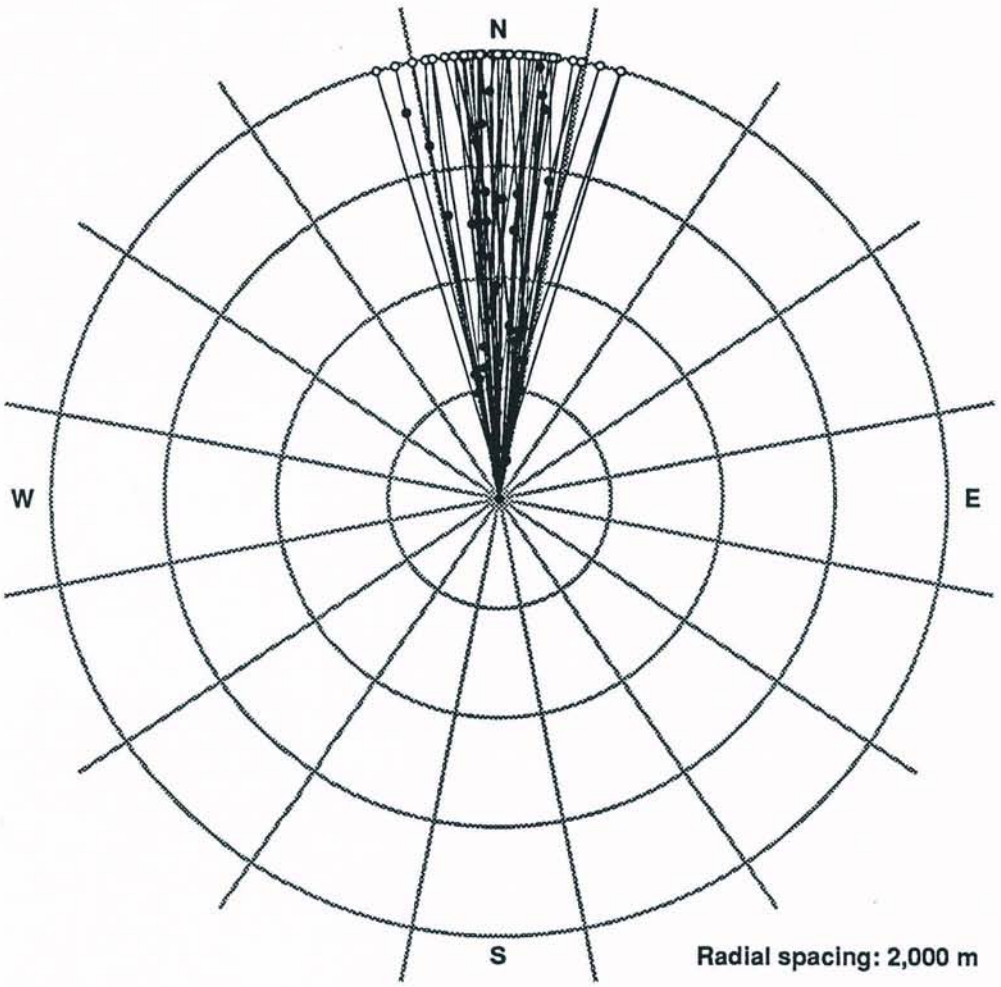

Figure F–9. Wind trajectories initially from S. The fraction remaining in sector N from the simulation shown was 90%.

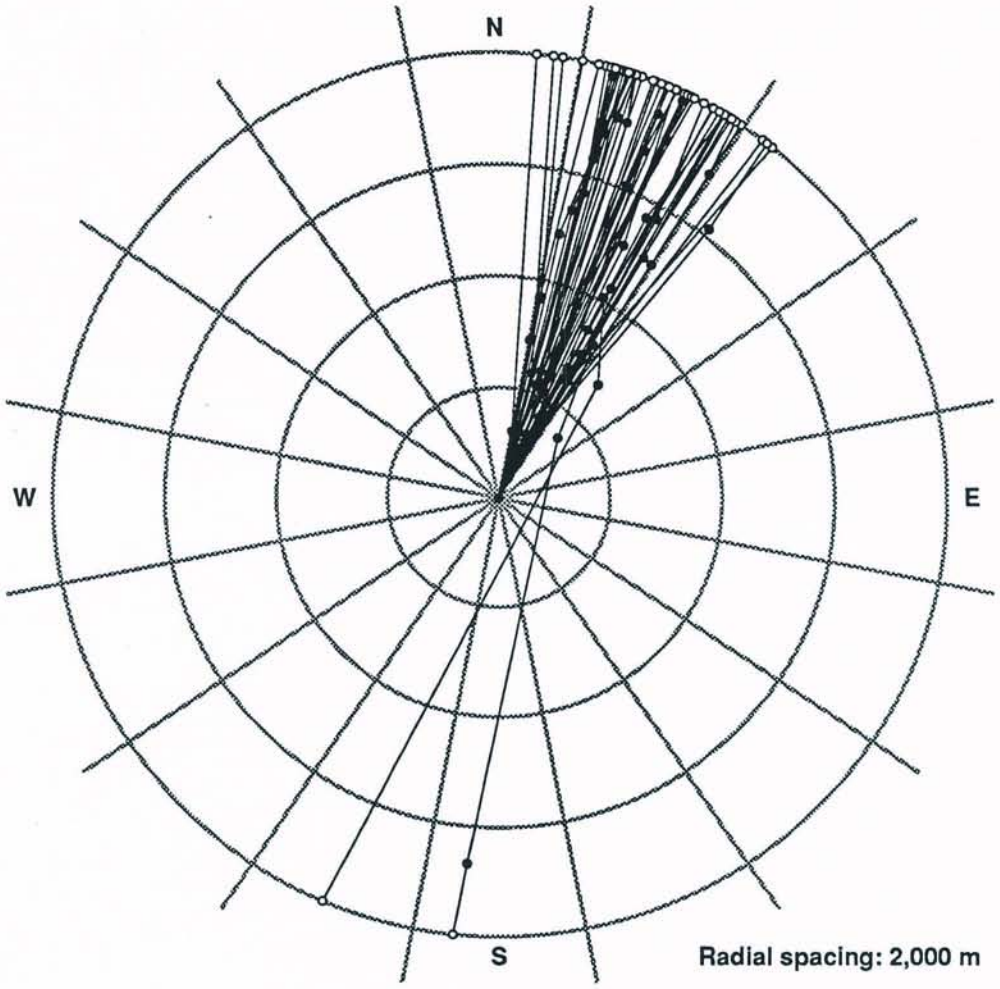

Figure F–10. Wind trajectories initially from SSW. The fraction remaining in sector NNE from the simulation shown was 84%.

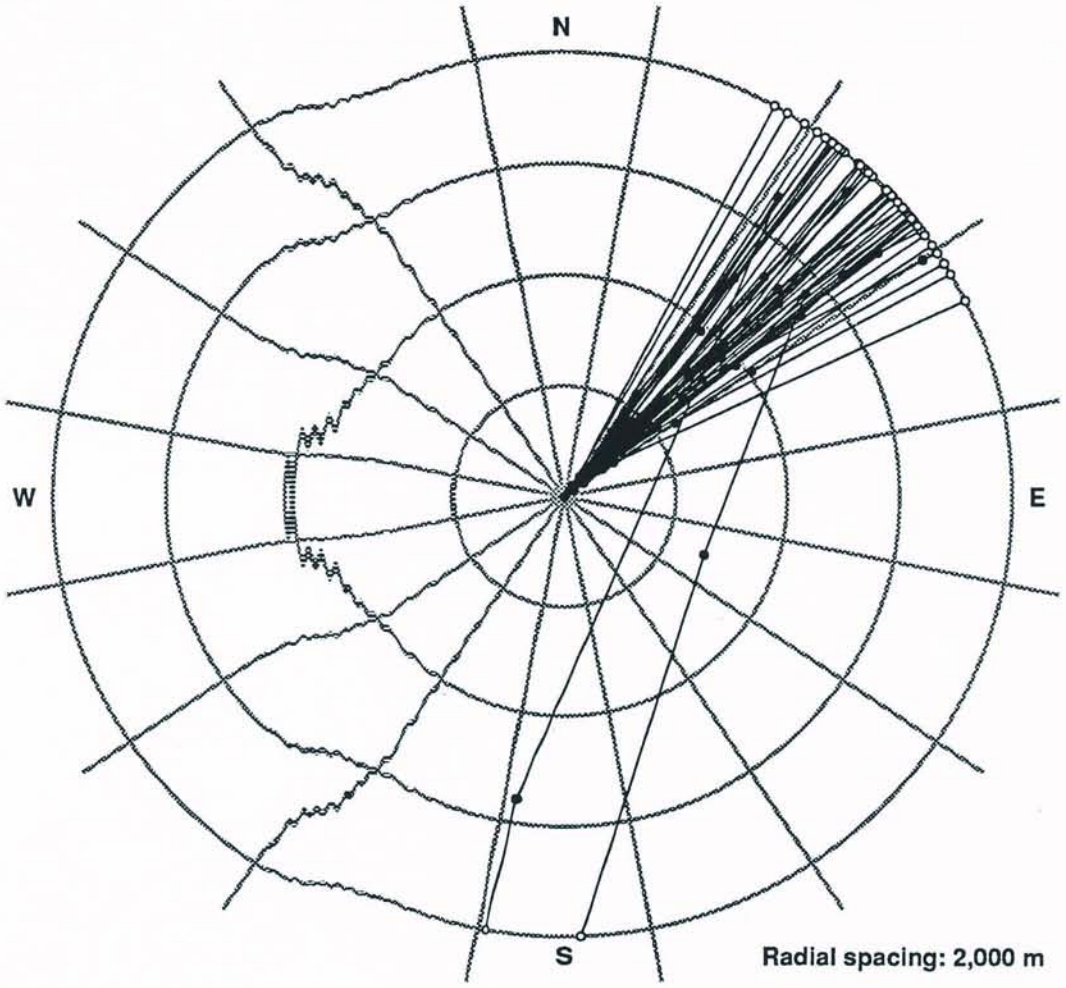

Figure F–11. Wind trajectories initially from SW. The fraction remaining in sector NE from the simulation shown was 82%.

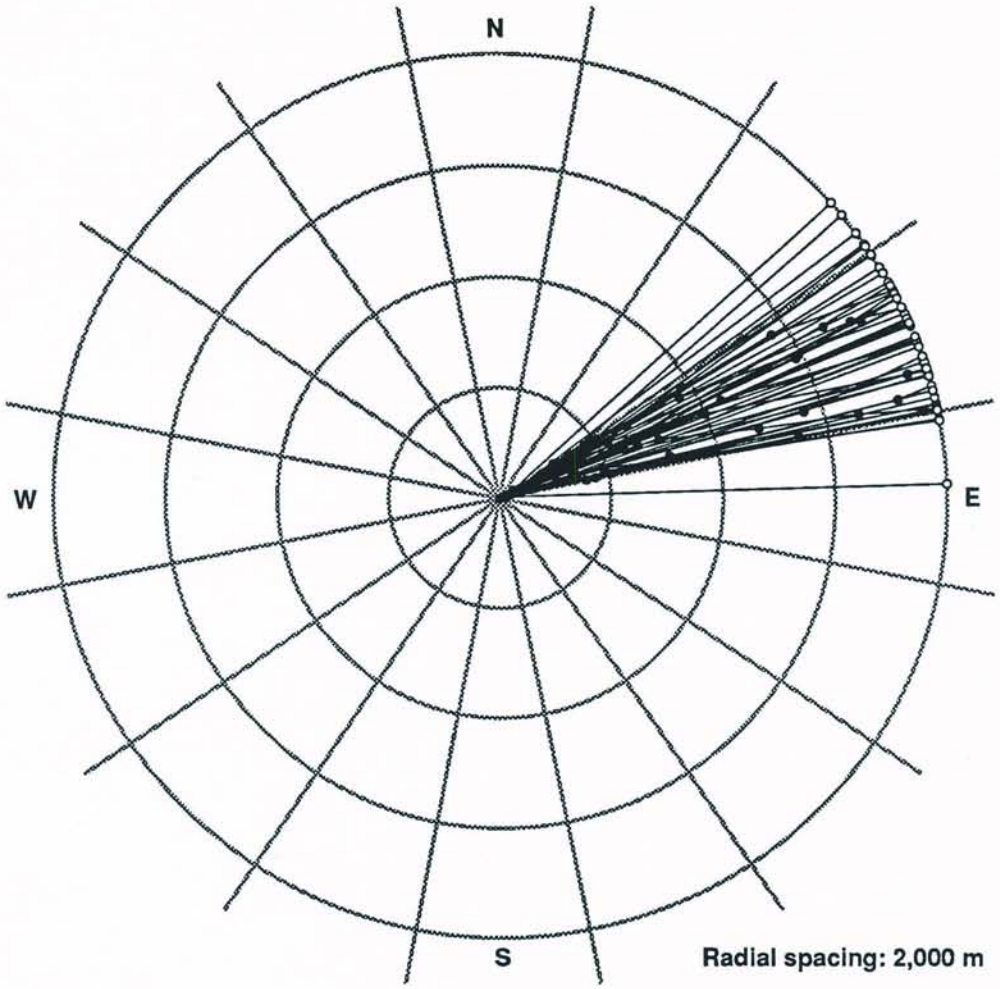

Figure F–12. Wind trajectories initially from WSW. The fraction remaining in sector ENE from the simulation shown was 84%.

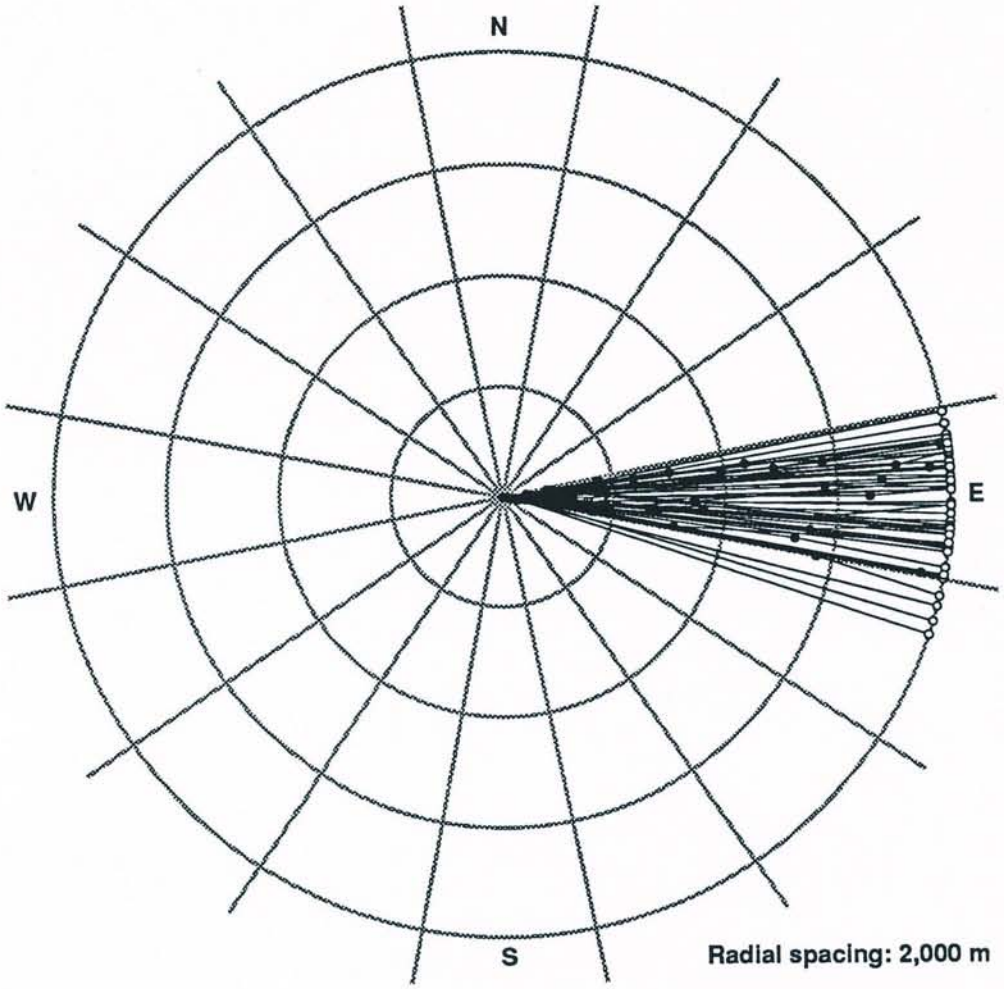

Figure F–13. Wind trajectories initially from W. The fraction remaining in sector E from the simulation shown was 92%.

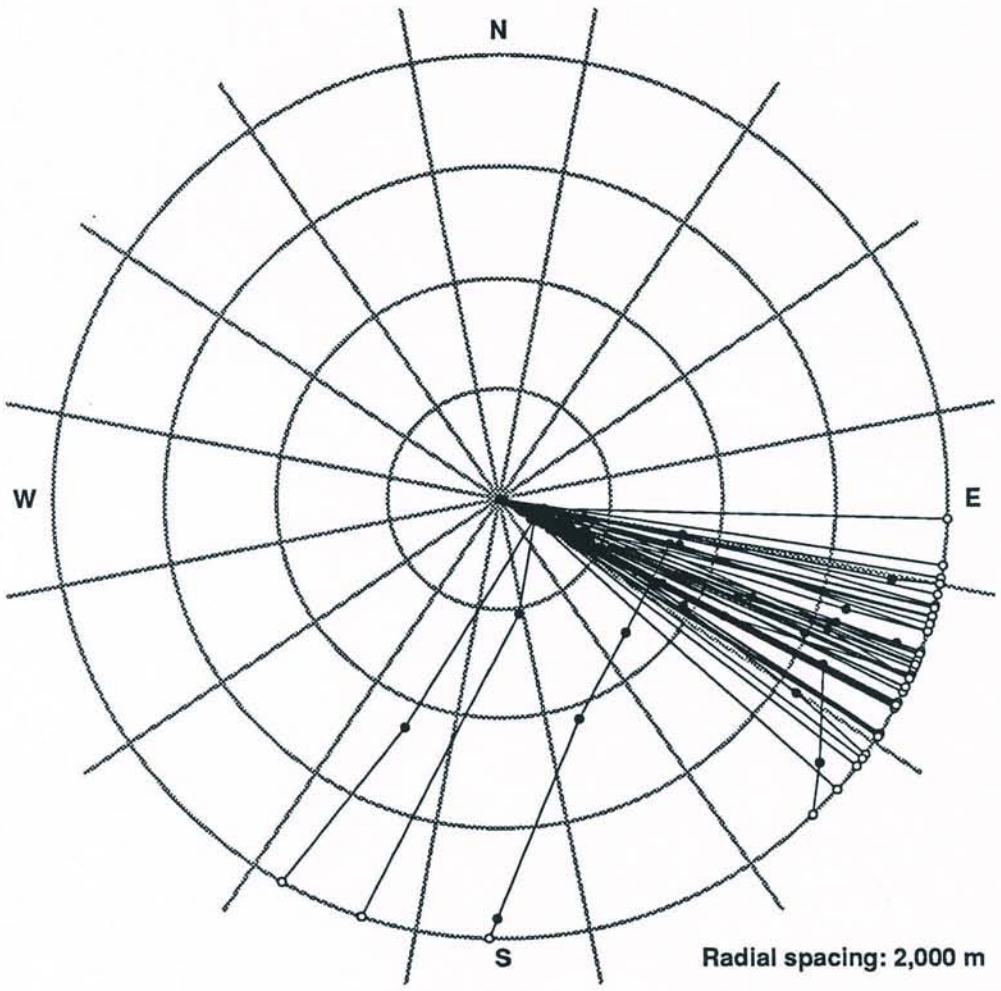

Figure F–14. Wind trajectories initially from WNW. The fraction remaining in sector ESE from the simulation shown was 76%.

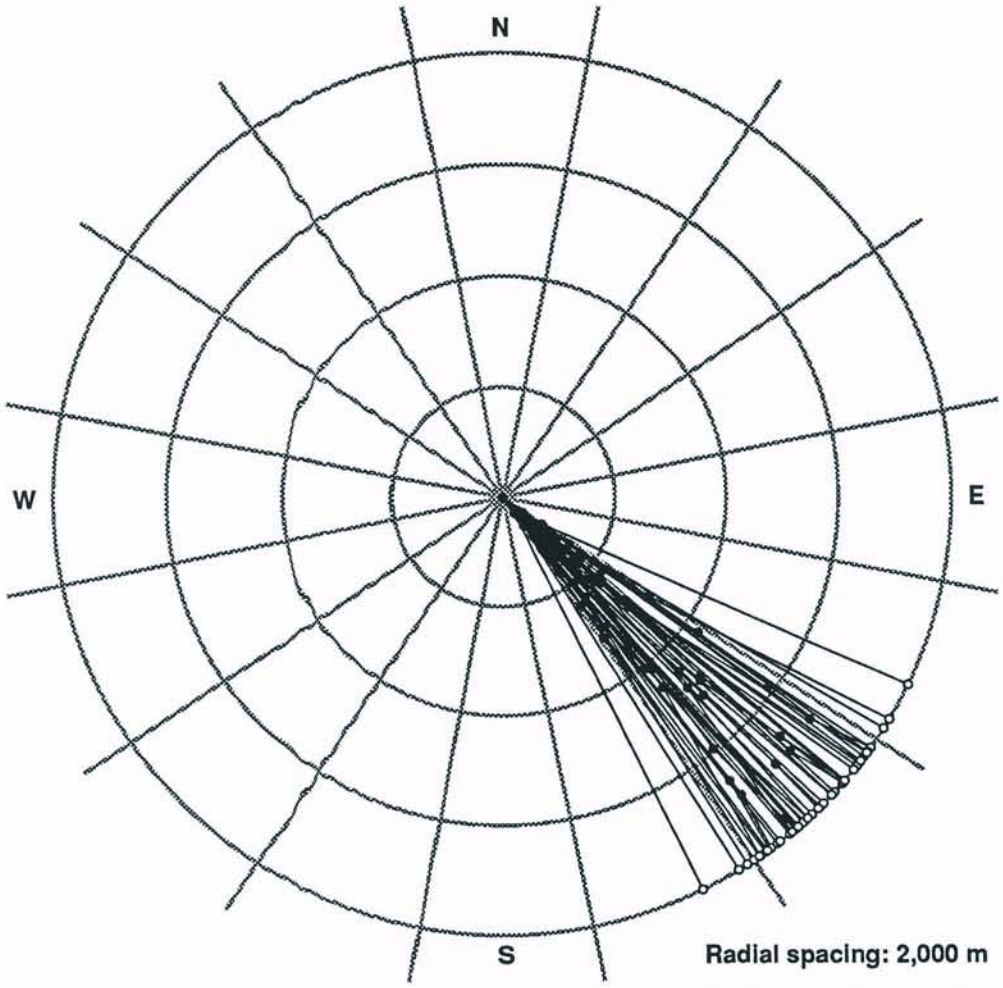

Figure F–15. Wind trajectories initially from NW. The fraction remaining in sector SE from the simulation shown was 88%.

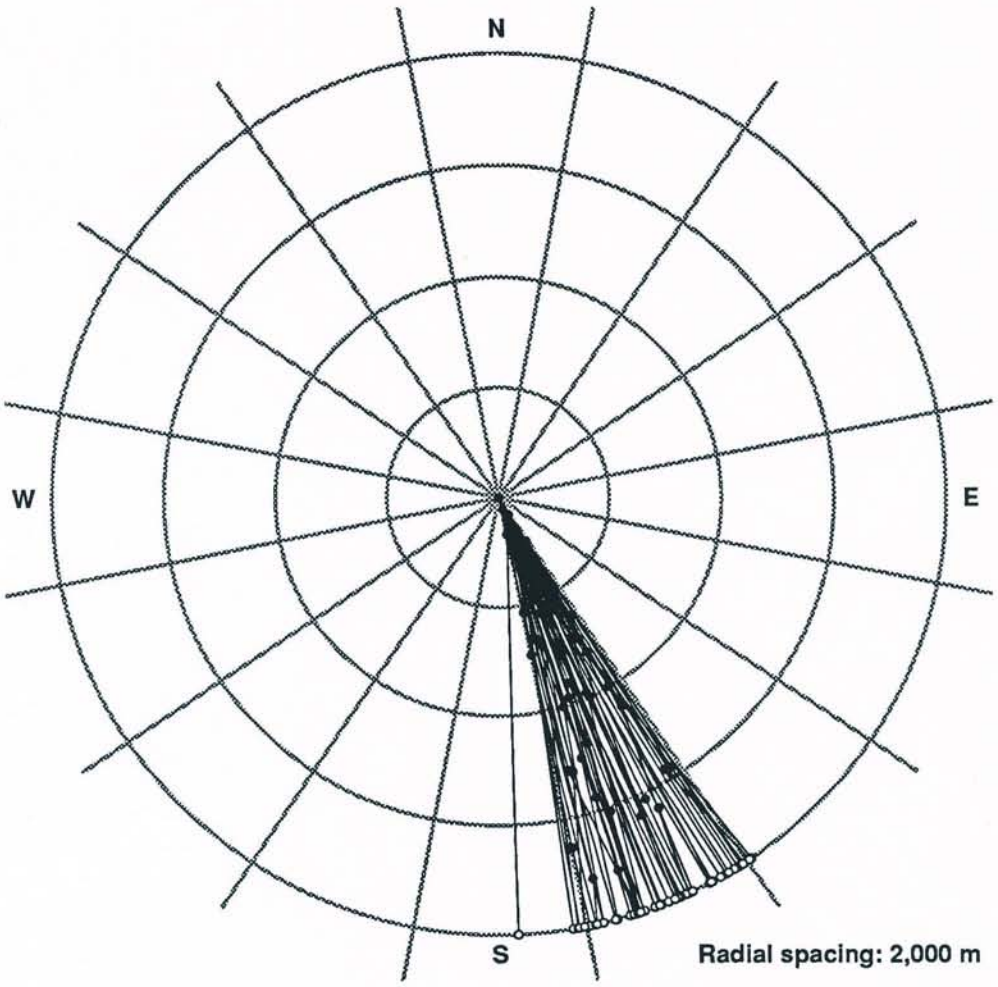

Figure F–16. Wind trajectories initially from NNW. The fraction remaining in sector SSE from the simulation shown was 86%.

APPENDIX G

DRY DEPOSITION AND PLUME DEPLETION

INTRODUCTION

Airborne contaminants in the form of small particles and gases are carried into contact with surfaces at or near ground-level by air turbulence and molecular diffusion and are fractionally retained on those surfaces as the result of chemical, physical, and biological processes. In addition, gravitational settling acts differentially on particles according to their size, density, and shape. These complex interactions are treated as a simple first-order removal process characterized by a coefficient v_d (m s^{-1}) called a DEPOSITION VELOCITY. The assumption is that the rate of deposition of radioactivity on the ground (pCi m^{-2} s^{-1}) is proportional to the concentration in the air at a specified reference height (assumed to be 1 m in this report). The proportionality factor is the deposition velocity v_d. Much effort has been devoted to the theoretical and experimental determination of deposition velocities, as review articles indicate (McMahon and Denison 1979, Sehmel 1980, Hosker and Lindberg 1982).

In this appendix, we describe theoretical and empirical approaches to estimating deposition velocity as a function of particle size and density, the nature of the surface, and micrometeorological variables. It is difficult to make direct reconciliation of deposition velocities estimated in this way with data from field studies, because field investigators often have not provided systematic observations of parameters that go into the theoretical calculation. Wind tunnel studies are more easily controlled but offer less meteorological reality.

Our defense of the models we have used rests on their physical plausibility and their role in the successful estimation of uranium deposition, which was measured by deployment of gummed film during the 1960s (Appendix M). We will show, however, that total deposition for the FMPC region is dominated by depositon of the effluent from the Plant 8 scrubbers, and thus the gummed-film validation can only be compared with the total but cannot validate minor components individually.

Depletion of the plume by deposition processes affects estimation of ground-level air concentrations and therefore dose. Two principal approaches to estimating depletion due to dry deposition may be called SOURCE DEPLETION and SURFACE DEPLETION. The former is substantially less costly to implement, but the latter is more satisfying to physical intuition. The claim to superiority of surface depletion models rests principally on theoretical arguments, whereas source depletion models continue to be used because of their computational efficiency and the lack of clear evidence of serious errors in their predictions, particularly for small domains.

In an order of presentation that we hope minimizes confusion, we begin by defining physical constants and meteorological quantities that repeatedly enter the formulas describing the deposition model. Then we present details of a generic wind profile, based on wind speed measured at a reference height and other meteorological variables, together with a parameter that characterizes surface roughness. These matters are preamble to a straightforward statement of the deposition model. Important results on empirical deposition velocities at the FMPC are presented, and we develop a special theory of deposition for the effluent from the

Plant 8 scrubbers. It is not our purpose to present a primer in any of the associated subject matter; we provide references to other sources for readers requiring a fuller discussion.

FUNDAMENTAL QUANTITIES

This section is primarily an annotated glossary of symbols for the physical constants and quantities that appear in the formulas defining our dry deposition model. For detailed and fundamental discussions of the context in which these quantities arise, we suggest Hanna et al. (1982) and Seinfeld (1986). We express units in the cgs system in this glossary, but please note that different units appear in other sections of this appendix.

μ_{air} = dynamic viscosity of air = 1.78×10^{-4} g s^{-1} cm^{-2}.

ρ_{air} = density of air, taken as 1.2×10^{-3} g cm^{-3}.

κ = von Kármán's constant, taken as 0.4 (dimensionless).

ν_{air} = μ_{air}/ρ_{air} (cm s^{-1}) = kinematic viscosity of air.

u_* = friction velocity (m s^{-1}), defined as the square root of the vertical momentum flux, which can be expressed as $K_{mz}(\partial u/\partial z)$, where the partial derivative is the gradient of the vertical profile of wind speed and K_{mz} is a vertical momentum flux rate coefficient (m^2 s^{-1}) (Hanna et al. 1982; also see the next section).

z_0 = roughness length (cm), which is related to roughness of the surface over which the wind moves. Hanna et al. (1982) suggest that $z_0 \approx 1/10$ of the height of the roughness elements. Table G–1 shows approximate values of the roughness length for different surfaces. We have used z_0 = 0.22 m, which is the geometric mean of values for uncut grass and trees. These ground covers represent extremes for most of the FMPC area.

L = Monin-Oboukhov length (cm), which is positive for stable conditions, negative for unstable conditions, and becomes infinite for neutral conditions. The correspondence with the Pasquill-Gifford stability categories A–F is indicated in Fig. G–1.

λ = mean free path length for air molecules = 9.322×10^{-6} cm.

C_c = Cunningham's slip correction = $1 + (2\lambda/d)[A + Q\exp(-bd/2\lambda)]$ (dimensionless), where d is the particle diameter (cm), $A = 1.234$, $Q = 0.413$, and $b = 0.904$ (Dennis 1976).

τ = characteristic particle relaxation time = $d^2\rho_p C_c/(18\mu_{air})$ (s), where d is the particle diameter (cm) and ρ_p is the particle density (g cm^{-3}).

St = Stokes' number = $\tau u_*^2/\nu_{air} = d^2\rho_p\rho_{air}C_c u_*^2/(18\mu_{air}^2)$ (cm).

k = Boltzmann's constant = 1.32×10^{-16} erg $(\text{molecule K})^{-1}$.

D = Brownian diffusivity = $kTC_c/(3\pi\mu_{air}d)$ (cm^2 s^{-1}) (Seinfeld 1986), where d is the particle diameter (cm) and T is the temperature (296 K was used).

Sc = Schmidt number = $\nu_{air}/D = 3\pi\mu_{air}^2 d/(kTC_c\rho_{air})$ (cm^{-1}).

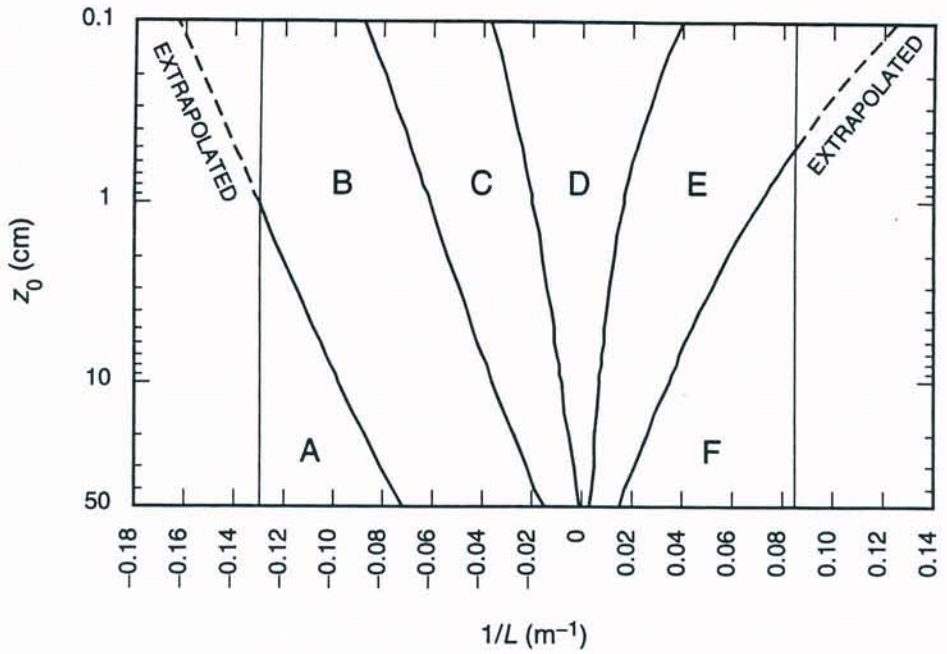

Figure G–1. Pasquill-Gifford turbulence classes as a function of roughness length z_0 and the reciprocal Monin-Obukhov length. Computerized conversion from $1/L$ to one of the classes A–F is based on a routine that stores digitized versions of the curves that separate the classes. (Redrawn from Hanna et al. (1982) with our extrapolations shown as dashed lines.)

Table G–1. Roughness Lengths for Various Surfaces[a]

Surface	z_0 (m)
Very smooth	10^{-5}
Snow	10^{-3}
Lawn	10^{-2}
Uncut grass	0.05
Mature root crops	0.1
Tree covered	1

[a] Excerpted from Seinfeld (1986), p. 495.

WIND SPEED PROFILE

Wind speed plotted as a function of the height z above the ground (say for a specific atmospheric stability category) is called a wind speed profile. Such profiles serve two purposes for the work described in this appendix: (1) they enable adjustment of wind speeds measured at a fixed reference height to the height of a release for purposes of modeling the downwind progress of the material (10 m is a typical reference height for airport measurements and is one of two instrumented levels for the tower at the FMPC site), and (2) profile expressions occur in formulas for the dry deposition model described in this appendix.

The formulas, which we state without proof, relate the wind speed at height z, $u(z)$, to the roughness length z_0 and the friction velocity u_*. They are

$$\begin{aligned}\frac{\kappa u(z)}{u_*} &= \ln\left(\frac{z}{z_0}\right) + \frac{4.7}{L}(z - z_0) \quad \text{for stable conditions } (1/L > 0) \\ &= \ln\left(\frac{z}{z_0}\right) \quad \text{for neutral conditions } (1/L = 0) \\ &= \ln\left(\frac{z}{z_0}\right) + \ln\left(\frac{(\eta_0^2 + 1)(\eta_0 + 1)^2}{(\eta^2 + 1)(\eta + 1)^2}\right) \\ &\quad + 2(\arctan\eta - \arctan\eta_0) \quad \text{for unstable conditions } (1/L < 0) \end{aligned} \tag{G–1}$$

where

$$\eta = \left(1 - 15\frac{z}{L}\right)^{1/4}, \quad \eta_0 = \left(1 - 15\frac{z_0}{L}\right)^{1/4},$$

κ is the von Kármán constant, u_* is the fraction velocity, and L is the Monin-Obukhov length (see the glossary of symbols above). This continuous variable is related to the Pasquill-Gifford stability categories by Fig. G–1. Note that Eq. G–1 is applicable only for $z > z_0$ and $u(z_0) = 0$. Equation G–1, as presented by Seinfeld (1986), shows three cases based on stability: the middle formula, for neutral conditions, is well known (Hanna et al. 1982); the others are the result of integrating empirical fits to $\partial u/\partial z$ obtained by Businger et al. (1971). To use the formulas for calculating the wind speed $u(z)$, one must know either u_* or the wind speed at some height $> z_0$. Typically, we have a value of the wind speed $u(10)$ measured at reference height 10 m, which we substitute into Eq G–1, solve for u_*, and then use the formula to obtain $u(z)$ for any other height. Figure G–2 shows a set of wind speed profiles that correspond to z_0 = 0.22 m.

GRAVITATIONAL SETTLING

For larger particles, an important component of deposition is gravitational settling. This component becomes dominant as the physical particle diameter increases above 10 μm. In the approach to dry deposition used in our simulations and presented in this appendix, gravitational settling is incorporated into the deposition velocity as one of several components. We denote this component by the symbol v_t and present formulas for it. The approach is adapted from Hanna et al. (1982).

Stokes' law gives the gravitational settling velocity for particles with physical diameters less than about 20 μm (the upper limit of validity depends on the particle density):

$$v_t = \frac{C_c d^2 g \rho_p}{18\mu_{air}} \tag{G–2}$$

where d is the particle physical diameter (μm), ρ_p is the particle density (g cm^{-3}), and g is the gravitational acceleration constant (cm s^{-2}). The Cunningham slip correction factor C_c has been added to the formula to account for the increased mobility of particles of diameter less than the mean free path of the air molecules (see the glossary of symbols above).

Larger particles require a different approach. Figure G–3 gives v_t as a function of diameter for density 5 g cm^{-3}. For other densities ρ_p we approximate the gravitational settling

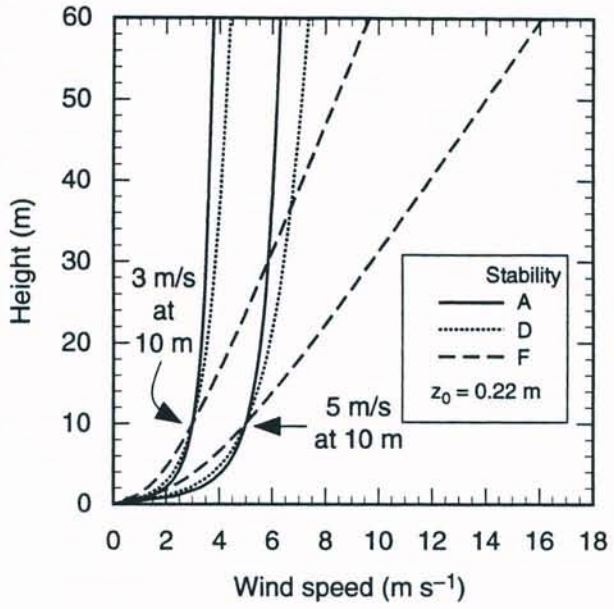

Figure G–2. Wind speed profiles for very unstable (class A), neutral (class D), and very stable (class F) conditions and roughness length z_0 = 0.22 m. Curves are shown that correspond to wind speeds of 3 and 5 m s^{-1} at reference height 10 m. The profiles are based on the formulas of Eq. G–1.

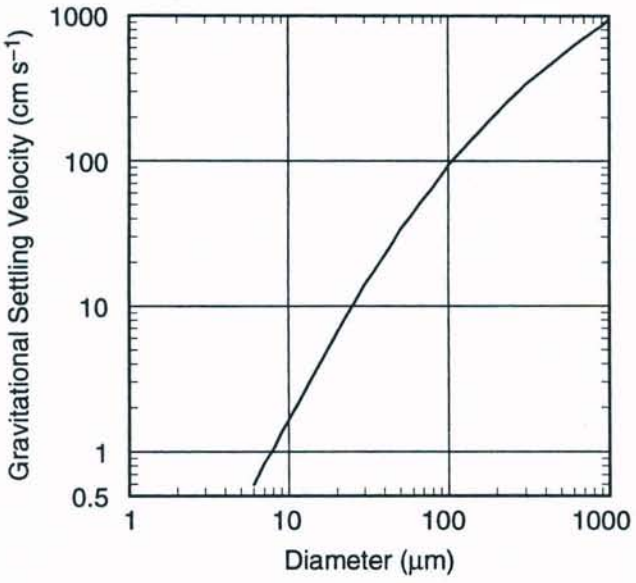

Figure G–3. Gravitational settling velocity for spherical particles with density 5 g cm^{-3} (redrawn from Hanna et al. (1982) with correction of the horizontal axis label).

velocity by using the plotted v_t times $\rho_p/5$. Our computer routines use Eq. G–2 for physical diameter $d \leq 6$ μm, a digitized version of Fig. G–3, corrected for particle density, for $d \geq 10$ μm, and logarithmic interpolation between the two in the transitional range $6 < d < 10$ μm.

DRY DEPOSITION VELOCITY

Our model for dry deposition can be expressed by the formula for the deposition rate

$$\omega = v_d \chi \tag{G–3}$$

where ω has units pCi m^{-2} s^{-1}, χ is the concentration of the airborne pollutant (pCi m^{-3}) at the reference level (taken as 1 m), and v_d (m s^{-1}) is the dry deposition velocity. Measurements of deposition velocities show a functional trend with physical particle diameter but more than an order of magnitude of scatter about this trend (Sehmel 1980).

We are aware of no measurements of deposition velocity in the vicinity of the FMPC during the facility's operation. The many field measurements at other locations provide insufficient information on concomitant variables to support empirical models. Using the results of wind tunnel studies, Sehmel and Hodgson (1980) provided a regression function for particulate deposition in the surface layer. We discuss this function further later in this section.

Electrical circuit analogies are a useful method of analyzing components of dry deposition (Seinfeld 1986, Hosker and Lindberg 1982). Our model of the dry deposition velocity is summarized by the resultant of three component resistances:

$$v_d = \frac{1}{r_{total}} = \frac{1}{r_a + r_s} + \frac{1}{r_t} \tag{G–4}$$

(Fig. G–4) where

r_{total} = total resistance,

r_a = momentum flux resistance associated with atmospheric turbulence above the laminar surface layer,

r_s = resistance of the surface layer,

r_t = resistance to gravitational settling = $1/v_t$.

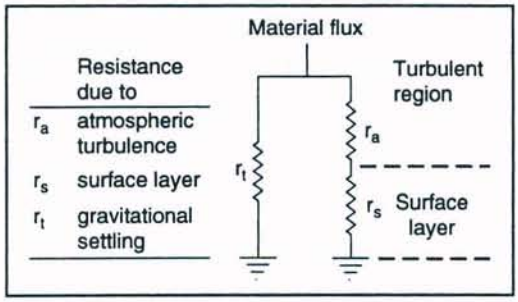

Figure G–4. Electrical resistance analogy for dry deposition.

The momentum transfer resistance r_a is represented by the equation

$$\frac{1}{r_a} = \frac{u_*^2}{\bar{u}_1} \tag{G–5}$$

(Seinfeld 1986), where u_* is the friction velocity (m s^{-1}) and $\bar{u}_1$ is the mean horizontal wind speed (m s^{-1}) at the reference height for deposition (1 m in this appendix). In general, we are

given the mean horizontal wind speed and calculate the friction velocity u_* from Eq. G–1. Note that through Eq. G–1 r_a depends on the roughness length z_0 and the Monin-Obukhov length L (or in rougher terms, the Pasquill-Gifford stability class). We return to this dependence below.

Various representations have been suggested for the surface layer resistance r_s. One version that accounts for both molecular diffusion of smaller particles and inertial effects of larger ones was suggested by Slinn (1976):

$$\frac{1}{r_s} = u_*(\mathrm{Sc}^{-2/3} + 10^{-3/\mathrm{St}}) \qquad \text{(G–6)}$$

where the Stokes number St is an increasing function of the particle diameter, and thus the term $10^{-3/\mathrm{St}}$ increases with particle diameter; this term represents the inertial effects of the larger particles. The Schmidt number Sc tends to zero with the particle diameter; thus the term $\mathrm{Sc}^{-2/3}$ increases without bound as the particle diameter tends to zero. This term expresses deposition by molecular diffusion of the smaller particles (see the glossary of fundamental quantities above for definitions of St and Sc).

Equations G–4 through G–6 — and the definition of the gravitational settling velocity v_t in the previous section — define our adopted model for the deposition velocity of particles. As noted, v_d is not a constant but depends on other variables. Through the momentum transfer resistance r_a, it depends on the roughness length z_0, the mean horizontal wind speed $\bar{u}_1$, and the Pasquill-Gifford stability class. And through the surface-layer resistance r_s and the gravitational settling velocity v_t, the depositon velocity v_d depends on the physical particle diameter and the particle density. Table G–2 illustrates some of these dependencies. The physical particle diameters are class medians from a lognormal distribution of physical particle diameter with GM = 4.0 μm, GSD = 2.0, and particle density = 7.0 g cm^{-3} (the density used for U_3O_8; see Appendix D). Deposition velocity is shown for the adjusted (1 m) wind speeds corresponding to the measured ranges at the 10-m height, and for Pasquill-Gifford stabilities A–F. All deposition velocities in Table G–2 are evaluated for the roughness length z_0 = 0.22 m.

Sehmel and Hodgson (1980) developed a model of dry deposition for which the surface layer resistance r_s is supplied by a regression function of several combinations of the variables that enter into the resistances we have defined above. The regression function for the surface resistance was fitted to data from wind tunnel experiments. The functional form of this model that we have implemented, as given in the 1980 reference, is

$$\mathrm{Int}_3 = -\exp\left(-378.051 + 16.498\ln\mathrm{Sc} + P\ln\tau^+ - 12.8044\ln d\right)$$

where

$$\tau^+ = \text{scaled dimensionless relaxation time} = \frac{\rho_p d^2}{18\mu}\frac{u_*^2}{\nu} \times 10^{-8},$$

$$P = -11.8178 - 0.28628\ln\tau^+ + 0.32262\ln(d/z_0) - 0.33850\ln(D/(z_0 u_*)),$$

d is the particle diameter (μm), and other symbols are defined in the glossary near the beginning of the appendix. The surface resistance is then given by

$$r_s = \frac{1 - \exp\left((v_t/u_*)\mathrm{Int}_3\right)}{v_t}. \qquad \text{(G–7)}$$

Table G–2. Dry Deposition Velocities[a] (m s^{-1}) and Adjusted Wind Speeds at 1 m (m s^{-1})

$\bar{u}$ (10m)	Physical diam. (μm)	Stability A	B	C	D	E	F
1 m s^{-1}	0.547	0.00013	0.00013	0.00012	0.00012	0.00011	0.00011
	0.874	0.00023	0.00023	0.00023	0.00022	0.00022	0.00022
	1.173	0.00037	0.00037	0.00037	0.00037	0.00036	0.00036
	1.512	0.00058	0.00058	0.00058	0.00058	0.00057	0.00057
	1.948	0.00092	0.00092	0.00092	0.00092	0.00092	0.00092
	2.617	0.0016	0.0016	0.0016	0.0016	0.0016	0.0016
	4.175	0.0039	0.0039	0.0039	0.0039	0.0039	0.0039
Adj. windsp. (m s^{-1})		0.47	0.46	0.43	0.4	0.35	0.3
3 m s^{-1}	0.547	0.0002	0.00019	0.00018	0.00017	0.00016	0.00015
	0.874	0.00028	0.00027	0.00027	0.00026	0.00025	0.00025
	1.173	0.00041	0.00041	0.0004	0.0004	0.00039	0.00038
	1.512	0.00065	0.00061	0.0006	0.0006	0.00059	0.00059
	1.948	0.0023	0.0013	0.00098	0.00094	0.00093	0.00093
	2.617	0.016	0.008	0.0034	0.0021	0.0017	0.0016
	4.175	0.065	0.049	0.032	0.022	0.01	0.0051
Adj. windsp. (m s^{-1})		1.4	1.4	1.3	1.2	1.0	0.91
5 m s^{-1}	0.547	0.00028	0.00026	0.00024	0.00023	0.00021	0.00019
	0.874	0.00041	0.00033	0.00031	0.0003	0.00028	0.00027
	1.173	0.0038	0.0013	0.00055	0.00044	0.00041	0.0004
	1.512	0.023	0.011	0.0034	0.0014	0.00067	0.00061
	1.948	0.065	0.041	0.02	0.0095	0.0026	0.0011
	2.617	0.11	0.086	0.058	0.039	0.017	0.0052
	4.175	0.15	0.13	0.1	0.086	0.062	0.038
Adj. windsp. (m s^{-1})		2.4	2.3	2.1	2.0	1.7	1.5
7 m s^{-1}	0.547	0.00038	0.00033	0.0003	0.00028	0.00025	0.00022
	0.874	0.0096	0.0032	0.00084	0.00042	0.00032	0.0003
	1.173	0.055	0.029	0.011	0.004	0.00083	0.00044
	1.512	0.12	0.079	0.044	0.024	0.0066	0.0013
	1.948	0.17	0.13	0.09	0.064	0.03	0.009
	2.617	0.2	0.17	0.13	0.11	0.07	0.037
	4.175	0.23	0.19	0.16	0.14	0.11	0.081
Adj. windsp. (m s^{-1})		3.3	3.2	3.0	2.8	2.4	2.1
9 m s^{-1}	0.547	0.0027	0.00086	0.0004	0.00034	0.0003	0.00026
	0.874	0.065	0.033	0.012	0.0042	0.00074	0.00033
	1.173	0.15	0.11	0.06	0.033	0.0093	0.0016
	1.512	0.22	0.17	0.12	0.084	0.04	0.012
	1.948	0.26	0.21	0.16	0.13	0.084	0.042
	2.617	0.28	0.24	0.19	0.16	0.12	0.083
	4.175	0.3	0.26	0.21	0.19	0.15	0.12
Adj. windsp. (m s^{-1})		4.3	4.1	3.8	3.6	3.1	2.7
11 m s^{-1}	0.547	0.022	0.0079	0.0019	0.00068	0.00035	0.0003
	0.874	0.16	0.11	0.054	0.027	0.0062	0.0009
	1.173	0.26	0.2	0.13	0.093	0.042	0.011
	1.512	0.31	0.25	0.19	0.15	0.095	0.044
	1.948	0.34	0.28	0.23	0.19	0.14	0.088
	2.617	0.36	0.3	0.25	0.21	0.17	0.12
	4.175	0.37	0.32	0.27	0.23	0.19	0.15
Adj. windsp. (m s^{-1})		5.2	5.0	4.7	4.4	3.8	3.3

[a] Surface transfer resistance based on Eq. G–6. Distribution of physical particle diameters is log-normal with GM = 4 μm and GSD = 2. Particle density is 7.0 g cm^{-3}.

Deposition velocities based on the surface resistance of Eq. G–7 are shown in Table G–3, with particle density and distribution of particle diameters the same as for Table G–2. Comparisons of the total deposition velocity models based on Eq. G–4 using the surfaces resistances given

Table G–3. Dry Deposition Velocities[a] (m s^{-1}) and Adjusted Wind Speeds at 1 m (m s^{-1})

$\bar{u}$ (10m)	Physical diam. (μm)	Stability A	B	C	D	E	F
1 m/s	0.547	0.00073	0.00077	0.00082	0.00088	0.00099	0.0012
	0.874	0.0012	0.0013	0.0013	0.0014	0.0016	0.0018
	1.173	0.0018	0.0019	0.002	0.002	0.0022	0.0025
	1.512	0.0026	0.0027	0.0028	0.0028	0.003	0.0033
	1.948	0.0038	0.0039	0.0039	0.004	0.0042	0.0045
	2.617	0.006	0.006	0.006	0.0061	0.0063	0.0065
	4.175	0.012	0.012	0.012	0.012	0.012	0.011
Adj. wind sp. (m s^{-1})		0.47	0.46	0.43	0.4	0.35	0.3
3 m/s	0.547	0.00071	0.00068	0.00066	0.00065	0.00064	0.00065
	0.874	0.0013	0.0012	0.0012	0.0011	0.0011	0.0011
	1.173	0.002	0.0019	0.0018	0.0018	0.0017	0.0017
	1.512	0.003	0.0028	0.0027	0.0026	0.0025	0.0025
	1.948	0.0045	0.0043	0.0041	0.004	0.0038	0.0037
	2.617	0.0075	0.0071	0.0067	0.0065	0.0062	0.006
	4.175	0.017	0.016	0.015	0.014	0.013	0.013
Adj. wind sp. (m s^{-1})		1.4	1.4	1.3	1.2	1.0	0.91
5 m/s	0.547	0.00095	0.00088	0.00081	0.00076	0.00071	0.00067
	0.874	0.0017	0.0016	0.0015	0.0014	0.0013	0.0012
	1.173	0.0027	0.0025	0.0023	0.0021	0.002	0.0018
	1.512	0.0042	0.0038	0.0035	0.0032	0.003	0.0028
	1.948	0.0065	0.0059	0.0053	0.005	0.0045	0.0042
	2.617	0.011	0.0099	0.0089	0.0083	0.0075	0.0069
	4.175	0.025	0.023	0.02	0.019	0.017	0.015
Adj. wind sp. (m s^{-1})		2.4	2.3	2.1	2.0	1.7	1.5
7 m/s	0.547	0.0013	0.0012	0.001	0.00095	0.00085	0.00076
	0.874	0.0024	0.0022	0.0019	0.0017	0.0015	0.0014
	1.173	0.0038	0.0034	0.003	0.0027	0.0024	0.0021
	1.512	0.0059	0.0053	0.0046	0.0042	0.0036	0.0032
	1.948	0.0094	0.0083	0.0072	0.0065	0.0056	0.005
	2.617	0.016	0.014	0.012	0.011	0.0095	0.0082
	4.175	0.038	0.033	0.028	0.025	0.021	0.018
Adj. wind sp. (m s^{-1})		3.3	3.2	3.0	2.8	2.4	2.1
9 m/s	0.547	0.0018	0.0016	0.0013	0.0012	0.001	0.00089
	0.874	0.0033	0.0029	0.0025	0.0022	0.0019	0.0016
	1.173	0.0054	0.0046	0.0039	0.0035	0.003	0.0025
	1.512	0.0084	0.0072	0.0061	0.0054	0.0045	0.0038
	1.948	0.013	0.011	0.0096	0.0085	0.0071	0.006
	2.617	0.023	0.02	0.017	0.014	0.012	0.01
	4.175	0.055	0.047	0.039	0.034	0.027	0.023
Adj. wind sp. (m s^{-1})		4.3	4.1	3.8	3.6	3.1	2.7
11 m/s	0.547	0.0024	0.0021	0.0017	0.0015	0.0013	0.001
	0.874	0.0045	0.0038	0.0032	0.0028	0.0023	0.0019
	1.173	0.0073	0.0062	0.0051	0.0045	0.0037	0.003
	1.512	0.012	0.0097	0.008	0.0069	0.0056	0.0046
	1.948	0.019	0.016	0.013	0.011	0.0088	0.0072
	2.617	0.033	0.027	0.022	0.019	0.015	0.012
	4.175	0.078	0.064	0.052	0.044	0.035	0.028
Adj. wind sp. (m s^{-1})		5.2	5.0	4.7	4.4	3.8	3.3

[a] Surface transfer resistance based on Sehmel and Hodgson (1980). Distribution of physical particle diameters is lognormal with GM = 4 μm and GSD = 2. Particle density is 7.0 g cm^{-3}.

by Eqs. G–6 and G–7 show important differences in the 0.2–2 μm range, with the latter model (i.e., Sehmel and Hodgson 1980) giving deposition velocities that are larger than those of the former. Figure G–5 shows a limited comparison based on z_0 = 0.22 m, $\bar{u}_1$ = 1 m s^{-1}, ρ_p = 7 g

cm^{-3}, and for neutral conditions (Pasquill-Gifford class D). The figure shows differences in excess of a factor of three, but for some combinations of parameters we have observed a factor of 14. We should note, however, that for the comparison shown in Fig. G–5, the model of Sehmel and Hodgson (1980) was based entirely upon the algorithm given in the reference and did not implement the combined resistances in the manner of Eqs. G–4 and G–5.

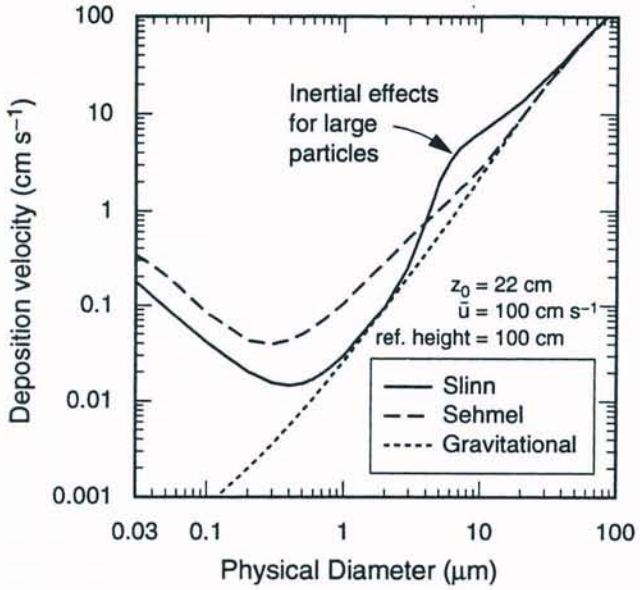

Figure G–5. Comparison of total deposition velocity computed with the model of Slinn (Eq. G–6) with that of Sehmel and Hodgson (1980) (Eq. G–7). Gravitational settling velocity is shown separately.

We choose as our standard the model of Sehmel and Hodgson (1980) for the surface resistance r_s as given by Eq. G–7, combined with Eqs. G–4 and G–5. With its calibration to a variety of wind tunnel data, this model has a clearer connection with a broader scope of data than does the model of Eq. G–6. Table G–4 shows a comparison of the models when each model is averaged over the FMPC composite annual meteorology and over lognormal distributions of physical particle diameters with different geometric means and geometric standard deviation 2. The table indicates the same general relationship between the two models as does Fig. G–5, namely that the Sehmel and Hodgson model dominates in the micron and submicron range, but that the magnitudes reverse for a range of larger particles where the impaction term of Eq. G–6 becomes important. For very large particles, gravitational settling is of overwhelming importance, and the two models give the same result. We note that the results of the averaging are sensitive to increases in the GSD of the particle size distribution.

Table G–4. Deposition Velocities (m s^{-1}) for Two Models Averaged Over FMPC Meteorology and Lognormal Distributions of Physical Particle Diameters with Various Geometric Means[a]

Median (GM) physical diameter (μm)	Surface resistance model	
	Eq. G–7[b]	Eq. G–6[c]
0.02	0.0048	0.0032
0.05	0.0030	0.0011
0.1	0.0016	0.00045
0.2	0.00092	0.00023
0.5	0.0011	0.00029
1	0.0025	0.0019
2	0.0068	0.0087
5	0.026	0.032
10	0.072	0.078
20	0.20	0.20

[a] For each distribution, the particle density is 7 g cm^{-3}, and the geometric standard deviation is 2.

[b] Sehmel and Hodgson (1980).

[c] Slinn (1976).

PLUME DEPLETION

Plume depletion resulting from deposition is of interest because it reduces air concentration progressively downwind from the point of release. Most plume calculations have made use of an approximate procedure based on the technique of SOURCE DEPLETION to account for reduced air concentrations due to dry deposition (Van der Hoven 1968). The basic assumption is that the release rate is viewed as a function of downwind distance and diminishes as airborne material is lost by deposition. We write $Q = Q(x)$, with $Q(0)$ equal to the given (constant) release rate. Then for the Gaussian plume model, the rate of change of $Q(x)$ with x is the total rate of deposition, integrated across the width of the plume (Eqs. F–3 and F–4):

$$\frac{dQ}{dx} = -\int_{-\infty}^{+\infty} \omega \, dy = -\frac{v_d Q}{u} Z(x,0,h) \exp\left(-\lambda \frac{x}{u}\right) = -\sqrt{\frac{2}{\pi}} \frac{Q v_d}{u \sigma_z} \exp\left(-\frac{h^2}{2\sigma_z^2}\right) \exp\left(-\lambda \frac{x}{u}\right), \quad \text{(G–7)}$$

where $z = 0$ has been used in Eq. F–3. The solution can be expressed as

$$Q(x) = Q(0) \exp\left(-\sqrt{\frac{2}{\pi}} \frac{v_d}{u} \int_0^x \frac{\exp(-\lambda x'/u)\, dx'}{\sigma_z \exp(h^2/2\sigma_z^2)}\right), \quad \text{(G–8)}$$

where the integral is evaluated numerically, utilizing the functional dependence of σ_z on x' (Table F–1). For the time-dependent model, the analog of Eq. G–8 is

$$Q(x) = Q(0) \exp\left(-\sqrt{\frac{2}{\pi}} \frac{v_d}{u} \int_0^x \frac{\exp(-\lambda x'/u)\, dx'}{\sigma_z'}\right), \quad \text{(G–9)}$$

where $\sigma'_z = [\sigma_z^2 + (KA/a^2u^2S^2)F(T_{sv})]^{1/2}$ with notations as defined following Eq. J–4. For the Gaussian model, the resulting estimate of ground-level concentration in the plume is then calculated from Eq. F–4 (or its sector-averaged counterpart Eq. F–6, as appropriate) with Q replaced by $Q(x)$ from Eq. G–8. In the case of the time-dependent model, the ratio $Q(x)/Q(0)$ from Eq. G–9 is applied to the formula of Eq. J–4 or an appropriate analog. The principal objection to source depletion is that material is removed uniformly from the full vertical extent of the plume rather than from the part near the ground as intuition suggests. But the fact that the plume retains its Gaussian cross section makes this method more tractable and computationally much less expensive than most alternative methods, even with the necessary numerical integration, which is carried out by interpolation in tables stored in the computer. Van der Hoven (1968) provides curves that give Q vs. x for different release heights h and stabilities A–F, but the curves are based on formulations of σ_z that are different from those in Table F–1; even so, the results are not qualitatively different from those obtained with the Briggs formulas).

EMPIRICAL DEPOSITION VELOCITIES

Near each of the four air monitoring stations located at the corners of the FMPC production area (designated NE, SE, SW, NW), gummed film (gumpaper) deposition samples were taken regularly during the period May 1960 through December 1962. Thus, at these locations, we may pair adjusted monthly averages of air concentrations (Appendix L) with monthly depositions and estimate total deposition velocities by the ratios. We have performed these calculations and tabulated the estimates of deposition velocity by station. Table G–5 shows the summary statistics.

Table G–5. Empirical Deposition Velocities to Gumpaper (m s^{-1}) Between May 1960 and December 1962

	Perimeter location			
	NE	SE	SW	NW
Number	30	28	25	29
Mean	0.11	0.20	0.19	0.13
St. dev.	0.06	0.13	0.18	0.09
Median	0.08	0.16	0.14	0.11
Minimum	0.04	0.07	0.03	0.02
Maximum	0.24	0.70	0.75	0.41

Dry deposition velocities for the generic particle size distribution corresponding to U_3O_8 released from the dust collectors (Appendix D, Table D–3 and Fig. D–3), averaged over the FMPC meteorology and over the particle size distribution, give $v_d \approx 0.01$ m s^{-1}. The wet deposition velocity, based on the assumption of annual rainfall of 100 cm and a washout ratio of 6×10^5 (Appendix H gives a median washout ratio of 5.6×10^5; see Fig. H–2), is $v_w \approx 0.02$ m s^{-1}. Clearly, the sum of these dry and wet deposition velocities is much too small to account

for the magnitudes of the empirical deposition velocities shown in Table G–5. It is the effluent of the Plant 8 scrubbers that primarily contributes to high rates of dry deposition. We discuss the deposition properties of this effluent in the next section.

ESTIMATE OF PLANT-8 SCRUBBER CONTRIBUTION TO TOTAL DEPOSITION

Appendix D develops a theory of reentrainment of uranium-containing liquid from mist eliminators into the exhaust gas as large droplets that subsequently escape from the scrubbers. It was estimated that 70% of the released mass of uranium from the Plant 8 scrubbers was in reentrained droplets, while the remainder penetrated the scrubbers without being scavenged and escaped as particles with physical diameters in the range 0–10 μm, with mean in the submicron range (Appendix D, Table D–11). Similarly, for the Plant 2/3 scrubbers, 54% of released uranium was reentrained, and the remaining solid particles that penetrated the scrubbers had a mean physical diameter of about 1 μm. Deposition velocities for different particle-size ranges in these discrete distributions are shown in Table G–6.

The initial water droplet diameters were estimated to be in the range 100–200 μm, which we interpreted as a lognormal distribution with these limits as 15th and 85th percentiles, respectively, giving geometric mean 141 μm and geometric standard deviation 1.4. For this distribution of droplets, we estimate a mean deposition velocity of 0.37 m s^{-1}. As the droplets move downwind, they evaporate and leave the uranium as a solid particle or agglomerate, with estimated effective diameter range and density indicated in Table G–6 for the scrubbers of Plant 2/3 and Plant 8.

We are going to estimate an average deposition velocity for airborne particulates released from the FMPC during 1960–1962 and compare the result with the empirical deposition velocities given in Table G–5. For this calculation, we estimate the percentages of uranium released from the Plant 2/3 and Plant 8 scrubbers during 1960–1962 as 13.7% and 59.2%, respectively. We compute two averages. The first considers the reentrained portions to be in the initial droplets before any evaporation took place, which would maximize the average deposition velocity. The second average is based on the diameter of the residual solid after all moisture has evaporated, which gives the more realistic value because of the high evaporation rate. The calculation of the two averages is summarized in Table G–7.

This analysis indicates that as the release moves downwind from the Plant 8 scrubbers, the dry deposition velocity that is applicable to that entrained component of the release decreases from 0.37 m s^{-1} to 0.28 m s^{-1}. Similarly, the part of the release from the Plant 2/3 scrubbers corresponds to deposition velocities ranging from 0.37 m s^{-1} down to 0.18 m s^{-1}. Averaged over all production sources, the corresponding range is 0.18 m s^{-1} to 0.13 m s^{-1} (Table G–7). These latter values are of a magnitude comparable to that of the empirical deposition velocities presented in Table G–5. This concurrence of estimates adds a measure of confidence to the general air-transport modeling approach, and in particular, to those aspects of the assessment that depend on deposition velocity.

Appendix M compares simulated deposition with gummed film measurements during 1960–1962. The overall impression of this comparison is that the simulations generally tend to underpredict the measured deposition values by factors of two to three, and the trend to underprediction increases with distance from the source. This observation, together with

Table G–6. Deposition Velocities for Emissions from the Scrubbers of Plant 2/3 and Plant 8

Aerodynamic diameter (μm)	Physical diameter (μm)	Frequency (%)	Deposition velocity (m s^{-1})
Plant 2/3 Scrubbers			
Reentrained — 54% of release from Plant 2/3 scrubbers density = 2.8 g cm^{-3}			
55	33	33.3	1.4×10^{-1}
69	41	33.3	1.8×10^{-1}
82	49	33.3	2.3×10^{-1}
			Mean 1.8×10^{-1}
Penetrating — 46% of release from Plant 2/3 scrubbers density = 7.3 g cm^{-3}			
2.7	1	89	1.7×10^{-3}
6.8	2.5	5.4	6.4×10^{-3}
9.5	3.5	2.2	1.1×10^{-2}
12	4.5	2.6	1.5×10^{-2}
15	5.5	0.7	2.1×10^{-2}
			Mean 2.6×10^{-3}
Plant 8 Scrubbers			
Reentrained — 70% of release from Plant 8 scrubbers density = 2 g cm^{-3}			
42	30	27	9.9×10^{-2}
82	58	30	2.2×10^{-1}
110	78	29	3.1×10^{-1}
219	155	14	7.3×10^{-1}
			Mean 2.8×10^{-1}
Penetrating — 30% of release from Plant 8 scrubbers density = 8.3 g cm^{-3}			
1.4	0.5	71.4	8.2×10^{-4}
4.3	1.5	11.8	3.1×10^{-3}
10	3.5	14.6	1.1×10^{-2}
22	7.5	2.2	3.6×10^{-2}
			Mean 3.3×10^{-3}

the overestimation of measured air concentrations by the model simulations (Appendix J), suggests that the deposition and plume depletion models may not be estimating sufficient removal of particles from the plume. The deposition velocity model is prone to underestimate the removal of particles near the source of an elevated release (before the plume "touches down"), but most of the sources for this study have been simulated with a dispersion model that treats the material as if it originated near the ground. Another explanation of the underestimation is that the deposition velocity model does not treat the fall of large particles with sufficient realism. The tilted-plume model is a modification of the Gaussian plume that

Table G–7. Average Dry Deposition Velocity (m s^{-1}) for FMPC Releases of Airborne Uranium

	Source % [a]	Droplets [b]	Residue [c]
Plant 2/3			
Reentrained	7.4	0.37	0.18
Penetrating	6.3	0.0026	0.0026
Plant 8			
Reentrained	41.3	0.37	0.28
Penetrating	17.7	0.0033	0.0033
Dust collectors	27.3	0.01	0.01
Means		0.18	0.13

[a] Percent of total uranium released during 1960–1962. The percentages of the total release that came from the Plant 2/3 and Plant 8 scrubbers during this period are assumed to be 13.7% and 59.2%, respectively. The estimated partition fractions between reentrained droplets and particles that penetrated the scrubbers are given in Table G–6.

[b] Assumes that the reentrained fraction of the scrubber releases is in the form of the initial liquid droplets.

[c] Assumes that the reentrained fraction of the scrubber releases is in the form of the solid residue particles after evaporation of liquid.

simulates the free-fall of the particles at their terminal velocities (Hanna et al. 1982), and this model (or an adaptation of it to the time-dependent model) will be considered for the final calculations. It is also possible that the predicted air concentrations decrease too rapidly with increasing distance from the point of release. These questions will be investigated, and any needed adjustments will be made before the final calculations are performed.

REFERENCES

Businger J.A., J.C. Wyngaard, Y. Izumi, and E.F. Bradley. 1971. "Flux-Profile Relationships in the Atmospheric Surface Layer." *J. Atmos. Sci.* **28**:181–189.

Dennis R. (Ed.) 1976. *Handbook on Aerosols.* Rep. TID-26608, Technical Information Center, Energy Research and Development Administration. Available from NTIS, Springfield, Virginia.

Hanna S.R., G.A. Briggs, and R.P. Hosker, Jr. 1982. *Handbook on Atmospheric Diffusion.* Rep. DOE/TIC-11223 (DE82002045) Technical Information Center, U.S. Department of Energy.

Hosker R.P., Jr., and S.E. Lindberg. 1982. "Review: Atmospheric Deposition and Plant Assimilation of Gases and Particles." *Atmos. Env.* **16**:889–910.

McMahon T.A. and P.J. Denison. 1979. "Empirical Atmospheric Deposition Parameters — A Survey." *Atmos. Env.* **13**:571–585.

Ramsdell J.V., Jr., and K.W. Burk. 1990. *MESOILT2, A Lagrangian Trajectory Climatological Dispersion Model.* Unpublished draft report PNL-7340 HEDR, Pacific Northwest Laboratory, Richland, Washington.

Sehmel G.A. 1980. "Particle and Gas Dry Deposition: A Review." *Atmos. Env.* **14**:983–1011.

Sehmel G.A. and W.H. Hodgson. 1980. "A Model for Predicting Dry Deposition of Particles and Gases to Environmental Surfaces," in *Implications of Clean Air Ammendments of 1977 and of Energy Considerations for Air Pollution Control.* Symposium Series #196, vol. 76, American Institute of Chemical Engineers Symposium Series.

Seinfeld J.H. 1986. *Atmospheric Chemistry and Physics of Air Pollution.* John Wiley and Sons, New York.

Slinn W.G.N. 1976. "Dry Deposition and Resuspension of Aerosol Particles — A New Look at Some Old Problems." In *Atmosphere-Surface Exchange of Particulate and Gaseous Pollutants (1974),* proceedings of a symposium held in Richland, Washington, Sep. 4–6, 1974. CONF-740921, Battelle Pacific Northwest Laboratories, Richland, Washington.

Van der Hoven I. 1968. "Deposition of Particles and Gases," Sect. 5–3 in *Meteorology and Atomic Energy 1968,* D. Slade, Ed. Rep. TID-24190, U.S. Atomic Energy Commission, Office of Information Services. Available from NTIS, Springfield, Va.

APPENDIX H

WET DEPOSITION AND PLUME DEPLETION

INTRODUCTION

In this appendix, we describe the use of the washout ratio to derive a "wet deposition velocity," which enters the deposition-rate and plume-depletion formulas in the same way as the dry deposition velocity v_d of Appendix G. We review the advantages and limitations of this approach, which we believe, on balance, best serves the needs of the estimates of longer-term averages of air concentrations and cumulative deposition.

THE WASHOUT RATIO

This formulation of the washout ratio is directly adapted from the presentation of Hanna et al. (1982). As they point out, two related quantities that are reported in the literature are often called washout ratios, that differ by about three orders of magnitude. The one we adopt is

$$W_r = C_r/C_a \tag{H–1}$$

where C_r is the concentration of the pollutant in precipitation (mg cm^{-3}) and C_a is the concentration in air (mg cm^{-3}) at a reference height (taken here to be 1 m). Both C_r and C_a are defined in terms of a unit of the medium. The alternate definition is

$$W'_r = C'_r/C'_a \tag{H–2}$$

where C'_r is the concentration of pollutant per unit mass of precipitation (e.g., mg per gH_2O) and C'_a is the concentration per unit mass of air. The concentrations C_a and C'_a are related by

$$C_a = \rho_a C'_a$$

where $\rho_a \approx 1.2 \times 10^{-3}$ g cm^{-3} is the density of air. Similarly

$$C_r = \rho_w C'_r$$

where ρ_w is the density of water (g cm^{-3}), and consequently

$$W'_r = \frac{\rho_a}{\rho_w} W_r . \tag{H–3}$$

To distinguish between the two definitions, one needs to be aware that the usual magnitude of W_r is 10^5–10^6.

If J denotes the precipitation rate (say cm s^{-1}), then the precipitation flux at the reference height is

$$F_w = C_r J = C_a W_r J \tag{H–4}$$

where the sample units of F_w are mg cm^{-2} s^{-1}. Equation H–4 indicates that the precipitation flux can be interpreted as the product of a coefficient with velocity units and the concentration C_a of the pollutant in air:

$$F_w = v_w C_a$$

where

$$v_w = W_r J . \tag{H–5}$$

Therefore, the coefficient v_w can be formally treated in the same manner as the dry depositon velocity v_d discussed in Appendix G. The total deposition rate is

$$\omega_{total} = (v_d + v_w)\chi \tag{H–6}$$

where χ is our other notation for concentration of the pollutant in air at ground level. And the source depletion formulas, analogous to Eqs. G–8 and G–9, are

$$Q(x)/Q(0) = \exp\left(-\sqrt{\frac{2}{\pi}}\frac{v_d + v_w}{u}\int_0^x \frac{\exp(-\lambda x'/u)\,dx'}{\sigma_z \exp(h^2/2\sigma_z^2)}\right), \tag{H–7}$$

for the Gaussian plume model and

$$Q(x)/Q(0) = \exp\left(-\sqrt{\frac{2}{\pi}}\frac{v_d + v_w}{u}\int_0^x \frac{\exp(-\lambda x'/u)\,dx'}{\sigma_z'}\right), \tag{H–8}$$

for the time-dependent wake effects model described in Appendix J, where the effective vertical dispersion parameter $\sigma_z' = [\sigma_z^2 + (KA/a^2u^2S^2)F(T_{sv})]^{1/2}$, with notations as defined following Eq. J–4.

Many field measurements of the washout ratio W_r exist. Hanna et al. (1982) note that more than half of the washout ratios in the survey of McMahon and Denison (1979) lie in the range 3×10^5 to 1×10^6, and that the median is about 6×10^5. We use this median as a nominal value and the indicated range as percentage points of a lognormal distribution in connection with estimates of uncertainty (Appendix K). Details are given in the next section.

EMPIRICAL DATA FOR DETERMINATION OF WASHOUT RATIO

A site-specific washout ratio for uranium in air at the FMPC was determined from measurements of uranium in air and rain in the 1960s. The main source of information for this analysis was the original analytical data sheets from National Lead Company of Ohio (NLCO 1961–1967). The analytical data sheets provided information on measurements of the concentration of uranium in precipitation as well as precipitation amounts. The time period examined was 1961–1967, during which a fairly complete dataset was collected using a standard technique. The precipitation collector was located on the east side of the Security Building, which is on the southern perimeter of the FMPC complex (Fig. H–1). The perimeter air monitoring stations that are closest to the FMPC Security building are the SW and SE stations. The SE station was chosen for computation of the washout ratio for two reasons:

- The SE air monitor is closest to the location where the precipitation was collected (about 200 m away)

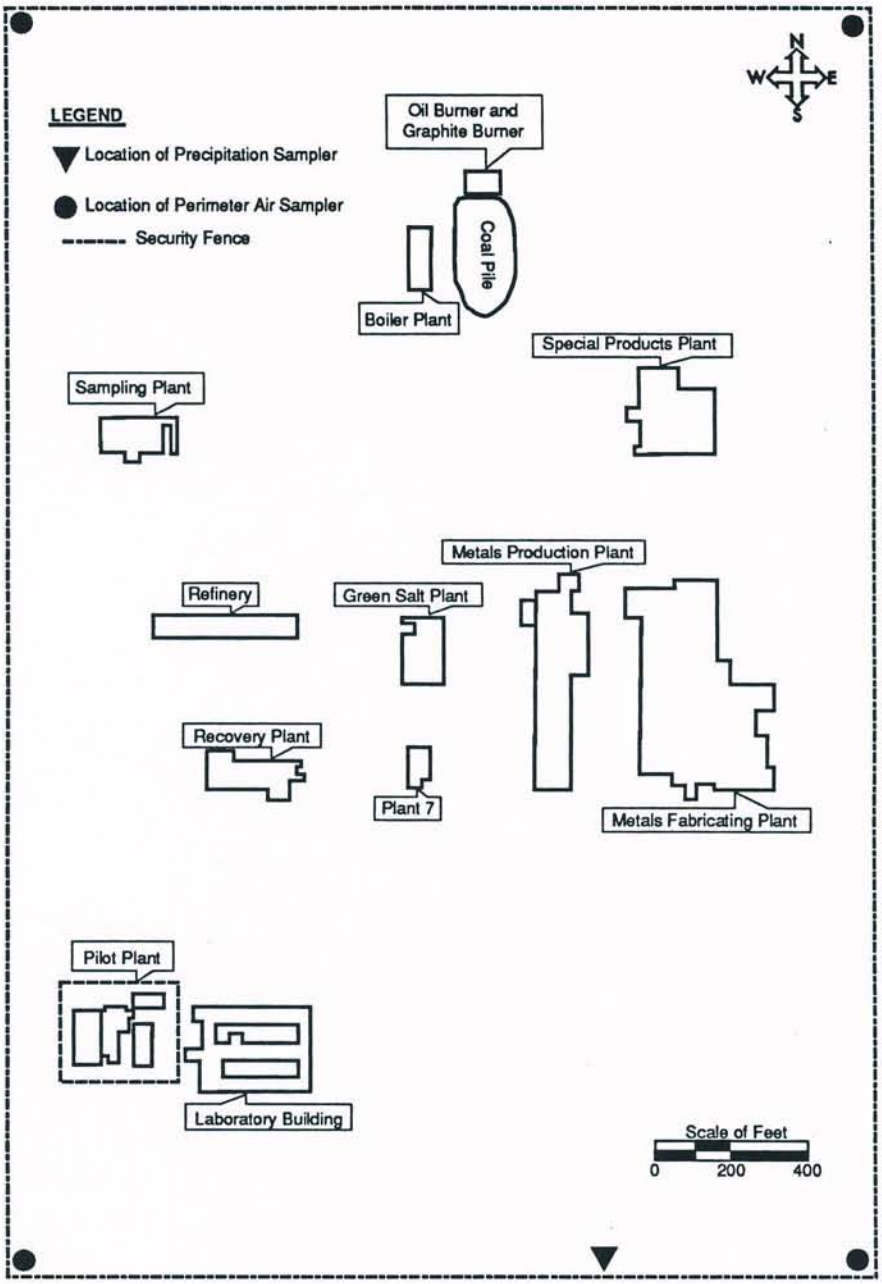

Figure H–1. Location of air and precipitation samplers relative to major release points in the production area at the FMPC.

- Both air and gumpaper from the SW location show higher and more erratic concentrations of U, compared with any other perimeter monitor, which suggests some local effects from operations in that part of the Production Area (probably the Pilot Plant).

The washout ratio was computed from the monthly uranium concentrations in air and precipitation according to Eq. H–1 above. There were 77 pairs of measurements during the seven-year period. The monthly measurements and ratios are listed in Table H–1, following the text of this appendix. A histogram of the results is shown in Fig. H–2.

Following the analysis of this dataset, the particle size characteristics of uranium in air at the perimeter sampling stations and the collection efficiency of the air samplers were thoroughly investigated (Appendix L). A significant portion of the total uranium in air at the FMPC perimeter was estimated to be in large particle size fractions, which would not have been efficiently collected by the perimeter air samplers. At the SE perimeter, 20–55% (range of monthly estimates) of the total uranium in air was associated with particles of aerodynamic diameter greater than 50 μm. Our estimate of the median collection efficiency for total uranium (all particle sizes) at the SE perimeter sampling station ranged from 40 to 64% for those 36 months, with an average of 51%. For computation of the washout ratio distribution, we assumed that the median collection efficiency of 51% applied to the air concentration measurements at the SE perimeter throughout the period. Multiplying the uncorrected washout ratios by 0.51 results in an estimated median value of 2.9×10^5 and interquartile range of 1.6×10^5 to 5.6×10^5, which is less by a factor of two than the data included in the survey of McMahon and Denison (1979), discussed in the previous section.

To adapt this distribution for uncertainty analysis, we note that the percentile ratios 75th : 50th = 1.9 and 50th : 25th = 1.8 are in good agreement, making the hypothesis of lognormality reasonable. We make this assumption, basing the shape on the first ratio. Thus, for the underlying normal distribution, the mean μ and standard deviation σ are estimated as

$$\mu = \ln 2.9 \times 10^5 \text{ and } 5.6 \times 10^5 = \exp(\mu + 0.67\sigma) = 2.9 \times 10^5 \exp(0.67\sigma)$$

so that

$$\sigma = \frac{1}{0.67} \ln \frac{5.6 \times 10^5}{2.9 \times 10^5} = 0.98 \text{ and GSD} = \exp(\sigma) = 2.7,$$

where GSD means the geometric standard deviation. This distribution will be applied to characterize the uncertainty of the washout ratio that represents monthly averages.

SUMMARY AND DISCUSSION

The washout ratio is appealing for its simplicity and the directness of methods for measuring it, and it is supported by a large number of field measurements. Its use in this application is well supported by local data taken on the FMPC site. For particular rainfall events, the uncertainty bounds of the washout ratio are wide, because of its implicit dependence on other parameters and factors, such as distributions of particle and raindrop diameter. Hanna et al. (1982) note that the washout ratio tends to decrease by a factor of two for each factor-of-ten increase in rainfall rate.

For longer-term average estimates of air concentrations and deposition, the washout ratio, incorporated into a wet deposition velocity along with average rainfall intensity (Eq. H–5), provides a plausible model of wet deposition, with uncertainty distribution based on the FMPC empirical data as shown in Fig. H–2. A distribution based on the literature cited earlier would give very similar results, except for the factor-of-two adjustment for sampling efficiency of large particles.

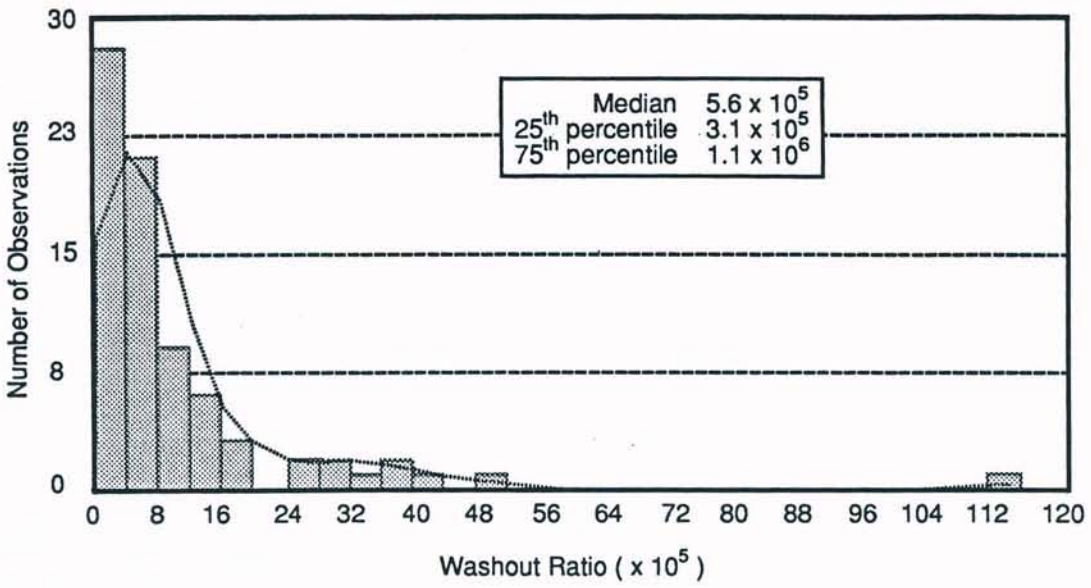

Figure H–2. Histogram of empirical washout ratios for uranium at the FMPC from 1961 through 1967. The solid line represents a "density trace" of the distribution, as determined and discussed in Hintze (1990). If the air concentrations are adjusted for the low collection efficiency for large particles (Appendix L), the washout ratio distribution is 0.51 times the values illustrated here.

REFERENCES

Hanna S.R., G.A. Briggs, and R.P. Hosker, Jr. 1982. *Handbook on Atmospheric Diffusion.* Rep. DOE/TIC-11223 (DE82002045) Technical Information Center, U.S. Department of Energy.

Hintze J.L. 1990. *Number Cruncher Statistical System. Version 5.1 Graphics. Reference Manual.* NCSS, Kaysville, UT.

McMahon T.A. and P.J. Denison. 1979. "Empirical Atmospheric Deposition Parameters — A Survey." *Atmos. Env.* **13**:571–585.

NLCO. 1961–1967. Analytical Data Sheets — Radioactivity in Precipitation. Health and Safety Division, Analytical Department. National Lead Company of Ohio, Cincinnati, Ohio.

Table H–1. Empirical Monthly Washout Ratios for Airborne Uranium at the FMPC, 1961–1967

Sampling Period	Concentration in Air (mg U cm^{-3}) [a]	Concentration in Rain (mg U cm^{-3})	Washout Ratio (unitless)
Jan-61	9.18×10^{-11}	4.0×10^{-4}	4.4×10^{6}
Feb-61	1.71×10^{-10}	1.2×10^{-4}	7.0×10^{5}
Mar-61	2.55×10^{-10}	1.3×10^{-4}	5.1×10^{5}
Apr-61	3.63×10^{-10}	4.0×10^{-4}	1.1×10^{6}
May-61	2.62×10^{-10}	6.2×10^{-5}	2.4×10^{5}
Jun-61	1.42×10^{-10}	2.8×10^{-5}	2.0×10^{5}
Jul-61	7.69×10^{-11}	3.0×10^{-5}	3.9×10^{5}
Aug-61	2.78×10^{-10}	2.0×10^{-5}	7.2×10^{4}
Sep-61	4.07×10^{-11}	2.3×10^{-5}	5.6×10^{5}
Oct-61	2.55×10^{-10}	4.4×10^{-5}	1.7×10^{5}
Nov-61	2.24×10^{-10}	1.1×10^{-4}	4.9×10^{5}
Dec-61	1.01×10^{-10}	6.5×10^{-5}	6.5×10^{5}
Jan-62	8.39×10^{-11}	4.0×10^{-5}	4.8×10^{5}
Feb-62	1.62×10^{-10}	2.9×10^{-5}	1.8×10^{5}
Mar-62	3.65×10^{-10}	1.3×10^{-4}	3.6×10^{5}
Apr-62	4.67×10^{-10}	5.8×10^{-4}	1.2×10^{6}
May-62	2.19×10^{-10}	1.8×10^{-4}	8.2×10^{5}
Jun-62	1.57×10^{-10}	1.2×10^{-4}	7.6×10^{5}
Jul-62	1.67×10^{-10}	1.8×10^{-5}	1.1×10^{5}
Aug-62	2.86×10^{-10}	1.2×10^{-4}	4.2×10^{5}
Sep-62	2.93×10^{-10}	2.7×10^{-4}	9.2×10^{5}
Oct-62	1.67×10^{-10}	1.1×10^{-4}	6.6×10^{5}
Nov-62	2.12×10^{-10}	NA[b]	NA
Dec-62	1.26×10^{-10}	6.5×10^{-4}	5.1×10^{6}
Jan-63	2.21×10^{-10}	2.7×10^{-4}	1.2×10^{6}
Feb-63	3.31×10^{-10}	1.0×10^{-3}	3.0×10^{6}
Mar-63	4.19×10^{-10}	8.0×10^{-5}	1.9×10^{5}
Apr-63	4.59×10^{-10}	2.0×10^{-4}	4.4×10^{5}
May-63	3.49×10^{-10}	1.3×10^{-4}	3.7×10^{5}
Jun-63	3.85×10^{-10}	1.6×10^{-4}	4.2×10^{5}
Jul-63	2.40×10^{-10}	7.0×10^{-5}	2.9×10^{5}
Aug-63	1.60×10^{-10}	5.0×10^{-5}	3.1×10^{5}
Sep-63	2.11×10^{-10}	NA	NA
Oct-63	3.31×10^{-10}	3.8×10^{-3}	1.2×10^{7}
Nov-63	3.96×10^{-10}	4.4×10^{-4}	1.1×10^{6}
Dec-63	2.26×10^{-10}	4.4×10^{-4}	2.0×10^{6}

Table H–1 (continued). Empirical Monthly Washout Ratios for Airborne Uranium at the FMPC, 1961–1967

Sampling Period	Concentration in Air (mg U cm^{-3}) [a]	Concentration in Rain (mg U cm^{-3})	Washout Ratio (unitless)
Jan-64	1.41×10^{-10}	2.2×10^{-4}	1.6×10^{5}
Feb-64	6.66×10^{-10}	1.2×10^{-3}	1.7×10^{6}
Mar-64	2.81×10^{-10}	2.0×10^{-4}	7.1×10^{5}
Apr-64	2.92×10^{-10}	2.2×10^{-4}	7.4×10^{5}
May-64	1.63×10^{-10}	1.4×10^{-4}	8.9×10^{5}
Jun-64	2.32×10^{-10}	7.0×10^{-5}	3.0×10^{5}
Jul-64	1.33×10^{-10}	1.1×10^{-4}	8.3×10^{5}
Aug-64	2.01×10^{-10}	9.5×10^{-5}	4.7×10^{5}
Sep-64	1.82×10^{-10}	NA	NA
Oct-64	2.07×10^{-10}	2.5×10^{-4}	1.2×10^{6}
Nov-64	2.77×10^{-10}	4.0×10^{-4}	1.4×10^{6}
Dec-64	6.90×10^{-11}	1.7×10^{-4}	2.5×10^{6}
Jan-65	1.69×10^{-10}	NA	NA
Feb-65	1.26×10^{-10}	NA	NA
Mar-65	1.59×10^{-10}	9.5×10^{-5}	6.0×10^{5}
Apr-65	9.62×10^{-11}	NA	NA
May-65	1.24×10^{-10}	1.2×10^{-4}	9.2×10^{5}
Jun-65	5.92×10^{-11}	1.5×10^{-4}	2.5×10^{6}
Jul-65	9.76×10^{-11}	3.0×10^{-5}	3.1×10^{5}
Aug-65	8.88×10^{-11}	5.0×10^{-5}	5.6×10^{5}
Sep-65	1.07×10^{-10}	4.0×10^{-5}	3.7×10^{5}
Oct-65	7.03×10^{-11}	2.5×10^{-5}	3.6×10^{5}
Nov-65	6.21×10^{-11}	2.2×10^{-4}	3.5×10^{6}
Dec-65	5.62×10^{-11}	2.1×10^{-4}	3.6×10^{6}
Jan-66	8.14×10^{-11}	8.5×10^{-5}	1.0×10^{6}
Feb-66	5.92×10^{-11}	7.5×10^{-5}	1.3×10^{6}
Mar-66	6.29×10^{-11}	2.3×10^{-4}	3.7×10^{6}
Apr-66	1.07×10^{-10}	3.4×10^{-5}	3.2×10^{5}
May-66	7.40×10^{-11}	7.5×10^{-5}	1.0×10^{6}
Jun-66	2.22×10^{-10}	4.5×10^{-5}	2.0×10^{5}
Jul-66	5.92×10^{-11}	1.6×10^{-5}	2.7×10^{5}
Aug-66	7.40×10^{-11}	2.3×10^{-5}	3.1×10^{5}
Sep-66	8.88×10^{-11}	1.3×10^{-5}	1.5×10^{5}
Oct-66	5.55×10^{-11}	NA	NA
Nov-66	1.81×10^{-10}	2.2×10^{-5}	1.2×10^{5}
Dec-66	2.90×10^{-10}	1.2×10^{-5}	4.1×10^{4}

Table H–1 (concluded). Empirical Monthly Washout Ratios for Airborne Uranium at the FMPC, 1961–1967

Sampling Period	Concentration in Air (mg U cm^{-3}) [a]	Concentration in Rain (mg U cm^{-3})	Washout Ratio (unitless)
Jan-67	1.26×10^{-10}	3.6×10^{-4}	2.9×10^{6}
Feb-67	5.55×10^{-11}	1.0×10^{-4}	1.8×10^{6}
Mar-67	1.33×10^{-10}	5.0×10^{-5}	3.8×10^{5}
Apr-67	1.33×10^{-10}	1.7×10^{-5}	1.3×10^{5}
May-67	2.18×10^{-10}	1.8×10^{-5}	8.2×10^{4}
Jun-67	9.62×10^{-11}	7.0×10^{-5}	7.3×10^{5}
Jul-67	1.07×10^{-10}	3.4×10^{-5}	3.2×10^{5}
Aug-67	1.04×10^{-10}	4.3×10^{-5}	4.2×10^{5}
Sep-67	6.21×10^{-11}	2.8×10^{-5}	4.5×10^{5}
Oct-67	3.00×10^{-10}	2.2×10^{-5}	7.3×10^{4}
Nov-67	2.14×10^{-10}	1.3×10^{-4}	6.1×10^{5}
Dec-67	1.75×10^{-10}	9.5×10^{-5}	5.4×10^{5}

[a] Converted from units on analytical data sheets (μCi mL^{-1}) using an activity to mass ratio of 6.8×10^{-7} Ci g^{-1}. These air concentrations are not adjusted for estimated collection efficiency of the air samplers (see text).

[b] NA = Data not available; data sheet was either not located or not legible.

APPENDIX I

PLUME RISE

INTRODUCTION

The release height parameter that appears in the Gaussian plume formula (Appendix F) should be viewed as an *effective* release height, which is the sum of the physical height of the stack or roof vent and an increment that depends on parameters associated with the stack as well as meteorological parameters. The increment is called the PLUME RISE (although it is sometimes negative), and many efforts to quantify it are recorded in the technical literature. The work of Briggs (1969, 1984) reviews previous work and suggests formulas that are currently widely adopted. We originally adopted these formulas for the purpose of simulating air transport of radionuclides released from the numerous stacks that vented FMPC process effluents, but subsequent analysis of building wake effects for the production complex has indicated that all rooftop releases should be treated as wake-entrained and therefore effectively originating at ground level (Appendix J). For entrained releases, considerations of plume rise are not ordinarily undertaken. The only remaining elevated source that is isolated from the complex is the old solid waste incinerator (OSWI), to which the plume-rise theory would be applicable. The oil burner is a special case, situated as it is north of the coal pile and northeast of the boiler plant. Because it is a hot source at a low height (2.4 m), we will plan to allow the plume rise calculation to determine whether its release should be treated as entrained or not (it is a small release, in any event). Our chief references are Briggs (1969) and Hanna et al. (1982). The material in this appendix is closely related to some aspects of building wake effects that are discussed in Appendix J.

BRIGGS' PLUME RISE FORMULAS

The two major cases considered are determined by whether the rise of the plume gas is dominated by buoyancy or by momentum. In our treatment, the plume gas is always assumed to be air, and this assumption removes some factors involving molecular weights and ratios of specific heat capacities from some of the formulas.

Buoyant Plumes

Plumes that rise under the predominant influence of buoyancy have been studied extensively, and reasonably good calibrations of formulas to observations exist for such plumes. For all cases in this category, the BUOYANCY FLUX is defined as

$$F = \frac{g}{T_p}(T_p - T_a)w_0 r_0^2 \qquad \text{(I–1)}$$

(Hanna et al. 1982) where

F = buoyancy flux ($m^4\ s^{-3}$)

g = gravitational acceleration = 9.807 m s^{-2}

T_p = absolute temperature of the plume gas (K)
T_a = absolute temperature of the ambient air (K)
w_0 = stack gas exit velocity (m s^{-1})
r_0 = radius of plume cross section at point of exit (m); this is taken as the interior radius of the mouth of a stack of circular cross section.

Neutral and unstable stratification. The plume rise is estimated by

$$\begin{aligned}\Delta h &= 1.6F^{1/3}u^{-1}x^{2/3} \quad \text{if } x/x^* < 1 \\ &= 1.6F^{1/3}u^{-1}(x^*)^{2/3}\left[\frac{2}{5}+\frac{16}{25}\frac{x}{x^*}+\frac{11}{5}\left(\frac{x}{x^*}\right)^2\right]\left(1+\frac{4}{5}\frac{x}{x^*}\right)^{-2} \quad \text{if } x/x^* \geq 1\end{aligned} \tag{I–2}$$

(Briggs 1969) where

$$x^* = \begin{cases} 2.2F^{2/5}h^{3/5} & \text{if } h < 300 \text{ m} \\ 67F^{2/5} & \text{if } h \geq 300 \text{ m} \end{cases}$$

where h is the physical release height (m), and the constants 2.2 and 67 have units $s^{6/5}\ m^{-6/5}$ and $s^{6/5}\ m^{-3/5}$, respectively; u is the wind speed (m s^{-1}) at height h, and x denotes the distance downwind from the source (m). Briggs (1969) estimated that Δh as estimated in Eq. I–2 has an uncertainty of ±10% for a flat and uniform site and ±40% for steep terrain or a nearby large body of water. We note that for our applications, h is always less than 300 m.

Stable stratification. Plume rise is given by

$$\begin{aligned}\Delta h &= 1.6F^{1/3}u^{-1}x^{2/3} \quad \text{for } x < 2.4us^{-1/2} \\ &= 2.9\left(\frac{F}{us}\right)^{1/3} \quad \text{for } x \geq 2.4us^{-1/2}\end{aligned} \tag{I–3}$$

(Briggs 1969) where the stability parameter s (s^{-2}) is given by

$$s = \frac{g}{T_a}\frac{\partial\theta}{\partial z}; \tag{I–4}$$

the partial derivative $\partial\theta/\partial z$ is the vertical potential temperature gradient of the air. A generic profile for this gradient can be obtained from the friction velocity u_* (which, operationally, is related to the wind-speed profile by Eq. G–1, Appendix G) and the Monin-Obukhov length L (Appendix G), as follows:

$$\frac{\partial\theta}{\partial z} = \frac{u_*^2 T_a}{g\kappa^2 Lz} \times \begin{cases} 0.74(1-9z/L)^{-1/2} & \text{for unstable conditions} \\ 0 & \text{for neutral conditions} \\ (0.74+5z/L) & \text{for stable conditions} \end{cases} \tag{I–5}$$

where z is the distance above the ground (m) and $\kappa = 0.4$ is the von Kármán constant (Hanna et al. 1982). For this application, only the stable case is applied.

NOTE: Equation I–5 is derived from Eqs. 1.32 and 1.36 on pp. 6–7 of Hanna et al. (1982), but an error of sign in their definition of the scaling temperature T_* would lead to a wrong sign in our result. Their definition on p. 6 should be $T_* = -\overline{W'T'}/u_*$.

Dense plume. If the plume is cooler than the ambient air ($T_p < T_a$), then it may descend below the release height and even to the ground. Briggs (1974) developed a method for

Table I–1. Briggs' Dense Plume Adjustment Factors, C

	Day	Night
$u < 3.5$ m s^{-1}	5	35
$u \geq 3.5$ m s^{-1}	10	15

such cases, which we have adapted for application to the FMPC site. In this event, if $u < 0.22C\sqrt{-gD\delta}$ (where C is given by Table I–1, δ is defined in Eqs. I–9 through I–11 below, and D is the stack diameter), the plume may touch ground near the source, at $x \approx 4.5hu/\sqrt{-gD\delta}$, and should be treated as a ground-level source with initial plume cross-sectional area $A = 0.2h^2$.

An alternate procedure is used at night for $u < 3.5$ m s^{-1}, when the descent is limited to about $100|F|^{1/4}$. If $h - 100|F|^{1/4} < 0.2h$, the plume is treated as a ground source as above, with initial area $A = 0.2h^2$. If $h - 100|F|^{1/4} \geq 0.2h$ but $h < \zeta$, where ζ is the minimum of the building's crosswind width and its height, the plume is again treated as a ground source but with initial area $A = \zeta^2$. Otherwise, it is treated as an elevated source with effective release height $h - 100|F|^{1/4}$. The reader is referred to the summary section below on application of the formulas and to Appendix J for further discussion of building wake effects.

Momentum-Dominated Plumes (Jets)

Plumes that rise principally from the momentum of the stack gas have been studied far less than buoyant plumes, and the associated formulas are advanced with less confidence.

We use the formulas for a momentum-dominated plume when $|F| < F_m \equiv w_0^2 r_0^2$ and $w_0/u \geq 4$. We apply the following formulas, recommended by Briggs (1969) for neutral conditions, to neutral and unstable stratifications:

$$\Delta h = 1.44D\left(\frac{w_0}{u}\right)^{2/3}\left(\frac{x}{D}\right)^{1/3} \tag{I–6a}$$

out to the downwind distance x for which

$$\Delta h = 3D\frac{w_0}{u} \tag{I–6b}$$

and beyond that distance, the plume remains level at the height determined by Eq. I–6b. In Eqs. I–6a and I–6b, D (m) is the inside stack diameter ($= 2r_0$). For stable conditions, Briggs (1969) gives the minimum expected theoretical plume rise as

$$\Delta h = 1.5\left(\frac{F_m}{u}\right)^{1/3} s^{-1/6} \tag{I–6c}$$

where s is the stability parameter defined by Eqs. I–4 and I–5. Briggs cautioned that this formula was unsupported by data.

EFFECTS OF STACK AND BUILDING

Building wake effects are discussed in Appendix J, and that discussion includes the application of special dispersion models to a plume that is entrained in the building wake cavity. Wake effects can also result in some downward displacement of a plume but not enough to entrain it in the wake cavity. In such cases, the plume remains elevated, and plume rise formulas are applied at the displaced height. Thus it is not practical to attempt a complete separation of the mechanisms that cause plumes to rise (i.e., momentum and buoyancy) from those wake effects that displace it downward. Therefore, we outline here the combined calculations that take into account both sets of mechanisms. This composite algorithm has been applied to all rooftop release points of the production plants in the FMPC complex, for all wind speed ranges and atmospheric stability categories. In all cases, the outcome was entrainment of the plume, calling for the use of the special dispersion models that incorporate wake effects.

First, we review the modifications of the plume rise algorithms due to stack downwash and building wake effects. For emissions from a stack of physical height h, the following downwash calculation is applied:

$$h' = \begin{cases} h & \text{if } w_0/u \geq 1.5 \\ h - 2D(1.5 - w_0/u) & \text{if } w_0/u < 1.5 \end{cases} \qquad \text{(I–7)}$$

Again, let ζ denote the smaller of the building's (crosswind) width W and height H. Then the initial effective height of the plume is

$$h'' = \begin{cases} h' & \text{(Case 1) if } h' > H + 1.5\zeta \\ 2h' - (H + 1.5\zeta) & \text{(Case 2) if } H \leq h' \leq H + 1.5\zeta \\ h' - 1.5\zeta & \text{(Case 3) if } h' < H. \end{cases} \qquad \text{(I–8)}$$

For Case 1, the plume is above the building wake, and plume rise formulas are applied with h'' as the baseline release height. In Cases 2 and 3, the plume is affected by the building wake, and if $h'' < 0.5\zeta$, the plume is considered to be trapped in the wake cavitation region of the building. In this case, it is treated as if it came from a ground-level source with initial cross-sectional area WH (Appendix J).

If the plume is not entrained in the building wake cavity and treated as a ground source, the effective release height h'' calculated from consideration of building wake effects is used as the basis for the final plume rise calculation (unless it is the resultant height of a dense plume that is not treated as a ground-level source).

NOTE ON THE DEFINITION OF THE MOMENTUM FLUX

The buoyancy flux F as defined by Eq. I–1 takes account only of plume buoyancy that is attributable to a difference between the ambient temperature T_a and that of the exhaust gas T_p. This is a reasonable representation if the gas is air and if its liquid water content is not appreciable. But component gases that are lighter (or heavier) than air at standard temperature and pressure clearly have the potential to affect the buoyancy of the plume. And in the case of scrubbed effluent gas it may not be appropriate to neglect the cooling of the plume as its liquid water content evaporates.

A more general definition of the buoyancy flux has been suggested by Briggs (1974). It may be stated as follows:

$$F = -g\,\delta\,w_0 r_0^2 \tag{I–9}$$

where

$$\delta = \delta_T + \delta_m + \delta_w \tag{I–10}$$

and

$$\delta_T = -\frac{(c_p)_p}{(c_p)_a}\frac{T_p - T_a}{T_a}, \quad \delta_m = \left(1 - \frac{28.9}{m_p}\right), \quad \delta_w = \frac{8Q_w}{M_p}, \tag{I–11}$$

where

$(c_p)_p$ = specific heat capacity of the plume gas (cal g^{-1} K^{-1})

$(c_p)_a$ = specific heat capacity of the ambient air (= 0.24 cal g^{-1} K^{-1})

28.9 = gram-molecular weight of air

m_p = gram-molecular weight of the plume gas ($m_p^{-1} = \sum_i f_i m_i^{-1}$, where f_i and m_i are the mass fraction and molecular weight of component gas i, respectively)

Q_w = mass release rate of liquid water in the plume (g s^{-1})

M_p = total mass release rate of plume gas and liquid water (g s^{-1}).

The terms δ_m and δ_w correspond to the contributions to buoyancy (positive and negative) of the plume's molecular weight and its cooling due to evaporation, respectively.

SUMMARY OF PROCEDURES

Interpretations of the plume-rise formulas of Briggs vary among practitioners who apply them. For the record, we have assembled the following procedural formulation from recommendations in the references (principally Hanna et al. 1982) and our judgment of the appropriate application to the characteristics of the FMPC site. The procedure also shows our manner of combining the plume rise treatment (buoyancy and momentum) with that of stack and building wake effects, although the combined form is effectively unused for the FMPC production complex because of the complete entrainment of rooftop releases (i.e., plume rise is pre-empted by wake effects).

Procedure. Carry out the plume displacement calculations of Eqs. I–7 and I–8 to obtain h''.

IF $h'' < 0.5\zeta$:

The plume is trapped in the downwind building wake cavity. Assume a ground source with effective cross-sectional plume area WH.

OTHERWISE:

The plume is buoyant (positively or negatively). Compute F according to Eq. I–1 or Eqs. I–9 through I–11.

IF $|F| \geq w_0^2 r_0^2$: (the plume is buoyancy dominated)

IF $F > 0$:

IF conditions are neutral or unstable (A–D):

Use Eq. I–2 to compute Δh; let $h_{eff} = h'' + \Delta h$.

OTHERWISE:

Use Eqs. I–3, I–4 and I–5 for stable conditions (E–F) to compute Δh; let $h_{\text{eff}} = h'' + \Delta h$.

OTHERWISE IF $F < 0$:

Use the **dense plume** procedure below.

OTHERWISE:

$F = 0$. Let $h_{\text{eff}} = h''$.

OTHERWISE:

The plume is momentum-dominated:

IF conditions are neutral or unstable (A–D):

Use Eqs. I–6a and I–6b.

OTHERWISE:

Use Eq. I–6c.

Dense plume procedure. The displaced height h'' is defined by Eqs. I–7 and I–8.
IF it is night:

IF $h'' - 100|F|^{1/4} < 0.2h''$:

The plume is a ground source with effective cross-sectional area $0.2(h'')^2$.

OTHERWISE:

IF $h'' < \zeta$: The plume is a ground source with area ζ^2.

OTHERWISE: The plume is elevated with $h_{\text{eff}} = h'' - 100|F|^{1/4}$.

OTHERWISE:

IF $u < 0.22C\sqrt{-gD\delta}$: The plume is a ground source with area $0.2(h'')^2$.

OTHERWISE: The plume is elevated with $h_{\text{eff}} = h''$ (from Eq. I–8).

AMBIENT AIR TEMPERATURES

Table I–2 shows averages of the hourly air temperatures measured at the FMPC tower from August 1986 through December 1991, together with the summary mean and standard deviation for each month. Please note that these tabular entries are based on data from the computer-controlled sampling system that have not been verified by WMCO personnel.

REFERENCES

Briggs G.A. 1969. *Plume Rise.* U.S. Atomic Energy Commission Office of Information Services. Available from NTIS, Springfield, Virginia.

Briggs G.A. 1974. "Diffusion Estimation for Small Emissions." In *Atmospheric Turbulence and Diffusion Laboratory 1973 Annual Report,* ATDL-106.

Briggs G.A. 1984. "Plume Rise and Buoyancy Effects." Chapter 8 in *Atomic Science and Power Production* (D. Randerson, Ed.). Rep. DOE/TIC-27601, U.S. Department of Energy, Office of Scientific and Technical Information.

Hanna S.R., G.A. Briggs, and R.P. Hosker, Jr. 1982. *Handbook on Atmospheric Diffusion.* Rep. DOE/TIC-11223 (DE82002045) Technical Information Center, U.S. Department of Energy.

Table I–2. FMPC Ambient Air Temperatures (°C) at 10-meter Height (Tabular Entries Are Means of the Hourly Averages)

Month	1986	1987	1988	1989	1990	1991	Mean	St. Dev.
Jan		−1.18	−2.19	3.21	4.24	−0.73	0.67	2.86
Feb		2.38	−0.81	−1.04	4.33	2.21	1.41	2.29
Mar		6.58	5.83	6.58	8.44	7.15	6.92	0.97
Apr		11.30	11.47	10.53	11.03	13.43	11.55	1.11
May		18.38	17.44	15.44	15.92	20.99	17.63	2.21
Jun		23.23	21.66	20.89	21.49	23.19	22.09	1.06
Jul		23.88	24.87	23.47	22.83	23.89	23.79	0.74
Aug	21.24	21.14	23.68	21.67	19.88	22.03	21.61	1.25
Sep	19.65	18.81	18.16	17.65		18.32	18.52	0.76
Oct	12.70	9.02	8.72	11.95	8.90	13.18	10.75	2.08
Nov	5.68	8.63	7.02	6.31	6.97	5.16	6.63	1.22
Dec	1.02	2.97	0.92	−5.06	3.61	2.60	1.01	3.16

APPENDIX J

BUILDING WAKE EFFECTS

INTRODUCTION

The unmodified Gaussian plume model does not account for the behavior of released material that is influenced by the leeward wake of a building. Most of the points of release from production plants at the FMPC are roof stacks that extend only a few meters above the roof of the building. When the ratio of the release height to the height of the building is not much greater than 1, experience shows that the plume (or some part of it) is likely to be entrained into the wake, drawn down near the ground, and diffused horizontally and vertically by the wake turbulence. The cross-sectional area of the plume is altered, and the wake effects persist to considerable distances downwind, possibly to a distance as great as 50 building heights. A building complex such as the FMPC site presents further complications, because most empirical rules apply to isolated structures of simple geometry. Careful studies of building complexes usually require field experiments, wind tunnel simulations, or supercomputer modeling of three-dimensional wind fields with turbulence.

Calculations with standard empirical rules indicate that for all roof-top stacks at the FMPC and for all representative wind speeds and stabilities, the release is expected to be entrained in the wake and to become, effectively, a release from an area approximately equal to that of the building's crosswind face. We refer to such releases as being effectively ground-level, in contrast to elevated releases from a point source. Hence a modification of the Gaussian plume model — or a different model altogether — is required to account for the wake effects. We have tested several models and combinations of assumptions, using the reconstructed uranium source term and the data collected by the air samplers at the four perimeter stations of the production area during the period 1960 through 1962. Of the applicable models tested, a new model of Ramsdell (1990) generally gave the best results in these tests, and we have provisionally adopted this model for use with releases from roof-top stacks at the FMPC.

In this appendix, we describe the models, with special attention to the so-called "time-dependent" model of Ramsdell, and we review the empirical criteria for distinguishing among releases with respect to their remaining elevated or being entrained in the building wake. Finally, we present the validation results for the 1960–1962 period.

APPROACH TO WAKE EFFECTS

We follow a set of criteria proposed by Briggs (1974) and recommended by Hanna et al. (1982) to determine the handling of wake effects. We are concerned with a rooftop stack with its top at height h (the physical release height, m) and a building of height H and crosswind width W (both m). The interior diameter of the stack is D (m), the exhaust gas velocity w_0 (m s^{-1}), and the wind speed u (m s^{-1}).

First a calculation is performed to estimate the plume downwash into the wake of the

stack. We compute

$$h' = \begin{cases} h & \text{if } w_0/u \geq 1.5 \\ h - 2D(1.5 - w_0/u) & \text{otherwise} \end{cases} \quad \text{(J–1)}$$

where h' is the adjusted plume height (m). For the second step, let ζ be the smaller of W and H. There are three cases:

If $h' \geq H + 1.5\zeta$, compute $h_{\text{eff}} = h'$.

If $H \leq h' < H + 1.5\zeta$, compute $h_{\text{eff}} = 2h' - (H + 1.5\zeta)$.

If $h' < H$, compute $h_{\text{eff}} = h' - 1.5\zeta$.

Finally, if the effective source height h_{eff} computed above is less than 0.5ζ, the plume should be treated as coming from a ground-level source. Otherwise, it is an elevated release from height h_{eff}. For dimensions of plant buildings in the FMPC production area, as interpreted and applied in our calculations, the value of ζ is always equal to the building height H.

> PLEASE NOTE: For all representative wind speeds and all rooftop stacks at FMPC production plants that were active during the 1960–1962 period, the algorithm described above invariably leads to the conclusion of effective ground-level releases.

THE STANDARD WAKE EFFECTS MODEL

One standard approach to estimating downwind concentrations of plumes entrained in building wakes makes use of a modified centerline version of the Gaussian plume model:

$$\chi/Q = \{u[\pi\sigma_y\sigma_z + cWH]\}^{-1} \quad \text{(J–2)}$$

where the constant c is an adjustable parameter for which a value of approximately 0.5 has been considered appropriate on various grounds (Hanna et al. 1982). Other quantities in the equation are

χ/Q = concentration (χ) normalized to release rate (Q) (s m^{-1})

u = wind speed (m s^{-1})

σ_y, σ_z = crosswind and vertical dispersion coefficients (m) as functions of the downwind distance, for which we used Briggs' formulas (Appendix F, Table F–1)

W, H = characteristic width and height (m) of the building.

The expression $\pi\sigma_y\sigma_z + cWH$ in the denominator of the right-hand term in Eq. J–2 is the cross-sectional area of the plume (discounting the interference with the ground) and is the sum of the "natural" elliptical cross section and a term proportional to the area of the building, which is dominant near the source where the product $\sigma_y\sigma_z$ is small.

Equation J–2 is one of a class of models that are applied to releases that are effectively from ground level, on the basis of the set of rules of plume displacement described in the previous section (if the release does not qualify to be treated as ground-level, a model such as the Gaussian plume for a positive effective release height is used). The model of Eq. J–2 is conservative in the sense of its tendency to overestimate concentrations near the point of release. Subsequent comparisons will quantify this tendency.

Because of the form of the standard wake effects model, the width of the plume (i.e., the crosswind distribution) is not clearly implied. Without knowing this quantity, it is not possible to do the crosswind integration that would be required for crosswind averaging or for applying deposition models to estimate depletion of the plume. Therefore, comparisons involving this model will be confined to estimates of centerline concentrations without adjustment for plume depletion due to deposition.

THE STATISTICAL MODEL

A second model that we include in this comparison was developed by Ramsdell (1990) from datasets from seven wake effects experiments. The regression function has the form

$$\chi/Q = \kappa x^{\alpha} A^{\beta} u^{\gamma} S^{\delta} \qquad \text{(J–3)}$$

where the coefficients $\kappa = 84.5$, $\alpha = -1.13$, $\beta = -1.25$, $\gamma = 0.720$, $\delta = 0.473$, were obtained from a least-squares procedure, and

x = downwind distance (m) from the point of release

A = characteristic area of the building (m^2)

u = wind speed (m s^{-1}) at the 10-m height, and

S = 1, 2, ..., 6 for stability class A, B, ..., F.

The data from which the model was derived covered various distance ranges, the greatest of which was $x = 1{,}200$ m. Thus Eq. J–3 should not be applied to estimating concentrations beyond that distance. We also note that the structure of this centerline model, like that of the standard wake effects model, implies no definite plume width (i.e., crosswind distribution). Consequently, unless the model is extended with arbitrary assumptions, one cannot perform the crosswind integration necessary for sector- or other crosswind averaging and for taking into account plume depletion due to deposition.

We must point out that the model of Eq. J–3 has been criticized, in part because of its dependence on a positive power of the wind speed, $u^{0.720}$. Briggs et al. (1992) argue that stability and wind speed are correlated and thus should not be treated as independent variables in a multiple regression; they suggest that the error from this correlation and from a failure to account for plume meander may have contributed to misleading results. Nevertheless, we include the model in our comparison because it summarizes the data from virtually all applicable wake effects experiments.

THE TIME-DEPENDENT PLUME MODEL

The time-dependent model of Ramsdell (1990) was to some extent inspired by the statistical model of Eq. J–2. The formulation of the time-dependent model is

$$\chi/Q = (\pi u \sigma_y' \sigma_z')^{-1} \qquad \text{(J–4)}$$

$$\sigma_y' = [\sigma_y^2 + (KA/a^2u^2)F(T_s)]^{1/2}$$

$$\sigma_z' = [\sigma_z^2 + (KA/a^2u^2S^2)F(T_{sv})]^{1/2}$$

where

$$F(T) = 1 - \left(1 + x/(uT)\right) \exp\left(-x/(uT)\right)$$

and

A = characteristic area of the building (m^2)

u = wind speed ($m\ s^{-1}$), which we have adjusted to the building height

x = downwind distance (m)

S = 1, 2, . . . , 6 for stabilities A, B, . . . , F, respectively (taken as a dimensionless parameter)

a = $0.4/\ln(z/z_0)$; z_0 is the roughness height (m) and we have taken z to be the building height; 0.4 is the von Kármán constant

u_* = au = friction velocity ($m\ s^{-1}$)

T_{sv} = $A^{1/2}/(Su_*)$ (s)

T_s = $A^{1/2}/u_*$ (s)

σ_y, σ_z = horizontal and vertical dispersion coefficients (m), expressed as functions of the downwind distance x; we used Briggs' formulas (Appendix F, Table F–1)

K = an adjustable parameter; Ramsdell (1990) obtained best fits with $K = 0.5$

The term "time dependent" refers to the approach used in deriving the model, but the time does not remain explicit in the final formula, except in the scaled quantities T_{sv} and T_s. The version of the model shown in Eq. J–4 is interpreted as the centerline concentration χ per unit release rate Q at downwind distance x from the source for wind speed u and for a stability that determines quantities σ_y, σ_z, S, and T_{sv}. We have followed the original paper in computing the friction velocity u_* for neutral conditions (see the definition of a in the above list), though this quantity could also be made specific to stability class.

The area A will be expressed as WH, where, as before, W is an effective crosswind width of the building and H is the height (both in m). The meaning of such characteristic dimensions blurs in the context of a complex of buildings such as exists at the FMPC site. Ideally, the model should be applied to releases that are entrained into the wakes of isolated buildings, in which case W and H might be actual dimensions of the building face. But in locations where the complex behaves like a larger structure, other interpretations may be appropriate. We discuss our approach to this ambiguity in a later section.

Briggs et al. (1992) included the time-dependent model in their criticism that we mentioned previously in connection with the statistical model. They objected on physical grounds to the time-dependent model's dependence on a positive power of wind speed. In a response included with the communication, Ramsdell conceded that some refinements of the model would be appropriate, but he took issue with most of the critics' conclusions. On pragmatic grounds, we retain the model because of its comparative practical success in predicting observed concentrations at the perimeter stations of the FMPC production area during the 1960–1962 period.

THE GAUSSIAN PLUME MODEL FOR ELEVATED RELEASES

If building wake effects are neglected and the standard Gaussian plume model is used for predicting downwind ground-level concentrations, the normalized centerline estimate is

$$\chi/Q = (\pi\sigma_y\sigma_z u)^{-1} \exp\left(-h_{\text{eff}}^2/(2\sigma_z^2)\right) \qquad \text{(J–5)}$$

where

h_{eff} = effective release height (m), computed as the sum of the physical release height and the plume rise that is estimated from the methods of Appendix I

u = wind speed (m s^{-1}) adjusted to the physical release height

σ_y, σ_z = crosswind and vertical dispersion coefficients (m), expressed as functions of downwind distance from the source.

This model is included in the comparison to permit an assessment of predictions when wake effects are neglected and all releases are treated as if they came directly from elevated point sources. As we noted previously, the empirical rules given by Eq. J–1 and the subsequent text point to the conclusion that plumes released from all rooftop stacks on FMPC production plants during 1960–1962 should be treated as having been entrained in the wake. Consequently, application of the standard Gaussian plume will likely be relegated to simulating emissions from the old solid waste incinerator, which is isolated from the complex and meets the criteria for an elevated source.

DETAILS AND RESULTS OF THE MODEL COMPARISON

Three of the models treated in our comparison consider wake effects through a parameter $A = WH$ representing the characteristic area (m^2) of the building that generates the wake; these models are the standard wake effects model, the statistical model, and the time-dependent model. The fourth model is the standard centerline Gaussian plume, which ignores wake effects and therefore is independent of this characteristic area. The distinction is important, because the complexity of the site complicates the analysis for the wake effects models, and a range of values of A will be considered for those models that contain it as a parameter.

The air concentration at each receptor station was predicted with each model by summing the result for each source (i.e., plant building), wind speed, and stability. For a source-receptor combination, it was assumed that the receptor was affected by the source only when the wind blew from the sector determined by the direction of the source-receptor vector, and that direction determined the frequencies of representative wind speeds and stabilities. Monthly meteorological data were taken from the 5-year composite FMPC dataset. Some approximations were made. In the first comparison of the four models, plume depletion due to wet and dry deposition was neglected because deposition could not be calculated for the statistical model or the standard wake effects model without making additional assumptions about the plume crosswind distribution. And for elevated releases treated by the Gaussian model, the stacks for each plant were consolidated into a single release source for the plant by averaging stack properties such as exit gas velocity, inside diameter, and physical release height (such considerations were not relevant to the wake effects models, and these models do not depend

on stack parameters). Each month's release of uranium for each plant was estimated by the mean value of the uncertainty distribution (Voillequé et al. 1991). Because of the highly skewed nature of the distributions for the Plant 8 scrubbers and the magnitude of this component relative to the total release, some upward bias may have resulted from the use of the mean values. Finally, the oil burner and the old solid waste incinerator were not included among the sources for the comparison.

For each wake effects model, we performed the calculations under two sets of assumptions and labeled the results "high" and "low" corresponding to the relative magnitudes of the predicted concentrations:

- HIGH. Each building was treated as if it were isolated. The area was estimated as the average of the north-south and the east-west building faces.
- LOW. The crosswind width of each building was assumed to be equal to the longer (north-south) dimension of the production area, which was estimated as 818 m. The height of each individual building and this common exaggerated width were used in computing the area. This assumption approximates considering the entire complex as a single building.

Inasmuch as the release estimates, and therefore the predicted concentrations, are available only only on a monthly basis, the air-monitoring data were combined into a weighted average for each month for which measurements were taken. The weights were proportional to the times that the samplers were operated for the respective samples. These averages were adjusted to account for the effects of reduced efficiency of the air samplers for particles of large aerodynamic diameters. Individual measurements of uranium in air at the four perimeter stations are tabulated in Appendix L, along with distributions of the factors for sampling efficiency. For the tabular comparisons, we used the medians of these distributions.

Table J–1 summarizes the model comparison in terms of two measures. The first is the multiplicative bias

$$B = \exp\left(\overline{\ln(P)} - \overline{\ln(O)}\right) \qquad \text{(J–6)}$$

where the overbars indicate averaging of the log-transformed predicted (P) and observed (O) values. A value of 1 corresponds to no bias; values greater than 1 indicate overprediction as an averaged multiple of the observed values, and values less than 1 indicate underprediction. The quantity B is equal to the geometric mean of the P/O ratios in the case of paired measurements. The second measure is the correlation coefficient r of the log-transformed P and O data. The bias and correlation are essentially the measures used by Ramsdell (1990) for similar comparisons. For the purpose of computing the measures, each wake effects model was represented by the geometric mean of its high and low versions. To avoid mixing models in the comparison of the four models, the old solid waste incinerator and the oil burner were excluded, because neither will be treated with a wake-effects model. Plume depletion due to deposition could not be applied consistently to the four models, because, as we noted previously, estimating plume widths for the statistical and the standard wake effects models would entail additional assumptions. Consequently, the comparison of the four models is shown in Table J–1 without deposition. At the bottom of the table, however, we show the results for the Gaussian and time-dependent models with adjustment for depletion due to deposition and with the inclusion of the old solid waste incinerator and the oil burner in the source term. In

Table J–1. Summary Table: Model Comparison for FMPC Perimeter Stations

Model	Quantity	NE	SE	SW	NW
Models applied only to production plant releases,[a] without plume depletion					
Statistical	Bias	0.94	1.05	0.67	0.35
	Correlation	0.47[b]	0.21	0.37	0.20
Standard wake effects	Bias	22.48	29.59	9.05	10.65
	Correlation	0.39[b]	0.19	0.41[b]	0.40[b]
Gaussian[c]	Bias	3.12	2.08	1.38	1.31
	Correlation	0.43[b]	0.14	0.42[b]	0.34
Time-dependent	Bias	3.46	4.03	2.51	1.37
	Correlation	0.49[b]	0.19	0.35	0.21
Models with full source term and plume depletion					
Time-dependent	Bias	1.72	2.10	1.50	0.70
	Correlation	0.55[b]	0.18	0.34	0.15
Gaussian[c]	Bias	3.50	2.17	1.08	1.32
	Correlation	0.47[b]	0.17	0.40[b]	0.24
Number of observations		31	29	26	30

[a] Specifically excluded from source term: old solid waste incinerator and oil burner.
[b] Significant at the 5% level.
[c] Plume rise.

calculating the tabular entries for the time-dependent model, we applied the Gaussian model to the old solid waste incinerator and the oil burner in order to treat them as point sources.

Table J–1 indicates generally low correlations for all models and stations. For the SE station, all correlations are statistically indistinguishable from zero, and the same is true for all but one of the correlations for the NW station. Estimates of the other correlations are in the range 0.14–0.55, which is not impressively high. One reason for the low-to-modest correlations is that month-to-month variations in the monitoring data do not match up well with corresponding variations in the reconstructed total source term. Table J–2 provides data on distances and directions from plant buildings to the four sampling stations that were used for the simulations.

The estimates of bias for the four models indicate disparate tendencies toward overprediction, with fewer underpredictions. The least bias is seen in the statistical model, with the Gaussian and time-dependent models exceeding its predictions by factors nearly as high as four. But note that the statistical model underpredicts the SW and NE stations by factors of 1.5 and 2.9, respectively. In its primitive form, the statistical model cannot be considered a viable contender on the practical grounds that it is not applicable beyond the 1,200-m range of the underlying data that were used in the regression that it represents. One must also realize that (1) plume depletion due to deposition has not been considered in the comparison

Table J–2. Distance (m) and Wind Direction[a] For Each Receptor and Plant

	NE		SE		SW		NW	
Plant	Dist.	Dir.	Dist.	Dir.	Dist.	Dir.	Dist.	Dir.
1	679	WSW	738	NW	467	N	373	SSE
2/3	690	SW	616	WNW	383	NNE	498	SSE
4	603	SSW	470	NW	456	NE	598	SE
5	595	SSW	363	NW	508	ENE	699	SE
6	553	SSW	314	NNW	603	ENE	761	SE
8	768	SW	532	WNW	286	NE	626	SSE
9	392	SSW	477	NNW	694	NE	647	ESE
Pilot	933	SW	612	W	123	NNE	716	S

[a] Sector indicates direction from which wind blows.

shown in the upper part of Table J–1, and (2) the models considered estimate sector-centerline concentrations, which typically exceed crosswind averages by a factor of two or more. The lower part of Table J–1 also shows the bias and correlation estimates for the time-dependent model after corrections for plume depletion have been made and the old solid waste incinerator and oil burner are included in the source term (the Gaussian model is applied to these sources, even even when the time-dependent model is applied to the production plants). In these latter calculations, the time-dependent model is seen in a more favorable light. The predictions of the Gaussian model change relatively little when plume depletion from deposition is considered (in fact, most of them increase slightly because of the addition of the two small sources). The reason is that the deposition-velocity model predicts little removal near an elevated source before the plume "touches down." Figures J–1 through J–4 show the high and low predictions of uranium air concentrations by the time-dependent model and the predictions of the Gaussian model, both with full source term and plume depletion, plotted on the same chart with the adjusted monthly averages of the monitoring results for 1960–1962 (Appendix L). The adjusted monitoring values are represented as shaded areas that comprehend the 5th to the 95th percentiles of the distributions for each month. We remind the reader that the "high" predictions of the time-dependent model are based on the assumption that each building is isolated, and the "low" predictions approximate treating the entire complex as a single building.

The standard wake effects model grossly overestimates the air monitoring data and presumably would do so after any reasonable adjustment for deposition and crosswind averaging. This fact is perhaps not surprising in view of the deliberate conservatism that was sought for models used in traditional radiation protection applications. Ramsdell (1990) plotted P/O ratios vs. wind speeds for this model with the seven datasets used in the development of his statistical model. The range of these ratios covers more than four orders of magnitude, with a preponderance of overpredictions at low wind speeds up to about 3 m s^{-1}.

The standard centerline Gaussian plume model for elevated releases represents the assumption that wake effects are negligible. This model also overestimates the measured concentrations at the perimeter stations, but its estimates (without deposition) are closer to the monitoring data than the estimates of the time-dependent model (Table J–1). To the extent

monitoring data than the estimates of the time-dependent model (Table J–1). To the extent that the time-dependent model represents the wake effects of buildings ("high" version) or the complex ("low" version), this comparison suggests that those effects are not as important in predicting air concentrations at the FMPC as might be expected. But one must bear in mind that this comparison is obscured by the idiosyncratic behavior of the deposition velocity model when it is applied to the Gaussian plume near the point of release. A somewhat more elaborate simulation would be required for a cleaner comparison.

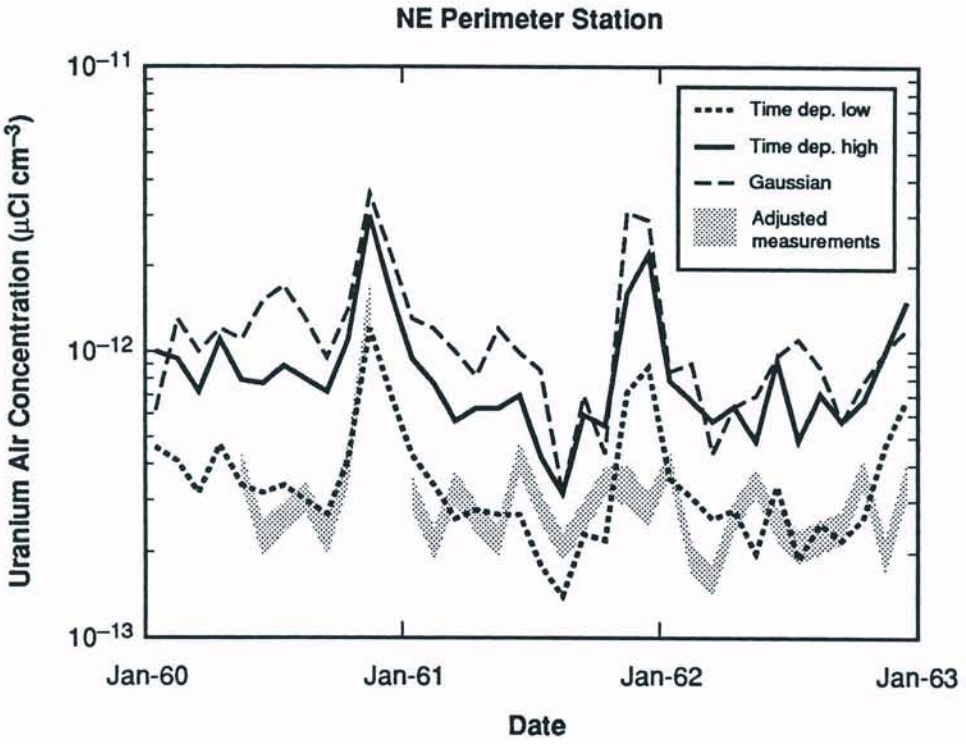

Figure J–1. The "time-dependent" model of Ramsdell (1990) and the Gaussian model compared with measured uranium concentrations at the perimeter station at the NE corner of the FMPC production area during the years 1960–1962. The model simulations accounted for plume depletion due to deposition and were based on a source term that included the old solid waste incinerator and the oil burner. The shaded areas represent the monthly averages of measured air concentrations, extending from the 5th to the 95th percentiles of their adjustment for sampling efficiency.

DISCUSSION AND CONCLUSIONS

We have described a set of simulations of releases of uranium from the FMPC to the atmosphere, using the reconstructed source term for 1960–1962 and sampling efficiency–adjusted air concentrations at the four monitoring stations at the four perimeter stations of the production area for the same period. The simulations were carried out with four different air dispersion models, three of which are specific to ground-level entrainment in building

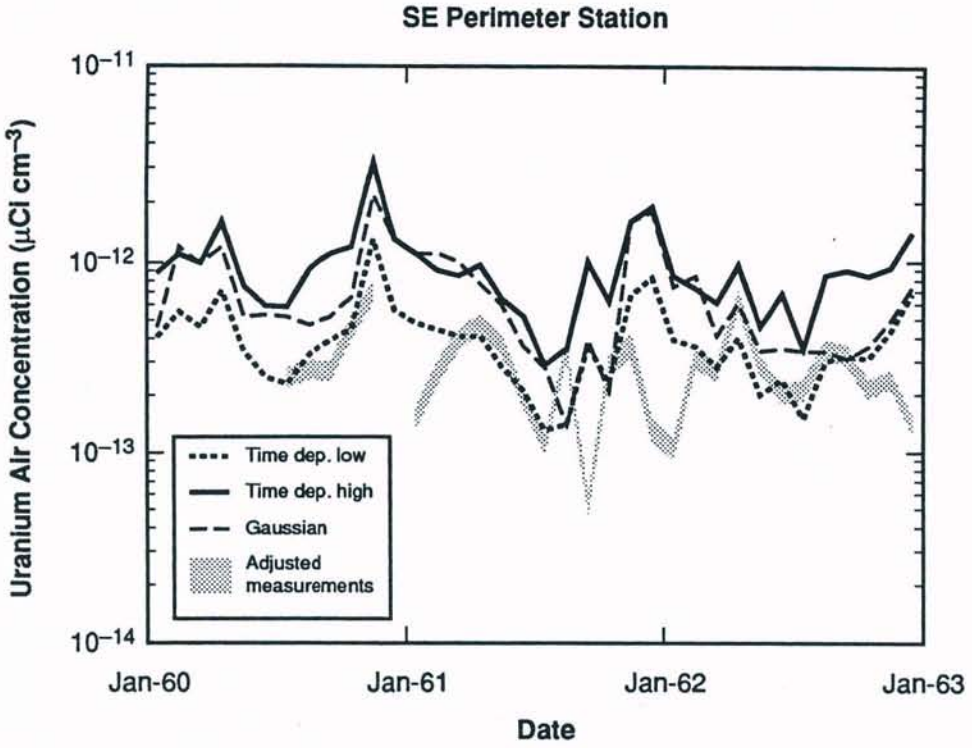

Figure J–2. The "time-dependent" model of Ramsdell (1990) and the Gaussian model compared with measured uranium concentrations at the perimeter station at the SE corner of the FMPC production area during the years 1960–1962. The model simulations accounted for plume depletion due to deposition and were based on a source term that included the old solid waste incinerator and the oil burner. The shaded areas represent the monthly averages of measured air concentrations, extending from the 5th to the 95th percentiles of their adjustment for sampling efficiency.

wakes. The statistical (regression) model of Ramsdell (1990) gives the least bias with the adjusted monitoring data, but the model is not applicable beyond 1,200 m, and deposition was not taken into account. The time-dependent wake-effects model developed by Ramsdell (1990) and the Gaussian plume model for elevated sources are at rough parity when plume depletion is considered, with the time-dependent model giving less-biased results on average, comparable correlations, and substantially less bias for the usually-downwind NE station. Both models are clearly superior in efficacy to the standard wake effects model.

We have noted that some degree of overestimation is associated with the use of the centerline version of a dispersion model for time-averaged meteorology. For the comparison, however, the use of the centerline prediction was satisfactory, because it applied to all models. For production simulations, however, the predicted concentrations will be averaged over the angle of the wind sector, and it may also be necessary to account for spillover from adjacent sectors. This smoothing process involves details that did not need to intrude into the comparison. Experience with sector-averaged Gaussian plume models indicates that overprediction by the certerline version is ordinarily about a factor of two.

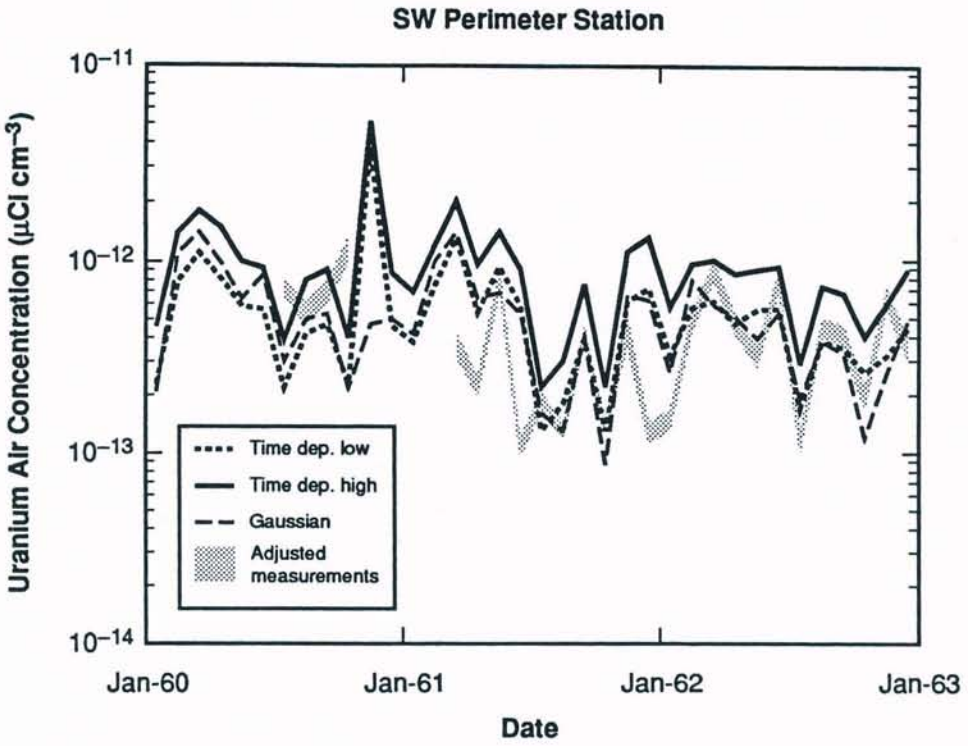

Figure J–3. The "time-dependent" model of Ramsdell (1990) and the Gaussian model compared with measured uranium concentrations at the perimeter station at the SW corner of the FMPC production area during the years 1960–1962. The model simulations accounted for plume depletion due to deposition and were based on a source term that included the old solid waste incinerator and the oil burner. The shaded areas represent the monthly averages of measured air concentrations, extending from the 5th to the 95th percentiles of their adjustment for sampling efficiency.

Some cautions are in order. A visual comparison of the curves with the plotted points in Fig. J–1, indicates that on short time scales (i.e., a few months), the reconstructed source term often leads to predictions that do not closely match the increases and decreases of measured air concentrations, although the agreement of longer-term averages is reasonably good (Table J–1). Thus it is plain that factor-of-two accuracy for certain specific months may be too much to claim. Interfering factors are numerous. Some of the obvious potential sources of error are the meteorological data (Appendix E), the source term, and errors associated with air sampling and the handling and analysis of the samples (Appendix L). Even so, we believe the results of the comparison of the time-dependent model predictions of air concentrations of uranium at the corner stations constitute an adequate (but limited) validation of the model.

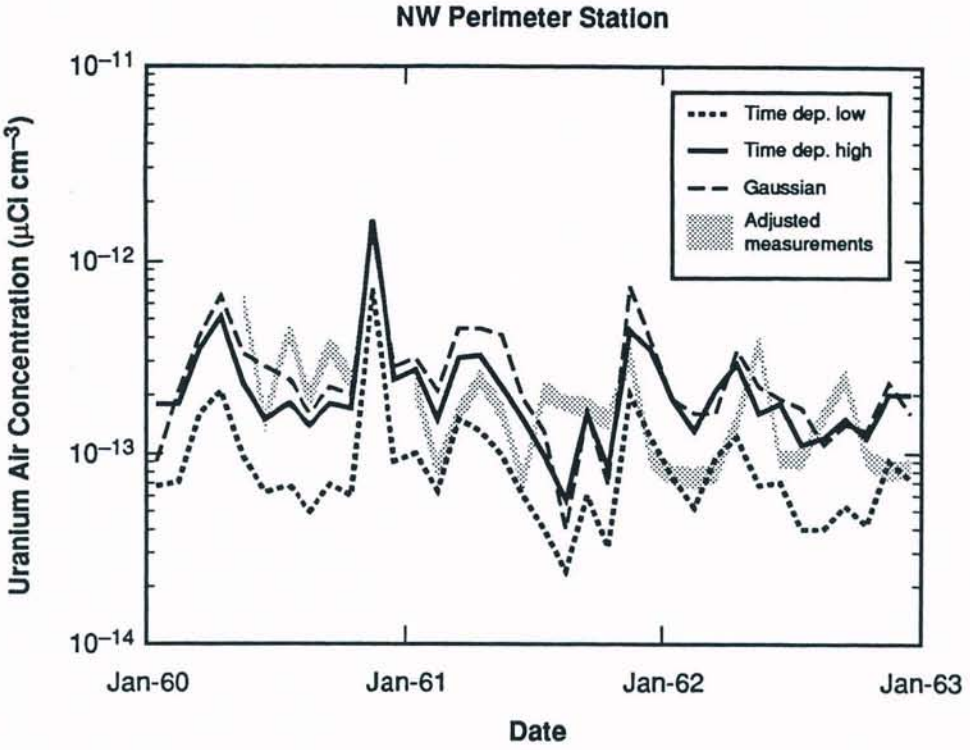

Figure J–4. The "time-dependent" model of Ramsdell (1990) and the Gaussian model compared with measured uranium concentrations at the perimeter station at the NW corner of the FMPC production area during the years 1960–1962. The model simulations accounted for plume depletion due to deposition and were based on a source term that included the old solid waste incinerator and the oil burner. The shaded areas represent the monthly averages of measured air concentrations, extending from the 5th to the 95th percentiles of their adjustment for sampling efficiency.

REFERENCES

Briggs G.A. 1974. "Diffusion Estimation for Small Emissions." In Atmospheric Turbulence and Diffusion Laboratory 1973 Annual Report, ATDL-106.

Briggs G.A., A.H. Huber, W.H. Snyder, and R.S. Thompson. 1992. Discussion of "Diffusion in Building Wakes for Ground-Level Releases," by J.V. Ramsdell, Jr. (1990), *Atmos. Env.* **24B**: 377–388. *Atmos. Env.* (in press).

Hanna S.R., G.A. Briggs, and R.P. Hosker, Jr. 1982. *Handbook on Atmospheric Diffusion.* Rep. DOE/TIC-11223 (DE82002045) Technical Information Center, U.S. Department of Energy.

Ramsdell J.V., Jr. 1990. "Diffusion in Building Wakes for Ground-Level Releases." *Atmos. Env.* **24B**: 377–388.

Voillequé P.G., K.R. Meyer, D.W. Schmidt, G.G. Killough, R.E. Moore, V.I. Ichimura, S.K. Rope, B. Shleien, and J.E. Till. 1991. *The Fernald Dosimetry Reconstruction Project, Tasks 2 and 3: Radionuclide Source Terms and Uncertainties — 1960–1962.* Rep. CDC-2, Radiological Assessments Corporation, Neeses, South Carolina 29107.

APPENDIX K

PARAMETRIC UNCERTAINTIES IN THE AIR TRANSPORT MODEL

INTRODUCTION

The term "parametric" in the title of this appendix is intended to convey the idea that we are concerned with one or more parameters of a model, each of which is associated with a certain range of values, and that we are uncertain about which value best represents the parameter in the context of what is being simulated. This uncertainty is expressed as a distribution of probability over the associated range of the parameter, and the analysis seeks to determine the corresponding distribution of values resulting from the simulation (the OUTPUT DISTRIBUTION). Thus we are studying the model's joint propagation of the parametric uncertainty distributions. Such an exercise furnishes more information than a sensitivity analysis, which provides only a matrix of partial derivatives of each result with respect to each parameter evaluated at the vector of "best" or "reference" parameter estimates.

One must be aware that this analysis says nothing directly about the appropriateness of the particular model to estimate the quantity of interest. It therefore cannot directly assess the ACCURACY of the model in its predictions. We deal with such questions in terms of the model's support by the relevant basic sciences and by validations, i.e., comparing results of simulations with data that were measured under conditions compatible with the assumptions governing the simulations. Departures of model predictions from data are measures of bias in the model. Examples are discussed in Appendices G, J, and M.

Our computational methodology is computer-implemented Monte Carlo analysis. (We use the term "Monte Carlo" in a generic sense to refer to any scheme of sampling of the parametric uncertainty distributions by computer-implemented techniques for pseudorandom numbers, rather than to mean a particular sampling scheme.) The well-known advantage of this approach is that it permits much greater generality than analytic techniques, which require restricted assumptions to permit solution of the equations in closed form or acceptable approximation of the solutions. The disadvantage is that the method produces an empirical distribution, and thus our estimates of means, variances, and percentiles are random variables, and if the model is computationally demanding, it may be difficult to generate a large enough number of trials to control the variances of these statistics (but nearly every application of statistics in the real world suffers from the same disadvantage).

In this discussion, a SIMULATION consists of a subdivision of the time of the FMPC's operation (1951–1988) into an integral number of PERIODS (years, quarters, or months) and application of the transport model to the airborne release for each period to estimate results, such as air concentrations and depositions at each receptor point in the region. The question of the duration of the fundamental period has not yet been settled. We have used one month (i.e., 1/12 of a year) as the standard for validation because of the availability of data at this resolution during 1960–1962, but for the purpose of dose estimation for the longer term, a different period may be chosen.

The purpose of this appendix is to sketch prospectively the application of this methodology to the air transport module to be used in our assessment. Our primary attention is to transport of releases of uranium and associated particulates from FMPC production plants and releases of radon gas and daughter products from the K-65 silos. A reference appropriate to the general context of this work is IAEA (1989).

THE AIR TRANSPORT MODEL IN THE CONTEXT OF UNCERTAIN PARAMETERS

There are two air transport and dispersion formulas to be implemented. One is the time-dependent model discussed by Ramsdell (1990), which we apply to all rooftop releases from the FMPC production area and to releases of radon from the K-65 silos. Equations for the model are given in Appendices F and J. Such releases are expected to be predominantly entrained into building wakes, and our comparisons of model-predicted air concentrations with data measured at the four perimeter stations indicated good agreement for this model (Appendix J). Two sources that are small in relation to the total are the old solid waste incinerator and the oil burner. Because they are hot sources, both will be treated as elevated releases with plume rise (Appendix I), and the Gaussian plume model will be applied.

Concentrations predicted by either model obviously depend multiplicatively on the release rate and on geometric factors associated with spatially-separated multiple sources. Both depend on the distance x (m) and direction from source to receptor point, wind speed, atmospheric stability, and depletion of the plume through wet and dry deposition (Appendices G and H). The time-dependent model takes wake effects into account through a parameter A (m^2) that represents an effective area of the building's crosswind face and treats the release as being from a vertical rectangle with the area of that face. The Gaussian plume depends on the effective release height of a point source, where "effective" indicates the physical release height h plus a term Δh to account for plume rise or sinkage (Appendix I).

The local meteorology is factored into the predictions both directly and indirectly. Only when the receptor point is downwind from the source is a nonzero concentration recorded, but for final calculations, some directional averaging may be used to account for spillover to and from adjacent sectors. This discussion does not consider the component of concentration resulting from resuspended material, which will be estimated from measurements (Appendix O). The horizontal and vertical dispersion coefficients σ_y and σ_z (m) depend on the distance x from the source and the stability class. The wind speed u (m s^{-1}) is a factor in the denominator of the Gaussian model, and it enters the time-dependent model in a more complicated way (Appendices F and J). The depletion of the plume depends on an integration from a point near the source to the receptor point, with the sum of the wet and dry deposition velocities ($v_w + v_d$) as a factor in the integrand. The rate of deposition on the ground is the product of this sum and the air concentration. Our model for the wet deposition velocity, v_w, depends on rainfall during the period of observation but not explicitly on other meteorological variables. The dry deposition velocity, v_d, is a function of wind speed, stability, and particle aerodynamic diameter. The distribution of particle aerodynamic diameter evolves as the released material moves downwind and hence depends on the sum of the deposition velocities. Figure K–1 summarizes these and other dependencies schematically.

It is an elementary observation that one should start at the far ends of dependency chains to assign uncertainties to variables that are "fundamental." Sometimes, however, our most

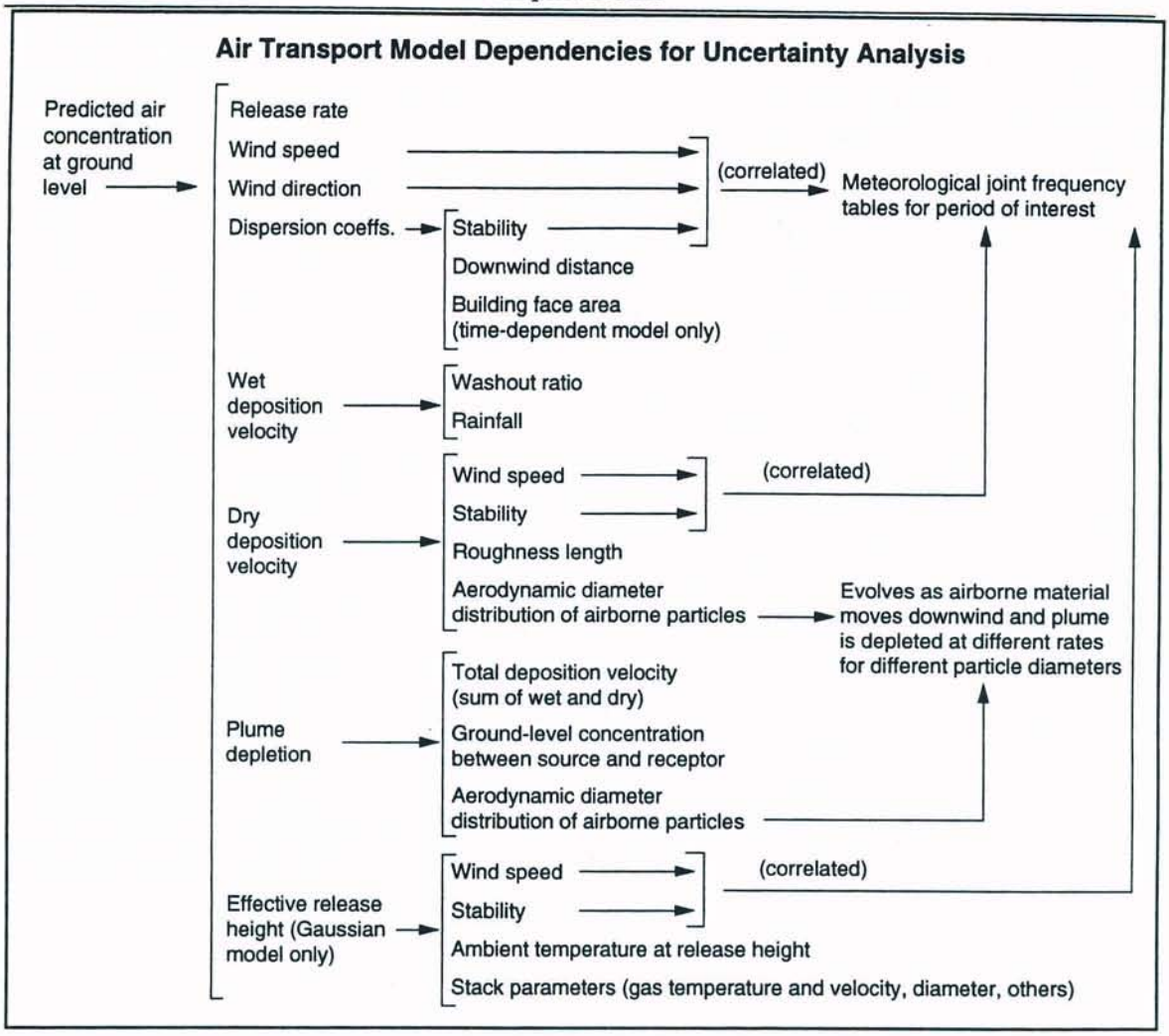

Figure K–1. Dependencies of predicted air concentrations on other variables.

confident quantification of uncertainty is at higher levels, and this situation may lead to revising the models. For example, early in the study, we examined a model of wet deposition that depended on distributions of particle and raindrop diameters. Difficulty in quantifying the latter distribution and the availability of local data for directly estimating the distribution of the washout ratio (Appendix H) led to our adopting the simpler model, which has no explicit dependence on diameters of particles or scavenging raindrops.

Uncertainty in Meteorological Joint Frequency Tables

In Fig. K–1, three paths lead to the meteorological joint frequency tables that characterize the wind speed, wind direction, and stability for the period of the plant's operation. For most of this period, the meteorological joint frequency tables for the FMPC are not strictly applicable (Appendix E), and we are obliged to estimate uncertainties that result from using these tables that are limited to a 1987–1991 data base. Appendix E has indicated an approach to estimating geometric standard deviations of a multiplicative error term for predicted air

concentrations at specific receptor points.

Unfortunately, air concentrations at different locations may be correlated in a way that is unknown to us *a priori*. As a preliminary and illustrative analysis, we have established a grid by using distances of 1 and 8 km from the center of the production area on the 8 radials with directions N, NE, E, SE, S, SW, W, and NW, for a total of 16 receptor points (Fig. K–2). For each of the years 1987–1991, with the annual-average joint frequency tables, we have used the time-dependent model with a nominal crosswind building-face area of 7,000 m^2 to estimate χ/Q at each receptor point. Statistics have been compiled on the log-transformed estimates, which are assumed to be normally distributed. Table K–1 shows the correlations and standard deviations.

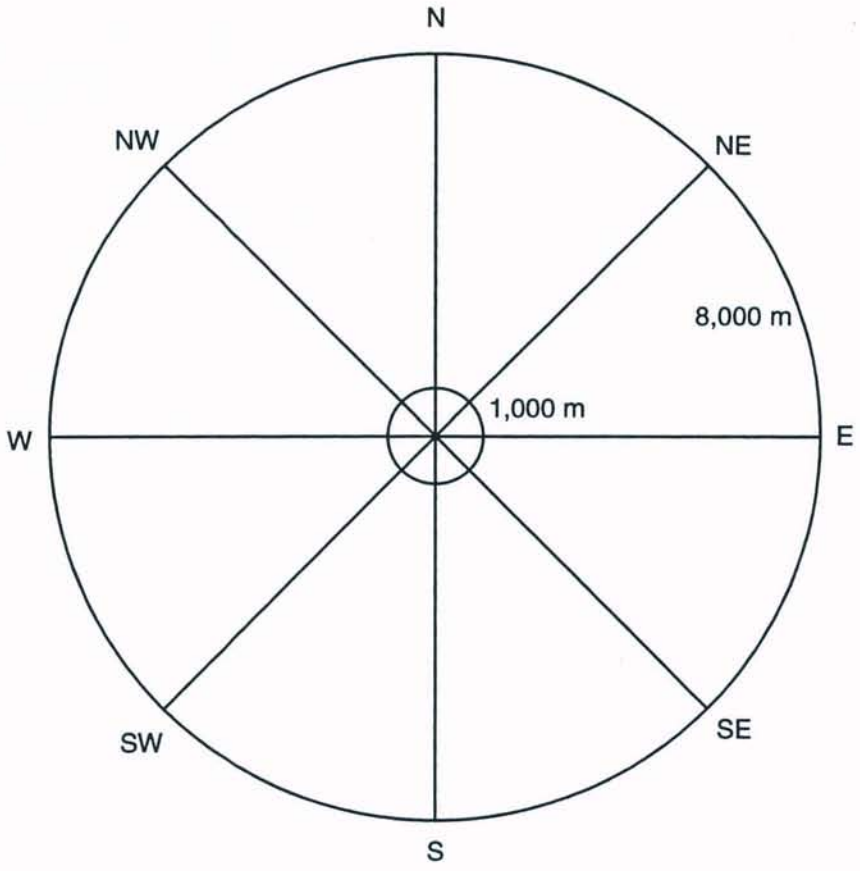

Figure K–2. Grid for locations at which air concentrations are computed to study the possible influence of year-to-year variability in the FMPC meteorological joint frequency tables. The central point is assumed to be the center of the production area of the FMPC.

The geometric standard deviations (GSDs) range from 1.1 to 1.4; the latter value corresponds to annual variations within the multiplicative range of ±74% (i.e., × or ÷ 1.74) with 90% confidence. The GSD for the computations with annual Cincinnati data for 1951–1991 at the NE-1,000-m point is 1.3 (Appendix E), though it may be higher for other points that we

have not yet sampled. The correlation matrix suggests that the assumption of independence of uncertainty distributions from one receptor point to another might be inappropriate. As we might expect, the pairs of receptor points in the same downwind direction from the source (e.g., N1 and N8) are usually strongly correlated. The exception is the pair S1 and S8, with a negative correlation that is small in magnitude (−0.086). One has to bear in mind that the correlation matrix of Table K–1 is itself based on a small sample (five successive years), and the temptation to use it as a basis for estimating a theoretical correlation matrix (assumed, perhaps incorrectly, to be stationary) should be resisted.

Table K–1. Estimated Variability of Model Predictions from Year to Year Based on Annual FMPC Meteorological Data for the Years 1987 through 1991[a]

	Correlation matrix																	
	N1	NE1	E1	SE1	S1	SW1	W1	NW1	N8	NE8	E8	SE8	S8	SW8	W8	NW8	GM[b]	GSD[c]
N1	1.000	0.190	−0.138	0.477	−0.052	−0.737	−0.282	−0.467	0.982	0.536	−0.316	0.381	−0.187	−0.745	−0.233	−0.406	1.3×10^{-6}	1.3
NE1		1.000	0.844	−0.240	0.581	0.507	0.576	0.702	0.177	0.847	0.671	−0.660	0.378	0.410	0.537	0.776	3.6×10^{-6}	1.1
E1			1.000	−0.662	0.248	0.657	0.365	0.729	−0.069	0.687	0.881	−0.858	0.370	0.671	0.311	0.819	2.9×10^{-6}	1.1
SE1				1.000	0.420	−0.469	−0.186	−0.575	0.389	0.005	−0.478	0.851	−0.586	−0.505	−0.174	−0.602	2.1×10^{-6}	1.1
S1					1.000	0.537	0.560	0.429	−0.138	0.433	0.388	−0.058	−0.086	0.416	0.502	0.429	1.0×10^{-6}	1.1
SW1						1.000	0.607	0.837	−0.733	0.132	0.753	−0.694	0.304	0.952	0.530	0.836	1.0×10^{-6}	1.3
W1							1.000	0.869	−0.410	0.082	0.149	−0.606	0.763	0.337	0.995	0.810	1.2×10^{-6}	1.2
NW1								1.000	−0.511	0.230	0.552	−0.894	0.742	0.671	0.834	0.989	5.2×10^{-7}	1.3
N8									1.000	0.577	−0.217	0.358	−0.264	−0.687	−0.369	−0.431	2.8×10^{-7}	1.2
NE8										1.000	0.610	−0.291	−0.070	0.159	0.047	0.350	8.5×10^{-7}	1.1
E8											1.000	−0.619	−0.035	0.855	0.061	0.647	8.0×10^{-7}	1.2
SE8												1.000	−0.751	−0.614	−0.581	−0.921	6.6×10^{-7}	1.2
S8													1.000	0.080	0.801	0.693	1.8×10^{-7}	1.1
SW8														1.000	0.247	0.697	1.9×10^{-7}	1.2
W8															1.000	0.769	4.1×10^{-7}	1.2
NW8																1.000	1.5×10^{-7}	1.4

[a] Codes indicate locations with N=north, NE=northeast, etc., 1=1,000 m, and 8=8,000 m.

[b] Sample geometric mean for χ/Q (s m^{-3}).

[c] Sample geometric standard deviation.

We have examined two other correlation matrices based on five-year composite annual datasets for Cincinnati, one for 1987–1991 and the other for 1960–1964. They differ qualitatively from the FMPC matrix of Table K–1 and from each other. They are presented in Tables K–2 and K–3.

The correlation matrices of Figs. K–1 and K–3 tend to support the hypothesis that receptors in the same sector are positively correlated. It is quite possible that correlations of some magnitude, positive and negative, exist between pairs of points in different sectors, but these patterns probably shift with time and are undetectable in our limited data base. A comparison of Tables K–1 and K–2 discourages the assumption that the Cincinnati correlations would apply to Fernald.

We propose to reduce the question of correlation to a simpler model for purposes of implementing the estimates of uncertainty due to year-to-year meteorological variations. We will assume that only the air concentrations at receptor points within the same sector are positively correlated, and that all other correlations are zero. Specifically, we apply a Markov-type assumption to the log-transformed uncertainty factors at the eight radial receptor points that are separated by 1-km intervals. It can be shown that for a chosen value of ρ $(-1 \leq \rho \leq 1)$ the recursion

$$v_1 = \epsilon_1$$

$$v_k = \rho v_{k-1} + \epsilon_k, \quad k = 2, 3, \ldots, 8,$$

Table K–2. Estimated Variability of Model Predictions from Year to Year Based on Annual Cincinnati Meteorological Data for the Years 1987 through 1991[a]

	Correlation matrix																	
	N1	NE1	E1	SE1	S1	SW1	W1	NW1	N8	NE8	E8	SE8	S8	SW8	W8	NW8	GM	GSD
N1	1.00	0.33	−0.31	−0.02	0.48	−0.43	−0.10	0.27	−0.32	−0.43	−0.85	−0.20	−0.74	−0.75	−0.37	−0.40	2.7×10^{-6}	1.1
NE1		1.00	−0.58	0.09	−0.13	−0.45	−0.13	−0.61	−0.62	0.27	−0.68	−0.09	−0.75	−0.34	−0.25	−0.91	3.0×10^{-6}	1.1
E1			1.00	−0.49	−0.65	−0.35	−0.36	−0.13	0.23	0.08	0.36	−0.16	0.21	−0.23	−0.06	0.38	2.1×10^{-6}	1.1
SE1				1.00	0.29	0.20	0.98	−0.06	0.68	0.57	0.28	0.94	0.30	0.50	0.88	0.34	1.2×10^{-6}	1.2
S1					1.00	0.58	0.31	0.82	0.05	−0.62	−0.20	0.01	0.08	0.15	−0.01	0.17	2.0×10^{-6}	1.1
SW1						1.00	0.30	0.63	0.27	−0.33	0.55	0.08	0.74	0.81	0.22	0.51	1.0×10^{-6}	1.2
W1							1.00	0.06	0.81	0.51	0.43	0.95	0.47	0.58	0.93	0.53	1.7×10^{-6}	1.1
NW1								1.00	0.16	−0.80	0.07	−0.20	0.33	0.14	−0.13	0.48	8.2×10^{-7}	1.1
N8									1.00	0.43	0.74	0.83	0.73	0.54	0.90	0.88	3.7×10^{-7}	1.1
NE8										1.00	0.36	0.73	0.14	0.28	0.70	0.05	4.1×10^{-7}	1.2
E8											1.00	0.48	0.96	0.82	0.65	0.82	2.3×10^{-7}	1.2
SE8												1.00	0.43	0.50	0.98	0.49	1.3×10^{-7}	1.4
S8													1.00	0.87	0.60	0.87	2.6×10^{-7}	1.2
SW8														1.00	0.63	0.56	1.3×10^{-7}	1.3
W8															1.00	0.63	2.1×10^{-7}	1.3
NW8																1.00	1.0×10^{-7}	1.2

[a] Codes indicate locations with N=north, NE=northeast, etc., 1=1,000 m, and 8=8,000 m.

[b] Sample geometric mean for χ/Q (s m^{-3}).

[c] Sample geometric standard deviation.

Table K–3. Estimated Variability of Model Predictions from Year to Year Based on Annual Cincinnati Meteorological Data for the Years 1960 through 1964[a]

	Correlation matrix																	
	N1	NE1	E1	SE1	S1	SW1	W1	NW1	N8	NE8	E8	SE8	S8	SW8	W8	NW8	GM	GSD
N1	1.00	−0.49	−0.62	−0.92	−0.33	−0.45	−0.59	−0.54	0.36	−0.79	−0.66	−0.57	−0.48	−0.67	−0.62	−0.73	2.8×10^{-6}	1.2
NE1		1.00	0.24	0.73	0.91	0.92	−0.39	−0.45	−0.89	0.92	0.54	0.73	0.75	0.89	−0.33	−0.20	2.7×10^{-6}	1.2
E1			1.00	0.63	−0.04	−0.06	0.58	0.46	0.12	0.47	0.84	0.40	−0.22	0.18	0.60	0.47	1.5×10^{-6}	1.1
SE1				1.00	0.61	0.65	0.34	0.28	−0.50	0.92	0.66	0.82	0.61	0.85	0.41	0.52	1.3×10^{-6}	1.1
S1					1.00	0.97	−0.49	−0.51	−0.83	0.77	0.17	0.81	0.88	0.92	−0.41	−0.23	1.6×10^{-6}	1.1
SW1						1.00	−0.42	−0.44	−0.92	0.83	0.23	0.73	0.94	0.95	−0.36	−0.14	1.7×10^{-6}	1.2
W1							1.00	0.99	0.53	−0.01	0.27	0.01	−0.28	−0.13	1.00	0.95	1.4×10^{-6}	1.5
NW1								1.00	0.55	−0.08	0.15	−0.04	−0.25	−0.16	0.98	0.95	1.1×10^{-6}	1.2
N8									1.00	−0.78	−0.34	−0.43	−0.82	−0.78	0.50	0.31	5.6×10^{-7}	1.1
NE8										1.00	0.70	0.76	0.71	0.90	0.05	0.18	3.8×10^{-7}	1.4
E8											1.00	0.31	0.02	0.34	0.27	0.21	1.9×10^{-7}	1.2
SE8												1.00	0.66	0.87	0.11	0.22	1.7×10^{-7}	1.2
S8													1.00	0.91	−0.22	0.04	2.4×10^{-7}	1.2
SW8														1.00	−0.05	0.15	2.8×10^{-7}	1.3
W8															1.00	0.96	2.5×10^{-7}	1.7
NW8																1.00	1.9×10^{-7}	1.3

[a] Codes indicate locations with N=north, NE=northeast, etc., 1=1,000 m, and 8=8,000 m.

[b] Sample geometric mean for χ/Q (s m^{-3}).

[c] Sample geometric standard deviation.

generates random variables v_k with the correlation between successive pairs v_k and v_{k+1} equal to ρ, provided the ϵ_k are independent random variables with zero mean (Kendall and Stuart 1968). We take the ϵ_k to be normally distributed with variances equal to 1 and define $\eta_k = \exp(X_k)$, where $X_k = \sigma_k v_k$ and the standard deviations σ_k are those estimated from the log-transformed ratios R_k of Appendix E. Then η_k can be shown to be lognormally distributed with geometric mean 1 and geometric standard deviation $\exp \sigma_k$, and the underlying normal random variables X_k are pairwise correlated as indicated. More generally, the correlation of η_k and η_{k+q} $(q \geq 0)$ is ρ^q (Kendall and Stuart 1968).

This procedure is applied to each sector, possibly with different values of ρ assigned to different sectors, although there is little basis for differentiating among the sectors. By starting the process for different sectors with independent random variables ϵ_1, we derive estimates of the uncertainty factors η_k that are uncorrelated between sectors.

The estimate of air concentration χ_k for location k in the sector may now be computed as

$$\chi_k = \chi_k^0 \eta_k ,$$

where χ_k^0 represents the unadjusted estimate. The stochastic multiplicative uncertainty factor η_k, as derived above, incorporates the year-to-year variability attributable to meteorology and the indicated correlations. More elaborate sampling schemes are necessary for general correlation matrices, but for the special case we have chosen, the one just outlined should be quite satisfactory and more efficient to implement.

Deposition Models and Parameters

In sampling for uncertainty, the deposition velocities will be treated as uncertain quantities. For the wet deposition velocity, v_w, the first source of uncertainty is in the washout ratio, for which a distribution has been characterized (Appendix H). A value of the washout ratio will be drawn from this distribution prior to each complete simulation (1951–1988) and the simulation performed with that value used for all years and all locations. Thus, for the simulation, the wet deposition velocity will vary only with the average rainfall rate for each period, which is the second source of uncertainty. Compilation of applicable rainfall data for the longer term (1951–1988) has not yet been completed, but the principal uncertainty is likely to derive from the use of surrogate rainfall data. Even data taken at the FMPC site cannot characterize rainfall at all locations within the eight-km domain. Uncertainty will be based on variability among different datasets from the greater Cincinnati region. Because of the dominance of dry deposition of large particles, the wet deposition velocity ($v_w \approx 0.01$ m s^{-1}) is unlikely to contribute a large component to the overall uncertainty of air concentrations.

As noted in Appendix G, dry deposition is highly uncertain, despite the somewhat elaborate theory that surrounds it. Although the various dependencies (wind speed, stability, roughness length, aerodynamic particle diameter) will be included in the calculation of the dry deposition velocity, v_d, we apply a systematic multiplicative uncertainty distribution, which is sampled at the beginning of each simulation and which will apply to all computed dry deposition velocities during the simulation. The uncertainty expressed applies principally to the model's ability to represent dry deposition rather than to uncertainty about specific parameter values. Sehmel (1980; see especially Fig. 2) reviewed numerous empirical studies of dry deposition and shows variability of measured deposition velocities for particulates spanning about three orders of magnitude, even when the estimates are plotted against particle diameter. We believe the three orders of magnitude just mentioned span too great an uncertainty range for our purpose because of uncontrolled factors in the studies reviewed (type of material, density, micrometeorological variables). The uranium particulate effluents from the FMPC are likely more homogeneous in properties that would affect deposition than the myriad particulate substances in the studies reviewed by Sehmel (1980). The spread of our applied uncertainty distribution has not been finally decided, but it is likely to comprehend at least an order of magnitude with 90% probability.

For larger particles, with aerodynamic diameters greater than about 20 μm, terminal velocity of gravitational fall is the dominant component in accounting for dry deposition, and we are inclined to associate relatively less uncertainty with this velocity than with deposition

velocities for smaller particles. A factor of two can be assigned to the effects of non-spherical shapes of particles and agglomerates (Hanna et al. 1982, Table 10.1), and perhaps an additional factor of two could be argued for to account for possible inaccuracy in graphical estimates used in the calculation (Appendix G, Table G–3). It should be mentioned that the *form* of the model for dry deposition of large particles — i.e., the use of a deposition velocity with source depletion — may not adequately address the removal of the particles from the plume, as is discussed at the end of Appendix G. This question will be investigated further before final calculations are undertaken, and consideration will be given to making use of a tilted-plume version of the model for particles in this size range. But the question concerns the structure of the model rather than parametric uncertainty.

Distributions of Particle Size

The study by Northern Kentucky Environmental Services (NKES) in 1985 furnished the basis of assigning distributions of particle diameter to the FMPC releases that passed through dust collectors (Appendix D). Particles in this size range (aerodynamic diameter < 20 μm) are in the respirable range and thus are the most important from the point of view of inhalation dosimetry. These releases, combined with particles of similar size that penetrate the scrubbers of Plant 2/3 and Plant 8, account for more than half of the uranium that was released to the air from the FMPC during 1960–1962.

Appendix D indicates methods that were used to consolidate the empirical distributions of dust-collector particles into a smaller number of distributions on the basis of the processes that produced them. The distributions are for U_3O_8 and UF_4, and each is subdivided according to inlet and outlet for the dust collector. A continuous-type distribution, based on a nonlinear cubic regression, was fitted to each empirical distribution for convenience in automated interpolation, extrapolation, and calculating percentage points (Appendix D).

The exact shapes, central measures, and quantiles of these distributions are, of course, uncertain, and we have developed tools to distort them randomly from their nominal configurations. By designating a fixed upper quantile (say the 90th percentile), denoted by x_u, and defining the parameter $S = x_u - x_{50\%}$ (which we call the SPREAD of the distribution), we may prescribe an arbitrary fractional increase or decrease in the spread (e.g., 50%) while keeping the median fixed. Alternatively, we may call for a similar increase or decrease of the median keeping the spread fixed. In this way, we apply random perturbations to the distributions in the Monte Carlo analysis and allow these distortions to propagate into the deposition and dose models. (We should note that for purposes of the Monte Carlo calculations, the particle size distributions are not considered probability distributions from which sampling is done. They are components of the deterministic model that underlies the simulations.)

Particles of similar size that penetrate the scrubbers have been represented by histograms with four and five class intervals (Tables D–11 and D–16). These particles represent about 24% of the uranium in airborne releases from the FMPC during 1960–1962 (Appendix D). This distribution and the allocation of uranium to particles of this class will be treated as uncertain quantities, but this implementation has not yet been carried out.

Reentrainment of uranium entering the scrubbers of Plant 2/3 and Plant 8 in the scrub liquor and the escape of the droplets to the atmosphere has resulted in distributions of large particles (physical diameters $>$ about 30 μm), which have been discussed in Appendix D.

About 49% of the uranium released from FMPC facilities to the atmosphere during 1960–1962 is believed to have been in these large-size distributions. These distributions and the allocation fraction will be treated as uncertain quantities. Implementation of the uncertainty mechanisms has not yet been worked out. Quantitative treatment of these particles is essential for total mass balance, and their deposition on crops and pasture introduces them into the ingestion dose pathway, but for inhalation dosimetry they are unimportant.

We consider the configurations of particle-size distributions and allocation fractions to be systematic quantities, which are varied only at the beginning of each simulation.

Roughness Length

The roughness length parameter, denoted by z_0 (m) is characteristic of the deposition surface (Appendix G). As a nominal value, we have taken 0.22 m, which is the geometric mean of the values for uncut grass (0.05 m) and tree cover (1 m). This range is suitable for the treatment of uncertainty of this parameter, although it must be truncated below 1 m, because that height is used as the reference height for the wind speed in estimating deposition velocities, and the use of the same value for z_0 creates a singularity in the formulas (the wind speed is taken to be zero at height z_0). In the simulations, the uncertainty of z_0 will be considered systematic, and the parameter will be varied only prior to each simulation of the 38 year plant history.

Parameters Influencing Plume Rise

Figure K–1 indicates a dependence of predicted air concentrations on point-of-release parameters that influence the rise or sinkage of the plume. Appendix I sets forth a methodology that was assembled primarily from the work of Briggs (1969, 1974, 1984). For buoyant plumes (the only ones with which we shall be concerned), Briggs (1969) suggests allowing for multiplicative deviations of $\pm 10\%$ from the estimates for a flat site and $\pm 40\%$ near a body of water or a prominent terrain irregularity, and we incorporate the latter estimate to account for terrain effects.

Because of our application of the building wake effects model to all releases from rooftop stacks, plume rise calculations will be applied only to two sources: the old solid waste incinerator and the oil burner. These facilities generated high temperatures, which are themselves uncertain, and further work remains to be done to quantify these sources. Their combined airborne release of uranium, however, was a small fraction of the total, and relatively large ranges of uncertainty can be assigned to their parameters without having a large effect on the overall uncertainty. The old solid waste incinerator is believed to have contributed significantly to contamination of the soil near it, but it is unclear how much of the contamination was spread by handling the ash during removal rather than from the stack itself.

Crosswind Building Area and Other Aspects of Wake Effects Modeling

Appendix J develops our approach to accounting for distortion of the plume by building wake effects. If the building generating the wake is isolated, the prediction of air concentration depends on the building's crosswind area. Simple models are not available for building complexes, but we also performed calculations based on the assumption that each building's width was approximately the longer dimension of the FMPC production area, thus treating the complex as a single large building. Calculations with these two extremes gives a range that tentatively serves as one component of uncertainty for the calculation. The range, generally within a factor of ±50%, is shown as the vertical extent of the shaded areas in Figs. J–1 through J–4. Other components of uncertainty associated with wake effects are more difficult to quantify in terms of model parameters, and we leave them in the category of residual uncertainty, which is discussed in the next subsection.

The validation simulations reported in Appendix J show a tendency of the wake effects model to overpredict the air concentrations at the perimeter stations. But the Gaussian plume, implemented in a form that ignored wake effects, produced comparable overpredictions, and thus one is not led to attribute the overpredictions to the particular treatment of building wake effects. As we pointed out at the end of Appendix G, and as the deposition results presented in Appendix M seem to confirm, at least part of the overprediction of air concentration is likely due to underestimation of the removal of large particles from the plume by dry deposition. As we have previously noted, the effect is probably the result of an inefficiency of the deposition velocity model with source depletion of the plume for particles in this size range.

Residual Uncertainty

It is possible that some observations of air concentration will lie outside of the range of uncertainty estimates even after the parametric variations described above have been incorporated into the Monte Carlo analysis. If this occurs to a significant extent, after the deposition models are given final adjustment and other fine-tuning is performed, similar comparisons to those depicted in Figs. J–1 through J–4 will be used as a basis for adding an uncertainty factor of such magnitude as is required to encompass the residual observed deviations of the model predictions from the measured values. The goal is that central values (means or medians) track observations as well as possible, minimizing bias in the predictions, and that necessary conservatism be put into the estimates of uncertainty.

CONCLUSION

We have summarized parametric uncertainties in the air transport models, together with existing or proposed methods of quantifying them for the final calculations. The result is a methodology that is designed to support different scenarios of exposure to airborne uranium and associated radionuclides, as well as to airborne radon and its daughters. The conceptual result of a Monte Carlo run of simulations is, for each period during the simulated plant operation (year or month), a correlated set of "observations" on air concentrations at receptor points in the assessment domain. These joint distributions, collectively, are our estimate of uncertainty in the air concentrations. The concentrations, however, are not the endpoint of the assessment. We qualified them as conceptual because there may not be an occasion to tabulate

them explicitly. Rather, any displayed tabulations would consist of estimates of incremental dose to several target organs for people residing near the receptor points (Appendix A).

REFERENCES

Briggs G.A. 1969. *Plume Rise.* U.S. Atomic Energy Commission Office of Information Services. Available from NTIS, Springfield, Virginia.

Briggs G.A. 1974. "Diffusion Estimation for Small Emissions." In *Atmospheric Turbulence and Diffusion Laboratory 1973 Annual Report,* ATDL-106.

Briggs G.A. 1984. "Plume Rise and Buoyancy Effects." Chapter 8 in *Atomic Science and Power Production* (D. Randerson, Ed.). Rep. DOE/TIC-27601, U.S. Department of Energy, Office of Scientific and Technical Information.

Hanna S.R., G.A. Briggs, and R.P. Hosker, Jr. 1982. *Handbook on Atmospheric Diffusion.* Rep. DOE/TIC-11223 (DE82002045) Technical Information Center, U.S. Department of Energy.

International Atomic Energy Agency (IAEA). 1989. *Evaluating the Reliability of Predictions Made Using Environmental Transfer Models,* Safety Series 100. Rep. STI/PUB/835, IAEA, Vienna.

Kendall M.G. and A. Stuart. 1968. *The Advanced Theory of Statistics. Volume 3 — Design and Analysis, and Time-Series.* Second Edition. Hafner Publishing Company, New York.

Ramsdell J.V., Jr. 1990. "Diffusion in Building Wakes for Ground-Level Releases." *Atmos. Environ.* **3**: 377–388.

Sehmel G.A. 1980. "Particle and Gas Dry Deposition: A Review." *Atmos. Env.* **14**: 983–1011.

APPENDIX L

AIR MONITORING DATA FROM STATIONS NEAR THE FMPC

INTRODUCTION

Examination of historical air monitoring data is important to the development of methodology used in the Fernald Dosimetry Reconstruction Project for several reasons. The air monitoring data can provide measurements to compare with environmental transport model predictions, and can assist in choosing appropriate models (e.g. of building wake effects, Appendix J, this report). In conjunction with other environmental measurements such as gumpaper and precipitation, air monitoring data can be used to derive site–specific parameter values for use in the models.

Although the environmental monitoring data are important to consider in developing methods for dose reconstruction, they are not complete enough, either temporally or spatially, to rely on exclusively for assessment of the exposure to surrounding populations from FMPC effluents. Rather, these data are used primarily to provide a quality check of the source term estimates and to calibrate or validate the transport models.

The material presented in this Appendix focuses on the early 1960's, in support of the model simulations performed for this time period. The complete set of air monitoring data will be included in the Task 5 verification report. A brief description of the air monitoring program is presented first along with data for the 1960–1962 period. Finally, factors affecting the quality of the measurements made during that time are discussed.

FMPC AIR MONITORING PROGRAM AND DATA FOR THE 1960–1962 PERIOD

From the earliest years of operation, ambient environmental air around the FMPC was sampled and analyzed for uranium. The amount and quality of data available has improved over the years. The objectives of the early perimeter air sampling program, as gathered from examination of historical memos and monthly reports, were twofold: 1) to determine the amount of uranium dust leaving the plant and 2) to compare the U concentration in air with the maximum permissible concentration in NBS Handbook 69 (NBS 1959). The latter objective was met in quarterly and annual reports of the monitoring data. Assessment of the amount of U leaving the plant were made generally in a qualitative way and were normally stated to be "small".

The basic air monitoring technique was to draw a known volume of air through a filter and to measure the amount of uranium collected by the filter. In the 1960–1962 period, samples of ambient air were obtained weekly from four locations located at the four corners of the production area (Figure L–1). In the first quarter of 1960, perimeter air sampling was not performed due to construction. Occasional samples of uranium in air at offsite locations were made during 1960–1962, but these offsite measurements are not complete enough to be useful for development of transport model methodology. Offsite air monitoring data for these and other years will be examined together in the Task 5 verification report.

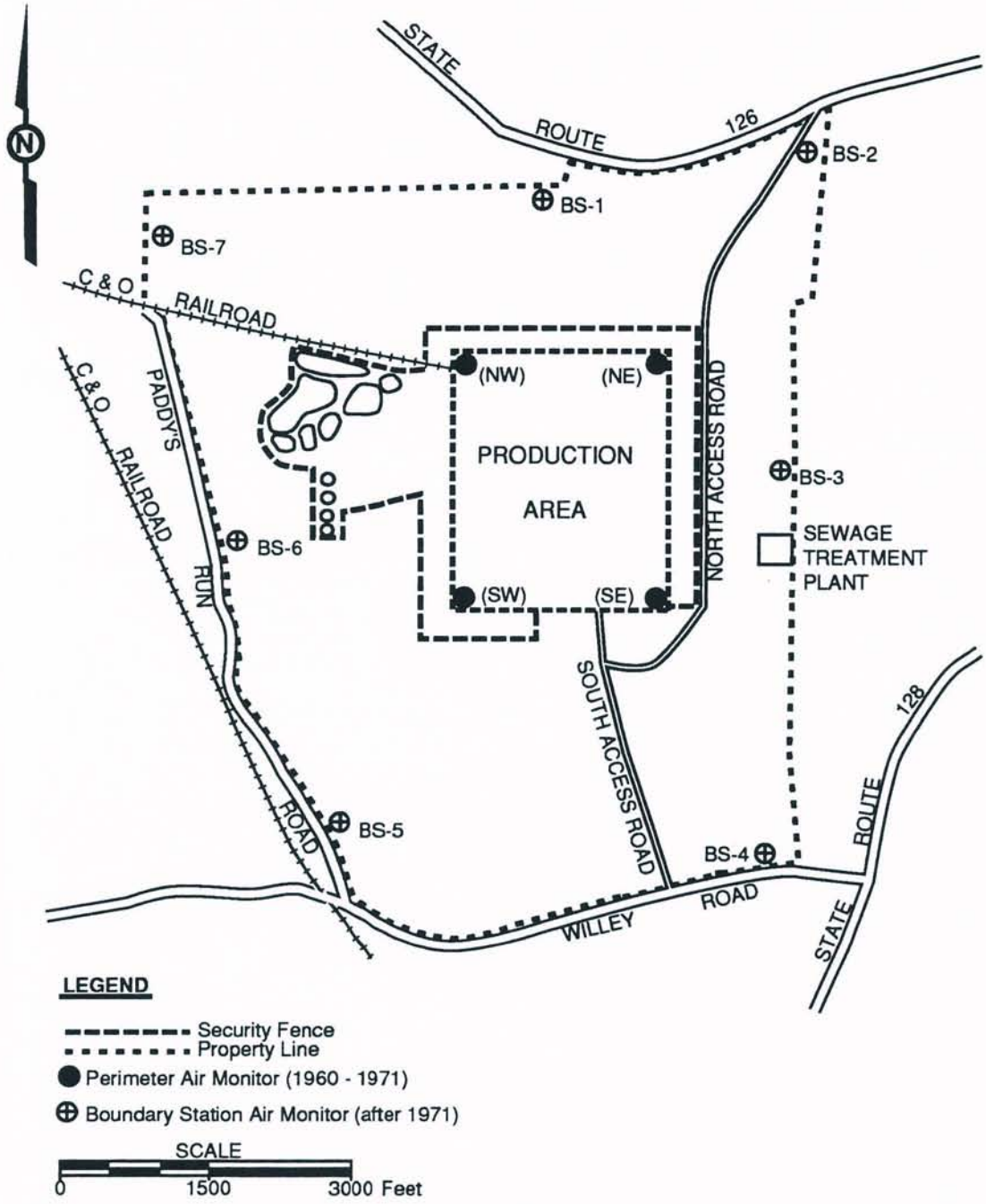

Figure L–1. Ambient air sampling locations around the FMPC.

For the dose reconstruction project, the measurements of uranium in air at the FMPC perimeter have been transcribed into computer spreadsheet format directly from the original Analytical Data Sheets from the Fernald site (NLCO 1960–1962). These data sheets record:

- location of the air sample
- sampling flow rate (m^3 min^{-1})
- sampling duration (min)
- total volume of air sampled (m^3)
- total U on the filter (μg)
- uranium concentration in air (μCi mL^{-1})
- alpha activity concentration in air (μCi mL^{-1})
- beta activity concentration in air (μCi mL^{-1})
- uncertainty on the alpha concentration at the 95% confidence level

The U mass on the air filter was determined by the FMPC Analytical Department using the fluorimetric analytical method. Numerous methods have been used for uranium analysis (Minczewski 1963), but fluorimetry has been most frequently adopted for routine analysis of samples containing very small quantities of uranium (usually 0.001 to 10 micrograms U). The U measurements are much more useful for our purposes than the gross alpha or beta analyses, which are strongly influenced by global fallout contributions.

A ratio of 6.8×10^{-7} Ci g^{-1} U was used by the FMPC staff to compute the activity concentrations, which were recorded on the data sheets. In the 1960–1962 period, and earlier, the volumetric flow rate of the sampler was recorded as a constant 1.5 m^3 min^{-1} (NLCO 1960–1962). The total volume of air drawn was computed by the product of this constant flow rate and the sampling time.

Although samples were taken generally at a frequency of one week, the air was not continuously sampled. A typical sampling was 3360 min (56 hours), or 33% of the week. One primary reason for the discontinuous sampling was that at these relatively high flow rates, the filters (approximately 4 inches in diameter) would load up with dust after several days, resulting in frequent pump failures. For two weeks in October 1960, a continuous air sampler (manufacturer: Unico, model 300) was tried along with the Staplex sampler at location PS-4 (SE corner). This test sampler had a flow rate of 15 cfm (0.47 m^3 min^{-1}), about 1/3 the flow rate of the Staplex high volume air samplers. After these two weeks, the new sampler was pulled in for maintenance, and there is no indication that the Staplex samplers were replaced. No routine continuous air monitors were employed at the FMPC until the *boundary* air monitoring stations were established in 1972 (Figure L–1). Examination of the data from the boundary stations will be included in the Task 5 verification report.

Until 1959 at the FMPC, the air samples were obtained in the open air at up to eight guard towers on the FMPC perimeter. Dodd (1958) indicated that protective covers were being constructed for the perimeter samplers and that "more frequent sampling and more reliable data will be available as soon as these are put in use". The perimeter guard towers were removed in late 1959, and permanent, wooden louvered-sided instrument shelters for the air samplers were completed by 22 April 1960 (Quigley 1960, 1961).

To summarize, from these written sources as well as personal communications with site personnel (Dugan 1992), we have deduced that the typical air sampler used at the FMPC perimeter during the 1960–1962 period was a Staplex high-volume air sampler inside a louvered weather shelter, drawing air at 1.5 m^3 min^{-1} through an MSA Type S pleated filter of approximately 4 inch (10 cm) diameter. The filter face was oriented perpendicular to the ground surface (Dugan 1992). The average inlet velocity through the sampler filter would have been 3.2 m s^{-1}.

A tabular presentation of the individual weekly measurements of uranium in air for 1960–1962 is included in Tables L–1 through L–3 below. Some measurements were invalidated due to conditions such as the following, which were noted by the sampling or analytical technicians on the analytical data sheets:

- defective pump
- uncertain sample volume or time
- partial loss of sample
- filters came loose

These invalidated data are indicated by "IV" in Tables L–1 through L–3.

Table L–1. Uranium in Air at Perimeter Monitoring Stations in 1960

Date/Time Off[a]	Sample Time (min)	Midpoint of Sampling Period	μCi U mL^{-1} ($\times 10^{-13}$) PS-1 (SW)	PS-2 (NW)	PS-3 (NE)	PS-4 (SE)
5/2/60 9:00	3360	1-May-60	NA[b]	1.71	1.71	NA
5/9/60 9:00	3360	8-May-60	NA	10.87	1.91	NA
5/16/60 9:00	3360	15-May-60	NA	0.18	1.27	NA
5/23/60 9:00	3360	22-May-60	NA	1.14	3.37	NA
5/30/60 12:00	3420	29-May-60	NA	1.64	1.23	NA
6/6/60 9:00	3300	5-Jun-60	NA	0.96	1.37	NA
6/13/60 9:00	3360	12-Jun-60	NA	0.46	0.82	NA
6/20/60 9:00	3360	19-Jun-60	NA	0.5	1.77	NA
6/27/60 10:00	3360	26-Jun-60	NA	0.68	0.09	NA
7/4/60 9:00	3360	3-Jul-60	NA	1.64	1.46	NA
7/11/60 9:00	3360	10-Jul-60	NA	2.59	NA	NA
7/18/60 9:00	3360	17-Jul-60	NA	2.05	1.09	NA
7/25/60 9:00	Varies	24-Jul-60	4.73	1.36	0.96	1.5
8/1/60 9:00	3360	31-Jul-60	2.41	2.32	1.5	0.96
8/8/60 9:00	3360	7-Aug-60	2.18	0.68	2.06	1.09
8/15/60 9:00	3360	14-Aug-60	1.64	0.96	1.5	1.91
8/22/60 9:00	3360	21-Aug-60	4.19	1.5	0.96	1.22
9/1/60 9:00	4800	30-Aug-60	2.09	0.68	1.32	1.05
9/8/60 9:00	3360	7-Sep-60	3.78	0.32	0.68	0.32

(continued next page)

Table L–1. (continued)

9/16/60 9:00	3840	15-Sep-60	1.18	2.59	1.54	2.5
9/22/60 9:00	2880	21-Sep-60	1.09	2.46	0.3	0.55
9/30/60 9:00	3360	29-Sep-60	6.37	1.37	1.23	1.41
10/7/60 9:00	3360	6-Oct-60	5.69	1.5	1.5	2.87
10/14/60 9:00	3360	13-Oct-60	7.71	1.37	2.74	1.64
10/21/60 9:00	NA	19-Oct-60	1.91	0.66	1.02	1.77
10/18/60 12:30	3360	17-Oct-60	NA	0.61	1.64	0.68
11/1/60 9:30	1920	31-Oct-60	NA	IV[c]	IV	4.03
11/8/60 9:00	3360	7-Nov-60	NA	NA	9.06	4.1

[a] If no time off is given, 9:00 AM is assumed, as this is a common recorded time.
[b] NA = Not available.
[c] IV= Invalid data.

Table L–2. Uranium in Air at Perimeter Monitoring Stations in 1961

			$\mu Ci\ U\ mL^{-1}\ (\times 10^{-13})$			
Date/Time Off[a]	Sample Time (min)	Midpoint of Sampling Period	PS-1 (SW)	PS-2 (NW)	PS-3 (NE)	PS-4 (SE)
1/11/61 14:00	120	11-Jan-61	NA[b]	NA	17.00	NA
1/27/61 15:30	3360	26-Jan-61	NA	2.39	1.21	0.20
2/1/61 9:00	2400	31-Jan-61	NA	0.191	3.03	0.70
2/8/61 9:00	3360	7-Feb-61	NA	0.15	0.80	0.70
2/15/61 14:00	3360	14-Feb-61	NA	NA	0.95	2.43
2/22/61 15:00	3360	21-Feb-61	NA	0.443	1.07	0.54
3/1/61 9:00	3360	28-Feb-61	NA	0.539	1.21	0.95
3/3/61 9:00	120	3-Mar-61	NA	NA	5.11	NA
3/8/61 14:30	3360	7-Mar-61	NA	0.75	2.32	0.56
3/15/61 15:30	3360	14-Mar-61	2.04	0.88	2.11	2.52
3/22/61 14:30	3360	21-Mar-61	2.25	0.68	0.27	1.56
3/29/61 9:00	3360	28-Mar-61	0.54	0.68	1.22	2.25
4/5/61 14:30	3360	4-Apr-61	IV[c]	IV	IV	IV
4/12/61 15:00	3360	11-Apr-61	2.32	0.34	0.41	3.89
4/19/61 14:30	3360	18-Apr-61	0.27	1.64	0.61	2.87
4/27/61 9:00	3720	26-Apr-61	0.75	1.57	2.80	0.61
5/3/61 9:00	2880	2-May-61	0.54	0.22	0.40	3.34
5/11/61 9:00	3840	10-May-61	3.68	0.96	0.68	1.09
5/18/61 10:00	3360	17-May-61	3.96	1.23	0.61	0.75
5/25/61 9:00	3360	24-May-61	8.1	1.08	0.95	1.49
6/1/61 9:30	3360	31-May-61	1.22	0.31	2.58	2.18
6/30/61 9:00	3840	29-Jun-61	0.53	0.37	2.12	0.96
7/7/61 19:00	120	7-Jul-61	0.18	11.4	0.14	0.35
7/7/61 9:30	3420	6-Jul-61	1.43	1.98	0.57	IV
7/14/61 9:00	3300	13-Jul-61	1.3	0.96	2.18	0.44

(continued next page)

Table L–2. (continued)

7/21/61 9:30	3300	20-Jul-61	0.6	1.09	2.59	0.68
7/31/61 9:30	4800	29-Jul-61	0.68	0.4	1.02	0.61
8/7/61 9:00	3360	6-Aug-61	0.61	0.54	0.38	4.98
8/14/61 9:00	3360	13-Aug-61	1.09	1.63	IV	1.23
8/21/61 9:30	3360	20-Aug-61	1.09	0.61	IV	1.09
8/28/61 9:00	3360	27-Aug-61	0.41	0.96	2.05	1.09
9/1/61 9:00	1920	31-Aug-61	0.29	1.71	1.09	1.02
9/8/61 9:00	3360	7-Sep-61	0.03	0.89	2.73	0.40
9/15/61 9:00	3360	14-Sep-61	2.87	1.37	1.23	0.15
9/22/61 9:00	3360	21-Sep-61	5.94	0.68	0.89	NA
10/2/61 9:00	4800	30-Sep-61	0.34	0.75	0.89	NA
10/9/61 9:00	3360	8-Oct-61	0.63	0.4	0.81	NA
10/16/61 9:00	3360	15-Oct-61	0.73	0.63	3.00	2.87
10/23/61 9:00	3360	22-Oct-61	1.64	0.75	1.64	2.18
11/1/61 9:00	4320	30-Oct-61	0.24	1.37	2.18	0.13
11/8/61 9:00	3360	7-Nov-61	1.64	IV	1.23	1.37
11/15/61 13:00	3420	14-Nov-61	3.07	1.23	1.98	1.57
11/22/61 9:00	3300	21-Nov-61	1.23	0.63	1.64	2.46
11/30/61 9:00	3840	29-Nov-61	1.09	2.05	0.82	0.66
12/7/61 9:30	3360	6-Dec-61	0.68	0.48	1.50	0.68

[a] If no time off is given, 9:00 AM is assumed, as this is a common recorded time.
[b] NA = Not available
[c] IV= Invalid data.

Table L–3. Uranium in Air at Perimeter Monitoring Stations in 1962

Date/Time Off[a]	Sample Time (min)	Midpoint of Sampling Period	μCi U mL^{-1} ($\times 10^{-13}$) PS-1 (SW)	PS-2 (NW)	PS-3 (NE)	PS-4 (SE)
1/5/62 9:00	3360	4-Jan-62	0.49	0.37	4.10	0.47
1/12/62 9:30	3360	11-Jan-62	0.39	0.68	1.64	0.53
1/19/62 9:00	3360	18-Jan-62	1.84	0.4	IV[c]	0.75
1/26/62 12:00	3420	25-Jan-62	0.52	0.18	1.23	0.52
2/2/62 9:00	3300	1-Feb-62	3.41	0.12	1.09	0.30
2/5/62 10:00	1440	4-Feb-62	0.16	0.47	0.82	0.68
2/12/62 9:00	3360	11-Feb-62	2.87	0.31	2.05	2.05
2/19/62 9:00	3360	18-Feb-62	2.18	0.048	0.08	1.36
2/26/62 9:00	3360	25-Feb-62	1.23	0.96	0.88	1.09
3/1/62 9:00	1440	28-Feb-62	4.71	0.06	0.18	5.66
3/8/62 9:00	3360	7-Mar-62	3.55	0.12	0.18	0.89
3/15/62 12:00	3420	14-Mar-62	1.36	1.23	0.82	1.57
3/22/62 8:30	3300	21-Mar-62	0.51	0.31	1.23	2.87

(continued next page)

Table L–3. (continued)

3/29/62 8:30	3360	28-Mar-62	16.24	0.27	1.77	1.36
4/4/62 8:30	2880	3-Apr-62	3.14	0.25	2.05	2.87
4/11/62 9:00	3360	10-Apr-62	0.57	0.96	1.23	0.48
4/18/62 9:00	3360	17-Apr-62	4.23	0.2	0.26	1.91
4/24/62 8:30	3360	23-Apr-62	1.43	1.23	1.84	7.37
5/2/62 9:00	3360	1-May-62	0.89	3.28	3.28	1.09
5/8/62 9:00	3360	7-May-62	0.46	1.77	1.16	1.71
5/16/62 9:00	3360	15-May-62	3.82	0.82	1.57	2.18
5/23/62 9:00	3360	22-May-62	1.84	1.77	1.3	1.91
6/15/62 9:00	3360	14-Jun-62	3.21	IV	1.71	0.96
6/22/62 9:00	3360	21-Jun-62	2.05	IV	1.84	IV
6/28/62 9:00	3360	27-Jun-62	4.84	0.54	0.61	IV
7/5/62 9:00	3360	4-Jul-62	1.09	0.68	0.51	0.31
7/12/62 9:00	3360	11-Jul-62	0.47	0.096	0.34	0.29
7/19/62 9:00	3360	18-Jul-62	0.54	IV	IV	1.16
7/26/62 9:00	3360	25-Jul-62	0.34	0.58	2.87	2.05
8/1/62 9:00	2880	31-Jul-62	0.5	0.55	0.55	1.84
8/8/62 9:00	3360	7-Aug-62	1.57	0.96	1.50	1.43
8/15/62 9:00	3360	14-Aug-62	4.1	1.09	0.68	3.68
8/22/62 9:00	3360	21-Aug-62	1.84	0.58	1.77	0.68
9/4/62 9:00	6240	2-Sep-62	1.57	IV	1.64	0.89
9/11/62 9:00	3360	10-Sep-62	2.59	0.82	1.98	0.41
9/20/62 9:00	4320	18-Sep-62	3.41	2.39	1.02	2.39
9/24/62 12:00	3420	23-Sep-62	2.25	0.96	1.16	1.77
10/1/62 9:00	2880	30-Sep-62	0.75	0.6	0.75	4.44
10/8/62 9:00	3360	7-Oct-62	1.09	0.57	1.23	1.57
10/15/62 9:00	3360	14-Oct-62	1.57	0.34	3.07	0.82
10/22/62 9:00	3360	21-Oct-62	0.68	0.89	2.46	0.63
10/29/62 9:00	3360	28-Oct-62	0.68	0.2	1.50	1.50
11/7/62 9:00	4320	5-Nov-62	1.36	0.61	1.02	1.57
11/14/62 9:00	3360	13-Nov-62	9.48	0.24	1.30	1.23
11/21/62 9:00	3360	20-Nov-62	0.34	0.57	IV	IV
11/30/62 9:00	4320	28-Nov-62	3.82	0.37	NA[b]	1.50
12/4/62 9:00	2040	3-Dec-62	2.52	0.82	NA	0.75
12/11/62 12:30	3420	10-Dec-62	0.89	0.14	1.91	NA
12/18/62 9:00	3300	17-Dec-62	0.59	IV	4.16	IV
12/25/62 9:00	3360	24-Dec-62	3.41	0.68	0.64	0.96
12/31/62 9:00	2940	30-Dec-62	3.46	0.58	1.85	NA

[a] If no time off is given, 9:00 AM is assumed, as this is a common recorded time.
[b] NA = Not available.
[c] IV= Invalid data.

EVALUATION OF QUALITY OF ENVIRONMENTAL MONITORING DATA FOR URANIUM IN AIR IN THE EARLY 1960s

For environmental monitoring programs in operation today, there are a number of measures which are taken to assure data quality. For air monitoring programs, these might include:

- maintenance of standard written procedures
- calibration of flow rate of sampling pumps
- collection of duplicate samples in the field
- laboratory analysis of blanks, duplicates, and known reference standards
- participation in interlaboratory comparison programs

In the early years of FMPC operation, there was not as much emphasis on quality assurance (QA) as we know it today. Although there probably were similar procedures and policies established, particularly for the laboratory handling and analysis of samples, minimal written documentation has been located. A general discussion of sources of uncertainty in early air monitoring measurements at the FMPC is presented below. Then, the next section includes a quantitative assessment of the bias and precision of the measurements.

Sources of Uncertainty in Measurements of Uranium in Air at the FMPC Perimeter

Determination of sample volume. The sample volume was determined from the product of the flow rate and the sampling time. As mentioned previously, the flow rate of the air samplers was assumed to be constant throughout the sampling period, when in fact, the flow rate can both decrease over the sampling period due to particulate loading on the filter and fluctuate with line voltage variation. Also different pumps may have had different average flow rates, whereas a single flow rate was used.

Collection efficiency of filter media. There are indications that different filter media were tested for use in the environmental air sampling program. The March 7, 1955 weekly report of the IH&R department discussed the newly established ambient air monitoring program for "obtaining information about fallout from atom bomb tests." This report indicated that Whatman 41 paper in high volume samplers proved unsatisfactory and that they changed to pleated filters in high volume samplers. Dugan (1992) indicated that the pleated filters were manufactured by MSA and were the same as those used for effluent sampling (Type S). These filters have been tested as 100% efficient for particles over 2.0 μm, dropping to a minimum of 47% for particles in the 0.4–0.6 μm range (Smith and Surprenant 1953). The calculations of uranium concentration in air on the Analytical Data Sheets (NLCO 1960–1962) implicitly assume that 100% of the uranium in the air drawn through the filter was collected.

Isokinetic sampling and particle size considerations. These factors can greatly affect what can be called the "inlet collection efficiency" as opposed to the filter collection efficiency. The inlet collection efficiency basically is concerned with how the particle size distribution and concentrations in the air stream entering the filter compare with the

surrounding air. It is widely observed that true isokinetic sampling under field conditions is impossible due to changing wind velocities and directions. The nature of sampling errors which may arise due to the anisokinetic sampling of airborne particles has been discussed in many texts on aerosols (e.g. Green and Lane 1957; Fuchs 1964; Vincent 1989). Small particles tend to behave like molecules and follow the air streams in non-linear motion, but large particles have sufficient inertia that they tend to move in straight lines and not follow curved air trajectories. Uranium was emitted from the FMPC production processes in a wide variety of particle sizes, from relatively small particles from the dust collectors to quite large particles resulting from evaporation of mist emitted from the scrubbers (Appendix D).

Garland and Nicholson (1991) summarize some important common features of studies of air sampler performance:

> "...all the published tests show some common features: the sampling efficiency declines with particle size and also with ambient wind speed. .... Orientation may be important for non-symmetrical inlets. The dependence of efficiency with so many parameters makes it improbable that any correction can be successfully applied to filter samplers operating in field conditions. Few of the filter samplers investigated have had a satisfactory sampling efficiency for particles larger than 30 μm, and it is unlikely that any can sample particles larger than 100 μm."

May et al. (1976) used a high volume air sampler positioned in a wind tunnel, as a standard for comparison with the collection characteristics of other air samplers. Results indicated negligible error in sampling of particles up to about 100 μm diameter for low ambient winds (2.5 m s^{-1}) and the device pointing into the wind. Although the wind speeds at FMPC are low, the sampler orientation would not have been continuously oriented to the wind, and the effect of the sampler housing is unknown. It is therefore unreasonable to expect high collection efficiencies for the large particle sizes.

The louvered sampler shelters could have acted as baffles in preventing the larger particles from entering the shelter. However, comparison of the data before and after installation of the shelters in early 1960 suggests that the louvered shelters did not result in a noticeable decrease in the concentration of uranium in sampled air. In fact, the concentrations in 1958–1959 appear lower (Figure L–2) even though the measurements were made in open air and the amounts of uranium released to air were reportly *larger* in 1958–1960 compared with 1961–1962 (Clark et al. 1989). (Limited air monitoring data from the first half of 1958 are omitted from this figure due to short total sampling times. No samples were taken in late 1959 and early 1960 due to construction.) It appears that the sampler inlet collection efficiency may have been more important than any shelter effect.

A summary of the direction of potential bias from these sources of error is presented in Table L–4.

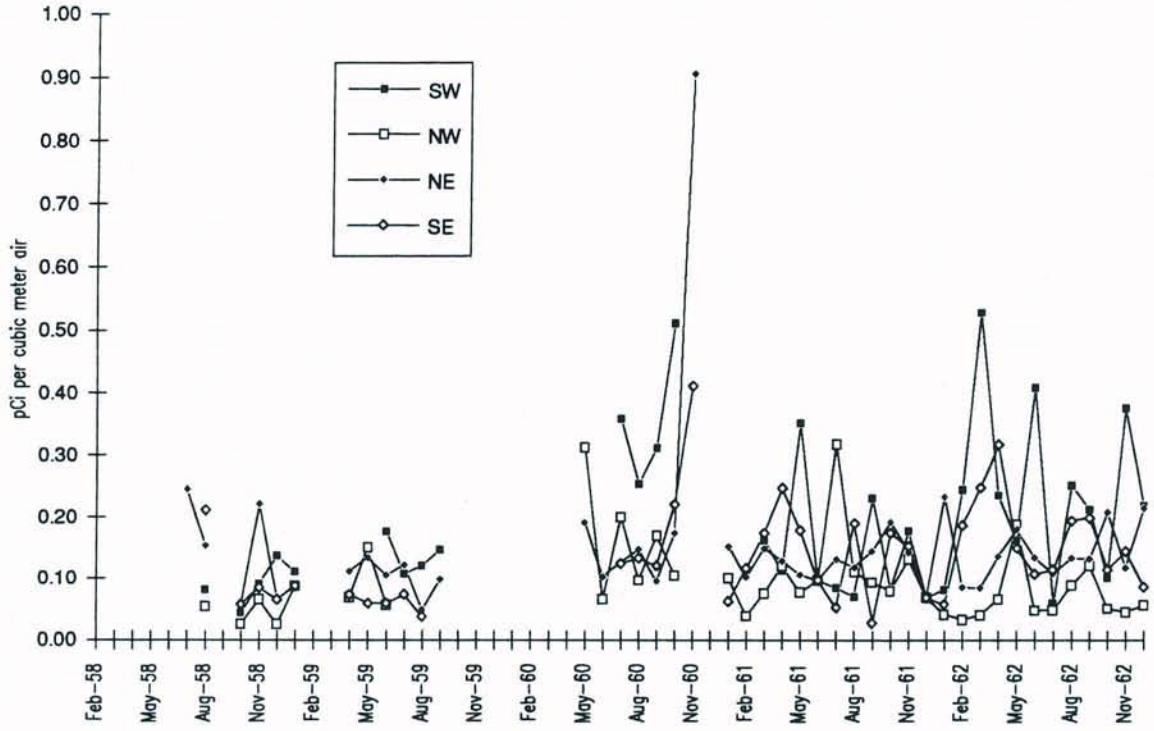

Figure L–2. Monthly average concentrations of total uranium in air at the perimeter stations between 1958 and 1962. Louvered shelters to house the samplers were installed in early 1960, whereas in 1958–1959 the samples were taken in the open at perimeter guard towers. The high values in November 1960 were presumably associated with the episodic release from the Pilot Plant (see Appendix V).

Table L–4. Direction of Bias for Potential Sources of Error in Measurements of Uranium in Air in the 1960s

Source of Error	Direction of Bias
Low collection efficiency for large particles	–
Flow rate decrease due to particulate loading on filter	–
Flow rate fluctuations due to line voltage	0
Less than 100% collection efficiency within filter media	–
Loss of particulate material from filter during collection or processing	–
Inadequate contamination control during collection/handling/analysis	+

– Indicates measurement would tend to underestimate true concentration.
0 Indicates no systematic bias.
+ Indicates measurement would tend to overestimate true concentration.

Quantitative Assessment of Bias and Precision

Bias. One important use of the air modeling data in methodology development for dose reconstruction is to compare measurements with model predictions. For this purpose, an estimate of the total uranium in air must be made, not just the concentration in the smaller, respirable size fractions. It is our judgment at this writing that the historical air monitoring data from the production area perimeter underestimate the total U in perimeter air, and that the largest bias is due to the low collection efficiency for large particles. The computation of large empirical deposition velocities to gumpaper (Appendix G) and an analysis of the particle sizes emitted by the scrubbers (Appendix D) point to the likelihood that a significant portion of airborne uranium at close distances is comprised of large particles. As discussed above, the collection efficiency for large particles declines with increasing particle size, because of inertial effects.

For these reasons, we have focused our assessment of the bias of the perimeter air samplers on the issue of collection efficiency of high volume air samplers as a function of particle size. Because there were no site-specific studies, we turned to the scientific literature for information. A number of literature sources on aerosol sampling of ambient air were reviewed (May et al. 1976, Pattenden and Wiffen 1977, Wedding et al. 1977, Agarwal and Liu 1980, Liu and Pui 1981, Vrins and Hofschreuder 1983, Vincent 1989, Garland and Nicholson 1991). The work of Wedding et al. proved most applicable to our situation, providing quantitative measurements of collection efficiency for the standard American High-Volume air sampler up to 50 μm aerodynamic diameter (Table L–5). (The aerodynamic diameter is the diameter of a sphere of unit density that has the same gravitational settling velocity as the particle. The physical diameter of a particle is its aerodynamic diameter divided by the square root of the particle density. See Appendix D.)

Table L–5. Sampling Effectiveness of Hi-Volume Air Sampler at 4.6 m s^{-1} (Wedding et al. 1977)

Particle aerodynamic diameter, μm							
5		15		30		50	
Sampler orientation[a]							
0°	45°	0°	45°	0°	45°	0°	45°
97%	100%	35%	55%	18%	41%	7%	34%

[a]Sampler orientation of 0° is defined as the situation with the Hi-Volume roof ridge parallel to the air flow. The Hi-Volume is extremely sensitive to the angle of approaching wind as is more efficient at 45° than 0° (Wedding et al. 1977).

In order to evaluate the Fernald sampler collection efficiency, we estimated the uranium particle size distributions at the locations of the perimeter air samplers. This calculation took into account the source term particle size characteristics, as well as the differential deposition of particles between the release points and the samplers according to particle diameters and densities. For Plants 2/3 and 8, the distances from the plant centers to each station were used, but the remainder of the release points were combined into a weighted

average coordinate pair, with the weights proportional to each plant's total release for the 36-month period. Separate weighted coordinate pairs were computed for the group of plants producing U_3O_8 and those producing UF_4. These simplifications were necessary to reduce computational time and are believed to introduce only minor errors for the purpose of this exercise.

The uranium particle size distribution was estimated on a monthly basis for each of the four perimeter sampler locations between 1960–1962. The distributions at the four stations were quite similar with an average of 30% of the total airborne U in the <5 μm fraction (aerodynamic diameter), 17% between 5 and 15 μm, 7% between 15 and 30 μm, 8% between 30 and 50 μm, and 38% over 50 μm. This qualitatively bimodal distribution arises from the fact that scrubber effluents contribute to the largest size fractions and the dust collectors contribute to the relatively small size fractions.

We used the Crystal Ball® software (Decisioneering 1992) to perform an uncertainty analysis of the collection efficiency of the perimeter air samplers, based on our estimates of the particle size distributions and the collection efficiencies published by Wedding et al. (Table L–5). The efficiency distribution shape was assumed to be triangular with the minimum, maximum, and most likely values shown in Table L–6. Minimum and maximum values for each interval were taken directly from Wedding et al., and the most likely value was obtained by averaging the sampler efficiencies bracketing that size range. For example, the most likely efficiency value for the 15–30 μm range was the average of 35, 55, 18, and 41% (Table L–5), or 37% (Table L–6). Monte Carlo sampling of the distributions was performed for 1000 trials.

Table L–6. Distributions of Collection Efficiency Used in Uncertainty Analysis

Particle Size (μm)	Collection Efficiency (%)		
	Minimum	Most Likely	Maximum
<5	97	98	100
5–15	35	72	100
15–30	18	37	55
30–50	7	25	41
>50	0	10	34

The result of the uncertainty analysis of sampler collection efficiency is included in Table L–7 for the NE perimeter station. The results from the other three stations were quite similar and are not tabulated here. The estimated median collection efficiency for sampling of total uranium ranged from 40% (SW station, November 1961), when uranium emissions from the scrubbers made up over 90% of the source term, to 65% (NE and SW stations, January 1960), when emissions from the scrubbers comprised less than half of the total uranium source term. The monthly distributions of sampler efficiency at each perimeter station were used to determine confidence intervals for the total uranium concentrations in air for each month, which were then compared to model predictions (Figures J–1 through J–4, Appendix J).

Table L–7. Collection Efficiency of Air Sampler for Total Airborne U at NE Perimeter Sampling Station During 1960–1962

	Percentiles of Efficiency Distribution				
	5%	25%	50%	75%	95%
Jan-60	57	61	65	69	73
Feb-60	44	47	50	53	56
Mar-60	44	47	50	53	56
Apr-60	42	45	47	50	53
May-60	44	47	50	53	56
Jun-60	40	43	46	49	52
Jul-60	42	45	47	50	53
Aug-60	42	45	47	50	53
Sep-60	38	42	44	47	50
Oct-60	37	40	43	46	50
Nov-60	53	58	62	65	70
Dec-60	38	41	43	46	50
Jan-61	38	41	43	46	50
Feb-61	42	45	47	50	53
Mar-61	40	43	46	49	52
Apr-61	45	48	50	53	57
May-61	42	45	48	50	54
Jun-61	44	47	50	53	56
Jul-61	47	50	53	56	60
Aug-61	51	54	57	59	63
Sep-61	46	50	53	55	59
Oct-61	49	52	55	58	62
Nov-61	35	38	41	44	48
Dec-61	47	50	53	56	60
Jan-62	52	55	58	60	63
Feb-62	44	47	50	53	56
Mar-62	55	59	62	66	70
Apr-62	44	47	50	53	56
May-62	46	49	51	54	57
Jun-62	47	50	53	56	60
Jul-62	46	50	53	55	59
Aug-62	51	55	59	62	66
Sep-62	49	53	56	59	63
Oct-62	49	52	55	58	62
Nov-62	51	55	59	62	66
Dec-62	53	58	62	65	70

This analysis of bias was particularly important for comparison of model predictions with estimates of total uranium in air. However, it should be emphasized again that the negative bias (roughly a factor of 2, due to collection efficiency of the air samplers) is not as important from a radiation protection standpoint. The particle size range which is important for internal dose assessment should have been efficiently collected by the samplers.

Precision. A site-specific data set was developed which allowed a quantitative analysis of the precision of measurements of uranium in ambient air in the early 1960's. This data set was obtained from the original analytical data sheets which recorded results of offsite air monitoring during 1963. At that time, it was standard procedure to take two air samples in the field at each offsite location. Prior to 1963, there were either too few measurements, there were no duplicate field measurements, or the duplicates appeared to be for the purpose of testing different filters or samplers, and thus were not true replicates. These data (there were a total of 87 pairs in 1963) provided a set of measurements which were used to assess the precision of the entire sampling procedure, including actual environmental variation, the field sampling method, sample preparation, and fluorimetric analysis.

This field replicate data set was analyzed by examining the distribution of the ratios of the paired measurements. That is,

$$R = C_1 / C_2 \qquad \text{(L–1)}$$

where C_1 and C_2 are the replicate measurements of uranium in air at the same location and time, and C_1 is the larger of the two measurements, so that $R \geq 1$.

The cumulative frequency distribution of R is shown in Figure L–3. Half of the replicate measurements (cumulative frequency = 0.5) resulted in a ratio less than 1.2, which corresponds to an 18% difference between the two measurements. The 75th and 90th percentiles of the distribution are 1.81 and 2.82, respectively, which correspond to percent differences of 58% and 95%. This analysis applies to the probable uncertainty of a single measurement of uranium in air. As several measurements are combined to produce, *e.g.*, a monthly average at a given location, the uncertainty on the central estimate is less.

The concentration range encompassed by this data set is 0.04 to 14×10^{-13} $\mu Ci\ mL^{-1}$. There was no clear relationship between the U concentration being measured and the magnitude of R. Although the two highest R values (R = 5) resulted from measurements of relatively low concentrations (0.3 and 0.6×10^{-13} $\mu Ci\ mL^{-1}$) and the highest concentration had a low R value (1.13), the relationship between these extremes is not consistent.

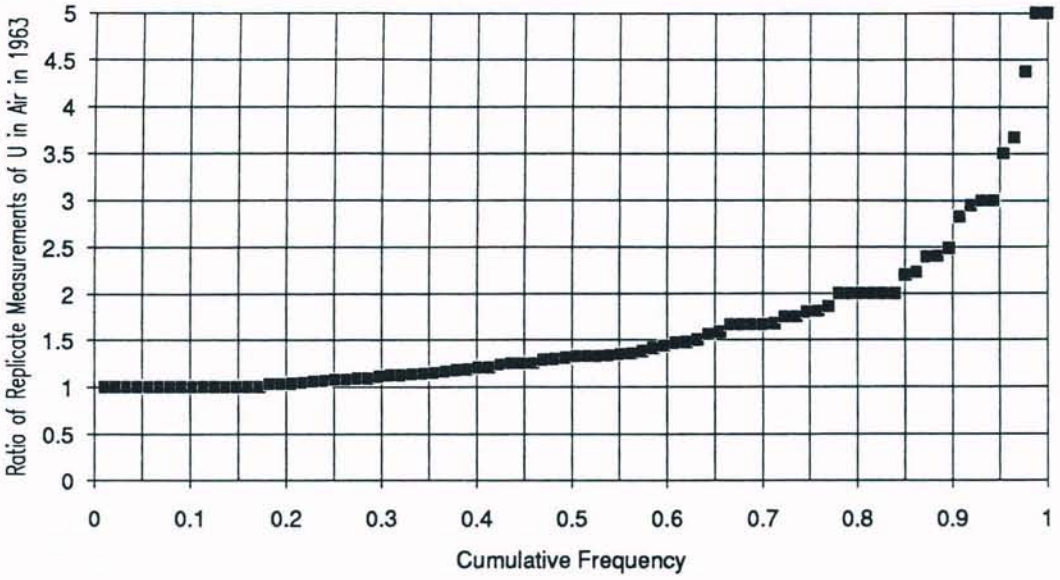

Figure L–3. Cumulative frequency distribution of the ratio between field replicates of uranium in offsite air in 1963. Perfect agreement between field replicates would result in a ratio of 1.00.

It is difficult to determine what portion of the variation is due to the different steps of the sampling procedure. However, the scientific literature indicates that the fluorimetric analysis of uranium at the levels indicated on the analytical data sheets should have standard deviations in the range of 3 to 10% (Rodden and Warf 1950, Steele and Taverner 1959, Price et al. 1953, Athavale et al. 1959, Hassialis and Musa 1956).

REFERENCES

Agarwal J.K. and B.Y.H. Liu. 1980. "A Criterion for Accurate Aerosol Sampling in Calm Air." *Am. Ind. Hyg. Assoc. J.* **41**:191–197.

Athavale V.T., L.M. Mahajan, N.R. Thakoor, and M.S. Varde. 1959. "Determination of Microgram Quantities of Uranium in Thorium." *Analyt. chim. Acta.* **21**:353–356.

Clark T.R., L. Elikan, C.A. Hill, and B.L. Speicher. 1989. *Addendum to FMPC–2082. History of FMPC Radionuclide Discharges. Revised Estimates of Uranium and Thorium Air Emissions from 1951–1987*. Westinghouse Materials Company of Ohio, Cincinnati, Ohio.

Decisioneering. 1992. *Crystal Ball® Version 2.0 for Windows. User's Manual*. Decisioneering, Inc., Boulder, Colorado.

Dodd A.O. 1958. "Monthly progress report for April 1958 — Radiation and Effluent Control." Internal memo of April 30, 1958 to R.H. Starkey. National Lead Company of Ohio, Cincinnati, Ohio.

Dugan T.A. 1992. Personal communication. Westinghouse Environmental Management Company of Ohio, Cincinnati, OH.

Fuchs N.A. 1964. *The Mechanics of Aerosols*. Pergamon Press, Oxford.

Garland J.A. and K.W. Nicholson. 1991. "A Review of Methods for Sampling Large Airborne Particles and Associated Radioactivity." *J. Aerosol Sci.* **22**:479–499.

Green H.L. and W.R. Lane. 1957. *Particulate Clouds: Dusts, Smokes and Mists*. Spor, London.

Hassialis M.D. and R.C. Musa. 1956. "The Analysis of Low–Grade Uranium Ores and their Products." *Proceedings of the International Conference on Peaceful Uses of Atomic Energy, Geneva*, Vol. VIII, pp. 216–221.

Liu B.Y.H. and D.Y.H. Pui. 1981. "Aerosol Sampling Inlets and Inhalable Particles." *Atmos. Environ.* **15**:589–600.

May K.R., M.P. Pomeroy and S. Hibbs. 1976. "Sampling Techniques for Large Windborne Particles." *J. Aerosol. Sci.* **7**:53–62.

Minczewski J. 1963. "Trace Impurity Analysis in Nuclear Materials, A Report to the Panel by Professor Dr. J. Minczewski." Part II in Analytical Chemistry of Nuclear Materials, *Report of the Panel on Analytical Chemistry of Nuclear Materials Held in Vienna 17–21 September 1962*, International Atomic Energy Agency, Vienna, p. 33.

NLCO. 1960–1962. Analytical Data Sheets. Health and Safety Division, Analytical Department. National Lead Company of Ohio. Cincinnati, OH.

NBS. 1959. "Maximum Permissible Body Burdens and Maximum Permissible Concentrations of Radionuclides in Air and Water for Occupational Exposure." NBS Handbook 69, National Bureau of Standards, Washington, DC.

Pattenden N.J. and R.D. Wiffen. 1977. "The Particle Size Dependence of the Collection Efficiency of an Environmental Aerosol Sampler." *Atmos. Environ.* **11**:677-81.

Price G.R., B.J. Ferretti, and S. Schwartz. 1953. "Fluorophotometric Determination of Uranium." *Anal. Chem.* **25**(2):322–331.

Quigley J.A. 1960. *IH&R Department Monthly Report for April 1960*. National Lead Company of Ohio, Cincinnati, Ohio.

Quigley J.A. 1961. *IH&R Department Annual Report for 1960*. National Lead Company of Ohio, Cincinnati, Ohio.

Rodden C.J. and J.D. Warf. 1950. "Uranium", Chapter 1 in *Analytical Chemistry of the Manhattan Project*. Clement J. Rodden (ed.), McGraw-Hill Book Company, p. 3.

Smith W.J. and N.F. Surprenant. 1953. "Properties of Various Filtering Media for Atmospheric Dust Sampling." *Proc. Amer. Soc. Testing Materials*. **53**:1122–1133.

Steele T.W. and L. Taverner. 1959. "A Review of the Chemical Methods for the Determination of Uranium in Ores, Residues, and Products Arising During Processing." In: *Progress in Nuclear Energy, Series IX, Analytical Chemistry, Volume I*, M.T. Kelley (ed.), Pergamon Press, pp 75–99.

Vincent J.H. 1989. "Sampling for Aerosols in the Ambient Atmosphere," Chapter 15 in *Aerosol Sampling: Science and Practice*. John Wiley, Chichester.

Vrins E. and P. Hofschreuder. 1983. "Sampling Total Suspended Particulate Matter." *J. Aerosol Sci*. **14**:318–322.

Wedding J.B., A.R. McFarland, and J.E. Cermak. 1977. "Large Particle Collection Characteristics of Ambient Aerosol Samplers." *Envir. Sci. Technol*. **11**:387–390.

APPENDIX M

DEPOSITION MEASUREMENTS USING GUMMED-FILM

INTRODUCTION

Gummed-film was used to measure fallout deposition at locations throughout the United States during the 1950s and 1960s (Eisenbud and Harley 1953, 1955, 1956, 1958; Harley et al. 1960). Deposition was measured daily at 40 to 95 locations during major periods of testing at the Nevada Test Site (Beck et al. 1990). Most of these data have been retrieved and compiled for use in an assessment of radioiodine doses to thyroids of persons in the continental United States from weapons testing at the NTS (Wachholz 1990).

At the FMPC, measurements of deposition of particles at locations within the plant boundaries and at offsite locations were performed using gummed-film from 1952 until 1965. Although the FMPC measurements were not part of the nationwide fallout monitoring effort, evidence indicates that the materials used were the same as in that program (Barry 1953, Yoder 1954).

Gummed-films, with an exposed area of 0.093 m^2 (1 ft^2), were mounted on pedestals that were about 0.9 m above ground. Most of the samples were exchanged monthly, although biweekly sampling was more common during the earlier years of the program.

At the FMPC, most samples were analyzed using the same fluorimetric technique that was employed for many other measurements of uranium. Gross beta and gross alpha analyses were also performed on most of the samples. The measurements of uranium deposition are of greatest interest for this project. The gross counting data are inherently of little interest, but were used when necessary to estimate the uranium depositions for some samples. Gross beta measurements reflected primarily the deposition of fallout from nuclear weapons testing that was underway at the NTS and subsequently in the South Pacific and in the Soviet Union.

The data presented in this appendix have been obtained from files of data sheets that contain the results of the laboratory analyses of the gummed films. The monitoring locations around the FMPC are discussed in the next section. An important aspect of the evaluation of the data was estimation of the gummed-film collection efficiency. That issue is discussed in the third section. The fourth section contains the results of deposition measurements that have been retrieved from the files and evaluated.

MONITORING LOCATIONS

During 1960–1962, the period of interest for this report, routine monthly deposition samples were obtained at about thirty locations within and around the FMPC production area. The locations are listed in Table M–1, together with the approximate directions and distances from the center of the production area. The latter were determined from a hand drawn map that was found in the archives that showed the 25 nearby locations and from

Table M–1. Approximate Locations of Deposition Measurements Near the FMPC During 1960–1962

Station Designation	Distance (m) from Center	Angle (deg) from North	Station Designation	Distance (m) from Center	Angle (deg) from North
N-1	337	6	A	217	201
N-2	720	2	S-1	246	178
N-3	1006	0	S-2	874	191
N-4	7200	~0	S-3	1429	183
NE-1	514	48	S-4	9500	188
NE-2	994	36	SW-1	520	219
NE-3	1200	26	SW-3	1223	224
NE-4[a]	4200	72	SW-4[b]	17000	148
E-1	323	89	W-1	326	262
E-2	732	89	W-2	623	260
E-4	14000	114	W-3	1086	264
B	103	135	W-4	12200	250
SE-1	509	142	C	109	292
SE-2	983	136	NW-1	514	319
SE-3	1606	147	NW-3	1623	304
SE-4	Unknown	Unknown			

[a] During 1960, this sampling station was located about 12500 m away at an angle of 73°.

[b] Actually located southeast of the facility center.

descriptions of the locations of more distant stations. The angles and distances given are best estimates from measurements using the map and its accompanying scale. The tabled values are best estimates, which have uncertainties in position that are estimated to be ±2-3 degrees and ±10-20 m. The positions of the 5 stations that were more than 2 km away from the plant center could not be shown on the small scale map and were estimated using another map of the Fernald area. Positional uncertainties for these locations are estimated to be ±5 degrees and ±500 m.

The table shows that although the locations were numbered as though they were along the compass lines, this was not exactly the case. When considered in terms of the 16-point compass sectors usually employed for meteroloogical dispersion calculations, a few of the locations are in sectors adjacent to those indicated by the station designation.

TABULATION OF REPORTED RESULTS

Recovery of data from the gummed-film monitoring program was good. Some samples, particularly at the distant locations, were not obtained routinely. These were in populated areas, so there are several possible reasons for lost samples; however, particular reasons were not given on the analysis sheets. Specific analyses were performed to determine the

amounts of uranium collected on the gummed-films. A few analytical sheets indicate that the sample was "lost during analysis" but do not provide additional information.

Table M–2 (in six parts) contains monitoring results taken from the analytical data sheets for the deposition samples. The fluorometric analyses for uranium were reported in units of $\mu g\ ft^{-2}$. On some analytical data sheets, the results appear to have been rounded; others are given to many significant figures.

Table M–2. Reported Uranium Deposition Near the FMPC for Indicated Exposure Period
(Part 1: 12-14-59 through 6-1-60)

	Reported Uranium Deposition (μg ft^{-2}) for Indicated Period					
Station	12-14-59 1-14-60	1-14-60 2-15-60	2-15-60 3-17-60	3-17-60 4-1-60	4-1-60 5-2-60	5-2-60 6-1-60
N-1	1033	1438	295	2570	3750	2250
N-2	398	438	220	700	975	900
N-3	238	385	145	675	650	575
N-4	73	200	108	130	170	200
NE-1	1545	1030	465	650	2000	1000
NE-2	690	490	270	425	1000	800
NE-3	265	388	270	275	575	450
NE-4			157	32	23	18
E-1	5150	15238	16250	2570	13750	5250
E-2	1545	2013	1250	925	2500	1750
E-4	33	29	15	13	34	27
SE-1	1288	1438	785	675	7250	5750
SE-2	293	490	220	425	375	825
SE-3	318	283	418	275	175	475
SE-4						
S-1	9595	11550	123	4500	9750	5000
S-2	318	1313	8000	2250	500	275
S-3	503	475	270	95	160	175
S-4	62	220*	75	160	120	190
SW-1	1113	1838	1750	225	2500	950
SW-3	715	425*	370	88	1250	350
SW-4		280	700	200	160	200
W-1	1288	2100	1715	1025	3250	2500
W-2	293	1313	1815		1100	2000
W-3	105	400	343	200	250	625
W-4	53	270	98	100	150	320
NW-1	558	400	143	375	625	4250
NW-3	198	225	195	98	225	300
A	11868	15225	14500	9750	13500	17500
B	20200	18900	11000	12000	19000	11250
C	11868	6563	8500	65000	26000	18250

Table M–2. Reported Uranium Deposition Near the FMPC for Indicated Exposure Period
(Part 2: 6-1-60 through 12-1-60)

	Reported Uranium Deposition (μg ft^{-2}) for Indicated Period					
Station	6-1-60 7-1-60	7-1-60 8-2-60	8-2-60 9-1-60	9-1-60 9-30-60	9-30-60 11-1-60	11-1-60 12-1-60
N-1	2250	4250	2250	1500	1750	9250
N-2	875	525	775	575	700	2250
N-3	725	575	775	475	475	2500
N-4	275		190	250	220	380
NE-1	1500	1000	1750	650	4250	4500
NE-2	875	750	1250	575	2250	2000
NE-3	525	800	800	650	1000	1500
NE-4		42				
E-1	12250	6750	7500	4750	6500	35000
E-2	1500	1750	1250	1500	2750	4750
E-4	43	23	14			51
SE-1	1000	4250	2250	2250	4750	10250
SE-2	325	2500	1075	1000	1750	4250
SE-3	275	525	550	550	525	2250
SE-4						
S-1	7750	19000	10750	13250	5250	20250
S-2	700	1200	1250	1750	1250	2750
S-3	375	625	525	725	6000	800
S-4	350	190	330	190	230	190
SW-1	3750	3250	6750	4250	1750	6500
SW-3	950	925	2250	1025	3750	750
SW-4		310	190	290	300	200
W-1	3500	8250	3500	1025	1500	12250
W-2	4500	10500	2500	7750	2250	2750
W-3	1250	927	775	2250	375	400
W-4	300	260	330	190	220	540
NW-1	775	2250	1250	950	1000	3000
NW-3	275	325	275	350	250	825
A	11250	26500	15500	18750	40000	43000
B	11250	39000	14500	11750	8750	26000
C	17500	30000	21000	9250	34000	46500

Table M–2. Reported Uranium Deposition Near the FMPC for Indicated Exposure Period
(Part 3: 12-1-60 through 6-1-61)

	Reported Uranium Deposition (μg ft^{-2}) for Indicated Period					
Station	12-1-60 1-5-61	1-5-61 2-14-61	2-14-61 3-15-61	3-15-61 4-18-61	4-18-61 5-19-61	5-19-61 6-1-61
N-1	2750	1250	4250	1075	1750	2250
N-2	825	675	925	400	300	275
N-3	900	575	600	425	325	375
N-4	250	150	190	120	330	140
NE-1	2750	1425	825	725	1075	475
NE-2	2250	550	725	575	2500	725
NE-3	1000	275	400	4002	250	475
NE-4				700	270	
E-1	10000	19250	14750	9000	10000	225
E-2	2500	1570	1025	1750	950	800
E-4	45		33		51	
SE-1	1600	3500	1400	3750	2500	1250
SE-2	2100	1375	600	1750	725	450
SE-3	1700	675	300	525	325	275
SE-4						170
S-1	13500	20000	9250	17750	10500	4750
S-2	1025	825	1025	750	775	475
S-3	925	425	275	300	275	625
S-4	588	230	190	120	270	210
SW-1	3750	5000	2000	2750	1750	975
SW-3	950	1250	375	725	425	425
SW-4	463	230	170	170	170	210
W-1				2750	2750	925
W-2	2000	2500	1500	2250	2000	1575
W-3	725	700	375	625	350	275
W-4	363	170	210	150	130	240
NW-1	1250	475	450	450	850	625
NW-3	425	133	300	450	300	425
A	24250	27500	13000	23250	14500	2750
B	12750	14350	8750	13500	7500	3250
C	30000	15750	24250	8000	8250	3000

Table M–2. Reported Uranium Deposition Near the FMPC for Indicated Exposure Period
(Part 4: 6-1-61 through 12-1-61)

	Reported Uranium Deposition (μg ft^{-2}) for Indicated Period					
Station	6-1-61 6-30-61	6-30-61 7-31-61	7-31-61 9-1-61	9-1-61 10-1-61	10-1-61 11-1-61	11-1-61 12-1-61
N-1	3250	2250	2250	425	2250	1600
N-2	725	1750	600	1875	475	575
N-3	600	825	600	475	475	400
N-4	230	700	900	530	350	150
NE-1		2000	1125	825	1475	1175
NE-2	3500	1175	775	725	725	525
NE-3	975	875	575	450	475	375
NE-4						
E-1	23750	7750	9250	7000	8000	6250
E-2	2250	1200	1500	1250	1250	1750
E-4						
SE-1		1000	4750	400	1200	2000
SE-2	825	475	875	825	475	625
SE-3	725	450	425	5000	250	250
SE-4	400	900	190	150	410	150
S-1	6250	5250	19250	175	4750	13250
S-2	525	1125	825	325	400	725
S-3	475	450	550	225	175	325
S-4	250	150	210	330	290	280
SW-1		1175	2500	925	5750	1775
SW-3	425	650	700	690	400	575
SW-4	200	110		225	120	90
W-1	1250	1750	2750	1525	1125	2250
W-2	875	700	400	750	225	1225
W-3	475	925	1025	225	70	375
W-4	170	250	370	140	2600	130
NW-1		675	1400	250	675	975
NW-3	425	425	500	825	325	2250
A	2750	5250	11750	7000	4250	16250
B	3250	9250	13000	7250	6250	8750
C	3000	15750	9750	11000	9250	9000

Table M–2. Reported Uranium Deposition Near the FMPC for Indicated Exposure Period
(Part 5: 12-1-61 through 6-1-62)

	Reported Uranium Deposition (μg ft^{-2}) for Indicated Period					
Station	12-1-61 12-29-61	12-29-61 2-5-62	2-5-62 3-1-62	3-1-62 4-4-62	4-4-62 5-2-62	5-2-62 6-1-62
N-1	800	1150	750	325	6250	4250
N-2	105	275	275	1450	1050	850
N-3	325	250	275	1100	625	750
N-4	220		180	450	130	175
NE-1	400	1750	425	275	3000	2250
NE-2	375	650	275	375	1175	825
NE-3	325	425	1175	275	700	575
NE-4	130		160	170	490	108
E-1	2250	6000	2250	3500	6000	6250
E-2	1025	1275	625	1575	3000	2000
E-4						
SE-1	875	775	1400	3000	3500	2750
SE-2	375	300	575	575	1500	425
SE-3	225	275	225	700	750	9500
SE-4						
S-1	6000	5500	6250	11750	12750	550
S-2	275	625	400	650	375	575
S-3	500	975	275	275	275	250
S-4	140		150	138	130	225
SW-1	625	1300	1525	6750	2500	3750
SW-3	850	325	450	350	900	650
SW-4	90		100	180	110	135
W-1	1025	1050	4250	2000	2250	3750
W-2	800	950	875	1050	3750	2500
W-3	350	250	225	350	1000	475
W-4	70		120	590	110	325
NW-1	400	475	375	475	1375	1175
NW-3	95	1225	225	85	325	625
A	8750	7250	10000	24250	17000	42500
B	5500	10250	6750	12750	11250	21000
C	4750	8250	3000	14500	14375	17250

Table M–2. Reported Uranium Deposition Near the FMPC for Indicated Exposure Period
(Part 6: 6-1-62 through 12-31-62)

	Reported Uranium Deposition (μg ft^{-2}) for Indicated Period						
Station	6-1-62 6-27-62	6-27-62 8-1-62	8-1-62 9-4-62	9-4-62 10-1-62	10-1-62 11-1-62	11-1-62 12-3-62	12-3-62 12-31-62
N-1	4500	1150	6250	4375	3438	2063	2063
N-2	825	240	1188	813	688	688	688
N-3	1025	260	1000	875	563	750	750
N-4	370	175	123	131	100	138	138
NE-1	2250	850	2950	2150	2750	2050	2050
NE-2	975	550	500	1563	1313	938	938
NE-3	575	400	1000	1000	1188	625	625
NE-4	460	16500	375	188	938	88	88
E-1	5000	2900	5000	7500	12500	2938	2938
E-2	4250	1400	2313	2875	2813	1250	1250
E-4							
SE-1	3750	1300	3150	5000	1900	2950	2950
SE-2	1450	500	1063	1563	813	1063	1063
SE-3	1750	250	331	1063	369	563	563
SE-4							
S-1	16500	6500	15000	28750	11875	13750	13750
S-2	475	220	938	2188	688	1000	1000
S-3	875	100	313	688	363	300	300
S-4	410	145	123	163	106	69	69
SW-1	8500	650	5500	12000	1850	12500	12500
SW-3	1425	400	1000	2688	1250	1563	1563
SW-4	240	120	68	231	231	131	131
W-1	3000	1550	168750	8750	2063	3063	3063
W-2	1350	850	51875	5625	1063	1125	1125
W-3	475	115	20625	938	375	325	325
W-4	1400	190	160	75	125	119	119
NW-1	1125	1250	2750	1400	1250	650	650
NW-3	450	230	3938	294	875	163	163
A	43750	1125	21875	50000	16250	27500	27500
B	15000	7500	15000	30000	18125	57500	57500
C	50000	338	25625	30000	14375	11875	11875

GUMMED-FILM COLLECTION EFFICIENCY

The collection effliciency for gummed-film is defined to be the ratio of the fallout activity collected by the gummed-film to the total amount deposited on a comparable ground surface. At the time of the measurements, the gummed-film collection efficiency was estimated to be about 60% (Harley et al. 1960). However, recent evaluations (Beck 1984; Beck et al. 1990) indicate that the efficiency varies with precipitation amount and is substantially lower than originally thought. Comparisons of gummed-film data against integrated deposition results from soil samples in relatively arid locations near the NTS yeilded an estimated efficiency of 20% for daily collections under dry conditions. Contemporary measurements of total deposition and deposition on gummed-film, including Chernobyl fallout and field experimental data, led Beck et al. (1990) to the following estimates of collection efficiencies for gummed-film as a function of daily precipitation amount. Beck et al. (1990) estimated that the 1-sigma fractional uncertainty for each collection efficiency in Table M–3 was about ±25%.

Table M–3. Estimated Collection Efficiencies for Gummed-Film Exchanged Daily

Daily precipitation (mm)	Collection efficiency
0 (dry)	0.20
0.01– 0.75	0.30
0.75–2.5	0.25
2.5–7.5	0.15
7.5–25	0.10
> 25	0.07

At the FMPC, gummed-film samples were exchanged biweekly or, more commonly, monthly. Direct application of the collection efficiencies for one-day sampling periods appeared inappropriate. Washoff of deposited material by subsequent precipitation or blowoff by wind would be expected to further reduce the amount retained at the end of the sampling period.

During a two-year period between March 1960 and March 1962, dailly, weekly, biweekly, and monthly measurements of uranium deposition on gummed-film were obtained for a location on the FMPC site, just north of the Health and Safety Building. This special study was undertaken by the Industrial Hygiene and Radiation Department at the FMPC to determine the collection efficiency of the gummed-film for various exposure times and weather conditions (Starkey 1960a, 1960b). No report describing the results of the study has been found; however, the FMPC data files contained the measurement results. We have analyzed these data to determine the gummed-film collection efficiencies for exposure periods longer than one day. The procedures used in the analysis and the results are described below.

National Weather Service daily precipitation measurements were obtained for both the Cincinnati airport, near Covington, Kentucky, and a downtown Cincinnati location (4th and Main Streets). Monthly precipitation totals at these two locations were compared with totals measured at the FMPC. From that comparison it appeared that the city location was more representative of the FMPC than the location at the airport.

The precipitation amount measured in downtown Cincinnati for a particular day was used to estimate the gummed-film collection efficiency for that day (using Table M–3). The measured deposition at the Health and Safety Building for the day was divided by the estimated collection efficiency to estimate the true daily deposition at that location. Those estimates were then summed for weekly, biweekly, and monthly periods for comparison with the total depositions measured for those periods. Weekly collections were compared with the sum of seven daily collections during the exposure period when the set of daily samples was complete. If only one daily value was missing a comparison was also made. However, if two or more daily depositions were unavailable, the weekly collection was not compared with the sum of daily values. The same approach to missing data was used for the longer collection periods. Comparisons of biweekly deposition results were made with the sums of 12–14 daily values. For monthly comparisons, a maximum of four missing daily measurements was tolerated.

The results of the comparisons of longer term deposition results with sums of the estimated true daily depositions are shown in Table M–4. Apparent mean collection efficiencies for the three longer exposure periods are comparable. The deposition-weighted average daily collection efficiency for the approximately three years of measurements was 0.16. This suggests that most losses occur during the day of deposition or that subsequent small losses on later days are counterbalanced by gains due to local effects or are masked.

Table M–4. Apparent Collection Efficiencies of Gummed-Film Exposed for Longer Collection Periods

Exposure duration	Number of comparisons	Apparent collection efficiency	
		Mean	Std. Dev.
1 Week	58	0.15	0.06
2 Weeks	31	0.16	0.06
1 Month	15	0.14	0.03

The collection efficiency of greatest interest is that for monthly exposure periods because, as can be seen from Table M–2, those were used most frequently in the gummed-film monitoring program during 1960–1962. However, biweekly sampling periods were used more frequently in the earlier years of monitoring. The distributions of the apparent collection efficiencies of gummed-film for these two exposure periods are shown in Fig. M–1, and M–2. As might be expected, the variability of the ratios is smallest for the longest averaging time.

If there are losses due to weathering of material deposited on the gummed film, these results suggest that there are approximately compensating depositions, presumably due to resuspension of material from the ground surface. An alternative explanation, which can not be excluded based on these results, is that the collection efficiency of the gummed-film depends primarily on the conditions at the time of deposition and that there is little removal of material fixed at that time.

TABULATION OF REVISED URANIUM DEPOSITION ESTIMATES

Table M-5 contains revised estimates of uranium deposition on gummed-film that were derived from the reported values (Table M–2) and the apparent collection efficiencies given in Table M–4. In Table M–5, which is in six parts, the revised deposition estimates have been converted to the metric units of mg m^{-2} for ease of presentation.

Uncertainties in the revised uranium depositions are estimated to be in the range of 20 to 30 percent of the tabulated values. Most of the uncertainty is associated with the estimates of the long term collection efficiencies (Table M–4). All values in Table M–5 have been rounded to a maximum of two significant figures.

COMPARISON OF DEPOSITION ESTIMATES WITH RESULTS OF SIMULATIONS

Simulations of air transport of uranium released from the FMPC site have been reported in Appendices G and J. In these simulations, a model of deposition and plume depletion was usually included to adjust predicted air concentrations to show the effect of loss of uranium from the plume by deposition. Similar calculations were performed for the purpose of comparing simulated deposition with the gummed film estimates. For most of the stations listed in Table M–1, Figs. M–3 through M–25 (placed at the end of this appendix) show the compared estimates as time series for the 36-month period 1960–1962, with "measured" denoting the efficiency-corrected gummed film estimates and "simulated" identifying the model predictions. Table M–6, located after the plots, tabulates the comparisons in terms of a measure of bias and the coefficients of correlation between the log-transformed gummed film estimates and the simulated values. Locations outside the 8-km assessment domain were excluded from these comparisons. The time-dependent model (Appendix J) was applied to all releases from rooftop stacks, and the Gaussian plume was used to predict transport from the old solid waste incinerator and the oil burner.

At nearly all locations, there is a tendency for the simulations to underpredict the gummed film estimates. A factor of two is a reasonable generalization of the degree of underprediction, although during 1962 a more pronounced divergence is apparent at some locations, and at station N–4, near the northern periphery of the assessment domain (Fig. M–6), the discrepancy is more than a factor of ten.

There is also a tendency for the relative difference to increase with the distance of the receptor from the source (Fig. M–26). This trend may be due to some combination of two

factors. The first is a possibly under-efficient deposition model, which would account for discrepancies near the source. The second is a model bias in predicting concentrations that tends increasingly toward underprediction with increasing distance. The second factor, if it is involved, could be caused by dispersion coefficients (σ_y, σ_z) that increase too rapidly with distance. One needs to bear in mind, however, that absolute deposition values at greater distances are usually smaller than at locations nearer the source, and it is possible for a relative difference to increase by an order of magnitude, while its absolute value remains constant or decreases. For example, the overall accuracy of prediction at station N–1 is within a factor of two (Table M–6 lists the bias as 0.68), corresponding to absolute differences of 100 mg m^{-2}, whereas at station N–4 (Fig. M–6), the underprediction by more than an order of magnitude (bias 0.05) corresponds to absolute differences of about 10 mg m^{-2}, on average.

The correlations between the log-transformed predicted and observed values that are given in Table M–6 (at the end of this appendix) are generally small in magnitude, and about half are negative. Much, but not all, of this effect is attributable to a tendency toward opposing secular trends in 1961 and 1962, but these are not observed uniformly in all plots. A peak in the simulated values near the end of 1961 corresponds, in many of the plots, to a dip in the gummed film data. In analyzing the air monitoring data at the perimeter stations for the 36-month period 1960–1962 (Appendix J), we have observed poor matching of the month-to-month fluctuations with those of the reconstructed source term (which the simulated values tend to follow closely), and it is not surprising to see similar effects in the comparison with deposition data.

The pattern of underprediction of deposition, coupled with the factor-of-two overpredictions by the models of air concentration at the NE perimeter station, suggests that the deposition model may be under-efficient in its prediction of the removal of the larger particles from the plume. This question, and the related question of the trend of increasing underprediction with distance (Fig. M–26), will be studied further as we prepare for the final calculations. The overall result, however, is a positive validation of the modeling approach, and for locations near the site, the underprediction of deposition fits logically with the overprediction of air concentration. Above all, one must realize that the general factor-of-two accuracy is quite good for the application of relatively simple models to atmospheric phenomena.

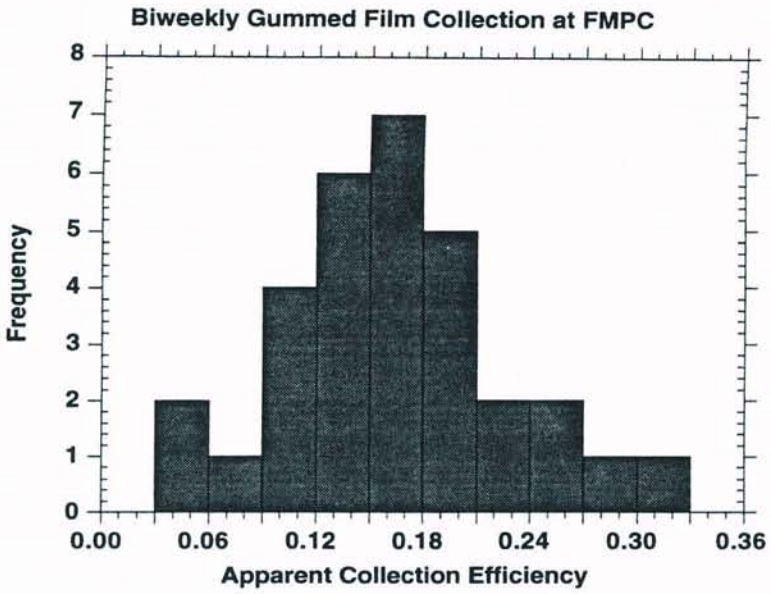

Figure M–1. Distribution of apparent collection efficiencies of gummed film exposed for a period of two weeks.

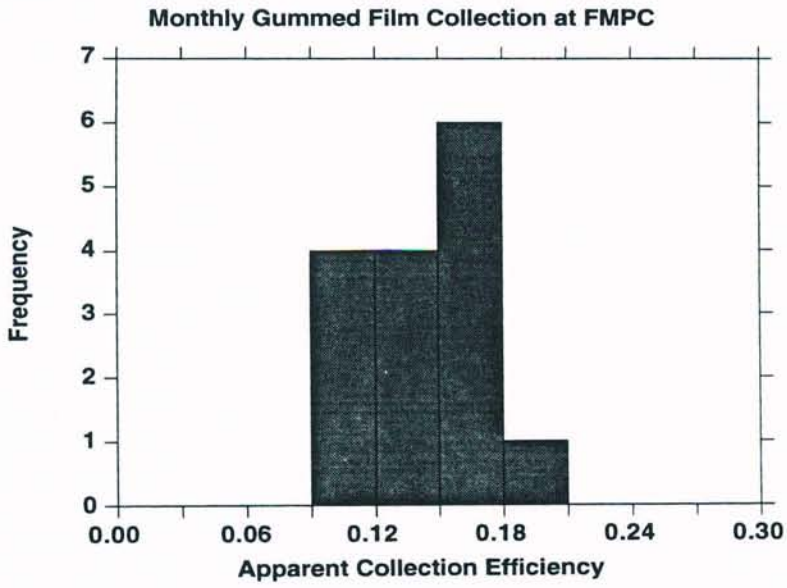

Figure M–2. Distribution of apparent collection efficiencies of gummed film exposed for a period of one month.

Table M–5. Revised Estimates of Uranium Deposition Near the FMPC for Indicated Exposure Period
(Part 1: 12-14-59 through 6-1-60)

	Revised Uranium Deposition (mg m^{-2}) for Indicated Period					
Station	12-14-59 1-14-60	1-14-60 2-15-60	2-15-60 3-17-60	3-17-60 4-1-60	4-1-60 5-2-60	5-2-60 6-1-60
N-1	78	110	22	200	280	170
N-2	30	33	17	53	74	68
N-3	18	22	11	51	49	44
N-4	6	15	8	10	13	15
NE-1	120	78	35	49	150	76
NE-2	52	37	20	32	76	61
NE-3	20	29	20	21	44	34
NE-4			12	2	2	1
E-1	390	1200	1200	200	1000	400
E-2	120	150	95	70	190	130
E-4	3	2	1	1	3	2
SE-1	98	110	60	51	550	440
SE-2	22	37	17	32	28	63
SE-3	24	21	32	21	13	36
SE-4						
S-1	730	880	9	340	740	380
S-2	24	100	610	170	38	21
S-3	38	36	20	7	12	13
S-4	5	17	6	12	9	14
SW-1	84	140	130	17	190	72
SW-3	54	32	28	7	95	27
SW-4		21	53	15	12	15
W-1	98	160	130	78	250	190
W-2	22	100	140		83	150
W-3	8	30	26	15	19	47
W-4	4	20	7	8	11	24
NW-1	42	30	11	28	47	320
NW-3	15	17	15	7	17	23
A	900	1200	1100	740	1000	1300
B	1500	1400	830	910	1400	850
C	900	500	640	4900	2000	1400

Table M–5. Revised Estimates of Uranium Deposition Near the FMPC for Indicated Exposure Period (Part 2: 6-1-60 through 12-1-60)

	Revised Uranium Deposition (mg m^{-2}) for Indicated Period					
Station	6-1-60 7-1-60	7-1-60 8-2-60	8-2-60 9-1-60	9-1-60 9-30-60	9-30-60 11-1-60	11-1-60 12-1-60
N-1	170	320	170	110	130	700
N-2	66	40	59	44	53	170
N-3	55	44	59	36	36	190
N-4	21		14	19	17	29
NE-1	110	76	130	49	320	340
NE-2	66	57	95	44	170	150
NE-3	40	61	61	49	76	110
NE-4		3				
E-1	930	510	570	360	490	2700
E-2	110	130	95	110	210	360
E-4	3	2	1			4
SE-1	76	320	170	170	360	780
SE-2	25	190	81	76	130	320
SE-3	21	40	42	42	40	170
SE-4						
S-1	590	1400	820	1000	400	1500
S-2	53	91	95	130	95	210
S-3	28	47	40	55	460	61
S-4	27	14	25	14	17	14
SW-1	280	250	510	320	130	490
SW-3	72	70	170	78	280	57
SW-4		23	14	22	23	15
W-1	260	620	260	590	110	930
W-2	340	800	190	170	170	210
W-3	95	70	59	40	28	30
W-4	23	20	25	14	17	41
NW-1	59	170	95	72	76	230
NW-3	21	25	21	27	19	63
A	850	2000	1200	1400	3000	3300
B	850	3000	1100	890	660	2000
C	1300	2300	1600	700	2600	3500

Table M–5. Revised Estimates of Uranium Deposition Near the FMPC for Indicated Exposure Period
(Part 3: 12-1-60 through 6-1-61)

	Revised Uranium Deposition (mg m^{-2}) for Indicated Period					
Station	12-1-60 1-5-61	1-5-61 2-14-61	2-14-61 3-15-61	3-15-61 4-18-61	4-18-61 5-19-61	5-19-61 6-1-61
N-1	210	95	320	81	130	170
N-2	63	51	70	30	23	21
N-3	68	44	45	32	25	28
N-4	19	11	14	9	25	11
NE-1	210	110	63	55	81	36
NE-2	170	42	55	44	190	55
NE-3	76	21	30	30	19	36
NE-4				53	20	13
E-1	760	1500	1100	680	760	17
E-2	190	120	78	130	72	61
E-4	3		3		4	
SE-1	120	260	110	280	190	95
SE-2	160	100	45	133	55	34
SE-3	130	51	23	40	25	21
SE-4						
S-1	1000	1500	700	1300	800	360
S-2	78	63	78	57	59	36
S-3	70	32	21	23	21	47
S-4	45	17	14	9	20	16
SW-1	280	380	150	210	130	74
SW-3	72	95	28	55	32	32
SW-4	35	17	13	13	13	16
W-1				210	210	70
W-2	150	190	110	170	150	120
W-3	55	53	28	47	27	21
W-4	28	13	16	11	10	18
NW-1	95	36	34	34	64	47
NW-3	32	10	23	34	23	32
A	1800	2100	980	1800	1100	210
B	970	1100	660	1000	570	250
C	2300	1200	1800	610	620	230

Table M–5. Revised Estimates of Uranium Deposition Near the FMPC for Indicated Exposure Period (Part 4: 6-1-61 through 12-1-61)

	Revised Uranium Deposition (mg m^{-2}) for Indicated Period					
Station	6-1-61 6-30-61	6-30-61 7-31-61	7-31-61 9-1-61	9-1-61 10-1-61	10-1-61 11-1-61	11-1-61 12-1-61
N-1	250	170	170	32	170	120
N-2	55	130	45	140	36	44
N-3	45	63	45	36	36	30
N-4	17	53	68	40	27	11
NE-1		152	85	63	110	89
NE-2	260	89	59	55	55	40
NE-3	74	66	44	34	36	28
NE-4	30	68	14	11	31	11
E-1	1800	590	700	530	610	470
E-2	170	91	110	95	95	130
E-4						
SE-1	0	76	360	30	91	150
SE-2	63	36	66	63	36	47
SE-3	55	34	32	380	19	19
SE-4						
S-1	470	400	780	13	360	1000
S-2	40	85	63	25	30	55
S-3	36	34	42	17	13	25
S-4	19	11	16	25	22	21
SW-1		89	190	70	440	140
SW-3	32	49	53	52	30	51
SW-4	15	8	11	17	9	7
W-1	95	130	210	120	85	170
W-2	66	53	30	57	17	93
W-3	36	70	78	17	5	28
W-4	13	19	28	11	200	10
NW-1		51	110	19	51	74
NW-3	32	32	38	63	25	170
A	210	400	890	530	320	1200
B	250	700	980	550	470	660
C	230	1200	740	830	700	680

Table M–5. Revised Estimates of Uranium Deposition Near the FMPC for Indicated Exposure Period (Part 5: 12-1-61 through 6-1-62)

	Revised Uranium Deposition (mg m^{-2}) for Indicated Period					
Station	12-1-61 12-29-61	12-29-61 2-5-62	2-5-62 3-1-62	3-1-62 4-4-62	4-4-62 5-2-62	5-2-62 6-1-62
N-1	61	87	57	25	470	320
N-2	8	21	21	110	80	64
N-3	25	19	21	83	47	57
N-4	17	0	14	34	10	13
NE-1	30	130	32	21	230	170
NE-2	28	49	21	28	89	63
NE-3	25	32	89	21	53	44
NE-4	10		12	13	37	8
E-1	170	460	170	260	460	470
E-2	78	97	47	120	230	150
E-4						
SE-1	66	59	110	230	260	210
SE-2	28	23	44	44	110	32
SE-3	17	21	17	53	57	42
SE-4						
S-1	460	420	470	890	970	720
S-2	21	47	30	49	28	44
S-3	38	74	21	21	21	19
S-4	11	0	11	10	10	17
SW-1	47	99	120	510	190	280
SW-3	64	25	34	27	68	49
SW-4	7	0	8	14	8	10
W-1	78	80	320	150	170	280
W-2	61	72	66	80	280	190
W-3	27	19	17	27	76	36
W-4	5	0	9	45	8	25
NW-1	30	36	28	36	100	89
NW-3	7	93	17	6	25	47
A	660	550	760	1800	1300	3200
B	420	780	510	970	850	1600
C	360	620	230	1100	1100	1300

Table M–5. Revised Estimates of Uranium Deposition Near the FMPC for Indicated Exposure Period
(Part 6: 6-1-62 through 12-31-62)

	Revised Uranium Deposition (mg m^{-2}) for Indicated Period						
Station	6-1-62 6-27-62	6-27-62 8-1-62	8-1-62 9-4-62	9-4-62 10-1-62	10-1-62 11-1-62	11-1-62 12-3-62	12-3-62 12-31-62
N-1	340	87	470	330	260	160	240
N-2	63	18	90	62	52	52	71
N-3	78	20	76	66	43	57	52
N-4	28	13	9	10	8	10	4
NE-1	170	64	220	160	210	160	190
NE-2	74	42	38	120	100	71	62
NE-3	44	30	76	76	90	47	62
NE-4	35	13	28	14	71	7	11
E-1	380	220	380	570	950	220	900
E-2	320	110	180	220	210	95	200
E-4							
SE-1	280	99	240	380	140	220	340
SE-2	110	38	81	120	62	81	110
SE-3	130	19	25	81	28	43	43
SE-4							
S-1	1300	460	1100	2200	900	1000	1500
S-2	36	17	71	170	52	76	95
S-3	66	8	24	52	28	23	430
S-4	31	11	9	12	8	5	4
SW-1	640	49	420	910	140	950	45
SW-3	110	30	76	200	95	120	140
SW-4	18	9	5	18	18	10	5
W-1	230	120	13000	660	160	230	290
W-2	100	64	3900	430	81	85	190
W-3	36	9	1600	71	28	25	71
W-4	110	14	12	6	9	9	4
NW-1	85	95	210	110	95	49	130
NW-3	34	17	300	22	66	12	17
A	3300	85	1700	3800	1200	2100	2000
B	1100	570	1100	2300	1400	4400	4500
C	3800	26	1900	2300	1100	900	1000

REFERENCES

Barry E.V. 1953. "Fallout Program." Memorandum to J.A. Quigley dated December 8. National Lead Company of Ohio, Cincinnati.

Beck H.L. 1984. *Estimates of Fallout from Nevada Weapons Testing in the Western United States based on Gummed-Film Monitoring Data*. New York: U. S. Department of Energy; Environmental Measurements Laboratoroy report EML-433.

Beck H.L., I.K. Helfer, A. Bouville, and M. Dreicer. 1990. "Estimates of Fallout in the Continental U. S. from Nevada Weapons Testing Based on Gummed-Film Monitoring Data." *Health Phys.* **59**: 565–576.

Eisenbud M. and J.H Harley. 1953. "Radioacctive Dust from Nuclear Detonations." *Science* **117**: 141–147.

Eisenbud M. and J.H Harley. 1955. "Radioacctive Fallout in the United States." *Science* **121**: 677–680.

Eisenbud M. and J.H Harley. 1956. "Radioacctive Fallout Through September 1955." *Science* 124: 251–255.

Eisenbud M. and J.H. Harley 1958. "Long-term Fallout." *Science* **128**: 399–402.

Harley J.H., N.A. Hallden, and L.S.Y. Ong, 1960. *Summary of Gummed-Film Results Through December 1959*. New York: U. S. Atomic Enery Commission; Health and Safety Laboratory report HASL-93.

Starkey R.H. 1960. "Special Fallout Study." Memorandum to All IH&R Personnel, dated March 17. National Lead Company of Ohio, Cincinnati.

Starkey R.H. 1960b. "IH&R Department Monthly Report for March, 1960." FMPC Memorandum to J. A. Quigley, dated April 5. National Lead Company of Ohio, Cincinnati.

Wachholz B.W. 1990. "Overview of the National Cancer Institute's Activities Related to Exposure of the Publid to Fallout from the Nevada Test Site." *Health Phys.* **59**: 511–514.

Yoder J.D. 1954. Letter to Dan Lynch, Coordinator of Special Projects, AEC New York Operations Office, requesting a source of continuing supply, dated August 26.

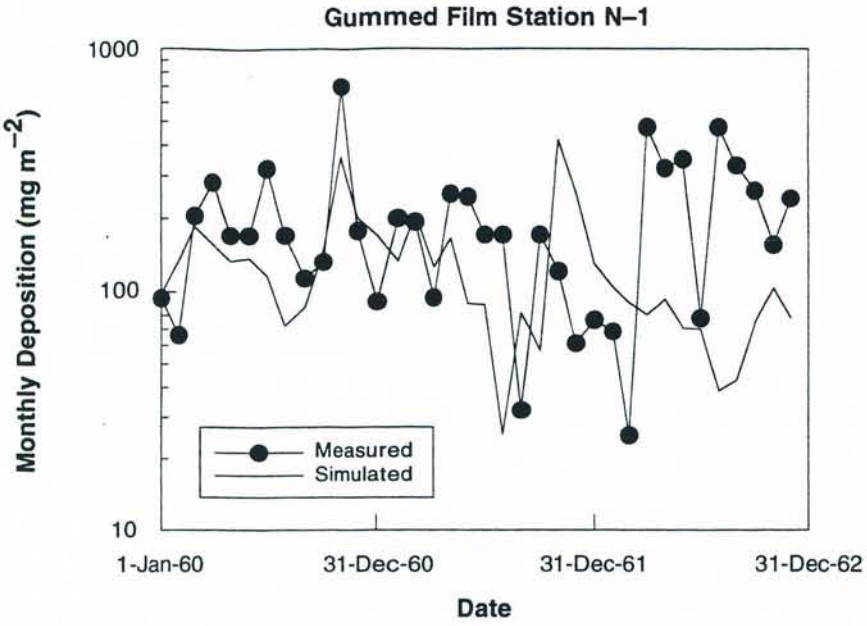

Figure M–3. Gummed film station N–1. Distance from the center of the production area was 337 m, and the direction was 6° from N.

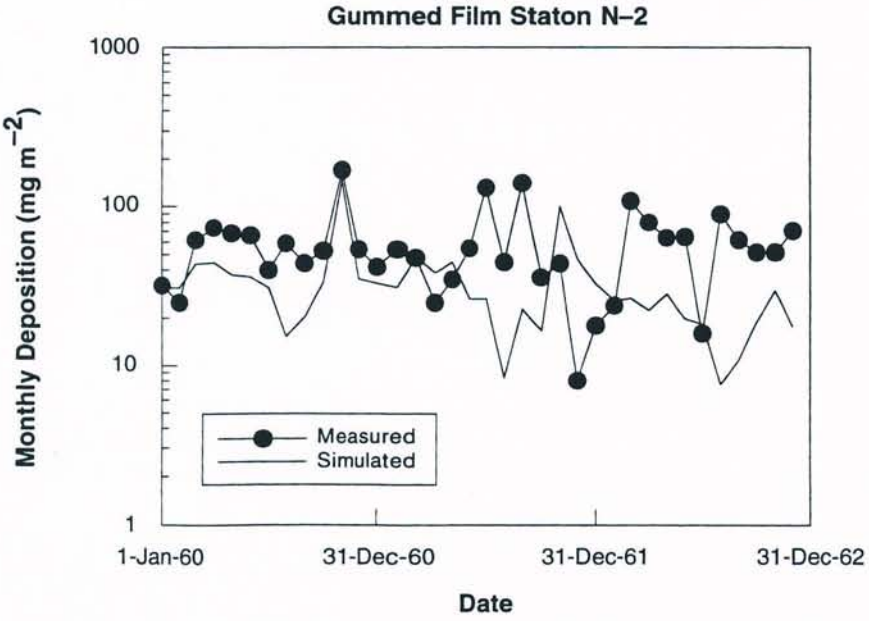

Figure M–4. Gummed film station N–2. Distance from the center of the production area was 720 m, and the direction was 2° from N.

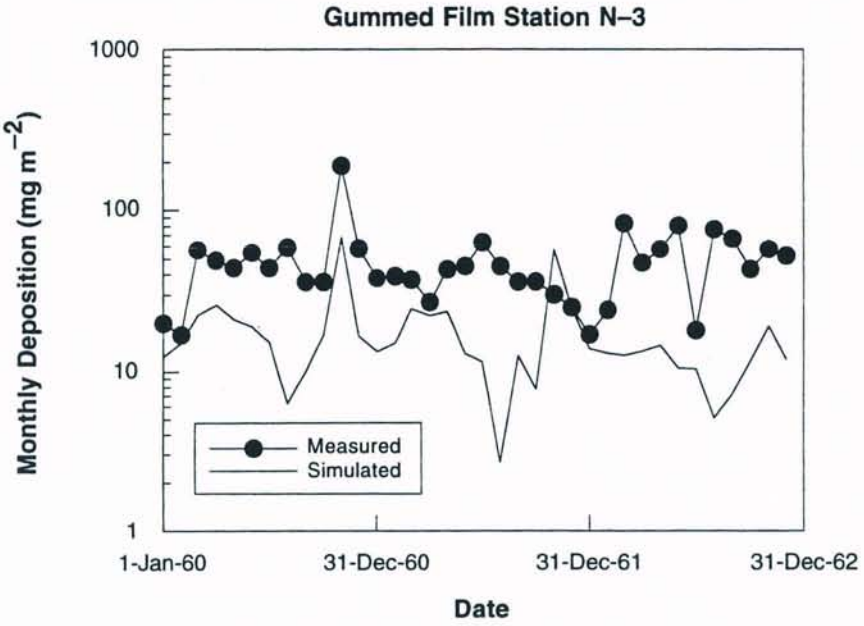

Figure M–5. Gummed film station N–3. Distance from the center of the production area was 1006 m, and the direction was N.

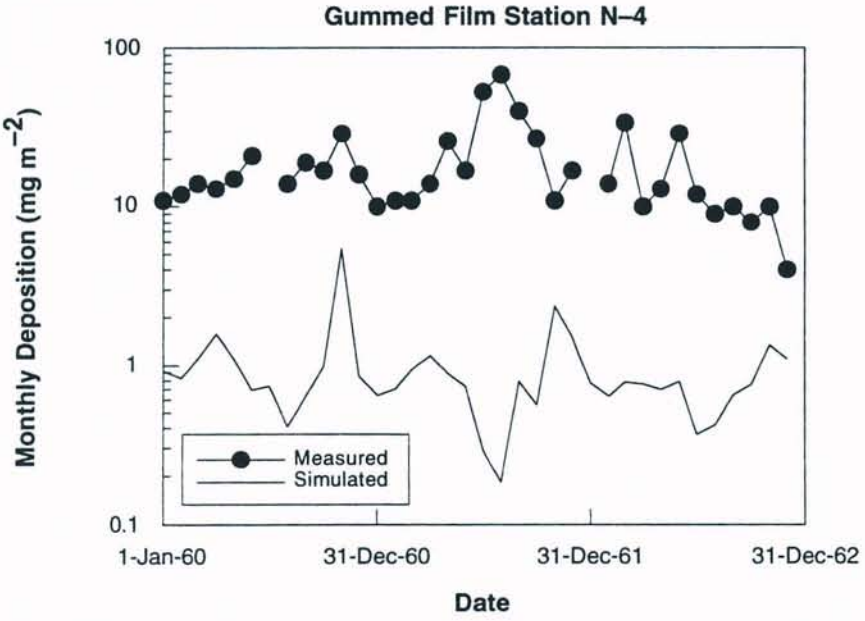

Figure M–6. Gummed film station N–4. Distance from the center of the production area was 7200 m, and the direction was N.

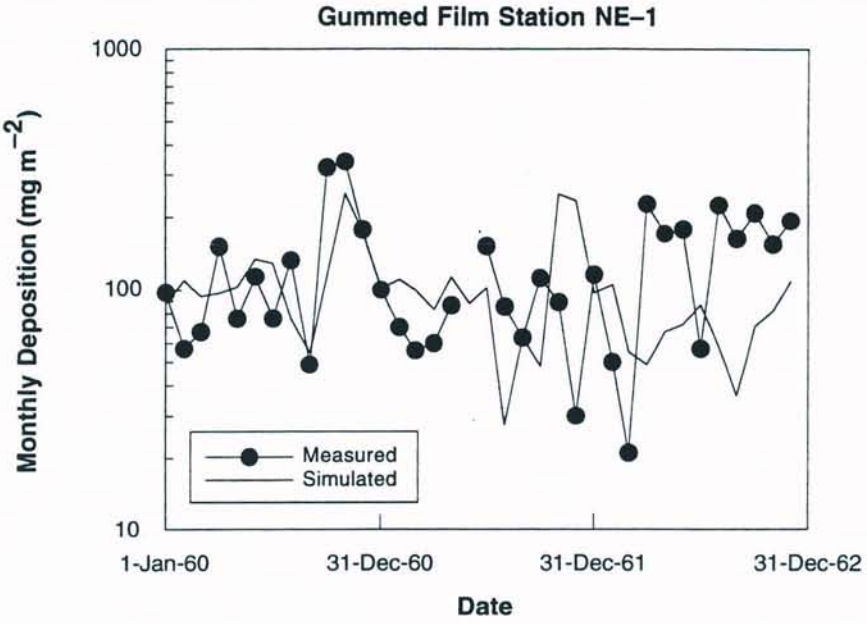

Figure M–7. Gummed film station NE–1. Distance from the center of the production area was 514 m, and the direction was 48° from N.

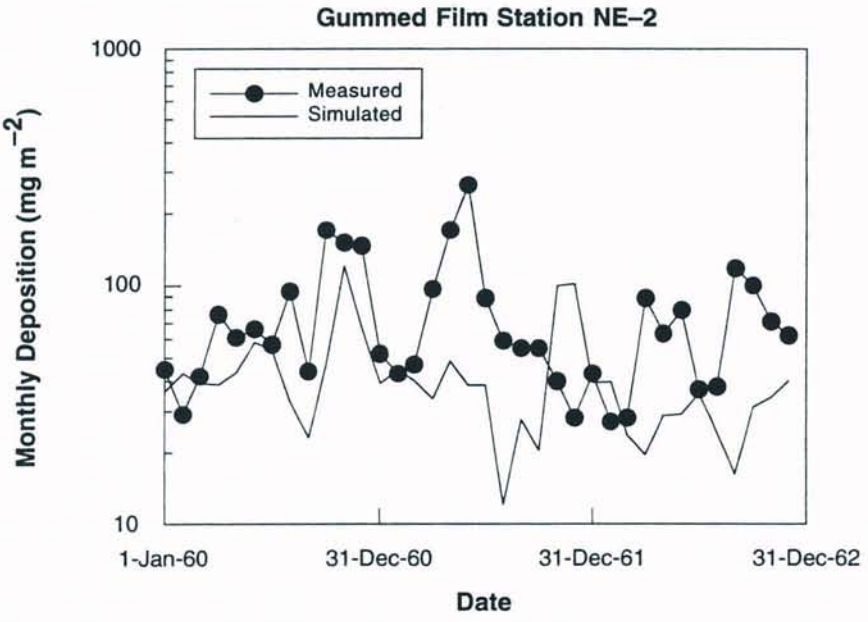

Figure M–8. Gummed film station NE–2. Distance from the center of the production area was 994 m, and the direction was 36° from N.

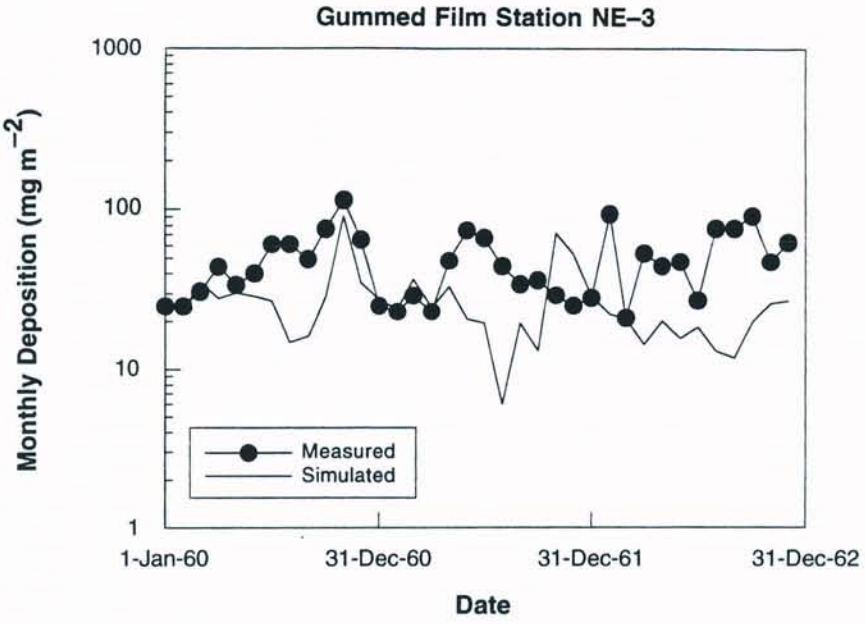

Figure M–9. Gummed film station NE–3. Distance from the center of the production area was 1200 m, and the direction was 26° from N.

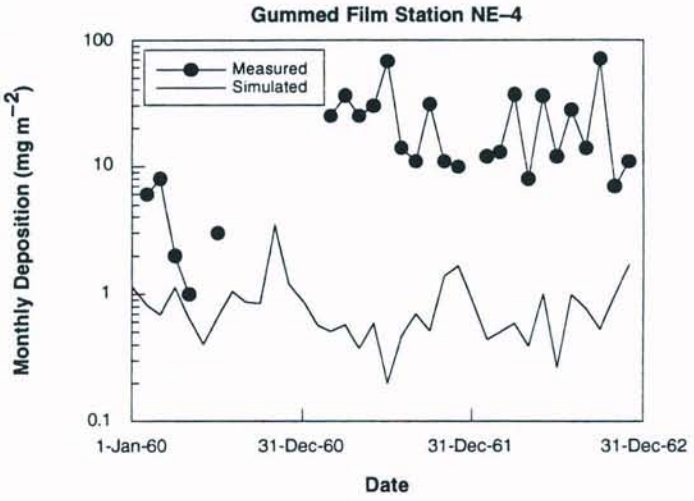

Figure M–10. Gummed film station NE–4. During 1960, the distance from the center of the production area was about 12,500 m, and the direction was 73° from N. For the remainder of the 36-month period, the station was located at a distance of 4200 m from the center of the production area, in the direction 72° from N. The simulation was based on the assumption that the longer distance was the correct one.

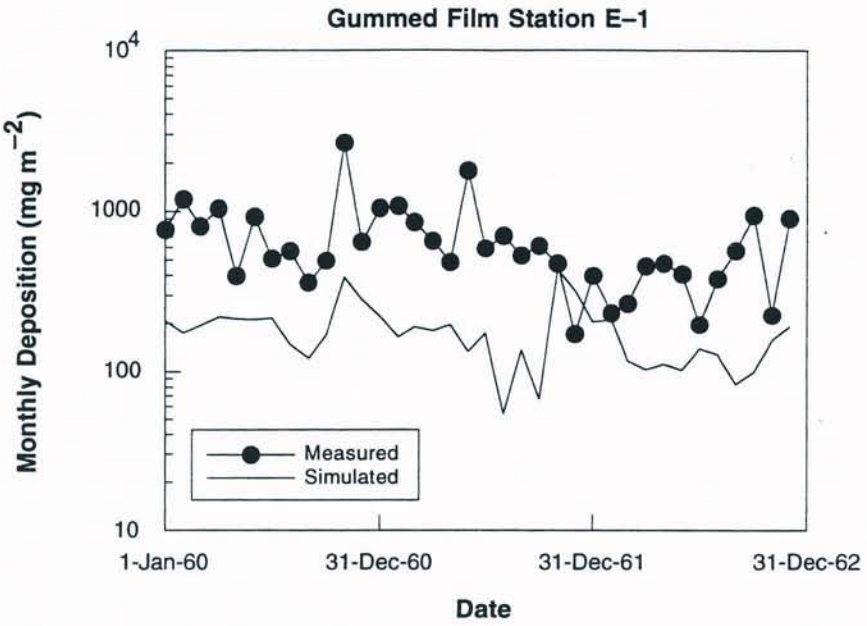

Figure M–11. Gummed film station E–1. Distance from the center of the production area was 323 m, and the direction was 89° from N.

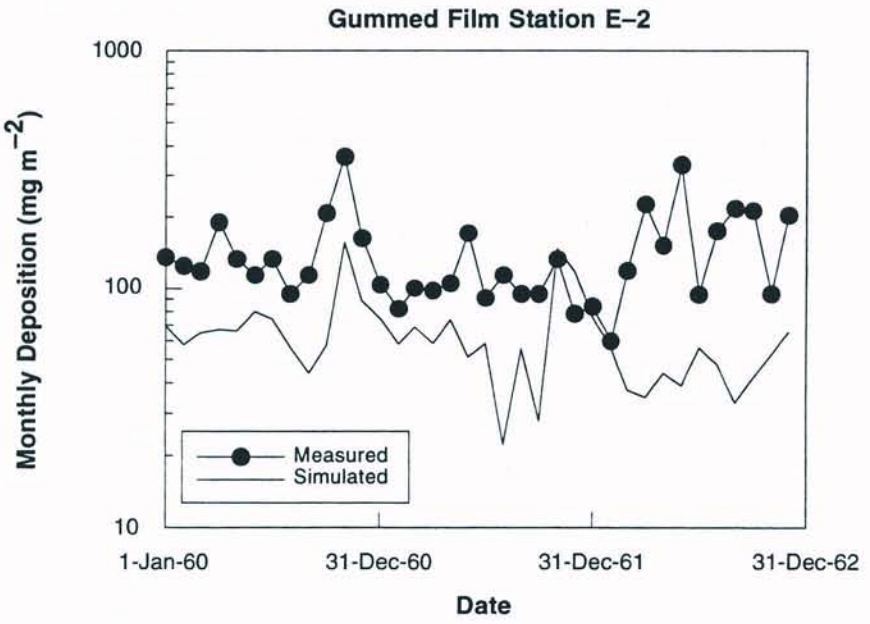

Figure M–12. Gummed film station E–2. Distance from the center of the production area was 732 m, and the direction was 89° from N.

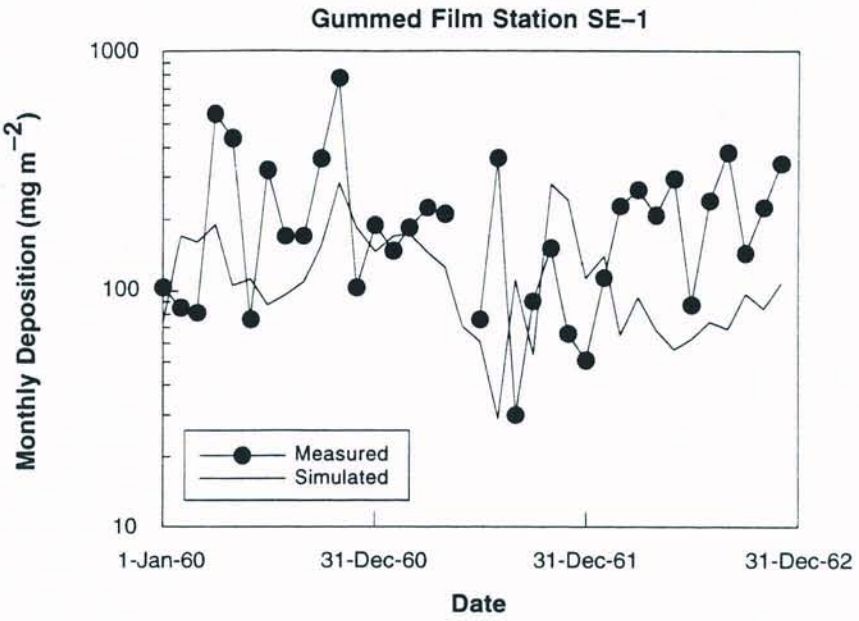

Figure M–13. Gummed film station SE–1. Distance from the center of the production area was 509 m, and the direction was 142° from N.

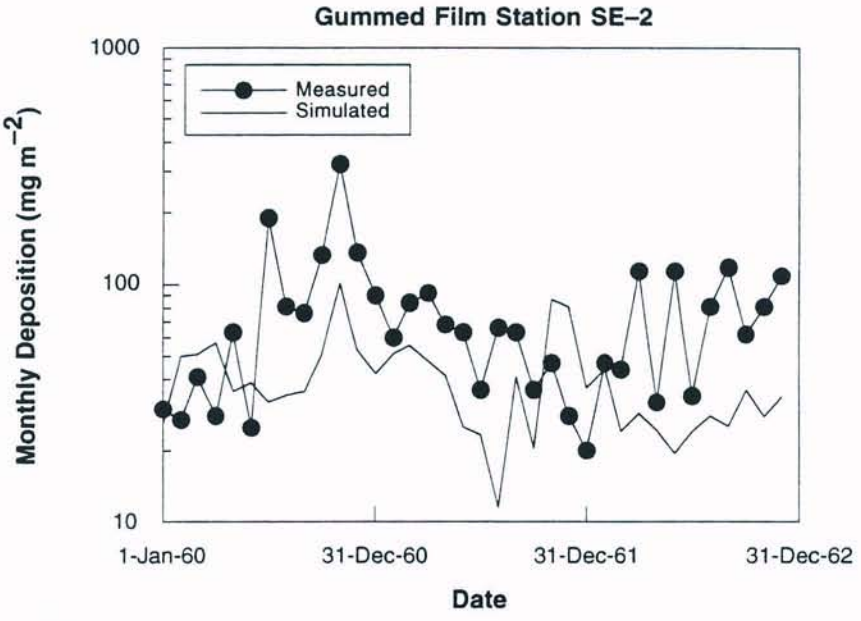

Figure M–14. Gummed film station SE–2. Distance from the center of the production area was 983 m, and the direction was 136° from N.

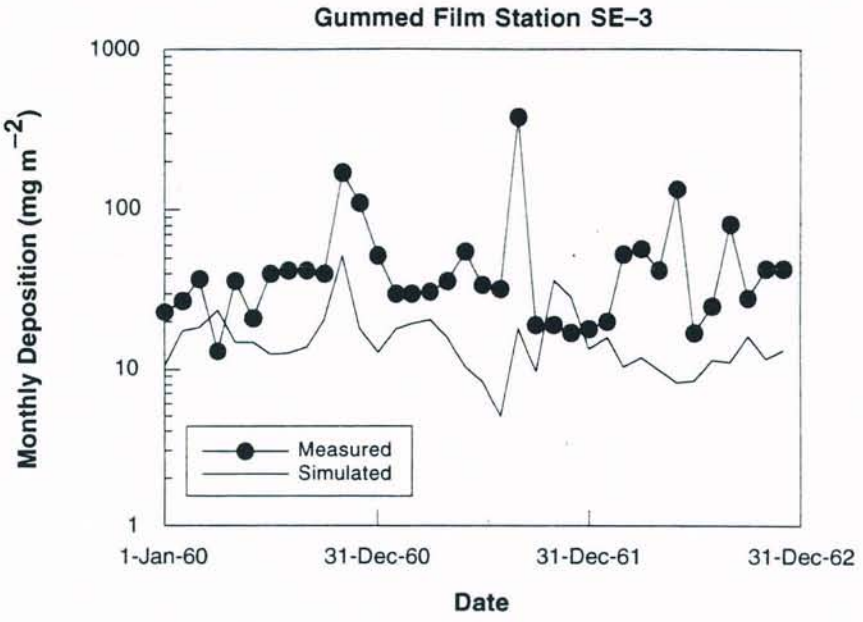

Figure M–15. Gummed film station SE–3. Distance from the center of the production area was 1606 m, and the direction was 147° from N.

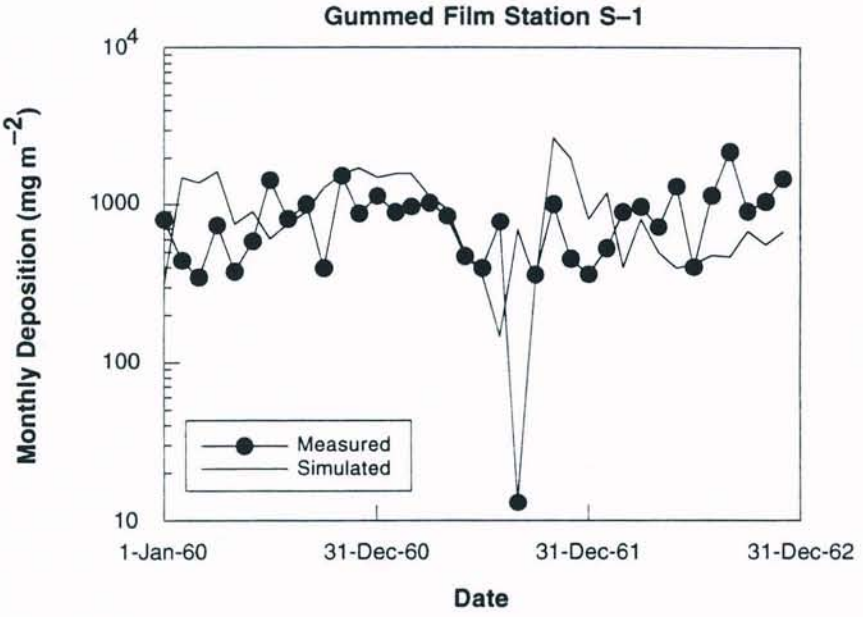

Figure M–16. Gummed film station S–1. Distance from the center of the production area was 246 m, and the direction was 178° from N.

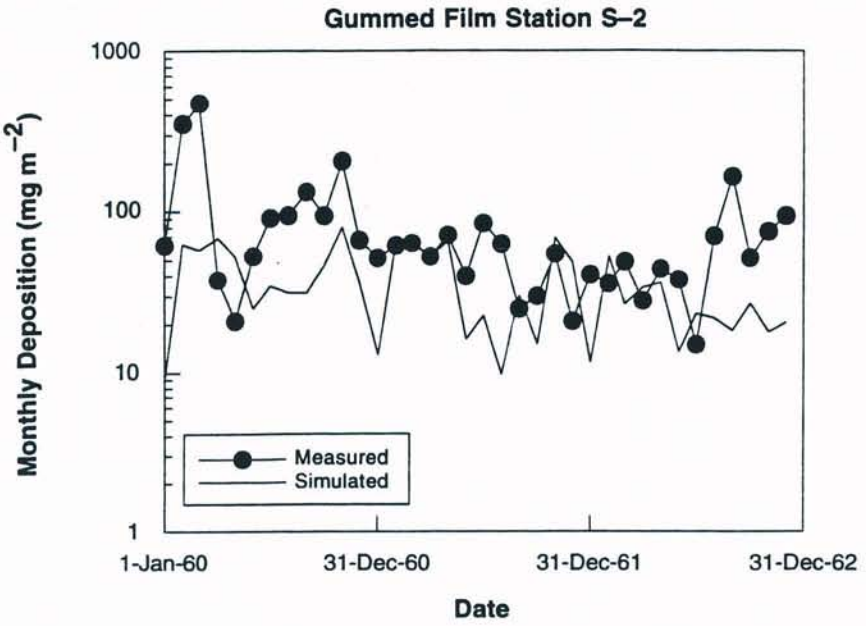

Figure M–17. Gummed film station S–2. Distance from the center of the production area was 874 m, and the direction was 191° from N.

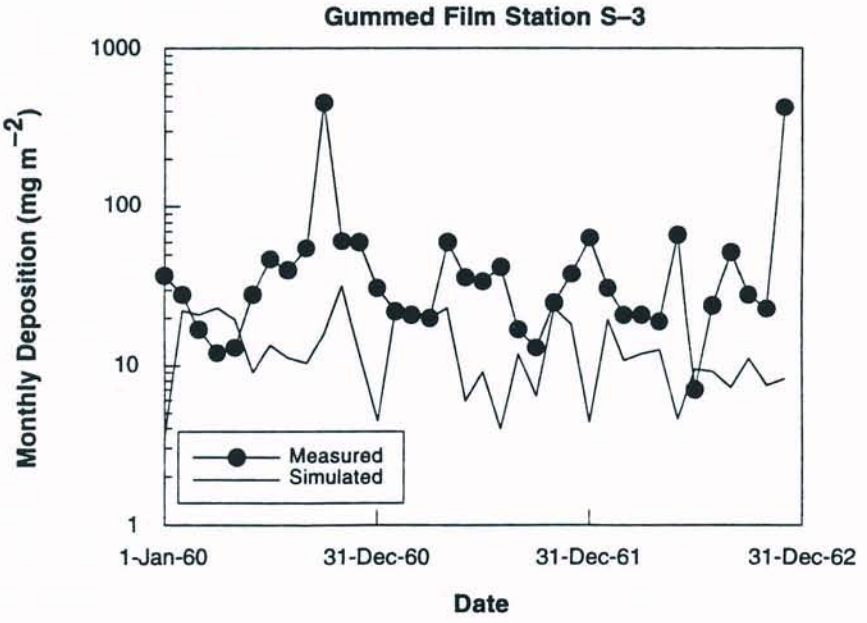

Figure M–18. Gummed film station S–3. Distance from the center of the production area was 1429 m, and the direction was 183° from N.

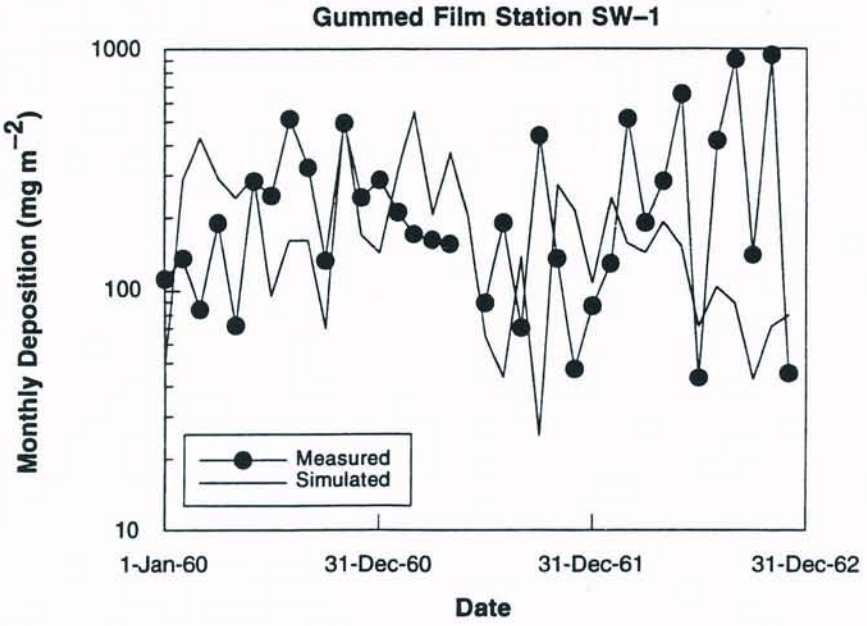

Figure M–19. Gummed film station SW–1. Distance from the center of the production area was 520 m, and the direction was 219° from N.

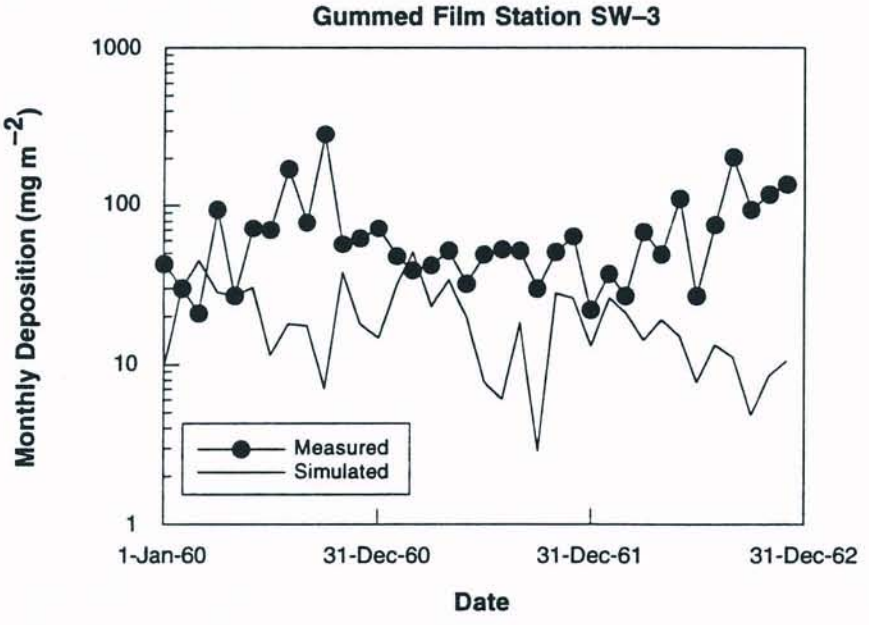

Figure M–20. Gummed film station SW–3. Distance from the center of the production area was 1223 m, and the direction was 224° from N.

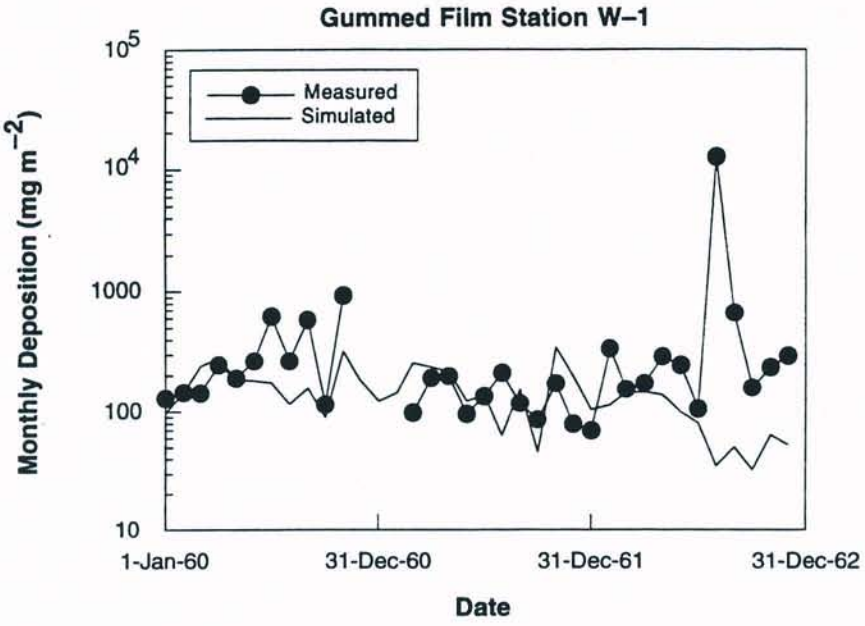

Figure M–21. Gummed film station W–1. Distance from the center of the production area was 326 m, and the direction was 262° from N.

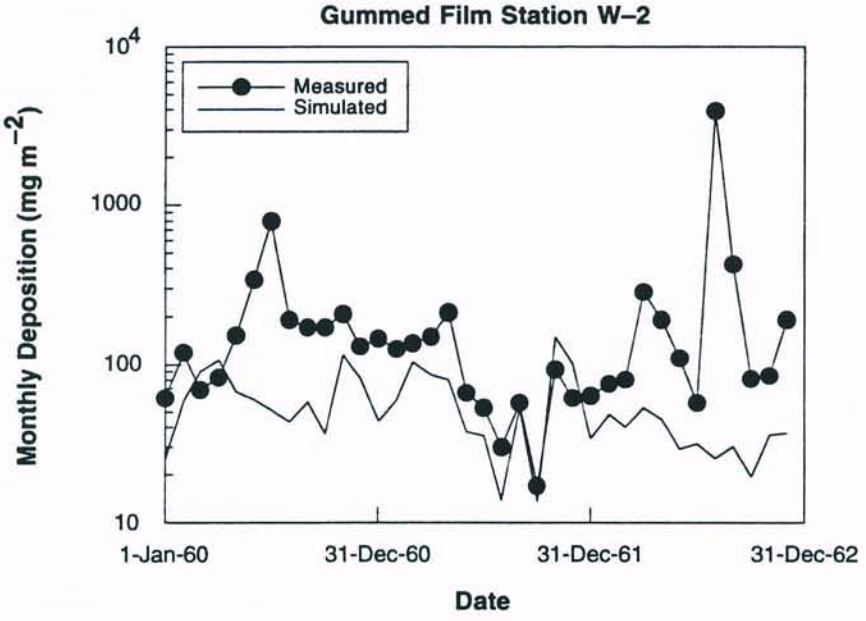

Figure M–22. Gummed film station W–2. Distance from the center of the production area was 623 m, and the direction was 260° from N.

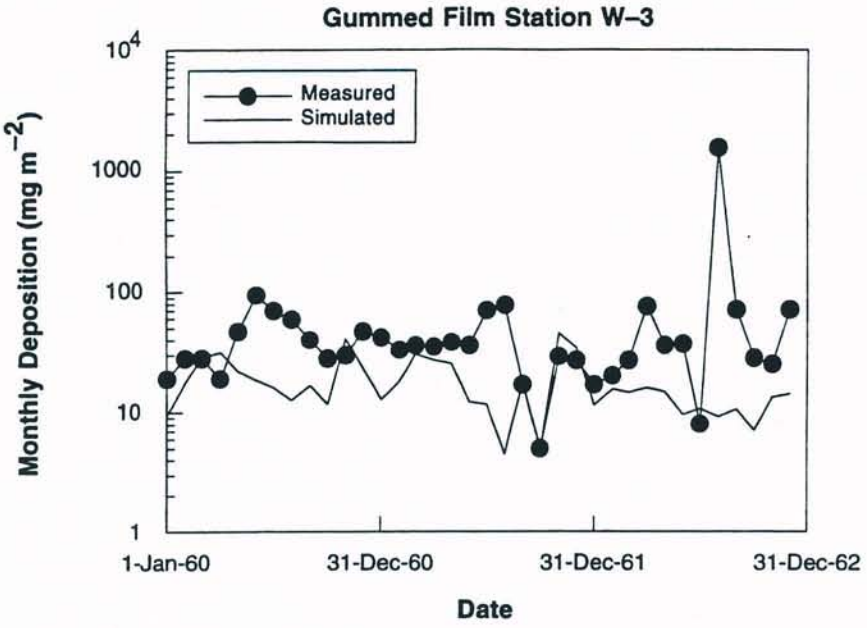

Figure M–23. Gummed film station W–3. Distance from the center of the production area was 1086 m, and the direction was 264° from N.

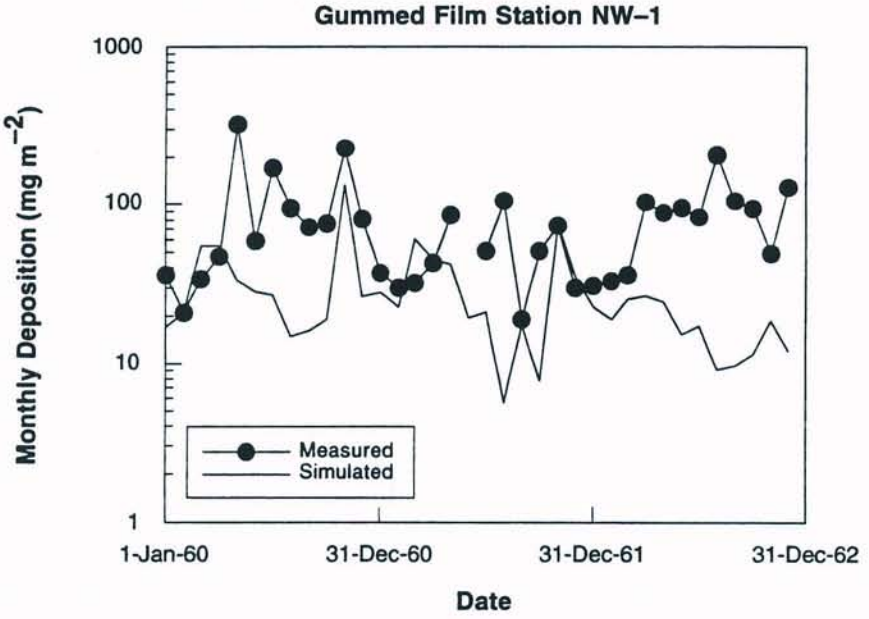

Figure M–24. Gummed film station NW–1. Distance from the center of the production area was 514 m, and the direction was 319° from N.

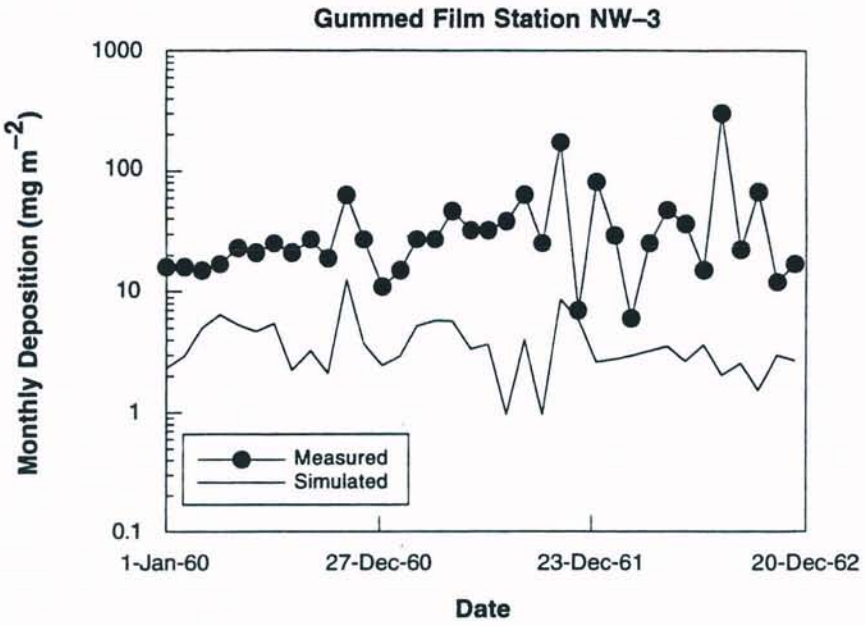

Figure M–25. Gummed film station NW–3. Distance from the center of the production area was 1623 m, and the direction was 304° from N.

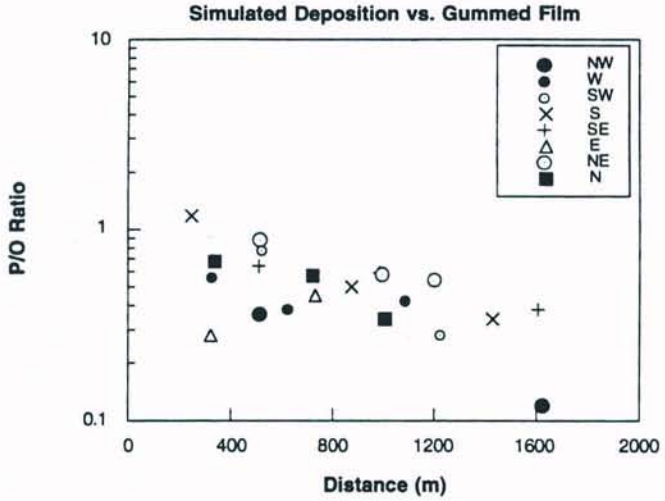

Figure M–26. Median predicted-to-observed ratios of monthly gummed-film measurements vs. distance from the site. There is a trend of increased underprediction of deposition with increasing distance, which may be due to some combination of an under-efficient deposition model and underprediction of air concentrations at greater distances. The station N–4 at distance 7,200 m was not plotted; its P/O ratio is 0.05.

Table M–6. Comparison of Simulated Deposition with Gummed Film Estimates

Station	Bias[a]	Correlation[b]
N-1	0.68	–0.08
N-2	0.57	–0.02
N-3	0.34	0.06
N-4	0.05	–0.25
NE-1	0.88	0.00
NE-2	0.58	0.05
NE-3	0.54	–0.11
NE-4	0.05	–0.33
E-1	0.28	0.12
E-2	0.45	–0.03
SE-1	0.64	–0.03
SE-2	0.59	0.11
SE-3	0.38	0.05
S-1	1.17	0.02
S-2	0.50	0.21
S-3	0.34	–0.15
SW-1	0.77	–0.03
SW-3	0.28	–0.27
W-1	0.56	–0.22
W-2	0.38	0.17
W-3	0.42	–0.05
NW-1	0.36	–0.08
NW-3	0.12	0.04

[a] Bias is defined here as the geometric mean of the predicted-to-observed ratios, with the mean taken over all (P,O) pairs for the 36-month period 1960–1962. Exact agreement would correspond to Bias = 1. Values <1 indicate underprediction.

[b] Correlation coefficients of the log-transformed predictions and observations.

APPENDIX N

SOIL DATA FOR LOCATIONS NEAR THE FMPC

INTRODUCTION

This appendix describes an approach to the interpretation of the variety of samples of uranium in soils near the FMPC that were available at the beginning of the study. Some samples had been taken at relatively few locations for much of the period of the plant's operation, some of which could be grouped as time series for particular locations. In the mid-1980s, considerable off-site soil sampling for uranium was undertaken over a wider area in the assessment domain of this study. These latter samples offer geographic extent but represent essentially a point in time. The challenge is to design an analysis that can make use of both spatial and temporal information and estimate critical parameters, including cumulative depostion of uranium over time in the area covered by the sampling. If we are prepared to make the assumption that nearly all of the uranium that was released to the atmosphere deposited within the assessment domain, then clearly an estimate of total cumulative deposition over the domain up to some specific time is an estimate of the total release up to that time.

Soil uranium may be employed to estimate or validate other estimates of uranium deposition if an adequate characterization of uranium concentration in soil over a specific time period exists. This quantity is referred to as the soil "inventory." Once the levels of uranium present in the soil at specific times are characterized by measurement, a model must be developed to describe the deposition of uranium on the soil and its removal over time by leaching and runoff. An important component of the model that we will describe is the soil-water partition coefficient K_d, which is related to the rate of removal of uranium from the soil by water, and conversely to the degree to which dissolved uranium becomes bound to the soil.

We estimated K_d by two methods. The first made use of observed inventories of uranium in the surface layer of the soil that had been taken at particular locations over a period of many years (time series) to estimate the rate of removal of uranium from the soil. The second method sought to estimate K_d directly from soil characteristics such as clay, organic content, and pH. The latter method is essentially derived from evaluations of K_d in the open literature. A third possible method, which has not been employed in this study, would attempt to determine K_d values for soil samples taken in the vicinity of the FMPC by a series of laboratory analyses.

METHODOLOGY

The Data Bases

We used six soil uranium data bases to obtain the information in this study. Table N–1 shows a list of these data bases and some information about each. The data were identified by sector, distance (within 1-km annuli, centered at the plant), year collected, type of

Table N–1. Soil Uranium Data Bases Used for Uranium Deposition Study

Database designation	Organization collecting	Date collected	Depth of stratum	Analysis	Results presented in
RI/FS[a]	IT Corp.	1988	0–2 in 2–4 in 4–6 in 0–6 in 6–12 in 12–18 in	U-238	Fig. N–3
SOIL-13	IT Corp.	1986	0–5 cm	Total U	Fig. N–2
FMPC	NLO NLO NLO/WMCO	1959 1965 1970–1988	 0–5 cm 5–10 cm	Total U	Figs. N–4 to N–10; Table N–2
ODH	Ohio Dept. of Health	1986	0–4 in	Total U	
EG&G	EG&G	1985		Total U U-238	
U of C	University of Cincinnati	1991		U-238	

[a] Remedial Investigation/Feasibility Study

analysis (total uranium or ^{238}U), the resultant value, number of samples represented by the value, and depth of the stratum sampled.

Initially, the data were organized into 16 sectors of 22.5° centered on the directions N, NNE, NE, etc. (the north sector was taken as the angular region $348.75° \leq \theta < 360°$ and $0° \leq \theta \leq 11.25°$). Coordinates in the data bases were either the Ohio State Plane or the UTM (Universal Transverse Mercator) system. All data were converted to UTM coordinates (with a margin of error of several meters). The coordinates for the FMPC Air Emission Center are shown in the following table:

	Ohio State Plane (ft)	UTM (m)
North	480,350	4,352,220
East	1,380,840	699,370
Deviation from North	1.5°W	1.4°E

Using Ohio State Plane or UTM coordinates, we arranged the data into sectors and specific distance intervals of 1 km.

Geographic Distribution, Time Sequence, and Stratification

Figure N–1 shows a layout of the plant property and the locations of the seven boundary stations where some of the time-series data were sampled. Figure N–2, based on the average

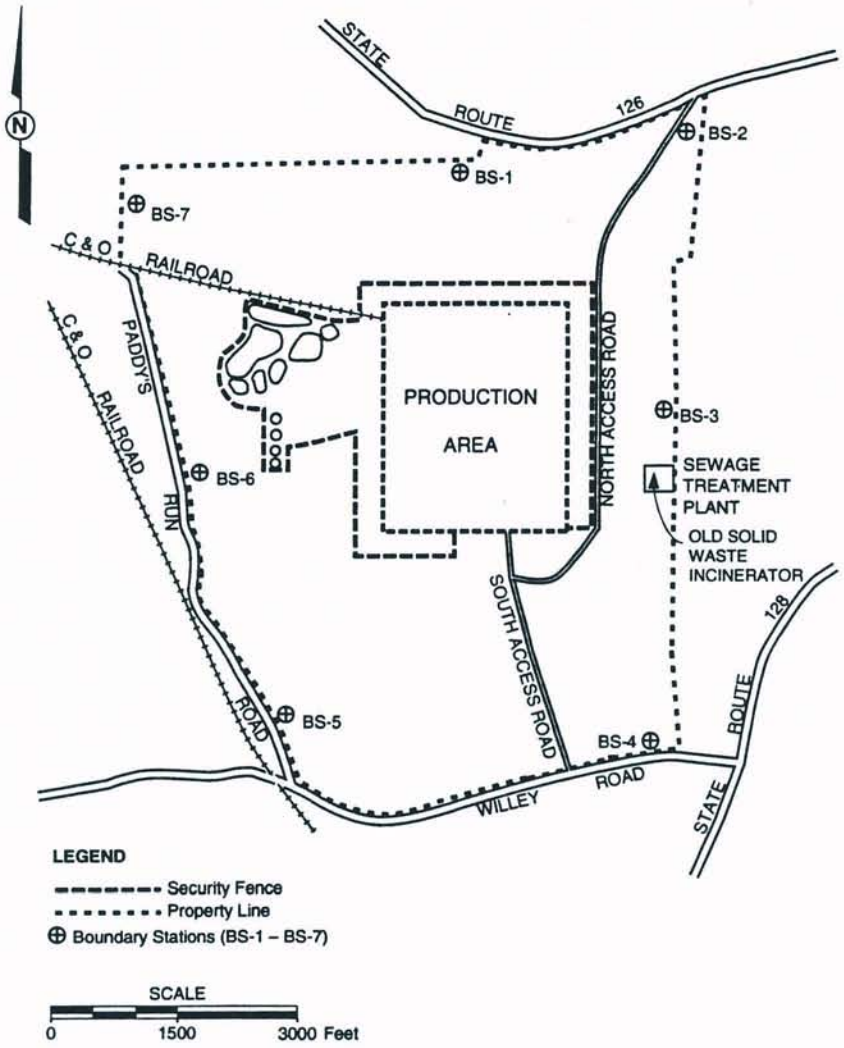

Figure N–1. FMPC Plant and property layout, showing the locations of the seven boundary stations BS-1 to BS-7.

results for "SOIL-13 1986 Total U," illustrates the geographic distribution of uranium in the soil. Of specific interest is evidence of uranium deposition in surface soil out to 6–7 km in the NNE and NE directions, directions toward which the prevailing winds blow. Closer to the plant itself is evidence of high uranium contamination (0–1 km, E, ESE, SSE, and NNW sectors) and to a lesser extent in the 1–2 km sectors corresponding to the S and NW directions.

These areas of high contamination near the plant could be due to spills of uranium-bearing materials or waste, or from airborne deposition. If they are the former, they need to be excluded from the total soil inventory used to estimate the airborne uranium source term; if they are the latter, they need to be included. Therefore, these areas merit closer inspection. Figure N–3 shows ^{238}U concentrations for 1989 in the immediate vicinity of the FMPC and some details of the site. The area immediately to the east is characterized by the presence of the old solid waste incinerator (OSWI) and was definitely a receptor of airborne uranium

	0–1	1–2	2–3	3–4	4–5	5–6	6–7	7–8	8–9	9–10
N		7.7		3.5	2.1	1.2	0.9	0.9	1.2	
NNE		7.3		4.4	1.8	2.3	2.1	1.3	1.1	
NE			2.3	1.7	1.1	1.3	2.2	1.3	0.8	
ENE			2.5	1.7	1.8	1.2	1.3	1.6		
E	59.1	3.7	1.7	2.5	2.0	1.8	1.2	1.1		
ESE	30.6	2.5	1.5	1.1	1.5	1.0	0.7	0.9	1.2	
SE		3.7		1.6	1.0	1.1	0.7	0.9	1.0	
SSE	25.1	3.5	1.5	1.1	1.0	0.9	1.2	1.1		
S		20.7	3.6	1.8	1.2	0.7	1.1	0.8	0.8	
SSW		4.2	0.8	1.5	0.9	1.4	1.3			
SW		6.5	5.0	1.3		1.0	1.0			
WSW			1.6	2.7	2.6	2.2	1.4	1.3	1.3	
W	6.3	8.5	0.6	2.0		0.8	1.1			
WNW										
NW		15.7		1.3	0.9	1.1	1.2	0.8	0.8	0.9
NNW	35.6	2.6	3.8	2.2	1.0	0.9	1.0	1.3	1.3	

Figure N–2. Schematic map of total uranium concentration (pCi g^{-1}) in SOIL-13 file by sector and 1-km distance increment. Concentration ranges are indicated by shading: 0–2 (none), 2–4 (light shaded area), and ≥4 (darker shaded area).

from that source. Extension of the ground contamination in a NE direction lends credence to this assumption. Contamination in the ESE and SSE are not in the direction of the prevailing winds. These areas are likely affected by ground contamination incidents and not by airborne deposition. The NNW contamination is associated with the onsite storage area of Plant 1, the sampling plant. A metal scrap area, the tank farm, and an unidentified source NE of Plant 9 (the special products plant) all show high levels of contamination. Except for the incinerator area, it appears reasonable to attribute levels of uranium in soil above about 100 pCi g^{-1} to causes other than airborne deposition.

Soil uranium concentrations from the early 1970s through 1988 were available at six of the seven FMPC boundary stations (see Figure N–1). The data collected at these stations over time are found in Table N–2. These data are employed later in this study as one method for determining the rate of removal of uranium from the soil.

Both surface data and stratified profiles (2 or 3 layers, with few exceptions) were used as input to one of the models presented in the next subsection.

Determination of K_d

As noted previously, the soil-water partition coefficient K_d (mL g^{-1}) can be estimated for a specified location from time series of uranium data in soil at that location, from the literature, or experimentally.

The time-series data at the boundary stations (Table N–2) were employed, together with a nonlinear regression procedure, to calculate a rate coefficient λ (y^{-1}) for removal of deposited uranium from the surface soil compartment. If such a rate coefficient can be obtained from regression on the uranium data, the value of K_d can be estimated from the rate coefficient. Conversely, given the value of K_d, an estimate of the removal rate coefficient λ can be calculated. The relationship between the two quantities is given by the equation

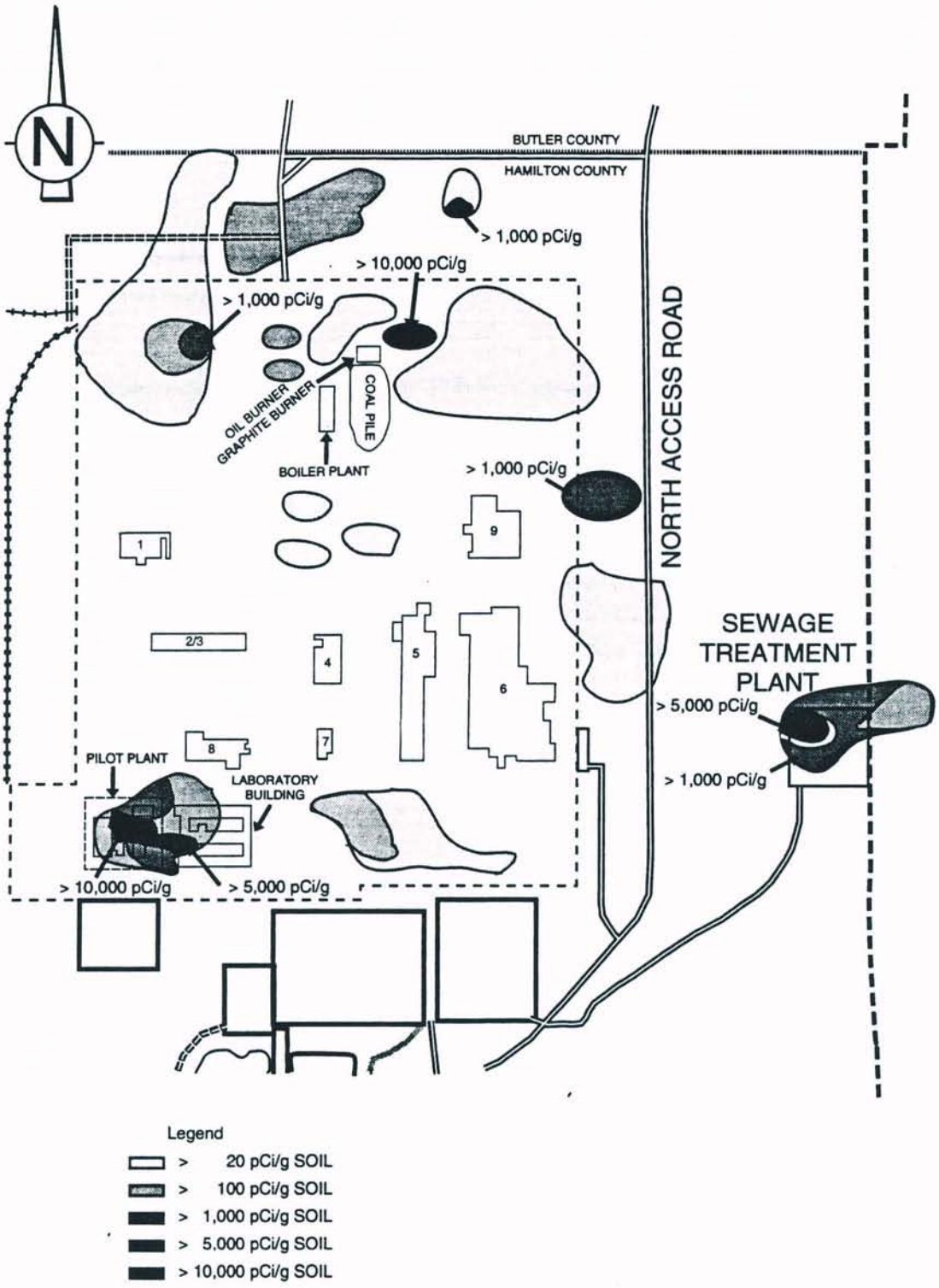

Figure N–3. Regions of higher radioactivity of uranium in the soil at the FMPC, based on plots from RI/FS measurements (Frazier 1990). The regions at the far right of the figure are associated with the old solid waste incinerator.

$$\lambda = \frac{R}{\Delta z(\theta + \rho K_d)} \quad \text{(N–1)}$$

where

R = water removal from the surface-soil compartment, taken to be the sum of infiltration and runoff (cm y^{-1}),
Δz = depth of surface layer (cm),
ρ = soil bulk density (taken as 1.6 g cm^{-3}),
K_d = soil-water partition coefficient for uranium (mL g^{-1})
θ = soil moisture content (assumed to be 0.1 mL cm^{-3}).

The regression depends on a simple one-box kinetic model given by the differential equation

$$\frac{dy}{dt} = -\lambda y + Mf(t) \quad \text{(N–2)}$$

where y denotes the mass (mg) of uranium in a surface-soil compartment one meter square by depth Δz. The source function $Mf(t)$ is the product of an undetermined multiplier M and a normalized function $f(t)$ whose shape is taken to represent the deposition of airborne uranium over time. By "normalized," we mean that that integral of $f(t)$ from 1951 to 1988 is 1. We have estimated the shape of this function by normalizing the annual estimates of release of uranium to the atmosphere between 1951 and 1988 from the Addendum to FMPC-2082 (Clark et al. 1989). The multiplier M, together with the removal coefficient λ, was determined by a nonlinear regression that incorporated the model of Eq. N–2.

It must be emphasized that this procedure does not assume the magnitude of deposition over time, but only its relative variation from year to year. The parameter M, which represents the total cumulative deposition per unit area at the location in question, comes from the regression, i.e., from the soil uranium data. Another point that must be emphasized is that this regression method requires time-series data, such as those shown in Table N–2 for the boundary stations. The procedure would not work if it were restricted to the spatially extensive data that were taken only in 1984 and 1986, for example.

The results of the regression just described are shown in Figs. N–4 through N–10. From the regression estimates of λ and by solving Eq. N–1 for K_d, we obtained the estimates of the soil-water partition coefficient for each boundary station (Table N–3). The K_d values for stations BS-1, BS-2, BS-5, and BS-6 average 17.5 mL g^{-1}, and the remaining stations are flagged because of special circumstances. BS-3 is near the old solid waste incinerator, and the data for BS-4 and BS-7 contained anomalous features. In the case of BS-4, the contrast of magnitudes between the 1959 observation and the data for all other years resulted in an anomalously high maximum and steep subsequent descent of the curve. An earlier regression that omitted the observations for 1959 and 1965 gave K_d = 18.3 mL g^{-1}. The data for BS-7 included no observations for the 1970s, and the curve appears to have been anomalously influenced by the relationship among the 1959, 1965, and remaining data points.

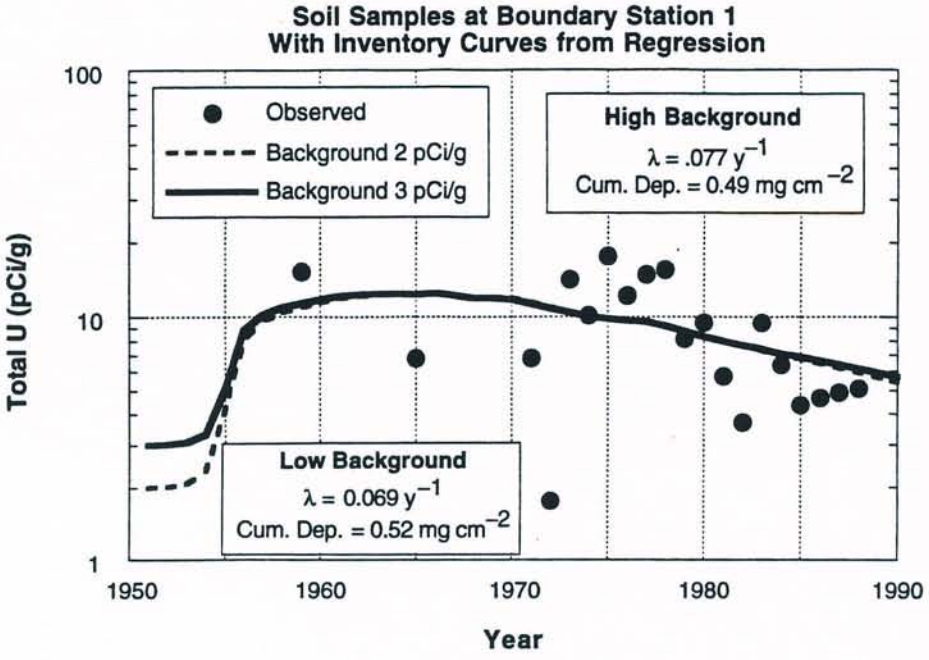

Figure N–4. Nonlinear regression curves for soil data taken at BS-1.

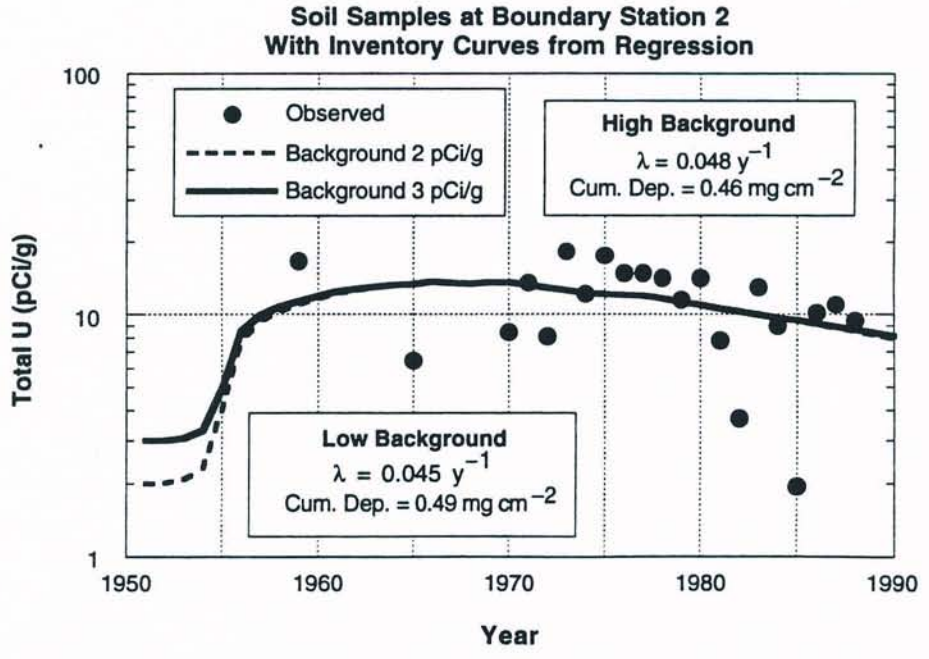

Figure N–5. Nonlinear regression curves for soil data taken at BS-2.

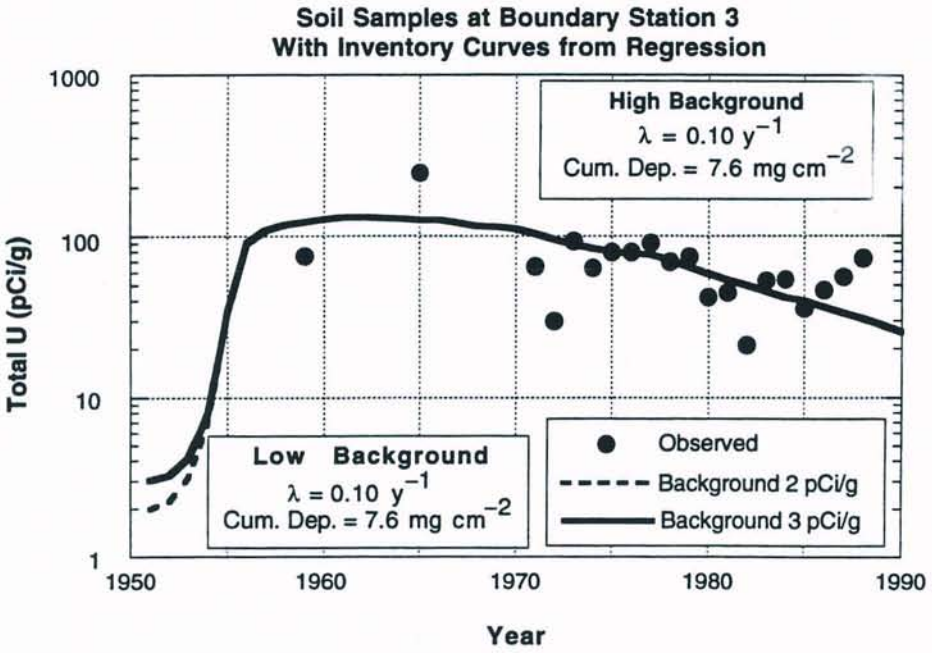

Figure N–6. Nonlinear regression curves for soil data taken as BS-3. This station is located near the old solid waste incinerator east of the production area.

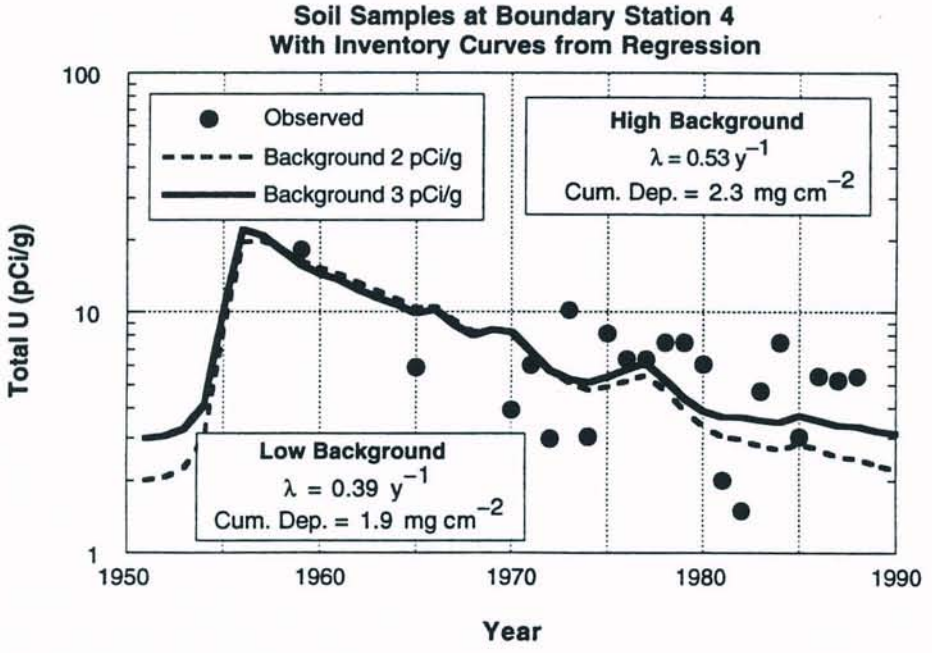

Figure N–7. Nonlinear regression curves for soil data taken at BS-4. The high value for 1959 appears anomalous in relation to the remaining data.

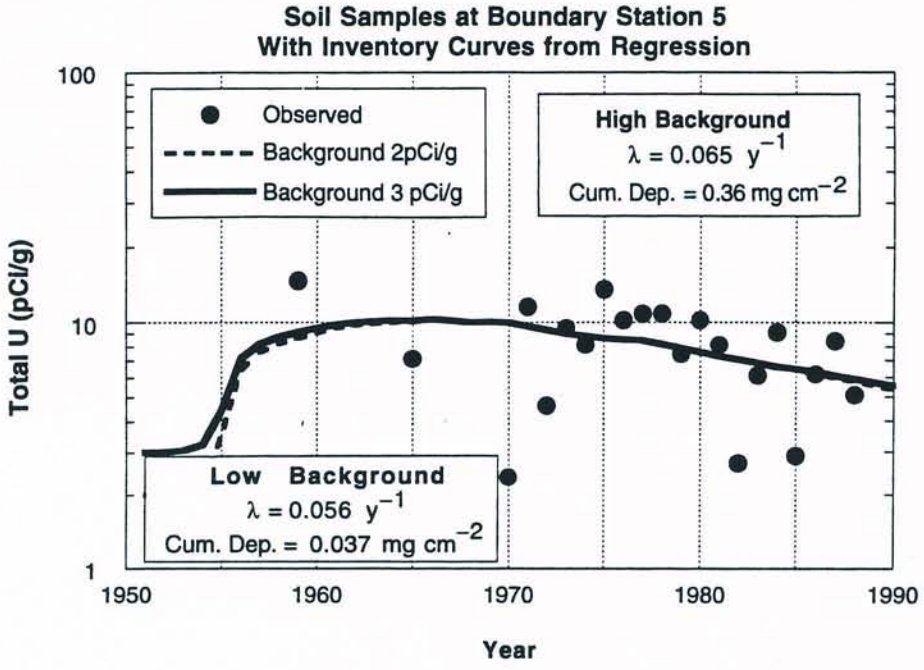

Figure N–8. Nonlinear regression curves for soil data taken at BS-5.

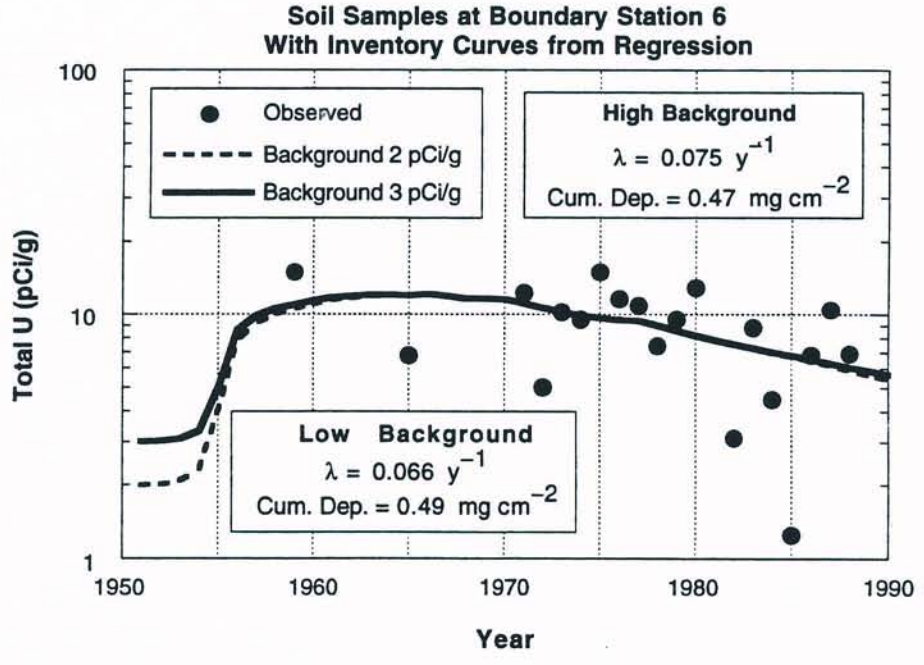

Figure N–9. Nonlinear regression curves for soil data taken at BS-6.

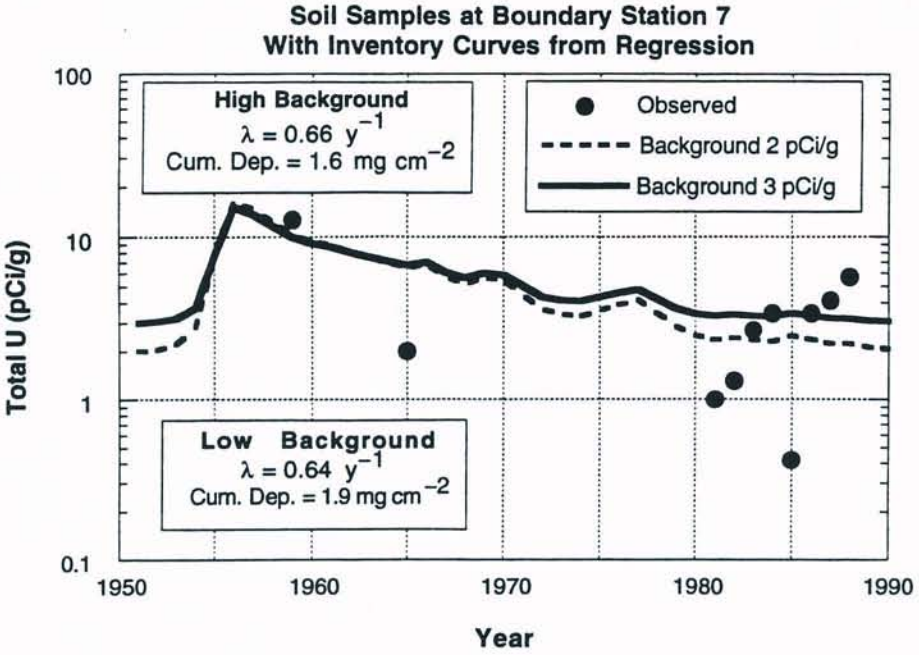

Figure N–10. Nonlinear regression curves for soil data taken at BS-7. The lack of data for the 1970s and the high value for 1959 contribute to a regression curve that is probably anomalous.

Table N–2. Total Uranium at Boundary Stations (pCi g^{-1} dry)
Depth 0–10 cm

	BS-1		BS-2		BS-3		BS-4		BS-5			BS-6		BS-7	
Year	FMPC	Soil 13	FMPC	Soil 13	FMPC	Soil 13	FMPC	Soil 13	FMPC	Soil 13	ODH	FMPC	Soil 13	FMPC	Soil 13
1959	15.2		17.0		75.3		18.1		14.6			14.9		12.7	
1965	6.8		6.4		245.0		5.9		7.1			6.8		2.0	
1970			8.5				3.9		2.4						
1971	6.8		13.5		65.0		6.0		11.5			12.2			
1972	1.8		8.1		29.8		3.0		4.6			5.0			
1973	14.2		18.3		92.8		10.2		9.5			10.2			
1974	10.2		12.2		63.6		3.1		8.1			9.5			
1975	17.6		17.6		79.2		8.1		13.5			14.9			
1976	12.2		14.9		79.2		6.4		10.2			11.5			
1977	14.9		14.9		90.0		6.4		10.8			10.8			
1978	15.6		14.2		69.1		7.5		10.8			7.5			
1979	8.1		11.5		74.5		7.5		7.5			9.5			
1980	9.5		14.2		42.0		6.1		10.2			12.9			
1981	5.7		7.8		45.0		2.0		8.1					1.0	
1982	3.7		3.7		21.0		1.5		2.7			3.1		1.3	
1983	9.5		13.0		53.0		4.7		6.1			8.8		2.7	
1984	6.4	8.2	9.0	7.2	54.2	16.6	7.5	5.4	9.1	11.2		4.5	4.1	3.4	8.1
1985	4.4		2.0		35.9		3.1		2.9			1.3		0.4	
1986	4.7	7.2	10.2	8.7	46.4	59.1	5.4	3.7	6.2		2.1	6.8	8.5	3.4	
1987	4.9		11.0		56.0		5.2		8.4			10.4		4.1	
1988	5.1		9.4		73.0		5.4		5.1			6.9		5.7	

The second approach employed was to search the literature for values of K_d for uranium in soils similar to those near the FMPC. Most of the information was relevant to geologic strata, rivers, or the marine environment. Only one set of data, the Multimedia Environmental Pollutant Assessment System (MEPAS), itself the result of an extensive literature review (Strenge and Peterson 1989), is applicable to surface soil. The MEPAS data for uranium isotopes, given in Table N–4, provide K_d values dependent on soil pH and composition.

County soil surveys for Butler and Hamilton Counties (Lerch et al. 1980; Lerch et al. 1982) provide the required information for use with the MEPAS data. Soil types were identified from these surveys at sixteen locations around the FMPC site. Table N–5 presents the locations of the sites, the soil types, and their characteristics. All of the pH values were between 5 and 9, with clay and organic matter between 10 and 30 percent. From the MEPAS values (Table N–4), 50 mL g^{-1} is the appropriate uranium K_d for these soil types.

Model for Estimation of Airborne Uranium Source Term

Values of the removal-rate coefficient λ having been determined by two methods, it is possible to develop a general model that can use these values and the total soil uranium data base to estimate total deposition of airborne uranium throughout the region surrounding the FMPC. This model has structural features in common with the earlier nonlinear regression model that was used to estimate the removal rate coefficient from the time-series soil uranium data at the boundary stations, but it is important to distinguish between the two. In the more general model, the removal rate coefficient λ is known in advance, whereas the regression model determines an estimate of λ. Both models make use of a normalized function $f(t)$ and determine a multiplier M such that $Mf(t)$ estimates deposition per unit area.

The general model works as follows. Given λ and the measured uranium mass Y (mg) in a square meter of surface soil, one solves the differential equation (Eq. N–2) with $M = 1$ to get $y(T)$, where T is the time the sample was taken, and one computes M from the equation

$$M = (Y - Y_b) / y(T) \qquad \text{(N–3)}$$

where Y_b is the background level of uranium in the compartment (mg).

As described previously, the region is divided into cells by using angular sectors and

Table N–3. Soil-Water Partition Coefficient K_d vs. Removal Coefficient λ

Boundary Station	Removal Coefficient (y^{-1})	K_d (mL g^{-1})	Other soil parameters	
BS-1	0.077	14.5	Depth Δz (cm)	10
BS-2	0.048	23.4	Bulk density (g cm^{-3})	1.6
BS-3	0.10	11.2 [b]	Moisture content (mL cm^{-3})	0.1
BS-4	0.53	2.1 [c]	Infiltration (cm y^{-1})	13[a]
BS-5	0.065	17.2	Runoff (cm y^{-1})	5[a]
BS-6	0.075	14.9		
BS-7	0.66	1.6 [c]		

[a] Infiltration and runoff parameters are from Voillequé et al. (1991).
[b] Near the old solid waste incinerator.
[c] Data questionable.

Table N–4 Values of Soil-Water Partition Coefficient K_d from MEPAS Data as a Function of pH and Soil Composition (mL g^{-1})[a,b]

	pH Range and Soil Composition								
	pH ≥ 9			pH 5–9			pH ≤ 5		
Isotope	<10%	10–30%	≥30%	<10%	10–30%	≥30%	<10%	10–30%	≥30%
U-233	0	5	50	0	50	500	0	5	50
U-234	0	5	50	0	50	500	0	5	50
U-235	0	5	50	0	50	500	0	5	50
U-236	0	5	50	0	50	500	0	5	50
U-238	0	5	50	0	50	500	0	5	50
U-239	0	5	50	0	50	500	0	5	50

[a] Excerpted from Table 4.1 of Strenge et al. (1989).

[b] Soil composition is percent by total weight of clay, organic matter, and iron and aluminum oxyhydroxides.

taking radial increments at intervals of 1 km. In each cell, for each observation Y, one computes the value of M as outlined above and then calculates cumulative deposition by integration of M times the normalized source function:

$$\text{Cumulative deposition} = M \quad \text{mg m}^{-2} \tag{N–4}$$

Note that in Eq. N–4 the cumulative deposition applies to the total period of the study (1951–1988); integration does not stop at the time T when the sample was taken. The cumulative deposition is then weighted by the number of sample points that went into calculating it, multiplied by the area of the cell, and accumulated into an average for the cell. Carrying out this procedure for all surface-soil data for each cell leads us to a table of deposition estimates — one for each cell — that can be summed to give an estimate of the total release. Of course, there may be cells with no data.

The approach summarized in Eqs. N–2, N–3, and N–4 works for surface-soil data but still does not provide a way of including soil-profile data. This is harder: it requires that Eq. N–2 be replaced by s system of differential equations. Consider the following system for N layers:

$$\frac{dy_1}{dt} = -(\lambda_1 + \lambda_{\text{roff}})y_1 + Mf(t) \tag{N–5}$$

$$\frac{dy_i}{dt} = -\lambda_i y_i + \lambda_{i-1} y_{i-1}, \quad i = 2, \ldots, N$$

where y_i is the uranium mass (mg) per m^2 in soil layer i, λ_{roff} is the removal-rate coefficient attributed to surface runoff, and λ_i is the removal-rate coefficient for material that moves from layer i to layer i+1. The procedure for estimating deposition at the location of the profile is the following:

1. Solve the system of Eq. N–5 with M = 1 to obtain $y_1(T), \ldots, y_N(T)$.
2. Compute

$$M_i = (Y_i - Y_b) / y_i(T), \quad i = 1, \ldots, N \tag{N–6}$$

3. Compute the N cumulative deposition estimates $\tilde{\omega}_i$ from the equation

$$\tilde{\omega}_i = M_i \quad \text{mg m}^{-2} \tag{N–7}$$

4. Multiply each $\tilde{\omega}_i$ by the area of the cell and by the number of samples that the measurement represents, and accumulate the products into the average for the cell.

This procedure uses the measurement from each layer to compute a separate estimate of deposition for the location of the profile. For a given profile, these estimates are not independent, because each is the result of solving the same coupled system of differential equations. The more nearly equal the N estimates of $\tilde{\omega}_i$ are, the more consistent are the measured data with the values of the λ_i and λ_{roff}. Perfect consistency, of course, is impossible, but intuition suggests that a fair degree of consistency is a desirable property for the calculation to possess. Working against such consistency are factors such as inhomogeneous soils, stratified horizontal movement of material, and different mechanisms contributing to the source function (e.g., a large spill superimposed on deposition from stack releases).

Estimating the Loss-Rate Coefficients

Equation N–1 characterizes the standard approach to estimating the rate coefficients for leaching of material from the soil. The approach is refined slightly for calculating the rate coefficients λ_i of Eq. N–5; this refinement is summarized by Eqs. N–8a and N–8b:

$$\lambda_i = \frac{R_q}{\Delta z_i(\theta + \rho K_d)} \quad y^{-1} \tag{N–8a}$$

where

R_q = net infiltration rate (cm y^{-1}) of water into the soil

Δz_i = vertical distance from top to bottom of layer i (cm)

θ = moisture content of soil (mL cm^{-3})

ρ = bulk density of soil (g cm^{-3})

K_d = soil-water partition coefficient (mL g^{-1}).

To account for surface runoff, the removal-rate coefficient for runoff, λ_{roff}, is defined as

$$\lambda_{\text{roff}} = \frac{R_r}{\Delta z_i(\theta + \rho K_d)} \quad y^{-1} \tag{N–8b}$$

where R_r = runoff rate from the surface layer (cm y^{-1}). For the calculations in this study, a value of 5 cm y^{-1} was used as the estimate of runoff (Voillequé et al. 1991).

It is important to note that in the formulation represented by Eqs. N–8a and N–8b, the parameters θ, ρ, and K_d do not vary from one soil layer to the next. In fact, in implementing the model, no allowance has been made for varying these parameters or the infiltration or the runoff from cell to cell. There is no logical reason that such variations cannot be accommodated, but it seems unlikely that sufficient information will be available to permit a credible calibration. Therefore, for now, soil parameters must be interpreted as representing average values for the entire region. The values of Δz_i are fixed by the depth of the sampled surface layer or the profile stratification at each sampling location.

Conversion from Radioactivity to Mass

Some of the data in the database measure total uranium; others measure ^{238}U. This dichotomy introduces a bit more tedium into the analysis.

The object is the calculation of the quantities $Y - Y_b$ in Eq. N–3 and $Y_i - Y_b$ in Eq. N–6. In each case, one is considering the mass of either total uranium or ^{238}U in a layer of soil (surface or subsurface) that is 1 meter square. Each quantity is the net mass (mg) above background. The data, however, are in activity concentration units (pCi g^{-1}), and the conversion depends on the isotopic interpretation. By convention, background is in terms of total uranium.

The specific activities and isotopic abundances for natural uranium are summarized in Table N–6. These data are used for converting the radioactivity concentration units (pCi g^{-1}) of the data to mass units for computation. The conversion factors are shown in the last row of Table N–6. They are based on the formula

Table N–5. Soil Characteristics Around the FMPC

			Surface				First subsurface			
Soil symbol	N	E	Depth (in)	Clay (%)	Soil reaction (pH)	Organic matter (%)	Depth (in)	Clay (%)	Soil reaction (pH)	Organic matter (%)
Ra	438350	1380600	0–12		6.1–7.3		12–15		6.1–7.3	
Butler – Ragsdale Silty Clay Loam										
XeB	48400	1383500	0–10		6.6–7.3		10–31		5.1–6.0	
Butler – Xenia silt loam										
FdA	481000	1383000	0–8	11–22	5.1–6.5	1–3	8–33	20–35	5.1–6.0	
Hamilton – Fincastle silt loam bedrock substratum										
XfB2	477250	1382600	0–9	11–22	6.6–7.3	1–3	9–26	27–35	5.1–6.0	
Hamilton – Xenia silt loam bedrock substratum										
McA	477500	1387700	0–9	8–17	5.6–7.3	1–3	9–34	18–30	5.1–6.0	
Hamilton – Martinsville silt loam										
MaB	480700	1377700	0–10	28–40	5.6–7.3	1–3	10–33	40–55	5.1–6.5	
Hamilton – Martinsville silt loam										
Gm	483600	1377100	0–8		6.1–7.8		8–34		6.1–8.4	
Butler – Genessee loam										
XeB	483100	1382900	0–10		6.6–7.3		10–31		5.6–6.0	
Butler – Genessee loam										
FeA	48200	1381800	0–8	11–12	5.1–6.5	1–3	8–33	20–35	5.1–6.0	
Hamilton – Fincastle										
EpB2	473300	1380000	0–7	15–25	5.6–7.3	1–3	7–36	35–48	5.6–7.8	
Hamilton – Eldean loam										
MaB	Off Grid		0–10	28–40	5.6–7.3	1–3	10–33	40–55	5.1–6.5	
Hamilton – Eldean loam										
RwB2	Off Grid		0–7		5.1–6.0		7–22		5.1–5.5	
Butler – Russell silt loam										
EuA	Off Grid		0–6		5.6–7.3		6–26		5.6–7.8	
Butler – Eldean loam										
EuA	Off Grid		0–6		5.6–7.3		6–26		5.6–7.8	
Butler – Eldean loam										
RtC	Off Grid		0–12	13–27	4.5–7.3	1–3	12–26	22–35	4.5–5.5	
Hamilton – Rossmoyre										
Gm	Off Grid		0–9	18–27	6.1–7.8	1–3	9–35	18–27	6.1–8.4	
Hamilton – Rossmoyre										

Table N–6. Activity-to-Mass Conversion of Natural Uranium and ^{238}U

		Natural uranium		U-238	
Isotope	Specific activity (Bq g^{-1} iso.)	Fractional abundance[a]	Bq (g U)$^{-1}$	Fractional abundance	Bq (g U)$^{-1}$ (r = 1)
U-234	2.3×10^8	0.000054	1.2×10^4	—	
U-235	8.0×10^4	0.0072	5.7×10^2	—	
U-238	1.2×10^4	0.99275	1.2×10^4	1.0	1.2×10^4
Total			2.5×10^4		1.2×10^4
Conversion (mg pCi^{-1})			1.5×10^{-3}		3.0×10^{-3}

[a] Based on data in a memorandum from Paul Voillequé dated March 10, 1991.

$$CF = \frac{3.7 \times 10^{-2}\ \text{Bq pCi}^{-1}}{\sum_i (SA)_i f_i\ \text{Bq g}^{-1} \times 10^{-3}\ \text{g mg}^{-1}}\ \text{mg pCi}^{-1} \qquad \text{(N–9)}$$

where the summation in the denominator represents the sum of the products of intrinsic specific activities $(SA)_i$ and fractional mass abundances (columns 2 and 3 of Table N–6).

Coding the Database for Input to the Program

The computer program that performs these calculations, which goes by the working name SOILCAL3, recognizes two categories of sample: surface soil only (code S) and profile (P). Each S entry requires a single line, which includes the code letter. A profile of N layers requires N lines of input, one for each layer, and these lines must be in the same order as the layers, top to bottom. The first line of a profile carries the code letter P and a number between 2 and 9 inclusive to indicate the number of layers. Each of the subsequent N–1 lines must contain the code letter L to indicate that it represents a subsurface layer.

To convert the data expressed in pCi g^{-1} to a mass (mg) of uranium in a soil layer, one may use the conversion factor CF of Eq. N–9 in the formula

$$Y - Y_b = (C - C_b \cdot r) \cdot CF \cdot \rho \cdot 10^6 \cdot \frac{\Delta z}{100} \qquad \text{(N–10)}$$

where C and C_b are the measured and background activity concentrations of uranium in the soil, r is the uranium isotopic activity ratio in the sample (r = 1 if C is the concentration of total uranium, and r = 0.5 was used for ^{238}U), ρ is the bulk density of the soil (g cm^{-3}), 10^6 is cm^3 per m^3, and $\Delta z/100$ is the distance (m) from the top to the bottom of the soil layer.

The eight fields in each line of the file may be summarized as follows:

Sector — An alphabetic code (N, NNE, NE, etc.) indicating one of 16 directional sectors, each of 22.5°, within which the sample was taken. These must agree for all layers of a profile sample.

Code — A letter code (S, P, L) indicating the type of sample the line represents. In case of code P (the first layer of a profile), the letter must be followed immediately with a number (2–9) indicating the number of layers in the profile (e.g., P3); no spaces may intervene. For subsurface layers of a profile, the code L may optionally be followed by a digit that indicates which layer it is (this digit is ignored by the program, however).

Annulus — This field indicates by a numeric code the radial distance interval from the center into which the sample location falls: 0–1,000 m, code 0; 1,000–2,000 m, code 1, etc.

Year — The calendar year in which the sample was taken. This may include a decimal fraction (e.g., 1985.25) to indicate the time more accurately, but the current data file does not incorporate this refinement.

Isotope — This field must contain either "TOT" or "238" to indicate, respectively, that total uranium or the isotope ^{238}U was measured.

pCi/g — The measured soil concentration of total uranium or ^{238}U, as the case may be, expressed in those units. This may be a single sample or an average of multiple samples.

Number — The number of samples summarized by the previous field. This value is used to weight the averages for the various cells.

Depth (cm) — The distance (cm) from the top to the bottom of the soil layer represented by the sample.

The fields are separated by tab characters, and identifying comments (introduced by a tab after the eighth field) may be inserted.

RESULTS AND DISCUSSION

Estimated Airborne Uranium Source Terms

The deposition function used in this study has the shape (but not the magnitude) of the airborne source term estimated by Clark et al. (1989). This normalized function provides a surrogate shape for the deposition rate at each sample point, with the magnitude being determined from the data and the removal rate coefficient calculated from the assumed value of the soil-water partition coefficient K_d.

Earlier, we concluded that with the exception of the old solid waste incinerator, areas of high contamination were not likely to be due to an airborne source. Therefore, except for the effect of the incinerator, we excluded all total uranium values (or ^{238}U equivalent) above 100

Table N–7. Estimated Total Cumulative Deposition (1951–1988) vs. Soil-Water Partition Coefficient K_d

K_d (mL g^{-1})	Deposition (kg U)	Sum of squares
1	6.01×10^7	3.3×10^{14}
10	1.98×10^6	1.1×10^{12}
15	8.91×10^5	3.2×10^{11}
25	3.68×10^5	4.4×10^{10}
50	1.67×10^5	2.3×10^9
100	1.10×10^5	2.6×10^8
500	6.88×10^4	1.4×10^9

Table N–8. Estimated Deposition of Airborne Uranium For Various Cutoffs and K_d Values

Cutoff ≥ pCi g^{-1}	K_d=50 mL g^{-1}	K_d=15 mL g^{-1}	Number of samples
20	1.42×10^5	7.71×10^5	846
100	1.67×10^5	8.91×10^5	906
300	1.92×10^5	9.47×10^5	913
1000	2.11×10^5	1.01×10^6	914

pCi g^{-1} from the input to the computational model (906 data points were processed on the basis of this constraint). The program processed samples of two types: surface soil only and profiles consisting generally of two or three strata. Table N–7 presents the estimates of the total uranium deposition from airborne releases (estimated as the total of the estimated deposition in all cells of the polar grid described earlier) for different K_d values.

The "Sum of squares" column in Table N–7 requires some explanation. When profile data are included in the analysis, Eqs. N–5 through N–7 are used to compute a deposition estimate from the data of each layer (stratum). When the resulting predicted concentrations for all of the layers are computed, they may or may not be consistent with the relative measured concentrations. If the consistency were perfect, the estimated depositions would be the same for all layers. In general, they are not. But in some cases, the discrepancies are greater than for others. We have used the following sum of squares as a measure of the discrepancy:

$$S = \sum_{i=1}^{N} (D_i - \overline{D})^2 \qquad \text{(N–11)}$$

where D_i is the estimate of deposition based on the data in layer i, and $\overline{D}$ is the average of these estimates of deposition over all of the layers. A total of these sums of squares is accumulated over all profiles in the data base. The reader is cautioned that the absolute significance of this measure is unclear, and that it probably is useful only in a comparative sense.

Varying K_d has a profound effect on the magnitude of the estimated total cumulative deposition A K_d of 15 mL g^{-1} is internally consistent with other data obtained during the course of this project, namely the regression based on the time-series data at four of the seven FMPC boundary stations. The resultant total cumulative deposition for airborne uranium is about three times the total release estimated by Clark et al. (1989). A similar ratio between the source term estimate of this project for the years 1960, 1961, and 1962 and the that of Clark et al. (1989) for the same three years was noted in the Task 2 and 3 report (Voillequé et al. 1991).

Table N–8 illustrates the effect of various cutoff levels for total uranium sample values on the estimate of the total cumulative deposition. For illustrative purposes, and because the K_d data were obtained either from this study or from the literature, we employed K_d values of 15 and 50 mL g^{-1}. Changing the cutoff level had a negligible effect compared to that of varying K_d.

Table N–9. Estimates of Total Deposition of Airborne Uranium, Adjusted for Levels of Non-Airborne Contamination Associated With the Old Solid Waste Incinerator

K_d (mL g^{-1})	Deposition (kg)
15	8.96×10^5
50	1.68×10^5

Contribution of Incinerator to the Airborne Uranium Source Term

With the same model described above (working name SOILCAL3) and K_d values of 15 and 50 mL g^{-1}, the entries in the uranium soil data base that were attributed to deposition from the incinerator were processed without cutoff for the quadrant consisting of the sectors E, ESE, SE, and SSE and for distances less than 1 km from the emission center. The respective estimates of deposition over the region were 4.4×10^7 and 1.2×10^7 kg. To correct for the approximate area contaminated by the incinerator, these numbers were adjusted by the ratio of that area (estimated to be 93 m^2) to that for the entire quadrant (7.85×10^5 m^2). The estimates of the possible additions to total deposition by the incinerator-related contamination are 5,200 and 1,400 kg of uranium for K_d values of 15 and 50 mL g^{-1}, respectively. Adding these estimates to the corresponding estimates of total deposition from Table N–7 gives the adjusted estimates shown in Table N–9. The effect for the sector as a whole is seen to be minor.

It is of interest to compare the values in Table N–9 with other estimates. The value corresponding to K_d = 50 mL g^{-1} underestimates the 178,000-kg source term given by Clark et al. (1989) by only about 11,000 kg (7%) and thus may be considered comparable to the earlier estimate. And the value corresponding to K_d = 15 mL g^{-1} exceeds the estimate of Clark et al. (1989) by a factor of five.

The Institute for Energy and Environmental Research (IEER) estimated an airborne uranium source term of 273,000 to 1,400,000 kg, the upper range of which is considerably higher than the total cumulative deposition estimate in Table N–7 that corresponds to K_d = 15 mL g^{-1} (Makhijani 1988; Makhijani 1989). The methodology of the IEER was previously reviewed (Shleien 1991). Although the IEER discussion left some uncertainty about the assumptions and procedure, the results obtained did not appear to contain an adjustment to account for uranium contamination by mechanisms other than deposition from airborne releases. Thus, it is difficult to compare their results to those of the present study.

We conclude that although the use of a K_d value from the literature leads to an estimate of total cumulative deposition and thus of the airborne source term that is approximately equal to the one given in the Addendum to FMPC-2082 (Clark et al. 1989), the higher estimate, which resulted from the use of a K_d that was derived from a subset of the uranium-in-soils data base of the present study, carries greater weight (both figuratively and literally). We caution, however, that there are factors that could introduce some degree of bias into both results:

1. The application of a single K_d and other soil parameters uniformly to a wide area may cause some distortion.
2. The possibility of substantial variation of K_d with depth in the soils has not been taken into account in the profile calculations.
3. We believe the use of the normalized airborne uranium source term from FMPC-2082 (Clark et al. 1989) is entirely reasonable for the long-term calculations described in this report. Nevertheless, it should be mentioned as a possible source of distortion.

On the basis of the work in this study, we believe the range 1.68×10^5 to 8.96×10^5 kg is likely to contain the true value of the quantity of uranium released to the air from the FMPC from 1951 through 1988 that was deposited within the assessment domain. We are more confident of values falling toward the upper end of this range because of the correspondence of these larger values to K_d values determined from time-series data taken from the data base of this study.

REFERENCES

Clark T.R., Elikan L., Hill C.A., and Speicher B.L. 1989. *History of FMPC Radionuclide Discharges: Revised Estimates of Uranium and Thorium Air Emissions from 1951–1987.* Rep. Addendum to FMPC-2082, Westinghouse Materials Company of Ohio.

Frazier J.R. 1990. Untitled letter to G.G. Killough, dated October 5, with enclosures that included maps of soil samples of uranium isotopes and other radionuclides.

Lerch N.K., Hale W.F., and Lemaster D.D. 1980. Soil Survey of Butler County, Ohio. U.S. Department of Agriculture Soil Conservation Service. Available from Butler Soil and Water Conservation District, 1810 Princeton Road, Hamilton, Ohio 45011.

Lerch N.K., Hale W.F., and Lemaster D.D. 1982. Soil Survey of Hamilton County, Ohio. U.S. Department of Agriculture Soil Conservation Service. Available from Hamilton County Soil and Water Conservation District, 20 Triangle Park Drive, Suite 2901, Cincinnati, Ohio 45246.

Makhijani A. 1988. *Release Estimates of Radioactive and Nonradioactive Materials to the Environment by the Feed Materials Production Center 1951–1985.* Institute for Energy and Environmental Research, Tacoma Park, Maryland.

Makhijani A. 1989. *Addendum to Release Estimates of Radioactive and Nonradioactive Materials to the Environment by the Feed Materials Production Center 1951–1985.* Institute for Energy and Environmental Research, Tacoma Park, Maryland.

Shleien B. 1991. Summary and Analysis of Previous Studies Applicable to Dose Reconstruction at the Feed Materials Production Center. SCINTA, Inc., Silver Spring, Maryland.

Strenge D.L. and Peterson S.R. 1989. Chemical Data Bases for the Multimedia Environmental Pollutant Assessment System (MEPAS): Version 1. PNL-7145, Pacific Northwest Laboratory, Richland, Washington.

Voillequé P.G., Meyer K.R., Schmidt D.W., Killough G.G., Moore R.E., Ichimura V.I., Rope S.K., Shleien B., and Till J.E. 1991. *The Fernald Dosimetry Reconstruction Project. Tasks 2 and 3: Radionuclide Source Terms and Uncertainties — 1960–1962.* Draft Interim Report for Comment. Radiological Assessments Corporation, Neeses, S.C.

APPENDIX O

RESUSPENSION OF PARTICULATES

INTRODUCTION

Airborne releases of uranium from the FMPC are eventually deposited on the ground surface through gravitational settling and wet and dry deposition processes. One subsequent transport process for this deposited material is RESUSPENSION, which refers to the reentry of previously deposited particles into the air. There are a number of approaches to estimating the magnitude of resuspension — Healy (1980) groups them into three basic types: (1) resuspension factor approach (2) resuspension rate approach and (3) mass loading approach. The mass loading approach was chosen for use in the reconstruction of pathways for airborne releases from the FMPC.

The mass loading concept is attractive for this purpose because of its empirical nature and its lack of dependence on detailed knowledge of soil characteristics and the resuspension process. Two parameters, the mass loading of dust in surface air (ML, in g soil m^{-3} air) and the concentration of the contaminant in the surface layer of soil (C_s, in Ci g^{-1} soil), are needed to provide an estimate of the air concentration of the contaminant (C_a, in Ci m^{-3} air), which is due to resuspension. That is:

$$C_a = C_s \times ML \qquad (O\text{–}1)$$

For the FMPC Dose Reconstruction, the environmental transport model is providing estimates of the uranium concentrations in surface soil (C_s) over time. This appendix examines the available data for the other variable in equation O–1 — mass loading in air (ML).

EXAMINATION OF SITE-SPECIFIC MASS LOADING DATA

In order to characterize the variations in particulate concentrations in air around the Fernald facility, we thoroughly examined weekly measurements for three years (1989–1991), which were readily available in electronic spreadsheet format from Westinghouse Environmental Management Company of Ohio (Byrne 1992). These spreadsheets contained a copy of the Radiological Environmental Monitoring data files, and represented raw data (data were in no way censored). The particulates were collected by 8 × 10 inch Whatman EPM-2000 glass fiber filters in high-volume air samplers, which were located within 6 km (4 mi) of the production center (Figure O–1). The distant air monitoring stations in Cincinnati were excluded from our analysis, because they may not be representative of resuspension within the area of greatest uranium deposition. The analytical and sample collection procedures are described by Grant (1992) and Kraps (1991), respectively.

For each week and location, we computed the μg particulate m^{-3} air from the measured total suspended particulate per sample and the volume of air sampled. Data for all locations were pooled into a monthly grand average and standard deviation. The monthly time scale was chosen to be consistent with that being used for the source term reconstruction. Tables O–1, O–2, and O–3 present the monthly averages and standard deviations for 1991, 1990, and 1989, respectively, and Table O–4 presents the 3–yr average and uncertainty.

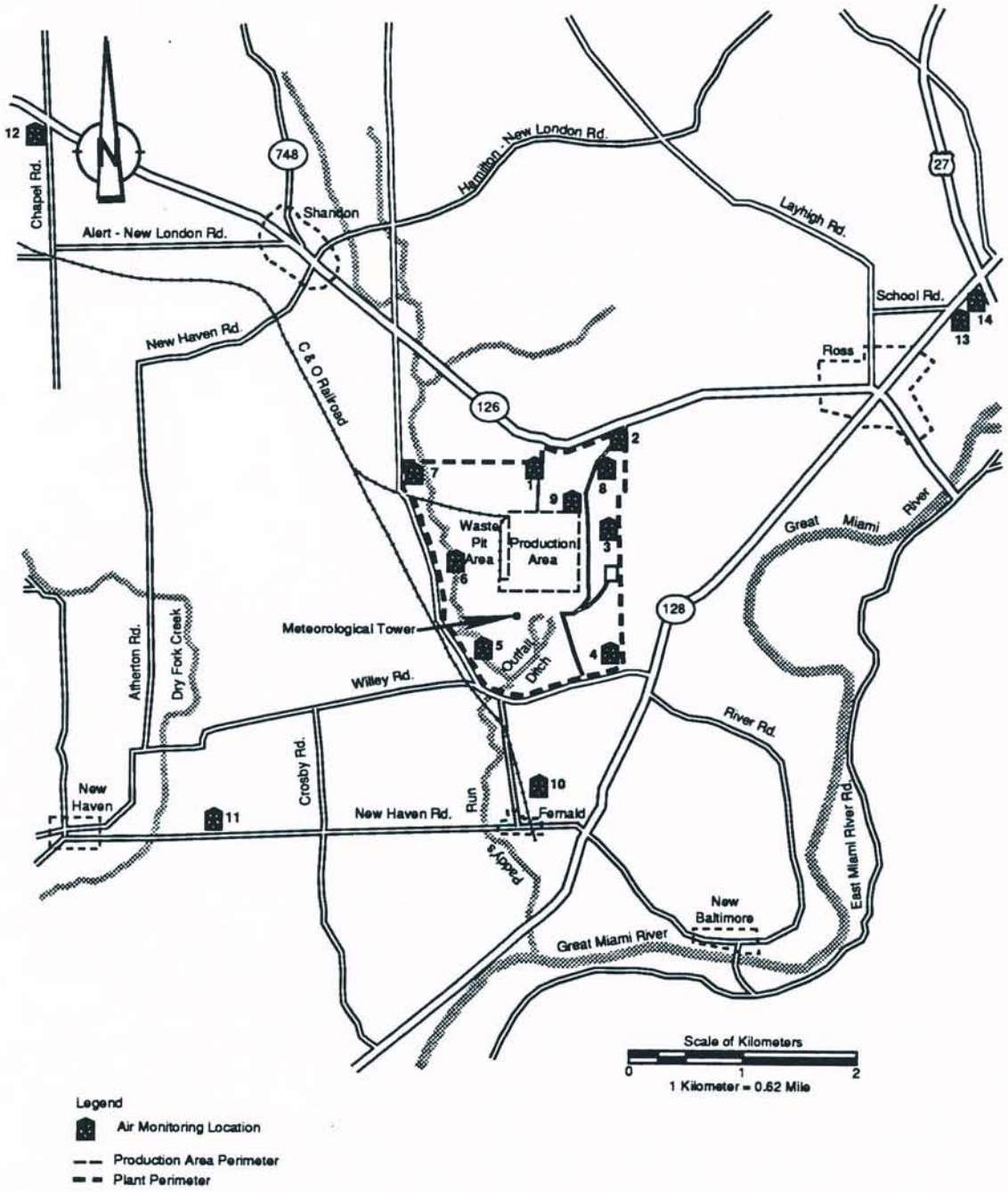

Figure O–1. Locations of high volume air samplers.

Table O–1. Total Suspended Particulates in Air (μg m^{-3}) Surrounding the FMPC in 1991[a]

Month	Number of Measurements	Average	Standard Deviation	Notes
January	56	25.4	5.7	
February	56	26.8	10.7	
March	55	23.6	4.0	
April	56	25.0	7.5	One week missing.
May	55	43.6	7.6	One outlier deleted.[b]
June	56	50.8	16	
July	69	44.8	15.1	One missing datum.
August	56	41.1	9.1	
September	56	45.4	19.6	
October	70	37.0	8.1	
November	56	33.2	12.1	
December	70	22.9	9.2	
All	711	35.1	14.7	

[a]Calculated from weekly measurements from high volume air samplers numbered 1–14 (Figure O–1) in the spreadsheet "1991.wk1" from Byrne (1992).
[b]Sampler only operated for two hours that week.

Table O–2. Total Suspended Particulates in Air (μg m^{-3}) Surrounding the FMPC in 1990[a]

Month	Number of Measurements	Average	Standard Deviation
January	45	25.6	7.8
February	36	21.3	3.1
March	36	26.5	7.1
April	36	23.0	4.1
May	45	32.9	8.6
June	36	34.6	11.4
July	45	38.8	8.9
August	36	41.4	4.0
September	36	33.5	9.7
October	45	27.6	7.2
November	36	31.1	8.1
December	36	22.2	6.3
All	468	30.0	9.8

[a]Calculated from weekly measurements from high volume air samplers 1–9 (Figure O–1) from the spreadsheet "ONAIR" received from Byrne (1992).

Table O–3. Total Suspended Particulates in Air (μg m^{-3}) Surrounding the FMPC in 1989[a]

Month	Number of Measurements	Average	Standard Deviation	Notes
January	45	27.7	6.1	
February	36	30.0	5.0	
March	36	43.4	14.6	
April	36	27.5	10.3	
May	45	35.0	6.2	
June	36	46.4	16.8	
July	36	41.5	10.8	
August	45	43.5	9.9	
September	36	32.0	6.9	
October	45	34.0	13.8	
November	36	25.4	6.4	
December	35	39.3	12.7	One outlier deleted.[b]
All	467	35.4	12.6	

[a]Calculated from weekly measurements from high volume air samplers 1–9 (Figure O–1) in the spreadsheet "89ONAIR" received from Byrne (1992).
[b]Sampler operated only one hour that week.

Table O–4. Summary of Total Suspended Particulates in Air (μg m^{-3}) Surrounding the FMPC by Month, 1989–1991

Month	1989	1990	1991	3–yr Average	Standard Error
January	27.7	25.6	25.4	26.2	0.7
February	30.0	21.3	26.8	26.0	2.5
March	43.5	26.5	23.6	31.2	6.2
April	27.5	23.0	25.0	25.2	1.3
May	35.0	32.9	43.6	37.2	3.3
June	46.4	34.6	50.8	43.9	4.8
July	41.5	38.8	44.8	41.7	1.7
August	43.5	41.4	41.1	42.0	0.8
September	32.0	33.5	45.4	37.0	4.2
October	34.0	27.6	37.0	32.9	2.8
November	25.4	31.1	33.2	29.9	2.3
December	39.3	22.2	22.9	28.1	5.6
All	35.4	30.0	35.1	33.5	1.8

The data for these three years show a factor of two variation between the minimum monthly average dust loading and the maximum monthly average. The annual averages are quite consistent, and are in good agreement with the 1966 National Air Surveillance Network, which showed a mean for all non urban locations of 38 μg m^{-3} (Healy 1980). The average for urban stations ranged from 33 to 254 μg m^{-3}.

USE OF 1989–1991 DATA FOR DOSE RECONSTRUCTION

The 1989–1991 data may be used to reconstruct the probable seasonal variation in dust loading from historical annual averages, if desired. For this purpose, the RELATIVE MASS LOADING is defined as the ratio of the monthly average mass loading to the annual average mass loading (Table O–5). The months May through September are relatively dustier than average, but are still within 30% of the annual average.

Table O–5. Relative Mass Loading[a] in Air Around the FMPC

Dustier than average:		Less dusty than average:	
May	1.11	October	0.98
June	1.30	November	0.90
July	1.25	December	0.83
August	1.26	January	0.79
September	1.10	February	0.77
		March	0.93
		April	0.75

[a] Ratio of monthly average to annual average mass loading.

Several modifying factors to the basic mass loading model deserve consideration and are discussed in the concluding section.

- the distribution of the contaminant among different size soil particles, described by an enrichment factor, EF
- the fraction of airborne dust which comes from the contaminated areas, f_c
- the fraction of the resuspended dust which is respirable, f_r

Equation O–1 may be expanded, to represent the concentration of uranium in air which is in respirable size fractions, $C_{a,r}$, as:

$$C_{a,r} = C_s \times ML \times EF \times f_c \times f_r \qquad (O–2)$$

Soil particles that are carried in suspension are the smaller ones, generally less than 30 μm. Thus, if the concentration of the contaminant in the soil fraction less than 30 μm is greatly different from that in the bulk soil, the airborne concentrations predicted by the mass-loading approach would not be a good estimate. The EPA proposed the use of an ENRICHMENT FACTOR to include these particle size considerations in resuspension calculations. The enrichment factor is defined as the summation of the products of g_i, the ratio of the fraction of the total activity in soil contained within the size increment i to the fraction of the total mass in that size, and f_i, the fraction of the airborne mass within each increment of particle size in the air. For the distribution of plutonium in soil sizes at Rocky Flats, CO, the EPA calculated an enrichment factor of 1.5 (Healy 1980).

The mass loading approach is most appropriate when applied to large areas of contamination. The smaller the contaminated area, the larger the fraction of the airborne dust which would not come from the contaminated area. Direct use of the mass loading equation O–1 without modification implies $f_c = 1.0$.

The measurements of total suspended particulates from the high-volume air samplers do not provide definitive information on the fraction of the particulate which is respirable, f_r; however they do exclude the largest particle sizes. (See Appendix L for estimates of collection efficiencies of high volume air samplers for different particle sizes.) The high volume air samplers used at the FMPC since the early 1970's are fundamentally the same as those described in the Reference Method for Determination of Suspended Particulate Matter in the Atmosphere (CFR 1985); the sample flow rate and the geometry of the shelter favor the collection of particles only up to 25–50 μm aerodynamic diameter.

For an initial analysis of the resuspension pathway at Fernald, it will be assumed that all of the measured particulate in air is respirable, and no enrichment factor will be used. If the resuspension pathway proves to be a relatively significant contributor to total exposure, quantification of these modifying factors in Equation O–2 may be necessary, perhaps by examination of data from other sites with similar soils and climate.

In addition to the above considerations for exposures to the general population, a higher mass loading would be used for specific assessments to individuals involved in particularly dusty activities, such as plowing. These special scenarios have not yet been defined.

REFERENCES

Byrne, J.M. 1992. *1991 Particulate Data*. Letter and disk transmission to S. K. Rope, dated July 24, 1992. Westinghouse Environmental Management Company of Ohio, Cincinnati, Ohio.

CFR, 1985. "Reference Method for the Determination of Suspended Particulate Matter in the Atmosphere (High-Volume Method)." Appendix B in *Code of Federal Regulations, Title 40 Protection of the Environment, Part 50 National Primary and Secondary Ambient Air Quality Standards*. General Printing Office, Washington DC.

Grant, D.L. circa 1992. "Determination of Airborne Particulates." Procedure ESH–P–30–068. Westinghouse Environmental Management Company of Ohio, Cincinnati, Ohio.

Healy, J.W. 1980. "Review of Resuspension Models." In: *Transuranic Elements in the Environment*, pp. 209-235 (W. C. Hanson, Ed.). DOE/TIC-22800. National Technical Information Service, Springfield, Virginia.

Kraps, P. 1991. "REMP Air Monitoring." Environmental Monitoring Section Procedure No. EM–RM–001. Westinghouse Materials Company of Ohio, Cincinnati, Ohio.

APPENDIX P

RADON, RADON DAUGHTERS, AND PENETRATING RADIATION FROM THE WASTE STORAGE SILOS: TRANSPORT MODELS AND MONITORING DATA

INTRODUCTION

In addition to the particulate releases from the FMPC stacks, there are two types of releases from the waste storage silos, located in the waste disposal area west of the FMPC production area, that must be considered. First, there is the release of ^{222}Rn and its short-lived daughters from the K-65 Silos, Silos 1 and 2. This release was described in our previous source term report (Voillequé et al. 1991). Second, there is gamma radiation that is emitted from the K-65 Silos and the Metal Oxide Silo, Silo 3. This gamma radiation represents a potential source of direct radiation exposure to people living near the Silos (see, for example, Dugan et al. 1990). The Metal Oxide Silo is not considered an important source of Rn releases (Voillequé et al. 1991). However, because it contains high concentrations of radioactive materials, it does represent a potentially significant source of direct radiation exposure.

In this appendix we discuss, for both the Rn releases and for the direct gamma exposures, (1) the methods and models used to estimate dispersion in the environment and doses to people, (2) the related environmental monitoring data, and (3) comparisons of our model predictions to the environmental measurements. Comparisons of the predicted and measured values were performed to evaluate the usefulness of our models.

MODIFICATIONS TO AIR DISPERSION MODEL SPECIFIC TO RADON

The general models for air dispersion of atmospheric releases, as described earlier in this report, particularly in Appendix J (Building Wake Effects), are also applied to Rn releases from the K-65 Silos.

Our typical compilations of meteorology data have included the meteorology for all observation times, and are thus best suited for use in modeling continuous releases occurring at all times of the day. However, the Rn source term from the K-65 Silos, as developed, includes both a continuous release component and a daylight-only release component (Voillequé et al. 1991). It is well known that daylight meteorology generally consists of more unstable conditions and higher wind speeds than does night-time meteorology. Thus, we believe it is reasonable to generate a meteorology data set to represent the daylight conditions, to better model the daylight-only Rn release.

A rule of thumb used in atmospheric dispersion modeling indicates that of the Pasquill-Gifford stability classes, classes A, B, and C occur primarily during daylight hours, classes E and F occur primarily during the night, and class D tends to occur equally during daylight and at night. Using this rule, a meteorology data set to approximate the daylight conditions was easily constructed. The joint frequency tables (JFTs) we use contain parameters that

designate the relative frequencies of each stability class. To construct the daylight JFT, we first set the relative frequencies of classes E and F to zero. We then set the frequency of class D to half of the value for 24-hour meteorology. We then renormalized, so that the sum of frequencies for classes A through D equals one. Table P–1 shows the result of this construction for an example case, using the composite FMPC meteorology, which was described in Appendix E.

Table P–1. Example Construction of Approximate Daylight-Only Meteorology Data Set, for FMPC Composite Data[a]

Stability class	Relative frequency of class	
	Normal (24-hour) data	Daylight-only approximation
A	0.0647574	0.212059
B	0.0304688	0.0997708
C	0.0435183	0.142502
D	0.333287	0.545678
E	0.291138	0
F	0.236831	0

[a] The FMPC composite dataset is described in Appendix E.

MONITORING DATA FOR RADON CONCENTRATIONS IN AIR

Data Obtained

A number of sources of environmental monitoring data for ^{222}Rn concentration in air have been located. The earliest monitoring in the FMPC environs appears to have been initiated in 1978 by the FMPC. A set of handwritten information (Boback circa 1984) indicates that these early measurements consisted primarily of grab samples, both of particulates to be analyzed for Rn daughters and of air to be analyzed for Rn. Some longer-term samples were taken using passive environmental radon monitors (PERMs). These early samples were taken at the FMPC site boundary air monitoring stations, primarily at boundary station 6, which was at the site boundary west of the K-65 Silos, and at locations very close to the K-65 Silos. The measurements continued into 1980.

Environmental monitoring data for ^{222}Rn concentrations in air are also provided in the site annual environmental reports, which present the results of environmental monitoring performed by FMPC staff. Radon monitoring is first mentioned in the 1979 environmental report (Boback and Ross 1980). This report provides maximum concentrations measured during "preliminary sampling," and indicates that the methods to be used for monitoring Rn were still under investigation at that time. We assume that this "preliminary sampling" and the early sampling described above are the same.

The FMPC established a routine Rn monitoring program in July 1980 at the (then) six boundary air monitoring stations (Boback and Ross 1981). Alpha track detectors, configured

as passive Rn gas detectors and supplied by a commercial vendor, were used. The routine program was intended to provide quarterly monitoring (i.e., the detectors were to be exposed for three-month periods), although there were significant variations in actual exposure times. In 1981 the program was expanded to include sampling at the (new) seventh boundary station and two background locations (Fleming et al. 1982). The initial results of the routine Rn monitoring program are included in the 1980 report. However, this report provides only the ranges of the measured concentrations. The 1981–1985 reports (Fleming et al. 1982, Fleming and Ross 1983, Fleming and Ross 1984, Facemire et al. 1985, and Aas et al. 1986) tabulate the maximum, minimum, and average concentrations measured at the seven boundary stations and at the background stations.

In 1986, the Rn monitoring program was expanded slightly to include sampling at two onsite air monitoring stations (AMS 8 and AMS 9) and three offsite locations (AMS 10, 11, and 13), in addition to the seven boundary stations (then called AMS 1–7) and two background stations (WMCO 1987). Maximum, minimum, and average concentrations were reported for each monitoring station. In 1987 the program was expanded greatly to include sampling at 16 locations on the site boundary, 16 locations on the fenceline around the K-65 Silos, 2 other onsite locations on the west side of the production area, four background stations, a few residences near the FMPC site, and air monitoring stations AMS 1–13 (WMCO 1988). The program continued with only minor changes through at least 1990 (WMCO 1989a, Dugan et al. 1990, and Byrne et al. 1991). The 1987–1990 reports only give results for the air monitoring stations and the site boundary stations; results for the K-65 Silos fenceline and the other two onsite locations were not reported (WMCO 1988, WMCO 1989a, Dugan et al. 1990, and Byrne et al. 1991). The 1987–1990 reports provide average results only.

Additional, more detailed results have been obtained for some periods of the FMPC Rn monitoring. A handwritten spreadsheet (Anonymous circa 1984) provides a compilation of the individual detector results of the routine FMPC monitoring for June 13, 1980, through December 27, 1983. We have also received computer file copies, directly from the site, of the FMPC alpha track monitoring data for 1987–1992 (only part of 1992) (Byrne 1992). These computer files include the individual measurements for locations reported in the environmental monitoring reports and also for the K-65 Silo fenceline locations. Starting in 1988, continuous Rn gas monitoring has been performed on the K-65 Silos fenceline and at other locations using active, powered, flow-through instruments. We have also received computer file copies of the data for these continuous Rn monitors for 1988–1992 (again, only part of 1992) (Byrne 1992).

Environmental Rn monitoring on and around the FMPC site has also been conducted by entities other than the FMPC operating contractor. The Mound facility, which is a DOE facility in Miamisburg, Ohio, established a Rn monitoring network at the FMPC in September 1984 (Hagee et al. 1985). Mound used Passive Environmental Radon Monitors (PERMs) with one- to two-week exposure periods. Mound initially monitored at six onsite locations, and later expanded to 17 onsite locations at varying distances from the K-65 Silos. The monitoring was performed through early October 1986. A Mound report summarized the results for September 20, 1984 through February 5, 1985 (Hagee et al. 1985). A letter with attached tables provides detailed results for July 2, 1985, through October 3, 1986

(Jenkins 1986). An Oak Ridge National Laboratory report (Berven and Cottrell 1987) summarizes results for the entire monitoring period.

The Ohio Department of Health performed environmental Rn monitoring at 12 locations on the FMPC site boundary and at 4 control locations, from June 1985 to November 1987 (Steva 1988). This monitoring used alpha track detectors that were changed after 3.5 to 8 months of exposure.

Data Chosen for Comparison to Model Predictions

One of our purposes in this appendix is to compare measured concentrations of Rn to predictions of our models in order to evaluate the usefulness of our models. To accomplish this objective, a data set with concentrations at different distances from the Silos will provide the best basis for comparison. Most of the data sets discussed above provide Rn concentrations measured primarily at the FMPC site boundary, or at the K-65 Silos fenceline, or both. In such cases, we have close-in locations, with significantly elevated concentrations, and relatively distant locations, with concentrations likely to be around background levels, but no intermediate locations, with intermediate concentrations. However, the Mound monitoring data were collected at a greater variety of distances from the Silos, and include a more complete range of Rn concentrations than the other available data sets. Thus, we have chosen to use the Mound data for comparison to our model predictions in this Task 4 report. The other data sets will be examined in more detail in the Task 5 Report.

The source terms for ^{222}Rn releases from the K-65 Silos were developed for an annual time resolution (Voillequé et al. 1991). Therefore, we wish to use annual average concentrations for our comparisons of models and measurements. From the Mound data we have obtained, the longest uninterrupted set of data is from July 2, 1985, through October 3, 1986. Within this period, monitoring at one of the intermediate distance locations was terminated on June 4, 1986. Thus, in order to use all of the data from this location, we will use the data from July 2, 1985, through July 2, 1986.

The results of the individual Mound measurements, from Jenkins (1986), are presented in Table PS–1, at the end of this Appendix. The monitoring locations are shown below in Figure P–1 (from Hagee et al. 1985). The time-integrated measurements were made with Passive Environmental Radon Monitors (PERMs), exposed for one to two weeks at the monitoring location (Hagee et al. 1985 and Jenkins 1986). The operating principle of the PERM involves, first, diffusion of Rn from ambient air through a porous barrier into a sensitive volume of the instrument (George 1977). Inside the sensitive volume, the positively charged ^{218}Po ions, formed from the decay of ^{222}Rn, are collected on a negative electrode. The cumulative alpha activity collected on the electrode is detected by an LiF thermoluminescent dosimeter (TLD) chip, which is very sensitive to alpha radiation, but relatively insensitive to beta and gamma radiation. After exposure, the TLD chip is removed and read in a TLD analyzer. The measured cumulative alpha activity is directly proportional to the time-integrated Rn concentration.

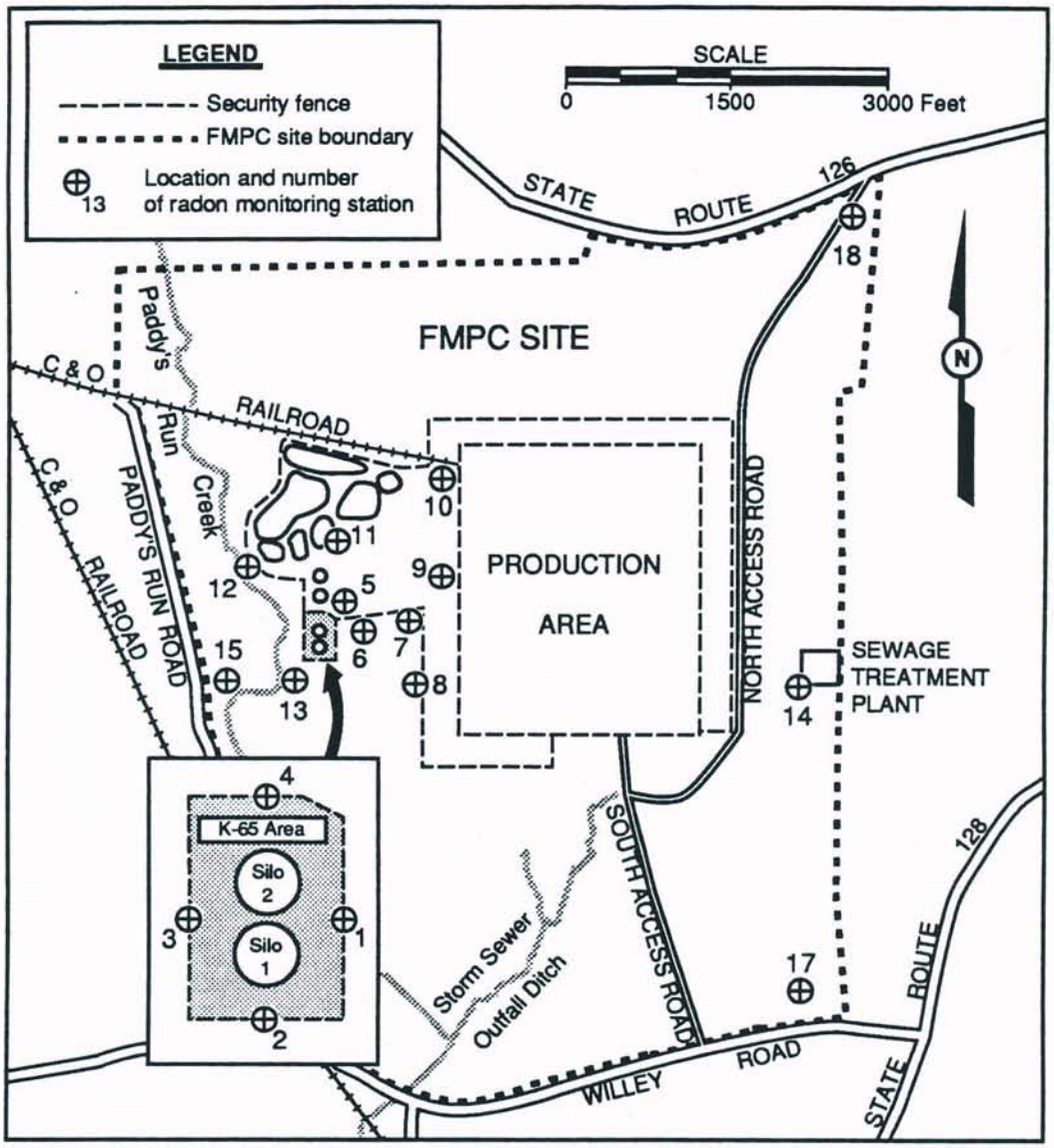

Figure P–1. Monitoring locations of the Mound Rn monitoring program on the FMPC site from September 1984 to October 1986 (from Hagee et al. 1985).

The quality of the Mound monitoring results is difficult to assess. Results of quality assurance exposures, such as replicates or exposures in known atmospheres, were not reported or mentioned with the Mound monitoring results (Hagee et al. 1985, Jenkins 1986, and Berven and Cottrell 1987). However, we have obtained a report of a contemporary U.S. DOE Environmental Measurements Laboratory (EML) intercomparison study of passive Rn detectors, in which Mound participated with PERMs (George et al. 1985). We assume that the measurements for this study occurred in late 1984 or early 1985 (the dates were not specified). In the study, each participant exposed its detectors to low concentrations of Rn (about 4 pCi L^{-1}) in a basement laboratory and to high concentrations (about 70 pCi L^{-1}) in

a special, controlled Rn room. For application to the FMPC monitoring, the exposures to lower concentrations are more relevant. For the test exposures, the "reference" Rn concentration was determined by continuous monitoring with flow-through scintillation cells, verified with periodic measurements using pulse ionization chambers. The pulse ionization chambers were the primary calibration instruments of the EML for Rn in air, traceable directly to the U.S. Department of Commerce, National Bureau of Standards (NBS) through use of NBS standard reference material ^{226}Ra solutions (George et al. 1985).

Results of the intercomparison study for PERMs at the low concentration, expressed as the ratio of the mean concentration measured by the participant to the reference concentration, are shown below in Table P–2. As given in the report, and in Table P–2, the results were listed by a random code assigned to each participant. From other information in the report, we were able to determine that Mound was either participant 5 or participant 6. Results for these two participants indicate a small underbias, with fair precision (relative standard deviations around 10%).

Table P–2. EML Intercomparison Results for PERMs at ^{222}Rn Concentrations About 4 pCi L^{-1}

	Measured concentration normalized to reference[a]	
Participant random code	Mean concentration	Standard deviation
5	0.59	0.06
6	0.78	0.09
7	2.00	1.10
8	0.95	0.45

[a] The values given are the mean and standard deviation of the concentrations measured by the participant, divided by the mean reference concentration.

To use the Mound monitoring data we must first calculate the annual average concentrations. In Table PS–1 it can be seen that from July 2, 1985, through July 2, 1986, there were a few cases when no measurement is recorded. In these cases no measurement was recorded in the source document (Jenkins 1986). We assume that, since there are only a small number of such occurrences, the lack of these data points does not contribute to any significant bias in an annual average concentration. Because individual measurements represent different exposure times, we calculated the annual averages as time-weighted averages of the individual measurements. Table P–3 presents the calculated annual average concentrations for July 2, 1985, through July 2, 1986.

As we are interested in Rn concentrations due to releases from the K-65 Silos, we must subtract a background concentration from the gross measurements made by Mound. In the Mound monitoring network, there were not any locations chosen to represent background

Table P–3. Annual Average (Time-Weighted) ^{222}Rn Concentrations Calculated from Mound Monitoring of July 2, 1985, to July 2, 1986 (pCi L^{-1})

Location	Gross	Net
1	5.94	5.5
2	2.29	1.8
3	8.11	7.6
4	4.78	4.3
5	5.69	5.2
6	1.79	1.3
7	1.37	0.91
8	1.34	0.88
9	0.919	0.46
10	0.817	0.36
11	1.33	0.87
12	1.62	1.2
13	0.605	0.14
14	0.364	
15	0.601	0.14
17	0.471	
18	0.559	

(Hagee et al. 1985). The FMPC did perform background radon monitoring during this time. However, their measurements were made using alpha track detectors. We feel that it is inappropriate to use a background concentration measured with a different instrument to calculate the net concentrations for the Mound monitoring. The first Mound report (Hagee et al. 1985) indicated that the concentrations measured at locations 14, 17, and 18 were in the background range. These locations, all on the east boundary of the FMPC site, are the farthest from the K-65 Silos. We will use the average of concentrations measured at these three locations to represent the background Rn concentration. (Later in this section we briefly discuss the predicted impact of the K-65 Silos releases on Rn concentrations at these locations.) This average background concentration is thus 0.46 pCi L^{-1}. For comparison we note that background concentrations measured by the FMPC program, at two locations, were 0.59 and 0.37 pCi L^{-1} in 1985 (Aas et al. 1986) and 0.60 and 0.57 pCi L^{-1} in 1986 (WMCO 1987). Table P–3 also shows the net Rn concentrations at each location, after background is subtracted.

COMPARISON OF MODELED TO MEASURED RADON CONCENTRATIONS

The Rn source term for releases from the K-65 Silos is described in the final report of Tasks 2 and 3 of this Project (in preparation). From the Tasks 2 and 3 work, estimated ^{222}Rn releases for 1980–1987 consist of two parts. First, a continuous release is estimated to occur at the uniform rate of 140 Ci y^{-1}. Second, there are releases that are estimated to occur only during daylight hours, with an annual release rate of 810 Ci y^{-1} (thus the

instantaneous release rate during daylight would be roughly twice as great, and the release rate during the night would be zero).

To use the Rn dispersion model, we must first determine the distances and directions of the monitoring locations from the release points. The Mound monitoring locations (Hagee et al. 1985) were plotted on larger scale drawings of the FMPC site that included the Ohio State Plane (OSP) coordinate system grid (Schwarzman 1992 and Woolpert circa 1988). The approximate OSP coordinates were then scaled from the drawings. The locations of the center of each K-65 Silo and the center of the two Silos (between the two) were determined similarly. Simple trigonometric relationships were used to calculate, from the coordinates, the distances and direction of the monitoring locations from the Silos. The Rn dispersion model requires as input the direction from which the wind would have to blow to expose the receptor to Rn from the Silos, expressed as one of the sixteen compass directions. The directions were translated into this format. (As an example, exposure of a receptor to the northeast of a Silo occurs with wind blowing from the southwest.) Table P–4 shows the results of these calculations.

Table P–4. Estimated Coordinate Locations of Mound Rn Monitoring Stations, with Distances (m) and "Wind from"[a] Directions from the K-65 Silos to the Monitoring Stations

	OSP Coordinates (ft)		From Silo 1		From Silo 2		From center of Silos	
Location	East	North	distance	wind from	distance	wind from	distance	wind from
Silo 1	1,378,484	480,400						
Silo 2	1,378,486	480,522						
Center of two Silos	1,378,485	480,461						
1	1,378,625	480,460	47	WSW	46	WNW	43	W
2	1,378,480	480,255	44	N	81	N	63	N
3	1,378,345	480,465	47	ESE	46	ENE	43	E
4	1,378,490	480,660	79	S	42	S	60	S
5	1,378,610	480,740	111	SSW	76	SSW	93	SSW
6	1,378,890	480,480	126	W	124	W	124	W
7	1,379,470	480,530	303	W	300	W	301	W
8	1,379,460	479,850	341	WNW	361	NW	351	WNW
9	1,379,810	481,140	463	WSW	445	WSW	454	WSW
10	1,379,810	481,910	613	SW	585	SW	598	SW
11	1,378,730	481,500	344	SSW	307	SSW	325	SSW
12	1,377,870	481,060	275	SE	249	SE	261	SE
13	1,378,300	480,110	105	NNE	138	NNE	121	NNE
14	1,382,980	479,950	1377	W	1381	W	1379	W
15	1,377,450	480,100	328	ENE	341	ENE	334	ENE
17	1,382,920	476,800	1741	NW	1765	NW	1753	NW
18	1,383,550	484,530	1992	SW	1968	SW	1980	SW

[a] The "wind from" direction is the direction from which the wind would have to blow to expose the receptor (the monitoring location) to Rn from the Silo(s). This direction format is used for consistency with our Rn dispersion model.

As discussed elsewhere, the Rn dispersion model evaluates concentrations at receptor points based on a point source release. We prefer to represent the Rn releases as single-point releases from a point centered between the two Silos. However, close in to the silos, the releases may be better represented as two point source releases from the centers of the two silos. Because some of the Mound monitoring points were located relatively close to the silos, preliminary calculations were performed to determine the difference between predicted χ/Q values assuming a single release point and those assuming two release points. The results of these calculations showed that this effect was only important relative to the Mound monitoring locations 1–5 and 8. In these cases, there was either a difference in direction or a significant difference in distance between the two approaches. For locations 6, 7, and 9–18 the χ/Q values based on a single release point, at the center of the two Silos, were not significantly different (less than 5%) from the χ/Q values based on two release points. Thus, for predictions for locations 1–5 and 8 we use two release points. For the other locations we use a single release point.

The building wake effects module of the Rn dispersion model requires the input of the effective height and width of the obstacle. In this case the obstacle is the combination of the Silos and the surrounding berms. As discussed in the Tasks 2 and 3 report (in preparation), the height of the Silos is 11 m, and the average of the north-south and east-west vertical cross sections of the Silos and berms is 600 m^2. We thus use an effective width of 55 m.

Because we are comparing to annual average measured Rn concentrations, we use the composite annual meteorology data sets for our predictions. The composite meteorology adjusted to daylight only conditions, as discussed earlier in this Appendix, is used for predictions for daylight releases.

Annual average values of χ/Q were calculated for the Mound monitoring locations for conditions of continual release and daylight-only release. These values are tabulated below in Table P–5.

The estimated Rn release rates are multiplied by the predicted χ/Q values to predict the Rn concentrations due to releases from the K-65 Silos. We then ratio the predicted concentrations to the net measured concentrations to form predicted to observed (P/O) ratios. The measured and predicted concentrations, and P/O ratios, are given in Table P–6, along with the distance of the monitoring location from the center of the two silos.

As seen in Table P–6, the geometric mean P/O ratio is 0.44 and there is a considerable range in P/O ratios (geometric standard deviation 2.9). To determine whether trends exist in these ratios, we plot the P/O ratios versus the distance of the monitoring location from the K-65 Silos, in Figure P–2 below. The plot shows that there is not a significant trend of P/O ratio with distance from the Silos. There also is not a significant trend of P/O ratio with Rn concentration, although there is much more scatter in the P/O values at lower concentrations. There does, however, appear to be some relationship between the P/O ratio and direction from the Silos. The only P/O ratios greater than 1 occur at locations 2, 13, and 15, which are all in the quadrant between south and west (winds from the north to east). We also note that the predicted impact of releases from the K-65 Silos on the Rn concentrations at locations 14, 17, and 18, which we chose to represent background, is small — only 6% to 14% of the measured concentrations (from Table P–3). This provides some additional support for the use of these locations as substitutes for background.

Table P–5. Predicted Annual Average χ/Q for Mound Monitoring Locations

Location	From center between Silos[a]		χ/Q (pCi m^{-3} per Ci y^{-1})	
	Distance (m)	Wind from direction[b]	Continual release	Daylight-only release
1	43	W	4.38	3.79
2	63	N	1.65	2.13
3	43	E	2.23	2.49
4	60	S	1.89	1.37
5	93	SSW	1.88	1.48
6	124	W	1.18	0.886
7	301	W	0.456	0.259
8	351	WNW	0.312	0.158
9	454	WSW	0.325	0.146
10	598	SW	0.312	0.131
11	325	SSW	0.405	0.235
12	261	SE	0.0871	0.0486
13	121	NNE	0.486	0.608
14	1379	W	0.142	0.0386
15	334	ENE	0.281	0.241
17	1753	NW	0.0939	0.0192
18	1980	SW	0.122	0.0307

[a] Relative to a point centered between the two Silos.

[b] The direction from which the wind would have to blow to expose the receptor (the monitoring location) to Rn from the Silos.

There are three monitoring locations, 12, 13, and 15, for which the P/O ratios deviate from the geometric mean P/O ratio by more than one geometric standard deviation. For location 12, the P/O ratio is extremely low, while the measured concentration was significantly above background. For locations 13 and 15, the P/O ratios are significantly greater than for other locations. At these two locations the measured concentrations were only slightly above background, so there is more uncertainty in the net concentrations. All of these locations are fairly close to Paddy's Run Creek, with location 12 upstream from the K-65 Silos and locations 13 and 15 downstream from the Silos (see Figure P–1). There may be localized, surface drainage air flow patterns along the creek channel, which may affect transport of releases from the Silos. The meteorological data we use was obtained at the FMPC meteorological tower, which is about 200 m south of the production area and 500 m northeast of Paddy's Run Creek. The Silos and monitoring locations 12, 13, and 15 are within about 100 m of Paddy's Run Creek.

Based on these comparisons of predictions to measurements for the Mound monitoring data, with geometric mean P/O ratio 0.44, it appears that the predicted concentrations are, in general, somewhat underbiased. It is impossible, using the available data, to precisely determine the sources of this bias. However, contributing factors could include inaccuracies in the Rn dispersion model and the associated input, meteorological data that are not

Table P–6. Comparison of Measured and Predicted ^{222}Rn Concentrations for Annual Average of Mound Monitoring for July 2, 1985, to July 2, 1986

	From center between Silos[a]		Rn concentration (pCi L^{-1})		
Location	Distance (m)	Wind from[b]	Measured[c]	Predicted	P/O ratio[d]
1	43	W	5.5	3.7	0.67
2	63	N	1.8	2.0	1.1
3	43	E	7.6	2.3	0.30
4	60	S	4.3	1.4	0.32
5	93	SSW	5.2	1.5	0.28
6	124	W	1.3	0.88	0.66
7	301	W	0.91	0.27	0.30
8	351	WNW	0.88	0.17	0.19
9	454	WSW	0.46	0.16	0.36
10	598	SW	0.36	0.15	0.42
11	325	SSW	0.87	0.25	0.28
12	261	SE	1.2	0.052	0.044
13	121	NNE	0.14	0.56	3.9
14	1379	W	[e]	0.051	[e]
15	334	ENE	0.14	0.24	1.7
17	1753	NW	[e]	0.029	[e]
18	1980	SW	[e]	0.042	[e]
GM[f]					0.44
GSD[f]					2.9

[a] Relative to a point centered between the two Silos.

[b] The direction from which the wind would have to blow to expose the receptor (the monitoring location) to Rn from the Silos.

[c] The net measured concentration, after subtraction of background.

[d] The P/O ratio is the predicted concentration divided by the measured (net) concentration.

[e] Locations 14, 17, and 18 were considered representative of background. Net measured concentrations and P/O ratios are not meaningful.

[f] GM is the geometric mean, and GSD is the geometric standard deviation.

properly representative of conditions around the Silos, or inaccurate source term estimates. We tentatively conclude that, relative to the measurements, and when the uncertainties involved are considered, the predicted concentrations are in a range considered acceptable. However, as mentioned earlier in this Appendix, additional environmental Rn monitoring data will be evaluated in the Task 5 Report. After analyzing those data, we will study further the agreement of predictions and measurements before making final conclusions about the performance of the Rn dispersion model. It should also be noted that these initial conclusions are based on comparisons for locations on the FMPC site, less than 1 km from the Silos, while the model will be used to predict offsite concentrations, generally at greater distances from the Silos.

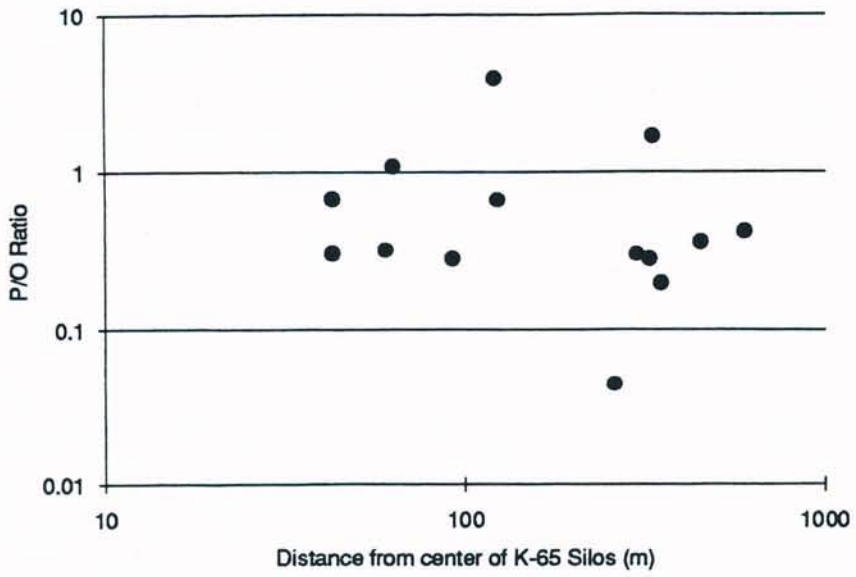

Figure P–2. Comparison of predicted to measured ^{222}Rn concentrations for Mound monitoring, annual average of data from July 2, 1985, through July 2, 1986. The P/O ratios are the predicted concentrations divided by the net measured concentrations. The geometric mean P/O ratio is 0.44, with geometric standard deviation 2.9.

MODEL FOR DIRECT EXPOSURE DUE TO SILOS SOURCES

It has been recognized that the K-65 Silos also present a potential source of direct radiation exposure to people living near the Silos (see, for example, Dugan et al. 1990). The large inventory of ^{226}Ra in the Silos produces a large inventory of ^{222}Rn and Rn daughters in the silo head space and also a large inventory of Rn and Rn daughters in the waste material itself. Two of these daughters, ^{214}Pb and ^{214}Bi, along with other radionuclides present in the Silos, emit gamma radiations that are the source of potential exposures. While the Metal Oxide Silo, Silo 3, is not considered an important source of Rn releases (Voillequé et al. 1991), the concentrations of radioactivity in Silo 3 are high enough that it may be a significant source of direct radiation exposures. Thus, our models for direct exposures must account for exposures from the K-65 Silos and the Metal Oxide Silo.

General Methodology

For estimating direct exposures to people from gamma radiation emitted from the waste storage silos, we have chosen to use a model, rather than to rely on environmental monitoring data. One reason for this is that exposure rate monitoring was performed primarily at the site boundary air monitoring stations. Thus, exposure rates at nearby residences would have to be estimated using some type of model (perhaps simple), anyway. In addition, the monitoring data do not cover all periods of interest.

We have chosen to use a readily available computer software package, MicroShield 4, to calculate exposure rates due to materials in the three Silos. MicroShield is designed to

perform shielding calculations and calculate exposure from gamma radiation sources (Negin and Worku 1992). The software was developed following standard verification and validation procedures, is used extensively in the radiation protection industry, and operates on IBM PC-compatible microcomputers. For finite volume source geometries, MicroShield uses Gauss quadrature methods for point-kernel numerical integration. We use the most recently available version of MicroShield, version 4.00.

Doses will be calculated using a simple model to incorporate factors describing the fractions of time the exposed person spends indoors, outdoors, and away from the exposure point (away from home).

In order to run MicroShield, input parameters are required for the following: (1) geometrical description of the exposure conditions, including geometry of the source, shielding, and source to receptor distance, (2) descriptions of the source material and shield materials, including densities and constituents, (3) quantities of radionuclides in the source material, either a total activity or a concentration by volume, and (4) the quadrature order to be used for the numerical integration.

Geometry Parameters for MicroShield

Figure P–3 shows the general cross section of the K-65 and Metal Oxide Silos. As shown, each silo is 80 ft in diameter with an overall height of 36 ft, of which about 26 ft 8 in is the tank wall and about 9 ft 4 in is the domed roof of the silo (Preload 1951, Shanks and Vogel 1988). The walls are 8 inch thick concrete and the domes are 4 inch thick concrete (Preload 1951, Shanks and Vogel 1988).

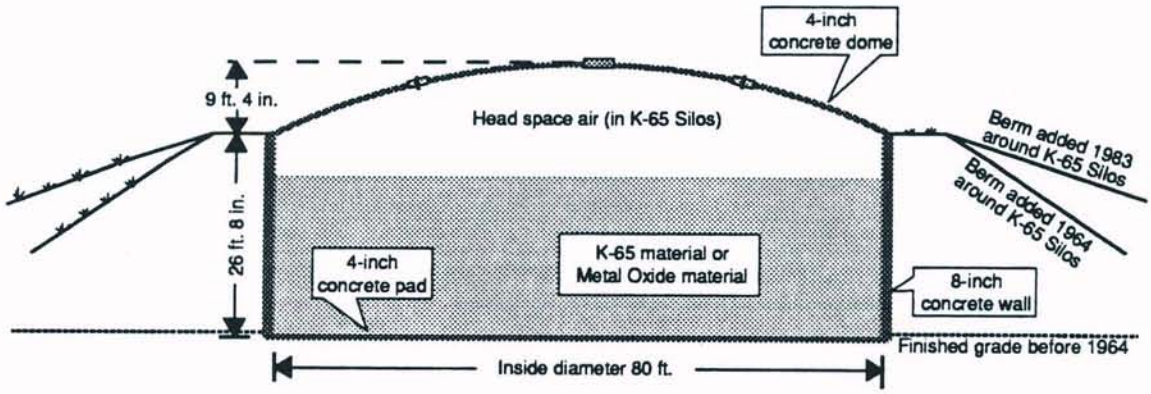

Figure P–3. General cross section of the K-65 and Metal Oxide Silos.

In our source term report (Voillequé et al. 1991), we concluded, based on the available information, that the volume in the K-65 Silos occupied by head space air was between 40,000 ft^3 and 62,000 ft^3 (average for the two Silos). For this work on direct exposures, we assume the head space volume is 51,000 ft^3. The volume of the dome of the Silo was calculated to be 23,900 ft^3 (Voillequé et al. 1991). This means that, on the average, the head space includes about 27,100 ft^3 that is in the cylindrical part of the Silo, which would be the top 5.4 ft of the cylindrical section. This implies that the average height of the K-65 material

in the Silos would be 21.3 ft. A 1990 draft Remedial Investigation Report (DOE 1990), which reported on the then recent sampling of the K-65 and Metal Oxide Silos, indicated that the Metal Oxide Silo was essentially full of metal oxide material. In 1972 the Metal Oxide Silo was estimated to contain 150,000 ft^3 of material (Nelson 1972). This is almost equal to the total volume of 158,000 ft^3 (sum of the dome volume, 23,900 ft^3, and the cylindrical volume, 134,000 ft^3).

The MicroShield program can evaluate exposures for several different volume source geometries, including sphere, cylinder, rectangular volume, truncated cone, and infinite slab. Of these, the geometry that most closely approximates the geometries of the Silos and Silo domes is the cylinder. We must deal with two different types of source material, the air of the K-65 Silos' head space and the solid K-65 and metal oxide waste materials. In 1964 earthen berms were constructed around the K-65 Silos (as indicated in Figure P–3), so two different configurations of the K-65 Silos must be considered: (1) without the surrounding berms, prior to 1964, and (2) with the berms, for 1964 and later. We thus envision three source and shield geometries, as shown in Figure P–4.

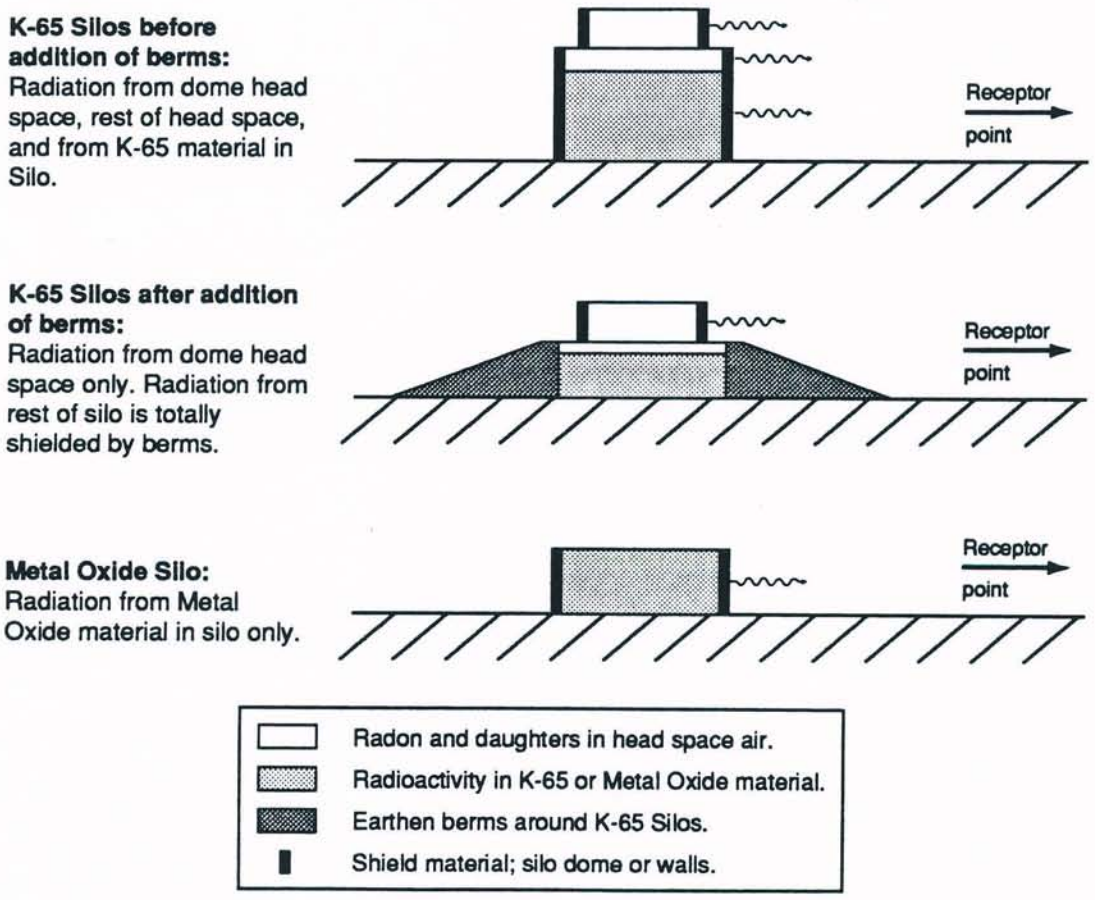

Figure P–4. Source and shield geometry models used for estimation of direct exposures from the K-65 and Metal Oxide Silos. As described in the text, we model the two K-65 Silos as a single Silo, but with twice the actual height.

We first consider the distance from the center of the source to the receptor point. This information will be variable, based on the receptor location of concern. In this assessment, we are interested in doses to people outside of the FMPC site boundary. The closest point on the boundary to the three Silos is slightly farther than 1000 ft from the Silos. At this distance we hypothesize that the two K-65 Silos could be treated as a single Silo, at the midpoint between the two. We tested this by performing two sets of exposure calculations for the Paddy's Run Road survey locations which are discussed later in this Appendix. These locations were all along Paddy's Run Road, southwest to northwest from the Silos.

The first set of calculations treated each of the two Silos separately, using the source activities and source to receptor distance applicable to each. The exposure rates due to each Silo were summed to give the total exposure rate at the receptor. The second set treated the two as a single Silo, using the average source activity concentrations and the distance from the midpoint between the two Silos to the receptor, but using a source height of twice the determined effective height. The use of a source height that is twice the actual source height effectively doubles the volume of the source and thus the total source activity, so that our effective source is equivalent to the two sources (the two Silos), stacked upon one another. The exposure rates for the two sets of calculations differed by less than 2% at all locations. Based on these results, we think it reasonable to treat the two K-65 Silos as a single Silo. Thus, we model the two K-65 Silos as a single Silo, using the average activity concentrations, the distance from the midpoint between the two Silos to the receptor, and a source height of twice the determined (based on physical heights) effective height. We note that we could accomplish the same result by using as the source activities for the single Silo the sum of the source activities for the two individual Silos. However, we actually will be using concentrations of radionuclides, and we would rather utilize the average concentration, which retains physical meaning. The Metal Oxide Silo will still be treated as a single, separate source, because the relative concentrations of radionuclides in the metal oxide material differ from those in the K-65 material.

Source geometry for K-65 Silos before addition of berms. The first geometry (see Figure P–4) is for the K-65 Silos before the berms were added. In this case, the source is modeled as three cylindrical sources. The bottom cylinder represents the K-65 material, and thus has a physical height of 21.3 ft, which we double for a modeled height of 42.6 ft. The second cylinder represents the head space that is in the cylindrical part of the Silo, and thus has a physical height of 5.4 ft, which we double for a modeled height of 10.8 ft. For both the bottom and second cylinders, the shield thickness is 8 in, as that is the thickness of the Silo walls.

The top cylinder represents the head space that is in the dome part of the Silos. This cylinder is modeled with a height of 18.67 ft, twice the physical height of the actual dome above the Silo walls (9.33 ft), and with radius 28.5 ft, to provide the same total volume as the two actual domes. Determination of the shield thickness for this cylinder is more difficult.

The prior source term work (Voillequé et al. 1991) concluded that the thickness of the concrete dome was between 3 and 4 in. We assume here a thickness of 3.5 in. However, the effective thickness in the horizontal direction is much greater, and varies with position on the dome, because the slope of the dome surface changes. To solve this, we wanted to

perform, once, a detailed exposure calculation for a complicated model of the dome, and use the results to determine an effective shield thickness value that could be used in a simpler model to provide the same results. The simpler model of the dome, that using the single, top cylinder discussed above, would then be used for further work. For the complicated model, we modeled the dome volume as broken into ten cylindrical volumes ("slices" of the dome), each of height 0.933 ft (one-tenth the total height), stacked on one another. The radii of these ten small cylinders were determined such that the overall shape of the stacked cylinders approximated the dome shape, and the total volume of the ten cylinders equalled the volume of the dome. The horizontal thickness of the dome material was determined based on standard trigonometric relationships.

The sum of the exposure rates, for this ten cylinder model, was assumed to be the correct exposure rate.

MicroShield was used to calculate the exposure rate due to each of the ten cylinder sources. For these calculations, we assumed a source concentration of 3×10^7 pCi L^{-1} in air (about the concentration measured in 1987) at a density of 0.001293 g cm^{-3}, assumed the shield (the dome material) to be normal concrete with density 2.35 g cm^{-3}, and assumed a receptor at 1000 ft from the source. The results of these calculations are shown below in Table P–7. We then made exposure calculations for the single cylinder model of the dome (9.33 ft height by 28.5 ft radius), and determined the shield thickness (horizontal dome material thickness) which resulted in an exposure rate equal to the sum of the exposure rates from the ten cylinder model. This equality occurred with a shield thickness of 9.805 in, which is thus considered the effective, horizontal thickness of the dome material. For further calculations we use our simple representation of the dome head space, the single cylinder model (9.33 ft height by 28.5 ft radius), with this effective shield thickness (9.805 in) for the dome material.

Table P–7. Calculations for Determining Effective Horizontal Thickness of Silo Dome for Modeling Dome Head Space as a Single Cylinder

Cylinder number	Source thickness (ft)	Source radius (ft)	Source volume (ft^3)	Effective dome thickness[a] (in)	Exposure rate (mR h^{-1})
1 (top)	0.933	9.2	247	34.6	8.219×10^{-8}
2	0.933	15.8	736	20.0	1.003×10^{-5}
3	0.933	20.4	1220	15.5	5.308×10^{-5}
4	0.933	24.1	1699	13.1	1.383×10^{-4}
5	0.933	27.2	2173	11.6	2.654×10^{-4}
6	0.933	30.0	2642	10.5	4.313×10^{-4}
7	0.933	32.6	3106	9.72	6.332×10^{-4}
8	0.933	34.9	3565	9.07	9.955×10^{-4}
9	0.933	37.0	4018	8.55	1.294×10^{-3}
10 (bottom)	0.933	39.0	4467	8.10	1.628×10^{-3}
sum	9.3		23870		5.449×10^{-3}

[a] Thickness of the dome in the horizontal direction, away from the Silo center.

Source geometry for K-65 Silos with berms. The second source geometry (see Figure P–4) is for the K-65 Silos after the berms are in place. The minimum horizontal thickness of the berms is eight ft. Screening level MicroShield calculations indicate that this thickness of earth would reduce the exposure rate due to radioactivity in the K-65 material by a factor of about 10^6. We thus assume that the berms provide total attenuation of radiation emitted through the Silo sides, so the K-65 material is neglected as a radiation source. Thus, the only source to consider is the dome head space. As for the previous geometry, we use a modeled height of 18.67 ft, a radius of 28.5 ft, and a shield thickness of 9.805 in.

Source geometry for Metal Oxide Silo. The third source geometry is for the Metal Oxide Silo, which has never had berms around it. Since this Silo is essentially full of metal oxide material, we model this Silo as a single cylinder, of radius 40 ft (as it actually exists) and with an effective height of 31.4 ft, to give the equivalent overall volume of 158,000 ft^3. Since the effective shield thickness calculated for the dome (9.805 in) is relatively close to the Silo wall thickness of 8 in, and since only about 15% of the material would be in the dome volume, we simply assume the wall thickness of 8 in can be applied to the whole cylinder.

Material Properties Parameters for MicroShield

The second type of information needed for input to MicroShield is the properties of the source and shield materials. For the Rn in the head space source, the basic source material is air. Air is also considered a shield material for all of our calculations, because air lies between the Silos and the receptor point. For the density of air we use the value for 0°C and atmospheric pressure of 0.001293 g cm^{-3} (HEW 1970). MicroShield includes air as a standard material, and we accept the default selection of the constituents in air.

For the K-65 and metal oxide materials, we found limited information about the constituents of the waste material in a Remedial Investigation Report (RIR) for restoration work on the Silos (DOE 1990). This RIR indicated that the K-65 material was primarily composed of silicates, carbonates, and sulfates. Other elements present at concentrations of at least 1% include Ca, Fe, Mg, and Pb. In particular, concentrations of Fe and Pb may be as high as 7% and 9% by weight, respectively. The major constituents present in the metal oxide material were similar, but also include Al and Na, and the relative concentrations differ from those in the K-65 material. The major constituents in concrete include silicates, Al, Ca, Na, K, and Fe (Negin and Worku 1992). The attenuation coefficients for many materials are similar when expressed on a per mass basis, although this does not hold for some of the heavier elements. In terms of gamma attenuation properties, the presence of very high concentrations of Fe and Pb appears to be the greatest difference between K-65 or metal oxide material and concrete.

We performed some test calculations with MicroShield, to see what difference the concentrations of 7% Fe and 9% Pb would make to gamma attenuation. Our test case used a source geometry of 20 ft height and 40 ft radius, with an 8 in concrete shield to represent the Silo wall. The source was 1000 Ci ^{226}Ra, 1000 Ci ^{222}Rn and equilibrium quantities of the Rn daughters, and the receptor dose point was 1000 ft from the "Silo." Two cases were run,

one with the source material assumed to be concrete, and one with the source material assumed to concrete, but with the addition of 7% Fe and 9% Pb. The calculated exposure rates differed by only about 0.2%. This difference is considered negligible, and so we assume that the K-65 and metal oxide materials are adequately represented, for shielding calculation purposes, by concrete.

The description of the source and shield materials also includes the density, and may include a water content, for the source material. For calculations of exposure and dose due to the K-65 and metal oxide materials, we will use the density and moisture content provided in the source term report (Tasks 2 and 3 Report, in preparation).

For the shield materials, which represent the concrete walls and dome of the Silo, we will use the default MicroShield density of 2.35 g cm^{-3} for concrete, and the default constituent makeup of concrete. We assume no additional water content.

Source Activities for MicroShield

The third type of information needed for input to MicroShield is the quantities of radionuclides present in the source materials. MicroShield allows the use of either total activity or activity concentrations. For our calculations, we use activity concentrations. The basic information will be provided in the final source term report (the Tasks 2 and 3 Report), although we will also make the assumption that the daughter products of source term radionuclides are also present at equilibrium concentrations. We have determined that ^{210}Pb, ^{210}Bi, and ^{210}Po, which are later daughters of ^{222}Rn, do not contribute to the calculated exposure rates, so these radionuclides will be neglected. For the case of the head space source, we only consider ^{222}Rn and its short-lived daughters. We assume that the daughters are uniformly distributed in the head space gas, although some of the daughters may plate out on the Silo walls and dome. However, since the source media in this case is air, which will provide little attenuation, the exact distribution of the radionuclides should not be important.

For the cases of K-65 or metal oxide materials, there are many radionuclides to consider. We consider those radionuclides that have been determined present in the waste materials, and daughter products. Table P–8 lists the radionuclides to be considered for these sources, along with the decay fractions for the daughters. More information about radionuclides considered will be provided in the final report of Tasks 2 and 3 (in preparation).

Integration Quadrature Order for Numerical Integration in MicroShield

The final input information needed for MicroShield is the integration quadrature order, which describes the number of increments into which the source is divided for the numerical integrations. For cylindrical sources, we must specify quadrature order for radial, circumferential, and axial directions. As recommended by the MicroShield manual (Negin and Worku 1992), we have made test calculations using a range of quadrature orders. The tests indicate that for both the head space source and a metal oxide source, the exposure rate results obtained with quadrature orders of 10 for the three parameters were within 1% of the results for higher quadrature order (finer "mesh" size). Thus, for all calculations we will use a quadrature order of 10 for the radial, circumferential, and axial directions.

Table P–8. Radionuclides Considered for K-65 and Metal Oxide Material Source Terms for MicroShield Direct Exposure Calculations

Radionuclide	Determination	Decay fraction	Radionuclide	Determination	Decay fraction
^{227}Ac	measurements		^{224}Ra	daughter of ^{228}Th	1.00
^{228}Ac	daughter of ^{232}Th	1.00	^{226}Ra	measurements	
^{212}Bi	daughter of ^{228}Th	1.00	^{228}Ra	daughter of ^{232}Th	1.00
^{214}Bi	daughter of ^{226}Ra	1.00	^{220}Rn	daughter of ^{228}Th	1.00
^{231}Pa	measurements[a] or		^{222}Rn	daughter of ^{226}Ra	1.00
	parent of ^{227}Ac [b]	1.00	^{228}Th	daughter of ^{232}Th	1.00
^{234}Pa	daughter of ^{238}U	0.0013	^{230}Th	measurements	
^{234m}Pa	daughter of ^{238}U	1.00	^{231}Th	daughter of ^{235}U	1.00
^{212}Pb	daughter of ^{228}Th	1.00	^{232}Th	measurements	
^{214}Pb	daughter of ^{226}Ra	1.00	^{234}Th	daughter of ^{238}U	1.00
^{212}Po	daughter of ^{228}Th	0.640	^{208}Tl	daughter of ^{228}Th	0.360
^{214}Po	daughter of ^{226}Ra	1.00	^{234}U	measurements	
^{216}Po	daughter of ^{228}Th	1.00	^{235}U	measurements	
^{218}Po	daughter of ^{226}Ra	1.00	^{238}U	measurements	

[a] For the metal oxide material, measurements are used.

[b] For the K-65 material, ^{231}Pa is assumed in equilibrium with its daughter, ^{227}Ac.

Summary of MicroShield Input Parameters

Table P–9 summarizes the input parameters that will be used in all the MicroShield calculations. In addition to those parameters, we also must input the source activity concentrations, densities, and moisture content, which will be taken from the final source term report (Tasks 2 and 3), and the source to receptor distances.

Table P–9. Summary of Input Parameters for MicroShield Exposure Rate Calculations

Cylinder geometry			Source properties		Shield properties			
designation	height (ft)	radius (ft)	material	density (g cm^{-3})	material	thickness (in)	density (g cm^{-3})	quadrature order[a]
K-65 Silos before Berms Added								
dome head space	18.67[b]	28.5	air	0.001293	concrete	9.805	2.35	10, 10, 10
cylinder air space	10.8[b]	40	air	0.001293	concrete	8	2.35	10, 10, 10
waste	42.6[b]	40	concrete	variable	concrete	8	2.35	10, 10, 10
K-65 Silos with Berms								
dome head space	18.67[b]	28.5	air	0.001293	concrete	9.805	2.35	10, 10, 10
Metal Oxide Silo								
waste	31.4	40	concrete	variable	concrete	8	2.35	10, 10, 10

[a] Integration quadrature orders for radial, circumferential, and axial directions.

[b] As mentioned in the text, this height is twice the physical height, to allow the treatment of the two K-65 Silos as a single Silo. This does not apply to the Metal Oxide Silo.

Calculation of Dose from Exposure Rates

For the calculations of dose to a receptor based on the exposure rate, we first estimate the total exposure with a simple model that incorporates factors for the fractions of time spent in the radiation field and for shielding provided by a home or other structure. Thus,

$$X = T\left(f_{out}\dot{X} + f_{in}f_R\dot{X}\right) \quad \text{(P–1)}$$

where

X = total exposure to the exposed person (mR)

$\dot{X}$ = exposure rate at the receptor, obtained from the MicroShield calculation (mR h^{-1})

f_{out} = fraction of time a person spends outdoors at the exposure point (generally at their home) (unitless)

f_{in} = fraction of time the person spends indoors at the exposure point (unitless)

f_R = exposure rate reduction factor, to account for the shielding provided by the structure (such as a home) (unitless)

T = time that the person is exposed to the conditions (years or fraction of year converted to hours)

The usage factors, f_{out} and f_{in}, and the exposure reduction factor for structures, f_R, have been reviewed by others (NCRP 1984 and Kocher 1983). For applications to generic exposure scenarios, we will use values recommended by the NCRP review.

For the conversion of total exposure to dose, external dose conversion factors are utilized in the following:

$$H_e = X \cdot (\text{DCF}) \quad \text{(P–2)}$$

where

H_e = effective dose equivalent to the exposed person (Sv)

DCF = external dose conversion factor, to convert exposure rate in air to effective dose equivalent (Sv mR^{-1}).

Dose conversion factors from exposure to effective dose equivalent are tabulated in the International Commission on Radiological Protection's (ICRP) Publication 51 (ICRP 1987). Publication 51 provides calculated factors for five irradiation geometries that used anthropomorphic male and female phantoms. Of the five irradiation geometries, the rotational geometry (abbreviated ROT) "...may be seen as an approximation to the irradiation pattern of a person moving around unsystematically relative to the location of the source" (ICRP 1987). Because the orientation of exposed persons around the FMPC vary considerably and are not known, the ROT geometry is considered the most applicable to our calculations.

Some of the dose conversion factors for the ROT geometry are shown in Table P–10. Preliminary MicroShield calculations indicate that roughly 90% of the exposure rates due to direct exposures from the waste storage silos are from photons of energy between 1 and 2 MeV. At these energies the dose conversion factors vary slowly with energy, so we use the average dose conversion factor for these energies, 0.0075 Sv R^{-1} (7.5×10^{-6} Sv mR^{-1}), to

represent the dose conversion factor for all energies. It is noted that the effective dose equivalent factors from Publication 51 (ICRP 1987) were based on the tissue weighting factors w_T of ICRP Publication 26 (ICRP 1977), which differ from the weighting factors of ICRP Publication 60 (ICRP 1991) which we generally use (see also Appendix T). The effective dose equivalent using the w_T from Publication 26 is expected to be very close to the effective dose using the w_T from Publication 60.

Table P–10. External Dose Conversion Factors: Effective Dose Equivalent per Unit Exposure for Rotational Geometry (ROT)[a]

Photon energy (MeV)	DCF (10^{-2} Sv R^{-1})
0.1	0.840
0.2	0.746
0.3	0.720
0.4	0.715
0.5	0.717
0.6	0.719
0.8	0.725
1.0	0.732
1.5	0.748
2.0	0.762
3.0	0.783

[a] Ref. ICRP 1987. Dose conversion factors based on calculations for male and female phantoms. Units are those of the ICRP report.

It is anticipated that, for people near the FMPC, doses from direct exposure from the waste storage silos will be small relative to the total doses due to FMPC emissions. Thus, the simplifying assumptions made for calculations of effective dose equivalent are thought to be adequate. If the relative importance of this exposure pathway is more significant than anticipated, it may be necessary to estimate organ doses. In that case, the method of equation P–2 would be applied, but with dose conversion factors for individual organs, and perhaps for individual photon energies, used to calculate organ doses H_T. Two sources of the kinds of additional details that would be required are ICRP Publication 51 (ICRP 1987) and an Oak Ridge National Laboratory report (Kerr et al. 1985).

PENETRATING RADIATION MONITORING DATA

Data Obtained

Only a few sources of environmental monitoring of penetrating radiation have been located. The most obvious source is exposure rate monitoring reported in FMPC environmental reports. External radiation monitoring was initiated in late 1975, using thermoluminescent dosimeters (TLDs) at locations along the FMPC site boundary (NLCO 1976). The first results of this penetrating radiation monitoring were presented in the 1976 annual report (Boback et al. 1977), which reported the minimum, maximum, and annual

average exposure rate for each of the six boundary air monitoring stations, BS-1 to BS-6, based on quarterly TLD measurements. The monitoring continued at the same locations through 1980 (Boback et al. 1978, Boback and Ross 1979, Boback and Ross 1980, and Boback and Ross 1981). In 1981, a new air monitoring station was added, BS-7, and exposure rate monitoring was also extended to this location (Fleming et al. 1982). This boundary monitoring continued unchanged through 1990, although four offsite locations were added in 1985, background measurements were added in 1986, and measurements at two additional onsite air monitoring stations, AMS 8 and AMS 9, were added in 1987 (Fleming and Ross 1983, Fleming and Ross 1984, Facemire et al. 1985, Aas et al. 1986, WMCO 1987, WMCO 1988, WMCO 1989a, Dugan et al. 1990, and Byrne et al. 1991).

In 1957 a survey of gamma exposure rates around the K-65 Silos was performed, to provide background information about potential personnel exposures that might result from the construction of an additional waste storage tank in the K-65 area (Ross 1957). Measurements were made at regular intervals in eight compass directions from each of the K-65 Silos, but only out to maximum distances of 320 ft or less.

In 1986 and 1987, exposure rate surveys were performed along Paddy's Run Road, along the west side of the FMPC site, near the K-65 Silos. We have obtained daily survey forms for the June 1987 measurements (FMPC 1987) and monthly spreadsheet summaries of the daily measurements for all of 1987 (Anonymous circa 1987). As far as we could determine, these data have not been published by FMPC.

Data Chosen for Comparison to Model Predictions

One of the purposes of this Appendix is to compare measurements of penetrating radiation to predicted exposure rates based on our model, to try to evaluate the performance of our model. For this purpose, a data set with measurements at a variety of distances from the Silos is desired. The 1957 survey around the K-65 Silos consisted only of measurements fairly close to the Silos, which would not be representative of the exposures expected offsite. The boundary air monitoring station measurements, reported in the annual environmental reports, show exposure rates clearly elevated above background at only one location, AMS 6 (or BS-6), with the other boundary station exposure rates indistinguishable from background and showing no trend with distance from the Silos (see, for example, Dugan et al. 1990 and Byrne et al. 1991). One of the onsite locations also showed an exposure rate above background, but this location was on the east side of the site, near production areas, and is likely due to production area radiation sources.

The data from the Paddy's Run Road surveys are also not ideal, as only five locations were monitored. However, these monitoring locations were close enough to the Silos that we expect to see exposure rates elevated above background. Unfortunately, the surveys apparently did not include measurements at a background location. Even with these problems, we think the Paddy's Run Road surveys are the best data available for comparisons with our modeled exposure rates, and we will use them for these comparisons. The other data sets will be examined in more detail in the Task 5 Report.

The locations of the Paddy's Run Road survey stations were obtained from the daily monitoring forms (FMPC 1987), and are shown in Figure P–5. We have tabulated the

monthly average exposure rates from these surveys (Anonymous circa 1987) below in Table P–11. We found that the daily results for June 1987 (FMPC 1987) agreed with the monthly summary data (Anonymous circa 1987). The daily monitoring forms (FMPC 1987) indicate that a Ludlum Model 19 Micro R Meter, a type of exposure rate survey meter, was used for the June 1987 measurements. The instruments used for the other measurements are not known to us.

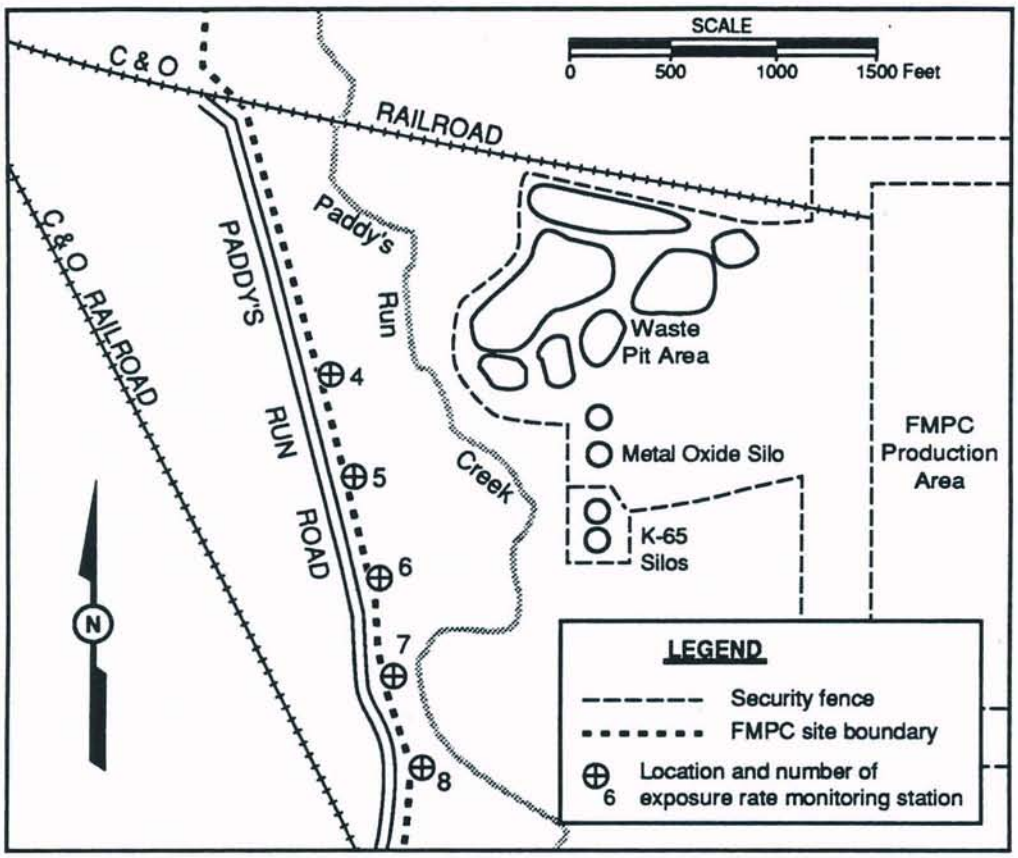

Figure P–5. Survey locations for Paddy's Run Road exposure rate surveys of 1986 and 1987, performed by the FMPC.

In Table P–11, there can be seen a significant change in recorded exposure rate between July and August, when the average exposure rates at all monitoring locations increased by 2 to 4 $\mu R\ h^{-1}$. We do not know of any change to the Silos, other significant change in radiation sources in this area, or seasonal effect that might have caused the change. One possible explanation is that the radiation survey instruments being used may have been changed (i.e., to a different type) or recalibrated at that time. It is well known that different types of radiation survey instruments have different energy response curves, and thus can produce different responses in a given condition, even when a calibration (which is usually only for a certain range of energies) has been performed. Since we did not obtain the daily survey forms for July and August 1987, we can only conjecture about the reasons for the change.

Table P–11. Monthly Average Exposure Rates ($\mu R\ h^{-1}$) from Paddy's Run Road Surveys of 1987

	Survey location				
Month	4	5	6	7	8
January	7	11	14	10	6
February	7	12	14	10	7
March	7	12	15	10	7
April	7	12	15	10	7
May	7	12	15	11	7
June	7	13	16	11	7
July	7	13	16	11	7
August	9	16	20	14	9
September	9	17	21	14	9
October	10	17	21	14	10
November	9	17	21	14	9
December	9	16	19	13	8
1987 Average	8	14	17	12	8

COMPARISONS OF MODELED TO MEASURED PENETRATING RADIATION EXPOSURE RATES

In 1987, the existence of the berms around the K-65 Silos means that Rn and daughters in the dome head space is the only source to be considered for the K-65 Silos (second geometry in Figure P–4). The Metal Oxide material is also a source (third geometry in Figure P–4).

The source activity concentrations, density, and moisture content data are compiled in the Tasks 2 and 3 report (in preparation). From that work, the average ^{222}Rn concentration in the K-65 Silos head space, for the 1980–1987 period, was estimated to be 2.62×10^7 pCi L^{-1}, or 0.0262 $\mu Ci\ cm^{-3}$ (the units required for MicroShield) (this was also previously developed in Voillequé et al. 1991). For the Metal Oxide Silo, the source term work (Tasks 2 and 3) compiles concentration measurement data for samples of the metal oxide. The density was determined to be 0.64 $g\ cm^{-3}$, and volume concentrations were calculated. Those concentrations are shown in Table P–12, along with the concentrations of daughter product radionuclides, that we assumed to be present at equilibrium concentrations. The moisture content was considered low enough to be negligible.

We determined the distances from the Silos to the monitoring locations by first plotting the monitoring locations on a detailed engineering drawing of the FMPC site (WMCO 1989b). We then scaled the distances between the monitoring location and Silo 3, and the midpoint between Silos 1 and 2 (see also Figure P–5). The results are given in Table P–13.

Using the source term and distance information, exposure rate calculations were performed using MicroShield. The results of these calculations are shown in Table P–14.

The Paddy's Run Road surveys did not include measurements of the background exposure rate, and no other background measurements using the same instruments are

Table P–12. Radionuclide Concentrations for Metal Oxide Material

Radionuclide	Concentration ($\mu Ci\ cm^{-3}$)	Basis	Radionuclide	Concentration ($\mu Ci\ cm^{-3}$)	Basis
^{227}Ac	3.72×10^{-4}	measured	^{226}Ra	1.90×10^{-3}	measured
^{228}Ac	5.01×10^{-4}	equilibrium	^{228}Ra	5.01×10^{-4}	equilibrium
^{212}Bi	5.01×10^{-4}	equilibrium	^{220}Rn	5.01×10^{-4}	equilibrium
^{214}Bi	1.90×10^{-3}	equilibrium	^{222}Rn	1.90×10^{-3}	equilibrium
^{231}Pa	3.57×10^{-4}	measured	^{228}Th	5.01×10^{-4}	equilibrium
^{234}Pa	1.25×10^{-6}	equilibrium	^{230}Th	3.28×10^{-2}	measured
^{234m}Pa	9.60×10^{-4}	equilibrium	^{231}Th	6.39×10^{-5}	equilibrium
^{212}Pb	5.01×10^{-4}	equilibrium	^{232}Th	5.01×10^{-4}	measured
^{214}Pb	1.90×10^{-3}	equilibrium	^{234}Th	9.60×10^{-4}	equilibrium
^{212}Po	3.21×10^{-4}	equilibrium	^{208}Tl	1.80×10^{-4}	equilibrium
^{214}Po	1.90×10^{-3}	equilibrium	^{234}U	9.46×10^{-4}	measured
^{216}Po	5.01×10^{-4}	equilibrium	^{235}U	6.39×10^{-5}	measured
^{218}Po	1.90×10^{-3}	equilibrium	^{238}U	9.60×10^{-4}	measured
^{224}Ra	5.01×10^{-4}	equilibrium			

Table P–13. Distance between Paddy's Run Road Survey Locations and Silos

Monitoring location	Distance from monitoring location (ft) to: Point between Silos 1 and 2	Center of Silo 3
4	1490	1520
5	1190	1210
6	1100	1090
7	1290	1250
8	1630	1580

known to us. Thus, for comparison purposes we used the measured and predicted values at location 8, in lieu of background data. We thus subtracted the values for location 8 from the other values before making comparisons. The predicted exposure rates, in excess of the prediction for location 8, are compared with the average measured exposure rates, in excess of the measured value for location 8, in Table P–15. For this survey data, the predicted excess exposure rates are roughly one half the measured excess exposure rates.

Based on these limited comparisons of predictions to measurements for the Paddy's Run Road surveys, it appears that our predicted exposure rates may be somewhat underbiased. With the available data, we cannot determine the sources of this bias. Contributing factors may include inaccuracies in the measurements, in the MicroShield model, or in parameter values used to describe the sources and shields (derived primarily from our source term). We tentatively conclude that, relative to the measurements, and when the uncertainties involved are considered, the predicted exposure rates are in a range considered acceptable.

Table P–14. Predicted Exposure Rates at Paddy's Run Road Survey Locations

	Predicted Exposure rate ($\mu R\ h^{-1}$) due to:		
Location	Silos 1 and 2	Silo 3	Total
4	1.68	0.0284	1.7
5	4.30	0.0523	4.4
6	5.83	0.0490	5.9
7	3.11	0.0212	3.1
8	1.12	0.00768	1.1

Table P–15. Comparison of Predicted and Measured Exposure Rates for Paddy's Run Road Survey Locations

	Excess exposure rate relative to location 8 ($\mu R\ h^{-1}$)	
Monitoring location	Predicted	Measured 1987 average
4	0.6	0
5	3.3	6
6	4.8	9
7	2.0	4

However, as mentioned earlier in this Appendix, additional environmental exposure rate data will be evaluated in the Task 5 Report. After analyzing those data, we will study further the agreement of predictions and measurements before making final conclusions about the performance of the MicroShield model for direct exposure calculations.

REFERENCES

Aas C.A., D.L. Jones, and R.W. Keys. 1986. *Feed Materials Production Center Environmental Monitoring Annual Report for 1985*. Rep. FMPC-2047, Special, UC-41, Westinghouse Materials Company of Ohio, Cincinnati, Ohio.

Anonymous. Circa 1984. *FMPC Radon (Terradex) Results*. Handwritten spreadsheet of Rn concentrations.

Anonymous. Circa 1987. *K-65/Paddy's Run Road Daily Surveys*. Twelve monthly summary spreadsheets for January through December 1987.

Berven B.A. and W.D. Cottrell. 1987. *Review of Radiological Data for the K-65 Storage Silos at the Feed Materials Production Center, Fernald, Ohio*. Rep. ORNL/M-2110, Oak Ridge National Laboratory, Oak Ridge, Tennessee.

Boback M.W. Circa 1984. File folder of information related to measurements of Rn and Rn daughters at the FMPC during 1978–1980. NLO, Inc., Cincinnati, Ohio.

Boback M.W. and K.N. Ross. 1979. *Feed Materials Production Center Environmental Monitoring Annual Report for 1978*. Rep. NLCO-1159, Special, National Lead Company of Ohio, Cincinnati, Ohio.

Boback M.W. and K.N. Ross. 1980. *Feed Materials Production Center Environmental Monitoring Annual Report for 1979*. Rep. NLCO-1164, Special, National Lead Company of Ohio, Cincinnati, Ohio.

Boback M.W. and K.N. Ross. 1981. *Feed Materials Production Center Environmental Monitoring Annual Report for 1980*. Rep. NLCO-1168, Special, NLO, Inc., Cincinnati, Ohio.

Boback M.W., K.N. Ross, and D.A. Fuchs. 1977. *Feed Materials Production Center Environmental Monitoring Annual Report for 1976*. Rep. NLCO-1142, Special, National Lead Company of Ohio, Cincinnati, Ohio.

Boback M.W., K.N. Ross, and D.A. Fuchs. 1978. *Feed Materials Production Center Environmental Monitoring Annual Report for 1977*. Rep. NLCO-1151, Special, National Lead Company of Ohio, Cincinnati, Ohio.

Byrne J.M. 1992. Letter, with enclosed computer disks, to Duane W. Schmidt, dated August 31, 1992. Reference number WEMCO:EM:EMON:92-1274, Westinghouse Environmental Management Company of Ohio, Cincinnati, Ohio.

Byrne J.M., T.A. Dugan, and J.S. Oberjohn. 1991. *Feed Materials Production Center Annual Environmental Report for Calendar Year 1990*. Rep. FMPC-2245, Special, UC-707, Westinghouse Materials Company of Ohio, Cincinnati, Ohio.

DOE (U.S. Department of Energy). 1990. *Remedial Investigation Report for Operable Unit 4, Task 6 Report, Feed Materials Production Center, Fernald, Ohio, Remedial Investigation and Feasibility Study*. Draft final, dated October 1990. U.S. Department of Energy, Oak Ridge, TN.

Dugan T.A., G.L. Gels, J.S. Oberjohn, and L.K. Rogers. 1990. *Feed Materials Production Center Annual Environmental Report for Calendar Year 1989*. Rep. FMPC-2200, Special, UC-707, Westinghouse Materials Company of Ohio, Cincinnati, Ohio.

Facemire C.F., D.L. Jones, and R.W. Keys. 1985. *Feed Materials Production Center Environmental Monitoring Annual Report for 1984*. Rep. NLCO-2028, Special, UC-41, NLO, Inc., Cincinnati, Ohio.

Fleming D.A. and K.N. Ross. 1983. *Feed Materials Production Center Environmental Monitoring Annual Report for 1982*. Rep. NLCO-1187, Special, UC-41, NLO, Inc., Cincinnati, Ohio.

Fleming D.A. and K.N. Ross. 1984. *Feed Materials Production Center Environmental Monitoring Annual Report for 1983*. Rep. NLCO-2018, Special, UC-41, NLO, Inc., Cincinnati, Ohio.

Fleming D.A., M.W. Boback, and K.N. Ross. 1982. *Feed Materials Production Center Environmental Monitoring Annual Report for 1981*. Rep. NLCO-1180, Special, UC-41, NLO, Inc., Cincinnati, Ohio.

FMPC (Feed Materials Production Center). 1987. *Perimeter Radiation Monitoring Report*. Twenty-nine radiation survey forms, dated June 1 through June 30, 1987. Environment, Safety & Health, Environmental & Radiological Monitoring Section.

George A.C. 1977. "A Passive Environmental Radon Monitor." In: A.J. Breslin, Ed. *Radon Workshop, February 1977*. Rep. HASL-325, published July 1977, Health and Safety Laboratory, Energy Research and Development Administration, New York, New York. pp. 25–30.

George A.C., L. Hinchliffe, I.M. Fisenne, and E.O. Knutson. 1985. *Intercomparison and Intercalibration of Passive Radon Detectors in North America*. Rep. EML-442, Environmental Measurements Laboratory, U.S. Department of Energy, New York, New York.

Hagee G.R., P.H. Jenkins, P.J. Gephart, and C.R. Rudy. 1985. *Radon and Radon Flux Measurements at the Feed Materials Production Center, Fernald, Ohio*. Rep. MLM-MU-85-68-0001, Mound, Monsanto Research Corporation, Miamisburg, Ohio.

HEW (U.S. Department of Health, Education, and Welfare). 1970. *Radiological Health Handbook*. Public Health Service, HEW, Rockville, Maryland.

ICRP (International Commission on Radiological Protection). 1977. *Recommendations of the ICRP*. ICRP Publication 26. *Ann. ICRP* 1(3).

ICRP (International Commission on Radiological Protection). 1987. *Data for Use in Protection Against External Radiation*. ICRP Publication 51. *Ann. ICRP* **17**(2/3).

ICRP (International Commission on Radiological Protection). 1991. *1990 Recommendations of the International Commission on Radiological Protection*. ICRP Publication 60. *Ann. ICRP* **21**(1–3).

Jenkins P.H. 1986. Letter to Woodrow D. Cottrell, Oak Ridge National Laboratory, dated November 21, 1986. Mound, Monsanto Research Corporation, Miamisburg, Ohio.

Kerr G.D., K.F. Eckerman, and J.C. Ryman. 1985. "Organ Doses from Exposure to Isotropic Fields of Gamma Rays with an Emphasis on Active Marrow and Osteogenic Tissue of the Skeleton." Pages 78–88 in Eckerman K.F., Ed. *Report of Current Work of the Metabolism and Dosimetry Research Group, January 1, 1984–June 30, 1985*. Rep. ORNL/TM-9690, Oak Ridge National Laboratory, Oak Ridge, Tennessee.

Kocher D.C. 1983. "External Dosimetry." Chapter 8 in: Till J.E. and H.R. Meyer, Eds. *Radiological Assessment, A Textbook on Environmental Dose Analysis*. Rep. NUREG/CR-3332, U.S. Nuclear Regulatory Commission, Washington, D.C.

NCRP (National Council on Radiation Protection and Measurements). 1984. *Radiological Assessment: Predicting the Transport, Bioaccumulation, and Uptake by Man of Radionuclides Released to the Environment*. NCRP Report No. 76, NCRP, Bethesda, Maryland.

Negin C.A. and G. Worku. 1992. *MicroShield, Version 4, User's Manual*. Rep. Grove 92-2, Grove Engineering, Inc., 15215 Shady Grove Road, Suite 200, Rockville, Maryland 20850.

Nelson, M.S. 1972. *U Content of Silos*. Letter to C.A. Keller, Uranium Enrichment Division, U.S. Atomic Energy Commission, dated September 21, 1972. National Lead Company of Ohio, Cincinnati, OH.

NLCO (National Lead Company of Ohio). 1976. *Feed Materials Production Center Environmental Monitoring Annual Report for 1975*. Rep. NLCO-1133, Special, NLCO, Cincinnati, Ohio.

Preload (Preload Enterprises, Inc.). 1951. *Two 125,000 c.f. Slurry Storage Tanks – Type K65, Atomic Energy Commission, Fernald, Ohio, Catalytic Construction Co.* Revision 4, engineering drawing dated September 15, 1951. Drawing number 51T20-3, FMPC drawing index code 34X-1450-A-00086, Preload, New York.

Ross K.N. 1957. *Storage of Residues from Processing Radium-Bearing Ores.* Internal memorandum to R.C. Heatherton, dated July 17, 1957. National Lead Company of Ohio, Cincinnati, Ohio.

Schwarzman G.E. 1992. *Quarterly Groundwater Sampling Locations and Private Wells.* FMPC drawing index code 00X-5500-G-02006, Westinghouse Environmental Management Company of Ohio, Cincinnati, Ohio.

Shanks P.A. and R.A. Vogel. 1988. *The K-65 Waste Storage Silos at the Feed Materials Production Center.* Paper for presentation at the DOE Model Conference, Oak Ridge, Tennessee, October 3–7, 1988. Rep. FMPC-2142, Westinghouse Materials Company of Ohio, Cincinnati, OH.

Steva D.P. 1988. *Ohio Department of Health Study of Radioactivity in Drinking Water and Other Environmental Media in the Vicinity of the U.S. Department of Energy's Feed Materials Production Center and Portsmouth Gaseous Diffusion Plant.* Ohio Department of Health, Columbus, Ohio.

Voillequé, P.G., K.R. Meyer, D.W. Schmidt, G.G. Killough, R.E. Moore, V.I. Ichimura, S.K. Rope, B. Shleien, and J.E. Till. 1991. *The Fernald Dosimetry Reconstruction Project, Tasks 2 and 3: Radionuclide Source Terms And Uncertainties — 1960–1962.* Draft interim report for comment, dated December 1991. Rep. CDC-2, Radiological Assessments Corporation, Neeses, South Carolina 29107.

WMCO (Westinghouse Materials Company of Ohio). 1987. *Feed Materials Production Center Environmental Monitoring Annual Report for 1986.* Rep. FMPC-2076, Special, UC-41, WMCO, Cincinnati, Ohio.

WMCO (Westinghouse Materials Company of Ohio). 1988. *Feed Materials Production Center Environmental Monitoring Annual Report for 1987.* Rep. FMPC-2135, Special, UC-41, WMCO, Cincinnati, Ohio.

WMCO (Westinghouse Materials Company of Ohio). 1989a. *Feed Materials Production Center Environmental Monitoring Annual Report for 1988.* Rep. FMPC-2173, Special, UC-707, WMCO, Cincinnati, Ohio.

WMCO (Westinghouse Materials Company of Ohio). 1989b. *Feed Materials Production Center.* Map of the FMPC site and immediate surroundings, dated June 27, 1989, WMCO, Cincinnati, Ohio.

Woolpert Consultants. Circa 1988. *Fernald Facility, Department of Energy, Fernald, Ohio.* Set of 17 topographic maps. FMPC drawing index codes 75X-5500-G-00112 through 75X-5500-G-00128, Woolpert Consultants, Dayton, Ohio.

Table PS–1. Concentrations of ^{222}Rn Measured by Mound Monitoring Program at the FMPC from July 2, 1985 through October 3, 1986 (pCi L^{-1})[a]

Monitoring period		Monitoring location									
From:	To:	1	2	3	4	5	6	7	8	9	10
07/02/85	07/18/85	4.7	1.7	2.8	2.7	6.4	1.6	1.9	0.80	1.1	0.69
07/18/85	08/02/85	4.0	1.3	5.8	2.2	3.2	1.3	1.5	0.71	0.73	0.37
08/02/85	08/08/85	1.4	1.1	8.0	6.3	2.5	0.74	1.6	0.76	0.93	0.78
08/08/85	08/15/85	5.0	1.7	8.1	3.9	5.2	1.2	0.87	0.88	0.97	0.28
08/15/85	08/29/85	4.2	1.6	5.7	4.2	3.8	1.2	1.2	0.57	1.2	0.79
08/29/85	09/05/85	8.0	1.7	5.1	3.9	8.2	1.4	1.4	0.67	0.56	0.61
09/05/85	09/12/85	5.4	1.9	2.1	4.0	7.0	1.4	1.9	1.1	1.3	0.69
09/12/85	09/19/85	3.8	2.1	25	5.5	5.9	2.4	3.9	2.7	2.1	1.1
09/19/85	10/01/85	6.4	2.7	9.9	11	8.3	2.8	3.2	1.7	2.1	2.3
10/01/85	10/09/85	8.4	2.0	14	4.3	6.5	3.4	4.2	2.5	1.4	1.0
10/09/85	10/23/85	3.7	2.9	9.3	5.6	5.7	1.2	1.9	1.4	1.6	1.3
10/23/85	11/06/85	1.6	2.0	19	1.7	1.3	0.88	0.55	0.75	0.38	
11/06/85	11/13/85	2.9	2.0	7.1	6.1	5.5	1.3	0.85	0.69	0.57	1.2
11/13/85	11/27/85	4.1	1.8	14	4.5	5.2	1.3	0.80	0.94	0.44	0.38
11/27/85	12/04/85	1.5	2.1	9.5	3.1	0.99	0.53	0.19	0.28	0.12	0.32
12/04/85	12/11/85	7.3	8.9	14	14	11	3.5	1.8	2.8	1.1	0.69
12/11/85	12/19/85	3.3	2.1	3.6	3.8	3.3	0.94	0.56	0.64	0.69	0.85
12/19/85	01/02/86	7.3	1.4	2.8	3.1	8.5	2.5	0.88	1.2	0.63	0.70
01/02/86	01/08/86	3.1	1.7	6.1	6.0	2.9	0.86	0.74	0.96	0.61	0.96
01/08/86	01/15/86	7.9	2.5	3.6	2.0	5.8	2.9	1.5	1.8	0.48	0.77
01/15/86	01/22/86	4.1	1.5	5.2	11	5.2	0.95	1.1	1.4	0.68	1.0
01/22/86	01/29/86	4.8	1.1	7	3.2	1.6	1.2	0.85	0.99	0.15	0.31
01/29/86	02/05/86	2.5	1.6	12	4.3	3.4	1.3	0.76	0.98	0.51	1.1
02/05/86	02/12/86	4.8	1.6	2.1	0.99	1.1	1.2	0.43	0.62	0.45	0.25
02/12/86	02/19/86	8.4	6.9	22	12	6.2	1.1	1.8	4.2	0.72	0.72
02/19/86	02/27/86	8.8	3.0	7.1	4.9	4.0	1.7	0.48	0.96	0.51	0.30
02/27/86	03/05/86	7.0	2.3	1.2	4.0	2.7	2.9	1.0	1.1	0.43	0.32
03/05/86	03/12/86	4.6	1.7	4.7	6.7	5.3	0.94	0.24	0.40	0.49	0.67
03/12/86	03/19/86	5.1	3.3	10.	4.4	4.8	2.4	0.56	0.93	0.56	0.48
03/19/86	03/26/86	7.3	2.7	3.4	5.2	6.1	2.2	0.47	1.1	0.69	0.67
03/26/86	04/02/86	7.5	2.7	4.1	3.3	15	3.5	1.5	2.6	0.97	1.3
04/02/86	04/09/86	9.7	2.2	12	3.8	9.2	1.8		1.5	1.5	1.2
04/09/86	04/16/86	8.6	1.2	6.8	3.0	2.7	2.6	1.9	1.5	0.86	0.74
04/16/86	04/29/86	12	4.4	6.3	5.1	5.1	2.0	1.9	2.4	1.2	1.2
04/29/86	05/07/86	7.6	5.3	2.4	5.2	7.4	2.7	1.6	2.5	0.54	1.2
05/07/86	05/14/86	7.0	1.9	18	2.2	4.6	1.6	0.97	1.2	0.97	0.67
05/14/86	05/21/86	4.5	0.61	1.5	5.5	6.7	1.4	0.54	1.1	0.83	0.48
05/21/86	05/28/86	7.2	1.8	9.9	5.4	5.2	2.3	1.5	1.8	1.1	1.1
05/28/86	06/04/86	9.1		11		7.4	2.9	1.6	2.6	1.2	0.91
06/04/86	06/11/86	7.4	0.97	5.8	5.5	9.5	1.1		1.1	0.76	0.60
06/11/86	06/18/86		1.9	3.1	4.3	13	2.0		1.4	1.6	0.79
06/18/86	06/25/86	12	1.7	9.3	3.8	7.7	2.9		1.6	1.4	1.1
06/25/86	07/02/86	11	1.6	7.1	5.1	6.8	2.5		1.7	1.6	0.76
07/02/86	07/08/86	8.0	2.7	1.4	5.4	10.	2.0		1.6	1.1	1.1
07/08/86	07/16/86	7.5	1.1	3.4	2.3	7.4	1.3		0.96	0.91	0.55
07/16/86	07/23/86	15	1.1	3.3	2.9	6.2	3.1		1.4	1.3	0.88
07/23/86	07/30/86	8.2	2.0	7.8	2.9	5.1	2.2		2.1	1.2	1.3
07/30/86	08/06/86	10.	1.5	6.2	3.0	3.8	2.6		2.2	2.0	1.4
08/06/86	08/13/86	8.4	1.9	3.4	2.8	5.2	2.9		2.2	1.1	1.1
08/13/86	08/20/86	5.5	1.3	4.9	3.0	5.5	1.7		1.8	1.5	0.93
08/20/86	08/27/86	4.2	1.9	7.3	2.6	4.7	1.4		1.4	1.6	1.1
08/27/86	09/03/86	2.3	2.5	11	3.0	2.2	1.8		2.4	2.0	1.2
09/03/86	09/10/86	7.5	1.8	5.7	4.4	5.5	2.8		1.8	1.7	1.2
09/10/86	09/17/86	4.0	0.77	5.6	3.7	5.2	0.67		0.74	0.36	1.1
09/17/86	09/24/86	4.2		6.3	2.7	6.1	1.7		1.1	1.0	0.78
09/24/86	10/03/86	4.8	0.85	3.2	4.3	9.5	1.3		1.2	1.2	0.85

[a] Ref: Jenkins 1986.

Table PS–1. Concentrations of ^{222}Rn Measured by Mound Monitoring Program at the FMPC from July 2, 1985 through October 3, 1986 (pCi L^{-1})[a] (continued)

Monitoring period		Monitoring location									
From:	To:	11	12	13	14	15	17	18	19	20	21
07/02/85	07/18/85	0.89	0.95	0.41	0.31	0.42	0.47	0.44			
07/18/85	08/02/85	0.72	0.95	0.45		0.65	0.51	0.68			
08/02/85	08/08/85	1.7	1.5	0.36	0.36	0.80	0.50	0.67			
08/08/85	08/15/85	0.59	0.73	0.58	0.35	0.67	0.58	0.47			
08/15/85	08/29/85	1.1	0.99	0.33	0.39	0.56	0.52	0.65			
08/29/85	09/05/85	0.93	1.5	0.39	0.56	0.73	0.59				
09/05/85	09/12/85	1.2	1.3	0.61	0.3	0.52	0.53	0.61			
09/12/85	09/19/85	2.1	2.5	1.1	1.1	2.1	1.0	2.2			
09/19/85	10/01/85	2.9	3.4	1.1	0.99	1.9	1.0	1.3			
10/01/85	10/09/85	2.6	2.7	1.2	1.1	1.5	1.1	1.4	1.1	1.1	2.1
10/09/85	10/23/85	2.2	2.1	0.84	0.43	0.82	0.58	0.83	0.96	0.86	1.6
10/23/85	11/06/85	0.86	1.1	0.40	0.28	0.82	0.35	0.37	0.50	0.30	0.56
11/06/85	11/13/85	0.94	1.7	0.47	0.2	0.43	0.19	0.30	0.32	0.19	0.41
11/13/85	11/27/85	0.49	0.81	0.57	0.27	0.58	0.24	0.33	0.54	0.32	0.55
11/27/85	12/04/85	0.31		0.30	0.17	0.25	0.57	0.16	0.18	0.19	0.14
12/04/85	12/11/85	1.3	2.2	2.4	0.69	0.67	0.98	0.59	0.85	0.63	1.2
12/11/85	12/19/85	0.84	0.87	0.51	0.18	0.21	0.22	0.23	0.35	0.15	0.29
12/19/85	01/02/86	0.73	0.70	0.48	0.29	0.34	0.34	0.29	0.42	0.24	0.29
01/02/86	01/08/86	0.85	1.6	0.66	0.23	0.28	0.25	0.39	0.44	0.34	0.25
01/08/86	01/15/86	0.70	1.4	0.69	0.42	0.39	0.44	0.39	0.63	0.32	0.60
01/15/86	01/22/86	1.2	2.2	0.38	0.38	0.44	0.36	0.27	0.72	0.44	0.40
01/22/86	01/29/86	0.44	1.1	0.27	0.26	0.43	0.25	0.32	0.41	0.25	0.41
01/29/86	02/05/86	0.74	1.2	0.51	0.34	0.65	0.30	0.31	0.41	0.38	0.26
02/05/86	02/12/86	0.24	0.36	0.26	0.11	0.15	0.15	0.18	0.26	0.17	0.17
02/12/86	02/19/86	2.6	4.7	0.83	0.29	0.54	0.38	0.37	0.67	0.43	0.88
02/19/86	02/27/86	0.89	1.2	0.38	0.18	0.22	0.21	0.24	0.35	0.23	0.32
02/27/86	03/05/86	0.66	1.0	0.27	0.30	0.20	0.27	0.15	0.27	0.29	
03/05/86	03/12/86	0.80	1.3	0.14	0.10	0.12	0.19	0.23	0.40	0.31	0.20
03/12/86	03/19/86	0.63	1.9	0.33	0.17	0.45	0.29	0.19	0.43	0.47	0.63
03/19/86	03/26/86	1.0	1.2	0.35	0.13	0.24	0.22	0.31	0.47	0.28	0.53
03/26/86	04/02/86	1.4	2.5	0.81	0.42	0.74	0.51	0.56	0.72	0.69	1.3
04/02/86	04/09/86	1.6	2.6	0.69	0.23	0.56	0.47	0.50	0.81	0.67	1.2
04/09/86	04/16/86	1.2	1.8	0.48	0.39	0.53	0.48	0.39	0.52	0.49	0.90
04/16/86	04/29/86	1.8	1.8	0.88	0.24	0.47	0.55	0.66	0.77	0.78	1.1
04/29/86	05/07/86	1.7	2.1	1.0	0.48	0.65	0.73		0.61	0.53	1.2
05/07/86	05/14/86	1.0	1.4	0.46	0.16	0.51	0.37	0.47	0.49	0.52	0.75
05/14/86	05/21/86	1.3	0.49	0.23	0.23	0.23	0.21	0.46	0.25	0.25	0.50
05/21/86	05/28/86	2.4	2.3	0.72	0.30	0.54	0.48	0.46	0.58	0.54	0.84
05/28/86	06/04/86	3.4	1.9	0.68	0.44	0.65	0.59	0.91	0.54	0.62	1.1
06/04/86	06/11/86	2.1	2.5	0.30	0.13	0.30	0.26	0.38	0.50	0.35	0.64
06/11/86	06/18/86	2.7	1.6	0.83	0.40	0.49	0.55	0.89	0.65	0.63	1.0
06/18/86	06/25/86	2.7	1.9	0.73	0.31	0.52	0.57	0.88	0.86	0.83	1.1
06/25/86	07/02/86	1.4	2.2	0.69	0.47	0.70	0.64	1.1	0.75	0.68	1.1
07/02/86	07/08/86	1.4	1.0	0.65	0.23	0.51	0.74	1.0	0.75	0.69	1.4
07/08/86	07/16/86	0.68	1.2	0.34	0.17	0.51	0.32	0.47	0.41	0.41	0.71
07/16/86	07/23/86	1.2	1.4	0.35		0.25	0.40	0.44	0.17	0.65	0.66
07/23/86	07/30/86	1.4	2.0	0.78	0.41	1.1	0.84	0.99	0.86	0.83	1.7
07/30/86	08/06/86	3.1	2.1	0.63	0.32	1.0	1.0	1.4	1.2	1.3	2.1
08/06/86	08/13/86	2.2	2.8	0.66	0.41	1.1	0.77	0.64	0.73	0.70	1.5
08/13/86	08/20/86	1.9	2.3	0.77	0.30	0.73	0.85	0.76	0.80	1.1	1.4
08/20/86	08/27/86	2.1	2.0	0.95	0.68	1.3	0.82	0.86	1.2	0.69	1.5
08/27/86	09/03/86	2.6	2.3	1.5	0.51	0.79	0.92	1.3	1.1	1.2	1.5
09/03/86	09/10/86	3.6	2.7	1.2	0.70	1.5	0.74	1.4	1.2	1.2	1.8
09/10/86	09/17/86	1.5	1.6	0.36	0.29	0.61	0.46	0.95	0.53	0.74	0.91
09/17/86	09/24/86	2.4	2.7	0.56	0.53	0.54	0.62	0.75	0.80	0.43	1.3
09/24/86	10/03/86	1.2	0.53	0.82	0.16	0.38	0.37	0.65	0.62	0.43	0.82

[a] Ref: Jenkins 1986.

APPENDIX Q

THE RAGTIME AGRICULTURAL MODEL

INTRODUCTION

Agricultural products (both commercial and those produced by individuals for their own consumption) constitute a node in a pathway for transport of released radionuclides to users of the products. In the context of the FMPC assessment domain, we consider radionuclide contamination of food crops and animal forage by deposition of airborne material and irrigation with water from contaminated sources. By these mechanisms, contamination is applied to plant surfaces and is also taken up through the roots from the soil. Translocation from the surface to interior plant tissues may also occur. The radioactivity may reach people who eat the vegetable matter or the products of animals that have consumed contaminated forage or water.

The RAGTIME model (Radionuclides in AGricultural systems, a TIME dependent model) was developed in the late 1970s and implemented on mainframe computers (Pleasant et al. 1980). The original goal was to provide a comprehensive agricultural model that would be useful for studying dynamic effects (e.g., time-dependent parameters, demographics of dairy and beef herds). In 1987, RAGTIME was revised and reprogrammed for participation in the international BIOMOVS model validation, in which data from the Chernobyl reactor accident were available from a number of sites for providing model inputs (air concentration data) and also resultant concentrations on crops for comparison with the model simulations. RAGTIME fared well in the validation exercise, where ^{131}I and ^{137}Cs were the radionuclides considered (Köhler et al. 1991).

This appendix gives background information on the RAGTIME approach and describes its proposed application to the FMPC region. Details of the implementation will depend, in some degree, on the relative contribution of ingestion pathways to the total dose to individuals living near the FMPC (including dose from inhalation, which is expected to dominate).

Much of this discussion is freely adapted from the reports Pleasant et al. (1980) and Pleasant et al. (1982), and we do not make further attributions to these sources. Inasmuch as one of us (G.G.K.) was one of the authors of these reports, we have made no particular effort to avoid identical or very similar phrasing where it best serves the purpose of our exposition.

ORIGINS OF RAGTIME

RAGTIME began as an adaptation of the earlier TERMOD (Booth and Kaye 1971), which treated response variables as dynamic quantities (i.e., the system was represented by a system of ordinary differential equations, in contrast to quasi–steady-state models based on transfer ratios). But TERMOD required a formulation for which the differential equations could be solved in closed form and therefore was unable to incorporate temporal refinements such as seasonal effects and time-varying parameters; nonlinearities were also precluded. To circumvent such limitations, the RAGTIME differential equations were solved numerically by a

discrete-variable technique. Ingrowth of radioactive daughters was also treated explicitly in the original RAGTIME.

In 1987, RAGTIME was revised and reprogrammed and, under the name RAGTIME87, participated, along with 20 other models, in the BIOMOVS program (BIOspheric MOdel Validation Study), an international cooperative study that was initiated by the Swedish National Institute of Radiation Protection. In Scenario A4 of the study, the models were tested using Chernobyl fallout data at 13 sites for ^{131}I and ^{137}Cs in forage, milk, beef, and grain. Predicted-to-observed ratios based on the RAGTIME87 simulations of resultant concentrations of radioactivity, based on daily records of radioactivity in the air, were extensively tabulated and plotted for all of the models (Köhler et al. 1991). When all predictions and observations are considered, we believe it is fair to say that RAGTIME87 was among the most successful of the models.

OVERVIEW OF RAGTIME

RAGTIME estimates radionuclide concentrations in food crops, pasture grass, beef, and milk, which are contaminated directly or indirectly by radionuclide deposition and irrigation with contaminated water. In the present structure, root crops are not explicitly represented and must be included by *ad hoc* methods. The model assumes a known rate of deposition of radioactivity (pCi m^{-2} s^{-1}) at a given location and uses interception fractions $\mathcal{S}_1$, $\mathcal{S}_2$, $\mathcal{S}_3$, and $\mathcal{S}_4$ to calculate radioactivity input rates to the model compartments representing above-ground food crops, the soil surface below the food crop, pasture grass, and pasture soil or root mat, respectively, at that location.

The model is shown schematically in Fig. Q–1. Although for the current dose reconstruction project it may not be necessary to represent explicitly the dynamics of daughter ingrowth, we retain the mechanisms in the formulas. Accordingly, the subscript i associated with the model compartments (E_i, S_i, P_i, etc.) refers to the ith nuclide of a decay chain ($i = 1, \ldots, N$). Alternatively, i can refer to the ith of a list of radionuclides that are not related by decay-chain relationships. Certain of the transfer coefficients are nuclide-, or element-, dependent; this dependence is also signified by the use of the subscript i (e.g., $(\tau_{p,t})_i$). The deposition source F_i (pCi m^{-2} s^{-1}) represents the input source of radioactivity corresponding to the ith nuclide in a decay chain. This source strength may vary with time according to a step function that is specified with the input. The interception fractions $\mathcal{S}_1, \ldots, \mathcal{S}_4$ may also be time-dependent with respect to growth dynamics of the crop land or pasture. Models for time-dependent interception fractions are discussed in a later section.

An outline of the terrestrial pathways considered in RAGTIME follows, along with brief descriptions of the parameters.

Transfer of Radioactivity to Food Crops

Radioactivity deposited on the surface of the above-ground food crop passes to the soil surface below the plants with an environmental half-time of usually less than 30 days (Witherspoon and Taylor 1970). We typically use 14 days for this parameter (Booth and Kaye 1971, Zimbrick and Voillequé 1968). For transfer from the soil surface below the food crop to the subsurface soil pool (root zone), we have assumed a 1,000-day environmental half-time. The

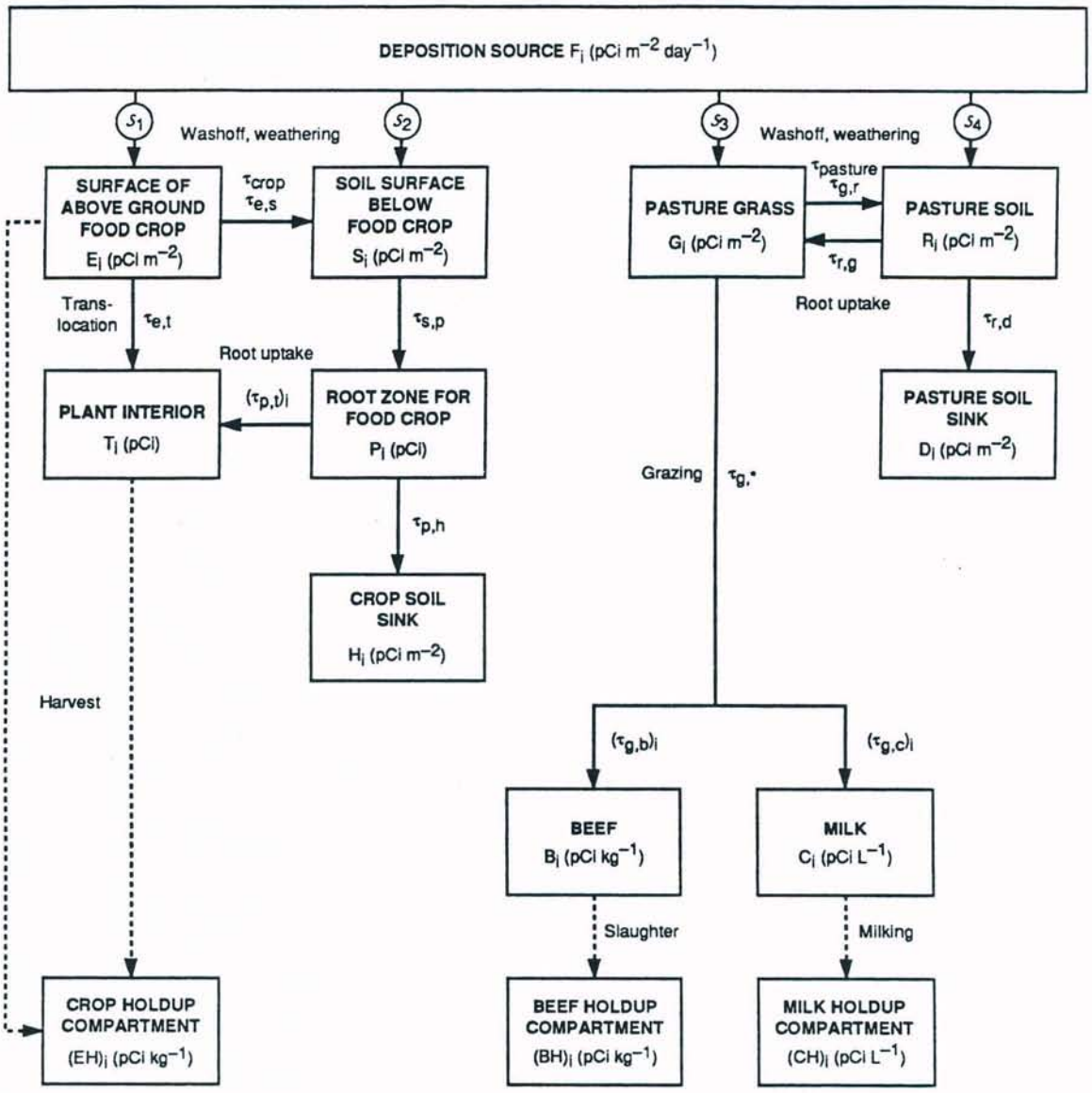

Figure Q–1. The RAGTIME schematic compartment diagram. Some details of the transfer mechanisms for food crops and pasture grass are elaborated in subsequent figures. Stored feed for beef and dairy cattle are not shown in the figure.

plant interior compartment T_i simulates radioactivity that is transferred to the edible parts of crops as a result of root uptake and translocation from the plant surface.

The rate coefficient $(\tau_{p,t})_i$ representing uptake to T_i through the roots of radioactivity from the root zone (P_i) is treated as a time-dependent quantity. The functional relationship is described in a subsequent section. For the loss of radioactivity from the root zone to the soil compartment below the roots H_i (soil sink), we have assumed a loss rate of 4% per year (Booth and Kaye 1971, Menzel 1963). The dotted lines in Fig. Q–1 from compartments E_i (surface of the above-ground food crop, expressed as the sum of components $(E_w)_i$ and $(E_d)_i$, as explained

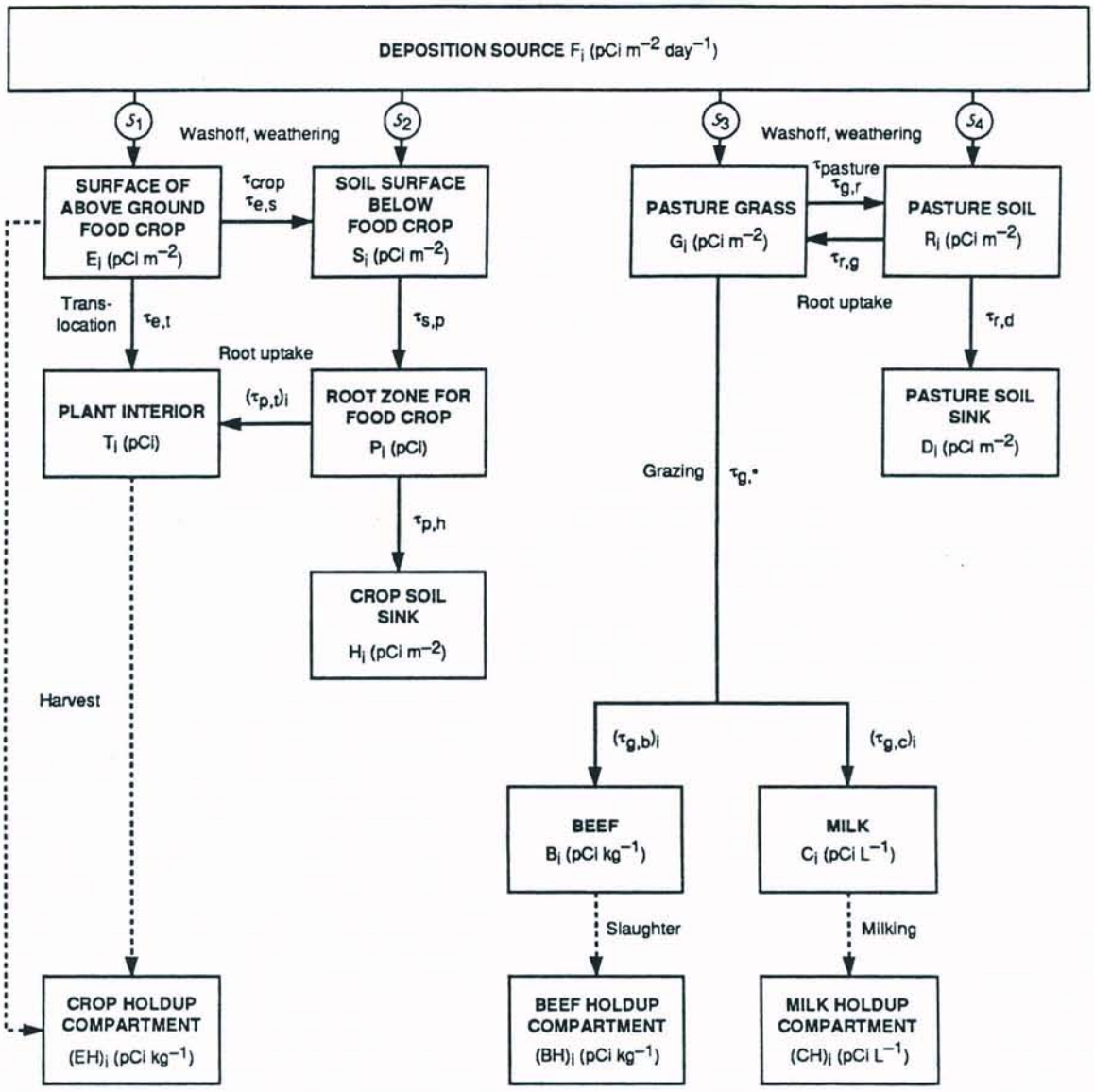

Figure Q–1. The RAGTIME schematic compartment diagram. Some details of the transfer mechanisms for food crops and pasture grass are elaborated in subsequent figures. Stored feed for beef and dairy cattle are not shown in the figure.

plant interior compartment T_i simulates radioactivity that is transferred to the edible parts of crops as a result of root uptake and translocation from the plant surface.

The rate coefficient $(\tau_{p,t})_i$ representing uptake to T_i through the roots of radioactivity from the root zone (P_i) is treated as a time-dependent quantity. The functional relationship is described in a subsequent section. For the loss of radioactivity from the root zone to the soil compartment below the roots H_i (soil sink), we have assumed a loss rate of 4% per year (Booth and Kaye 1971, Menzel 1963). The dotted lines in Fig. Q–1 from compartments E_i (surface of the above-ground food crop, expressed as the sum of components $(E_w)_i$ and $(E_d)_i$, as explained

below) and T_i (plant interior) to compartment $(EH)_i$ (crop holdup) represent harvesting of crops.

The level of radioactivity in all compartments associated with crops at a given time is dependent on the histories of both the deposition source strength and on the growth of the crops. The effect of crop growth on the radioactivity level on the plant surfaces (compartment E_i) is simulated through the use of the time-dependent interception fraction S_1. The time-dependent transfer coefficient $(\tau_{p,t})_i$ plays a similar role as the principal source for the plant interior T_i. (The translocation coefficient $(\tau_{e,t})_i$ is not currently parameterized.) Before the emergence of plants, the value of S_1 is zero, as is that for $(\tau_{p,t})_i$. At harvest time, the entire food crop is assumed to be stored in a holdup compartment $(EH)_i$, after which time the radioactivity concentration level in this food is assumed to be affected only by the dynamics of radioactive decay. Thus, the activity level in the compartments representing crops in the field (compartments E_i and T_i) is zero except at times between the emergence and harvest of crops.

Transfer of Radioactivity to Beef and Milk

As in the case of transfer from the surface of the above-ground food crop to the soil surface, we have assumed a 14-day environmental half-time for the loss of radioactivity from pasture grass to pasture soil (Booth and Kaye 1971, Zimbrick and Voillequé 1968). To account for uptake of radioactivity by pasture grass from soil, we have used a transfer rate of 1% per year from R_i to G_i (Booth and Kaye 1971, Menzel 1963). As in the determination of $\tau_{p,h}$, a transfer rate of 4% per year from the pasture soil compartment R_i to the soil below the roots D_i was assumed (Booth and Kaye 1971, Menzel 1963).

The rate coefficient for loss of radioactivity from pasture grass resulting from grass consumption by a cow is denoted by $\tau_{g,*}$. This coefficient is calculated as $V_c/(A_g D_g)$, where V_c is the average ingestion rate of grazing cows (kg day^{-1}), D_g is the dry-weight areal grass density (kg m^{-2}), and A_g is the pasture area required to graze one cow (m^2).

The beef compartment B_i represents the concentration of radioactivity in the muscle of a steer, and C_i simulates the concentration of radioactivity in the milk in a cow's udder. It is not assumed that the total loss from the pasture grass compartment, G_i, due to a cow's grass consumption is accounted for by gains to the beef and milk compartments B_i and C_i. Rather, the transfer coefficients $(\tau_{g,b})_i$ and $(\tau_{g,c})_i$ account for only the portions of the total activity transferred to the cow through consumption of grass, those portions being the activity transferred to beef (B_i) and milk (C_i), respectively.

The dotted lines in Fig. Q–1 from the beef and milk compartments B_i and C_i to the holdup compartments $(BH)_i$ and $(CH)_i$, respectively, represent the effect of storage on the radionuclide concentration in these foods.

Refinements

In the foregoing summary, we passed over certain details in order to avoid unnecessarily intricate exposition. Two of these refinements are summarized here.

The plant-surface compartments of food crops and grass have been subdivided to account for the different dynamics of retention and loss for the components of wet and dry deposition. Material deposited in the wet deposition compartment during rain is fractionally subject to

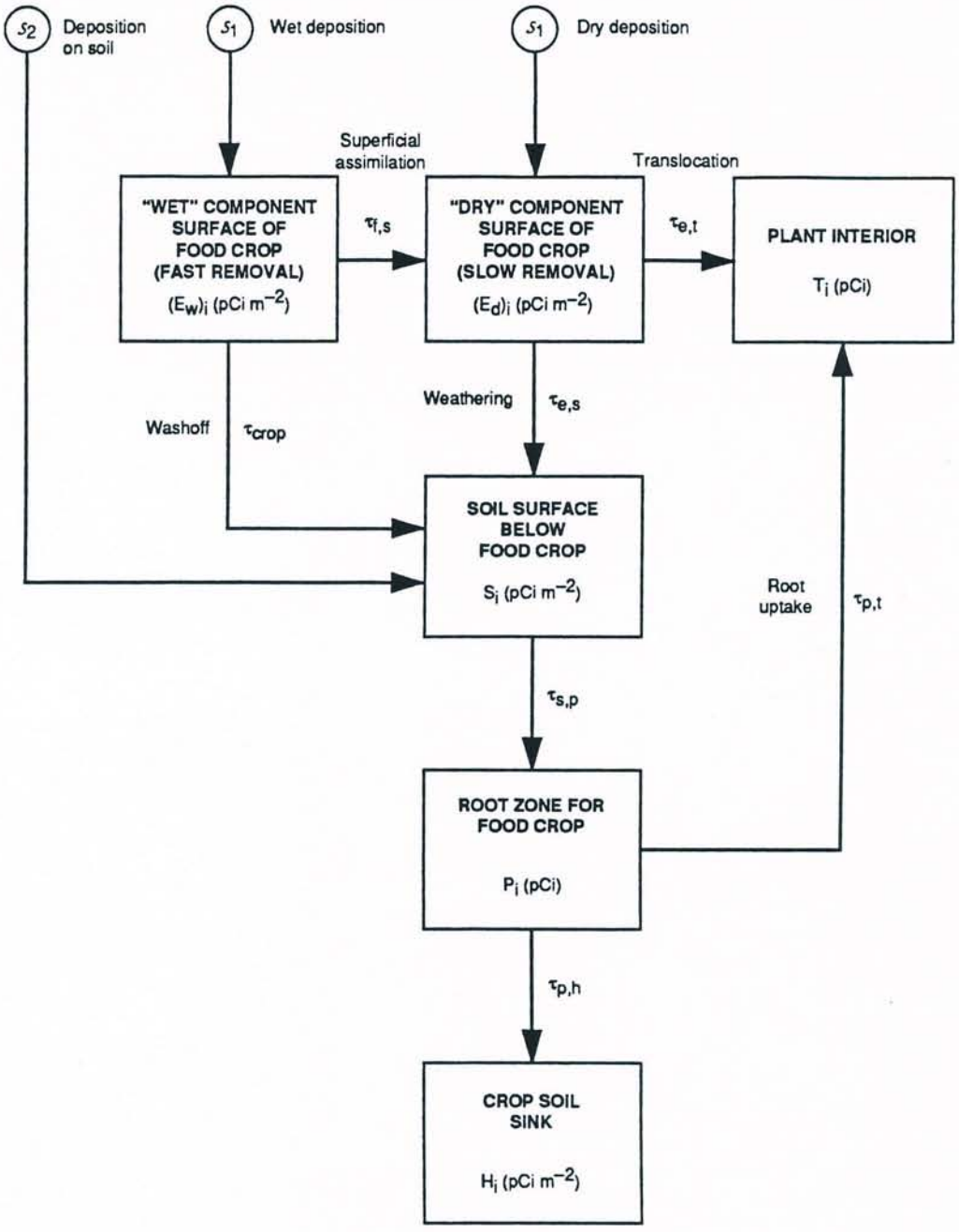

Figure Q–2. Detail of the RAGTIME above-ground food crop model. The plant surface compartment E_i is subdivided into "fast" and "slow" components, associated with wet and dry deposition, respectively.

rapid washoff, and the remaining fraction of the compartment's content transfers to the surface compartment associated with dry deposition, which is depleted by weathering that occurs more slowly than washoff. Notation for these compartments for food crops are $(E_w)_i$ and $(E_d)_i$ for wet and dry, respectively (Fig. Q–2). For pasture grass, they are $(G_w)_i$ and $(G_d)_i$ (Fig. Q–3).

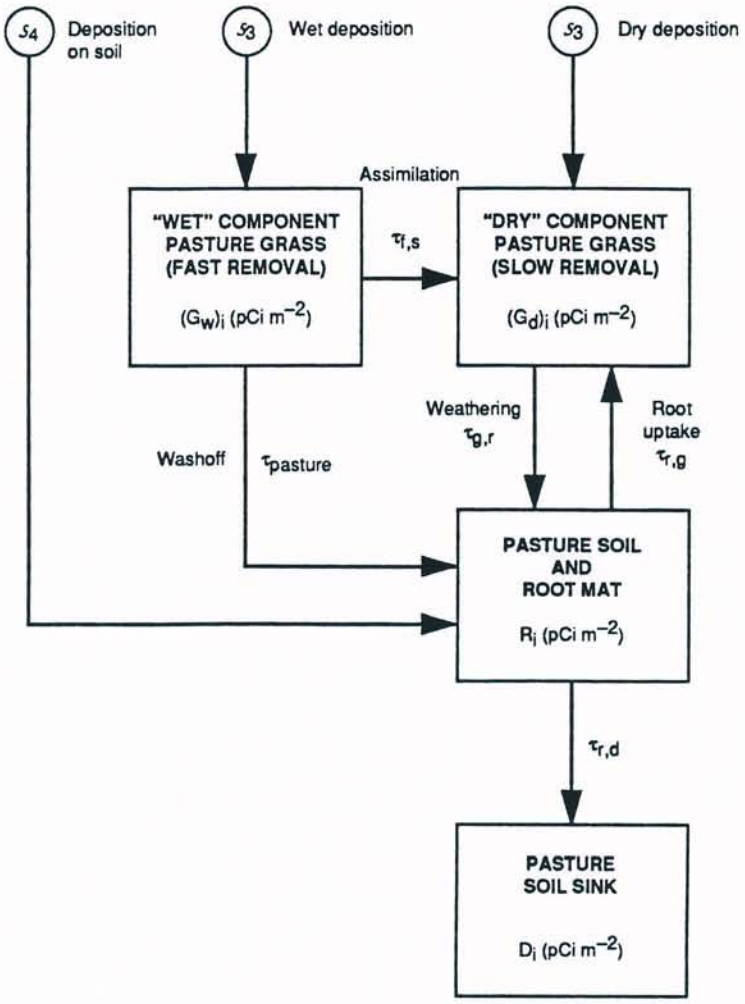

Figure Q–3. Detail of the RAGTIME pasture grass model. The grass compartment G_i is subdivided into "fast" and "slow" components, associated with wet and dry deposition, respectively.

Resuspension was incorporated into RAGTIME as an explicit mechanism, but the capability will not be used for the dose reconstruction project, and we are omitting it from the discussion in order to simplify the equations and parameter lists. Appendix O describes the approach to resuspension that is planned for this project.

The first of the foregoing modifications is discussed in more detail in subsequent sections.

Differential Equations and Glossary of Symbols

The following system of equations describes the transfer of deposited radioactivity to food crops, pasture grass, beef, and milk as depicted in Figs. Q–1 through Q–3. Definitions of the compartments used in the RAGTIME model follow the system of equations. Each equation includes a summation term that accounts for buildup of the current radionuclide from decay of precursors in a decay chain; the quantity β_{ij} represents the branching ratio from nuclide j to nuclide i. Descriptions of all quantities used in these equations, along with default values

used for certain of those that currently represent constants, are given in the next section in a glossary.

Crop surface: wet deposition

$$\frac{d(E_w)_i}{dt} = S_1\left(v_w(\chi_{air})_i - \left((\lambda_r)_i + \tau_{crop} + (\tau_{f,s})_i\right)(E_w)_i + (\lambda_r)_i \sum_{j=1}^{i-1} \beta_{ij}(E_w)_j \right. \quad \text{(Q–1)}$$

Crop surface: dry deposition

$$\frac{d(E_d)_i}{dt} = S_1\left(v_d(\chi_{air})_i + (\tau_{f,s})_i(E_w)_i - \left((\lambda_r)_i + \tau_{e,s}\right)(E_d)_i + (\lambda_r)_i \sum_{j=1}^{i-1} \beta_{ij}(E_w)_j \right. \quad \text{(Q–2)}$$

Crop surface soil

$$\frac{dS_i}{dt} = S_2(v_d + f_w v_w)(\chi_{air})_i + \tau_{e,s}(E_d)_i + f_w \tau_{crop}(E_w)_i - \left((\lambda_r)_i + \tau_{s,p}\right)S_i + (\lambda_r)_i \sum_{j=1}^{i-1} \beta_{ij} S_j \quad \text{(Q–3)}$$

Crop root soil

$$\frac{dP_i}{dt} = A\tau_{s,p}S_i - \left((\lambda_r)_i + (\tau_{p,t})_i + \tau_{p,h}\right)P_i + (\lambda_r)_i \sum_{j=1}^{i-1} \beta_{ij} P_j \quad \text{(Q–4)}$$

Pasture grass: wet deposition

$$\frac{d(G_w)_i}{dt} = S_3 v_w(\chi_{air})_i - \left((\lambda_r)_i + \tau_{pasture} + \tau_{f,s} + \tau_{g,*}\right)(G_w)_i + (\lambda_r)_i \sum_{j=1}^{i-1} \beta_{ij}(G_w)_j \quad \text{(Q–5)}$$

Pasture grass: dry deposition

$$\frac{d(G_d)_i}{dt} = S_3 v_d(\chi_{air})_i + \tau_{f,s}(G_w)_i - \left((\lambda_r)_i + \tau_{g,r} + \tau_{g,*}\right)(G_d)_i + \tau_{r,g}R_i + (\lambda_r)_i \sum_{j=1}^{i-1} \beta_{ij}(G_d)_j \quad \text{(Q–6)}$$

Pasture soil

$$\frac{dR_i}{dt} = S_4(v_d + f_w v_w)(\chi_{air})_i + \tau_{g,r}(G_d)_i + \tau_{pasture}(G_w)_i - \left((\lambda_r)_i + \tau_{r,g} + \tau_{r,d}\right)R_i + (\lambda_r)_i \sum_{j=1}^{i-1} \beta_{ij} R_j \quad \text{(Q–7)}$$

Pasture soil sink

$$\frac{dD_i}{dt} = \tau_{r,d}R_i - (\lambda_r)_i D_i + (\lambda_r)_i \sum_{j=1}^{i-1} \beta_{ij} D_j \quad \text{(Q–8)}$$

Milk

$$\frac{dC_i}{dt} = (\tau_{g,c})_i\, p_c(t)\left((G_d)_i + (G_w)_i\right) - \left((\lambda_r)_i + \tau_{milk}\right)C_i + (\lambda_r)_i \sum_{j=1}^{i-1} \beta_{ij} C_j \qquad \text{(Q–9)}$$

Beef

$$\frac{dB_i}{dt} = (\tau_{g,b})_i\, p_b(t)\left((G_d)_i + (G_w)_i\right) - \left((\lambda_r)_i + \tau_{beef} + (\tau_{exc})_i\right)B_i + (\lambda_r)_i \sum_{j=1}^{i-1} \beta_{ij} B_j \qquad \text{(Q–10)}$$

Interior of crops

$$\frac{dT_i}{dt} = (\tau_{p,t})_i P_i + (\tau_{e,t})_i\left((E_d)_i + (E_w)_i\right) - (\lambda_r)_i T_i + (\lambda_r)_i \sum_{j=1}^{i-1} \beta_{ij} T_j \qquad \text{(Q–11)}$$

Crop soil sink

$$\frac{dH_i}{dt} = (\tau_{p,h}/A)P_i - (\lambda_r)_i H_i + (\lambda_r)_i \sum_{j=1}^{i-1} \beta_{ij} H_j \qquad \text{(Q–12)}$$

Stored crops

$$\frac{d(EH)_i}{dt} = -(\lambda_r)_i (EH)_i + (\lambda_r)_i \sum_{j=1}^{i-1} \beta_{ij} (EH)_j \qquad \text{(Q–13)}$$

A summary of the RAGTIME compartments follows.

$(E_w)_i$ "Wet" component of radioactivity present on the surface of the above-ground food crop per unit land surface (pCi m^{-2}). This component receives deposition only during rain and is subject to rapid removal by washoff, but its content is also transferred fractionally to the "dry" surface component, which weathers more slowly. Translocation to compartment T_i can occur.

$(E_d)_i$ "Dry" component of radioactivity present on the surface of the above-ground food crop per unit land surface (pCi m^{-2}). This component receives deposition at all times and is subject to slow removal by weathering. Translocation to compartment T_i can occur.

E_i The sum of the compartments $(E_w)_i$ and $(E_d)_i$ (pCi m^{-2}).

S_i Radioactivity present at the soil surface below food crops (pCi m^{-2}).

P_i Radioactivity present in the subsurface soil pool (root zone) associated with one person's food supply (pCi).

$(G_w)_i$ "Wet" component of radioactivity present on pasture grass (pCi m^{-2}). This component receives deposition only during rain and is subject to rapid removal by washoff, but its content is also transferred fractionally to the "dry" component, which weathers more slowly.

$(G_d)_i$	"Dry" component of radioactivity present on pasture grass (pCi m^{-2}). This component receives deposition at all times and is subject to slow removal by weathering.
G_i	The sum of the compartments $(G_w)_i$ and $(G_d)_i$ (pCi m^{-2}).
R_i	Radioactivity present in pasture soil from ground surface to the root depth of the grass (pCi m^{-2}).
D_i	Radioactivity present in pasture soil beneath the root depth (pasture soil sink) (pCi m^{-3}).
C_i	Concentration of radioactivity in milk (pCi L^{-1}).
B_i	Concentration of radioactivity in beef (pCi kg^{-1}).
T_i	Radioactivity present in the interior tissue of plants produced for human consumption (pCi).
H_i	Radioactivity present in the crop soil below the root depth (crop soil sink) (pCi m^{-2}).
$(EH)_i$	Concentration of radioactivity in food that is stored following harvest of crops (pCi kg^{-1}).
$(BH)_i$	Concentration of radioactivity in the beef holdup compartment (pCi kg^{-1}).
$(CH)_i$	Concentration of radioactivity in the milk holdup compartment (pCi L^{-1}).

Glossary of RAGTIME Symbols

The following list contains symbols (other than those for compartments) that occur in the differential equations (Eqs. Q–1 through Q–13), as well as others required in the definitions.

A	Surface area (m^2) required to furnish the food crop for one person.
A_g	Pasture area per cow (m^2).
β_{ij}	Radioactive branching ratio from nuclide j to nuclide i ($j < i$).
B_{iv}	Concentration of nuclide i per unit wet weight of vegetables and fruits and dry weight of pasture grass (pCi kg^{-1}) divided by concentration of nuclide per unit dry weight in soil (pCi kg^{-1}).
d	Depth of plow layer (cm).
D_g	Dry-weight areal grass density (kg m^{-2}).
$(F_f)_i$	Fraction of the daily intake of nuclide i by a beef cow that appears per kg of flesh at time of slaughter (day kg^{-1}).
$(F_m)_i$	Fraction of the daily intake of nuclide i by a dairy cow that appears per liter of milk at equilibrium (day L^{-1}).
f_w	In dynamic mode, a coefficient that equals 1 during rain and 0 otherwise. When a specific rainfall schedule is not available, f_w can be taken as the fraction of time that rain falls during the period under study.
$(\lambda_r)_i$	Radioactive decay-rate coefficient for the ith radionuclide (day^{-1}).
M_b	Muscle mass of a steer at the time of slaughter (kg).

$p_b(t)$ Fraction of a beef cow's feed that is contaminated pasture grass at time t.

$p_c(t)$ Fraction of a dairy cow's feed that is contaminated pasture grass at time t.

ρ Bulk density of the soil (g cm^{-3}).

S_1 Interception fraction for surface of above-ground food crop (dimensionless).

S_2 Interception fraction for soil surface below food crop ($= 1 - S_1$).

S_3 Interception fraction for pasture grass (taken as 0.25).

S_4 Interception fraction for soil surface or root mat below pasture grass (taken as 0.75).

τ_{beef} Fractional rate of slaughter of the beef herd (day^{-1}).

τ_{crop} Washoff rate coefficient for material that is wet-deposited on food crops during rainfall (day^{-1}). Expressed as $S_1 r/(K_w(r)Y)$, where r is rainfall rate (mm day^{-1} = L day^{-1} m^{-2}), Y is the crop yield (kg m^{-2}), and $K_w(r) = ar^b$ L kg^{-1} for experimentally determined regression coefficients a and b; for particulates, $a = 2.574$, $b = -0.457$ have been used. For elemental iodine and other reactive gases, we have used the constant value $K_w = 2.5$ L kg^{-1}.

$\tau_{e,s}$ Transfer rate coefficient from $(E_d)_i$ to S_i (day^{-1}).

$(\tau_{exc})_i$ Excretion rate of stable isotope of the nuclide from the muscle of a steer (i.e., radioactive decay is not counted in the removal).

$\tau_{f,s}$ Rate coefficient (day^{-1}) for removal of wet-deposited material from the "wet" component of above-ground food crop and pasture grass surface to the "dry" component. For elemental iodine and other reactive gases, we have used 4 day^{-1}; for particulates, 2 day^{-1} is suggested.

$\tau_{g,*}$ Rate coefficient representing loss of radioactivity from pasture grass due to cow's consumption of grass (day^{-1}); defined to be $V_c/(A_g D_g)$.

$(\tau_{g,b})_i$ Transfer rate coefficient from $(G_d)_i + (G_w)_i$ to B_i (m^2 kg^{-1} day^{-1}).

$(\tau_{g,c})_i$ Transfer rate coefficient from $(G_d)_i + (G_w)_i$ to C_i (m^2 L^{-1} day^{-1}).

$\tau_{g,r}$ Transfer rate coefficient from $(G_d)_i$ to R_i (day^{-1}).

τ_{milk} Transfer rate of milk from the udder (day^{-1}).

$\tau_{pasture}$ Washoff rate coefficient for material that is wet-deposited on pasture grass during rainfall (day^{-1}). Expressed as $S_3 r/(K_w(r)D_g)$, where r is rainfall rate (mm day^{-1} = L day^{-1} m^{-2}) and $K_w(r) = ar^b$ for experimentally determined regression coefficients a and b; for particulates, $a = 2.574$, $b = -0.457$ have been used. For elemental iodine and other reactive gases, we have used the constant value $K_w = 2.5$ L kg^{-1}.

$\tau_{p,h}$ Transfer rate coefficient from P_i to H_i (day^{-1}).

$(\tau_{p,t})_i$ Transfer coefficient from P_i to T_i (day^{-1}).

$\tau_{r,d}$ Transfer rate coefficient from R_i to D_i (day^{-1}) (day^{-1}).

$\tau_{r,g}$ Transfer rate coefficient from R_i to $(G_d)_i$) (day^{-1}).

$\tau_{s,p}$ Transfer rate coefficient from S_i to P_i (day^{-1}).

U Milk capacity of the udder (L).

V_c Dry weight consumption per day by a cow (kg day^{-1}).

PARAMETERS DESCRIBING TRANSFER TO CROPS

Modes of contamination of edible portions of crop plants include the interception and retention of aerially depositing radionuclides by crops as well as root uptake following deposition onto crop soils. In addition, interception and retention by crops of radionuclides resuspended from soil may contribute to the contamination of foodstuffs, although, as previously noted, this pathway is not included in the model for purposes of the dose reconstruction.

In describing these pathways of contamination, RAGTIME considers seasonal cycles of crops (i.e., when the crops are and are not present during the year), as well as time dependency of parameters describing contamination. Much of this time dependency is due to physical and morphological changes in plants due to growth and maturation. Time dependency of the interception parameters $\mathcal{S}_1$ and $\mathcal{S}_2$ and of the root uptake parameter $(\tau_{p,t})_i$ have been incorporated into the model. Both parameters are based on a curve adapted from Miller (1967):

$$M = M_f^0\left(1 - \exp(-a_\tau(t^2 - t_0^2))\right) \qquad \text{(Q–14)}$$

describing the mass M of edible crop per plant (g) at time $t \geq t_0$, where M_f^0 is the final mass of grain at harvest (g per plant), t_0 is the time of emergence of the grain (day), and a_τ is the growth coefficient (day^{-2}). The use of this function in the representation of the crop interception fraction and the parameter $(\tau_{p,t})_i$ is described in the next two subsections.

Time-Dependent Aerosol Interception ($\mathcal{S}_1$ and $\mathcal{S}_2$)

The interception of airborne radionuclides by edible portions of crop plants depends on the following major factors:

1. the surface area exposed to depositing particles,
2. the shape of the edible portion and its orientation to depositing particles, and
3. the particle density of the depositing material.

The form of time-dependent interception fraction for food crops is

$$\mathcal{S}_1 = s_L^0 M^{(1-n_L)w} \qquad \text{(Q–15)}$$

where M is from Eq. Q–14, s_L^0 and n_L are empirical constants and w is the number of plants per square meter of land. For grains, values of the parameters used were the following: M_f^0 = 1 g plant^{-1}, $a_\tau = 1.24 \times 10^{-4}$ day^{-2}, $s_L^0 = 0.00075$, $n_L = 0.455$, and $w = 250$ plants m^{-2}.

Time-Dependent Root Uptake $(\tau_{p,t})_i$

Literature reviewed indicates a paucity of data regarding time-dependent root uptake of most elements. What is available indicates that the shape of the uptake curve, however, is similar to that of the growth curve for some elements and crop species studied (Belcher and Ragland 1972, Brewster et al. 1975, Pacques et al. 1975, Jones and Handreck 1977, Miller et al. 1977, Page et al. 1977, and Parks et al. 1970). The approach followed in RAGTIME is either to characterize uptake rates by edible portions of crops on the basis of any empirical data available, or to assume that the uptake rate follows the growth curve for the edible portion in the absence of empirical uptake data.

The time-dependent formulation of the root-uptake parameter is

$$(\tau_{p,t})_i = \frac{\dot{M} B_{iv}}{10{,}000 A d \rho} \qquad \text{(Q–16)}$$

where $\dot{M}$ is the time derivative of the growth curve (Eq. Q–14), where B_{iv} is the concentration ratio for fresh weight of plant divided by dry weight of soil (dimensionless), A is the soil surface area required to furnish food crops for one person (m^2), d is the depth of the plow layer (cm), ρ is the soil bulk density (g cm^{-3}), and 10,000 converts m^2 to cm^2. The value for B_{iv} is obtained from empirical studies that measure the final crop concentration with respect to a soil concentration believed to be approximately constant throughout the growth cycle.

Time-Independent Parameters ($\tau_{e,s}$, $\tau_{s,p}$, and $\tau_{p,h}$)

Retention, both initial and long-term, of intercepted radionuclides depends on

1. the surface characteristics of the edible portion,
2. the particle size,
3. the wind speed, and
4. the relative humidity and amount of rainfall

(Miller and Lee 1966). The effect of each of these factors on retention varies from site to site, and thus the value of $\tau_{e,s}$, the retention coefficient, may vary greatly. We have assumed an average, time-independent value of $\tau_{e,s}$ of 0.0495 day^{-1}, consistent with that provided in TERMOD (Booth and Kaye 1971).

The movement of radionuclides deposited on surface soil to the root zone has been characterized by TERMOD as $\tau_{s,p}$. The definition and value of this parameter has been carried over to RAGTIME.

The downward movement of radionuclides out of the root zone into the soil sink is again characterized by a time- and nuclide-independent parameter, $\tau_{p,h}$, adopted from TERMOD.

PARAMETERS DESCRIBING TRANSFER TO BEEF AND MILK

Contamination of beef and milk may occur as a result of the interception or root uptake of depositing radionuclides by forage crops, and the subsequent ingestion by beef or dairy cattle. RAGTIME considers direct consumption by cattle of pasture grass as well as stored feeds and hay. The previous versions of RAGTIME do not account directly for the ingestion of contaminated soil by cattle, but it may be possible to add this mechanism for the final calculations in this study. Inhalation of radioactivity by cattle has not been treated explicitly in past versions, but BIOMOVS experience indicated that this mechanism may require further study.

Contamination of Pasture Grasses

As with food crops, discussed in the previous section, pasture grass ($(G_w)_i + (G_d)_i$) may be contaminated through interception of depositing radionuclides, including resuspended particulates, and through root uptake of nuclides deposited on the soil or root mat (R_i) beneath the pasture grass. In the present version of the model, we assume that a pasture exposed to depositing radionuclides maintains a constant biomass throughout the year, and that the interception fraction for grasses, S_3, remains constant. The assumed value $S_3 = 0.25$ is equal to the value originally used in TERMOD (Booth and Kaye 1971) and falls in the range of empirical measurements reported by Chamberlain (1970) for initial retention (where sampling is done immediately after contamination) of grasslands. This parameter would be expected to vary with plant density and other environmental factors and thus represents an average value as it is used in RAGTIME. The fraction S_3 is applied directly to the total aerosol deposition rate, and thus the model does not explicitly account for interception of radionuclides resuspended from the soil or root mat beneath the pasture grass.

The fraction S_4 represents the fraction of depositing radioactivity that is not initially intercepted by grass leaves, and thus it is the fraction deposited on the surface soil or root mat beneath the leaves. Therefore, this fraction is assigned the value $S_4 = 1 - S_3 = 0.75$.

The value of the parameter $\tau_{r,g}$, representing additional input into the pasture grass compartment from surface soil, is consistent with the TERMOD value adopted from a paper by Menzel (1963), which indicates that an upper limit for uptake of radionuclides in the surface soil by a single crop is 1%. Considered on an annual basis, $\tau_{r,g}$ becomes 2.74×10^{-5} day^{-1}.

Three aspects of root uptake by pasture grasses have not been considered at present. First, the element dependency of the parameter $\tau_{r,g}$ has been neglected; yet it may be important when root uptake is significant in comparison with foliar contamination. Second, an additional mode of root absorption of radionuclides that has not been considered involves their availability for uptake from the root mat, which is a "thatch" of dead and decomposing tissues around the plant-base region in which grasses may root. This mode could be significant. Finally, the time dependency of $\tau_{r,g}$ has not been investigated.

Loss of radionuclides from the grass compartments $(G_w)_i$ and $(G_d)_i$ may occur through ingestion of grass by grazing cattle ($\tau_{g,*}$), radioactive decay ($(\lambda_r)_i$), by washoff of recently deposited material during rain ($\tau_{pasture}$ applied to $(G_w)_i$), and by weathering of surface-deposited radionuclides ($\tau_{g,r}$ applied to $(G_d)_i$). The value of $\tau_{g,r}$ is assumed to be equivalent to the weath-

ering coefficient $\tau_{e,s}$ for food crops, discussed in a previous section, and thus represents a 14-day half-time for retention of intercepted materials. This value is consistent with data reported by Chamberlain (1970) for grasslands, although it may vary with seasons and climatic factors. In particular, this weathering coefficient, when measured, incorporates loss of surface material due to shedding of the protective leaf cuticle during plant growth (Chamberlain 1970), thus suggesting a seasonal and species dependency of $\tau_{g,r}$. As with $\tau_{e,s}$, $\tau_{g,r}$ is assumed to be time independent until further research dictates that a different approach should be taken.

The value of $\tau_{g,*}$ (day^{-1}) is the coefficient of loss of radionuclides from pasture grass through consumption by grazing beef and dairy cattle. For the RAGTIME model, an average ingestion rate, V_c, of 10 kg day^{-1} dry matter is assumed, consistent with the value used in TERMOD (Booth and Kaye 1971). The coefficient is computed as $\tau_{g,*} = V_c/(A_g D_g)$, where D_g is the dry-weight areal grass density, for which 0.15 kg m^{-2} is used (Booth and Kaye 1971), and A_g is the pasture area per cow (m^2). At present, it is assumed that $\tau_{g,*}$ is constant throughout the year.

The rate of loss of radionuclides from the surface soil (R_i) beneath pasture grass is represented by the parameter $\tau_{r,d}$. As for the similarly defined parameter $\tau_{p,h}$ for crop soil, an element-independent rate of 1.1×10^{-1} day^{-1} is used, as given in TERMOD documentation (Booth and Kaye 1971). Future research may indicate a more appropriate value or representation for this process.

Contamination of Beef and Milk

Transfer of radionuclides from pasture grass to beef or milk is parameterized by $(\tau_{g,b})_i$, in m^2 kg^{-1} day^{-1}, or $(\tau_{g,c})_i$, in m^2 L^{-1} day^{-1}, respectively (Fig. Q–1). These parameters represent transfer rates and are provisionally assumed to be time-independent. Element-specific values of $(\tau_{g,b})_i$ and $(\tau_{g,c})_i$ were calculated from the empirically-derived transfer coefficients $(F_f)_i$ and $(F_m)_i$, which characterize the ratios between beef or milk concentrations of an element and the equilibrium concentration of that element in pasture grass or feed (Moore et al. 1979, Ng et al. 1977). By definition

F_f = the fraction of the daily intake of an element by a beef cow which appears per kg of flesh at time of slaughter (day kg^{-1})

F_m = the fraction of the daily intake of an element by a dairy cow which appears per liter of milk at equilibrium (day L^{-1}).

Therefore, the empirical coefficients represent the theoretical coefficients only if pasture grass (or feed) is the only source of the element in question in the cow's diet. The parameter $(\tau_{g,b})_i$ was derived by assuming that the concentration in beef at the time of slaughter approximates an equilibrium concentration with a steady-state concentration in pasture grass. Thus, if $(B^{eq}_{cow})_i$ is taken to represent the equilibrium concentration of element i in the muscle of a single cow (pCi kg^{-1}), and G^{eq}_i is the steady-state concentration in grass (pCi m^{-2}), then from the equilibrium equation

$$(\tau_{g,b})_i G^{eq}_i - (\tau_{exc})_i (B^{eq}_{cow})_i = 0$$

it follows that

$$\frac{(B_{cow}^{eq})_i}{G_i^{eq}} = \frac{(\tau_{g,b})_i}{(\tau_{exc})_i}$$

where $(\tau_{exc})_i$ is the loss rate of the element i from the muscle of a steer (day^{-1}), and thus

$$(\tau_{g,b})_i = \frac{(B_{cow}^{eq})_i}{G_i^{eq}}(\tau_{exc})_i . \qquad (Q–17)$$

We also have

$$(F_f)_i = \frac{(B_{cow}^{eq})_i}{G_i^{eq} V_c / D_g} \qquad (Q–18)$$

where

V_c = dry-weight grass consumption per day by a cow (10 kg day^{-1})

D_g = dry-weight areal grass density (0.15 kg m^{-2}).

It follows from Eqs. Q–17 and Q–18 that $(\tau_{g,b})_i$ is related to $(F_f)_i$ by the equation

$$(\tau_{g,b})_i = \frac{(F_f)_i (\tau_{exc})_i V_c}{D_g} . \qquad (Q–19)$$

If one assumes that the animal's diet consists solely of pasture grass, the loss rate of the element from the muscle of a steer, $(\tau_{exc})_i$, may be interpreted to represent both the element-specific metabolic turnover and the element-independent dilution of the concentration due to increase in muscle mass during growth. Dilution due to growth is handled explicitly in the RAGBEEF model (Pleasant et al. 1982) but has not been implemented in RAGTIME.

In a manner similar to the foregoing, we obtain

$$(\tau_{g,c})_i = \frac{(F_m)_i \tau_{milk} V_c}{D_g} \qquad (Q–20)$$

where τ_{milk} is the element-independent loss rate from the udder (2 day^{-1}). Derivation of Eq. Q–20 was based on the equilibrium equation

$$(\tau_{g,c})_i G_i^{eq} - \tau_{milk} (C_{cow}^{eq})_i = 0$$

and the relationship

$$(F_m)_i = \frac{(C_{cow}^{eq})_i}{G_i^{eq} V_c / D_g}$$

where $(C_{cow}^{eq})_i$ is the equilibrium concentration of element i in milk. Again, dynamics related to maturation and milking practices for a single cow have been neglected at this time, though they have been considered in the RAGBEEF model (Pleasant et al. 1982).

As in TERMOD, the compartmental equation (Eq. Q–10) considers losses from beef in the herd as a whole by including the term τ_{beef} to account for slaughter of contaminated cattle. This interpretation then implies instantaneous replacement of the slaughtered portion with uncontaminated cattle and a subsequent reduction or loss of radioactivity from the compartment. The uncontaminated cattle then begin to accumulate radioactivity at a rate determined

by $(\tau_{g,b})_i$. If, however, the radionuclide concentration in the beef compartment is to be used as an indication of radiation exposure by ingestion of beef, the present methodology could underestimate concentrations in beef cattle being slaughtered. That is, this latter portion of the herd will likely be the more mature segment, which has been exposed to contaminated pasture for the greatest length of time, although the concentration calculated will be an average of all members of the herd. The RAGBEEF model (Pleasant et al. 1982) addressed this problem.

The milk compartment may also be interpreted to represent concentrations in milk obtained from the dairy herd as a whole. In this case, however, instantaneous replacement of milk removed from the udder by uncontaminated milk does not result in a reduction in concentration below that to which people might be exposed, because each lactating cow, as well as the herd, is subject to this same removal process. That is, while slaughtering will not affect the radionuclide concentration in beef of any particular cow, milking will affect the concentration in milk of each individual lactating cow in the herd, and thus can be considered as applying to the herd as a whole.

For both milk and beef compartments, radionuclide loss and buildup of daughters due to radioactive decay during storage prior to human consumption is considered. Compartments $(CH)_i$ and $(BH)_i$, representing concentrations of each nuclide in milk and beef, respectively, following storage were devised to provide this information.

RADIONUCLIDE-SPECIFIC PARAMETERS FOR RAGTIME

In this section we summarize parameter values for RAGTIME that are specific to the elements for which radioisotopes are considered in the source term. The parameters are distribution coefficients for pasture and garden produce (B_{iv1} and B_{iv2}) and transfer coefficients for beef and other animal products (F_f) and milk (F_m).

Plant/Soil Distribution Coefficients for Pasture and Garden Produce

Most listings of plant/soil distribution coefficients for root uptake found in the literature apply to dry pasture grass (B_{iv1}) and wet weight of garden vegetables or orchard fruits (B_{iv2}). These listings are neither site-specific nor plant-specific, but they apply to average garden consumption of a variety of vegetables grown in an average garden soil. It would be preferable, of course, to be able to use site-specific values for specific types of plants grown in gardens near the FMPC. In lieu of site-specific information, however, an attempt was made to locate values in the literature obtained from growing plants in similar types of soils.

The soil in Hamilton and Butler counties in southwestern Ohio where the FMPC is located consists mainly of Fincastle and Henshaw silt loam (Appendix N). A summary report by Ng et al. (1982a) of a comprehensive review of measured distribution coefficients was found to contain data for only three of the elements (Sr, Cs, Ru) released as radionuclides from the FMPC for loam or silt loam soils, and these data applied only to a few vegetables. Because of the sparsity of soil-specific and plant-specific information, it was concluded that the best available values are probably those values recently certified by the U.S. Environmental Protection Agency for administration of the Clean Air Act (Parks 1991). The computer program, CAPP88-PC, described in this reference contains computer files of B_{iv1} and B_{iv2} for nearly all

elements. Table Q–1 lists distribution coefficients from this source for the most important radionuclide elements discharged to the atmosphere from the FMPC. These values apply to average pasture grass and garden or orchard produce grown in average U.S. soil.

Table Q–1. Plant/Soil Distribution Coefficients B_{iv1} and B_{iv2} for Pasture and Produce for Elements Released as Radionuclides from the FMPC

Element	B_{iv1} [a]	B_{iv2} [b]
U	8.50×10^{-3}	1.71×10^{-3}
Pu	4.50×10^{-4}	1.93×10^{-5}
Th	8.50×10^{-4}	3.64×10^{-5}
Np	1.00×10^{-1}	4.28×10^{-3}
Pa	2.50×10^{-3}	1.07×10^{-4}
Ra	1.50×10^{-2}	6.42×10^{-4}
Po	2.50×10^{-3}	1.71×10^{-4}
Pb	4.50×10^{-2}	3.85×10^{-3}
Bi	3.50×10^{-2}	2.14×10^{-3}
Cs	8.00×10^{-2}	1.28×10^{-2}
Ru	7.50×10^{-2}	8.56×10^{-3}
Sr	2.50	1.07×10^{-1}
Tc	9.50	6.42×10^{-1}

[a] Relative to dry pasture grass.

[b] Relative to wet weight of garden vegetables or orchard fruits.

Transfer Coefficients for Milk and Beef

Element-specific feed-to-milk transfer coefficients for dairy cattle (d L^{-1}) were computed by Ng et al. 1977. Table Q–2 lists their values for elements released from the FMPC as radionuclides. These milk transfer values are nearly identical to recent U.S. EPA–certified values in the computer code CAP88-PC (Parks 1991). The beef transfer coefficients (day kg^{-1}) listed in the table are also U.S. EPA–certified values from CAP88-PC.

Transfer Coefficients for Other Animal Products

Besides beef and milk, other animal products that may have been produced and consumed in the immediate area surrounding the FMPC include pork, lamb, chicken, and eggs. Transfer coefficients for some of the elements released as radionuclides at the FMPC are listed in Table Q–3.

The RAGTIME model, as described, does not accommodate these food items, but is being extended to consider them.

Table Q–2. Feed-to-Milk and Feed-to-Beef Transfer Coefficients

Element	Milk Transfer Coefficient[a] (day L^{-1})	Beef Transfer Coefficient[b] (day kg^{-1})
U	6.1×10^{-4}	2.0×10^{-4}
Pu	1.0×10^{-7}	5.0×10^{-7}
Th	5.0×10^{-6}	6.0×10^{-6}
Np	5.0×10^{-6}	5.5×10^{-5}
Pa	5.0×10^{-6}	1.0×10^{-5}
Ra	4.5×10^{-4}	2.5×10^{-4}
Po	1.4×10^{-4}	9.5×10^{-5}
Pb	2.6×10^{-4}	3.0×10^{-4}
Bi	5.0×10^{-4}	4.0×10^{-4}
Cs	7.1×10^{-3}	2.0×10^{-2}
Ru	6.1×10^{-7}	2.0×10^{-3}
Sr	1.4×10^{-3}	3.0×10^{-4}
Tc	9.9×10^{-3}	8.5×10^{-3}

[a] Ng et al.1977.

[b] Values are from the computer code CAP88-PC (Parks 1991).

Table Q–3. Transfer Coefficients for Other Animal Products[a]

Element	Transfer Coefficient (day kg^{-1})			
	Pork	Lamb	Chicken	Eggs
Sr	2.9×10^{-3}	1.9×10^{-3}	3.2×10^{-2}	2.2×10^{-1}
Ru	6.8×10^{-3}	1.3×10^{-2}	2.4×10^{-1}	4.0×10^{-3}
Cs	3.0×10^{-1}	1.2×10^{-1}	4.4	4.3×10^{-1}
Ce	2.5×10^{-3}	5.0×10^{-3}	9.0×10^{-2}	3.1×10^{-3}
Pu	3.4×10^{-6}	6.7×10^{-6}	2.0×10^{-5}	3.3×10^{-5}
Am	1.2×10^{-5}	2.4×10^{-5}	7.2×10^{-5}	3.9×10^{-3}
U[b]	1.4×10^{-3}	2.7×10^{-3}	8.0×10^{-3}	1.3×10^{-2}

[a] From Ng (1982) unless otherwise noted.

[b] Uranium values were estimated from the listed plutonium values by using an assumed U/Pu ratio of 400, calculated from coefficients derived from computer code CAP88-PC Parks (1991).

Interception Fractions

The interception fraction (S_1 and S_3 for food crops and pasture grass, respectively, in the notation of the RAGTIME model) is defined as the fraction of the total deposit of an airborne pollutant on ground surfaces that is initially intercepted by vegetation. Baes et al. (1984)

estimated interception fractions for leafy vegetables and exposed produce from theoretical considerations. Their values are listed in Table Q–4. A single interception fraction was calculated for all leafy vegetables as a class, while values for five typical examples of exposed produce were calculated separately. These interception fractions could possibly be used to approximate fractions for other garden or orchard crops with similar characteristics. The values in Table Q–4 are used to calibrate the time dependence of interception fraction S_1 (Eqs. Q–14 and Q–15).

Table Q–4. Interception Fractions for Gardens and Orchards[a]

Crop	Interception Fraction (mature crop)	Interception Fraction (average during season)
Leafy vegetables (lettuce, cabbage, greens, etc.)	0.30	0.15
Exposed Produce		
Apples	0.045	0.034
Snap beans	0.097	0.073
Tomatoes	0.091	0.068
Peaches	0.048	0.036
Cherries	0.036	0.027

[a] Baes et al. 1984.

AGRICULTURAL PRODUCTION AND GROWING PERIODS FOR CROPS IN AREAS NEAR THE FMPC

We give some specific agricultural data for Butler and Hamilton Counties in southwestern Ohio. Table Q–5 lists agricultural products of the two counties with annual yields. Table Q–6 lists the approximate planting dates and growing seasons of principal crops grown in gardens in Butler County.

POSSIBLE AGRICULTURAL SCENARIOS FOR THE FMPC AREA

A comparison of inhalation doses with food ingestion doses in the FMPC area using RAGTIME will indicate the extent of detail that will be necessary in treating the food-chain pathway. Such a comparison will require the adoption of scenarios for production and consumption of various agricultural products by individuals living in various parts of the FMPC assessment domain. One comparison could use a hypothetical individual living near the FMPC boundary, who only eats beef, milk, pork, lamb, chicken, and eggs produced on his property, and who only eats vegetables produced in his own garden. This scenario, described in detail below, may serve as a starting point, which may be subject to later refinement and modification. It is reasonable, for purposes of the comparison, first to use assumptions that would tend to

Table Q–5. Agricultural Production in Butler and Hamilton Counties of Southwestern Ohio in 1987[a]

Product	Butler County	Hamilton County
Corn (bushels)	4.458×10^6	5.12×10^5
Wheat (bushels)	3.61×10^5	2.1×10^4
Oats (bushels)	2.5×10^4	not avail.
Soybeans (bushels)	9.2×10^5	1.83×10^5
Apples (acres)	114	93
Vegetables for sale (acres)	236	562
Cattle sold	11,008	1,365
Hogs sold	48,950	2,344
Sheep sold	1,514	279
Chickens sold	1,020	not avail.
Number of milk cows	3,426	454
Eggs	not avail.	not avail.

[a] Data taken from *1987 Census of Agriculture,* Vol.1, Geographic Area Series, Part 35, Ohio, State and County Data, 1989, U.S. Department of Commerce, Bureau of the Census, AC87-A-35.

maximize the estimate of dose to such an individual. If the resulting estimates of dose by ingestion are small in comparison with those for inhalation, one could justify allocating fewer resources to the agricultural pathway.

The food pathway offers considerable practical difficulties for the assessment. If commercial food products are produced within the domain, it is very difficult (perhaps impossible) to trace food produced at different locations, with different levels of contamination, to consumers within the domain. It is usually the case that commercially produced food products are much more widely distributed than in such a small and sparsely-populated area as the assessment domain. Traditional practice in radiation protection assessments is to focus attention on individual gardens that would provide the local source of radioactive food contamination. Few families live entirely from their own gardens and livestock, and the conservatism of this scenario for a garden and pasture near the source of radioactivity has been considered appropriate for radiation protection assessments. Such an approach is, of course, at variance with the philosophy of dose reconstruction, in which it is desirable to minimize the bias in estimating dose and risk. But it can be justified for the purpose of determining which pathways contribute negligibly to total dose and risk, and it is in this spirit that we consider it here.

Table Q–6. Growing Periods and Usual Planting Times for Garden Crops in Butler County, Ohio[a]

Garden Crop	Usual Planting Period		Growing Period (days)
	From	To	
Lettuce	4/1	8/1	40 to 50
Onions	4/1		110 to 150
Winter onions	9/1	10/1	110 to 150
Peas	4/1		50 to 60
Potatoes	4/1	5/15	90 to 140
Radishes	4/1	8/1	25 to 35
Carrots	4/1	7/15	55 to 75
Sweet corn	4/15	7/1	65 to 90
Snap beans	5/15		50 to 60
Lima beans	5/20	6/10	65 to 85
Pole beans	5/15	6/1	65 to 90
Beets	4/15	7/15	50 to 70
Cucumbers	5/10	6/1	50 to 70
Squash	5/1	6/1	50 to 65
Winter squash	later		60 to 110
Cauliflower	7/15		about 100
Tomatoes	5/15		about 50

[a] Information presented in this table is derived from telephone discussions on September 22, 1992, with Steve Bartell, Agricultural Agent for Butler County, Ohio.

Animal Products

Table Q–2 listed feed-to-animal transfer coefficients for various animal products and plant/soil distribution coefficients for produce and pasture. To maximize the radiation dose from consuming beef, pork, lamb, chicken, and eggs, it should be assumed that all food ingested by animals, except for commercial food supplements, was produced on the property of the hypothetical individual.

Beef and milk cattle, and sheep, eat pasture grass primarily, and therefore plant/soil distribution coefficients for pasture should be used for calculation of radiation doses from consumption of beef, lamb, and milk.

Corn is the basic feed for hogs, but a high-protein supplement is required for maximum meat production. This supplement usually consists of soybean meal, meat scraps, fish meal, and other inexpensive high-protein substances. It is reasonable to assume that an individual may grow his own corn for feeding a few hogs, but that any high-protein supplementary feed would come from a non-local commercial source.

Commercial chicken feed containing mainly corn and wheat, with meat scraps and fish meal added to increase the protein content to 20%, is used for commercial production of chicken meat and eggs. To maximize the radiation dose to a hypothetical individual from

chicken and egg consumption, it can be assumed that he grows his own corn for chicken feed, but that any protein supplement would be obtained from a non-local commercial source. Plant/soil distribution coefficients for corn ideally should be used in the calculation of radiation doses for ingestion of pork, chicken, and eggs. Distribution coefficients for corn have been reported for only a few elements, however, and these values are not greatly different from those certified by the U.S. EPA for produce from a typical garden. Therefore, these U.S. EPA–certified distribution coefficients for produce as listed in Table Q–2 will be used in the dose calculations.

Garden Vegetables

Table Q–6 lists the usual planting and growing periods for 17 vegetables typically grown in gardens in Butler County, Ohio. Information is not available on average percentages by weight of these vegetables grown in gardens in the area. A strict monthly resolution of the radiation dose calculations, however, would require a specific knowledge of percentage contributions by weight of each of the vegetables.

An approximate solution to the problem is to assume that six vegetables contribute the bulk of the garden consumption of the hypothetical individual and that each of these six vegetables contributes about equally. Table Q–7 lists six vegetables that possibly contribute most of the average garden production, and it also lists the earliest planting date, the approximate last harvest date, and average the growing period for each of the vegetables.

Table Q–7. Planting and Harvest Information for Garden Crops in Butler County, Ohio

Garden Crop	Earliest Planting date	Last Harvest date	Average Growing Period (days)
Lettuce	4/1	9/15	45
Onions	4/1	8/10	130
Potatoes	4/1	9/10	115
Sweet corn	4/15	9/15	75
Beans	5/15	8/20	70
Tomatoes	5/15	7/20	50

The information listed in Table Q–7 may be used to construct a distribution of vegetable planting times that would maximize the aerial deposition on edible parts of garden plants and root uptake from contaminated soil. The only leafy vegetable listed in the table is lettuce, which has an average interception fraction of 0.15 during its growing period. The average interception fractions of beans and tomatoes are 0.073 and 0.068, respectively. The edible portion of sweet corn is covered with a husk, and the edible parts of onions and potatoes grow mostly underground. Accordingly, zero interception should probably be assumed for these vegetables, and contamination should be attributed to root uptake and direct absorption from the soil. The latter mechanism has not yet been incorporated into RAGTIME but requires attention for root vegetables.

ADDENDUM: UNCERTAINTIES IN AGRICULTURAL TRANSFER PARAMETERS

This section provides a compilation of uncertainty estimates for agricultural transfer parameters tabulated elsewhere in this appendix.

Plant/Soil Distribution Coefficients

Most listings of plant/soil distribution coefficients for root uptake found in the literature apply to dry pasture grass (B_{iv1}) and wet weight of garden vegetables or orchard fruits (B_{iv2}). The definitions of these distribution coefficients are as follows:

B_{iv1} = pCi radionuclide/kg dry pasture grass per pCi radionuclide/kg dry soil

B_{iv2} = pCi radionuclide/kg wet weight edible parts of crops per pCi radionuclide/kg dry soil.

Because of the sparsity of soil-specific and plant-specific information, it was concluded that the best available values are probably those values recently certified by the U.S. Environmental Protection Agency for administration of the Clean Air Act (Parks 1991). The computer code (CAP88-PC) described in the reference contains computer files of B_{iv1} and B_{iv2} for nearly all elements.

Table Q–8 lists the uncertainties in the distribution coefficients. The footnotes in the table refer to the references to the values upon which the uncertainty calculations were based or explain how the uncertainties were calculated. In some cases, where the distribution coefficients were calculated by averaging two values from other elements with close atomic numbers, the uncertainties were calculated by averaging the uncertainties of these other elements.

Transfer Coefficients for Milk and Beef

Element-specific feed-to-misk transfer coefficients (F_m) for dairy cattle (days L^{-1}) were computed by Ng et al. (1977). The beef transfer coefficients F_f (days kg^{-1}) are EPA-certified values from CAP88-PC (Parks 1991). Table Q–9 contains uncertainties in some of these transfer coefficients based on ranges of observed values given in references in the table footnotes. An average of these calculated uncertainties is listed as a default value for each element for which no information could be found.

Transfer Coefficients for Other Animal Products

Besides beef and milk, other animal products that may have been produced and consumed in the immediate area surrounding the FMPC include pork, lamb, chicken, and eggs. Strontium and cesium are the only radionuclides for which there is any information from which uncertainties may be calculated for transfer coefficients for these animal products. Table Q–10 lists these uncertainties based on ranges of observed values taken from Ng (1982). Average values for strontium and cesium listed in the table could possibly be used as default uncertainties for other radionuclides.

Table Q–8. Uncertainties in Plant/Soil Distribution Coefficients

Element	Uncertainty	Footnote
U	+70, −90	a
Pu	+600, −90	b
Th	+50, −95	a
Np	+200, −65	c
Pa	+60, −95	d
Ra	+300, −50	b
Po	+30, −30	e
Pb	+140, −90	f
Bi	+85, −60	g
Cs	+150, −65	b
Ru	+300, −80	b
Sr	+250, −75	b
Tc	+120, −70	b

[a] Estimated from data presented in Garten (1978).

[b] From GSD value in Baes et al. (1984).

[c] From GSD value in Ng et al. (1982a).

[d] An average of U and Th uncertainties.

[e] From standard deviation in Watters et al. (1969).

[f] A geometric mean of 0.045 was reported by Baes et al. (1984) based on values ranging from 0.13 to 0.9. A close examination of original references (Dedolph et al. 1970, Ter Haar 1970), however, revealed that a pertinent range of experimental values corresponding to the listed uncertainties was much smaller (0.006 to 0.110).

[g] An average of Po and Pb uncertainties.

DISCUSSION AND CONCLUSIONS

This appendix has set out the principal features of the RAGTIME agricultural model in moderate detail. In addition, a review of parameter values and uncertainties has been undertaken, and the results have been added to the database. The reader should bear several points in mind in reviewing the features of the model.

First is that RAGTIME is still an evolving methodology. It is not defined by a computer program that cannot be altered because its author is no longer available and no one understands it. Rather, RAGTIME consists of an approach that grew out of earlier experiences (e.g., TERMOD) and was developed further while preserving a useful inheritance from the earlier work. In each modification, the model has grown to accommodate features that new experience has shown to be desirable or necessary.

Second, the valuable BIOMOVS experience in 1987 gave us confidence in some parameters and pathways of RAGTIME, but at the same time it pointed to some refinements that were needed. It must be remembered that BIOMOVS tested RAGTIME with only two radionuclides. The model has not yet accumulated an extensive data base.

Table Q–9. Uncertainties in Feed-to-Milk (F_m) and Feed-to-Beef (F_f) Transfer Coefficients

Element	Uncertainty in F_m	Uncertainty in F_f
U	+95, −70 [a]	+230, −80 [f]
Pu	+75, −90 [a]	+480, −80 [d]
Th	+85, −80 [b]	+230, −80 [f]
Np	+110, −75 [e]	+230, −80 [f]
Pa	+110, −75 [e]	+230, −80 [f]
Ra	+95, −75 [c]	+230, −80 [f]
Po	+110, −75 [e]	+230, −80 [f]
Pb	+110, −75 [e]	+75, −75 [g]
Bi	+110, −75 [e]	+230, −80 [f]
Cs	+185, −75 [c]	+255, −70 [g]
Ru	+110, −75 [e]	+230, −80 [f]
Sr	+130, −60 [c]	+120, −90 [g]
Tc	+110, −75 [e]	+230, −80 [f]

[a] Garten (1978).

[b] Average of U and Pu uncertainties.

[c] Based on overall range of observed values for which averages were calculated. From Ng et al. (1977).

[d] From the range of observed values in Ng (1982).

[e] An average of uncertainties in F_m for U, Pu, Th, Ra, Cs, and Sr.

[f] An average of uncertainties in F_f for Pu, Pb, Cs, and Sr..

[g] From range of observed values in Ng et al. (1982b).

Table Q–10. Uncertainties (%) in Transfer Coefficients for Other Animal Products

Element	Pork	Lamb	Chicken	Eggs
Sr	+40, −60	+95, −40	+150, −45	+20, −30
Cs	+30, −15	+110, −50	+2, −2	+25, −20
Average	+35, −40	+100, −45	+75, −25	+25, −25

Third, for each major application, it is our practice to do extensive revising and reprogramming of RAGTIME for the specific problems at hand. In this way, the model is given a thorough review, any errors that surface are corrected, and innovations that grow out of the new application are incorporated. For example, in the present study, it is possible that we will add an explicit module for root crops, which is not present in the existing structure.

RAGTIME, as its acronym advertises, is a time-dependent or dynamic model. Thus the system evolves gradually in small time steps (at substantial computational cost) and is capable of giving information at various times. The other principal class of compartment models consists of quasi–steady-state models that depend on transfer factors and generally can de-

liver only time-integrated quantities to be converted into consumption and dose. There is nothing inherently superior about the time-dependent models if the quasi–steady-state models deliver the information that is needed. For long-term estimates of the consequences of low-level releases of radionuclides, these models may be entirely adequate. But in applying such a model to a dose reconstruction, one must examine its structure and parameterization to determine how much conservatism is inherent in the implementation. For the analysis of episodic events, however, dynamic models have the advantage of being able to simulate the transfer of the radioactivity through the environmental compartments over time, and the more complete picture enables the investigator to have more (or sometimes less) confidence in the conclusions reached.

REFERENCES

Baes C.F., III, R.D. Sharp, A.L. Sjoreen, and R.W. Shor. 1984. *A Review and Analysis of Parameters for Assessing Transport of Environmentally Released Radionuclides through Agriculture.* Rep. ORNL-5786, Oak Ridge National Laboratory, Oak Ridge, Tennessee.

Belcher C.R. and J.L. Ragland. 1972. "Phosphorus Absorption by Sod-Planted Corn (*Zea mays L.*) from Surface-Applied Phosphorus." *Agronomy J.* **64**: 754–756.

Booth R.S. and S.V. Kaye. 1971. *A Preliminary Systems Analysis Model of Radioactivity Transfer to Man from Deposition in a Terrestrial Environment.* Rep. ORNL/TM-3135, Oak Ridge National Laboratory, Oak Ridge, Tennessee.

Brewster J.L., K.K.S. Bhat, and P.H. Nye. 1975. "The Possibility of Predicting Solute Uptake and Plant Growth Response from Independently Measured Soil and Plant Characteristics." *Plant and Soil* **42**: 197–226.

Chamberlain A.C. 1970. "Interception and Retention of Radioactive Aerosols by Vegetation." *Atmos. Environ.* **4**: 57–78.

Dedolph R., G. ter Haar, R. Holtzman, and H. Lucas, Jr. 1970. "Sources of Lead in Perennial Ryegrass and Radishes." *Env. Sci. and Tech.* 4(3): 217.

Garten C.T., Jr. 1978. "A Review of Parameter Values Used to Assess the Transport of Plutonium, Uranium, and Thorium in Terrestrial Food Chains." *Env. Res.* **17**: 437–452.

Jones L.H.P. and K.A. Handreck. 1977. "Studies of Silica in the Oat Plant." *Plant and Soil* **23**: 79–96.

Köhler H., S.-R. Peterson, and F.O. Hoffman. 1991. *Multiple Model Testing Using Chernobyl Fallout Data of I-131 in Forage and Milk and Cs-137 in Forage, Milk, Beef and Grain.* BIOMOVS Technical Report 13, Part 1. National Institute of Radiation Protection, Stockholm, Sweden.

Menzel R.G. 1963. "Factors Influencing the Biological Availability of Radionuclides for Plants." *Fed. Am. Soc. Exptl. Biol. Proc.* **22**: 1398–1401.

Miller C.F. 1967. *Operation Ceniza-Arena: Retention of Fallout Particles from Volcan Irazu (Costa Rica) by Plants and People,* Part 3. Rep. SRI-MU-4890, Stanford Research Institute, Menlo Park, California.

Miller J.E., J.J. Hassett, and D.E. Koeppe. 1977. "Interactions of Lead and Cadmium on Metal Uptake and Growth of Corn Plants." *J. Environ. Qual.* **6**: 18–20.

Moore R.E., C.F. Baes, III, L.M. McDowell-Boyer, A.P. Watson, F.O. Hoffman, J.C. Pleasant, and C.W. Miller. 1979. *AIRDOS-EPA: A Computerized Methodology for Estimating Environmental Concentrations and Dose to Man from Airborne Releases of Radionuclides.* Rep. ORNL-5532, Oak Ridge National Laboratory, Oak Ridge, Tennessee.

Ng Y.C. 1982. "A Review of Transfer Factors for Assessing the Dose from Radionuclides in Agricultural Products." *Nucl. Safety* **23**(1): 57–71.

Ng Y.C., S.E. Thompson, and C.S. Colsher. 1982a. *Soil-to-Plant Concentration Factors for Radiological Assessments.* Rep. NUREG/CR-2975, Lawrence Livermore Laboratory, Livermore, California.

Ng Y.C., S.E. Thompson, and C.S. Colsher. 1982b. *Transfer Coefficients for Assessing the Dose from Radionuclides in Meat and Eggs.* Rep. NUREG/CR-2976, Lawrence Livermore National Laboratory, Livermore, California.

Ng Y.C., C.S. Colsher, D.J. Quinn, and S.E. Thompson. 1977. *Transfer Coefficients for the Prediction of the Dose to Man via the Forage-Cow-Milk Pathway from Radionuclides Released to the Biosphere.* Rep. UCRL-51939, Lawrence Livermore Laboratory, Livermore, California.

Pacques G.L., R.L. Vanderlip, and D.A. Whitney. 1975. "Growth and Nutrient Accumulation and Distribution in Grain Sorghum. I. Dry Matter Production and Ca and Mg Uptake and Distribution." *Agronomy J.* **67**: 607–616.

Page M.B., J.L. Smalley, and O. Talibudeen. 1977. "The Growth and Nutrient Uptake of Winter Wheat." *Plant and Soil* **49**: 149–160.

Parks Barry S. 1991. *User's Guide for CAP88-PC, Version 1.0.* Rep. EPA 520/6-91-022, U.S. Environmental Protection Agency, Washington, D.C.

Parks C.L., A.W. White, and F.C. Boswell. 1970. "Effect of a Plastic Barrier Under the Nitrate Band on Nitrogen Uptake by Plants." *Agronomy J.* **62**: 437–439.

Pleasant J.C., L.M. McDowell-Boyer, and G.G. Killough. 1980. *RAGTIME: A FORTRAN IV Implementation of a Time-Dependent Model for Radionuclides in Agricultural Systems. First Progress Report.* Rep. NUREG/CR-1196, ORNL/NUREG/TM-371, Oak Ridge National Laboratory, Oak Ridge, Tennessee.

Pleasant J.C., L.M. McDowell-Boyer, and G.G. Killough. 1982. *RAGBEEF: A FORTRAN IV Implementation of a Time-Dependent Model for Radionuclide Contamination of BEEF.* Rep. NUREG/CR-2610, ORNL/TM-8011, Oak Ridge National Laboratory, Oak Ridge, Tennessee.

Ter Haar G. 1970. "Air as a Source of Lead in Edible Crops." *Env. Sci. and Tech.* **4**(3): 226–229.

Watters R.L., J.E. Johnson, and W.R. Hansen. 1969. "A Study of Unsupported Polonium-210 for Ion Exchange in Soil and Uptake in Vegetation," in *Second Technical Progress Report of the Department of Radiology and Radiation Biology.* Rep. COO-1733-3, Colorado State University, Fort Collins, Colorado 80521.

Witherspoon J.P. and F.G. Taylor, Jr. 1970. "Interception and Retention of a Simulated Fallout by Agricultural Plants." *Health Phys.* **19**: 493–499.

Zimbrick J.D. and P.G. Voillequé (Eds.). 1968. *1967 CERT Progress Report, Controlled Environmental Radioiodine Tests at the National Reactor Testing Station,* Progress Report Number Four. Rep. IDO-12065, Idaho National Engineering Laboratory, Idaho Falls, Idaho.

APPENDIX R

SURFACE WATER TRANSPORT

INTRODUCTION

This appendix describes important environmental exposure pathways for the surface water transport of radionuclides from the FMPC, and the methods that will be used to determine radiation doses to individuals in the vicinity of the FMPC from these pathways. Source term estimates for 1960–1962, which were reported earlier, are used in this appendix to illustrate the methodology (Voillequé et al. 1991). Figure R–1 shows that there are two distinct points of release of radionuclides to surface water from the FMPC:

- The main effluent line to the Great Miami River
- Runoff and spills that enter Paddy's Run Creek.

Basic hydrologic characteristics of the surface water receiving the discharge effluent from the site must be known for this pathway analysis. With this information, we can determine the environmental concentrations of the radionuclides (for the 1960–1962 period only uranium is considered) in surface water from both the Great Miami River and Paddy's Run Creek. Our methodology involves applying the 1960–1962 source term to several surface water pathway models to evaluate the magnitude of doses from the surface water pathway, and the relative contribution of various pathways to dose. The three approaches we used are:

- National Council on Radiation Protection and Measurements (NCRP) Screening Model for releases to surface water (NCRP 1991);
- The GENII model developed by Battelle for the Hanford Environmental Project (Napier et al. 1988); and finally,
- A basic surface water monthly dilution (MD) model combining our monthly estimates of source term with uncertainty estimates using a statistical risk management program (Crystal Ball™).

Initially, we used the NCRP Screening Model and the GENII Model to determine the key surface water exposure pathways on an annual basis. Once the major pathways were identified based on annual source term estimates, more refined calculations were made using our monthly source term and uncertainty estimates for 1960, 1961, and 1962.

With these three approaches to surface water dosimetry for the Fernald Dosimetry Reconstruction Project, the modeling is simple, environmental radionuclide concentrations and ultimately, radiation doses are being checked three different ways, and estimates of uncertainties are being included. We list several tables of original data of river flow characteristics and uranium measurements in water and sediment near the FMPC. These tables of data are presented in Tables RS–1 through RS–10 ("S" for "Special") at the end of the appendix.

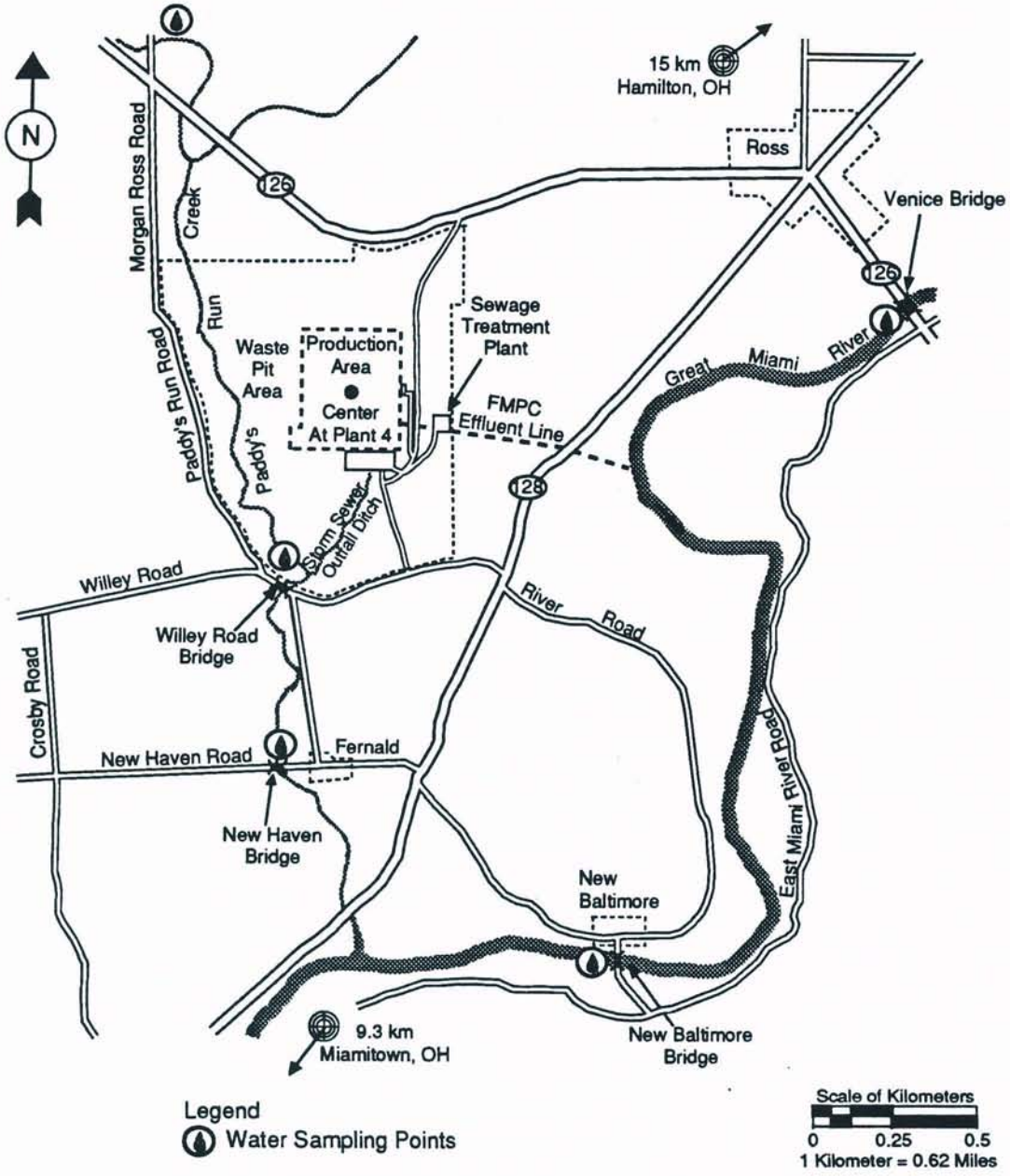

Figure R–1. Diagram of the FMPC showing the liquid effluent release points and the main water sampling locations in the early years of operations.

HYDROLOGIC CHARACTERISTICS OF SURFACE WATER FLOW

Since the most important factor for dispersion of radioactivity released to surface water is dilution in a receiving body of water, site-specific hydrologic parameters are utilized as much as possible to determine radionuclide concentrations after mixing has occurred. The major water flow near the Feed Materials Production Center (FMPC) is the Great

Miami River which enters the Ohio River approximately 18 miles (29 km) downstream of Cincinnati. The river, located about a half mile east and south of the FMPC, runs in a southerly direction. Upstream of the FMPC on the Great Miami River lie the communities of Fairfield, Hamilton, Middletown, and Dayton. Downstream areas are sparsely populated and have a few small industries. The Great Miami River is not a source of public drinking water between the FMPC and its confluence with the Ohio River. It is considered unsafe for swimming due to turbulence, but some people do fish the river.

The main effluent line from the FMPC discharges into the Great Miami River through a 4650-foot-long, 16 inch diameter cast-iron pipe, constructed in 1952 (Catalytic 1953). Seven concrete manholes are located along the line for access and maintenance purposes. Various physical characteristics of the Great Miami River have been studied extensively over the years (IT 1988; USGS 1991; Starkey 1955–1962).

The U.S. Geological Survey has measured river flow parameters such as flow rates and drainage areas on a daily basis since 1910 at several stations along the river, and all records are available for this project (USGS 1991). For flow estimates in the vicinity of the FMPC effluent discharge point, the Miami Conservancy District has routinely adjusted the USGS flow measurements of the Great Miami River for the contribution from the intervening drainage area between Hamilton, Ohio and Ross or New Baltimore. These adjustments are necessary because wastewater, from the Champion Papers Company and the Fairfield Wastewater Treatment Plant, is returned to the river below the Hamilton gauge. In addition, groundwater pumped by the City of Cincinnati and the Southwestern Ohio Water Company (SOWC) is diverted out of the drainage basin. The diversion by Cincinnati is above Ross and the diversion by SOWC was installed in 1952 below Ross. When these adjustments are made, the mean discharge for the FMPC vicinity is approximately 5% higher than that measured at the Hamilton gauge (Rozelle 1991).

The cyclical nature of the river flow rate is shown clearly in Figure R–2 for 1959 through 1963 with higher flows during the first half of the year, and lower rates during the fall months. Table RS–1 at the end of this appendix lists the high, average and low monthly discharge rates for 1960–1962. The flow of the river at the Hamilton gauge averages 3300 cubic feet per second (cfs) (93.4 $m^3\ s^{-1}$) with a maximum of 352,000 cfs (9970 $m^3\ s^{-1}$) measured in March 1913 and a minimum of 100 cfs (2.8 $m^3\ s^{-1}$) measured in September 1941. Five retarding basins were constructed on the river in 1922, and the maximum discharge since that time was 108,000 cfs (3058 $m^3\ s^{-1}$) on January 21, 1959 (USGS 1991).

Figure R–3 shows the relative magnitude of the river flow rate compared to the liquid effluent flow rate from the FMPC from January 1960 through December 1962. Whereas the river flow rate varies seasonally between 300 and 30,000 million gallons per day (MGD), the effluent discharge rate in the early sixties was fairly constant month to month at about one million gallons per day. Data were not located to determine maximum and minimum effluent flow rates for all months in 1962; nevertheless, the difference in magnitude between the river and the effluent flow is clear. As the flow rate decreases the dilution of the radioactive material decreases and, consequently, the concentration of the radionuclides increases.

Natural drainage from the FMPC to the Great Miami River is primarily by way of Paddy's Run, a small creek which begins north of the FMPC and flows southward along the

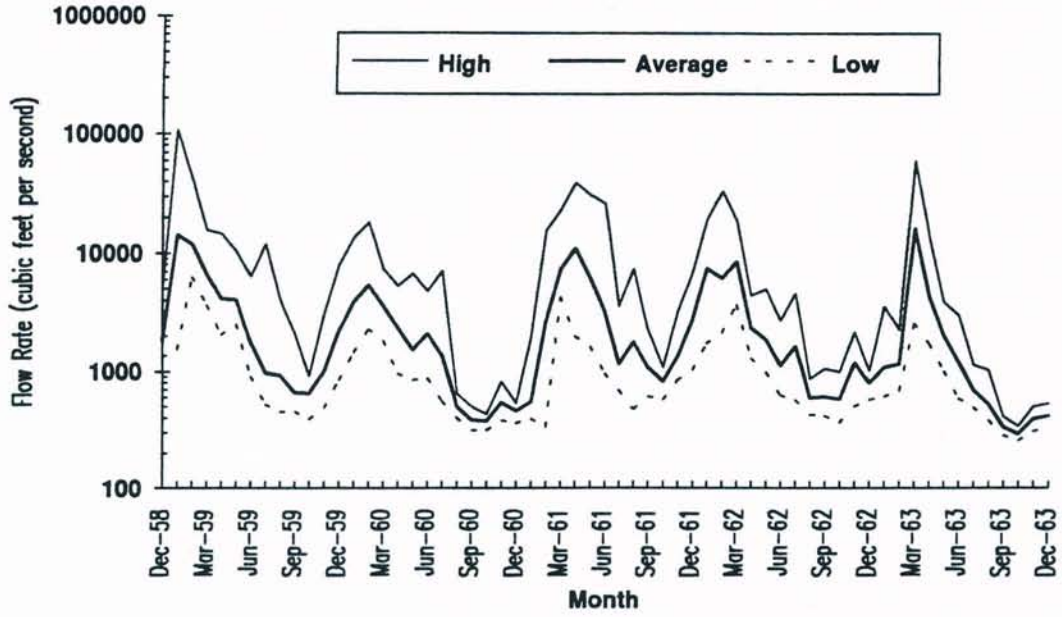

Figure R–2. Monthly high, average and low flow rates for the Great Miami River in the vicinity of the FMPC. The daily USGS discharge is measured in cubic feet per second (cfs), and adjusted for the FMPC area by the Miami Conservancy District.

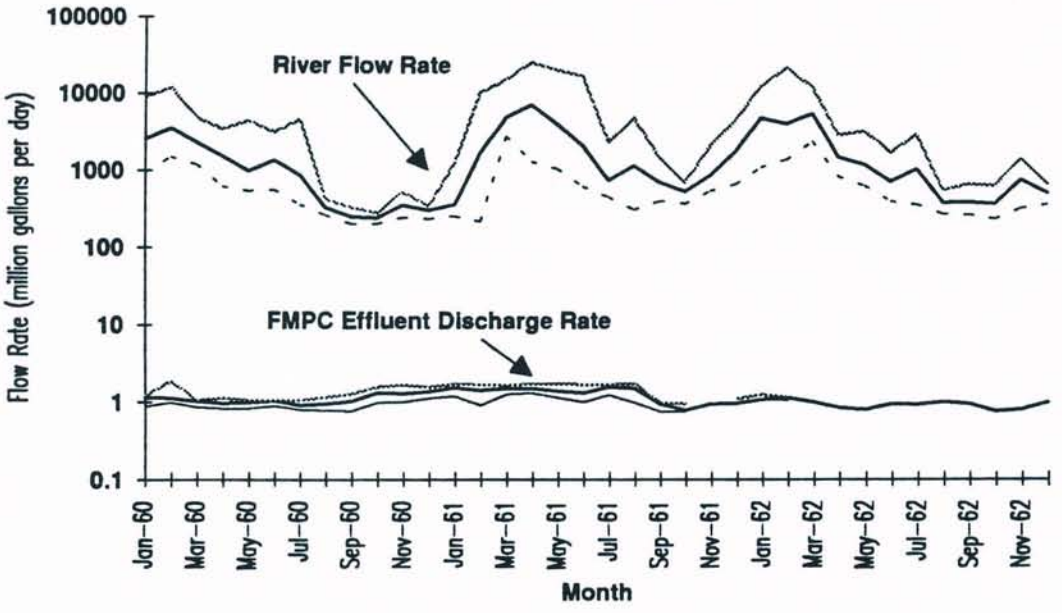

Figure R–3. The relative magnitude of the flow rates of the Great Miami River and the liquid effluent from the FMPC. The average flow is shown as the center black line, with the high and low flow shown above and below, respectively. The effluent discharge was routinely measured in gallons, or million gallons per day (MGD).

western edge of the site. This intermittent stream begins losing flow to the underlying sand and gravel aquifer south of the waste pit area (Dames and Moore 1985). Its flow is erratic and seasonal, and serves principally to catch runoff from the west area of the site during heavy rains. The flow in Paddy's Run Creek is not gauged. Water movement is generally slow in the frequent riffles and pools in this area, which range in depth from 5 to 15 inches (Facemire et al., 1990). The mean drainage discharge of gauged streams in Butler and Hamilton counties ranged between 11.7 and 13.3 inches per year through the sixties (ODNR, 1968).

Occasionally, when there is water flow above and below the FMPC, Paddy's Run can be dry from the K-65 storage area to a point below the Willey Road Bridge (Facemire et al., 1990). Consequently, determining an average flow rate and volume through Paddy's Run Creek is quite uncertain. However, estimates of flow rate and volume were made occasionally over the operating history of the FMPC (For example, NLCO 1961–1962, Klein 1965) and the average uranium concentration in water moving through the creek could be estimated. The flow in Paddy's Run Creek, which generally exists only during January to May, averaged 2 to 4 cfs (0.065 to 0.1 m^3 s^{-1}). These values for Paddy's Run are approximately 0.1% of the flow in the Great Miami River. Since flow in Paddy's Run is dependent upon rainfall, discharges from the site to Paddy's Run generally occurred during periods of heavy rain and runoff when the storm sewer outfall overflowed, or when runoff from the west side the of site flowed into the Paddy's Run Creek.

SURFACE WATER EXPOSURE PATHWAYS

Environmental pathway analysis addresses the movement of radionuclides from their release from a facility, their movement through air, water and soil, and eventual uptake by plants, animals and humans. Mathematical models of aquatic radionuclide transport quantify these pathways and estimate concentrations of radioactivity in food and drinking water by simulating the movement of the released radioactivity through the water, its transfer to aquatic organisms, and its uptake by crops, garden produce or farm animals.

From releases of radionuclides in liquid effluent, two modes of radiation exposures can occur: external and internal. External exposure can occur from ground contamination, shoreline activities or swimming. Internal exposures can occur when the radionuclides are ingested into the body, either directly in water, or indirectly through ingestion of fish, agricultural or garden produce, animal products or through inadvertent ingestion of soil. River or creek water used for irrigation or for watering animals may introduce radionuclides into food crops and animal products such as milk or eggs that people ultimately consume. We have considered a variety of potential exposure pathways from materials released from the FMPC to surface water, and discuss them in the following sections.

Drinking Water Ingestion

Although the Great Miami River is not used as a drinking water source, this pathway was considered in the initial radiation dose analysis for an individual who may drink water

from the river. The dose from the ingestion of water is calculated from the water concentrations and water ingestion rate. For our purposes, no correction was made for transport through the water distribution system (which adjusts for removal of radionuclides during treatment in municipal water supply facilities), because no water treatment facilities are located along the Great Miami River from the FMPC to the Ohio River 18 miles (30 km) to the south.

Ingestion of Fish

Ingestion of fish is a potential surface water exposure pathway. Although the river is turbulent, some people do fish the river. A variety of fish species live in the Great Miami River including river carpsucker, drum, long nose gar, gizzard shad, large mouth bass, longear sunfish, and channel catfish (Miller 1989). Paddy's Run is home to over 20 taxa of fish, with three species, creek chubs, central stoneroller minnows, and bluntnose minnow most common both upstream and downstream of the FMPC (Facemire *et al.*, 1990). A 1973 survey by the Miami Conservancy District (Conn 1976) indicated that aquatic invertebrate populations in the Great Miami River from approximately Dayton, Ohio (upriver) to the confluence with the Ohio River were characteristic of those of stressed streams. In 1969, fish populations in the lower portions of the Great Miami River contained low proportions of sport and pollution intolerant species (MCD 1969). Sport fish are principally sunfish species while the forage fish, characteristic of the Great Miami River in the FMPC area, are mainly carp, goldfish and shiners. An ecological study done by Battelle Columbus Laboratories in 1977 supported the Miami Conservancy District's conclusions about species composition. In the same study, they also found a large number of fish and a variety of species in Paddy's Run, indicating a "fairly clean water stream" (Battelle 1977).

Animal Product and Crop Ingestion

Human exposure to radionuclides in surface water can also occur when contaminated water is used to irrigate crops or garden products. Farming has been one of the major economic activities of Hamilton and Butler counties, especially in the rural area surrounding the plant site (Battelle 1981). Dairy farming, raising beef cattle, and crops such as sweet corn, grain corn, soybeans, and wheat predominate in the area. Garden produce is grown in the area and sold at local produce stands. The animal product exposure pathway assumes that animals are fed contaminated crops or contaminated water. With the GENII and NCRP models, we considered four animal products in the initial surface water pathway assessment: beef, poultry, cow's milk and eggs.

The State of Ohio records irrigation usage information for all counties in Ohio. They record the location of use by latitude and longitude, the volume withdrawn, and whether water is drawn from wells, from the river, or from a combination. Some crops and garden produce are irrigated in this area; however, most irrigation water comes from wells (Luczyk 1992). Site-specific information, which is incorporated into our surface water pathway analysis, is described more fully in the GENII MODEL section of this appendix. Furthermore, Appendix Q summarizes agricultural parameters such as vegetable planting times and growing periods, for Butler and Hamilton counties.

Battelle Columbus Laboratories conducted environmental assessments at several different times at the FMPC that provide insights on the environs of the FMPC (Battelle 1977; Battelle 1981). Generally, four major vegetation communities occur in the FMPC area: grazed pasture along the east, south and north sides, mowed area (pasture) along the northeast portions, wooded areas along the stream beds and on the north side and forb-shrub area near Paddy's Run and in the northwest portion (Battelle 1977). Portions of the mowed areas outside the inner fence were planted with approximately 131,000 pine and spruce tree seedlings in 1972.

Inadvertent Ingestion of Soil and Water

Uptake of radionuclides may result from inadvertent ingestion of soil with foods or of water during recreational swimming. The GENII model used conservative estimates of average soil ingestion over the lifetime of an individual of approximately 400 mg per day. Inadvertent ingestion of water may occur during recreational swimming. In the GENII model, the amount ingested is assumed to be 10 mL per hour of swimming. The length of time of swimming is used to estimate the dose to an individual from this pathway.

Aquatic Recreational Activities

Recreational activities near water include boating, swimming and external exposure from shoreline activities. Environmental pathway analysis considers concentrations of the radionuclides in water, the time spent in each of these activities, as well as the sediment concentration deposited on shoreline from contaminated water following a long period of deposition.

The next major sections provide details of the methods and key conclusions reached from our three approaches to surface water dosimetry: the NCRP Screening Method, the GENII model, and our estimates based on our MD model using monthly source terms and uncertainties.

NCRP SCREENING MODEL

The screening techniques developed by the National Council on Radiation Protection and Measurements (NCRP 1991) represent an approach that combines important transport mechanisms, exposure pathways, and dosimetry methods to a few calculation steps that require a minimum amount of site-specific data.

We used the NCRP Level II screening methods for surface water releases in which some site-specific data are used to account for dispersion in surface waters and to estimate annual average radionuclide concentrations in the river, and important exposure pathways. Table R–1 lists the annual low, average, and high river flow rates for 1960 to 1962 in the vicinity of the FMPC (USGS 1991; Rozelle 1991). The annual average low river flow rate for each year is used in the screening calculations as a conservative assumption, since dilution of the radioactive material is minimized.

Table R–1. Average River Flow for the Great Miami River

	Average River Discharge ($m^3 s^{-1}$)		
Year	Low Flow	Average Flow	High Flow
1960	25	53	157
1961	33	95	384
1962	32	146	224

The IT Corporation (1988) determined representative values for the river in the vicinity of the FMPC for water depth, velocity, and channel width using the HEC–2 computer model developed by the Hydrological Engineering Center of the U.S. Army Corps of Engineers. These values, listed below, are used as site-specific parameters for the screening Level II calculations:

- channel width = 345 feet (105 m)
- water depth = 5.4 feet (1.65 m)
- flow velocity = 2.1 feet per second (0.64 m s^{-1}).

Table R–2 presents the annual surface water source terms and data on effluent volumes calculated previously (Voillequé et al. 1991). The source terms to the river were 5600 kg uranium (U) for 1960, 7300 kg U for 1961 and 6200 kg U for 1962, with a total for the three-year period of 19,000 kg uranium. For Paddy's Run the source terms were 1300, 1400, and 1500 kg U for 1960, 1961 and 1962, respectively. Using a conversion factor of 6.8 x 10^{-7} Ci U per g U, Table R–2 lists the source term in curies (Ci). Similarly, the effluent volume, recorded by the FMPC in gallons is converted to liters using the conversion factor of 3.785 L per gallon. Using these values for the NCRP screening, we obtained the annual average concentration at the point of release and downstream in the Great Miami River and in Paddy's Run Creek.

Results of the NCRP screening methods are presented in Table R–3. This methodology showed that the important exposure pathways for uranium releases to the river are drinking water (26%), consuming vegetables from a garden that has been irrigated with contaminated water from the river (33%), and from external exposure to garden soil and shoreline deposits (31%). These calculations are based on a 30–year buildup time for the uranium daughter products.

The high contribution from ground and shoreline contamination does not appear to be a major exposure pathway, however, when one considers the sediment sampling data from the Great Miami River. Figure R–4 shows the analyses for total uranium that were done on sediment samples from the Great Miami River from 1974 through 1986 (NLCO 1974–1986). These data are listed in Table RS–2 at the end of this appendix as total uranium (pCi g^{-1} dry weight) in sediment, where samples were generally taken from near shore and midstream locations, and the results averaged. The top two inches (5.1 cm) of sediment were scraped; only that portion passing a 50-mesh screen was analyzed for uranium (NLCO 1976; NLCO 1975). The minimum detection level was 0.5 μg U g^{-1}.

Table R–2. Calculated Uranium Concentrations in the Great Miami River and in Paddy's Run Creek Based Upon the NCRP Screening Methods

Year	Source Term (Ci U)	Effluent Volume (L)	Average Concentration (pCi L^{-1}) At discharge point	After mixing[a]
		Great Miami River		
1960	3.8	1.5×10^9	2500	4.9
1961	4.9	1.8×10^9	2700	4.6
1962	4.1	1.3×10^9	3200	4.1
3–yr.	12.8	4.6×10^9	2700	4.6
		Paddy's Run		
1960	0.86	1.1×10^8	7800	600
1961	0.92	1.6×10^8	5700	440
1962	1.08	2.3×10^8	4600	350
3–yr.	2.70	4.9×10^8	5400	420

[a] Based on average low flow rate for year.

Table R–3. Relative Importance of Exposure Pathways for Uranium Releases to the Great Miami River for 1960 to 1962 Based Upon the NCRP Screening Model [a]

Surface Water Pathways	Screening Value Sv	Screening Value mrem	Relative Contribution (%)
External			
Boat & Swim	3.1×10^{-12}	3.1×10^{-7}	<0.001
Ground & Shore [b]	1.1×10^{-5}	1.1×10^{0}	31
Internal			
Drinking Water	9.1×10^{-6}	9.1×10^{-1}	26
Fish Consumption	1.1×10^{-6}	1.1×10^{-1}	3
Irrigated garden [c]	1.2×10^{-5}	1.2×10^{0}	33
Milk	1.7×10^{-6}	1.7×10^{-1}	5
Meat	8.6×10^{-7}	8.6×10^{-2}	2
Total	3.6×10^{-5}	3.6×10^{0}	100

[a] Based on uranium surface water source term from Voillequé et al. 1991.

[b] Contributions from ground irradiation from garden soil and shoreline deposits; assumes a 30-year build-up time.

[c] Assumes consumption of vegetables irrigated only with contaminated river water.

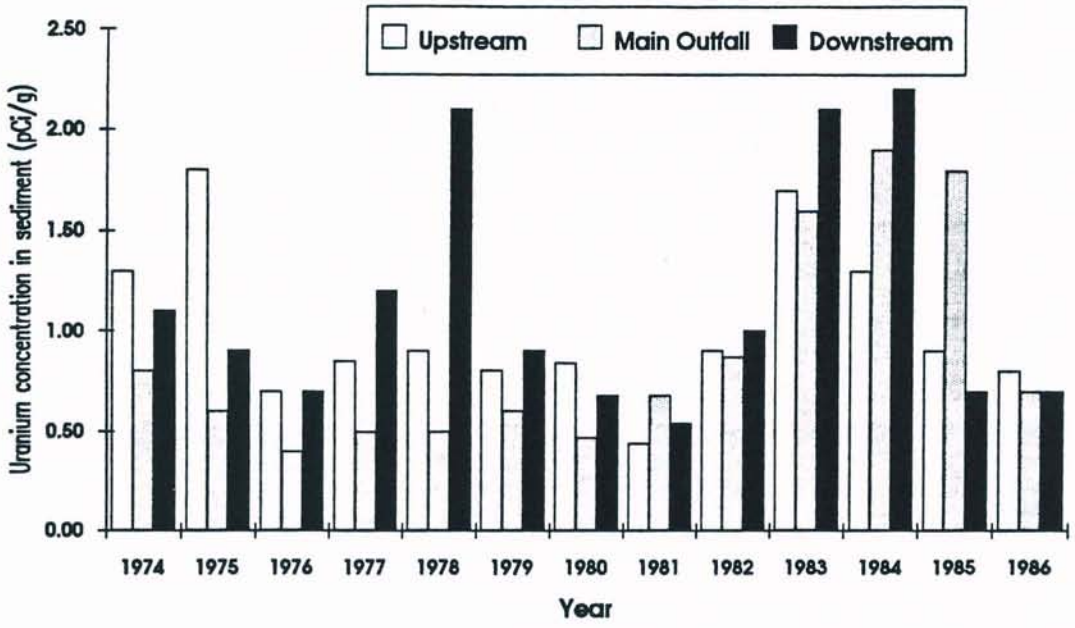

Figure R–4. Average uranium concentrations in sediment samples taken upstream, at the main effluent outfall, and downstream where Paddy's Run enters the river.

The data indicate no clear difference between uranium in sediment measured upstream, just downstream of the effluent discharge point, or further downstream below the point where Paddy's Run Creek flows into the Great Miami River. The results from 1974 onward indicate no build-up of uranium in the sediments where settling might be expected to occur. Most of the uranium present in the site effluent is soluble, probably existing as a carbonate complex, and remains soluble, probably after mixing in the river. Furthermore, periodic flooding may scour the river bed and banks, preventing any long-term sediment accumulation (NLCO 1974, 1978; USGS 1991). Consequently, for our methodology, we do not consider a 30–year build-up factor for uranium in the sediments.

GENII MODEL

The GENII model was also used to evaluate the importance of various exposure pathways. In addition, the GENII code allows one to calculate, at selected locations downstream, the concentration of radionuclides in water, as well as, radiation doses resulting from releases of radionuclides to nontidal rivers and near-shore lake environment. GENII incorporates the internal dosimetry models recommended by the International Commission on Radiological Protection (ICRP) in updated versions of the environmental pathway analysis models used at the Hanford Laboratories in Richland, Washington (Napier 1988). The surface water program in GENII solves for radionuclide concentrations in a river under the following assumptions:

- constant flow depth
- constant downstream longshore velocity
- straight river channel
- constant lateral dispersion coefficient
- continuous point discharge release of effluent
- constant river width.

For the initial runs of the GENII model, we used the uranium source term estimates for calendar years 1960, 1961 and 1962 (Table R–2) (Voillequé et al. 1991). Radiation doses were calculated for a hypothetical individual who was assumed to be exposed through the various pathways to maximum or average exposure levels. Table R–4 lists the exposure scenario parameters that differ for the hypothetical "average" individual and the "maximum" individual that were utilized in the GENII model calculations. For internal exposure pathways, ingestion of drinking water, fish, agricultural products, meat, milk, eggs, and inadvertent soil ingestion were considered. The external exposure pathways considered were: ground contamination from irrigation, recreation such as swimming, boating and shoreline activities. Irrigation is assumed to occur over a 6 month period at a rate of 40 inches per year.

Table R–4. Exposure Pathway Parameters Used in the GENII Model For Hypothetical Individuals

Exposure Pathway	"Average" Individual	"Maximum" Individual
External	Hours of exposure per year	
To ground contamination	2900	4400
For swimming	10	100
For boating	5	100
For shoreline activities	17	500
Internal Consumption	Consumption rate (kg y^{-1})	
Fish	6.9	40
Leafy vegetables	15	30
Other vegetables	140	220
Fruit	64	330
Meat	70	80
Poultry	8.5	18
Eggs	20	30
Cow's milk	230 L y^{-1}	270 L y^{-1}
Drinking water	440 L y^{-1}	730 L y^{-1}

For comparison, the NCRP method assumes values that are similar to those assigned to the maximum individual listed in Table R–4. An exception to this is the assumed 8000 hours of exposure per year to ground contamination, compared to 4400 hours in the GENII model.

In addition, the NCRP screening model combines the consumption of fruits, vegetables and grains (200 kg y^{-1}), and assumes 10 kg per year of freshwater fish are consumed, which represents approximately the 99th percentile of adult consumption in the U.S. (Rupp et al. 1980).

Results of the GENII model calculations are listed in Table R–5. Drinking river water, and consuming garden produce and fish from the river each contribute approximately 25 to 30% of the radiation dose to an individual. The total dose to a maximally-exposed individual, calculated with the GENII model (0.2 mrem), is roughly 20 times less than the NCRP screening value of 3.6 mrem.

Table R–5. Relative Importance of Exposure Pathways for Uranium Releases to the River Based on the GENII Model [a]

Surface Water Pathways	Annual Maximum Radiation Dose		Relative Contribution(%)
	Sv	mrem	
External[b]	4×10^{-9}	4×10^{-4}	<0.01
Internal	2×10^{-6}	2×10^{-1}	
Drinking Water			25
Fish Consumption			24
Vegetables[c]			30
Fruit			5
Milk			10
Meat			5
Inadvertent Soil & Water Ingestion			<0.05
Total	2×10^{-6}	2×10^{-1}	100

[a] Based on uranium surface water source term for 1960, 1961 and 1962 from Voillequé et al. 1991.
[b] Contributions from ground irradiation from garden soil and shoreline deposits; assumes no build-up time.
[c] Assumes consumption of vegetables and fruit irrigated with 40 inches (102 cm) of contaminated river water per year.

Based upon the information obtained from the NCRP Screening Model and the GENII code, we concluded that the major pathways contributing to radiation dose from uranium in the surface water would be from the consumption of drinking water, the ingestion of fish and local garden produce. The importance of the consumption of garden produce depends greatly on the extent of irrigation with river water. Accordingly, to determine the extent of irrigation with river water in this area, we obtained County water usage information for Butler and Hamilton Counties from the Ohio Department of Natural Resources, Division of Water (Luczyk 1992). In April 1990 they began a water withdrawal registration program in which facilities and individuals were required to register with the State of Ohio if over 100,000 gallons per day (70 gallons per minute) were withdrawn from surface and groundwater. In addition, the relative contribution by category is tabulated. The categories include industrial, power generation, public water supply, miscellaneous as well as

agricultural/irrigation. The agricultural/irrigation category includes not only crop and livestock production, but also landscaping, fish and waterfowl propagation, and golf course irrigation. For 1991, large quantities of water were withdrawn in both Butler and Hamilton Counties for industry (greater than 25 MGD) and for public water supplies (greater than 25 MGD) (Luczyk 1992). Most of the water withdrawn in Hamilton County is for power generation (greater than 250 MGD). However, Butler and Hamilton Counties withdrew less than one million gallons per day (MGD) from surface water for agriculture and irrigation, and from 1 to 5 MGD from groundwater for these purposes.

Even if we assume that the 1 MGD withdrawn from surface water in Butler and Hamilton counties is used only for irrigation purposes, this is an extremely small volume of water for irrigation in comparison to the forty inches of irrigation per year assumed in the GENII model. An assumed irrigation rate of 40 inches of river water per year for Butler (471 square miles) and Hamilton (413 square miles) Counties represents a volume of water at least three orders of magnitude greater than the 0 to 1 MGD actually recorded by the state for these counties in 1991. Clearly, the model assumption is orders of magnitude greater than the actual quantity of river water used for irrigation, and we conclude that this pathway is not one of the major pathways of exposure for this area.

MONTHLY SURFACE WATER DOSIMETRY METHODOLOGY

The NCRP and GENII models allowed us to do initial screening of surface water exposure pathways on annual source term estimates. Based upon these models along with site-specific irrigation and sediment sampling data, we concluded that the ingestion of drinking water and fish were key pathways for exposure to uranium from the FMPC during the early sixties. Consequently, we calculated monthly estimates of uranium concentrations and intake of uranium by individuals via these pathway using a basic monthly dilution model (MD)

This approach requires that we account for dilution and transport of the material in the receiving body of water, *i.e.*, either the Great Miami River or Paddy's Run Creek. These aquatic transport calculations assume that the radionuclide concentration at the downstream receptor of interest in a receiving surface water (C_m) is equal to the radionuclide concentration at the point of radionuclides release, *i.e.*, the radionuclide concentration at the discharge point into the Great Miami River (C_0) divided by the dilution factor (S):

$$C_m = C_0 / S \qquad \text{(R–1)}$$

where,

C_m = radionuclide concentration in the receiving surface water (Bq m^{-3}),

C_0 = radionuclide concentration of an effluent at the point of release (Bq m^{-3})

S = the dilution factor, a ratio of the flow rate of the receiving body of water to the flow rate of the waste effluent.

The effluent concentration (C_0) is the radionuclide release rate divided by the effluent flow rate:

$$C_0 = W_0 / Q_0 \qquad \text{(R–2)}$$

where,

W_0 = radionuclide release rate at the point of release (Bq s^{-1}), and

Q_0 = flow rate of the effluent discharge at the point of release (m^3 s^{-1}).

The dilution factor, S, is based upon the river flow characteristics of the Great Miami River, and FMPC discharge volumes for the site. When the quantity of effluent is small relative to the receiving water body (*i.e.*, dilution on the order of 10 to 100), initial mixing is relatively rapid, and reduces the radionuclide concentration (Jirka et al., 1983).

The MD model incorporated a statistical uncertainty analysis computer program (CrystalBall™) to provide bounds around our central estimates. We assumed a distribution of values for monthly discharge of uranium and monthly discharge volume based upon the source term values reported in Task 2 and 3. For the monthly dilution factors, we assume a distribution of values based upon the daily flow measurements made by USGS (Table R–1).

Figure R–5 compares the median uranium concentrations in the river from the MD model, with the surface water source terms for January 1960 through December 1962. In addition, the figure compares the calculated uranium concentrations to reported background levels in domestic drinking water in the U.S. of 0.8 to about 3 pCi U L^{-1} (NCRP 1984b). The river has not been used as a drinking water source but this is a convenient measure to show the relative contribution of the FMPC effluents to uranium in the river. The background concentrations of uranium in drinking water are taken from an extensive study by the National Uranium Resource Evaluation (NURE) program plus data prepared for the US EPA, in which over 90,000 drinking water samples were evaluated.

For this time period, the highest uranium concentrations in the river occurred from August 1960 through January 1961 and in September 1962 when it exceeded 20 pCi L^{-1}. There is good agreement for these times between the source term and concentration estimates. However, in mid-1961 the higher source term estimates are not reflected in higher uranium concentrations in the river. Generally, the highest uranium concentrations in the river were calculated for 1960, although the lowest quantity of uranium was discharged that year, compared to 1961 and 1962. These observations emphasize the importance of the river flow rate on the dilution of the uranium in estimating environmental concentrations in the river. The average river flow in 1960 was less than half (1650 cfs) that measured in 1961 (3570 cfs). Consequently, the uranium concentrations were lower in 1961 because the river flow rate was high. Table RS–3 summarizes the monthly uranium concentrations in river water and in fish, with the standard deviations calculated with CrystalBall™ shown in parentheses.

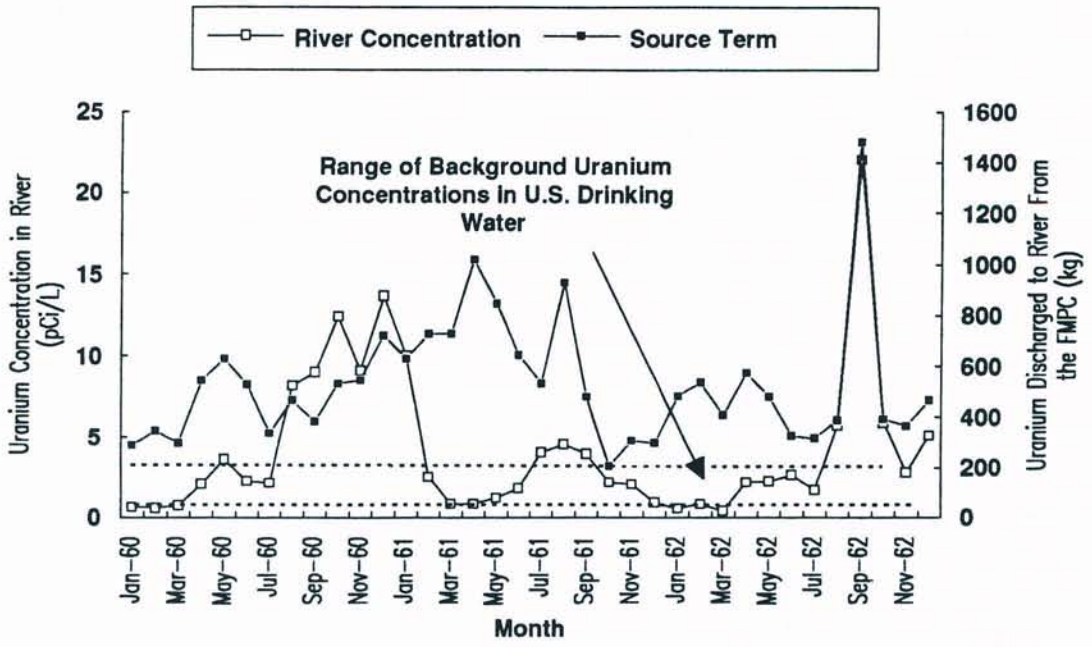

Figure R-5. Comparison of the quantity of uranium discarded from the FMPC to the Great Miami River with the uranium concentration measured in the river after dilution during 1960–1962. The dotted lines indicate the approximate average range of background uranium concentrations in U.S. drinking water.

The concentration of a particular radionuclide in fish is related to the radionuclide concentration in the water through concentration ratios. The concentration ratio (CR) is a ratio of the concentration of the radionuclide in the fish to that in the water. It is based upon the intake rate and biological elimination of the radionuclide by the fish, and the mass of the fish. The CR assumes that equilibrium has been reached between the organism and its environment. Neither freshwater nor marine fish accumulate uranium to a great degree (Poston and Klopfer 1986), and it appears that very little uranium is accumulated in muscle tissue. Published CR values for uranium in freshwater fish range from less than 1 to almost 100 depending upon the type of fish and its environment (NCRP 1984; Peterson 1983; Wahlgren et al. 1976; Poston and Klopfer 1986). The NCRP and GENII models assume a CR of 10. However, in a literature review on the uptake and distribution of selected radionuclides in fish, Poston and Klopfer recommended a CF of 50 for uranium in freshwater fish. They based their recommendation on several experimental studies, and on the observation that omnivorous fish such as carp and catfish, had higher CR values than piscivorous species such as trout for which more studies have been done. Since the predominant species of fish from the Great Miami River include carp, shad and catfish, we assumed a distribution of CR from 1 to 100, with a mean of 50 for our monthly estimates of uranium concentrations in fish.

The intake of uranium in drinking water by individuals is given by the product of the concentration of uranium in river water and the ingestion rate of water. For our purposes, no correction was made for transport through the water distribution system (which adjusts for removal of radionuclides during treatment in municipal water supply facilities), because no water treatment facilities are located along the Great Miami River from the FMPC to the Ohio River 18 miles (30 km) to the south. We assumed a normal distribution of ingestion rates for river water of 0 to 2 L per day with a mean of 1 L, to determine a monthly intake of uranium for this period. Similarly, the intake of uranium via fish consumption is given by the product of the uranium concentration in fish and the intake rate of fish for a particular time period. We assumed a lognormal distribution of fish consumption rates of 1 to 10 kg per year with a mean of 5 kg for this area. The resulting monthly intake of uranium from the ingestion of river water and from the consumption of fish from the river is compiled in Table RS–4, along with the results of the uncertainty analysis using the CrystalBall™ program.

COMPARISON OF MODELED TO MEASURED URANIUM CONCENTRATIONS IN SURFACE WATER FOR 1960–1962

The validation process involves comparing model-calculated uranium concentrations with actual environmental sampling measurements that were done in the Great Miami River and in Paddy's Run Creek. This procedure provides a measure of proof that our models of calculating environmental concentrations and ultimately radiation doses are reasonable. It should be emphasized that the actual environmental measurements were not used in our model development. The sources of information for the sampling measurements are the original analytical data sheets from the Analytical Department of National Lead Company of Ohio (NLCO 1960–1962). For the early sixties, water samples were collected upstream and downstream in Paddy's Run, and analyzed routinely for total uranium (mg U L^{-1}), gross alpha and beta activity, total suspended solids, some chemical constituents, and occasionally for radium. Three-day composite samples were analyzed from the New Haven Road Bridge and the Willey Road Bridge south of the FMPC, while weekly samples were taken at the Paddy's Run bridge north of Route 126. Figure R–1 shows the locations of water sampling points in Paddy's Run Creek and the Great Miami River during this time.

In the Great Miami River, weekly water samples were taken upstream at the Venice Bridge in Ross, about a mile (1.6 km) north of the effluent discharge point, and at the New Baltimore Bridge, about 2 miles (3.2 km) downstream. There was no reported minimum detectable concentration for uranium although the minimum reported value in the data sheets is approximately 0.001 mg U L^{-1}. Tables RS–5, RS–6, and RS–7 at the end of this appendix list the original results in units of mg U L^{-1} from analytical data sheets located for this time period. These tables show the large amount of water sampling data that were collected, and still available for our study. For the Great Miami River, there is not a consistent difference between upriver and downriver locations. Although there is much scatter of data points, especially in 1962, the majority of measurements cluster around the 0.015 mg L^{-1} (10 pCi U L^{-1}) level. Figure R–6 displays the data as monthly averages in units of pCi U L^{-1}, to compare with our MD model results. We can compare the model-predicted

(P) to observed (O) concentrations by calculating the P/O ratio as a measure of bias. A ratio of 1 indicates no bias. The median P/O ratio for this period is approximately 0.70, indicating that the model underpredicts the concentrations measured in the river somewhat. The sources of this slight bias can be attributed to lack of knowledge about the sampling and analytical protocol, and to missing data for some time periods. However, the reasonable agreement between the measured uranium concentrations in the river and those calculated with our model using monthly source term estimates supports our dosimetric methods.

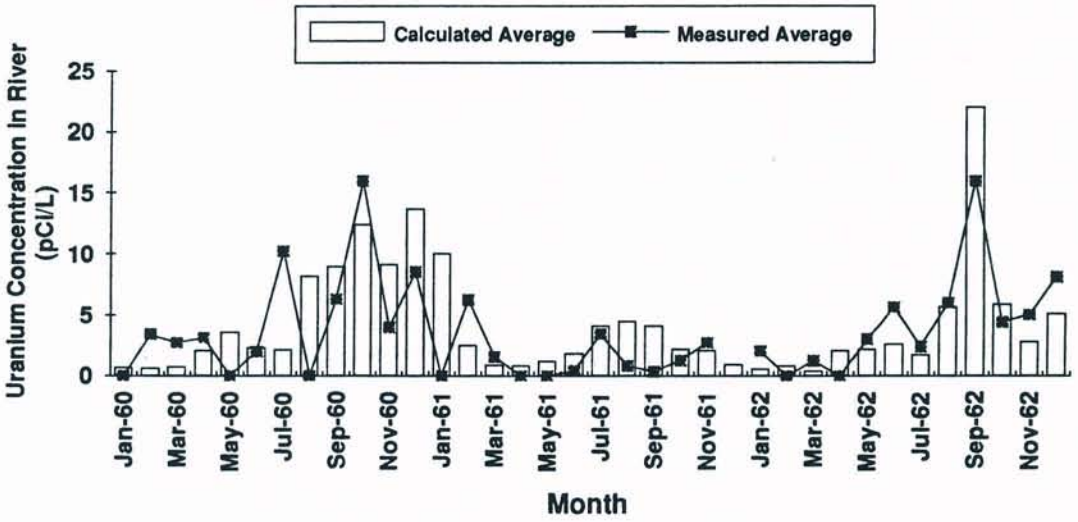

Figure R–6. Comparison of calculated and measured average monthly uranium concentrations downstream of the FMPC in the Great Miami River during 1960, 1961 and 1962.

In a similar fashion, Figure R–7 shows monthly averages in pCi U L^{-1} for Paddy's Run Creek sampling locations downstream of the FMPC for 1960, 1961 and 1962. The original data, recorded in mg U L^{-1} on the analytical data sheets, are tabulated in Tables RS–8, RS–9, and RS–10 at the end of the appendix. For Paddy's Run Creek water samples, there is much more scatter in uranium measurements than with those from the Great Miami River, but the upriver samples from north of Route 126 tend to be lower than the Willey Road and the New Haven Road measurements. The median P/O ratio for Paddy's Run is approximately 3, indicating that our model overpredicts the measured uranium concentration values in Paddy's Run Creek during this time. This overprediction is probably due to the extreme seasonal variation in flow, causing difficulty in estimating an average flow in the creek over an extended period of time. However, the relative contribution of Paddy's Run to surface water pathway exposures is relatively small compared to the river. If Paddy's Run Creek is a key source of exposure relative to other pathways, these methods will be further refined. Nevertheless, Figure R–7 shows that the general pattern between calculated and measured concentrations is quite similar.

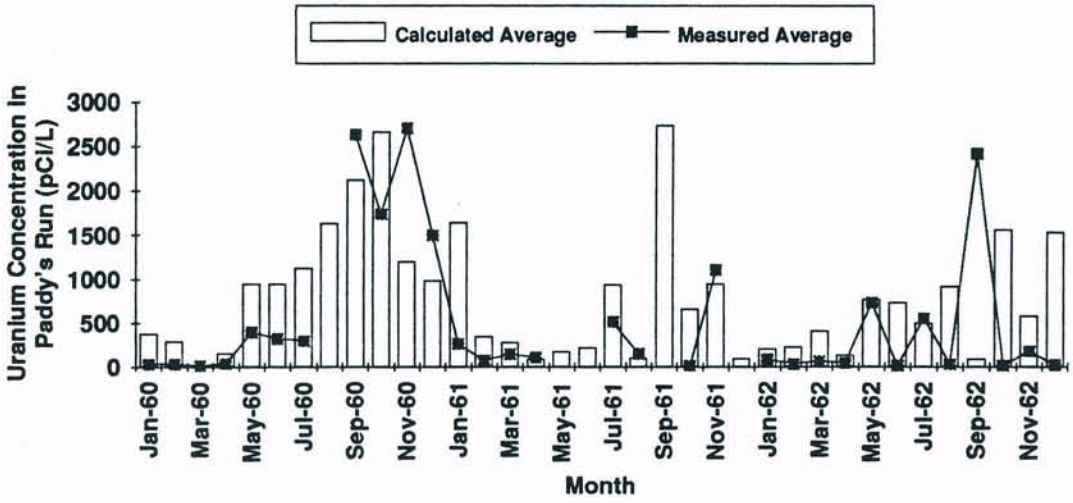

Figure R–7. Comparison of calculated and measured average monthly uranium concentrations in Paddy's Run Creek downstream of the FMPC during 1960, 1961, and 1962. Uranium concentration measurements were not located for all months.

While Figures R–6 and R–7 compare monthly averages, Tables R–6 and R–7 provide comparisons between the annual averages of measured concentrations and calculated uranium concentrations in the river and in Paddy's Run based on the GENII model and on our MD model. For the river, there is good agreement between measured and calculated uranium concentrations for this three-year period, although the standard deviation about the mean is rather broad. For the Paddy's Run Creek the range of concentrations is much greater, most likely due to erratic water flow in the creek much of the year. Because of the large seasonal fluctuations in Paddy's Run, computation of an annual average results in a large standard deviation about the mean. Nevertheless, the calculated concentrations of uranium in Paddy's Run, based on high and low flow rates for the creek do encompass the range of concentrations measured in Paddy's Run during 1960–1962. This agreement suggests that the methods we have developed to determine environmental concentrations of uranium and other radionuclides based on our monthly source term data are acceptable.

CONCLUSIONS

Our three approaches to surface water dosimetry have provided an efficient process to evaluate the importance of environmental transport pathways for discharges from the FMPC to surface water. The NCRP screening approach and the GENII model allowed us to examine all possible pathways, including some that had been suggested to us by local residents. In addition, the GENII model provided radionuclide concentrations in river water from radionuclides discharged from the site. The initial analysis using the NCRP Screening

Table R–6. Measured vs. Calculated Uranium Concentrations (pCi L^{-1}) in the Great Miami River (standard deviation)

Year	# Samples	Average Measured Concentration			Calculated FMPC Contribution	
		Upstream[a]	Downstream[b]	FMPC Contribution[c]	GENII Model[d]	MD Model[e]
1960	76	12.8 (18.5)	15.5 (14.3)	5.0 (12.5)	2.3	5.3 (4.8)
1961	53	10.9 (9.2)	11.3 (5.7)	0.1 (9.9)	1.6	2.9 (2.6)
1962	64	10.3 (9.2)	14.0 (13.9)	3.6 (12.6)	1.7	4.4 (5.9)

[a] Average concentration in water at Venice Bridge in Ross.
[b] Average concentration in water at New Baltimore Bridge south of the FMPC.
[c] Average difference between individual downstream and upstream measurements.
[d] Expected concentrations using GENII model based on annual source term to river and average river flow rate for that year.
[e] Calculated uranium concentrations from our monthly dilution model with monthly source term estimates and CrystalBall™ uncertainty analysis.

Table R–7 . Measured vs. Calculated Uranium Concentrations (pCi L^{-1}) in Paddy's Run Creek Downstream of the FMPC (standard deviation)

Year	Measured Uranium Concentration		FMPC Calculated Contribution	
	# of Samples	Average[a]	GENII[b]	MD[c]
1960	106	770 (1300)	(225–1030)	1040 (1700)
1961	103	350 (630)	(160–1000)	690 (1600)
1962	162	350 (740)	(200–1300)	640 (1900)

[a] Average concentration of samples taken at Willey Road and at the New Haven Bridge. Upstream uranium concentrations, taken just north of Route 126, were subtracted. Upstream concentrations ranged from 10 to 15 pCi L^{-1}.
[b] Paddy's Run is an ungauged stream, but flow was occasionally measured. The values in parentheses represent calculated concentrations from the GENII model based on the annual source term to Paddy's Run, and high and low flow rates, respectively.
[c] Calculated uranium concentrations from our monthly dilution model with monthly source term estimates and CrystalBall™ uncertainty analysis.

and the GENII models identified drinking water from the river, the consumption of produce from gardens irrigated with river water, and fish consumption as the key internal exposure pathways. We concluded that consumption of produce irrigated with river water was not a key pathway based on recorded irrigation rates for Hamilton and Butler Counties obtained from the State of Ohio.

We determined that the inadvertent ingestion of soil is a very minor pathway with respect to potential human exposure. External exposure to contaminated ground near the river shoreline contributed about 25% to the total dose if a 30-year buildup factor for uranium was assumed, or less than 0.01% of the dose when buildup was not included in the calculations. The buildup of uranium in sediments in the river is not supported by sampling data from the mid-seventies onward.

Although the calculation of radiation doses for all years of operation will be reported in the Task 6 report, this initial analysis indicated that the annual effective dose equivalent to a maximally-exposed individual from all pathways is approximately 2×10^{-6} Sv (0.2 mrem) based on the conservative assumptions of the GENII model. This initial analysis shows that the radiation dose to a maximally-exposed individual is quite low even with this conservative approach. Our final dose estimates for surface water pathways will be "best estimates" with uncertainties, based on the MD dilution model.

Our third approach appears to be a good one. We incorporated uncertainty analysis using CrystalBall™ to establish bounds around our median estimates. The results showed that the calculated average uranium concentration in river water and in Paddy's Run during this period agree well with that measured in the early sixties. Clearly, our simple MD model which utilizes our monthly source term data and site-specific parameters is adequate for calculating radiation doses from radionuclide releases to surface water for all years of operation.

REFERENCES

Battelle. 1977. *Environmental Impact Assessment of Feed Materials Production Center.* Prepared for US DOE. Columbus, OH: Battelle Columbus Laboratories.

Battelle. 31 January 1981. *Environmental Report of the Feed Material Production Center Fernald, Ohio.* Columbus, OH: Battelle Columbus Laboratories.

Catalytic Construction Company. 1952. *Completion Report for the Feed Materials Production Center.* For the Atomic Energy Commission.

Conn, C. C. 1976. *Biological survey of the Great Miami River.* Dayton, OH: The Miami Conservancy District.

Dames & Moore. July 1985. *Feed Materials Production Center Groundwater Study – Task C Report.* Prepared for U.S. Department of Energy. White Plains, NY: Dames & Moore.

Facemire, C.F.; Guttman, S.I.; Osborne, D.R.; Sperger, R.H. January 1990. *Biological and Ecological Site Characterization of the Feed Materials Production Center*. Oxford, OH: Miami University.

IT (IT Corporation). 1 August 1988. *Hydrologic Study of FMPC Discharge to the Great Miami River. Final Report*. Prepared for the FMPC Westinghouse Materials Company of Ohio. Pittsburgh, PA: IT Corporation.

Jirka, G. H., A. N. Findikakis, Y. Onishi, P.J. Ryan. 1983. "Transport of Radionuclides in Surface Waters", page 3–1 in *Radiological Assessment*. Edited by J. E. Till and H. R. Meyer. NUREG/CR–3332.

Klein, F.J. 1965. Sampling Storm Sewer Outfall Water to Paddy's Run. Handwritten memorandum to K.N. Ross. Cincinnati, OH: National Lead Company of Ohio.

Luczyk, A. September 1992. Personal communication. Columbus, OH: Ohio Department of Natural Resources, Division of Water.

MCD (Miami Conservancy District). 1969. *Fish Survey of the Miami River – Regional Water Quality Management Program.* Technical Note 4; Dayton, OH.

Miller, M.C. 19 September 1989. *Electrofishing Survey of the Great Miami River*. Cincinnati, OH: University of Cincinnati Department of Biological Sciences.

Napier, B.A.; Peloquin, R.A.; Strenge, D.L.; Ramsdell, J.V. GENII – The Hanford Environmental Radiation Dosimetry Software System Volume 1: Conceptual Representation. Richland, WA: Pacific Northwest Laboratory. December 1988.

NCRP (National Council on Radiation Protection and Measurements). 1984a. "Soil Content and Transport", page 15 in *Exposures from the Uranium Series with Emphasis on Radon and its Daughters*. Report No. 77. Bethesda, MD 20814.

NCRP (National Council on Radiation Protection and Measurements). 1984b. "Drinking Water", page 45 in *Exposures from the Uranium Series with Emphasis on Radon and its Daughters*. Report No. 77. Bethesda, MD 20814.

NCRP (National Council on Radiation Protection and Measurements). 1985. "Assessment of Radionuclides Released to Surface Waters", page 96 in *Radiological Assessment: Predicting the Transport, Bioaccumulation, and Uptake by Man of Radionuclides Released to the Environment*. Report No. 76. Bethesda, MD 20814.

NCRP (National Council on Radiation Protection and Measurements). December 1991. "Screening Models for Releases of Radionuclides to Air, Surface Water, and Ground Water," NCRP Report No. XX Volume 1, Draft Document, Bethesda, MD.

NLCO. 1960–1962. Analytical data sheets for three-day composite or weekly water samples taken from Paddy's Run and the Great Miami River, respectively. Analytical Department, Cincinnati, OH: National Lead Company of Ohio.

NLCO. 1974 – 1990. Annual Environmental Monitoring Reports. Cincinnati, OH: National Lead Company of Ohio.

ODNR (Ohio Department of Natural Resources). 1968. "Flow Duration of Ohio Streams Based on Gaging Station Records Through 1965", Division of Water. Water Bulletin 42.

Peterson, H.T. 1983. "Terrestrial and Aquatic Food Chain Pathways" page 5–1 in *Radiological Assessment A Textbook on Environmental Dose Analysis*. Edited by J. E. Till and H. R. Meyer. NUREG/CR–3332.

Poston T. M., D. C. Klopfer. September 1986. *A Literature Review of the Concentration Ratios of Selected Radionuclides in Freshwater and Marine Fish.* PNL–5484, UC–11, pp. 206–212. Pacific Northwest Laboratory.

Rozelle, J.L. 23 July 1991. *Discharge in Great Miami River.* Letter to John Byrne, Westinghouse Materials Company of Ohio. Dayton, OH: The Miami Conservancy District.

Rupp, E. M., Miller, F.L. and Baes, C.F., III. 1980. "Some results of recent surveys of fish and shellfish consumption by age and region of U.S. residents," *Health Phys.* 39: 1965.

Starkey, R.H. 1955–1962. *Industrial Hygiene & Radiation Monthly Reports to J.A. Quigley.* Cincinnati, OH: National Lead Company of Ohio.

USGS (U.S. Geological Survey) 1991. *Water Resources Data Ohio Water Year 1991.* Volume 1. Ohio River Basin. U.S. Geological Survey Water–Data Report OH–91–1. Prepared in cooperation with the State of Ohio and with other agencies.

Voillequé, P.G.; Meyer, K. R.; Schmidt, D.W.; Killough G.G.; Moore, R.E., Ichimura, V.I., Rope, S.K.; Shleien, B.; Till, J.E. December 1991. *The Fernald Dosimetry Reconstruction Project Tasks 2 and 3 Radionuclide Source Terms and Uncertainties — 1960– 1962.* Neeses, S.C.: Radiological Assessments Corporation.

Wahlgren, M.A., Alberts, J.J., Nelson, D.M. and Orlandini, K.A. 1976. "Study of the behavior of transuranics and possible chemical homologues in Lake Michigan water and biota", page 9 in *Transuranium Nuclides in the Environment*, Report No. IAEA–STI/PUB/410 (International Atomic Energy Agency, Vienna).

Table RS–1. Dilution Factor Determination for Surface Water Transport Calculations Based on Liquid Effluent and the Great Miami River Flow Rates

	FMPC Discharges [a]			Great Miami River Flow Rate [b]			
Date	Source Term (kg U)	Volume (MG)	Flow Rate (MGD)	High (MGD)	Average (MGD)	Low (MGD)	Dilution Factor[c] (S)
Jan 60	286	35.2	1.14	8820	2510	945	2201
Feb 60	343	32.3	1.11	11865	3507	1491	3149
Mar 60	295	31.5	1.02	4791	2325	1179	2288
Apr 60	544	28.8	0.96	3465	1523	620	1586
May 60	629	30.1	0.97	4410	987	546	1017
Jun 60	528	31.1	1.04	3119	1355	567	1307
Jul 60	334	28.2	0.91	4610	882	357	970
Aug 60	466	29.0	0.94	420	322	258	344
Sep 60	381	30.3	1.01	322	248	204	245
Oct 60	530	40.7	1.31	278	242	204	184
Nov 60	544	38.1	1.27	523	350	245	275
Dec 60	720	42.2	1.36	343	298	234	219
Jan 61	629	47.0	1.52	1260	356	255	235
Feb 61	727	41.9	1.40	10185	1701	217	1218
Mar 61	728	45.9	1.48	15225	4820	2783	3255
Apr 61	1018	45.1	1.50	25515	7140	1292	4755
May 61	845	43.2	1.39	20055	4032	1050	2895
Jun 61	644	39.1	1.30	17010	2090	621	1603
Jul 61	533	47.6	1.54	2342	746	445	485
Aug 61	927	46.0	1.48	4820	1155	309	778
Sep 61	481	28.1	0.94	1486	706	399	754
Oct 61	205	24.3	0.78	706	532	372	679
Nov 61	307	28.3	0.94	2090	866	544	919
Dec 61	297	29.9	0.97	4500	1797	669	1860
Jan 62	480	33.5	1.08	12557	4846	1127	4487
Feb 62	535	31.9	1.14	21584	4040	1398	3550
Mar 62	407	31.0	1.00	12353	5544	2389	5535
Apr 62	572	25.2	0.84	2871	1522	842	1811
May 62	478	24.6	0.79	3265	1210	634	1524
Jun 62	325	28.5	0.95	1744	717	404	755
Jul 62	315	28.6	0.92	2973	1049	367	1138
Aug 62	387	30.9	1.00	552	383	274	385
Sep 62	1481	28.4	0.95	675	393	267	416
Oct 62	390	23.2	0.75	634	375	235	501
Nov 62	365	23.9	0.80	1398	758	326	953
Dec 62	465	30.1	0.97	652	514	367	530

a From Voillequé et al. 1991.

b From USGS 1991; river flow rates are based on Hamilton, OH discharge adjusted for the river in the vicinity of the FMPC by the Miami Conservancy District.

c The Dilution Factor, S, is the average river flow rate divided by the average effluent flow rate.

Table RS–2. Sediment Sampling in the Great Miami River

	Total Uranium (pCi g^{-1} dry wt)[a]		
Year	Upstream of the FMPC	Downstream of Discharge Point	Downstream of Paddy's Run
1974	1.30	0.80	1.10
1975	1.80	0.60	0.90
1976	0.70	0.40	0.70
1977	0.85	0.50	1.20
1978	0.90	0.50	2.10
1979	0.80	0.60	0.90
1980	0.84	0.47	0.68
1981	0.44	0.68	0.54
1982	0.90	0.87	1.00
1983	1.70	1.60	2.10
1984	1.30	1.90	2.20
1985	0.90	1.80	0.70
1986	0.80	0.70	0.70
Average	1.02	0.88	1.14
Stdev	0.39	0.53	0.60

[a] The FMPC Environmental Reports stated that "the 95% CI was ± 25%" for all samples.

Table RS–3. Calculated Median Estimates of Uranium Concentration for 1960–1962 (Standard Deviation) [a]

	Great Miami River After Dilution ($pCi\ L^{-1}$)			Fish From The River ($pCi\ g^{-1}$)		
Month	1960	1961	1962	1960	1961	1962
Jan	0.65 (0.09)	10 (1.4)	0.56 (0.07)	0.033 (0.006)	0.50 (0.08)	0.027 (0.005)
Feb	0.59 (0.08)	2.5 (0.32)	0.83 (0.11)	0.030 (0.005)	0.120 (0.021)	0.042 (0.007)
Mar	0.72 (0.10)	0.86 (0.11)	0.42 (0.06)	0.036 (0.006)	0.042 (0.007)	0.021 (0.004)
Apr	2.1 (0.28)	0.83 (0.1)	2.1 (0.3)	0.104 (0.018)	0.042 (0.006)	0.110 (0.015)
May	3.6 (0.46)	1.2 (0.15)	2.2 (0.34)	0.18 (0.031)	0.060 (0.016)	0.110 (0.019)
Jun	2.3 (0.32)	1.8 (0.24)	2.60 (0.34)	0.12 (0.022)	0.090 (0.015)	0.130 (0.022)
Jul	2.1 (0.28)	4.1 (0.52)	1.7 (0.24)	0.11 (0.018)	0.20 (0.033)	0.085 (0.014)
Aug	8.2 (1.1)	4.5 (0.66)	5.7 (0.74)	0.41 (0.069)	0.220 (0.039)	0.280 (0.048)
Sep	9.1 (1.2)	4.1 (0.53)	22 (4.6)	0.45 (0.081)	0.20 (0.030)	1.10 (0.25)
Oct	12 (1.6)	2.2 (0.3)	5.9 (0.8)	0.62 (0.091)	0.11 (0.018)	0.290 (0.05)
Nov	8.6 (1.1)	2.1 (0.29)	2.8 (0.39)	0.43 (0.072)	0.10 (0.018)	0.140 (0.025)
Dec	14 (1.7)	0.93 (0.12)	5.1 (0.8)	0.68 (0.13)	0.050 (0.007)	0.260 (0.053)

[a] Estimates based on monthly source term data from Voillequé et al. 1991, with uncertainty analysis using CrystalBall™.

Table RS–4. Ingestion of Uranium (pCi per month) in Water and Fish From the Great Miami River During 1960–1962 (Standard Deviation)[a]

	Water[b]	Fish[c]		Water[b]	Fish[c]
Jan 60	19	13	Jul 61	120	81
	(3.2)	(2.3)		(20)	(15)
Feb 60	17	12	Aug 61	136	91
	(2.9)	(2.3)		(25)	(17)
Mar 60	22	14	Sep 61	120	80
	(3.5)	(2.8)		(20)	(16)
Apr 60	63	42	Oct 61	65	44
	(11)	(8.2)		(11)	(8.3)
May 60	108	72	Nov 61	62	41
	(17)	(15)		(10)	(8.5)
Jun 60	68	46	Dec 61	28	19
	(11)	(10)		(4.1)	(3.5)
Jul 60	64	43	Jan 62	17	11
	(11)	(8.2)		(2.9)	(2.3)
Aug 60	245	164	Feb 62	25	17
	(45)	(32)		(4.4)	(3.4)
Sep 60	270	180	Mar 62	12	8
	(43)	(41)		(2.1)	(1.5)
Oct 60	372	248	Apr 62	66	44
	(57)	(48)		(10)	(6.5)
Nov 60	273	182	May 62	67	45
	(44)	(32)		(12)	(9.2)
Dec 60	410	270	Jun 62	80	53
	(68)	(50)		(13)	(10)
Jan 61	300	200	Jul 62	51	34
	(50)	(41)		(9.2)	(6.4)
Feb 61	75	50	Aug 62	170	110
	(13)	(11)		28)	(21)
Mar 61	26	17	Sep 62	660	440
	(4.1)	(3.4)		(149)	(106)
Apr 61	25	17	Oct 62	177	120
	(4.1)	(3.0)		(29)	(26)
May 61	36	24	Nov 62	84	56
	(6.0)	(4.3)		(14)	(12)
Jun 61	54	36	Dec 62	153	100
	(8.2)	(6.9)		(31)	(22)

[a] Estimates based on monthly source term data from Voillequé et al. 1991, with uncertainty analysis using CrystalBall™.

[b] Assumed a lognormal distribution of ingestion of river water from 0 to 60 L, with mean of 30 L (8 gal) per month.

[c] Assumed a lognormal distribution of fish ingestion from the river of 0 to 800 g, with a mean of 400 g (0.9 lb), per month. 800 g per month approximates the 99th percentile of adult consumption in the U.S. (Rupp et al. 1980).

Table RS–5. Measured Uranium Concentrations (mg L^{-1}) in Miami River Water in 1960

1960 Collection Date	Venice Bridge (Upriver)	New Baltimore (Downriver)	1960 Collection Date	Venice Bridge (Upriver)	New Baltimore (Downriver)
6-Jan	0.05	0.03	17-Aug	0.04	0.01
13-Jan	0.004	0.006	25-Aug	0.022	0.031
20-Jan	0.038	0.015	30-Aug	0.018	0.03
27-Jan	0.026	0.016	1-Sep	0.015	0.012
1-Feb	0.018	0.028	8-Sep	0.003	0.021
3-Feb	0.016	0.03	15-Sep	0.019	0.028
11-Feb	0.064	0.066	16-Sep	0.006	0.011
18-Feb	0.002	0.004	20-Sep	0.018	0.021
25-Feb	0.002	0.005	21-Sep	0.019	0.022
26-Feb	0.003	0.01	22-Sep	0.007	0.034
29-Feb	0.006	0.003	22-Sep	0.028	0.02
4-Mar	0.01	0.04	23-Sep	0.013	0.08
10-Mar	0.006	0.01	26-Sep	0.014	0.018
17-Mar	0.008	0.006	27-Sep	0.008	0.021
24-Mar	0.014	0.014	28-Sep	0.016	0.026
28-Mar	0.006	0.008	29-Sep	0.026	0.012
31-Mar	0.03	0.02	29-Sep	0.027	0.023
7-Apr	0.01	0.02	6-Oct	0.003	0.002
14-Apr	0.016	0.018	6-Oct	0.005	0.013
21-Apr	0.008	0.021	11-Oct	0.011	0.012
25-Apr	0.01	0.011	13-Oct	0.016	0.024
28-Apr	0.013	0.1	19-Oct	0.017	0.11
6-May	0.029	0.017	20-Oct	0.008	0.016
12-May	0.008	0.008	24-Oct	0.019	0.025
19-May	0.006	0.011	25-Oct		0.07
31-May	0.008	0.008	27-Oct	0.008	0.009
2-Jun	0.008	0.008	31-Oct	0.006	0.047
9-Jun	0.016	0.011	3-Nov	0.014	0.014
16-Jun	0.005	0.011	10-Nov	0.007	0.024
23-Jun	0.009	0.028	17-Nov	0.014	0.025
30-Jun	0.013	0.01	24-Nov	0.21	0.15
27-Jun	0.016	0.015	28-Nov	0.014	0.015
29-Jun	0.009	0.013	8-Dec	0.024	0.022
7-Jul	0.009	0.037	15-Dec	0.09	0.014
14-Jul	0.017	0.019	22-Dec	0.014	0.057
21-Jul	0.017	0.049	27-Dec	0.008	0.024
26-Jul	0.012	0.016	29-Dec	0.008	0.014
28-Jul	0.011	0.02	Avg (mg L^{-1})	0.018	0.024
4-Aug	0.031	0.019	Stdev (mg L^{-1})	0.030	0.024
11-Aug	0.001	0.012	Avg (pCi L^{-1})	12.5	16.7
10 Aug	0.04	0.015	Stdev (pCi L^{-1})	17.8	16.7

Table RS–6. Measured Uranium Concentrations (mg L^{-1}) in Miami River Water in 1961

1961 Collection Date	Venice Bridge (Upriver)	New Baltimore (Downriver)	1961 Collection Date	Venice Bridge (Upriver)	New Baltimore (Downriver)
5-Jan	0.019	0.022	22-Jun	0.015	0.011
12-Jan	0.027	0.013	29-Jun	0.008	0.01
19-Jan	0.09	0.011	6-Jul	0.013	0.027
26-Jan	0.009	0.018	13-Jul	0.005	0.017
31-Jan	0.023	0.027	20-Jul	0.008	0.007
2-Feb	0.013	0.026	25-Jul	0.008	0.006
9-Feb	0.004	0.014	10-Aug	0.01	0.01
16-Feb	0.009	0.013	17-Aug	0.006	0.015
23-Feb	0.017	0.016	24-Aug	0.02	0.03
27-Feb	0.022	0.042	28-Aug	0.012	0.019
2-Mar	0.009	0.017	31-Aug	0.03	0.01
9-Mar	0.013	0.015	7-Sep	0.002	0.01
15-Mar	0.011	0.013	14-Sep	0.008	0.027
23-Mar	0.007	0.012	21-Sep	0.04	0.02
24-Mar	0.012	0.007	28-Sep	0.013	0.008
27-Mar	0.015	0.013	5-Oct	0.007	0.007
30-Mar	0.006	0.012	12-Oct	0.007	0.012
6-Apr	0.042	0.012	19-Oct	0.022	0.024
13-Apr	0.02	0.016	26-Oct	0.01	0.01
20-Apr	0.01	0.013	30-Oct	0.008	0.01
24-Apr	0.017	0.01	2-Nov	0.016	0.01
27-Apr	0.016	0.014	9-Nov	0.014	0.012
18-May	0.014	0.002	16-Nov	0.014	0.035
22-May	0.01	0.02	23-Nov	0.016	0.023
25-May	0.02	0.02	30-Nov	0.02	0.02
1-Jun	0.04	0.04	Avg (mg L^{-1})	0.016	0.016
8-Jun	0.015	0.017	Stdev (mg L^{-1})	0.013	0.008
15-Jun	0.01	0.013	Avg (pCi L^{-1})	10.9	11.0
			Stdev (pCi L^{-1})	9.2	5.6

Table RS–7. Measured Uranium Concentrations (mg L^{-1}) in Miami River Water in 1962

1962 Collection Date	Venice Bridge (Upriver)	New Baltimore (Downriver)	1962 Collection Date	Venice Bridge (Upriver)	New Baltimore (Downriver)
1-Jan	0.008	0.011	26-Jul	0.004	0.005
11-Jan	0.003	0.002	2-Aug	0.007	0.011
18-Jan	0.02	0.01	9-Aug	0.007	0.014
25-Jan	0.02	0.04	16-Aug	0.006	0.008
2-Feb	0.05	0.04	23-Aug	0.004	0.014
8-Feb	0.008	0.006	30-Aug	0.005	0.021
15-Feb	0.01	0.011	6-Sep	0.005	0.012
22-Feb	0.004	0.007	13-Sep	0.027	0.135
1-Mar	0.024	0.006	20-Sep	0.03	0.01
9-Mar	0.005	0.003	27-Sep	0.006	0.021
15-Mar	0.009	0.008	4-Oct	0.003	0.014
22-Mar	0.02	0.03	11-Oct	0.006	0.012
29-Mar	0.01	0.03	18-Oct	0.03	0.034
5-Apr	0.05	0.03	25-Oct	0.02	0.017
12-Apr	0.014	0.008	1-Nov	0.01	0.026
19-Apr	0.06	0.04	8-Nov	0.005	0.011
26-Apr	0.04	0.04	15-Nov	0.028	0.035
4-May	0.005	0.007	22-Nov	0.031	0.045
10-May	0.008	0.025	29-Nov	0.02	0.02
17-May	0.007	0.01	6-Dec	0.01	0.01
24-May	0.008	0.008	13-Dec	0.02	0.02
31-May	0.01	0.01	27-Dec	0.007	0.03
7-Jun	0.02	0.01	Avg (mg L^{-1})	0.02	0.02
14-Jun	0.01	0.03	Stdev (mg L^{-1})	0.01	0.02
21-Jun	0.015	0.017	Avg (pCi L^{-1})	10.3	14.0
19-Jul	0.001	0.022	Stdev (pCi L^{-1})	9.2	13.9

Table RS–8. Measured U Concentrations (mg L^{-1}) in Paddy's Run in 1960

1960 Collection Date	North of Rte 126 (Upstream)	Willey Road	New Haven Road	1960 Collection Date	North of Rte 126 (Upstream)	Willey Road	New Haven Road
2-Jan		0.12		14-Apr	0.02		
5-Jan		0.07		21-Apr	0.01		
6-Jan	0.007	0.011		28-Apr	0.01		
8-Jan		0.117		6-May	0.07		
11-Jan		0.191		12-May	0.014		
13-Jan	0.005	0.31		13-May		4.90	
14-Jan		0.46		19-May		0.04	
17-Jan		0.042		20-May		6.00	
20-Jan		0.007		26-May	0.008		
18-Jan		0.074		27-May		2.70	
21-Jan		0.11		30-May		0.80	
26-Jan		0.14		2-Jun	0.003	2.10	
27-Jan	0.009	0.02		5-Jun		0.23	
29-Jan		0.089		6-Jun	0.007		0.03
1-Feb		0.04		9-Jun	0.02		
3-Feb	0.015	0.019		15-Jun	0.015	1.20	0.15
4-Feb		0.22		16-Jun	0.01		
7-Feb		0.24		18-Jun		0.50	
10-Feb		0.18		23-Jun	0.02		
11-Feb	0.009	0.007		24-Jun		1.30	
13-Feb		0.08		27-Jun		0.70	
18-Feb	0.005	0.007	0.05	29-Jun	0.01		0.40
19-Feb		0.13		30-Jun	0.01	0.27	
22-Feb		0.09		1-Jul	0.02		
25-Feb	0.029	0.02		3-Jul		0.5	
26-Feb		0.08		6-Jul		1	
28-Feb		0.07		7-Jul	0.01		
2-Mar		0.07		9-Jul		0.6	
4-Mar	0.01	0.007		13-Jul		1.1	
10-Mar	0.008	0.007		16-Jul		0.3	
15-Mar		0.2		15-Jul		0.013	0.15
16-Mar		0.08		19-Jul		1.9	
17-Mar	0.006			21-Jul	0.011		
18-Mar		0.07		28-Jul	0.005		
22-Mar		0.04		4-Aug	0.015		
24-Mar	0.01			12-Aug	0.08		
25-Mar		0.04		18-Aug	0.014		
28-Mar		0.04		30-Aug		23.00	
31-Mar	0.03	0.03		1-Sep	0.015		
3-Apr		0.27		15-Sep	0.04		
6-Apr		0.07		15-Sep	0.023		
7-Apr		0.02		21-Sep	0.014	0.019	
9-Apr		0.16		22-Sep	0.07		0.11

Table RS–8. Measured Uranium Concentrations (mg L^{-1}) in Paddy's Run Water in 1960 (continued)

1960 Collection Date	North of Rte 126 (Upstream)	Willey Road	New Haven Road	1960 Collection Date	North of Rte 126 (Upstream)	Willey Road	New Haven Road
25-Sep			0.016	13-Nov			
23-Sep	0.017	0.13		16-Nov			
28-Sep	0.009			17-Nov	0.019		
29-Sep	0.01		0.015	19-Nov			0.036
1-Oct				22-Nov			0.031
4-Oct				24-Nov	0.14		
6-Oct	0.012	3.50	0.012	25-Nov		7.30	0.12
7-Oct				28-Nov		8.5	0.019
10-Oct				1-Dec	0.007		0.029
13-Oct	0.045		0.045	4-Dec			0.042
16-Oct				7-Dec			0.028
19-Oct		6.60		8-Dec	0.058		
20-Oct	0.01		0.01	10-Dec			0.008
20-Oct				14-Dec			0.031
23-Oct				15-Dec	0.034		
26-Oct				17-Dec			0.025
27-Oct	0.007		0.007	20-Dec			0.09
29-Oct				26-Dec		4.20	0.13
1-Nov				28-Dec			1.9
3-Nov	0.017		0.017	Avg (mg L^{-1})	0.02	1.6	0.14
4-Nov				Stdev (mg L^{-1})	0.02	3.3	0.33
7-Nov				Avg (pCi L^{-1})	14	1050	95
10-Nov	0.017	8.00	0.017	Stdev (pCi L^{-1})	14	2200	224

Table RS–9. Measured U Concentrations (mg L^{-1}) in Paddy's Run in 1961

1961 Collection Date	North of Rte 126 (Upstream)	Willey Road	New Haven Road	1960 Collection Date	North of Rte 126 (Upstream)	Willey Road	New Haven Road
1-Jan			0.17	15-Jul			0.23
4-Jan	0.019		0.043	18-Jul		0.33	0.24
7-Jan			0.11	21-Jul	0.014	0.51	0.4
10-Jan			0.04	24-Jul		0.17	0.16
13-Jan	0.018		0.022	27-Jul	0.007		0.11
16-Jan			0.18	30-Jul			0.35
19-Jan	0.037		0.2	1-Aug		0.18	0.5
17-Jan		1.2		2-Aug	0.02	0.7	
20-Jan		0.31		4-Aug		0.14	0.14
22-Jan			0.072	7-Aug		0.3	0.11
25-Jan			0.09	10-Aug	0.02		0.09
28-Jan			0.041	13-Aug			0.12
31-Jan			0.018	16-Aug			0.06
3-Feb			0.08	17-Aug	0.09		
6-Feb			0.017	20-Aug			0.06
9-Feb			0.09	22-Aug			0.08
18-Feb			0.11	24-Aug	0.04		
28-Feb		0.21		28-Aug			0.17
2-Mar	0.005	1.4		1-Sep			0.06
3-Mar			0.11	7-Oct			0.11
5-Mar		0.31	0.19	10-Oct			0.09
8-Mar	0.008	0.046	0.034	12-Oct	0.008		
11-Mar		0.06	0.06	13-Oct			0.11
14-Mar	0.031	0.33	0.08	16-Oct			0.11
18-Mar		1.1	0.13	19-Oct	0.028		0.06
20-Mar		0.19	0.2	22-Oct			0.05
23-Mar	0.005	0.062	0.07	25-Oct	0.009		0.03
26-Mar		0.11	0.11	26-Oct			0.09
29-Mar	0.005	0.23	0.1	31-Oct			0.02
1-Apr		0.23	0.1	3-Nov	0.02		0.021
4-Apr		0.3	0.09	9-Nov	0.012		0.09
7-Apr	0.026		0.08	12-Nov			0.044
10-Apr		0.7	0.11	15-Nov	0.007		1
13-Apr	0.002	0.21	0.25	17-Nov		6.8	2.5
16-Apr		0.34	0.09	21-Nov			0.23
19-Apr	0.023	0.14	0.044	24-Nov	0.018	1.1	0.27
22-Apr		0.11	0.14	27-Nov		0.53	0.27
25-Apr		0.09	0.09	30-Nov	0.03		0.08
30-Jun			0.016	Avg (mg L^{-1})	0.03	0.69	0.20
3-Jul			0.047	Stdev(mg L^{-1})	0.05	1.31	0.45
6-Jul		4	2.9	Avg (pCi L^{-1})	20	470	140
9-Jul	0.25	0.29	0.17	Stdev (pCi L^{-1})	33	890	300

Table RS–10. Measured Uranium Concentrations (mg L^{-1}) in Paddy's Run Water in 1962

1962 Collection Date	North of Rte 126 (Upstream)	Willey Rd.	New Haven	1962 Collection Date	North of Rte 126 (Upstream)	Willey Rd.	New Haven
2-Jan			0.05	5-Apr			
4-Jan	0.008			6-Apr	0.002	0.02	0.03
5-Jan			0.1	9-Apr		0.15	0.09
8-Jan		0.09	0.09	12-Apr		0.032	0.09
11-Jan	0.002	0.11	0.05	15-Apr	0.007	0.06	0.1
14-Jan			0.05	19-Apr		0.09	0.11
17-Jan		0.07	0.05	21-Apr	0.3		0.11
18-Jan	0.02			24-Apr			0.11
20-Jan		0.07	0.11	27-Apr			0.05
23-Jan		0.07	0.06	30-Apr	0.002		0.09
25-Jan	0.02			2-May		0.42	
26-Jan		0.44	0.09	2-May		0.9	
29-Jan		0.07	0.09	3-May	0.01	5	0.27
31-Jan		0.8	0.09	6-May			0.04
2-Feb	0.018			9-May	0.01		0.06
4-Feb		0.11	0.1	12-May			0.09
7-Feb		0.03	0.05	15-May			0.05
8-Feb	0.003			18-May	nd		0.04
10-Feb		0.13	0.12	21-May			0.04
14-Feb		0.04	0.1	24-May	0.005		0.04
15-Feb	0.011			27-May		3.5	1
17-Feb		0.04	0.06	31-May	0.006	0.23	0.18
20-Feb		0.1	0.1	2-Jun			0.1
22-Feb	0.008			5-Jun			0.05
25-Feb		0.035	0.031	7-Jun	0.01		0.09
26-Feb		0.018	0.039	11-Jun			0.03
1-Mar	0.006	0.18	0.037	14-Jun	0.02		0.09
4-Mar		0.05	0.04	17-Jun			0.13
7-Mar		0.02	0.03	20-Jun	0.003		0.034
8-Mar	0.005			23-Jun			0.018
10-Mar		0.04	0.03	26-Jun			0.02
11-Mar		0.023	0.034	28-Jun	0.006		
15-Mar	0.013			29-Jun			0.03
16-Mar	0.013	0.017	0.48	2-Jul			0.03
19-Mar		0.03	0.19	7-Jul			0.27
22-Mar		0.09	0.05	11-Jul			0.12
25-Mar	0.02	0.03	0.03	12-Jul	0.004		
28-Mar		0.03	0.04	13-Jul			
29-Mar				14-Jul			1.3
31-Mar	0.03	0.32	0.7	17-Jul		1.4	0.53
3-Apr		0.11	0.09	19-Jul	0.002		0.06

Table RS–10. Measured Uranium Concentrations (mg L^{-1}) in Paddy's Run Water in 1962 (continued)

1962 Collection Date	North of Rte 126 (Upstream)	Willey Rd.	New Haven	1962 Collection Date	North of Rte 126 (Upstream)	Willey Rd.	New Haven
23-Jul			0.1	15-Oct			0.024
26-Jul	0.003		0.016	18-Oct	0.013		0.014
29-Jul			0.056	21-Oct			0.013
1-Aug			0.006	25-Oct	0.008		0.08
2-Aug	0.002			28-Oct			0.23
4-Aug			0.11	31-Oct	0.018		0.055
7-Aug			0.17	3-Nov			0.051
10-Aug	0.002		0.041	6-Nov			0.017
13-Aug			0.8	9-Nov	0.018		0.012
16-Aug	0.014		0.031	8-Nov			
29-Aug			0.021	12-Nov		0.57	0.41
23-Aug	0.005		0.016	15-Nov	0.001		0.022
25-Aug			0.02	18-Nov			0.019
28-Aug			0.055	21-Nov	0.009	0.38	0.032
30-Aug	0.003			24-Nov			0.16
31-Aug			0.024	27-Nov			0.14
3-Sep		7.1	0.09	30-Nov	0.031		0.02
6-Sep	0.015		0.25	3-Dec			0.03
9-Sep			0.13	6-Dec	0.01		0.06
13-Sep	0.019		0.04	9-Dec			0.1
15-Sep			0.02	12-Dec	0.01	0.03	
18-Sep			0.027	15-Dec			0.15
21-Sep	0.001		0.018	18-Dec			0.11
24-Sep			0.08	21-Dec	0.01		0.02
27-Sep	0.008		0.036	24-Dec			0.04
30-Sep			0.02	27-Dec			0.04
4-Oct	0.018		0.019	30-Dec			0.11
6-Oct			0.042	Avg (mg L^{-1})	0.02	0.54	0.11
9-Oct			0.19	Stdev (mg L^{-1})	0.04	1.38	0.18
11-Oct	0.009		0.031	Avg (ugL^{-1})	10.8	364.4	74.8
				Avg (pCi L^{-1})	28.6	937.9	122.4

APPENDIX S

GROUNDWATER TRANSPORT

INTRODUCTION

In our previous source term report (Voillequé et al. 1991), we concluded that uranium contamination in the groundwater had not migrated outside the FMPC boundary by 1962. Byrne et al. (1991) provides a brief history of the measurement of offsite U contamination of groundwater. Significant U contamination in groundwater south of the site, due to releases from the FMPC, was discovered in late 1981, and concentrations in these locations remain elevated. Thus, for an undetermined length of time, which could be as long as about three decades, U from the FMPC in groundwater south of the site was a source of potential radiation exposures to nearby residents. The contaminated groundwater of this South Plume remains an important issue to local residents.

In this Appendix, we discuss the reasons for applying simple methods to estimate concentrations of U in groundwater wells for times when no measurements are available. We then describe the exposure pathways considered, and describe the dosimetry methods. Because we will not apply detailed transport models to estimate concentrations of U in the groundwater, we consider the source term to include the calculation of U concentrations in groundwater at receptor wells. Those calculations and estimated concentrations will be described in the report of Tasks 2 and 3 of this Project.

JUSTIFICATION FOR SIMPLE APPROACH TO U CONCENTRATIONS

Since the discovery of the U contamination of the South Plume, groundwater samples have been taken from existing, private wells and specifically-installed monitoring wells. Sampling of private wells has been performed by the FMPC, the Ohio Department of Health (ODH), and the U.S. Geological Survey (USGS).

The FMPC site has maintained a program of monitoring U concentrations in water from private wells around the site, particularly south of the site, since early 1982, after the U contamination in groundwater was discovered (Byrne et al. 1991). In addition, many monitoring wells were installed around the site to assist in characterizing the South Plume. Figure S–1 shows the locations of these monitored private wells (from Schwarzman 1992a), along with the approximate boundary of the South Plume U contamination at the end of 1991 (Schwarzman 1992b). The area of the South Plume U contamination has been estimated by the FMPC based on monitoring of the private wells and the recently-installed monitoring wells, which are not shown in Figure S–1. There are additional known areas of groundwater contamination on the FMPC site, but only the South Plume area extends outside the site boundary at this time (Byrne et al. 1991). Since this Project is concerned only with past doses to people around the site, the groundwater contamination to be considered in the Project is limited to the South Plume.

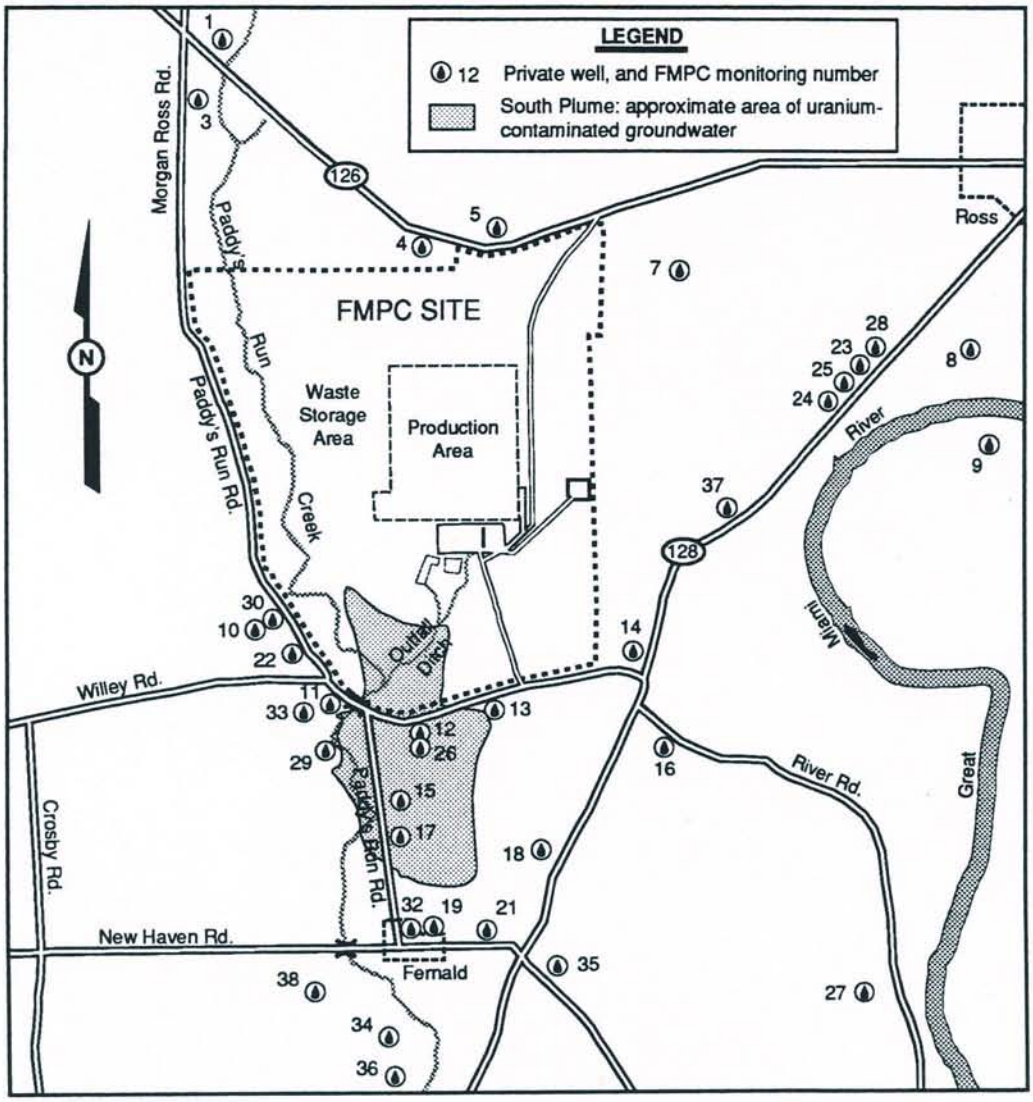

Figure S–1. Locations of the private wells around the FMPC that are monitored by the FMPC, and the approximate area of U contamination in the South Plume. Although well 26 is within the area of groundwater contamination, the U concentrations from this well are at background levels (Byrne et al. 1991).

Of the private wells that have been monitored by the FMPC through 1990, only three, numbers 12, 15, and 17, have shown U concentrations above the range of background (Fleming and Ross 1984, Facemire et al. 1985, Aas et al. 1986, WMCO 1987, WMCO 1988, WMCO 1989, Dugan et al. 1990, and Byrne et al. 1991). These wells are within the South Plume, as shown in Figure S–1. Note that well 26, which is also within the areal extent of the South Plume, has had U concentrations at background levels (Aas et al. 1986, WMCO 1987, WMCO 1988, WMCO 1989, Dugan et al. 1990, and Byrne et al. 1991). This well was installed in 1985 much deeper in the aquifer than the nearby well 12 (Dames and Moore 1985).

The ODH and USGS studies (Steva 1988 and Sedam 1984) included water sampling from many of the same wells as those monitored by the FMPC, as well as additional wells. The results of analyses from these two studies showed U contamination in the same three wells as indicated by the FMPC sampling.

Because only three wells have been impacted by elevated U concentrations of the South Plume, the number of people potentially receiving radiation doses from contaminated groundwater is extremely limited. Thus, these doses would have negligible importance toward the main objective of this Project, the determination of the feasibility of an epidemiological study. For this reason, we believe that a detailed assessment of the transport of radionuclides in the groundwater and detailed assessments of doses to potentially exposed individuals, through groundwater pathways, are not warranted. Instead, simple methods will be used to estimate the likely concentrations of U in wells within the South Plume at different times between 1962 and 1988. The analyses of exposure pathways and potential doses will also be relatively simple.

URANIUM CONCENTRATIONS IN GROUNDWATER AT RECEPTOR WELLS

The source term work of Tasks 2 and 3 of this Project (in progress) will develop estimates of the U concentrations in wells in the South Plume, as a function of time. That work will use two major types of information, measured U concentrations in the plume, and information about the source of the contamination. For perspective, Table S–1 shows annual average concentrations of U in the three contaminated private wells, as measured by the FMPC (Fleming and Ross 1984, Facemire et al. 1985, Aas et al. 1986, WMCO 1987, WMCO 1988, WMCO 1989, Dugan et al. 1990, and Byrne et al. 1991). Those concentrations can be compared to the background U concentration in groundwater, which has been estimated by the FMPC to be between 0.068 and 2.2 pCi L^{-1} (Byrne et al. 1991). More detailed sampling results (individual samples, rather than just average values) are available from the FMPC. As mentioned earlier, some additional data are available from the ODH and USGS studies. The Tasks 2 and 3 work will use the available measured concentrations, including the details of the individual measurements, to determine whether any significant trends exist in the data that might be helpful in estimating concentrations for earlier time periods. If a reasonable trend cannot be identified, a maximum annual average U concentration may be used for the dose assessment, with large uncertainty bounds applied.

Recent studies of the groundwater around the FMPC site (Dames and Moore 1985, and DOE 1990) have concluded that the primary source of the U contamination in the groundwater is U in waters released to the storm sewer outfall ditch and to Paddy's Run Creek (see Figure S–1). The soils in parts of the outfall ditch and Paddy's Run Creek are very permeable, and apparently allow contaminated water to move directly downward into the aquifer. The Tasks 2 and 3 work will also develop estimates of the concentrations of U in water released to the storm sewer outfall ditch and to Paddy's Run Creek. Trends in the estimated discharges will be examined. This information will be combined with the U concentrations measured in the plume to help determine estimated concentrations in the plume for other time periods.

Table S–1. Concentrations of Uranium Measured in the Wells within the Contaminated Area of the South Plume[a]

	Average U concentration (pCi L^{-1})		
Year	Well 12	Well 15	Well 17
1983	141	293	39
1984	165	219	36
1985	140	204	31
1986	147	193	31
1987	201	201	40
1988	170	190	38
1989	170	190	27
1990	130	190	30

[a] Ref: Fleming and Ross 1984, Facemire et al. 1985, Aas et al. 1986, WMCO 1987, WMCO 1988, WMCO 1989, Dugan et al. 1990, and Byrne et al. 1991

EXPOSURE PATHWAYS AND DOSIMETRY

Our assessment of potential exposure pathways and doses to people around the FMPC begins with concentrations of U in the groundwater (which will be provided in the Tasks 2 and 3 report). For this reason, the considerations of exposure pathways and dosimetry are similar to those of the surface water releases, discussed in Appendix R, and so we use, in general, the same methods used for surface water releases. We next briefly summarize the methods utilized for surface water releases, and describe differences required for the releases to groundwater.

In Appendix R we discussed the potential exposure pathways relevant to doses originating from radioactivity in surface water. These pathways included ingestion of contaminated drinking water, ingestion of fish from the contaminated water source, ingestion of vegetables and animal products grown using contaminated irrigation water, inadvertent ingestion of contaminated soil or water, and external exposures from recreational swimming and boating in or on the contaminated water or from radioactivity deposited on soils. Because the use of groundwater does not involve a large, accessible source of the contaminated water, some of these pathways are not reasonable for a groundwater source. These pathways, ingestion of fish and external exposures from boating activities, are eliminated from consideration as potential exposure pathways for the groundwater sources. The remaining pathways are plausible, based on conceivable uses of groundwater.

The analyses in Appendix R, using the NCRP screening model approach and using the GENII model, resulted in the conclusion that the important exposure pathways for surface water discharges were ingestion of contaminated drinking water, ingestion of fish from the contaminated water source, and ingestion of produce from gardens irrigated with the contaminated water. With elimination of the fish ingestion pathway, these analyses apply

equally well to the assessment of important exposure pathways for radioactivity in groundwater. The ingestion of produce from gardens irrigated with contaminated water was later eliminated as a plausible pathway for exposure to surface water releases, based on very limited use of surface water for irrigation in the two counties around the FMPC (see Appendix R). For the small number of groundwater users within the South Plume area, however, irrigation of gardens with well water is plausible, so this exposure pathway is retained. We thus conclude that the important exposure pathways for releases of radioactivity to the groundwater from the FMPC are ingestion of drinking water and ingestion of produce from irrigated gardens.

The dosimetry for these two exposure pathways will be performed using the same methods used for surface water releases, although the calculations will start with the concentrations of radionuclides in the groundwater. The transfer factors and usage factors used for assessments of doses to generic individuals will be the same as for surface water releases. However, for calculation of dose to a specific individual using contaminated groundwater, usage factors, such as the quantities of well water used for drinking and irrigation, can be based on the individual's habits and lifestyle. Doses, for generic or specific individuals, will only be calculated for people who used contaminated groundwater.

REFERENCES

Aas C.A., D.L. Jones, and R.W. Keys. 1986. *Feed Materials Production Center Environmental Monitoring Annual Report for 1985*. Rep. FMPC-2047, Special, UC-41, Westinghouse Materials Company of Ohio, Cincinnati, Ohio.

Byrne J.M., T.A. Dugan, and J.S. Oberjohn. 1991. *Feed Materials Production Center Annual Environmental Report for Calendar Year 1990*. Rep. FMPC-2245, Special, UC-707, Westinghouse Materials Company of Ohio, Cincinnati, Ohio.

Dames and Moore. 1985. *Department of Energy, Feed Materials Production Center, Groundwater Study, Task C Report*. Dames and Moore, White Plains, New York.

DOE (U.S. Department of Energy). 1990. *Engineering Evaluation/Cost Analysis, South Plume, Feed Materials Production Center, Fernald, Ohio*. Rep. FMPC-0003-6, Oak Ridge Operations Office, DOE.

Dugan T.A., G.L. Gels, J.S. Oberjohn, and L.K. Rogers. 1990. *Feed Materials Production Center Annual Environmental Report for Calendar Year 1989*. Rep. FMPC-2200, Special, UC-707, Westinghouse Materials Company of Ohio, Cincinnati, Ohio.

Facemire C.F., D.L. Jones, and R.W. Keys. 1985. *Feed Materials Production Center Environmental Monitoring Annual Report for 1984*. Rep. NLCO-2028, Special, UC-41, NLO, Inc., Cincinnati, Ohio.

Fleming D.A. and K.N. Ross. 1984. *Feed Materials Production Center Environmental Monitoring Annual Report for 1983*. Rep. NLCO-2018, Special, UC-41, NLO, Inc., Cincinnati, Ohio.

Schwarzman G.E. 1992a. *Quarterly Groundwater Sampling Locations and Private Wells*. FMPC drawing index code 00X-5500-G-02006, Westinghouse Environmental Management Company of Ohio, Cincinnati, Ohio.

Schwarzman G. 1992b. *Contour Area ≥ 20 ppb Total Uranium, 4th Quarter 1991.* Drawing, preliminary. Westinghouse Environmental Management Company of Ohio, Cincinnati, Ohio.

Sedam A.C. 1984. *Occurrence of Uranium in Ground Water in the Vicinity of the U.S. Department of Energy Feed Materials Production Center, Fernald, Ohio.* Open-File Report 85-099, U.S. Geological Survey, Columbus, Ohio.

Steva D.P. 1988. *Ohio Department of Health Study of Radioactivity in Drinking Water and Other Environmental Media in the Vicinity of the U.S. Department of Energy's Feed Materials Production Center and Portsmouth Gaseous Diffusion Plant.* Ohio Department of Health, Columbus, Ohio.

WMCO (Westinghouse Materials Company of Ohio). 1987. *Feed Materials Production Center Environmental Monitoring Annual Report for 1986.* Rep. FMPC-2076, Special, UC-41, WMCO, Cincinnati, Ohio.

WMCO (Westinghouse Materials Company of Ohio). 1988. *Feed Materials Production Center Environmental Monitoring Annual Report for 1987.* Rep. FMPC-2135, Special, UC-41, WMCO, Cincinnati, Ohio.

WMCO (Westinghouse Materials Company of Ohio). 1989. *Feed Materials Production Center Environmental Monitoring Annual Report for 1988.* Rep. FMPC-2173, Special, UC-707, WMCO, Cincinnati, Ohio.

APPENDIX T

DOSE CONVERSION FACTORS

INTRODUCTION

This appendix is a reference for the dosimetric factors and related information that will be used to convert predicted exposure of individuals to radionuclides into dose. Such quantities are often generically called DOSE CONVERSION FACTORS, and it is this usage that we have adopted for this report (an alternative usage is DOSE COEFFICIENT). Typical units are mrem pCi^{-1} or Sv Bq^{-1} (internal dose per unit activity inhaled or ingested; factors of this form are frequently called DOSE RATE CONVERSION FACTORS) and mrem s^{-1} $(pCi\ m^{-3})^{-1}$ or Sv s^{-1} $(Bq\ m^{-3})^{-1}$ (external dose rate per unit concentration in air or water). We have chosen not to convert all units to a single system, but rather to present reference tabulations in their original form; accordingly, we include a conversion table (Table T–1) to assist the reader.

Dose conversion factors are specific to numerous dependencies, which include the radionuclide and its physical and chemical form, exposure mode, target organ or tissue, and the age (and possibly sex) of the exposed individual. Exposure modes vary according to whether the source of the radiation is internal or external to the body. Examples of exposure modes for internal dose are ingestion of contaminated food or water and inhalation of contaminated air. For external dose resulting from proximity to sources of penetrating radiations, we consider immersion in contaminated air and water and direct exposure to radionuclides in the soil. In the case of internal exposure by inhalation of particulate matter, the dose conversion factor also depends on the distribution of particle diameters.

Historically, the dosimetry of ^{222}Rn (usually called radon in this appendix) and its decay progeny (daughters) has been separated from the treatment of other internal emitters. We maintain that separation in this discussion, although final reported doses (Task 6) may or not maintain it.

Dose conversion factors summarize extensive dynamic calculations with complex physicochemical, anatomical, and metabolic models. This appendix cannot be a textbook of the models and methodology. We refer readers to our specific citations to reports of the International Commission on Radiological Protection (ICRP) and the National Council on Radiation Protection and Measurements (NCRP), and to Killough and Eckerman (1983) and Kocher (1983) for general background.

DECAY CHAINS

Computation of dose requires that the dynamics of decay and formation of radioactive progeny (or "daughters") of radionuclides be considered. In the case of internal dose, the dose conversion factor accounts for the formation and decay of radioactive daughters after the radionuclide has entered the body. Daughters formed during transport must be accounted for by the transport model, and those formed while the radioactive progenitors are resident in the production facility must be included in the source term.

Table T–1. Useful Multipliers for Converting Dose and Activity Units

From	To									
	Sv	mSv	rem	mrem	Ci	μCi	pCi	Bq	Sv Bq^{-1}	mrem pCi^{-1}
Sv	1	10^{3}	10^{2}	10^{5}						
mSv	10^{-3}	1	10^{-1}	10^{2}						
rem	10^{-2}	10	1	10^{3}						
mrem	10^{-5}	10^{-2}	10^{-3}	1						
Ci					1	10^{6}	10^{12}	3.7×10^{10}		
μCi					10^{-6}	1	10^{6}	3.7×10^{4}		
pCi					10^{-12}	10^{-6}	1	3.7×10^{-2}		
Bq					2.7×10^{-11}	2.7×10^{-5}	27	1		
Sv Bq^{-1}									1	3.7×10^{3}
mrem pCi^{-1}									2.7×10^{-4}	1

For purposes of reference, we show all decay chains that include radionuclides shown by the analysis of Appendix C to be relevant to estimation of dose from FMPC releases. These chains are presented as Figures T–1, T–2, and T–3. In general, the subchains actually used in the calculations are the result of truncation of the chain at a point beyond which the inclusion of further daughter species would not affect the dose estimate.

INTERPRETATION OF DOSE CONVERSION FACTORS

It is anticipated that most risk resulting from radionuclides released from the FMPC will be associated with internal dose. Accordingly, internal dose conversion factors are developed in somewhat more detail than those for external dose.

Internal Dose

The internal dosimetry chosen for this project is based principally on the methodology of the International Commission on Radiological Protection (ICRP) as described in ICRP Publication 30 (ICRP 1979), with some anatomical and physiological data based on data from ICRP Publication 23 (the "Reference Man" document, ICRP 1975). This methodology specifies models for estimating 50-year COMMITTED DOSE EQUIVALENT (CDE) to each of a list of organs and tissues of the body and refers to ICRP Publication 26 (ICRP 1977) for the definition of a risk-weighted average of these organ CDEs, called the EFFECTIVE DOSE EQUIVALENT (EDE). This concept has been superseded by a different set of organs and risk-proportional weights specified in ICRP Publication 60 (ICRP 1991), and the new risk-weighted dose is called simply EFFECTIVE DOSE (ED). Table T–2 shows the organs and weighting factors for the effective dose, which is defined by the equation

$$\mathrm{ED} = \sum_{\mathrm{T}} w_{\mathrm{T}} H_{\mathrm{T}} \quad \mathrm{Sv\ Bq^{-1}} \qquad \text{(T–1)}$$

where T denotes each irradiated organ or tissue and H_{T} is the dose equivalent to the organ or tissue (truncated after 50 years for the dose conversion factors in this appendix).

The units of dose equivalent to specific organs and tissues and of the ED are Sv Bq^{-1} or the equivalent in conventional units. The interpretation is the dose equivalent to the

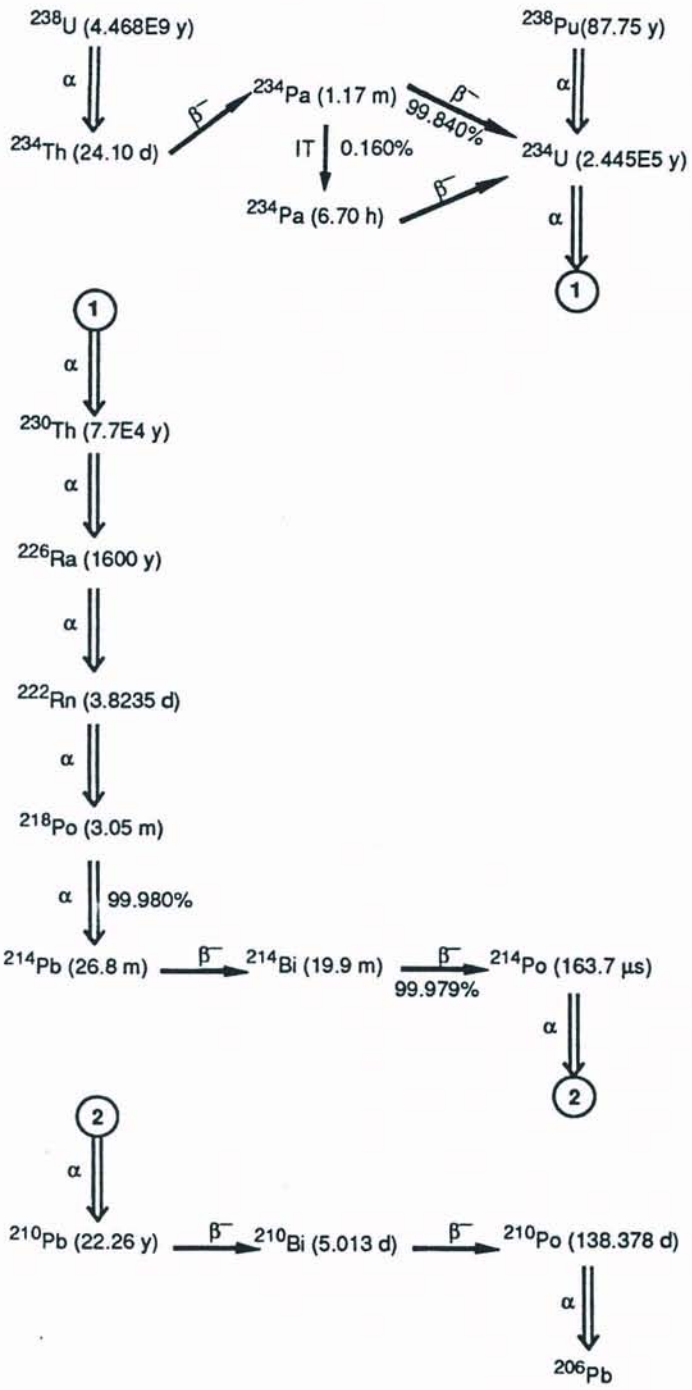

Figure T–1. Radioactive decay chains including ^{234}U, ^{238}U, ^{230}Th, and ^{234}Th. (Source: Kocher 1981).

irradiated tissue per unit intake of radioactivity into the body. The dose equivalent is generally averaged over the target tissue (i.e., is proportional to the emitted energy absorbed by the

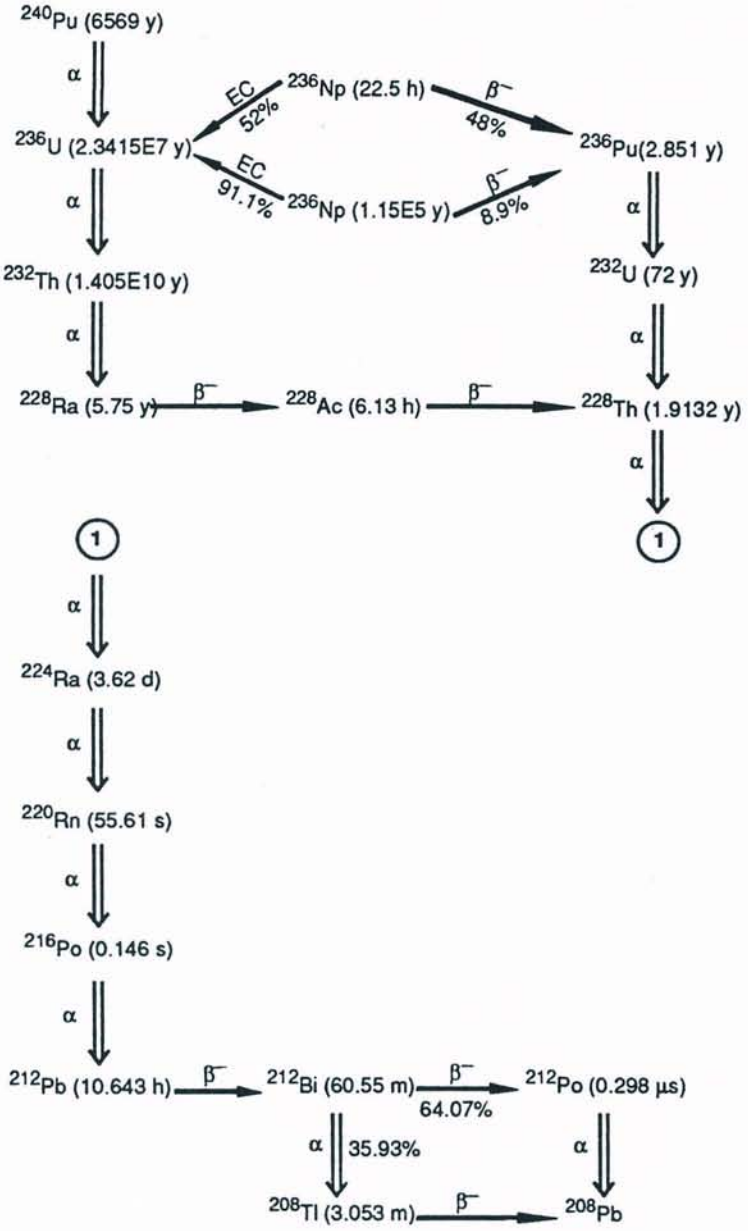

Figure T–2. Radioactive decay chains including ^{228}Th and ^{232}Th. (Source: Kocher 1981).

tissue and divided by the tissue mass). The factors are calculated on the basis of a model for an individual who is a young adult at the time of an acute or instantaneous intake, and the dose is accumulated for a period of 50 years after the intake.

The fundamental dose conversion factors for adults that we have selected for this study are listed in Tables T–1S through T–12S at the end of this appendix. Based on the methodology of ICRP Publication 30, with some corrections and enhancements, these tables were prepared

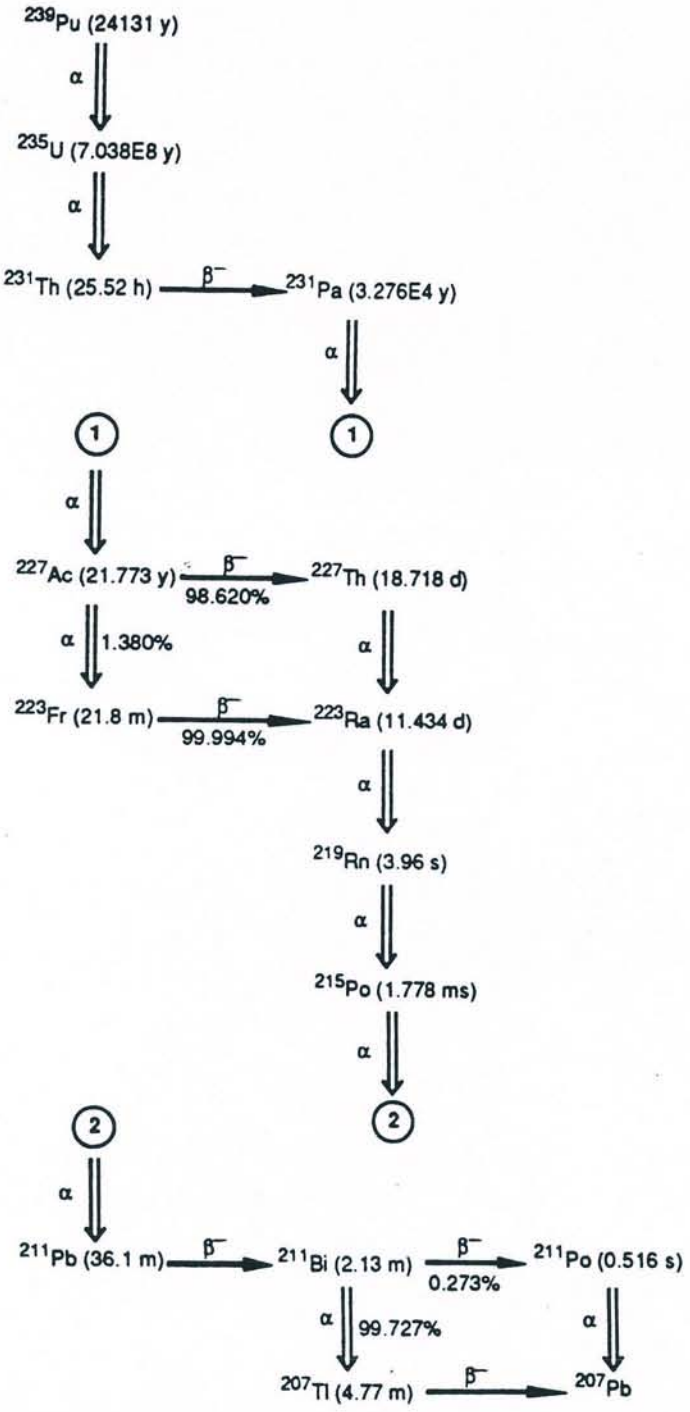

Figure T–3. Radioactive decay chains including ^{235}U and ^{239}Pu. (Source: Kocher 1981).

from the same data base that supplied the corresponding factors given by Eckerman et al.

Table T–2. ICRP Tissue Weighting Factors[a]

Tissue or Organ	Weighting factor ω_T
Gonads	0.20
Bone marrow (red)	0.12
Colon	0.12
Lung	0.12
Stomach	0.12
Bladder	0.05
Breast	0.05
Liver	0.05
Esophagus	0.05
Thyroid	0.05
Skin	0.01
Bone surface	0.01
Remainder	0.05

a From ICRP Publication 60 (ICRP 1991). These weighting factors apply to "a reference population of equal numbers of both sexes and a wide range of ages. In the definition of effective dose, they apply to workers, to the whole population, and to either sex."

(1988). The factors require modification for application to younger age groups., as we discuss next.

Age and sex dependence. The dosimetric methodology of ICRP Publication 30 (ICRP 1979) is based on models for a hypothetical young male, although gonadal dose to males and females is separated according to dose to testes and ovaries. Breast and uterus are also included as target tissues. With ICRP Publication 56 Part 1 (ICRP 1990) the Commission has begun the publication of dose conversion factors with dependence on age at the time of intake, broken down into six groups represented by the ages 3 months, 1, 5, 10, and 15 years, and adult. The newer factors do not further distinguish sexes, except as mentioned previously.

For this study, a complication that arises in connection with age dependence is the limited set of radionuclides treated by Part 1 of ICRP Publication 56 (ICRP 1990). These radionuclides do not include uranium or thorium isotopes, although the necessary isotopes of plutonium, neptunium, and americium are included. For the uranium and thorium isotopes pertinent to our study, it is necessary to resort to other sources of information if age dependence is to be considered. It is fortunate that some tabulations of age-dependent factors were prepared at the Oak Ridge National Laboratory for the U.S. Nuclear Regulatory Commission (Cristy et al. 1986). These tabulations include age-specific factors for the uranium isotopes ^{234}U, ^{235}U, ^{238}U, ^{228}Th, ^{230}Th, and ^{232}Th, but not ^{234}Th. The factors are presented as ratios for conversion of the adult dose to that of the desired juvenile group. In the case of the effective dose, however, the earlier definition was used, and we accept this limitation, which we do not consider serious in the ratios. The relevant age-specific factors are shown in Tables T–13S through T–20S.

Inhalation. It is anticipated that the respiratory model of ICRP Publication 30 (ICRP 1979) will be replaced by a more elaborate age-specific version that is currently under devel-

Region	Compartment	Clearance Class D T (day)	D F	W T (day)	W F	Y T (day)	Y F
N-P	a	0.01	0.5	0.01	0.1	0.01	0.01
(D_{N-P} = 0.30)	b	0.01	0.5	0.40	0.9	0.40	0.99
T-B	c	0.01	0.95	0.01	0.5	0.01	0.01
(D_{T-B} = 0.08)	d	0.2	0.05	0.2	0.5	0.2	0.99
	e	0.5	0.8	50	0.15	500	0.05
P	f	n.a.	n.a.	1.0	0.4	1.0	0.4
(D_P = 0.25)	g	n.a.	n.a.	50	0.4	500	0.4
	h	0.5	0.2	50	0.05	500	0.15
L	i	0.5	1.0	50	1.0	1000	0.9
	j	n.a.	n.a	n.a.	n.a.	infinite	0.1

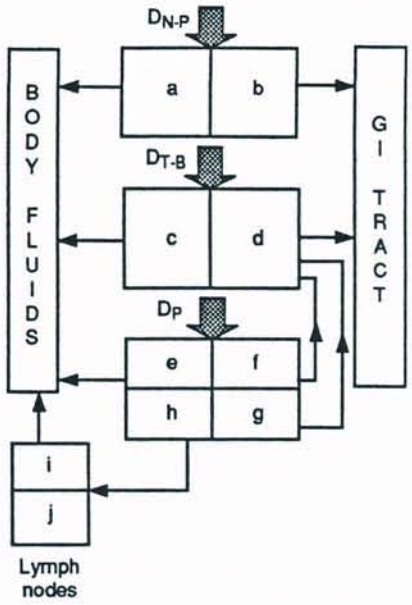

Figure T–4. The lung model of ICRP Publication 30. The columns D, W, and Y correspond, respectively, to rapid (days), intermediate (weeks), and slow (months) clearance of inspired material. The symbols T and F denote the biological half-time (days) and the fractional coefficient, respectively, corresponding to the compartment indicated by the subscript. The regional deposition fractions D_{N-P}, D_{T-B}, and D_P correspond to the nasal pharynx, tracheobronchial tree, and pulmonary regions, respectively, of the respiratory tract, and the values shown in the table are for particulate activity median aerodynamic diameter (AMAD) of 1 μm. Corresponding fractions for other values of the AMAD may be read from the graphs in Fig. T–5. The notation "n.a." means "not applicable."

opment (Bair 1991). The dose conversion factors of ICRP Publication 56 Part 1, however, are based on the current lung model, which is not age-specific, and all dose conversion factors for inhalation that are listed in this appendix (except, to some degree, those for radon) suffer the same limitation. It is not possible, within the schedule of the current project, to incorporate the newer lung model.

The ICRP lung model of ICRP Publication 30 (ICRP 1979) is defined schematically by the table and diagram in Fig. T–4. The model separates the respiratory tract into four major regions: the nasal pharynx (N-P), the tracheobronchial tree (T-B), the pulmonary region (P), and the respiratory lymph nodes (L). Each of the major regions is subdivided into two or more dynamic compartments, labelled by the letters a through j. Deposition is allocated first to the three major regions exposed to the airways by the three fractions D_{N-P}, D_{T-B}, and D_P. Within each region, allocation to the compartments is specified by the tabular fractions F indicated in the table in Fig. T–4. For example, fractional deposition in compartments a and b would be given by $D_{N-P}F_a$ and $D_{N-P}F_b$, respectively. Removal from these two compartments over time (without radioactive decay) is represented by the exponential functions $\exp(-(\ln 2/T_a)t)$ and $\exp(-(\ln 2/T_b)t)$. The values shown in the table for the major deposition fractions correspond to particulate distributions with activity median aerodynamic diameter (AMAD) 1 μm. Sets

of regional deposition fractions corresponding to other values of the AMAD may be read from the curves shown in Fig. T–5, and some sets of deposition fractions are given in Table T–3.

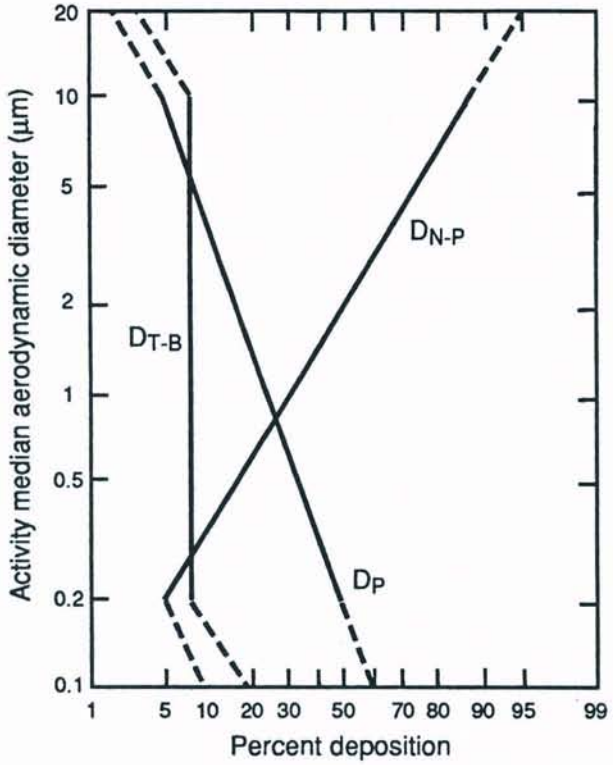

Figure T–5. Particulate deposition in the respiratory tract for the lung model of ICRP Publication 30 (ICRP 1979). The three curves are labelled to correspond to the three regional deposition fractions, for nasal pharynx (N-P), tracheobronchial tree (T-B), and pulmonary region (P). The model is defined for activity median aerodynamic diameters (AMAD) in the range from 0.2 to 10 μm, but the dashed segments of the curves indicate "provisional" extensions. The model is not recommended for use for distributions with AMAD less than 0.1 μm. The model assumes that each distribution is lognormal with geometric standard deviation less than 4.5.

Just as regional deposition within the respiratory tract is a function of median aerodynamic particle diameter, the dose conversion factors for inhalation also depend on this parameter. To avoid the necessity of huge tabulations, dose conversion factors have been computed for AMAD = 1 μm, together with fractions F_{N-P}, F_{T-B}, and F_P that correspond to the respiratory regions indicated by the subscripts. Using the regional deposition fractions D_{N-P}, D_{T-B}, and D_P for the desired AMAD, the correction factor

$$CF = \frac{D_{N-P}}{0.30} F_{N-P} + \frac{D_{T-B}}{0.08} F_{T-B} + \frac{D_P}{0.25} F_P , \qquad \text{(T–2)}$$

which adjusts the tabulated dose conversion factor to its counterpart for the desired AMAD. For example, in Table T-1S, the entries for bone surface under Class Y are 1.01×10^{-6} (7,

2, 91). (The parenthesized fractions are expressed as percentages.) If we wish to estimate the dose equivalent to bone following the intake by inhalation of 1 Bq of Class-Y ^{238}U as an aerosol with AMAD = 5 μm, we may consult Table T–3 and find $D_{N-P} = 0.74$, $D_{T-B} = 0.08$, and $D_P = 0.088$. Substitution in Eq. T–2 gives

$$CF = \frac{0.74}{0.30} \times 0.07 + \frac{0.08}{0.08} \times 0.02 + \frac{0.088}{0.25} \times 0.91 = 0.513$$

so that the adjusted dose conversion factor for bone surface is

$$0.513 \times 1.01 \times 10^{-6} = 5.18 \times 10^{-7}.$$

The deposition model that is part of the ICRP lung model applies to an aerosol with particle equivalent aerodynamic diameters assumed to be lognormally distributed with geometric standard deviation less than 4.5. "Equivalent aerodynamic diameter" refers to the diameter of a sphere of unit density (1 g cm^{-3}) with the same gravitational settling velocity as the particle of interest. The term "equivalent" refers to the spherical reference geometry and is frequently omitted. Distributions of aerodynamic particle diameters can be tabulated with respect to particle count, mass, radioactivity, or other properties. The ICRP respiratory deposition model is based on distribution of aerodynamic diameters with respect to radioactivity, and the median or geometric mean of such a distribution is the activity median aerodynamic diameter (AMAD).

Table T–3. Regional Deposition Fractions vs. Aerosol AMAD

	Deposition fractions[a]	
AMAD (μm)	N-P	P
0.2	0.050	0.50
0.3	0.088	0.43
0.4	0.13	0.39
0.5	0.16	0.35
0.6	0.19	0.32
0.7	0.23	0.30
0.9	0.26	0.28
1.0	0.30	0.25
2.0	0.50	0.17
3.0	0.61	0.13
4.0	0.69	0.10
5.0	0.74	0.088
6.0	0.78	0.076
7.0	0.81	0.067
8.0	0.84	0.060
9.0	0.86	0.055
10.0	0.87	0.050

[a] The deposition fraction $D_{T-B} = 0.08$ for all AMAD.

Measurements of particle diameter distributions at inlet and outlet ducts of selected dust collectors by Northern Kentucky Environmental Services (NKES) in 1985 revealed some distributions that did not appear to be lognormal (Appendix D). We have chosen to generalize

our methodology for inhalation dosimetry in order to admit distributions that are not restricted to lognormality.

Our approach is to partition the given distribution into a number N of subpopulations, based on the aerodynamic diameter intervals $0 < d \leq d_1, d_1 \leq d \leq d_2, \ldots, d_{N-1} \leq d$. In each interval, we use the median aerodynamic diameter (i.e., the number d_i' in the interval $d_{i-1} < d \leq d_i$ that divides the mass or activity for that interval in half) to represent the interval and assume that all particles of this ith subpopulation have the aerodynamic diameter d_i'. This assumption can be interpreted as a degenerate lognormal distribution with geometric mean d_i' and geometric standard deviation 1. Let p_i denote the fraction of activity (or mass) in the ith interval ($\sum_{i=1}^{N} p_i = 1$), and let $(\mathrm{DCF})_i$ denote the inhalation dose conversion factor for the desired organ corresponding to median aerodynamic diameter d_i'. Then the composite factor representing the given distribution of aerodynamic particle diameters is

$$\mathrm{DCF} = p_1(\mathrm{DCF})_1 + p_2(\mathrm{DCF})_2 + \ldots + p_N(\mathrm{DCF})_N . \qquad \text{(T–3)}$$

The values of the $(\mathrm{DCF})_i$ are computed from the application of Eq. T–2 to the 1-μm factors given in Tables T–1S through T–12S. Generally, we have chosen the interval boundaries d_i to partition the distribution into equal mass fractions ($p_1 = \ldots = p_N = 1/n$). Note that DCF, as given by Eq. T–3, has units like Sv Bq^{-1}, so that it still must be multiplied by the quantity of activity that was inhaled to give the estimate of dose to the organ.

The numbers labelled as f1 in Tables T–1S through T–12S are fractional uptakes from the gastrointestinal (GI) tract (the mathematical notation f_1 has been used in ICRP publications for many years to denote this fraction). They apply both to material that is ingested directly and to material that is brought up from the pulmonary airways by ciliary action (from compartments f and g in the diagram in Fig. T–1) and swallowed.

It is unlikely that a meaningful discrimination among transuranic radionuclides in the source term can be accomplished (Appendix C). Accordingly, for purposes of transport and dosimetry, we are treating the transuranic group generically. For internal dose, it is reasonable to choose the dose conversion factors for ^{239}Pu as representative of the group because of the similarity of these factors among the transuranic radionuclides that are indicated in the source term (compare Tables T–8S through T–12S).

Dose to the lungs from the radon decay chain is handled in a manner different from that just described for inhaled particulates. Radon dosimetry has been worked out for the radon daughters ^{218}Po (radium A), ^{214}Pb (radium B), and ^{214}Bi (radium C) for tissue at a depth of 22 μm below the surface of the bronchial epithelium, which is believed to be the shallowest locus of bronchial cell nuclei associated with bronchiogenic cancer (NCRP 1984). The NCRP dose conversion factors are given for the adult male and female and the ten-year-old child. Other ages are not given explicit treatment, but a calculation is reported that supports using the dose for the adult female as a surrogate for that of the one-year-old infant (NCRP 1984). The factors are expressed as follows:

Male Adult:

Light activity: $\mathrm{DRF} = 0.98\mathrm{RaA}^* + 0.029\mathrm{RaA} + 0.16\mathrm{RaB} + 0.14\mathrm{RaC}$ (T–4)

Resting: $\mathrm{DRF} = 0.32\mathrm{RaA}^* + 0.022\mathrm{RaA} + 0.12\mathrm{RaB} + 0.10\mathrm{RaC}$ (T–5)

Female Adult:

Light activity: $DRF = 0.82RaA^* + 0.029RaA + 0.16RaB + 0.14RaC$ (T–6)

Resting: $DRF = 0.29RaA^* + 0.019RaA + 0.10RaB + 0.09RaC$ (T–7)

Child (ten-year-old):

Light activity: $DRF = 2.36RaA^* + 0.06RaA + 0.26RaB + 0.28RaC$ (T–8)

Resting: $DRF = 0.54RaA^* + 0.04RaA + 0.17RaB + 0.18RaC$ (T–9)

In Eqs. T–4 through T–9, the dose-rate factors (DRF) are in mrad y^{-1}, and RaB, and RaC denote concentrations of radium A, radium B, and radium C, respectively, in pCi m^{-3}. The notations RaA and RaA* denote the fractional concentrations of radium A that are unattached and attached, respectively, to airborne particles; the units are pCi m^{-3}. To convert these doses to mrem (dose equivalent), it is necessary to multiply by the quality factor 20 that is associated with alpha decay (ICRP 1991).

As the coefficients of RaA and RaA* in Eqs. T–4 through T–9 indicate, a given activity concentration of unattached radium A can be considerably more effective in depositing energy in the tracheobronchial epithelium than the same concentration of its attached counterpart. Estimation of the concentration of unattached radium A (the unattached fraction) is tied into the more general problem of estimating dynamically the concentrations of radon and each daughter as the decay and buildup progresses. For the unattached fraction, we have adapted a model of Raabe (1969) for incorporation into our air transport model. The mechanisms expressed by the model are summarized as follows. Radon gas decays to radium A, which initially is unattached, but becomes attached (i.e., is removed from the "unattached" compartment) by a first-order process governed by a rate coefficient λ_S that depends on properties of the ambient aerosol. The attached ions undergo alpha decay and a fraction α_a are detached from their aerosol particles by the recoil; this fraction of the transformed ions become unattached radium B. Further transformations are similar. The following equations express the model:

$$\frac{dA_r}{dt} = -\lambda_r A_r - v[A_r] \quad \text{(T–10)}$$

$$\frac{dA_a}{dt} = -\lambda_a(A_a - A_r) - v[A_a - A_{af}] \quad \text{(T–11)}$$

$$\frac{dA_{af}}{dt} = \lambda_a A_r + \alpha_a \lambda_a (A_a - A_{af}) - (\lambda_a + \lambda_S)A_{af} - v_f[A_{af}] \quad \text{(T–12)}$$

$$\frac{dA_b}{dt} = -\lambda_b(A_b - A_a) - v[A_b - A_{bf}] \quad \text{(T–13)}$$

$$\frac{dA_{bf}}{dt} = \lambda_b A_{af} + \alpha_b \lambda_b (A_a - A_{af}) - (\lambda_b + \lambda_S)A_{bf} - v_f[A_{bf}] \quad \text{(T–14)}$$

$$\frac{dA_c}{dt} = -\lambda_c(A_c - A_b) - v[A_c] \quad \text{(T–15)}$$

where A_r, A_a, A_b, and A_c are the total radioactivities of radon, radium A, radium B, and radium C, respectively (pCi), and A_{af} and A_{bf} are the unattached radioactivities of radium A

and radium B, respectively. The quantities λ_r, λ_a, λ_b, and λ_c are the corresponding radioactive decay-rate coefficients (s^{-1}). The terms such as $v[A_a - A_{af}]$ are estimates of environmental deposition rates (air-to-ground), where v is a deposition velocity appropriate to the species (m s^{-1}) and the bracketed quantity is the concentration of the species in air (pCi m^{-3}). This concentration must be estimated by an air dispersion model. In practice, the depositions have proved to have a negligible effect on the concentrations, and without them, the equations may be solved in closed form. NCRP Publication 78 (NCRP 1984) cites other sources for the value $\alpha_a = 0.81 \pm 0.07$, and we have adopted this value for both recoil fractions α_a and α_b. The attachment coefficient λ_S is given by

$$\lambda_S = \frac{S\bar{v}}{4} \text{ s}^{-1} \qquad \text{(T–16)}$$

where

$S = n\pi\bar{D}$ = particle surface area per unit volume (cm^2 cm^{-3}),

$\bar{D}$ = diameter corresponding to the mean surface area of aerosol particles (cm),

n = number concentration of aerosol particles (cm^{-3}),

4 = ratio of spherical surface area to area of plane circular projection,

$\bar{v}$ = average velocity of unattached radon daughters = 1.38×10^4 cm s^{-1}.

These parameter values were taken from NCRP (1984).

Initial conditions for the differential equations of Eq. T–10 through T–15 specify the relative state of equilibrium of radon and its daughters near the release source (the K-65 silos in the present study). The initial conditions also set the initial state of the attached and unattached fractions of radium A and radium B. (We note that although Raabe's model considers this partitioning for radium B, the NCRP dose model applies it only to radium A.) As the radon and daughter products move downwind, the differential equations govern the evolution of the decay of radon and the buildup of the daughters.

Dose to the embryo/fetus. Dose to the embryo/fetus from radionuclides taken into the body of a pregnant woman is based on methods and data given in Regulatory Guide 8.36 of the Nuclear Regulatory Commission (USNRC 1992). Tables in Appendix C of this reference list monthly incremental estimates of dose to the embryo/fetus from an introduction of radioactivity into maternal blood at the beginning of each gestational month. Such tables have been computed for the uranium and transuranic isotopes of interest to this study but not for the thorium isotopes. A cruder method based on the 9-month gestation dose equivalent to the embryo/fetus is outlined in the reference, and we provisionally adopt this method for the thorium isotopes pertinent to this study. This method can be expected to overestimate the dose to the embryo/fetus, and this inconsistency with the more refined methodology used for the other radionuclides will be reviewed if dose from thorium turns out to be of significant magnitude relative to the other radionuclides.

Tables T–38S through T–41S display the incremental dose numbers to the embryo/fetus by gestational month for the isotopes ^{234}U, ^{235}U, ^{238}U, and ^{239}Pu (which is treated as the transuranic surrogate). Factors for the 9-month gestation dose equivalent are given in Table T–42S for ^{228}Th, ^{230}Th, ^{232}Th, and ^{234}Th.

External Dose

Our treatment of external dose from immersion in contaminated air and water is based on dose-rate conversion factors developed at the Oak Ridge National Laboratory and tabulated in U.S. Department of Energy report DOE/EH-0070 (USDOE 1988). External dose-rate conversion factors documented in this reference are shown in Tables T–27S through T–36S. To estimate dose from exposure to contaminated soil, we have adopted the method of Kocher and Sjoreen (1985). This methodology is based on dose-rate conversion factors at 1 m above the ground surface from monoenergetic sources uniformly distributed in horizontally infinite slabs of soil from the surface to various depths. The relevant numbers from their paper are reproduced in Table T–37S. Tables T–27S through T–36S also present dose-rate conversion factors for concentrations of radionuclides on the ground surface, and such factors would be appropriate for pavement and other ground surfaces where radionuclides would have little opportunity to migrate downward. For soils, the model of Kocher and Sjoreen (1985) is applicable to any predicted vertical profile of radioactivity at a particular time. Their factors are stated in terms of a range of discrete monoenergetic photon energies and consequently must be interpolated and folded into the photon spectrum for each radionuclide of interest.

Age-dependent external dose-rate conversion factors are not available to us at this time. It is anticipated that external dose will constitute a minor component of the total dose to residents near the FMPC, and therefore the model for adults will serve. If subsequent experience proves this assumption incorrect, refinements will have to be undertaken at the appropriate time.

Plutonium-239 was selected as the surrogate for transuranic radionuclides for internal dosimetry. An examination of Tables T–34S through T–36S indicates, however, that this choice is not appropriate for external dose. The higher effective dose rates of ^{237}Np make it the more suitable choice for a generic transuranic emitter until the question of negligible magnitude of the external dose component is settled.

Dose rate from an external source to an embryo/fetus will be estimated by the dose rate to the uterus of the pregnant woman (ICRP 1990). For purposes of radiation protection, a more conservative approach is called for in USNRC (1992).

DYNAMIC CONSIDERATIONS FOR DOSE CONVERSION FACTORS

The internal dose conversion factor can be interpreted as committed dose equivalent (truncated to 50 years) per unit acute intake of radioactivity at time zero (i.e., the varying dose rate to the organ is integrated from 0 to 50 years). What is sometimes wanted, for a strict interpretation, is dose rate over time, but such numbers are seldom published because of the resulting bulk of the tabulations and the infrequent demand for them in radiological assessments.

A common interpretation of the DCF is dose rate per unit intake rate (e.g., Sv year^{-1} per Bq year^{-1}). This interpretation is an approximation, but it is reasonable for many applications if one bears in mind that for radionuclides that are persistently retained in the body, the realization of the dose from a given year's intake may be completed long after the passing of that year, and in some instances we may be taking credit for dose that is never delivered because of the death of the individual. On the other hand, the 50-year truncation of the

dose can potentially underestimate the committed dose equivalent from persistently retained materials, but as we shall see, the tendency toward overestimation likely predominates. We present a brief analysis that gives some sense of the possible misprediction of the internal dose as a result of using the 50-year DCFs.

A simplified prototype of the dose model represents dose rate to an organ as

$$\dot{D}_{\text{acute}}(t) = k \exp(-\lambda_{\text{eff}} t) \tag{T–17}$$

where t is time after intake (days), and k is a constant with units such as Sv day^{-1}, and which we also assume to contain the necessary uptake fraction of ingested or inhaled material that reaches the organ. The effective rate coefficient λ_{eff} (day^{-1}) combines removal by radioactive decay and biological processes in terms of the respective half-lives, T_{r} and T_{b} (days):

$$\lambda_{\text{eff}} = \frac{\ln 2}{T_{\text{r}}} + \frac{\ln 2}{T_{\text{b}}} . \tag{T–18}$$

The dose rate after exposure from time 0 to time t resulting from a continuous intake rate (chronic exposure), $I(t)$ (Bq day^{-1}), that may vary over time is given by the convolution integral

$$\dot{D}(t) = \int_0^t I(t-\tau)\dot{D}_{\text{acute}}(\tau)\, d\tau = k \int_0^t I(t-\tau) \exp(-\lambda_{\text{eff}}\tau)\, d\tau . \tag{T–19}$$

If the intake rate in Eq. T–19 is constant, (= I) the dose rate can be expressed as

$$\dot{D}(t) = \frac{Ik}{\lambda_{\text{eff}}} \left(1 - \exp(-\lambda_{\text{eff}} t)\right) . \tag{T–20}$$

Integration of Eq. T–20 gives the dose delivered from time 0 to time t:

$$D(t) = \frac{Ik}{\lambda_{\text{eff}}} \left(t - \frac{1 - \exp(-\lambda_{\text{eff}} t)}{\lambda_{\text{eff}}} \right) . \tag{T–21}$$

On the other hand, if an acute intake at time zero is I^* Bq and no further radioactivity is taken into the body, the dose after t days is

$$D_{\text{acute}}(t) = \frac{I^* k}{\lambda_{\text{eff}}} \left(1 - \exp(-\lambda_{\text{eff}} t)\right) . \tag{T–22}$$

Note that we have an equivalence between dose rate from chronic exposure at a constant rate (Eq. T–20) and dose from a single acute exposure (Eq. T–22) for this simple dose model, provided the chronic intake rate (Bq day^{-1}) is numerically equal to the acute intake (Bq). Because the chronic dose rate increases with the time t, this result indicates that the 50-year DCF estimates the maximum dose rate for a chronic intake that is constant over time.

The DCF corresponding to our model is Eq. T–22 with t = 18,250 days (50 years) and I^* = 1. The dose estimate corresponding to a particular intake is given with I^* = total intake. But if the intake occurs over an extended period, it is clear that the use of the acute-intake model may introduce some degree of distortion, depending on the desired interpretation. For example, if an individual is exposed for 5 years and dies at the end of that period, the DCF method would include a component of dose for a period of 45 years after the individual's death.

How this distortion varies with the parameters λ_{eff} and the length t of the intake period is what we propose to investigate.

We revert to the notation I for the constant intake rate; the total intake is It, and the DCF estimate of dose, E, is

$$E = It \cdot (\text{DCF}) = \frac{Itk}{\lambda_{eff}} \left(1 - \exp(-\lambda_{eff} t_{50})\right) \qquad \text{(T–23)}$$

where t_{50} represents 50 years in whatever units are being used. The quantity that we are estimating is given by $D(t)$ in Eq. T–21. We use the ratio

$$r = \frac{E}{D(t)} = \frac{1 - \exp(-\lambda_{eff} t_{50})}{1 - \left(1 - \exp(-\lambda_{eff} t)\right)(\lambda_{eff} t)^{-1}} \qquad \text{(T–24)}$$

to investigate the degree of approximation of the DCF-computed estimate to the more realistic dynamic quantity.

Table T–4 shows values of the ratio $r = E/D(t)$ of Eq. T–24 for a range of values of the intake period and the effective half-life $T_{eff} = \ln 2/\lambda_{eff}$, each shown in years. Ratios larger than 1 indicate overestimation by the DCF method. It is necessary to bear in mind that DCFs are based on a variety of effective half-lives; for uranium, for example, the single-exponential model was not used in ICRP Publication 30 (ICRP 1979). Thus Table T–4 by itself cannot be expected to give a realistic sense of the overprediction that could result from the DCF method.

Table T–4. Ratios of DCF-Estimated Dose to Time-Integrated Dose for Various Effective Half-Lives and Exposure (Intake) Periods: Single-Exponential Model

Intake period (years)	Effective half-life (years)														
	0.125	0.5	1	2	3	4	5	10	20	30	40	50	60	70	80
0.125	3.59	12.22	23.75	46.84	69.92	92.98	115.97	224.26	380.60	474.83	535.50	577.41	607.98	631.23	649.48
0.5	1.51	3.59	6.46	12.22	17.99	23.75	29.50	56.55	95.56	119.05	134.17	144.60	152.22	158.00	162.55
1	1.22	2.18	3.59	6.46	9.34	12.22	15.09	28.60	48.06	59.75	67.28	72.47	76.25	79.13	81.39
2	1.10	1.51	2.18	3.59	5.02	6.46	7.89	14.63	24.31	30.11	33.83	36.40	38.27	39.70	40.81
3	1.06	1.31	1.73	2.64	3.59	4.54	5.49	9.97	16.39	20.22	22.68	24.38	25.61	26.55	27.29
4	1.05	1.22	1.51	2.18	2.88	3.59	4.30	7.65	12.43	15.28	17.11	18.37	19.28	19.98	20.52
5	1.04	1.17	1.39	1.90	2.46	3.02	3.59	6.25	10.06	12.32	13.77	14.76	15.49	16.04	16.47
10	1.02	1.08	1.17	1.39	1.64	1.90	2.18	3.48	5.31	6.39	7.08	7.55	7.89	8.15	8.35
20	1.01	1.04	1.08	1.17	1.27	1.39	1.51	2.11	2.95	3.44	3.74	3.95	4.10	4.21	4.30
30	1.01	1.02	1.05	1.11	1.17	1.24	1.31	1.67	2.18	2.46	2.63	2.75	2.83	2.90	2.94
40	1.00	1.02	1.04	1.08	1.12	1.17	1.22	1.46	1.79	1.97	2.08	2.15	2.20	2.24	2.27
50	1.00	1.01	1.03	1.06	1.09	1.13	1.17	1.34	1.57	1.68	1.75	1.79	1.83	1.85	1.87
60	1.00	1.01	1.02	1.05	1.08	1.11	1.14	1.27	1.42	1.49	1.53	1.56	1.57	1.59	1.60
70	1.00	1.01	1.02	1.04	1.07	1.09	1.11	1.22	1.32	1.36	1.38	1.39	1.40	1.40	1.41
80	1.00	1.01	1.02	1.04	1.06	1.08	1.10	1.18	1.24	1.26	1.26	1.26	1.26	1.26	1.26

To improve our perspective on the question, we consider specific retention functions for uranium in bone and kidneys (for present purposes, a retention function is analogous to a normalized version of Eq. T–17). DCFs for uranium given in this appendix (other than for lungs and gastrointestinal tract) were based on these retention functions (ICRP 1979):

$$R_{BONE}(t) = 0.897e^{-(\ln 2)t/20} + 0.103e^{-(\ln 2)t/5000} \qquad \text{(T–25)}$$

$$R_{KIDNEY} = 0.996e^{-(\ln 2)t/6} + 0.004e^{-(\ln 2)t/1500} \qquad \text{(T–26)}$$

where time units are expressed in days. (Note that the coefficients of the exponential terms are normalized to sum to 1, so that $R(0) = 1$.) The function for the kidney is used for other soft tissues, apart from the exceptions noted above. The $E/D(t)$ ratio for such two-term models has the form

$$r = \frac{c_1 F_1(t_{50}) + c_2 F_2(t_{50})}{(c_1/\lambda_1)(1 - F_1(t)/t) + (c_2/\lambda_2)(1 - F_2(t)/t)} \qquad \text{(T–27)}$$

where

$$F_i(t) = \frac{1 - \exp(-\lambda_i t)}{\lambda_i}.$$

Table T–5 shows the $E/D(t)$ ratios for these two organ models for uranium, tabulated over the same range of exposure (or intake) periods. Note that for the earlier example of an individual who died at the end of a five-year exposure, the overestimation of dose to the bone from uranium by the DCF method would be by a factor of more than six. If the individual were one of the cases in an epidemiological study, the error could bias the results by taking credit for a component of dose that could not have contributed to the condition. Similar remarks would apply to a component of dose delivered after the onset of the disease for which the relationship to the radiation is being investigated. Note that for the kidney and most other soft tissues, the overestimation is by only 55 percent.

Table T–5. Ratios of DCF-Estimated Uranium Dose to Time-Integrated Dose for Bone and Kidney

Intake period (years)	Organ	
	Bone	Kidney
0.125	46.67	2.53
0.5	22.83	2.09
1	16.78	1.96
2	11.60	1.81
3	9.00	1.70
4	7.42	1.62
5	6.34	1.55
10	3.82	1.34
20	2.35	1.18
30	1.84	1.11
40	1.58	1.08
50	1.42	1.07
60	1.32	1.05
70	1.26	1.05
80	1.21	1.04

One would avoid this problem by using dosimetric data in the form of dose-rate tables, but as we have mentioned, such tables are not systematically available. Our present plan is to estimate approximate adjustments only to those factors that involve effective half-lives that would lead to error ratios above an acceptable limit. The need for application of such methods depends on the exact use made of the dosimetric results. For example, in the case of estimating the average chronic dose over a lifetime to a population of all ages, the error would likely be less than a factor of two.

REFERENCES

Bair W.J. 1991. "Overview of ICRP Respiratory Tract Model." *Rad. Prot. Dosim.* **38**(1/3): 147–152.

Cristy M.W., R.W. Leggett, D.E. Dunning, Jr., and K.F. Eckerman. 1986. *Relative Age-Specific Radiation Dose Commitment Factors for Major Radionuclides Released from Nuclear Fuel Facilities.* Rep. NUREG/CR-4628, ORNL/TM-9890, Oak Ridge National Laboratory, Oak Ridge, Tennessee.

Eckerman K.F., A.B. Wolbarst, and C.B. Richardson. 1988. *Limiting Values of Radionuclide Intake and Air Concentration and Dose Conversion Factors for Inhalation, Submersion, and Ingestion.* Federal Guidance Report No. 11, EPA-520/1-88-020, U.S. Environmental Protection Agency.

International Commission on Radiological Protection (ICRP). 1991. *1990 Recommendations of the International Commission on Radiological Protection.* ICRP Publication 60. *Ann. ICRP* **21**(1–3).

International Commission on Radiological Protection (ICRP). 1990. *Age-Dependent Doses to Members of the Public from Intake of Radionuclides: Part 1.* ICRP Publication 56. *Ann. ICRP* **20**(2).

International Commission on Radiological Protection (ICRP). 1979. *Limits for Intakes of Radionuclides by Workers.* ICRP Publication 30 Part 1, *Ann. ICRP* **2**(3/4).

International Commission on Radiological Protection (ICRP). 1975. *Report of the Task Group on Reference Man.* ICRP Publication 23. Pergamon Press, Oxford.

Killough G.G. and K.F. Eckerman. 1980. "Internal Dosimetry." Chapter 7 in *Radiological Assessment — A Textbook on Environmental Dose Analysis,* J.E. Till and H.R. Meyer, Eds. Rep. NUREG/CR-3332, ORNL-5968, U.S. Nuclear Regulatory Commission, Washington, D.C.

Kocher D.C. 1981. *Radioactive Decay Tables — A Handbook of Decay Data for Application to Radiation Dosimetry and Radiological Assessments.* Rep. DOE/TIC-11026, Technical Information Center, U.S. Department of Energy, Oak Ridge, Tennessee.

Kocher D.C. 1980. "External Dosimetry." Chapter 8 in *Radiological Assessment — A Textbook on Environmental Dose Analysis,* J.E. Till and H.R. Meyer, Eds. Rep. NUREG/CR-3332, ORNL-5968, U.S. Nuclear Regulatory Commission, Washington, D.C.

Kocher D.C. and A.L. Sjoreen. 1985. "Dose-Rate Conversion Factors for External Exposure to Photon Emitters in Soil." *Health Phys.* **48**(2): 193–205.

National Council on Radiation Protection and Measurements (NCRP). 1984. *Evaluation of Occupational and Environmental Exposures to Radon and Radon Daughters in the United States,* NCRP Report No. 78. NCRP, Bethesda, Maryland.

Raabe O.G. 1969. "Concerning the Interactions that Occur between Radon Decay Products and Aerosols." *Health Phys.* **17**(2): 177–185.

U.S. Department of Energy (USDOE). 1988. *External Dose-Rate Conversion Factors for Calculation of Dose to the Public.* Rep. DOE/EH–0070. Assistant Secretary for Environment, Safety, and Health, Office of Environmental Guidance and Compliance, Washington, D.C.

U.S. Nuclear Regulatory Commission (USNRC). 1992. *Radiation Dose to the Embryo/Fetus.* Regulatory Guide 8.36, Office of Nuclear Regulatory Research, Washington, D.C.

Table T–1S. Internal Dose Conversion Factors for ^{238}U (Sv Bq^{-1})

U-238 T1/2 = 4.468E9y

	Inhalation			Oral	
	Class D f1 = 5.0E-02	Class W f1 = 5.0E-02	Class Y f1 = 2.0E-03	f1 = 5.0E-02	f1 = 2.0E-03
Adrenals	2.24E-08 (33 16 51)	6.77E-09 (30 29 41)	3.22E-09 (5 1 94)	2.31E-09	9.28E-11
Bld wall	2.22E-08 (33 16 51)	6.70E-09 (30 29 41)	2.38E-09 (7 2 91)	2.30E-09	9.46E-11
BSurface	9.78E-06 (33 16 51)	2.94E-06 (30 29 41)	1.01E-06 (7 2 91)	1.01E-06	4.04E-08
Breast	2.23E-08 (33 16 51)	6.74E-09 (30 29 41)	2.91E-09 (6 2 92)	2.31E-09	9.33E-11
ST wall	2.24E-08 (33 16 51)	7.30E-09 (31 27 42)	3.74E-09 (12 3 85)	3.28E-09	1.07E-09
SI wall	2.26E-08 (34 16 50)	8.09E-09 (33 25 42)	4.14E-09 (22 6 72)	4.65E-09	2.56E-09
ULI wall	2.44E-08 (38 15 47)	1.48E-08 (39 17 44)	1.24E-08 (37 10 53)	1.61E-08	1.46E-08
LLI wall	2.90E-08 (47 13 40)	3.20E-08 (43 12 45)	3.32E-08 (42 11 47)	4.57E-08	4.57E-08
Kidneys	4.01E-06 (33 16 51)	1.21E-06 (30 29 41)	4.27E-07 (7 2 91)	4.15E-07	1.66E-08
Liver	2.22E-08 (33 16 51)	6.73E-09 (30 29 41)	3.13E-09 (5 1 94)	2.30E-09	9.26E-11
Lungs	2.80E-07 (3 2 95)	1.42E-05 (0 0 100)	2.66E-04 (0 0 100)	2.30E-09	9.22E-11
Ovaries	2.23E-08 (33 16 51)	6.71E-09 (30 29 41)	2.42E-09 (7 2 91)	2.31E-09	1.02E-10
Pancreas	2.23E-08 (33 16 51)	6.74E-09 (30 29 41)	3.18E-09 (5 1 94)	2.30E-09	9.30E-11
R Marrow	6.58E-07 (33 16 51)	1.98E-07 (30 29 41)	6.88E-08 (7 2 91)	6.80E-08	2.72E-09
Skin	2.23E-08 (33 16 51)	6.71E-09 (30 29 41)	2.58E-09 (6 2 92)	2.30E-09	9.24E-11
Spleen	2.23E-08 (33 16 51)	6.74E-09 (30 29 41)	3.12E-09 (5 1 94)	2.30E-09	9.27E-11
Testes	2.22E-08 (33 16 51)	6.70E-09 (30 29 41)	2.37E-09 (7 2 91)	2.30E-09	9.39E-11
Thymus	2.22E-08 (33 16 51)	6.76E-09 (30 29 41)	3.78E-09 (4 1 95)	2.30E-09	9.20E-11
Thyroid	2.22E-08 (33 16 51)	6.71E-09 (30 29 41)	2.73E-09 (6 2 92)	2.30E-09	9.20E-11
Uterus	2.22E-08 (33 16 51)	6.70E-09 (30 29 41)	2.40E-09 (7 2 91)	2.30E-09	9.51E-11
Effective (ICRP60)	2.30E-07 (29 14 57)	1.77E-06 (1 1 98)	3.19E-05 (0 0 100)	2.58E-08	6.42E-09

Table T–2S. Internal Dose Conversion Factors for ^{235}U (Sv Bq^{-1})

U-235 T1/2 = 703.8E6y

	Inhalation			Oral	
	Class D f1 = 5.0E-02	Class W f1 = 5.0E-02	Class Y f1 = 2.0E-03	f1 = 5.0E-02	f1 = 2.0E-03
Adrenals	2.41E-08 (33 16 51)	7.50E-09 (29 28 43)	7.42E-09 (2 1 97)	2.50E-09	1.09E-10
Bld wall	2.35E-08 (33 16 51)	7.10E-09 (30 29 41)	2.60E-09 (7 2 91)	2.49E-09	1.65E-10
BSurface	1.01E-05 (33 16 51)	3.05E-06 (30 29 41)	1.05E-06 (7 2 91)	1.05E-06	4.20E-08
Breast	2.38E-08 (33 16 51)	7.33E-09 (29 28 43)	5.37E-09 (3 1 96)	2.49E-09	1.21E-10
ST wall	2.37E-08 (33 16 51)	7.90E-09 (31 26 43)	6.76E-09 (8 2 90)	3.56E-09	1.23E-09
SI wall	2.41E-08 (34 16 50)	8.67E-09 (34 25 41)	4.66E-09 (23 6 71)	5.24E-09	3.03E-09
ULI wall	2.61E-08 (39 15 46)	1.57E-08 (42 17 41)	1.31E-08 (41 11 48)	1.84E-08	1.69E-08
LLI wall	3.17E-08 (48 13 39)	3.38E-08 (48 12 40)	3.42E-08 (47 13 40)	5.31E-08	5.33E-08
Kidneys	4.19E-06 (33 16 51)	1.26E-06 (30 29 41)	4.45E-07 (7 2 91)	4.33E-07	1.73E-08
Liver	2.36E-08 (33 16 51)	7.37E-09 (29 28 43)	7.36E-09 (2 1 97)	2.46E-09	1.14E-10
Lungs	2.95E-07 (3 2 95)	1.48E-05 (0 0 100)	2.76E-04 (0 0 100)	2.46E-09	1.01E-10
Ovaries	2.37E-08 (33 16 51)	7.24E-09 (30 28 42)	2.84E-09 (9 2 89)	2.67E-09	3.34E-10
Pancreas	2.39E-08 (33 16 51)	7.44E-09 (29 28 43)	7.34E-09 (3 1 96)	2.49E-09	1.23E-10
R Marrow	6.58E-07 (33 16 51)	1.98E-07 (30 29 41)	7.15E-08 (7 2 91)	6.81E-08	2.78E-09
Skin	2.36E-08 (33 16 51)	7.17E-09 (30 29 41)	3.56E-09 (5 1 94)	2.45E-09	1.04E-10
Spleen	2.37E-08 (33 16 51)	7.36E-09 (29 28 43)	6.97E-09 (3 1 96)	2.46E-09	1.15E-10
Testes	2.36E-08 (33 16 51)	7.10E-09 (30 29 41)	2.52E-09 (7 2 91)	2.45E-09	1.15E-10
Thymus	2.35E-08 (33 16 51)	7.49E-09 (28 27 45)	1.04E-08 (2 0 98)	2.43E-09	9.81E-11
Thyroid	2.37E-08 (33 16 51)	7.22E-09 (30 29 41)	4.11E-09 (4 1 95)	2.45E-09	9.82E-11
Uterus	2.36E-08 (33 16. 51)	7.14E-09 (30 29 41)	2.71E-09 (7 2 91)	2.52E-09	1.89E-10
Effective (ICRP60)	2.36E-07 (29 14 57)	1.84E-06 (1 1 98)	3.31E-05 (0 0 100)	2.73E-08	7.43E-09

Table T–3S. Internal Dose Conversion Factors for ^{234}U (Sv Bq^{-1})

U-234 T1/2 = 2.445E5y

	Inhalation			Oral	
	Class D f1 = 5.0E-02	Class W f1 = 5.0E-02	Class Y f1 = 2.0E-03	f1 = 5.0E-02	f1 = 2.0E-03
Adrenals	2.50E-08 (33 16 51)	7.52E-09 (30 29 41)	2.66E-09 (7 2 91)	2.58E-09	1.03E-10
Bld wall	2.50E-08 (33 16 51)	7.52E-09 (30 29 41)	2.65E-09 (7 2 91)	2.58E-09	1.03E-10
BSurface	1.09E-05 (33 16 51)	3.29E-06 (30 29 41)	1.13E-06 (7 2 91)	1.13E-06	4.52E-08
Breast	2.50E-08 (33 16 51)	7.52E-09 (30 29 41)	2.68E-09 (7 2 91)	2.58E-09	1.03E-10
ST wall	2.52E-08 (33 16 51)	8.09E-09 (32 27 41)	3.30E-09 (16 4 80)	3.70E-09	1.22E-09
SI wall	2.54E-08 (34 16 50)	8.87E-09 (33 26 41)	4.25E-09 (24 6 70)	5.23E-09	2.88E-09
ULI wall	2.74E-08 (38 15 47)	1.53E-08 (42 18 40)	1.19E-08 (42 11 47)	1.79E-08	1.62E-08
LLI wall	3.22E-08 (47 13 40)	3.15E-08 (47 13 40)	3.11E-08 (47 13 40)	4.95E-08	4.94E-08
Kidneys	4.52E-06 (33 16 51)	1.36E-06 (30 29 41)	4.79E-07 (7 2 91)	4.68E-07	1.87E-08
Liver	2.50E-08 (33 16 51)	7.52E-09 (30 29 41)	2.67E-09 (7 2 91)	2.58E-09	1.03E-10
Lungs	3.18E-07 (3 2 95)	1.60E-05 (0 0 100)	2.98E-04 (0 0 100)	2.58E-09	1.03E-10
Ovaries	2.50E-08 (33 16 51)	7.52E-09 (30 29 41)	2.65E-09 (7 2 91)	2.59E-09	1.06E-10
Pancreas	2.50E-08 (33 16 51)	7.52E-09 (30 29 41)	2.65E-09 (7 2 91)	2.58E-09	1.03E-10
R Marrow	6.98E-07 (33 16 51)	2.10E-07 (30 29 41)	7.22E-08 (7 2 91)	7.21E-08	2.88E-09
Skin	2.50E-08 (33 16 51)	7.52E-09 (30 29 41)	2.65E-09 (7 2 91)	2.58E-09	1.03E-10
Spleen	2.50E-08 (33 16 51)	7.52E-09 (30 29 41)	2.66E-09 (7 2 91)	2.58E-09	1.03E-10
Testes	2.50E-08 (33 16 51)	7.52E-09 (30 29 41)	2.65E-09 (7 2 91)	2.58E-09	1.03E-10
Thymus	2.50E-08 (33 16 51)	7.52E-09 (30 29 41)	2.66E-09 (7 2 91)	2.58E-09	1.03E-10
Thyroid	2.50E-08 (33 16 51)	7.52E-09 (30 29 41)	2.65E-09 (7 2 91)	2.58E-09	1.03E-10
Uterus	2.50E-08 (33 16 51)	7.52E-09 (30 29 41)	2.65E-09 (7 2 91)	2.58E-09	1.04E-10
Effective (ICRP60)	2.53E-07 (29 14 57)	1.99E-06 (1 1 98)	3.58E-05 (0 0 100)	2.82E-08	6.96E-09

Table T–4S. Internal Dose Conversion Factors for ^{234}Th (Sv Bq^{-1})

Th-234 T1/2 = 24.10d

	Inhalation		Oral
	Class W f1 = 2.0E-04	Class Y f1 = 2.0E-04	f1 = 2.0E-04
Adrenals	1.14E-10 (32 43 25)	2.24E-11 (18 5 77)	1.64E-12
Bld wall	1.02E-10 (37 46 17)	1.00E-11 (62 17 21)	9.15E-12
BSurface	7.83E-09 (35 47 18)	6.29E-10 (44 12 44)	2.08E-11
Breast	1.08E-10 (34 44 22)	1.66E-11 (28 8 64)	3.57E-12
ST wall	5.50E-10 (56 16 28)	4.99E-10 (61 16 23)	9.95E-10
SI wall	1.21E-09 (60 12 28)	1.21E-09 (62 17 21)	2.55E-09
ULI wall	6.48E-09 (61 10 29)	6.94E-09 (62 17 21)	1.47E-08
LLI wall	1.87E-08 (62 9 29)	2.03E-08 (62 17 21)	4.30E-08
Kidneys	1.06E-10 (35 45 20)	1.31E-11 (36 10 54)	3.71E-12
Liver	7.77E-10 (35 47 18)	5.91E-11 (48 13 39)	4.17E-12
Lungs	4.66E-08 (0 0 100)	6.39E-08 (0 0 100)	7.05E-13
Ovaries	1.13E-10 (39 43 18)	2.11E-11 (61 16 23)	3.12E-11
Pancreas	1.13E-10 (33 42 25)	2.33E-11 (20 6 74)	3.49E-12
R Marrow	4.18E-09 (36 47 17)	2.56E-10 (60 16 24)	1.84E-11
Skin	1.01E-10 (35 46 19)	9.93E-12 (39 11 50)	1.31E-12
Spleen	1.11E-10 (33 42 25)	2.15E-11 (21 6 73)	2.90E-12
Testes	9.93E-11 (36 48 16)	6.58E-12 (65 17 18)	2.53E-12
Thymus	1.19E-10 (30 39 31)	3.36E-11 (11 3 86)	4.15E-13
Thyroid	1.03E-10 (34 45 21)	1.27E-11 (28 8 64)	2.88E-13
Uterus	1.05E-10 (37 46 17)	1.21E-11 (61 16 23)	1.26E-11
Effective (ICRP60)	8.57E-09 (19 7 74)	1.02E-08 (15 5 80)	5.30E-09

Table T–5S. Internal Dose Conversion Factors for ^{232}Th (Sv Bq^{-1})

Th-232 T1/2 = 1.405E10y

	Inhalation		Oral
	Class W f1 = 2.0E-04	Class Y f1 = 2.0E-04	f1 = 2.0E-04
Adrenals	8.02E-07 (25 33 42)	6.34E-07 (3 1 96)	1.31E-09
Bld wall	7.41E-07 (25 33 42)	5.88E-07 (3 1 96)	1.21E-09
BSurface	1.11E-02 (25 33 42)	4.99E-03 (6 2 92)	1.85E-05
Breast	7.72E-07 (25 33 42)	6.14E-07 (3 1 96)	1.26E-09
ST wall	7.41E-07 (25 33 42)	6.06E-07 (3 1 96)	2.14E-09
SI wall	7.55E-07 (25 33 42)	5.98E-07 (3 1 96)	3.56E-09
ULI wall	7.58E-07 (25 32 43)	6.05E-07 (4 1 95)	1.47E-08
LLI wall	7.87E-07 (25 32 43)	6.27E-07 (5 1 94)	4.27E-08
Kidneys	7.65E-07 (25 33 42)	6.07E-07 (3 1 96)	1.25E-09
Liver	6.23E-06 (25 33 42)	5.04E-06 (3 1 96)	1.02E-08
Lungs	1.44E-05 (1 2 97)	9.40E-04 (0 0 100)	1.25E-09
Ovaries	7.62E-07 (25 33 42)	5.98E-07 (3 1 96)	1.25E-09
Pancreas	7.66E-07 (25 33 42)	6.21E-07 (3 1 96)	1.25E-09
R Marrow	8.93E-04 (25 33 42)	4.01E-04 (6 2 92)	1.48E-06
Skin	7.57E-07 (25 33 42)	6.01E-07 (3 1 96)	1.24E-09
Spleen	7.52E-07 (25 33 42)	6.12E-07 (3 1 96)	1.23E-09
Testes	7.55E-07 (25 33 42)	5.94E-07 (3 1 96)	1.23E-09
Thymus	7.51E-07 (25 33 42)	6.29E-07 (3 1 96)	1.23E-09
Thyroid	7.44E-07 (25 33 42)	5.99E-07 (3 1 96)	1.21E-09
Uterus	7.47E-07 (25 33 42)	5.92E-07 (3 1 96)	1.22E-09
Effective (ICRP60)	2.21E-04 (25 33 42)	2.11E-04 (3 1 96)	3.69E-07

Table T–6S. Internal Dose Conversion Factors for ^{230}Th (Sv Bq^{-1})

Th-230 T1/2 = 7.7E4y

	Inhalation		Oral
	Class W f1 = 2.0E-04	Class Y f1 = 2.0E-04	f1 = 2.0E-04
Adrenals	4.09E-07 (25 33 42)	1.73E-07 (6 2 92)	6.80E-10
Bld wall	4.08E-07 (25 33 42)	1.72E-07 (6 2 92)	6.80E-10
BSurface	2.16E-03 (25 33 42)	8.71E-04 (6 2 92)	3.60E-06
Breast	4.08E-07 (25 33 42)	1.72E-07 (6 2 92)	6.80E-10
ST wall	4.09E-07 (25 33 42)	1.73E-07 (6 2 92)	1.77E-09
SI wall	4.10E-07 (25 33 42)	1.74E-07 (6 2 92)	3.41E-09
ULI wall	4.16E-07 (26 33 41)	1.81E-07 (8 2 90)	1.65E-08
LLI wall	4.33E-07 (27 32 41)	2.00E-07 (12 3 85)	4.93E-08
Kidneys	4.08E-07 (25 33 42)	1.72E-07 (6 2 92)	6.80E-10
Liver	3.57E-06 (25 33 42)	1.51E-06 (6 2 92)	5.94E-09
Lungs	1.61E-05 (1 1 98)	3.00E-04 (0 0 100)	6.80E-10
Ovaries	4.08E-07 (25 33 42)	1.72E-07 (6 2 92)	6.82E-10
Pancreas	4.08E-07 (25 33 42)	1.73E-07 (6 2 92)	6.80E-10
R Marrow	1.73E-04 (25 33 42)	6.99E-05 (6 2 92)	2.89E-07
Skin	4.08E-07 (25 33 42)	1.72E-07 (6 2 92)	6.80E-10
Spleen	4.08E-07 (25 33 42)	1.72E-07 (6 2 92)	6.80E-10
Testes	4.08E-07 (25 33 42)	1.72E-07 (6 2 92)	6.80E-10
Thymus	4.08E-07 (25 33 42)	1.73E-07 (6 2 92)	6.80E-10
Thyroid	4.08E-07 (25 33 42)	1.72E-07 (6 2 92)	6.80E-10
Uterus	4.08E-07 (25 33 42)	1.72E-07 (6 2 92)	6.80E-10
Effective (ICRP60)	4.48E-05 (24 32 44)	5.33E-05 (2 1 97)	7.75E-08

Table T–7S. Internal Dose Conversion Factors for ^{228}Th (Sv Bq^{-1})

Th-228 T1/2 = 1.9131y

	Inhalation		Oral
	Class W f1 = 2.0E-04	Class Y f1 = 2.0E-04	f1 = 2.0E-04
Adrenals	1.35E-06 (26 34 40)	2.35E-07 (15 4 81)	2.32E-09
Bld wall	1.34E-06 (26 34 40)	2.25E-07 (16 4 80)	2.38E-09
BSurface	1.37E-03 (26 34 40)	2.29E-04 (16 4 80)	2.37E-06
Breast	1.35E-06 (26 34 40)	2.32E-07 (15 4 81)	2.33E-09
ST wall	1.35E-06 (26 34 40)	2.36E-07 (15 4 81)	3.64E-09
SI wall	1.35E-06 (26 34 40)	2.31E-07 (16 4 80)	6.07E-09
ULI wall	1.37E-06 (26 34 40)	2.53E-07 (18 5 77)	3.11E-08
LLI wall	1.44E-06 (27 32 41)	3.23E-07 (25 6 69)	1.32E-07
Kidneys	1.35E-06 (26 34 40)	2.30E-07 (15 4 81)	2.33E-09
Liver	1.17E-05 (26 34 40)	1.97E-06 (16 4 80)	2.01E-08
Lungs	9.48E-05 (0 1 99)	6.91E-04 (0 0 100)	2.31E-09
Ovaries	1.35E-06 (26 34 40)	2.26E-07 (16 4 80)	2.53E-09
Pancreas	1.35E-06 (26 34 40)	2.37E-07 (15 4 81)	2.32E-09
R Marrow	1.12E-04 (26 34 40)	1.87E-05 (16 4 80)	1.93E-07
Skin	1.34E-06 (26 34 40)	2.28E-07 (15 4 81)	2.31E-09
Spleen	1.34E-06 (26 34 40)	2.36E-07 (15 4 81)	2.32E-09
Testes	1.34E-06 (26 34 40)	2.25E-07 (16 4 80)	2.33E-09
Thymus	1.35E-06 (26 34 40)	2.44E-07 (14 4 82)	2.31E-09
Thyroid	1.34E-06 (26 34 40)	2.30E-07 (15 4 81)	2.30E-09
Uterus	1.34E-06 (26 34 40)	2.26E-07 (16 4 80)	2.38E-09
Effective (ICRP60)	4.01E-05 (19 24 57)	8.77E-05 (1 0 99)	6.55E-08

Table T–8S. Internal Dose Conversion Factors for ^{240}Pu (Sv Bq^{-1})

Pu-240 T1/2 = 6537y

	Inhalation		Oral		
	Class W f1 = 1.0E-03	Class Y f1 = 1.0E-05	f1 = 1.0E-03	f1 = 1.0E-04	f1 = 1.0E-05
Adrenals	1.02E-09 (25 33 42)	4.33E-10 (6 2 92)	8.46E-12	8.48E-13	8.63E-14
Bld wall	9.01E-10 (25 33 42)	3.74E-10 (6 2 92)	7.55E-12	8.23E-13	1.50E-13
BSurface	2.11E-03 (25 33 42)	8.21E-04 (6 2 92)	1.76E-05	1.76E-06	1.76E-07
Brain	9.53E-10 (25 33 42)	3.94E-10 (6 2 92)	7.91E-12	7.91E-13	7.91E-14
Breast	9.51E-10 (25 33 42)	4.33E-10 (5 1 94)	7.97E-12	8.82E-13	1.73E-13
ST wall	1.53E-09 (36 23 41)	1.08E-09 (35 9 56)	1.21E-09	1.20E-09	1.20E-09
SI wall	2.44E-09 (43 17 40)	2.11E-09 (43 12 45)	3.01E-09	3.01E-09	3.00E-09
ULI wall	9.78E-09 (51 10 39)	1.04E-08 (50 13 37)	1.74E-08	1.74E-08	1.74E-08
LLI wall	2.81E-08 (52 9 39)	3.11E-08 (51 14 35)	5.33E-08	5.34E-08	5.34E-08
Kidneys	9.41E-10 (25 33 42)	3.90E-10 (6 2 92)	7.82E-12	7.90E-13	8.69E-14
Liver	3.78E-04 (25 33 42)	1.51E-04 (6 2 92)	3.14E-06	3.14E-07	3.14E-08
Lungs	1.73E-05 (0 0 100)	3.23E-04 (0 0 100)	8.07E-12	8.08E-13	8.22E-14
Ovaries	3.18E-05 (25 33 42)	1.20E-05 (7 2 91)	2.64E-07	2.64E-08	2.64E-09
Pancreas	9.44E-10 (25 33 42)	3.94E-10 (6 2 92)	7.87E-12	8.22E-13	1.17E-13
R Marrow	1.69E-04 (25 33 42)	6.57E-05 (6 2 92)	1.41E-06	1.41E-07	1.41E-08
Skin	9.28E-10 (25 33 42)	3.86E-10 (6 2 92)	7.71E-12	7.80E-13	8.68E-14
Spleen	9.21E-10 (25 33 42)	3.95E-10 (6 2 92)	7.64E-12	7.72E-13	8.50E-14
Testes	3.18E-05 (25 33 42)	1.20E-05 (7 2 91)	2.64E-07	2.64E-08	2.64E-09
Thymus	9.10E-10 (25 33 42)	3.87E-10 (6 2 92)	7.55E-12	7.55E-13	7.56E-14
Thyroid	9.05E-10 (25 33 42)	3.76E-10 (6 2 92)	7.51E-12	7.51E-13	7.51E-14
Uterus	9.02E-10 (25 33 42)	3.74E-10 (6 2 92)	7.57E-12	8.35E-13	1.61E-13
Effective (ICRP60)	6.87E-05 (24 32 44)	6.48E-05 (2 1 97)	5.62E-07	6.21E-08	1.21E-08

Table T-9S. Internal Dose Conversion Factors for ^{239}Pu (Sv Bq^{-1})

Pu-239 T1/2 = 24065y

	Inhalation		Oral		
	Class W f1 = 1.0E-03	Class Y f1 = 1.0E-05	f1 = 1.0E-03	f1 = 1.0E-04	f1 = 1.0E-05
Adrenals	9.54E-10 (25 33 42)	4.01E-10 (6 2 92)	7.92E-12	7.95E-13	8.28E-14
Bld wall	9.01E-10 (25 33 42)	3.74E-10 (6 2 92)	7.52E-12	7.98E-13	1.25E-13
BSurface	2.11E-03 (25 33 42)	8.21E-04 (6 2 92)	1.76E-05	1.76E-06	1.76E-07
Brain	9.23E-10 (25 33 42)	3.83E-10 (6 2 92)	7.66E-12	7.66E-13	7.66E-14
Breast	9.22E-10 (25 33 42)	3.99E-10 (6 2 92)	7.69E-12	8.09E-13	1.21E-13
ST wall	1.52E-09 (36 23 41)	1.07E-09 (35 9 56)	1.20E-09	1.19E-09	1.19E-09
SI wall	2.43E-09 (43 17 40)	2.10E-09 (43 12 45)	2.99E-09	2.99E-09	2.99E-09
ULI wall	9.72E-09 (51 10 39)	1.03E-08 (50 13 37)	1.73E-08	1.73E-08	1.73E-08
LLI wall	2.79E-08 (52 9 39)	3.10E-08 (51 14 35)	5.30E-08	5.31E-08	5.31E-08
Kidneys	9.21E-10 (25 33 42)	3.83E-10 (6 2 92)	7.66E-12	7.76E-13	8.78E-14
Liver	3.78E-04 (25 33 42)	1.51E-04 (6 2 92)	3.14E-06	3.14E-07	3.14E-08
Lungs	1.73E-05 (0 0 100)	3.23E-04 (0 0 100)	7.74E-12	7.75E-13	7.89E-14
Ovaries	3.18E-05 (25 33 42)	1.20E-05 (7 2 91)	2.64E-07	2.64E-08	2.64E-09
Pancreas	9.23E-10 (25 33 42)	3.86E-10 (6 2 92)	7.68E-12	7.89E-13	9.95E-14
R Marrow	1.69E-04 (25 33 42)	6.57E-05 (6 2 92)	1.41E-06	1.41E-07	1.41E-08
Skin	9.12E-10 (25 33 42)	3.79E-10 (6 2 92)	7.57E-12	7.63E-13	8.17E-14
Spleen	9.09E-10 (25 33 42)	3.84E-10 (6 2 92)	7.55E-12	7.64E-13	8.47E-14
Testes	3.18E-05 (25 33 42)	1.20E-05 (7 2 91)	2.64E-07	2.64E-08	2.64E-09
Thymus	9.05E-10 (25 33 42)	3.82E-10 (6 2 92)	7.51E-12	7.51E-13	7.54E-14
Thyroid	9.03E-10 (25 33 42)	3.75E-10 (6 2 92)	7.49E-12	7.49E-13	7.50E-14
Uterus	9.01E-10 (25 33 42)	3.74E-10 (6 2 92)	7.54E-12	8.11E-13	1.38E-13
Effective (ICRP60)	6.87E-05 (24 32 44)	6.48E-05 (2 1 97)	5.62E-07	6.20E-08	1.21E-08

Table T-10S. Internal Dose Conversion Factors for ^{238}Pu (Sv Bq^{-1})

Pu-238 T1/2 = 87.74y

	Inhalation		Oral		
	Class W f1 = 1.0E-03	Class Y f1 = 1.0E-05	f1 = 1.0E-03	f1 = 1.0E-04	f1 = 1.0E-05
Adrenals	1.06E-09 (25 33 42)	4.37E-10 (6 2 92)	8.84E-12	8.85E-13	8.97E-14
Bld wall	9.58E-10 (25 33 42)	3.85E-10 (6 2 92)	8.03E-12	8.70E-13	1.54E-13
BSurface	1.90E-03 (25 33 42)	7.25E-04 (7 2 91)	1.58E-05	1.58E-06	1.58E-07
Brain	1.00E-09 (25 33 42)	4.02E-10 (6 2 92)	8.34E-12	8.34E-13	8.34E-14
Breast	1.00E-09 (25 33 42)	4.40E-10 (6 2 92)	8.41E-12	9.28E-13	1.80E-13
ST wall	1.62E-09 (36 23 41)	1.13E-09 (36 10 54)	1.29E-09	1.28E-09	1.28E-09
SI wall	2.60E-09 (43 17 40)	2.23E-09 (44 12 44)	3.20E-09	3.20E-09	3.20E-09
ULI wall	1.04E-08 (51 10 39)	1.10E-08 (50 13 37)	1.85E-08	1.85E-08	1.85E-08
LLI wall	2.99E-08 (52 9 39)	3.30E-08 (51 14 35)	5.67E-08	5.68E-08	5.68E-08
Kidneys	9.93E-10 (25 33 42)	3.99E-10 (6 2 92)	8.26E-12	8.33E-13	9.03E-14
Liver	3.51E-04 (25 33 42)	1.37E-04 (6 2 92)	2.92E-06	2.92E-07	2.92E-08
Lungs	1.84E-05 (0 0 100)	3.20E-04 (0 0 100)	8.49E-12	8.50E-13	8.64E-14
Ovaries	2.80E-05 (25 33 42)	1.04E-05 (7 2 91)	2.33E-07	2.33E-08	2.33E-09
Pancreas	9.96E-10 (25 33 42)	4.02E-10 (6 2 92)	8.31E-12	8.66E-13	1.22E-13
R Marrow	1.52E-04 (25 33 42)	5.80E-05 (7 2 91)	1.27E-06	1.27E-07	1.27E-08
Skin	9.81E-10 (25 33 42)	3.95E-10 (6 2 92)	8.16E-12	8.25E-13	9.14E-14
Spleen	9.75E-10 (25 33 42)	4.04E-10 (6 2 92)	8.10E-12	8.17E-13	8.89E-14
Testes	2.80E-05 (25 33 42)	1.04E-05 (7 2 91)	2.33E-07	2.33E-08	2.33E-09
Thymus	9.66E-10 (25 33 42)	3.96E-10 (6 2 92)	8.02E-12	8.02E-13	8.02E-14
Thyroid	9.62E-10 (25 33 42)	3.86E-10 (6 2 92)	7.99E-12	7.99E-13	7.99E-14
Uterus	9.59E-10 (25 33 42)	3.85E-10 (6 2 92)	8.05E-12	8.81E-13	1.64E-13
Effective (ICRP60)	6.26E-05 (24 32 44)	6.15E-05 (3 0 97)	5.10E-07	5.73E-08	1.20E-08

Table T–11S. Internal Dose Conversion Factors for ^{237}Np (Sv Bq^{-1})

Np-237 T1/2 = 2.14E6y	Inhalation	Oral
	Class W f1 = 1.0E-03	f1 = 1.0E-03
Adrenals	2.75E-08 (25 33 42)	2.28E-10
Bld wall	8.29E-09 (25 33 42)	8.39E-11
BSurface	3.27E-03 (25 33 42)	2.72E-05
Brain	2.54E-08 (25 33 42)	2.11E-10
Breast	1.69E-08 (25 33 42)	1.45E-10
ST wall	1.25E-08 (26 31 43)	1.29E-09
SI wall	1.54E-08 (28 31 41)	3.13E-09
ULI wall	2.38E-08 (35 23 42)	1.74E-08
LLI wall	4.30E-08 (42 17 41)	5.32E-08
Kidneys	1.94E-08 (25 33 42)	1.65E-10
Liver	1.17E-04 (25 33 42)	9.73E-07
Lungs	1.61E-05 (0 0 100)	1.53E-10
Ovaries	2.96E-05 (25 33 42)	2.46E-07
Pancreas	2.11E-08 (25 33 42)	1.78E-10
R Marrow	2.62E-04 (25 33 42)	2.18E-06
Skin	1.19E-08 (25 33 42)	9.97E-11
Spleen	1.19E-08 (25 33 42)	1.00E-10
Testes	2.96E-05 (25 33 42)	2.46E-07
Thymus	1.02E-08 (24 32 44)	8.18E-11
Thyroid	1.34E-08 (25 33 42)	1.10E-10
Uterus	9.27E-09 (25 33 42)	9.69E-11
Effective (ICRP60)	7.79E-05 (24 33 43)	6.38E-07

Table T–12S. Internal Dose Conversion Factors for ^{241}Am (Sv Bq^{-1})

Am-241 T1/2 = 432.2y	Inhalation	Oral
	Class W f1 = 1.0E-03	f1 = 1.0E-03
Adrenals	5.47E-09 (25 33 42)	4.62E-11
Bld wall	1.34E-09 (25 33 42)	2.29E-11
BSurface	2.17E-03 (25 33 42)	1.81E-05
Brain	2.71E-09 (25 33 42)	2.25E-11
Breast	2.67E-09 (25 33 42)	2.62E-11
ST wall	3.25E-09 (31 28 41)	1.34E-09
SI wall	4.20E-09 (36 23 41)	3.34E-09
ULI wall	1.28E-08 (46 14 40)	1.90E-08
LLI wall	3.16E-08 (52 9 39)	5.82E-08
Kidneys	4.38E-09 (25 33 42)	3.99E-11
Liver	3.91E-04 (25 33 42)	3.25E-06
Lungs	1.84E-05 (0 0 100)	3.36E-11
Ovaries	3.25E-05 (25 33 42)	2.70E-07
Pancreas	4.70E-09 (25 33 42)	4.24E-11
R Marrow	1.74E-04 (25 33 42)	1.45E-06
Skin	1.83E-09 (25 33 42)	1.61E-11
Spleen	2.03E-09 (25 33 42)	1.94E-11
Testes	3.25E-05 (25 33 42)	2.70E-07
Thymus	1.71E-09 (24 32 44)	1.36E-11
Thyroid	1.60E-09 (25 33 42)	1.32E-11
Uterus	1.47E-09 (25 33 42)	3.00E-11
Heff	7.08E-05 (24 32 44)	5.79E-07

Table T–13S. Age-Specific Ingestion DCFs for ^{238}U, Normalized to the Adult[a]

MODE	AGE	F1	EFF	ADREN	BL WALL	BRAIN	B SURF	BREAST	ST W	SI W	ULI W	LLI W	KIDNEY
S	NB	1.6E-1	110.	54.	54.	54.	180.	54.	51.	48.	35.	25.	53.
	3M	1.5E-1	74.	40.	40.	40.	120.	40.	38.	36.	27.	20.	39.
	1Y	1.0E-1	16.	15.	15.	15.	23.	15.	14.	13.	11.	8.6	11.
	5Y	7.0E-2	3.9	4.8	4.8	4.8	4.3	4.8	4.7	4.6	4.3	3.9	3.9
	10Y	8.0E-2	3.2	3.3	3.3	3.3	3.8	3.3	3.2	3.1	2.7	2.4	3.0
	15Y	9.0E-2	3.1	2.3	2.3	2.3	4.3	2.3	2.3	2.2	1.7	1.4	2.5
	20Y	5.0E-2	1.0	1.0	1.0	1.0	1.0	1.0	1.0	1.0	1.0	1.0	1.0
I	NB	6.4E-3	56.	54.	53.	54.	180.	53.	33.	25.	21.	20.	53.
	3M	6.0E-3	40.	40.	40.	40.	120.	40.	26.	20.	17.	16.	39.
	1Y	4.0E-3	11.	15.	14.	15.	23.	15.	9.4	8.6	8.0	7.4	11.
	5Y	2.8E-3	3.8	4.8	4.7	4.8	4.3	4.8	3.8	3.9	3.9	3.7	3.9
	10Y	3.2E-3	2.6	3.3	3.3	3.3	3.8	3.3	2.4	2.4	2.3	3.2	3.0
	15Y	3.6E-3	2.0	2.3	2.3	2.4	4.3	2.3	1.6	1.4	1.3	1.2	2.5
	20Y	2.0E-3	1.0	1.0	1.0	1.0	1.0	1.0	1.0	1.0	1.0	1.0	1.0

MODE	AGE	F1	LIVER	LUNGS	OVARIES	PANCR	ACT MAR	SKIN	SPLEEN	TESTES	THYMUS	THYROID	UTERUS
S	NB	1.6E-1	51.	54.	54.	54.	71.	54.	71.	54.	54.	54.	54.
	3M	1.5E-1	38.	40.	40.	40.	51.	40.	46.	40.	40.	40.	40.
	1Y	1.0E-1	13.	15.	15.	15.	9.8	15.	15.	15.	15.	15.	15.
	5Y	7.0E-2	4.4	4.8	4.8	4.8	2.4	4.8	5.0	4.8	4.8	4.8	4.8
	10Y	8.0E-2	3.3	3.3	3.3	3.3	2.1	3.3	3.8	3.3	3.3	3.3	3.3
	15Y	9.0E-2	2.5	2.4	2.3	2.3	2.0	2.3	3.1	2.3	2.3	2.3	2.3
	20Y	5.0E-2	1.0	1.0	1.0	1.0	1.0	1.0	1.0	1.0	1.0	1.0	1.0
I	NB	6.4E-3	51.	54.	52.	53.	71.	54.	71.	53.	54.	54.	53.
	3M	6.0E-3	38.	40.	39.	40.	51.	40.	46.	40.	40.	40.	40.
	1Y	4.0E-3	13.	15.	14.	15.	9.8	15.	15.	14.	15.	15.	14.
	5Y	2.8E-3	4.3	4.8	4.7	4.8	2.4	4.8	5.0	4.8	4.8	4.8	4.7
	10Y	3.2E-3	3.3	3.3	3.2	3.3	2.1	3.3	3.8	3.3	3.3	3.3	3.3
	15Y	3.6E-3	2.5	2.3	2.3	2.3	2.0	2.3	3.1	2.3	2.3	2.3	2.3
	20Y	2.0E-3	1.0	1.0	1.0	1.0	1.0	1.0	1.0	1.0	1.0	1.0	1.0

[a] Cristy et al. (1986).

Table T-14S. Age-Specific Ingestion DCFs for ^{235}U, Normalized to the Adult[a]

MODE	AGE	F1	EFF	ADREN	BL WALL	BRAIN	B SURF	BREAST	ST W	SI W	ULI W	LLI W	KIDNEY
S	NB	1.6E-1	110.	55.	55.	55.	190.	55.	53.	48.	34.	25.	55.
	3M	1.5E-1	77.	41.	41.	41.	130.	41.	39.	36.	26.	20.	41.
	1Y	1.0E-1	16.	15.	15.	15.	23.	15.	14.	13.	11.	8.5	11.
	5Y	7.0E-2	4.0	4.8	4.8	4.8	4.3	4.8	4.7	4.6	4.2	3.8	3.9
	10Y	8.0E-2	3.2	3.3	3.3	3.3	3.8	3.3	3.2	3.1	2.7	2.4	3.0
	15Y	9.0E-2	3.1	2.4	2.3	2.4	4.3	2.4	2.3	2.1	1.7	1.4	2.5
	20Y	5.0E-2	1.0	1.0	1.0	1.0	1.0	1.0	1.0	1.0	1.0	1.0	1.0
I	NB	6.4E-3	55.	55.	50.	55.	190.	53.	33.	24.	21.	19.	55.
	3M	6.0E-3	40.	41.	37.	41.	130.	39.	26.	19.	17.	16.	41.
	1Y	4.0E-3	11.	14.	13.	15.	23.	14.	9.2	8.4	7.9	7.4	11.
	5Y	2.8E-3	3.8	4.8	4.5	4.8	4.3	4.6	3.8	3.9	3.9	3.7	3.9
	10Y	3.2E-3	2.6	3.3	3.2	3.3	3.8	3.2	2.3	2.4	2.3	2.2	3.0
	15Y	3.6E-3	1.9	2.3	2.2	2.4	4.3	2.3	1.6	1.4	1.3	1.2	2.5
	20Y	2.0E-3	1.0	1.0	1.0	1.0	1.0	1.0	1.0	1.0	1.0	1.0	1.0

MODE	AGE	F1	LIVER	LUNGS	OVARIES	PANCR	ACT MAR	SKIN	SPLEEN	TESTES	THYMUS	THYROID	UTERUS
S	NB	1.6E-1	53.	55.	55.	55.	76.	55.	74.	55.	55.	55.	55.
	3M	1.5E-1	39.	41.	41.	41.	54.	41.	48.	41.	41.	41.	41.
	1Y	1.0E-1	13.	15.	14.	15.	10.	15.	15.	15.	15.	15.	15.
	5Y	7.0E-2	4.4	4.8	4.8	4.8	2.4	4.8	5.0	4.8	4.8	4.8	4.8
	10Y	8.0E-2	3.4	3.3	3.3	3.3	2.1	3.3	3.9	3.3	3.3	3.3	3.3
	15Y	9.0E-2	2.5	2.4	2.3	2.4	2.1	2.4	3.1	2.4	2.4	2.4	2.3
	20Y	5.0E-2	1.0	1.0	1.0	1.0	1.0	1.0	1.0	1.0	1.0	1.0	1.0
I	NB	6.4E-3	51.	55.	41.	53.	75.	55.	73.	54.	55.	55.	49.
	3M	6.0E-3	38.	41.	31.	40.	53.	41.	47.	40.	41.	41.	36.
	1Y	4.0E-3	13.	15.	11.	14.	9.9	15.	15.	14.	15.	15.	13.
	5Y	2.8E-3	4.4	4.8	4.1	4.7	2.4	4.8	5.0	4.8	4.8	4.8	4.5
	10Y	3.2E-3	3.3	3.3	2.8	3.3	2.1	3.3	3.8	3.3	3.3	3.3	3.1
	15Y	3.6E-3	2.4	2.4	2.0	2.3	2.0	2.3	3.1	2.3	2.4	2.4	2.2
	20Y	2.0E-3	1.0	1.0	1.0	1.0	1.0	1.0	1.0	1.0	1.0	1.0	1.0

[a] Cristy et al. (1986).

Table T–15S. Age-Specific Ingestion DCFs for ^{234}U, Normalized to the Adult[a]

MODE	AGE	F1	EFF	ADREN	BL WALL	BRAIN	B SURF	BREAST	ST W	SI W	ULI W	LLI W	KIDNEY
S	NB	1.6E-1	110.	56.	56.	56.	190.	56.	53.	49.	36.	26.	55.
	3M	1.5E-1	78.	41.	41.	41.	130.	41.	40.	37.	27.	20.	41.
	1Y	1.0E-1	16.	15.	15.	15.	23.	15.	14.	13.	11.	8.7	11.
	5Y	7.0E-2	4.0	4.8	4.8	4.8	4.3	4.8	4.7	4.6	4.3	3.9	3.9
	10Y	8.0E-2	3.2	3.4	3.4	3.4	3.8	3.4	3.2	3.2	2.8	2.4	3.0
	15Y	9.0E-2	3.1	2.4	2.4	2.4	4.3	2.4	2.3	2.2	1.8	1.5	2.5
	20Y	5.0E-2	1.0	1.0	1.0	1.0	1.0	1.0	1.0	1.0	1.0	1.0	1.0
I	NB	6.4E-3	59.	56.	56.	56.	190.	56.	34.	25.	21.	20.	55.
	3M	6.0E-3	42.	41.	41.	41.	130.	41.	26.	20.	17.	16.	41.
	1Y	4.0E-3	11.	15.	15.	15.	23.	15.	9.5	8.7	8.0	7.4	11.
	5Y	2.8E-3	3.8	4.8	4.8	4.8	4.3	4.8	3.8	3.9	3.9	3.7	3.9
	10Y	3.2E-3	2.6	3.4	3.4	3.4	3.8	3.4	2.4	2.4	2.3	2.2	3.0
	15Y	3.6E-3	2.0	2.4	2.4	2.4	4.3	2.4	1.6	1.4	1.3	1.2	2.5
	20Y	2.0E-3	1.0	1.0	1.0	1.0	1.0	1.0	1.0	1.0	1.0	1.0	1.0

MODE	AGE	F1	LIVER	LUNGS	OVARIES	PANCR	ACT MAR	SKIN	SPLEEN	TESTES	THYMUS	THYROID	UTERUS
S	NB	1.6E-1	53.	56.	56.	56.	76.	56.	74.	56.	56.	56.	56.
	3M	1.5E-1	39.	41.	41.	41.	54.	41.	48.	41.	41.	41.	41.
	1Y	1.0E-1	14.	15.	15.	15.	10.	15.	15.	15.	15.	15.	15.
	5Y	7.0E-2	4.4	4.4	4.8	4.8	2.4	4.8	5.0	4.8	4.4	4.8	4.4
	10Y	8.0E-2	3.4	3.4	3.4	3.4	2.1	3.4	3.9	3.4	3.4	3.4	3.4
	15Y	9.0E-2	2.5	2.4	2.4	2.4	2.1	2.4	3.1	2.4	2.4	2.4	2.4
	20Y	5.0E-2	1.0	1.0	1.0	1.0	1.0	1.0	1.0	1.0	1.0	1.0	1.0
I	NB	6.4E-3	53.	56.	56.	56.	76.	56.	74.	56.	56.	56.	56.
	3M	6.0E-3	39.	41.	41.	41.	54.	4.1	48.	41.	41.	41.	41.
	1Y	4.0E-3	14.	15.	15.	15.	10.	15.	15.	15.	15.	15.	15.
	5Y	2.8E-3	4.4	4.8	4.8	4.8	2.4	4.8	5.0	4.4	4.8	4.8	4.8
	10Y	3.2E-3	3.4	3.4	3.3	3.4	2.1	3.4	3.9	3.4	3.4	3.4	3.4
	15Y	3.6E-3	2.5	2.4	2.4	2.4	2.1	2.4	3.1	2.4	2.4	2.4	2.4
	20Y	2.0E-3	1.0	1.0	1.0	1.0	1.0	1.0	1.0	1.0	1.0	1.0	1.0

[a] Cristy et al. (1986).

Table T-16S. Age-Specific Ingestion DCFs for ^{232}Th, Normalized to the Adult[a]

MODE	AGE	F1	EFF	ADREN	BL WALL	BRAIN	B SURF	BREAST	ST W	SI W	ULI W	LLI W	KIDNEY
G	NB	1.0E-2	95.	160.	160.	160.	77.	160.	140.	120.	58.	34.	210.
	3M	5.0E-3	44.	73.	74.	73.	36.	73.	65.	56.	32.	22.	95.
	1Y	5.0E-4	4.0	6.4	6.4	6.3	3.3	6.4	6.5	6.8	7.4	7.3	8.1
	5Y	5.0E-4	3.1	4.5	4.5	4.5	2.7	4.5	4.4	4.3	4.1	3.8	5.5
	10Y	5.0E-4	2.6	3.6	3.6	3.6	2.5	3.6	3.3	3.2	2.7	2.3	4.0
	15Y	5.0E-4	2.4	2.6	2.6	2.6	2.3	2.6	2.4	2.2	1.6	1.4	2.8
	20Y	2.0E-4	1.0	1.0	1.0	1.0	1.0	1.0	1.0	1.0	1.0	1.0	1.0

MODE	AGE	F1	LIVER	LUNGS	OVARIES	PANCR	ACT MAR	SKIN	SPLEEN	TESTES	THYMUS	THYROID	UTERUS
G	NB	1.0E-2	240.	160.	160.	160.	170.	160.	300.	160.	160.	160.	160.
	3M	5.0E-3	110.	74.	74.	74.	76.	74.	140.	74.	74.	74.	74.
	1Y	5.0E-4	9.3	6.4	6.4	6.4	6.5	6.4	11.	6.4	6.4	6.4	6.4
	5Y	5.0E-4	5.9	4.5	4.5	4.5	4.3	4.5	6.7	4.5	4.5	4.5	4.5
	10Y	5.0E-4	4.1	3.6	3.6	3.6	3.1	3.6	4.3	3.6	3.6	3.6	3.6
	15Y	5.0E-4	2.8	2.6	2.6	2.6	2.4	2.6	2.9	2.6	2.6	2.6	2.6
	20Y	2.0E-4	1.0	1.0	1.0	1.0	1.0	1.0	1.0	1.0	1.0	1.0	1.0

[a] Cristy et al. (1986).

Table T-17S. Age-Specific Ingestion DCFs for ^{230}Th, Normalized to the Adult[a]

MODE	AGE	F1	EFF	ADREN	BL WALL	BRAIN	B SURF	BREAST	ST W	SI W	ULI W	LLI W	KIDNEY
G	NB	1.0E-2	88.	230.	230.	230.	69.	230.	170.	120.	51.	31.	280.
	3M	5.0E-3	40.	100.	100.	100.	32.	100.	78.	59.	29.	21.	120.
	1Y	5.0E-4	3.7	8.0	8.0	8.0	2.9	8.0	7.7	7.8	7.8	7.4	10.
	5Y	5.0E-4	2.8	4.7	4.7	4.7	2.4	4.7	4.3	4.2	4.0	3.7	6.1
	10Y	5.0E-4	2.4	3.1	3.1	3.1	2.3	3.1	2.8	2.7	2.4	2.2	3.9
	15Y	5.0E-4	2.2	2.3	2.3	2.3	2.2	2.3	2.0	1.8	1.4	1.3	2.7
	20Y	2.0E-4	1.0	1.0	1.0	1.0	1.0	1.0	1.0	1.0	1.0	1.0	1.0

MODE	AGE	F1	LIVER	LUNGS	OVARIES	PANCR	ACT MAR	SKIN	SPLEEN	TESTES	THYMUS	THYROID	UTERUS
G	NB	1.0E-2	320.	230.	230.	230.	200.	230.	380.	230.	230.	230.	230.
	3M	5.0E-3	140.	100.	100.	100.	87.	100.	170.	100.	100.	100.	100.
	1Y	5.0E-4	12.	8.1	8.1	8.0	7.2	8.1	13.	8.1	8.1	8.1	8.0
	5Y	5.0E-4	6.6	4.7	4.7	4.7	4.5	4.7	7.5	4.7	4.7	4.7	4.7
	10Y	5.0E-4	4.1	3.1	3.1	3.1	3.1	3.1	4.4	3.1	3.1	3.1	3.1
	15Y	5.0E-4	2.7	2.3	2.3	2.3	2.4	2.3	2.8	2.3	2.3	2.3	2.3
	20Y	2.0E-4	1.0	1.0	1.0	1.0	1.0	1.0	1.0	1.0	1.0	1.0	1.0

[a] Cristy et al. (1986).

Table T–18S. Age-Specific Ingestion DCFs for ^{228}Th, Normalized to the Adult[a]

MODE	AGE	F1	EFF	ADREN	BL WALL	BRAIN	B SURF	BREAST	ST W	SI W	ULI W	LLI W	KIDNEY
G	NB	1.0E-2	450.	150.	150.	150.	510.	150.	140.	110.	51.	27.	190.
	3M	5.0E-3	180.	71.	70.	71.	200.	70.	64.	55.	29.	19.	85.
	1Y	5.0E-4	14.	7.9	7.9	7.9	15.	7.9	7.8	7.7	7.7	7.3	8.0
	5Y	5.0E-4	6.4	4.3	4.3	4.3	6.5	4.3	4.2	4.1	4.0	3.7	4.4
	10Y	5.0E-4	3.8	2.7	2.7	2.7	4.1	2.7	2.6	2.5	2.4	2.2	3.1
	15Y	5.0E-4	2.6	1.9	1.9	1.9	2.9	1.9	1.9	1.7	1.4	1.3	2.4
	20Y	2.0E-4	1.0	1.0	1.0	1.0	1.0	1.0	1.0	1.0	1.0	1.0	1.0

MODE	AGE	F1	LIVER	LUNGS	OVARIES	PANCR	ACT MAR	SKIN	SPLEEN	TESTES	THYMUS	THYROID	UTERUS
G	NB	1.0E-2	250.	150.	150.	150.	800.	150.	390.	150.	150.	150.	150.
	3M	5.0E-3	110.	71.	69.	71.	300.	71.	160.	71.	71.	71.	70.
	1Y	5.0E-4	10.	7.9	7.9	7.9	20.	7.9	14.	7.9	7.9	7.9	7.9
	5Y	5.0E-4	5.3	4.3	4.3	4.3	9.1	4.3	7.1	4.3	4.3	4.3	4.3
	10Y	5.0E-4	3.5	2.7	2.7	2.7	4.7	2.7	4.3	2.7	2.7	2.7	2.7
	15Y	5.0E-4	2.5	1.9	1.9	1.9	2.9	1.9	2.8	1.9	1.9	1.9	1.9
	20Y	2.0E-4	1.0	1.0	1.0	1.0	1.0	1.0	1.0	1.0	1.0	1.0	1.0

[a] Cristy et al. (1986).

Table T–19S. Age-Specific Ingestion DCFs for ^{239}Pu, Normalized to the Adult[a,b]

Pu-239 Ingestion

	3 months	1 year	5 years	10 years	15 years	Adult
f1	1E-2	1E-3	1E-3	1E-3	1E-3	1E-3
Effective	14.43	1.44	1.13	1.03	1.01	1.00
Adrenals	46.15	3.77	2.31	1.46	1.08	1.00
Bl. Wall	46.15	3.77	2.31	1.46	1.08	1.00
Bone Surf.	10.00	1.00	1.00	0.94	1.06	1.00
Brain	46.15	3.77	2.31	1.46	1.08	1.00
Breast	46.15	3.77	2.31	1.46	1.08	1.00
S Wall	43.57	4.07	2.43	1.57	1.14	1.00
SI Wall	39.38	4.44	2.63	1.63	1.13	1.00
ULI Wall	26.67	6.00	3.23	1.97	1.20	1.00
LLI Wall	18.18	6.67	3.48	2.12	1.21	1.00
Kidneys	36.51	3.02	2.06	1.48	1.13	1.00
Liver	17.75	1.85	1.43	1.13	0.98	1.00
Lungs	46.15	3.77	2.38	1.54	1.08	1.00
Ovaries	9.58	1.00	1.04	1.04	1.13	1.00
Pancreas	46.15	3.77	2.31	1.46	1.08	1.00
R. Marrow	24.72	2.02	1.46	1.12	0.99	1.00
Skin	46.15	3.77	2.31	1.46	1.08	1.00
Spleen	46.15	3.77	2.31	1.46	1.08	1.00
Testes	15.00	1.46	1.29	1.13	1.13	1.00
Thymus	46.15	3.77	2.31	1.46	1.08	1.00
Thyroid	46.15	3.77	2.31	1.46	1.08	1.00
Uterus	46.15	3.77	2.31	1.46	1.08	1.00

[a] Cristy et al. (1986).

[b] Entries correspond to AMAD = 1 μm.

Table T-20S(a). Age-Specific Inhalation DCFs for ^{238}U, Normalized to the Adult[a]

MODE	AGE	AMAD	F1	EFF	ADREN	BL WALL	BRAIN	B SURF	BREAST	ST W	SI W	ULI W	LLI W	KIDNEY
D	NB	0.3	1.6E-1	34.	17.	17.	17.	58.	17.	17.	17.	17.	17.	17.
	3M	0.3	1.5E-1	25.	13.	13.	13.	42.	13.	13.	13.	13.	13.	13.
	1Y	0.3	1.0E-1	8.1	7.3	7.3	7.3	11.	7.3	7.3	7.3	7.3	7.3	5.5
	5Y	0.3	7.0E-2	2.9	3.4	3.4	3.4	3.1	3.4	3.4	3.4	3.4	3.4	2.8
	10Y	0.3	8.0E-2	2.1	2.1	2.1	2.1	2.4	2.1	2.1	2.1	2.1	2.1	1.9
	15Y	0.3	9.0E-2	1.8	1.3	1.3	1.3	2.4	1.3	1.3	1.3	1.3	1.3	1.4
	20Y	0.3	5.0E-2	1.0	1.0	1.0	1.0	1.0	1.0	1.0	1.0	1.0	1.0	1.0
D	NB	1.0	1.6E-1	35.	17.	17.	17.	59.	17.	17.	17.	17.	17.	17.
	3M	1.0	1.5E-1	26.	14.	14.	14.	43.	14.	14.	14.	14.	14.	14.
	1Y	1.0	1.0E-1	8.3	7.4	7.4	7.3	12.	7.4	7.4	7.4	7.4	7.4	5.6
	5Y	1.0	7.0E-2	2.9	3.4	3.4	3.4	3.1	3.4	3.4	3.4	3.4	3.4	2.8
	10Y	1.0	8.0E-2	2.1	2.1	2.1	2.1	2.4	2.1	2.1	2.1	2.1	2.1	1.9
	15Y	1.0	9.0E-2	1.8	1.3	1.3	1.3	2.4	1.3	1.3	1.3	1.3	1.3	1.4
	20Y	1.0	5.0E-2	1.0	1.0	1.0	1.0	1.0	1.0	1.0	1.0	1.0	1.0	1.0
D	NB	5.0	1.6E-1	37.	18.	18.	18.	62.	18.	18.	18.	18.	18.	18.
	3M	5.0	1.5E-1	27.	14.	14.	14.	44.	14.	14.	14.	14.	14.	14.
	1Y	5.0	1.0E-1	8.4	7.5	7.5	7.5	12.	7.5	7.5	7.5	7.5	7.5	5.7
	5Y	5.0	7.0E-2	2.9	3.5	3.5	3.5	3.1	3.5	3.5	3.5	3.5	3.5	2.8
	10Y	5.0	8.0E-2	2.1	2.1	2.1	2.1	2.4	2.1	2.1	2.1	2.1	2.1	1.9
	15Y	5.0	9.0E-2	1.8	1.3	1.3	1.3	2.4	1.3	1.3	1.3	1.3	1.3	1.4
	20Y	5.0	5.0E-2	1.0	1.0	1.0	1.0	1.0	1.0	1.0	1.0	1.0	1.0	1.0
W	NB	0.3	1.6E-1	18.	20.	20.	20.	64.	20.	20.	20.	19.	19.	19.
	3M	0.3	1.5E-1	14.	15.	15.	15.	43.	15.	15.	15.	15.	15.	15.
	1Y	0.3	1.0E-1	6.9	8.1	8.1	8.1	12.	8.1	8.1	8.1	8.0	8.0	6.2
	5Y	0.3	7.0E-2	3.3	3.6	3.6	3.6	3.2	3.6	3.6	3.6	3.6	3.6	2.9
	10Y	0.3	8.0E-2	2.2	2.2	2.2	2.2	2.6	2.2	2.2	2.2	2.2	2.2	2.0
	15Y	0.3	9.0E-2	1.5	1.4	1.4	1.4	2.6	1.4	1.4	1.4	1.4	1.4	1.5
	20Y	0.3	5.0E-2	1.0	1.0	1.0	1.0	1.0	1.0	1.0	1.0	1.0	1.0	1.0
W	NB	1.0	1.6E-1	20.	22.	22.	22.	72.	22.	22.	21.	21.	21.	21.
	3M	1.0	1.5E-1	15.	17.	17.	17.	49.	17.	17.	17.	16.	16.	16.
	1Y	1.0	1.0E-1	7.0	8.4	8.4	8.4	13.	8.4	8.4	8.4	8.2	8.2	6.4
	5Y	1.0	7.0E-2	3.3	3.6	3.6	3.6	3.2	3.6	3.6	3.6	3.7	3.7	2.9
	10Y	1.0	8.0E-2	2.2	2.3	2.3	2.3	2.6	2.3	2.3	2.3	2.3	2.3	2.1
	15Y	1.0	9.0E-2	1.6	1.5	1.5	1.5	2.7	1.5	1.5	1.5	1.4	1.4	1.5
	20Y	1.0	5.0E-2	1.0	1.0	1.0	1.0	1.0	1.0	1.0	1.0	1.0	1.0	1.0
W	NB	5.0	1.6E-1	26.	25.	25.	25.	84.	25.	25.	24.	23.	23.	24.
	3M	5.0	1.5E-1	20.	19.	19.	19.	58.	19.	19.	19.	18.	18.	19.
	1Y	5.0	1.0E-1	7.6	8.9	8.9	8.9	14.	8.9	8.9	8.8	8.6	8.6	6.7
	5Y	5.0	7.0E-2	3.3	3.7	3.7	3.7	3.3	3.7	3.7	3.7	3.7	3.7	3.0
	10Y	5.0	8.0E-2	2.2	2.4	2.4	2.4	2.7	2.4	2.4	2.3	2.3	2.3	2.1
	15Y	5.0	9.0E-2	1.7	1.5	1.5	1.5	2.8	1.5	1.5	1.5	1.5	1.5	1.6
	20Y	5.0	5.0E-2	1.0	1.0	1.0	1.0	1.0	1.0	1.0	1.0	1.0	1.0	1.0
Y	NB	0.3	6.4E-3	5.7	5.5	5.7	5.7	11.	5.6	5.8	6.3	8.6	8.6	4.9
	3M	0.3	6.0E-3	4.9	4.9	5.1	5.0	8.5	5.0	5.1	5.6	7.4	7.4	4.3
	1Y	0.3	4.0E-3	3.8	4.0	4.1	4.1	5.1	4.0	4.0	4.3	5.0	5.0	3.3
	5Y	0.3	2.8E-3	2.3	2.3	2.3	2.3	2.5	2.4	2.3	2.4	2.7	2.7	2.1
	10Y	0.3	3.2E-3	1.6	1.5	1.5	1.5	2.1	1.5	1.5	1.5	1.7	1.7	1.5
	15Y	0.3	3.6E-3	1.2	1.1	1.1	1.1	1.5	1.1	1.1	1.1	1.1	1.1	1.1
	20Y	0.3	2.0E-3	1.0	1.0	1.0	1.0	1.0	1.0	1.0	1.0	1.0	1.0	1.0
Y	NB	1.0	6.4E-3	5.7	6.6	6.8	6.8	15.	6.7	7.2	7.9	11.	11.	6.1
	3M	1.0	6.0E-3	4.9	5.7	5.9	5.9	12.	5.8	6.2	6.8	9.4	9.4	5.2
	1Y	1.0	4.0E-3	3.8	4.3	4.4	4.3	5.6	4.3	4.3	4.7	5.6	5.6	3.5
	5Y	1.0	2.8E-3	2.3	2.4	2.4	2.4	2.6	2.4	2.4	2.6	3.0	3.0	2.1
	10Y	1.0	3.2E-3	1.6	1.5	1.6	1.6	2.1	1.6	1.5	1.6	1.8	1.8	1.5
	15Y	1.0	3.6E-3	1.2	1.1	1.1	1.1	1.6	1.1	1.1	1.1	1.2	1.2	1.2
	20Y	1.0	2.0E-3	1.0	1.0	1.0	1.0	1.0	1.0	1.0	1.0	1.0	1.0	1.0
Y	NB	5.0	6.4E-3	5.7	11.	12.	12.	35.	12.	13.	14.	17.	17.	11.
	3M	5.0	6.0E-3	5.0	9.3	9.6	9.6	25.	9.4	10.	11.	14.	14.	9.0
	1Y	5.0	4.0E-3	3.8	5.5	5.6	5.6	8.0	5.6	5.6	6.1	7.0	7.0	4.4
	5Y	5.0	2.8E-3	2.3	2.8	2.8	2.8	2.8	2.8	2.8	3.0	3.5	3.5	2.4
	10Y	5.0	3.2E-3	1.6	1.8	1.8	1.8	2.3	1.8	1.8	1.9	2.1	2.1	1.7
	15Y	5.0	3.6E-3	1.2	1.2	1.2	1.2	1.9	1.2	1.2	1.2	1.3	1.3	1.3
	20Y	5.0	2.0E-3	1.0	1.0	1.0	1.0	1.0	1.0	1.0	1.0	1.0	1.0	1.0

[a] Cristy et al. (1986).

Table T-20S(b). Age-Specific Inhalation DCFs for ^{238}U, Normalized to the Adult[a]

MODE	AGE	AMAD	F1	LIVER	LUNGS	OVARIES	PANCR	ACT MAR	SKIN	SPLEEN	TESTES	THYMUS	THYROID	UTERUS
D	NB	0.3	1.6E-1	16.	19.	17.	17.	22.	17.	22.	17.	17.	17.	17.
	3M	0.3	1.5E-1	13.	16.	13.	13.	17.	13.	16.	13.	13.	13.	13.
	1Y	0.3	1.0E-1	6.7	7.0	7.3	7.3	4.9	7.3	7.4	7.3	7.3	7.3	7.3
	5Y	0.3	7.0E-2	3.1	3.4	3.4	3.4	1.7	3.4	3.6	3.4	3.4	3.4	3.4
	10Y	0.3	8.0E-2	2.1	2.2	2.1	2.1	1.3	2.1	2.4	2.1	2.1	2.1	2.1
	15Y	0.3	9.0E-2	1.4	1.5	1.3	1.3	1.1	1.3	1.7	1.3	1.3	1.3	1.3
	20Y	0.3	5.0E-2	1.0	1.0	1.0	1.0	1.0	1.0	1.0	1.0	1.0	1.0	1.0
D	NB	1.0	1.6E-1	16.	19.	17.	17.	23.	17.	23.	17.	17.	17.	17.
	3M	1.0	1.5E-1	13.	15.	14.	14.	17.	14.	16.	14.	14.	14.	14.
	1Y	1.0	1.0E-1	6.8	7.1	7.4	7.4	5.0	7.4	7.4	7.4	7.4	7.4	7.4
	5Y	1.0	7.0E-2	3.1	3.4	3.4	3.4	1.7	3.4	3.6	3.4	3.4	3.4	3.4
	10Y	1.0	8.0E-2	2.1	2.2	2.1	2.1	1.3	2.1	2.4	2.1	2.1	2.1	2.1
	15Y	1.0	9.0E-2	1.4	1.5	1.3	1.3	1.1	1.3	1.8	1.3	1.3	1.3	1.3
	20Y	1.0	5.0E-2	1.0	1.0	1.0	1.0	1.0	1.0	1.0	1.0	1.0	1.0	1.0
D	NB	5.0	1.6E-1	17.	19.	18.	18.	24.	18.	24.	18.	18.	18.	18.
	3M	5.0	1.5E-1	14.	15.	14.	14.	18.	14.	16.	14.	14.	14.	14.
	1Y	5.0	1.0E-1	6.9	7.3	7.5	7.5	5.1	7.5	7.6	7.5	7.5	7.5	7.5
	5Y	5.0	7.0E-2	3.2	3.4	3.5	3.5	1.7	3.5	3.6	3.5	3.5	3.5	3.5
	10Y	5.0	8.0E-2	2.1	2.2	2.1	2.1	1.3	2.1	2.4	2.1	2.1	2.1	2.1
	15Y	5.0	9.0E-2	1.4	1.4	1.3	1.3	1.2	1.3	1.8	1.3	1.3	1.3	1.3
	20Y	5.0	5.0E-2	1.0	1.0	1.0	1.0	1.0	1.0	1.0	1.0	1.0	1.0	1.0
W	NB	0.3	1.6E-1	18.	17.	20.	20.	25.	20.	25.	20.	20.	20.	20.
	3M	0.3	1.5E-1	14.	14.	15.	15.	18.	15.	17.	15.	15.	15.	15.
	1Y	0.3	1.0E-1	7.4	6.8	8.1	8.1	5.5	8.1	8.2	8.1	8.1	8.1	8.1
	5Y	0.3	7.0E-2	3.2	3.4	3.6	3.6	1.8	3.6	3.8	3.6	3.6	3.6	3.6
	10Y	0.3	8.0E-2	2.2	2.2	2.2	2.2	1.4	2.2	2.6	2.2	2.2	2.2	2.2
	15Y	0.3	9.0E-2	1.5	1.5	1.4	1.4	1.3	1.4	1.9	1.4	1.4	1.4	1.4
	20Y	0.3	5.0E-2	1.0	1.0	1.0	1.0	1.0	1.0	1.0	1.0	1.0	1.0	1.0
W	NB	1.0	1.6E-1	20.	17.	22.	22.	28.	22.	28.	22.	22.	22.	22.
	3M	1.0	1.5E-1	16.	14.	17.	17.	20.	17.	19.	17.	17.	17.	17.
	1Y	1.0	1.0E-1	7.7	6.8	8.4	8.4	5.7	8.4	8.5	8.4	8.4	8.4	8.4
	5Y	1.0	7.0E-2	3.3	3.4	3.6	3.6	1.9	3.6	3.8	3.6	3.6	3.6	3.6
	10Y	1.0	8.0E-2	2.3	2.2	2.3	2.3	1.4	2.3	2.6	2.3	2.3	2.3	2.3
	15Y	1.0	9.0E-2	1.6	1.5	1.5	1.5	1.3	1.5	1.9	1.5	1.5	1.5	1.5
	20Y	1.0	5.0E-2	1.0	1.0	1.0	1.0	1.0	1.0	1.0	1.0	1.0	1.0	1.0
W	NB	5.0	1.6E-1	23.	17.	25.	25.	32.	25.	33.	25.	25.	25.	25.
	3M	5.0	1.5E-1	18.	14.	19.	19.	24.	19.	22.	19.	19.	19.	19.
	1Y	5.0	1.0E-1	8.1	6.8	8.9	8.9	6.0	8.9	9.0	8.9	8.9	8.9	8.9
	5Y	5.0	7.0E-2	3.4	3.4	3.7	3.7	1.9	3.7	3.9	3.7	3.7	3.7	3.7
	10Y	5.0	8.0E-2	2.4	2.2	2.4	2.4	1.5	2.4	2.7	2.4	2.4	2.4	2.4
	15Y	5.0	9.0E-2	1.6	1.5	1.5	1.5	1.3	1.5	2.0	1.5	1.5	1.5	1.5
	20Y	5.0	5.0E-2	1.0	1.0	1.0	1.0	1.0	1.0	1.0	1.0	1.0	1.0	1.0
Y	NB	0.3	6.4E-3	5.1	5.7	5.7	5.5	4.8	5.6	6.2	5.7	5.3	5.6	5.7
	3M	0.3	6.0E-3	4.6	4.9	5.1	4.9	3.9	5.0	5.3	5.1	4.7	5.0	5.1
	1Y	0.3	4.0E-3	3.7	3.8	4.1	3.9	2.6	4.0	4.2	4.1	3.8	4.0	4.1
	5Y	0.3	2.8E-3	2.2	2.3	2.3	2.3	1.5	2.3	2.6	2.3	2.2	2.3	2.3
	10Y	0.3	3.2E-3	1.5	1.6	1.5	1.5	1.2	1.5	1.8	1.5	1.4	1.5	1.5
	15Y	0.3	3.6E-3	1.1	1.2	1.1	1.1	1.1	1.1	1.2	1.1	1.1	1.1	1.1
	20Y	0.3	2.0E-3	1.0	1.0	1.0	1.0	1.0	1.0	1.0	1.0	1.0	1.0	1.0
Y	NB	1.0	6.4E-3	6.1	5.7	6.8	6.6	6.4	6.7	7.7	6.8	6.3	6.7	6.8
	3M	1.0	6.0E-3	5.3	4.9	5.9	5.7	5.1	5.8	6.3	5.9	5.5	5.8	5.9
	1Y	1.0	4.0E-3	3.9	3.8	4.3	4.2	2.8	4.3	4.5	4.4	4.1	4.3	4.4
	5Y	1.0	2.8E-3	2.3	2.3	2.4	2.4	1.5	2.4	2.7	2.4	2.3	2.4	2.4
	10Y	1.0	3.2E-3	1.6	1.6	1.6	1.5	1.2	1.5	1.8	1.6	1.5	1.5	1.6
	15Y	1.0	3.6E-3	1.2	1.2	1.1	1.1	1.1	1.1	1.3	1.1	1.1	1.1	1.1
	20Y	1.0	2.0E-3	1.0	1.0	1.0	1.0	1.0	1.0	1.0	1.0	1.0	1.0	1.0
Y	NB	5.0	6.4E-3	10.	5.7	12.	11.	14.	12.	15.	12.	11.	12.	12.
	3M	5.0	6.0E-3	8.5	4.9	9.6	9.3	10.	9.5	11.	9.6	9.0	9.5	9.6
	1Y	5.0	4.0E-3	5.0	3.8	5.6	5.5	3.7	5.6	5.7	5.6	5.4	5.6	5.6
	5Y	5.0	2.8E-3	2.6	2.3	2.8	2.8	1.6	2.8	3.0	2.8	2.7	2.8	2.8
	10Y	5.0	3.2E-3	1.8	1.6	1.8	1.8	1.3	1.8	2.1	1.8	1.7	1.8	1.8
	15Y	5.0	3.6E-3	1.3	1.2	1.2	1.2	1.1	1.2	1.5	1.2	1.2	1.2	1.2
	20Y	5.0	2.0E-3	1.0	1.0	1.0	1.0	1.0	1.0	1.0	1.0	1.0	1.0	1.0

[a] Cristy et al. (1986).

Table T-21S(a). Age-Specific Inhalation DCFs for ^{235}U, Normalized to the Adult[a]

MODE	AGE	AMAD	F1	EFF	ADREN	BL WALL	BRAIN	B SURF	BREAST	ST W	SI W	ULI W	LLI W	KIDNEY
D	NB	0.3	1.6E-1	35.	17.	17.	17.	58.	17.	17.	17.	17.	17.	17.
	3M	0.3	1.5E-1	26.	13.	13.	13.	42.	13.	13.	13.	13.	13.	13.
	1Y	0.3	1.0E-1	8.2	7.3	7.3	7.3	11.	7.3	7.3	7.3	7.3	7.3	5.6
	5Y	0.3	7.0E-2	2.9	3.4	3.4	3.4	3.1	3.4	3.4	3.4	3.4	3.4	2.8
	10Y	0.3	8.0E-2	2.1	2.1	2.1	2.1	2.4	2.1	2.1	2.1	2.1	2.1	1.9
	15Y	0.3	9.0E-2	1.8	1.3	1.3	1.3	2.4	1.3	1.3	1.3	1.3	1.3	1.4
	20Y	0.3	5.0E-2	1.0	1.0	1.0	1.0	1.0	1.0	1.0	1.0	1.0	1.0	1.0
D	NB	1.0	1.6E-1	36.	17.	17.	17.	60.	17.	17.	17.	17.	17.	17.
	3M	1.0	1.5E-1	26.	14.	14.	14.	43.	14.	14.	14.	14.	14.	14.
	1Y	1.0	1.0E-1	8.3	7.4	7.4	7.4	12.	7.4	7.4	7.4	7.4	7.4	5.6
	5Y	1.0	7.0E-2	2.9	3.4	3.4	3.4	3.1	3.4	3.4	3.4	3.4	3.4	2.8
	10Y	1.0	8.0E-2	2.1	2.1	2.1	2.1	2.4	2.1	2.1	2.1	2.1	2.1	1.9
	15Y	1.0	9.0E-2	1.8	1.3	1.3	1.3	2.4	1.3	1.3	1.3	1.3	1.3	1.4
	20Y	1.0	5.0E-2	1.0	1.0	1.0	1.0	1.0	1.0	1.0	1.0	1.0	1.0	1.0
D	NB	5.0	1.6E-1	38.	18.	18.	18.	62.	18.	18.	18.	18.	18.	18.
	3M	5.0	1.5E-1	28.	14.	14.	14.	45.	14.	14.	14.	14.	14.	14.
	1Y	5.0	1.0E-1	8.5	7.5	7.5	7.5	12.	7.5	7.5	7.5	7.5	7.5	5.7
	5Y	5.0	7.0E-2	2.9	3.5	3.5	3.5	3.1	3.5	3.5	3.5	3.5	3.5	2.8
	10Y	5.0	8.0E-2	2.1	2.1	2.1	2.1	2.4	2.1	2.1	2.1	2.1	2.1	1.9
	15Y	5.0	9.0E-2	1.8	1.3	1.3	1.3	2.4	1.3	1.3	1.3	1.3	1.3	1.4
	20Y	5.0	5.0E-2	1.0	1.0	1.0	1.0	1.0	1.0	1.0	1.0	1.0	1.0	1.0
W	NB	0.3	1.6E-1	18.	20.	20.	20.	65.	20.	20.	20.	19.	18.	19.
	3M	0.3	1.5E-1	14.	15.	15.	15.	44.	15.	15.	15.	15.	15.	15.
	1Y	0.3	1.0E-1	6.9	8.1	8.1	8.1	13.	8.1	8.1	8.1	8.0	7.7	6.2
	5Y	0.3	7.0E-2	3.4	3.6	3.6	3.6	3.2	3.6	3.6	3.6	3.6	3.6	2.9
	10Y	0.3	8.0E-2	2.2	2.2	2.2	2.2	2.6	2.2	2.2	2.2	2.2	2.2	2.0
	15Y	0.3	9.0E-2	1.5	1.4	1.4	1.5	2.6	1.5	1.4	1.4	1.4	1.3	1.5
	20Y	0.3	5.0E-2	1.0	1.0	1.0	1.0	1.0	1.0	1.0	1.0	1.0	1.0	1.0
W	NB	1.0	1.6E-1	20.	22.	22.	22.	73.	22.	22.	21.	21.	20.	21.
	3M	1.0	1.5E-1	15.	17.	17.	17.	50.	17.	17.	17.	16.	16.	16.
	1Y	1.0	1.0E-1	7.1	8.4	8.4	8.4	13.	8.4	8.4	8.4	8.2	7.8	6.4
	5Y	1.0	7.0E-2	3.4	3.6	3.6	3.6	3.3	3.6	3.6	3.6	3.7	3.6	2.9
	10Y	1.0	8.0E-2	2.2	2.3	2.3	2.3	2.6	2.3	2.3	2.3	2.3	2.2	2.1
	15Y	1.0	9.0E-2	1.6	1.5	1.5	1.5	2.7	1.5	1.5	1.5	1.4	1.4	1.6
	20Y	1.0	5.0E-2	1.0	1.0	1.0	1.0	1.0	1.0	1.0	1.0	1.0	1.0	1.0
W	NB	5.0	1.6E-1	26.	25.	25.	25.	85.	25.	25.	24.	23.	21.	24.
	3M	5.0	1.5E-1	20.	19.	19.	19.	59.	19.	19.	19.	18.	17.	19.
	1Y	5.0	1.0E-1	7.6	8.9	8.9	8.9	14.	8.9	8.8	8.8	8.5	8.0	6.8
	5Y	5.0	7.0E-2	3.3	3.7	3.7	3.7	3.3	3.7	3.7	3.7	3.7	3.7	3.0
	10Y	5.0	8.0E-2	2.2	2.4	2.4	2.4	2.7	2.4	2.3	2.3	2.3	2.2	2.2
	15Y	5.0	9.0E-2	1.7	1.5	1.5	1.5	2.8	1.5	1.5	1.5	1.5	1.4	1.6
	20Y	5.0	5.0E-2	1.0	1.0	1.0	1.0	1.0	1.0	1.0	1.0	1.0	1.0	1.0
Y	NB	0.3	6.4E-3	5.7	5.6	5.7	5.7	11.	6.0	5.5	6.5	8.8	11.	5.0
	3M	0.3	6.0E-3	4.9	5.0	5.1	5.1	8.5	5.4	4.9	5.7	7.6	9.6	4.3
	1Y	0.3	4.0E-3	3.9	4.0	4.1	4.1	5.1	4.4	3.8	4.3	5.0	5.6	3.3
	5Y	0.3	2.8E-3	2.3	2.4	2.4	2.3	2.5	2.7	2.3	2.5	2.8	3.0	2.1
	10Y	0.3	3.2E-3	1.6	1.6	1.5	1.5	2.1	1.7	1.5	1.6	1.7	1.8	1.5
	15Y	0.3	3.6E-3	1.2	1.1	1.1	1.1	1.5	1.2	1.1	1.1	1.2	1.2	1.1
	20Y	0.3	2.0E-3	1.0	1.0	1.0	1.0	1.0	1.0	1.0	1.0	1.0	1.0	1.0
Y	NB	1.0	6.4E-3	5.7	6.4	6.9	6.8	16.	6.9	6.7	8.1	12.	14.	6.1
	3M	1.0	6.0E-3	5.0	5.6	6.0	5.9	12.	6.0	5.8	6.9	9.8	12.	5.2
	1Y	1.0	4.0E-3	3.9	4.2	4.4	4.4	5.7	4.6	4.1	4.7	5.7	6.2	3.5
	5Y	1.0	2.8E-3	2.3	2.5	2.4	2.4	2.6	2.7	2.3	2.6	3.0	3.2	2.1
	10Y	1.0	3.2E-3	1.6	1.6	1.6	1.6	2.1	1.7	1.5	1.6	1.8	2.0	1.5
	15Y	1.0	3.6E-3	1.2	1.2	1.1	1.1	1.6	1.2	1.1	1.2	1.2	1.2	1.2
	20Y	1.0	2.0E-3	1.0	1.0	1.0	1.0	1.0	1.0	1.0	1.0	1.0	1.0	1.0
Y	NB	5.0	6.4E-3	5.8	11.	12.	12.	36.	11.	12.	14.	17.	18.	11.
	3M	5.0	6.0E-3	5.0	8.6	9.6	9.6	25.	9.2	9.7	11.	14.	15.	9.0
	1Y	5.0	4.0E-3	3.9	5.3	5.7	5.6	8.1	5.7	5.4	6.1	7.0	7.1	4.4
	5Y	5.0	2.8E-3	2.3	2.8	2.8	2.8	2.8	3.0	2.7	3.1	3.5	3.5	2.4
	10Y	5.0	3.2E-3	1.6	1.8	1.8	1.8	2.3	1.9	1.7	1.9	2.1	2.1	1.7
	15Y	5.0	3.6E-3	1.2	1.2	1.2	1.2	1.9	1.3	1.2	1.2	1.3	1.2	1.3
	20Y	5.0	2.0E-3	1.0	1.0	1.0	1.0	1.0	1.0	1.0	1.0	1.0	1.0	1.0

[a] Cristy et al. (1986).

Table T–21S(b). Age-Specific Inhalation DCFs for ^{235}U, Normalized to the Adult[a]

MODE	AGE	AMAD	F1	LIVER	LUNGS	OVARIES	PANCR	ACT MAR	SKIN	SPLEEN	TESTES	THYMUS	THYROID	UTERUS
D	NB	0.3	1.6E-1	16.	19.	17.	17.	23.	17.	22.	17.	17.	17.	17.
	3M	0.3	1.5E-1	13.	16.	13.	13.	17.	13.	16.	13.	13.	13.	13.
	1Y	0.3	1.0E-1	6.7	7.1	7.3	7.3	5.0	7.3	7.4	7.3	7.3	7.3	7.3
	5Y	0.3	7.0E-2	3.1	3.5	3.4	3.4	1.7	3.4	3.6	3.4	3.4	3.4	3.4
	10Y	0.3	8.0E-2	2.1	2.2	2.1	2.1	1.3	2.1	2.4	2.1	2.1	2.1	2.1
	15Y	0.3	9.0E-2	1.4	1.5	1.3	1.3	1.1	1.3	1.7	1.3	1.3	1.3	1.3
	20Y	0.3	5.0E-2	1.0	1.0	1.0	1.0	1.0	1.0	1.0	1.0	1.0	1.0	1.0
D	NB	1.0	1.6E-1	16.	19.	17.	17.	23.	17.	23.	17.	17.	17.	17.
	3M	1.0	1.5E-1	13.	15.	14.	14.	18.	14.	16.	14.	14.	14.	14.
	1Y	1.0	1.0E-1	6.8	7.1	7.4	7.4	5.1	7.4	7.5	7.4	7.4	7.4	7.4
	5Y	1.0	7.0E-2	3.1	3.5	3.4	3.4	1.8	3.4	3.6	3.4	3.4	3.4	3.4
	10Y	1.0	8.0E-2	2.1	2.2	2.1	2.1	1.3	2.1	2.4	2.1	2.1	2.1	2.1
	15Y	1.0	9.0E-2	1.4	1.5	1.3	1.3	1.2	1.3	1.8	1.3	1.3	1.3	1.3
	20Y	1.0	5.0E-2	1.0	1.0	1.0	1.0	1.0	1.0	1.0	1.0	1.0	1.0	1.0
D	NB	5.0	1.6E-1	17.	19.	18.	18.	24.	18.	24.	18.	18.	18.	18.
	3M	5.0	1.5E-1	14.	15.	14.	14.	18.	14.	16.	14.	14.	14.	14.
	1Y	5.0	1.0E-1	6.9	7.3	7.5	7.5	5.2	7.5	7.6	7.5	7.5	7.5	7.5
	5Y	5.0	7.0E-2	3.2	3.5	3.5	3.5	1.8	3.5	3.6	3.5	3.5	3.5	3.5
	10Y	5.0	8.0E-2	2.1	2.2	2.1	2.1	1.4	2.1	2.5	2.1	2.1	2.1	2.1
	15Y	5.0	9.0E-2	1.4	1.4	1.3	1.3	1.2	1.3	1.8	1.3	1.3	1.3	1.3
	20Y	5.0	5.0E-2	1.0	1.0	1.0	1.0	1.0	1.0	1.0	1.0	1.0	1.0	1.0
W	NB	0.3	1.6E-1	18.	17.	20.	20.	26.	20.	25.	20.	19.	20.	20.
	3M	0.3	1.5E-1	14.	14.	15.	15.	18.	15.	17.	15.	15.	15.	15.
	1Y	0.3	1.0E-1	7.4	6.8	8.1	8.1	5.5	8.1	8.2	8.1	8.0	8.1	8.1
	5Y	0.3	7.0E-2	3.3	3.4	3.6	3.6	1.8	3.6	3.8	3.6	3.5	3.6	3.6
	10Y	0.3	8.0E-2	2.2	2.2	2.2	2.2	1.4	2.2	2.6	2.2	2.2	2.2	2.2
	15Y	0.3	9.0E-2	1.5	1.5	1.4	1.4	1.3	1.4	1.9	1.4	1.4	1.4	1.4
	20Y	0.3	5.0E-2	1.0	1.0	1.0	1.0	1.0	1.0	1.0	1.0	1.0	1.0	1.0
W	NB	1.0	1.6E-1	20.	17.	22.	22.	29.	22.	28.	22.	21.	22.	22.
	3M	1.0	1.5E-1	16.	14.	17.	17.	21.	17.	19.	17.	17.	17.	17.
	1Y	1.0	1.0E-1	7.7	6.8	8.4	8.4	5.7	8.4	8.5	8.4	8.4	8.4	8.4
	5Y	1.0	7.0E-2	3.3	3.4	3.6	3.6	1.9	3.6	3.8	3.6	3.6	3.6	3.6
	10Y	1.0	8.0E-2	2.3	2.2	2.3	2.3	1.5	2.3	2.6	2.3	2.3	2.3	2.3
	15Y	1.0	9.0E-2	1.6	1.5	1.5	1.5	1.3	1.5	2.0	1.5	1.5	1.5	1.5
	20Y	1.0	5.0E-2	1.0	1.0	1.0	1.0	1.0	1.0	1.0	1.0	1.0	1.0	1.0
W	NB	5.0	1.6E-1	23.	17.	25.	25.	33.	25.	33.	25.	25.	25.	25.
	3M	5.0	1.5E-1	18.	14.	19.	19.	24.	19.	22.	19.	19.	19.	19.
	1Y	5.0	1.0E-1	8.2	6.8	8.9	8.9	6.1	8.9	9.0	8.9	8.9	8.9	8.9
	5Y	5.0	7.0E-2	3.4	3.4	3.7	3.7	1.9	3.7	3.9	3.7	3.7	3.7	3.7
	10Y	5.0	8.0E-2	2.4	2.2	2.4	2.4	1.5	2.4	2.7	2.4	2.4	2.4	2.4
	15Y	5.0	9.0E-2	1.6	1.5	1.5	1.5	1.3	1.5	2.0	1.5	1.5	1.5	1.5
	20Y	5.0	5.0E-2	1.0	1.0	1.0	1.0	1.0	1.0	1.0	1.0	1.0	1.0	1.0
Y	NB	0.3	6.4E-3	4.8	5.6	5.8	5.2	4.8	5.4	6.0	5.7	4.5	5.8	5.8
	3M	0.3	6.0E-3	4.3	5.0	5.1	4.7	3.9	4.8	5.1	5.1	4.0	5.2	5.1
	1Y	0.3	4.0E-3	3.5	4.0	4.1	3.8	2.5	4.0	4.1	4.1	3.3	4.2	4.1
	5Y	0.3	2.8E-3	2.2	2.4	2.4	2.2	1.5	2.3	2.5	2.4	2.1	2.4	2.4
	10Y	0.3	3.2E-3	1.5	1.6	1.5	1.5	1.2	1.5	1.7	1.5	1.4	1.6	1.5
	15Y	0.3	3.6E-3	1.2	1.1	1.1	1.1	1.1	1.1	1.2	1.1	1.1	1.1	1.1
	20Y	0.3	2.0E-3	1.0	1.0	1.0	1.0	1.0	1.0	1.0	1.0	1.0	1.0	1.0
Y	NB	1.0	6.4E-3	5.4	6.4	6.9	6.1	6.4	6.3	7.3	6.9	5.2	6.8	6.9
	3M	1.0	6.0E-3	4.8	5.6	6.0	5.3	5.1	5.5	6.0	5.9	4.6	5.9	6.0
	1Y	1.0	4.0E-3	3.7	4.2	4.4	4.0	2.7	4.3	4.3	4.4	3.5	4.5	4.4
	5Y	1.0	2.8E-3	2.2	2.5	2.4	2.3	1.5	2.4	2.6	2.4	2.1	2.5	2.4
	10Y	1.0	3.2E-3	1.6	1.6	1.6	1.5	1.2	1.5	1.8	1.6	1.4	1.6	1.6
	15Y	1.0	3.6E-3	1.2	1.2	1.1	1.1	1.1	1.1	1.3	1.1	1.1	1.2	1.1
	20Y	1.0	2.0E-3	1.0	1.0	1.0	1.0	1.0	1.0	1.0	1.0	1.0	1.0	1.0
Y	NB	5.0	6.4E-3	8.8	11.	12.	10.	14.	11.	14.	12.	9.1	11.	12.
	3M	5.0	6.0E-3	7.3	8.6	9.6	8.4	11.	8.9	10.	9.7	7.5	9.4	9.6
	1Y	5.0	4.0E-3	4.5	5.3	5.6	5.1	3.7	5.5	5.5	5.7	4.6	5.6	5.7
	5Y	5.0	2.8E-3	2.5	2.8	2.8	2.6	1.6	2.8	2.9	2.8	2.5	2.8	2.8
	10Y	5.0	3.2E-3	1.7	1.8	1.8	1.7	1.3	1.8	2.0	1.8	1.6	1.8	1.8
	15Y	5.0	3.6E-3	1.3	1.2	1.2	1.2	1.2	1.2	1.5	1.2	1.2	1.2	1.2
	20Y	5.0	2.0E-3	1.0	1.0	1.0	1.0	1.0	1.0	1.0	1.0	1.0	1.0	1.0

[a] Cristy et al. (1986).

Table T-22S(a). Age-Specific Inhalation DCFs for ^{234}U, Normalized to the Adult[a]

MODE	AGE	AMAD	F1	EFF	ADREN	BL WALL	BRAIN	B SURF	BREAST	ST W	SI W	ULI W	LLI W	KIDNEY
D	NB	0.3	1.6E-1	35.	17.	17.	17.	58.	17.	17.	17.	17.	17.	17.
	3M	0.3	1.5E-1	26.	14.	14.	14.	42.	14.	14.	14.	14.	14.	13.
	1Y	0.3	1.0E-1	8.2	7.4	7.4	7.4	11.	7.4	7.4	7.4	7.4	7.4	5.6
	5Y	0.3	7.0E-2	2.9	3.4	3.4	3.4	3.1	3.4	3.4	3.4	3.4	3.4	2.8
	10Y	0.3	8.0E-2	2.1	2.1	2.1	2.1	2.4	2.1	2.1	2.1	2.1	2.1	1.9
	15Y	0.3	9.0E-2	1.8	1.3	1.3	1.3	2.4	1.3	1.3	1.3	1.3	1.3	1.4
	20Y	0.3	5.0E-2	1.0	1.0	1.0	1.0	1.0	1.0	1.0	1.0	1.0	1.0	1.0
D	NB	1.0	1.6E-1	36.	17.	17.	17.	60.	17.	17.	17.	17.	17.	17.
	3M	1.0	1.5E-1	26.	14.	14.	14.	43.	14.	14.	14.	14.	14.	14.
	1Y	1.0	1.0E-1	8.3	7.4	7.4	7.4	12.	7.4	7.4	7.4	7.4	7.4	5.6
	5Y	1.0	7.0E-2	2.9	3.5	3.5	3.5	3.1	3.5	3.5	3.5	3.5	3.5	2.8
	10Y	1.0	8.0E-2	2.1	2.1	2.1	2.1	2.4	2.1	2.1	2.1	2.1	2.1	1.9
	15Y	1.0	9.0E-2	1.8	1.3	1.3	1.3	2.4	1.3	1.3	1.3	1.3	1.3	1.4
	20Y	1.0	5.0E-2	1.0	1.0	1.0	1.0	1.0	1.0	1.0	1.0	1.0	1.0	1.0
D	NB	5.0	1.6E-1	38.	18.	18.	18.	62.	18.	18.	18.	18.	18.	18.
	3M	5.0	1.5E-1	28.	14.	14.	14.	44.	14.	14.	14.	14.	14.	14.
	1Y	5.0	1.0E-1	8.5	7.6	7.6	7.6	12.	7.6	7.6	7.6	7.6	7.5	5.7
	5Y	5.0	7.0E-2	2.9	3.5	3.5	3.5	3.1	3.5	3.5	3.5	3.5	3.5	2.8
	10Y	5.0	8.0E-2	2.1	2.1	2.1	2.1	2.4	2.1	2.1	2.1	2.1	2.1	1.9
	15Y	5.0	9.0E-2	1.8	1.3	1.3	1.3	2.4	1.3	1.3	1.3	1.3	1.3	1.4
	20Y	5.0	5.0E-2	1.0	1.0	1.0	1.0	1.0	1.0	1.0	1.0	1.0	1.0	1.0
W	NB	0.3	1.6E-1	18.	20.	20.	20.	65.	20.	20.	20.	19.	19.	19.
	3M	0.3	1.5E-1	14.	15.	15.	15.	44.	15.	15.	15.	15.	15.	15.
	1Y	0.3	1.0E-1	6.9	8.2	8.2	8.2	13.	8.2	8.2	8.1	8.1	7.8	6.2
	5Y	0.3	7.0E-2	3.4	3.6	3.6	3.6	3.2	3.6	3.6	3.6	3.6	3.6	2.9
	10Y	0.3	8.0E-2	2.2	2.2	2.2	2.2	2.6	2.2	2.2	2.2	2.2	2.2	2.0
	15Y	0.3	9.0E-2	1.5	1.4	1.4	1.4	2.6	1.4	1.4	1.4	1.4	1.4	1.5
	20Y	0.3	5.0E-2	1.0	1.0	1.0	1.0	1.0	1.0	1.0	1.0	1.0	1.0	1.0
W	NB	1.0	1.6E-1	20.	22.	22.	22.	73.	22.	22.	22.	21.	20.	21.
	3M	1.0	1.5E-1	15.	17.	17.	17.	50.	17.	17.	17.	16.	16.	16.
	1Y	1.0	1.0E-1	7.1	8.5	8.5	8.5	13.	8.5	8.4	8.4	8.3	7.9	6.4
	5Y	1.0	7.0E-2	3.4	3.6	3.6	3.6	3.3	3.6	3.6	3.6	3.7	3.6	2.9
	10Y	1.0	8.0E-2	2.2	2.3	2.3	2.3	2.6	2.3	2.3	2.3	2.3	2.2	2.1
	15Y	1.0	9.0E-2	1.6	1.5	1.5	1.5	2.7	1.5	1.5	1.5	1.4	1.4	1.6
	20Y	1.0	5.0E-2	1.0	1.0	1.0	1.0	1.0	1.0	1.0	1.0	1.0	1.0	1.0
W	NB	5.0	1.6E-1	26.	25.	25.	25.	85.	25.	25.	24.	23.	21.	24.
	3M	5.0	1.5E-1	20.	19.	19.	19.	59.	19.	19.	19.	18.	17.	19.
	1Y	5.0	1.0E-1	7.7	9.0	9.0	9.0	14.	9.0	8.9	8.9	8.6	8.4	6.8
	5Y	5.0	7.0E-2	3.3	3.7	3.7	3.7	3.3	3.7	3.7	3.7	3.7	3.7	3.0
	10Y	5.0	8.0E-2	2.2	2.4	2.4	2.4	2.7	2.4	2.4	2.4	2.3	2.3	2.2
	15Y	5.0	9.0E-2	1.7	1.5	1.5	1.5	2.8	1.5	1.5	1.5	1.5	1.4	1.6
	20Y	5.0	5.0E-2	1.0	1.0	1.0	1.0	1.0	1.0	1.0	1.0	1.0	1.0	1.0
Y	NB	0.3	6.4E-3	5.7	5.7	5.7	5.7	11.	5.7	6.0	6.3	8.6	11.	5.0
	3M	0.3	6.0E-3	4.9	5.1	5.1	5.1	8.6	5.1	5.3	5.6	7.4	9.3	4.3
	1Y	0.3	4.0E-3	3.8	4.1	4.1	4.1	5.1	4.1	4.1	4.3	4.9	5.5	3.3
	5Y	0.3	2.8E-3	2.3	2.4	2.4	2.4	2.6	2.4	2.4	2.4	2.7	3.0	2.1
	10Y	0.3	3.2E-3	1.6	1.5	1.5	1.5	2.1	1.5	1.5	1.5	1.7	1.8	1.5
	15Y	0.3	3.6E-3	1.2	1.1	1.1	1.1	1.5	1.1	1.1	1.1	1.1	1.2	1.1
	20Y	0.3	2.0E-3	1.0	1.0	1.0	1.0	1.0	1.0	1.0	1.0	1.0	1.0	1.0
Y	NB	1.0	6.4E-3	5.7	6.9	6.9	6.9	16.	6.8	7.5	8.0	11.	14.	6.1
	3M	1.0	6.0E-3	5.0	5.9	5.9	5.9	12.	5.9	6.4	6.8	9.6	12.	5.2
	1Y	1.0	4.0E-3	3.8	4.4	4.4	4.4	5.7	4.4	4.5	4.7	5.6	6.2	3.5
	5Y	1.0	2.8E-3	2.3	2.4	2.4	2.4	2.6	2.4	2.5	2.6	3.0	3.2	2.1
	10Y	1.0	3.2E-3	1.6	1.6	1.6	1.6	2.1	1.6	1.6	1.6	1.8	1.9	1.5
	15Y	1.0	3.6E-3	1.2	1.1	1.1	1.1	1.6	1.1	1.1	1.1	1.2	1.2	1.2
	20Y	1.0	2.0E-3	1.0	1.0	1.0	1.0	1.0	1.0	1.0	1.0	1.0	1.0	1.0
Y	NB	5.0	6.4E-3	5.8	12.	12.	12.	36.	12.	13.	17.	17.	18.	11.
	3M	5.0	6.0E-3	5.0	9.7	9.7	9.7	25.	9.7	11.	11.	14.	15.	9.1
	1Y	5.0	4.0E-3	3.9	5.7	5.7	5.7	8.1	5.7	5.8	6.1	7.0	7.1	4.4
	5Y	5.0	2.8E-3	2.3	2.8	2.8	2.8	2.8	2.8	2.9	3.1	3.5	3.5	2.4
	10Y	5.0	3.2E-3	1.6	1.8	1.8	1.8	2.3	1.8	1.8	1.9	2.1	2.1	1.7
	15Y	5.0	3.6E-3	1.2	1.2	1.2	1.2	1.9	1.2	1.3	1.2	1.3	1.2	1.3
	20Y	5.0	2.0E-3	1.0	1.0	1.0	1.0	1.0	1.0	1.0	1.0	1.0	1.0	1.0

[a] Cristy et al. (1986).

Table T-22S(b). Age-Specific Inhalation DCFs for ^{234}U, Normalized to the Adult[a]

MODE	AGE	AMAD	F1	LIVER	LUNGS	OVARIES	PANCR	ACT MAR	SKIN	SPLEEN	TESTES	THYMUS	THYROID	UTERUS
D	NB	0.3	1.6E-1	16.	19.	17.	17.	23.	17.	23.	17.	17.	17.	17.
	3M	0.3	1.5E-1	13.	16.	14.	14.	18.	14.	16.	14.	14.	14.	14.
	1Y	0.3	1.0E-1	6.8	7.1	7.4	7.4	5.0	7.4	7.4	7.4	7.4	7.4	7.4
	5Y	0.3	7.0E-2	3.1	3.4	3.4	3.4	1.8	3.4	3.6	3.4	3.4	3.4	3.4
	10Y	0.3	8.0E-2	2.1	2.2	2.1	2.1	1.3	2.1	2.4	2.1	2.1	2.1	2.1
	15Y	0.3	9.0E-2	1.4	1.5	1.3	1.3	1.1	1.3	1.7	1.3	1.3	1.3	1.3
	20Y	0.3	5.0E-2	1.0	1.0	1.0	1.0	1.0	1.0	1.0	1.0	1.0	1.0	1.0
D	NB	1.0	1.6E-1	17.	19.	17.	17.	24.	17.	23.	17.	17.	17.	17.
	3M	1.0	1.5E-1	13.	15.	14.	14.	18.	14.	16.	14.	14.	14.	14.
	1Y	1.0	1.0E-1	6.9	7.1	7.4	7.4	5.1	7.4	7.5	7.4	7.4	7.4	7.4
	5Y	1.0	7.0E-2	3.2	3.5	3.5	3.5	1.8	3.5	3.6	3.5	3.5	3.5	3.5
	10Y	1.0	8.0E-2	2.1	2.2	2.1	2.1	1.3	2.1	2.4	2.1	2.1	2.1	2.1
	15Y	1.0	9.0E-2	1.4	1.5	1.3	1.3	1.2	1.3	1.8	1.3	1.3	1.3	1.3
	20Y	1.0	5.0E-2	1.0	1.0	1.0	1.0	1.0	1.0	1.0	1.0	1.0	1.0	1.0
D	NB	5.0	1.6E-1	17.	19.	18.	18.	24.	18.	24.	18.	18.	18.	18.
	3M	5.0	1.5E-1	14.	15.	14.	14.	19.	14.	17.	14.	14.	14.	14.
	1Y	5.0	1.0E-1	7.0	7.3	7.6	7.6	5.2	7.6	7.6	7.6	7.6	7.6	7.6
	5Y	5.0	7.0E-2	3.2	3.5	3.5	3.5	1.8	3.5	3.6	3.5	3.5	3.5	3.5
	10Y	5.0	8.0E-2	2.1	2.2	2.1	2.1	1.4	2.1	2.5	2.1	2.1	2.1	2.1
	15Y	5.0	9.0E-2	1.4	1.4	1.3	1.3	1.2	1.3	1.8	1.3	1.3	1.3	1.3
	20Y	5.0	5.0E-2	1.0	1.0	1.0	1.0	1.0	1.0	1.0	1.0	1.0	1.0	1.0
W	NB	0.3	1.6E-1	19.	17.	20.	20.	26.	20.	25.	20.	20.	20.	20.
	3M	0.3	1.5E-1	15.	14.	15.	15.	18.	15.	17.	15.	15.	15.	15.
	1Y	0.3	1.0E-1	7.5	6.8	8.2	8.2	5.6	8.2	8.2	8.2	8.2	8.2	8.2
	5Y	0.3	7.0E-2	3.3	3.4	3.6	3.6	1.8	3.6	3.8	3.6	3.6	3.6	3.6
	10Y	0.3	8.0E-2	2.3	2.2	2.2	2.2	1.4	2.2	2.6	2.2	2.2	2.2	2.2
	15Y	0.3	9.0E-2	1.5	1.5	1.4	1.4	1.3	1.4	1.9	1.4	1.4	1.4	1.4
	20Y	0.3	5.0E-2	1.0	1.0	1.0	1.0	1.0	1.0	1.0	1.0	1.0	1.0	1.0
W	NB	1.0	1.6E-1	21.	17.	22.	22.	29.	22.	28.	22.	22.	22.	22.
	3M	1.0	1.5E-1	16.	14.	17.	17.	21.	17.	19.	17.	17.	17.	17.
	1Y	1.0	1.0E-1	7.8	6.8	8.5	8.5	5.8	8.5	8.5	8.5	8.5	8.5	8.5
	5Y	1.0	7.0E-2	3.3	3.4	3.6	3.6	1.9	3.6	3.8	3.6	3.6	3.6	3.6
	10Y	1.0	8.0E-2	2.3	2.2	2.3	2.3	1.5	2.3	2.7	2.3	2.3	2.3	2.3
	15Y	1.0	9.0E-2	1.6	1.5	1.5	1.5	1.3	1.5	2.0	1.5	1.5	1.5	1.5
	20Y	1.0	5.0E-2	1.0	1.0	1.0	1.0	1.0	1.0	1.0	1.0	1.0	1.0	1.0
W	NB	5.0	1.6E-1	24.	17.	25.	25.	33.	25.	33.	25.	25.	25.	25.
	3M	5.0	1.5E-1	18.	14.	19.	19.	25.	19.	22.	19.	19.	19.	19.
	1Y	5.0	1.0E-1	8.2	6.8	9.0	9.0	6.1	9.0	9.0	9.0	9.0	9.0	9.0
	5Y	5.0	7.0E-2	3.4	3.4	3.7	3.7	1.9	3.7	3.9	3.7	3.7	3.7	3.7
	10Y	5.0	8.0E-2	2.4	2.2	2.4	2.4	1.5	2.4	2.7	2.4	2.4	2.4	2.4
	15Y	5.0	9.0E-2	1.6	1.5	1.5	1.5	1.4	1.5	2.0	1.5	1.5	1.5	1.5
	20Y	5.0	5.0E-2	1.0	1.0	1.0	1.0	1.0	1.0	1.0	1.0	1.0	1.0	1.0
Y	NB	0.3	6.4E-3	5.4	5.7	5.7	5.7	4.8	5.7	6.3	5.7	5.7	5.7	5.7
	3M	0.3	6.0E-3	4.8	4.9	5.1	5.1	3.9	5.1	5.4	5.1	5.1	5.1	5.1
	1Y	0.3	4.0E-3	3.9	3.8	4.1	4.1	2.5	4.1	4.3	4.1	4.1	4.1	4.1
	5Y	0.3	2.8E-3	2.3	2.3	2.4	2.4	1.5	2.4	2.6	2.4	2.4	2.4	2.4
	10Y	0.3	3.2E-3	1.6	1.6	1.5	1.5	1.2	1.5	1.8	1.5	1.5	1.5	1.5
	15Y	0.3	3.6E-3	1.1	1.2	1.1	1.1	1.1	1.1	1.3	1.1	1.1	1.1	1.1
	20Y	0.3	2.0E-3	1.0	1.0	1.0	1.0	1.0	1.0	1.0	1.0	1.0	1.0	1.0
Y	NB	1.0	6.4E-3	6.5	5.7	6.9	6.9	6.6	6.9	7.9	6.9	6.9	6.9	6.9
	3M	1.0	6.0E-3	5.6	4.9	5.9	5.9	5.2	5.9	6.4	5.9	5.9	5.9	5.9
	1Y	1.0	4.0E-3	4.1	3.8	4.4	4.4	2.8	4.4	4.6	4.4	4.4	4.4	4.4
	5Y	1.0	2.8E-3	2.4	2.3	2.4	2.4	1.5	2.4	2.7	2.4	2.4	2.4	2.4
	10Y	1.0	3.2E-3	1.6	1.6	1.6	1.6	1.2	1.6	1.9	1.6	1.6	1.6	1.6
	15Y	1.0	3.6E-3	1.2	1.2	1.1	1.1	1.1	1.1	1.3	1.1	1.1	1.1	1.1
	20Y	1.0	2.0E-3	1.0	1.0	1.0	1.0	1.0	1.0	1.0	1.0	1.0	1.0	1.0
Y	NB	5.0	6.4E-3	11.	5.7	12.	12.	14.	12.	15.	12.	12.	12.	12.
	3M	5.0	6.0E-3	9.2	4.9	9.7	9.7	11.	9.7	11.	9.7	9.7	9.7	9.7
	1Y	5.0	4.0E-3	5.3	3.8	5.7	5.7	3.7	5.7	5.8	5.7	5.7	5.7	5.7
	5Y	5.0	2.8E-3	2.7	2.3	2.8	2.8	1.6	2.8	3.1	2.8	2.8	2.8	2.8
	10Y	5.0	3.2E-3	1.8	1.6	1.8	1.8	1.3	1.8	2.1	1.8	1.8	1.8	1.8
	15Y	5.0	3.6E-3	1.3	1.2	1.2	1.2	1.2	1.2	1.5	1.2	1.2	1.2	1.2
	20Y	5.0	2.0E-3	1.0	1.0	1.0	1.0	1.0	1.0	1.0	1.0	1.0	1.0	1.0

[a] Cristy et al. (1986).

Table T-23S(a). Age-Specific Inhalation DCFs for ^{232}Th, Normalized to the Adult[a]

MODE	AGE	AMAD	F1	EFF	ADREN	BL WALL	BRAIN	B SURF	BREAST	ST W	SI W	ULI W	LLI W	KIDNEY
W	NB	0.3	1.0E-2	2.2	3.2	3.2	3.2	1.6	3.2	3.2	3.2	3.2	3.3	4.1
	3M	0.3	5.0E-3	2.0	2.9	2.9	2.9	1.4	2.9	2.9	2.9	2.9	3.0	3.7
	1Y	0.3	5.0E-4	1.7	2.5	2.5	2.5	1.3	2.5	2.5	2.5	2.5	2.5	3.2
	5Y	0.3	5.0E-4	1.3	1.8	1.8	1.8	1.1	1.8	1.8	1.8	1.8	1.8	2.2
	10Y	0.3	5.0E-4	1.1	1.4	1.4	1.4	0.98	1.4	1.4	1.4	1.4	1.4	1.6
	15Y	0.3	5.0E-4	0.96	1.0	1.0	1.0	0.94	1.0	1.0	1.0	1.0	1.0	1.1
	20Y	0.3	2.0E-4	1.0	1.0	1.0	1.0	1.0	1.0	1.0	1.0	1.0	1.0	1.0
W	NB	1.0	1.0E-2	2.2	3.2	3.3	3.2	1.6	3.2	3.3	3.3	3.3	3.4	4.2
	3M	1.0	5.0E-3	2.0	2.9	3.0	2.9	1.5	2.9	3.0	3.0	0.00	3.0	3.8
	1Y	1.0	5.0E-4	1.7	2.5	2.5	2.5	1.3	2.5	2.5	2.5	2.5	2.6	3.2
	5Y	1.0	5.0E-4	1.2	1.8	1.8	1.8	1.1	1.8	1.8	1.8	1.8	1.8	2.2
	10Y	1.0	5.0E-4	1.1	1.4	1.4	1.4	0.98	1.4	1.4	1.4	1.4	1.4	1.6
	15Y	1.0	5.0E-4	0.96	1.0	1.0	1.0	0.94	1.0	1.0	1.0	1.0	1.0	1.1
	20Y	1.0	2.0E-4	1.0	1.0	1.0	1.0	1.0	1.0	1.0	1.0	1.0	1.0	1.0
W	NB	5.0	1.0E-2	2.1	3.3	3.4	3.3	1.6	3.4	3.4	3.4	3.4	3.5	4.4
	3M	5.0	5.0E-3	1.9	3.0	3.0	3.0	1.5	3.0	3.0	3.0	3.1	3.1	3.9
	1Y	5.0	5.0E-4	1.6	2.5	2.6	2.5	1.3	2.5	2.6	2.6	2.6	2.6	3.2
	5Y	5.0	5.0E-4	1.2	1.8	1.8	1.8	1.1	1.8	1.8	1.8	1.8	1.8	2.2
	10Y	5.0	5.0E-4	1.1	1.4	1.4	1.4	0.99	1.4	1.4	1.4	1.4	1.4	1.6
	15Y	5.0	5.0E-4	0.95	1.0	1.0	1.0	0.94	1.0	1.0	1.0	1.0	1.0	1.1
	20Y	5.0	2.0E-4	1.0	1.0	1.0	1.0	1.0	1.0	1.0	1.0	1.0	1.0	1.0
Y	NB	0.3	1.0E-2	2.5	2.0	2.0	2.0	1.3	2.0	2.0	2.0	2.0	2.1	2.5
	3M	0.3	5.0E-3	2.3	1.9	1.9	1.9	1.2	1.9	1.9	1.9	1.9	2.0	2.3
	1Y	0.3	5.0E-4	2.0	1.7	1.7	1.7	1.2	1.7	1.7	1.7	1.7	1.8	2.1
	5Y	0.3	5.0E-4	1.5	1.4	1.4	1.4	1.0	1.4	1.4	1.4	1.4	1.4	1.6
	10Y	0.3	5.0E-4	1.2	1.2	1.2	1.2	1.0	1.2	1.2	1.2	1.2	1.2	1.3
	15Y	0.3	5.0E-4	1.0	1.0	1.0	1.0	1.0	1.0	1.0	1.0	1.0	1.0	1.1
	20Y	0.3	2.0E-4	1.0	1.0	1.0	1.0	1.0	1.0	1.0	1.0	1.0	1.0	1.0
Y	NB	1.0	1.0E-2	2.5	2.2	2.2	2.2	1.4	2.2	2.2	2.2	2.3	2.4	2.8
	3M	1.0	5.0E-3	2.3	2.0	2.2	2.0	1.3	2.0	2.0	2.0	2.1	2.2	2.5
	1Y	1.0	5.0E-4	2.0	1.8	1.8	1.8	1.2	1.8	1.8	1.8	1.8	1.8	2.2
	5Y	1.0	5.0E-4	1.5	1.4	1.4	1.4	1.0	1.4	1.4	1.4	1.4	1.4	1.6
	10Y	1.0	5.0E-4	1.2	1.2	1.2	1.2	1.0	1.2	1.2	1.2	1.2	1.2	1.3
	15Y	1.0	5.0E-4	1.0	1.0	1.0	1.0	0.99	1.0	1.0	1.0	1.0	1.0	1.1
	20Y	1.0	2.0E-4	1.0	1.0	1.0	1.0	1.0	1.0	1.0	1.0	1.0	1.0	1.0
Y	NB	5.0	1.0E-2	2.7	3.2	3.2	3.2	1.9	3.2	3.2	3.2	3.4	3.9	4.1
	3M	5.0	5.0E-3	2.4	2.6	2.6	2.5	1.5	2.6	2.6	2.6	2.8	3.2	3.3
	1Y	5.0	5.0E-4	2.0	2.0	2.0	2.0	1.2	2.0	2.0	2.0	2.1	2.2	2.5
	5Y	5.0	5.0E-4	1.4	1.5	1.5	1.5	1.1	1.5	1.5	1.5	1.5	1.6	1.8
	10Y	5.0	5.0E-4	1.2	1.3	1.3	1.3	1.0	1.3	1.3	1.3	1.3	1.3	1.4
	15Y	5.0	5.0E-4	1.0	1.0	1.0	1.0	0.99	1.0	1.0	1.0	1.1	1.1	1.1
	20Y	5.0	2.0E-4	1.0	1.0	1.0	1.0	1.0	1.0	1.0	1.0	1.0	1.0	1.0

[a] Cristy et al. (1986).

Table T–23S(b). Age-Specific Inhalation DCFs for ^{232}Th, Normalized to the Adult[a]

MODE	AGE	AMAD	F1	LIVER	LUNGS	OVARIES	PANCR	ACT MAR	SKIN	SPLEEN	TESTES	THYMUS	THYROID	UTERUS
W	NB	0.3	1.0E-2	4.8	15.	3.2	3.2	3.3	3.2	5.9	3.2	3.2	3.2	3.2
	3M	0.3	5.0E-3	4.3	12.	2.9	2.9	3.0	2.9	5.3	2.9	2.9	2.9	2.9
	1Y	0.3	5.0E-4	3.7	6.3	2.5	2.5	2.6	2.5	4.4	2.5	2.5	2.5	2.5
	5Y	0.3	5.0E-4	2.3	3.2	1.8	1.8	1.7	1.8	2.7	1.8	1.8	1.8	1.8
	10Y	0.3	5.0E-4	1.6	2.1	1.4	1.4	1.2	1.4	1.7	1.4	1.4	1.4	1.4
	15Y	0.3	5.0E-4	1.1	1.5	1.0	1.0	0.97	1.0	1.1	1.0	1.0	1.0	1.0
	20Y	0.3	2.0E-4	1.0	1.0	1.0	1.0	1.0	1.0	1.0	1.0	1.0	1.0	1.0
W	NB	1.0	1.0E-2	4.9	14.	3.3	3.2	3.4	3.3	6.1	3.3	3.3	3.3	3.3
	3M	1.0	5.0E-3	4.4	12.	3.0	2.9	3.0	3.0	5.4	0.00	3.0	3.0	3.0
	1Y	1.0	5.0E-4	3.7	6.0	2.5	2.5	2.6	2.5	4.4	2.5	2.5	2.5	2.5
	5Y	1.0	5.0E-4	2.4	3.1	1.8	1.8	1.7	1.8	2.7	1.8	1.8	1.8	1.8
	10Y	1.0	5.0E-4	1.6	2.0	1.4	1.4	1.2	1.4	1.7	1.4	1.4	1.4	1.4
	15Y	1.0	5.0E-4	1.1	1.4	1.0	1.0	0.97	1.0	1.1	1.0	1.0	1.0	1.0
	20Y	1.0	2.0E-4	1.0	1.0	1.0	1.0	1.0	1.0	1.0	1.0	1.0	1.0	1.0
W	NB	5.0	1.0E-2	5.1	11.	3.4	3.4	3.5	3.4	6.3	3.4	3.4	3.4	3.4
	3M	5.0	5.0E-3	4.5	9.2	3.0	3.0	3.1	0.00	5.5	3.0	3.0	3.0	3.0
	1Y	5.0	5.0E-4	3.7	5.1	2.5	2.5	2.6	2.6	4.4	2.6	2.6	2.6	2.6
	5Y	5.0	5.0E-4	2.4	2.7	1.8	1.8	1.7	1.8	2.7	1.8	1.8	1.8	1.8
	10Y	5.0	5.0E-4	1.6	1.9	1.4	1.4	1.3	1.4	1.7	1.4	1.4	1.4	1.4
	15Y	5.0	5.0E-4	1.1	1.3	1.0	1.0	0.98	1.0	1.1	1.0	1.0	1.0	1.0
	20Y	5.0	2.0E-4	1.0	1.0	1.0	1.0	1.0	1.0	1.0	1.0	1.0	1.0	1.0
Y	NB	0.3	1.0E-2	2.8	2.9	2.0	2.0	2.3	2.0	3.4	2.0	2.0	2.0	2.0
	3M	0.3	5.0E-3	2.6	2.7	1.9	1.9	2.2	1.9	3.1	1.9	1.9	1.9	1.9
	1Y	0.3	5.0E-4	2.3	2.3	1.7	1.7	2.0	1.7	2.8	1.7	1.7	1.7	1.7
	5Y	0.3	5.0E-4	1.7	1.6	1.4	1.4	1.4	1.4	1.9	1.4	1.4	1.4	1.4
	10Y	0.3	5.0E-4	1.3	1.3	1.2	1.2	1.2	1.2	1.4	1.2	1.2	1.2	1.2
	15Y	0.3	5.0E-4	1.1	1.1	1.0	1.0	1.0	1.0	1.1	1.0	1.0	1.0	1.0
	20Y	0.3	2.0E-4	1.0	1.0	1.0	1.0	1.0	1.0	1.0	1.0	1.0	1.0	1.0
Y	NB	1.0	1.0E-2	3.1	2.9	2.2	2.2	2.6	2.2	3.8	2.2	2.2	2.2	2.2
	3M	1.0	5.0E-3	2.8	2.7	2.0	2.0	2.3	2.0	3.4	2.0	2.0	2.0	2.0
	1Y	1.0	5.0E-4	2.4	2.3	1.8	1.8	2.0	1.8	2.8	1.8	1.8	1.8	1.8
	5Y	1.0	5.0E-4	1.7	1.6	1.4	1.4	1.5	1.4	1.9	1.4	1.4	1.4	1.4
	10Y	1.0	5.0E-4	1.3	1.3	1.2	1.2	1.2	1.2	1.4	1.2	1.2	1.2	1.2
	15Y	1.0	5.0E-4	1.1	1.1	1.0	1.0	1.0	1.0	1.1	1.0	1.0	1.0	1.0
	20Y	1.0	2.0E-4	1.0	1.0	1.0	1.0	1.0	1.0	1.0	1.0	1.0	1.0	1.0
Y	NB	5.0	1.0E-2	4.7	2.9	3.2	3.2	3.7	3.2	5.9	3.2	3.2	3.2	3.2
	3M	5.0	5.0E-3	3.7	2.7	2.6	2.6	2.9	2.6	4.6	2.9	2.5	2.6	2.6
	1Y	5.0	5.0E-4	2.8	2.3	2.0	2.0	2.2	2.0	3.3	2.0	2.0	2.0	2.0
	5Y	5.0	5.0E-4	1.9	1.6	1.5	1.5	1.5	1.5	2.1	1.5	1.5	1.5	1.5
	10Y	5.0	5.0E-4	1.4	1.3	1.3	1.3	1.2	1.3	1.5	1.3	1.3	1.3	1.3
	15Y	5.0	5.0E-4	1.1	1.1	1.0	1.0	1.0	1.0	1.1	1.0	1.0	1.0	1.0
	20Y	5.0	2.0E-4	1.0	1.0	1.0	1.0	1.0	1.0	1.0	1.0	1.0	1.0	1.0

[a] Cristy et al. (1986).

Table T-24S(a). Age-Specific Inhalation DCFs for ^{230}Th, Normalized to the Adult[a]

MODE	AGE	AMAD	F1	EFF	ADREN	BL WALL	BRAIN	B SURF	BREAST	ST W	SI W	ULI W	LLI W	KIDNEY
W	NB	0.3	1.0E-2	2.1	4.3	4.3	4.3	1.4	4.3	4.3	4.3	4.3	4.4	5.2
	3M	0.3	5.0E-3	1.9	3.8	3.8	3.8	1.2	3.8	3.8	3.8	3.8	3.9	4.6
	1Y	0.3	5.0E-4	1.5	3.1	3.1	3.1	1.1	3.1	3.1	3.1	3.1	3.1	3.8
	5Y	0.3	5.0E-4	1.1	1.8	1.8	1.8	0.95	1.8	1.8	1.8	1.8	1.9	2.4
	10Y	0.3	5.0E-4	0.99	1.2	1.2	1.2	0.90	1.2	1.2	1.2	1.2	1.2	1.5
	15Y	0.3	5.0E-4	0.91	0.92	0.92	0.92	0.88	0.92	0.92	0.92	0.92	0.92	1.1
	20Y	0.3	2.0E-4	1.0	1.0	1.0	1.0	1.0	1.0	1.0	1.0	1.0	1.0	1.0
W	NB	1.0	1.0E-2	2.0	4.4	4.4	4.4	1.4	4.4	4.4	4.4	4.5	4.6	5.4
	3M	1.0	5.0E-3	1.8	3.9	3.9	3.9	1.3	3.9	3.9	3.9	3.9	4.0	4.7
	1Y	1.0	5.0E-4	1.5	3.1	3.1	3.1	1.1	3.1	3.1	3.1	3.1	3.2	3.9
	5Y	1.0	5.0E-4	1.1	1.8	1.8	1.8	0.95	1.8	1.8	1.8	1.9	1.9	2.4
	10Y	1.0	5.0E-4	0.98	1.2	1.2	1.2	0.90	1.2	1.2	1.2	1.2	1.3	1.6
	15Y	1.0	5.0E-4	0.91	0.91	0.91	0.91	0.88	0.91	0.91	0.91	0.92	0.92	1.1
	20Y	1.0	2.0E-4	1.0	1.0	1.0	1.0	1.0	1.0	1.0	1.0	1.0	1.0	1.0
W	NB	5.0	1.0E-2	1.9	4.6	4.6	4.6	1.4	4.6	4.6	4.6	4.7	4.9	5.6
	3M	5.0	5.0E-3	1.7	4.0	4.0	4.0	1.3	4.0	4.0	4.0	4.0	4.2	4.9
	1Y	5.0	5.0E-4	1.4	3.1	3.1	3.1	1.1	3.1	3.1	3.1	3.2	3.2	3.9
	5Y	5.0	5.0E-4	1.1	1.9	1.9	1.9	0.95	1.9	1.9	1.9	1.9	1.9	2.4
	10Y	5.0	5.0E-4	0.96	1.2	1.2	1.2	0.90	1.2	1.2	1.2	1.2	1.3	1.6
	15Y	5.0	5.0E-4	0.89	0.91	0.91	0.91	0.88	0.91	0.91	0.91	0.91	0.92	1.1
	20Y	5.0	2.0E-4	1.0	1.0	1.0	1.0	1.0	1.0	1.0	1.0	1.0	1.0	1.0
Y	NB	0.3	1.0E-2	3.4	2.5	2.5	2.5	1.1	2.5	2.5	2.5	2.6	2.8	3.1
	3M	0.3	5.0E-3	3.0	2.3	2.3	2.3	1.0	2.3	2.3	2.3	2.4	2.5	2.9
	1Y	0.3	5.0E-4	2.4	2.0	2.0	2.0	0.98	2.0	2.0	2.0	2.0	2.1	2.5
	5Y	0.3	5.0E-4	1.6	1.4	1.4	1.4	0.93	1.4	1.4	1.4	1.4	1.4	1.8
	10Y	0.3	5.0E-4	1.3	1.1	1.1	1.1	0.95	1.1	1.1	1.1	1.1	1.1	1.3
	15Y	0.3	5.0E-4	1.1	0.99	0.99	0.99	0.98	0.99	0.99	0.99	0.99	1.0	1.0
	20Y	0.3	2.0E-4	1.0	1.0	1.0	1.0	1.0	1.0	1.0	1.0	1.0	1.0	1.0
Y	NB	1.0	1.0E-2	3.4	2.9	2.9	2.9	1.2	2.9	2.9	2.9	3.1	3.4	3.6
	3M	1.0	5.0E-3	3.0	2.5	2.5	2.5	1.1	2.5	2.5	2.5	2.7	3.0	3.1
	1Y	1.0	5.0E-4	2.4	2.1	2.1	2.1	1.0	2.1	2.1	2.1	2.1	2.3	2.6
	5Y	1.0	5.0E-4	1.6	1.4	1.4	1.4	0.93	1.4	1.4	1.4	1.5	1.5	1.8
	10Y	1.0	5.0E-4	1.3	1.1	1.1	1.1	0.95	1.1	1.1	1.1	1.1	1.1	1.3
	15Y	1.0	5.0E-4	1.1	0.99	0.99	0.99	0.98	0.99	0.99	0.99	0.99	1.0	1.1
	20Y	1.0	2.0E-4	1.0	1.0	1.0	1.0	1.0	1.0	1.0	1.0	1.0	1.0	1.0
Y	NB	5.0	1.0E-2	3.4	4.5	4.5	4.5	1.6	4.5	4.6	4.6	5.1	6.2	5.6
	3M	5.0	5.0E-3	2.8	3.4	3.4	3.4	1.3	3.4	3.5	3.5	3.9	4.8	4.2
	1Y	5.0	5.0E-4	2.2	2.4	2.4	2.4	1.1	2.4	2.4	2.4	2.6	3.0	3.0
	5Y	5.0	5.0E-4	1.5	1.6	1.6	1.6	0.95	1.6	1.6	1.6	1.7	1.8	2.0
	10Y	5.0	5.0E-4	1.2	1.2	1.2	1.2	0.94	1.2	1.2	1.2	1.2	1.3	1.4
	15Y	5.0	5.0E-4	1.0	0.97	0.97	0.97	0.95	0.97	0.97	0.98	0.99	1.0	1.1
	20Y	5.0	2.0E-4	1.0	1.0	1.0	1.0	1.0	1.0	1.0	1.0	1.0	1.0	1.0

[a] Cristy et al. (1986).

Table T–24S(b). Age-Specific Inhalation DCFs for ^{230}Th, Normalized to the Adult[a]

MODE	AGE	AMAD	F1	LIVER	LUNGS	OVARIES	PANCR	ACT MAR	SKIN	SPLEEN	TESTES	THYMUS	THYROID	UTERUS
W	NB	0.3	1.0E-2	6.0	16.	4.3	4.3	3.7	4.3	7.0	4.3	4.3	4.3	4.3
	3M	0.3	5.0E-3	5.3	13.	3.8	3.8	3.3	3.8	6.2	3.8	3.8	3.8	3.8
	1Y	0.3	5.0E-4	4.4	6.6	3.1	3.1	2.8	3.1	5.0	3.1	3.1	3.1	3.1
	5Y	0.3	5.0E-4	2.6	3.3	1.8	1.8	1.8	1.8	2.9	1.8	1.8	1.8	1.8
	10Y	0.3	5.0E-4	1.6	2.1	1.2	1.2	1.2	1.2	1.7	1.2	1.2	1.2	1.2
	15Y	0.3	5.0E-4	1.1	1.5	0.92	0.92	0.97	0.92	1.1	0.92	0.92	0.92	0.92
	20Y	0.3	2.0E-4	1.0	1.0	1.0	1.0	1.0	1.0	1.0	1.0	1.0	1.0	1.0
W	NB	1.0	1.0E-2	6.2	16.	4.4	4.4	3.8	4.4	7.3	4.4	4.4	4.4	4.4
	3M	1.0	5.0E-3	5.4	13.	3.9	3.9	3.3	3.9	6.3	3.9	3.9	3.9	3.9
	1Y	1.0	5.0E-4	4.4	6.4	3.1	3.1	2.8	3.1	5.1	3.1	3.1	3.1	3.1
	5Y	1.0	5.0E-4	2.6	3.3	1.8	1.8	1.8	1.8	2.9	1.8	1.8	1.8	1.8
	10Y	1.0	5.0E-4	1.6	2.1	1.2	1.2	1.2	1.2	1.7	1.2	1.2	1.2	1.2
	15Y	1.0	5.0E-4	1.1	1.5	0.91	0.91	0.96	0.91	1.1	0.91	0.91	0.91	0.91
	20Y	1.0	2.0E-4	1.0	1.0	1.0	1.0	1.0	1.0	1.0	1.0	1.0	1.0	1.0
W	NB	5.0	1.0E-2	6.4	14.	4.6	4.6	4.0	4.6	7.6	4.6	4.6	4.6	4.6
	3M	5.0	5.0E-3	5.6	11.	4.0	4.0	3.4	4.0	6.5	4.0	4.0	4.0	4.0
	1Y	5.0	5.0E-4	4.5	5.9	3.1	3.1	2.8	3.1	5.1	3.1	3.1	3.1	3.1
	5Y	5.0	5.0E-4	2.6	3.0	1.9	1.9	1.8	1.9	2.9	1.9	1.9	1.9	1.9
	10Y	5.0	5.0E-4	1.6	2.0	1.2	1.2	1.2	1.2	1.8	1.2	1.2	1.2	1.2
	15Y	5.0	5.0E-4	1.1	1.4	0.91	0.91	0.96	0.91	1.1	0.91	0.91	0.91	0.91
	20Y	5.0	2.0E-4	1.0	1.0	1.0	1.0	1.0	1.0	1.0	1.0	1.0	1.0	1.0
Y	NB	0.3	1.0E-2	3.5	5.7	2.5	2.5	2.3	2.5	4.0	2.5	2.5	2.5	2.5
	3M	0.3	5.0E-3	3.2	4.9	2.3	2.3	2.1	2.3	3.6	2.3	2.3	2.3	2.3
	1Y	0.3	5.0E-4	2.8	3.8	2.0	2.0	1.9	2.0	3.1	2.0	2.0	2.0	2.0
	5Y	0.3	5.0E-4	1.9	2.3	1.4	1.4	1.4	1.4	2.0	1.4	1.4	1.4	1.4
	10Y	0.3	5.0E-4	1.3	1.6	1.1	1.1	1.1	1.1	1.4	1.1	1.1	1.1	1.1
	15Y	0.3	5.0E-4	1.0	1.2	0.99	0.99	1.0	0.99	1.1	0.99	0.99	0.99	0.99
	20Y	0.3	2.0E-4	1.0	1.0	1.0	1.0	1.0	1.0	1.0	1.0	1.0	1.0	1.0
Y	NB	1.0	1.0E-2	4.0	5.7	2.9	2.9	2.6	2.9	4.6	2.9	2.9	2.9	2.9
	3M	1.0	5.0E-3	3.5	4.9	2.5	2.5	2.3	2.5	4.0	2.5	2.5	2.5	2.5
	1Y	1.0	5.0E-4	2.9	3.8	2.1	2.1	2.0	2.1	3.3	2.1	2.1	2.1	2.1
	5Y	1.0	5.0E-4	1.9	2.3	1.4	1.4	1.4	1.4	2.1	1.4	1.4	1.4	1.4
	10Y	1.0	5.0E-4	1.3	1.6	1.1	1.1	1.1	1.1	1.4	1.1	1.1	1.1	1.1
	15Y	1.0	5.0E-4	1.1	1.2	0.99	0.99	1.0	0.99	1.1	0.99	0.99	0.99	0.99
	20Y	1.0	2.0E-4	1.0	1.0	1.0	1.0	1.0	1.0	1.0	1.0	1.0	1.0	1.0
Y	NB	5.0	1.0E-2	6.3	5.7	4.5	4.5	4.1	4.5	7.4	4.5	4.5	4.5	4.5
	3M	5.0	5.0E-3	4.8	4.9	3.4	3.4	3.1	3.4	5.5	3.4	3.4	3.4	3.4
	1Y	5.0	5.0E-4	3.4	3.8	2.4	2.4	2.2	2.4	3.8	2.4	2.4	2.4	2.4
	5Y	5.0	5.0E-4	2.1	2.3	1.6	1.6	1.5	1.6	2.4	1.6	1.6	1.6	1.6
	10Y	5.0	5.0E-4	1.4	1.6	1.2	1.2	1.2	1.2	1.5	1.2	1.2	1.2	1.2
	15Y	5.0	5.0E-4	1.1	1.2	0.97	0.97	1.0	0.97	1.1	0.97	0.97	0.97	0.97
	20Y	5.0	2.0E-4	1.0	1.0	1.0	1.0	1.0	1.0	1.0	1.0	1.0	1.0	1.0

[a] Cristy et al. (1986).

Table T-25S(a). Age-Specific Inhalation DCFs for ^{228}Th, Normalized to the Adult[a]

MODE	AGE	AMAD	F1	EFF	ADREN	BL WALL	BRAIN	B SURF	BREAST	ST W	SI W	ULI W	LLI W	KIDNEY
W	NB	0.3	1.0E-2	13.	3.8	3.8	3.8	9.9	3.8	3.8	3.8	3.9	4.0	4.6
	3M	0.3	5.0E-3	10.	3.4	3.4	3.4	7.7	3.4	3.4	3.4	3.4	3.5	3.9
	1Y	0.3	5.0E-4	6.1	2.8	2.8	2.8	5.5	2.8	2.8	2.8	2.8	2.9	3.1
	5Y	0.3	5.0E-4	3.0	1.7	1.7	1.7	2.6	1.7	1.7	1.7	1.7	1.7	1.9
	10Y	0.3	5.0E-4	1.8	1.0	1.0	1.0	1.6	1.0	1.0	1.0	1.0	1.1	1.3
	15Y	0.3	5.0E-4	1.2	0.81	0.81	0.81	1.1	0.81	0.81	0.81	0.81	0.81	0.99
	20Y	0.3	2.0E-4	1.0	1.0	1.0	1.0	1.0	1.0	1.0	1.0	1.0	1.0	1.0
W	NB	1.0	1.0E-2	12.	3.9	3.9	3.9	10.	3.9	3.9	3.9	4.0	4.1	4.7
	3M	1.0	5.0E-3	9.7	3.4	3.4	3.4	8.0	3.4	3.4	3.4	3.5	3.6	4.0
	1Y	1.0	5.0E-4	6.0	2.8	2.8	2.8	5.5	2.8	2.8	2.8	2.8	2.9	3.1
	5Y	1.0	5.0E-4	2.9	1.7	1.7	1.7	2.6	1.7	1.7	1.7	1.7	1.7	1.9
	10Y	1.0	5.0E-4	1.8	1.0	1.0	1.0	1.6	1.0	1.0	1.0	1.0	1.1	1.3
	15Y	1.0	5.0E-4	1.2	0.80	0.80	0.80	1.1	0.80	0.80	0.80	0.81	0.81	0.99
	20Y	1.0	2.0E-4	1.0	1.0	1.0	1.0	1.0	1.0	1.0	1.0	1.0	1.0	1.0
W	NB	5.0	1.0E-2	12.	4.0	4.0	4.0	11.	4.0	4.0	4.0	4.1	4.3	4.9
	3M	5.0	5.0E-3	9.1	3.5	3.5	3.5	8.3	3.5	3.5	3.5	3.5	3.7	4.1
	1Y	5.0	5.0E-4	5.9	2.8	2.8	2.8	5.5	2.8	2.8	2.8	2.8	2.9	3.1
	5Y	5.0	5.0E-4	2.8	1.7	1.7	1.7	2.6	1.7	1.7	1.7	1.7	1.8	1.9
	10Y	5.0	5.0E-4	1.7	1.0	1.0	1.0	1.6	1.0	1.0	1.0	1.1	1.1	1.3
	15Y	5.0	5.0E-4	1.2	0.80	0.80	0.80	1.1	0.80	0.80	0.80	0.80	0.81	0.99
	20Y	5.0	2.0E-4	1.0	1.0	1.0	1.0	1.0	1.0	1.0	1.0	1.0	1.0	1.0
Y	NB	0.3	1.0E-2	9.7	3.5	3.4	3.4	7.3	3.5	3.4	3.4	3.6	4.2	3.9
	3M	0.3	5.0E-3	8.0	3.0	2.9	2.9	5.8	3.0	3.0	3.0	3.1	3.6	3.3
	1Y	0.3	5.0E-4	5.7	2.5	2.4	2.4	4.3	2.5	2.4	2.4	2.5	2.7	2.6
	5Y	0.3	5.0E-4	3.0	1.5	1.5	1.5	2.3	1.6	1.5	1.5	1.6	1.7	1.7
	10Y	0.3	5.0E-4	2.0	1.0	0.98	0.98	1.5	1.0	0.98	0.98	1.0	1.1	1.2
	15Y	0.3	5.0E-4	1.4	0.91	0.90	0.90	1.1	0.91	0.90	0.90	0.91	0.92	1.0
	20Y	0.3	2.0E-4	1.0	1.0	1.0	1.0	1.0	1.0	1.0	1.0	1.0	1.0	1.0
Y	NB	1.0	1.0E-2	9.9	4.1	4.0	4.0	9.4	4.1	4.1	4.1	4.4	5.4	4.7
	3M	1.0	5.0E-3	8.1	3.4	3.3	3.3	6.8	3.3	3.3	3.3	3.6	4.4	3.7
	1Y	1.0	5.0E-4	5.7	2.5	2.5	2.5	4.5	2.5	2.5	2.5	2.6	3.0	2.7
	5Y	1.0	5.0E-4	3.0	1.6	1.5	1.5	2.4	1.6	1.6	1.6	1.6	1.8	1.7
	10Y	1.0	5.0E-4	2.0	1.0	1.0	1.0	1.5	1.0	1.0	1.0	1.0	1.1	1.2
	15Y	1.0	5.0E-4	1.4	0.90	0.89	0.89	1.1	0.90	0.89	0.89	0.90	0.92	1.0
	20Y	1.0	2.0E-4	1.0	1.0	1.0	1.0	1.0	1.0	1.0	1.0	1.0	1.0	1.0
Y	NB	5.0	1.0E-2	11.	6.0	6.0	6.0	15.	6.0	6.0	6.1	6.6	8.3	7.2
	3M	5.0	5.0E-3	8.4	4.4	4.3	4.3	9.7	4.4	4.4	4.4	4.9	6.4	5.0
	1Y	5.0	5.0E-4	5.7	2.8	2.8	2.8	5.2	2.8	2.8	2.8	3.0	3.7	3.0
	5Y	5.0	5.0E-4	3.0	1.7	1.7	1.7	2.6	1.7	1.7	1.7	1.8	2.1	1.8
	10Y	5.0	5.0E-4	2.0	1.1	1.1	1.1	1.6	1.1	1.1	1.1	1.1	1.3	1.3
	15Y	5.0	5.0E-4	1.4	0.87	0.86	0.86	1.1	0.87	0.87	0.87	0.88	0.93	1.0
	20Y	5.0	2.0E-4	1.0	1.0	1.0	1.0	1.0	1.0	1.0	1.0	1.0	1.0	1.0

[a] Cristy et al. (1986).

Table T-25S(b). Age-Specific Inhalation DCFs for ^{228}Th, Normalized to the Adult[a]

MODE	AGE	AMAD	F1	LIVER	LUNGS	OVARIES	PANCR	ACT MAR	SKIN	SPLEEN	TESTES	THYMUS	THYROID	UTERUS
W	NB	0.3	1.0E-2	5.9	17.	3.8	3.8	16.	3.8	8.6	3.8	3.8	3.8	3.8
	3M	0.3	5.0E-3	5.0	13.	3.4	3.4	12.	3.4	7.2	3.4	3.4	3.4	3.4
	1Y	0.3	5.0E-4	4.0	6.7	2.8	2.8	8.2	2.8	5.4	2.8	2.8	2.8	2.8
	5Y	0.3	5.0E-4	2.2	3.3	1.7	1.7	3.8	1.7	3.0	1.7	1.7	1.7	1.7
	10Y	0.3	5.0E-4	1.4	2.1	1.0	1.0	1.9	1.0	1.8	1.0	1.0	1.0	1.0
	15Y	0.3	5.0E-4	1.0	1.5	0.81	0.81	1.2	0.81	1.2	0.81	0.81	0.81	0.81
	20Y	0.3	2.0E-4	1.0	1.0	1.0	1.0	1.0	1.0	1.0	1.0	1.0	1.0	1.0
W	NB	1.0	1.0E-2	6.1	16.	3.9	3.9	17.	3.9	9.0	3.9	3.9	3.9	3.9
	3M	1.0	5.0E-3	5.1	13.	3.4	3.4	12.	3.4	7.4	3.4	3.4	3.4	3.4
	1Y	1.0	5.0E-4	4.0	6.6	2.8	2.8	8.3	2.8	5.4	2.8	2.8	2.8	2.8
	5Y	1.0	5.0E-4	2.2	3.3	1.7	1.7	3.8	1.7	3.0	1.7	1.7	1.7	1.7
	10Y	1.0	5.0E-4	1.4	2.1	1.0	1.0	1.9	1.0	1.8	1.0	1.0	1.0	1.0
	15Y	1.0	5.0E-4	1.0	1.5	0.80	0.80	1.2	0.80	1.2	0.80	0.80	0.80	0.80
	20Y	1.0	2.0E-4	1.0	1.0	1.0	1.0	1.0	1.0	1.0	1.0	1.0	1.0	1.0
W	NB	5.0	1.0E-2	6.3	15.	4.0	4.0	18.	4.0	9.4	4.0	4.0	4.0	4.0
	3M	5.0	5.0E-3	5.3	12.	3.5	3.5	13.	3.5	7.6	3.5	3.5	3.5	3.5
	1Y	5.0	5.0E-4	4.0	6.3	2.8	2.8	8.3	2.8	5.5	2.8	2.8	2.8	2.8
	5Y	5.0	5.0E-4	2.2	3.2	1.7	1.7	3.8	1.7	3.0	1.7	1.7	1.7	1.7
	10Y	5.0	5.0E-4	1.4	2.0	1.0	1.0	1.9	1.0	1.8	1.0	1.0	1.0	1.0
	15Y	5.0	5.0E-4	1.0	1.4	0.80	0.80	1.2	0.80	1.2	0.80	0.80	0.80	0.80
	20Y	5.0	2.0E-4	1.0	1.0	1.0	1.0	1.0	1.0	1.0	1.0	1.0	1.0	1.0
Y	NB	0.3	1.0E-2	4.9	9.9	3.4	3.4	11.	3.4	6.8	3.4	3.4	3.4	3.4
	3M	0.3	5.0E-3	4.1	8.2	2.9	3.0	8.6	2.9	5.6	2.9	2.9	3.0	2.9
	1Y	0.3	5.0E-4	3.2	5.7	2.4	2.4	6.3	2.4	4.4	2.4	2.4	2.4	2.4
	5Y	0.3	5.0E-4	2.0	3.1	1.5	1.5	3.2	1.5	2.6	1.5	1.5	1.5	1.5
	10Y	0.3	5.0E-4	1.3	2.0	0.98	0.99	1.7	0.98	1.6	0.98	0.99	0.99	0.98
	15Y	0.3	5.0E-4	1.0	1.4	0.90	0.91	1.1	0.90	1.1	0.90	0.91	0.90	0.90
	20Y	0.3	2.0E-4	1.0	1.0	1.0	1.0	1.0	1.0	1.0	1.0	1.0	1.0	1.0
Y	NB	1.0	1.0E-2	6.0	9.9	4.0	4.1	14.	4.0	8.4	4.0	4.0	4.1	4.0
	3M	1.0	5.0E-3	4.7	8.2	3.3	3.3	10.	3.3	6.5	3.3	3.3	3.3	3.3
	1Y	1.0	5.0E-4	3.4	5.7	2.5	2.5	6.7	2.5	4.6	2.5	2.5	2.5	2.5
	5Y	1.0	5.0E-4	2.0	3.1	1.5	1.6	3.3	1.5	2.7	1.5	1.6	1.6	1.5
	10Y	1.0	5.0E-4	1.3	2.0	1.0	1.0	1.7	1.0	1.6	1.0	1.0	1.0	1.0
	15Y	1.0	5.0E-4	1.0	1.4	0.89	0.90	1.1	0.89	1.1	0.89	0.90	0.89	0.89
	20Y	1.0	2.0E-4	1.0	1.0	1.0	1.0	1.0	1.0	1.0	1.0	1.0	1.0	1.0
Y	NB	5.0	1.0E-2	9.1	9.9	6.0	6.0	24.	6.0	13.	6.0	5.9	6.0	6.0
	3M	5.0	5.0E-3	6.3	8.2	4.3	4.3	14.	4.3	8.9	4.3	4.3	4.3	4.3
	1Y	5.0	5.0E-4	3.8	5.7	2.8	2.8	7.6	2.8	5.2	2.8	2.8	2.8	2.8
	5Y	5.0	5.0E-4	2.2	3.1	1.7	1.7	3.6	1.7	2.9	1.7	1.7	1.7	1.7
	10Y	5.0	5.0E-4	1.4	2.0	1.1	1.1	1.9	1.1	1.7	1.1	1.1	1.1	1.1
	15Y	5.0	5.0E-4	1.0	1.4	0.86	0.86	1.2	0.86	1.2	0.86	0.87	0.86	0.86
	20Y	5.0	2.0E-4	1.0	1.0	1.0	1.0	1.0	1.0	1.0	1.0	1.0	1.0	1.0

[a] Cristy et al. (1986).

Table T-26S. Age-Specific Inhalation DCFs for ^{239}Pu, Normalized to the Adult[a]

Pu-239 Class W AMAD=1 micron

	3 months	1 year	5 years	10 years	15 years	Adult
Effective	1.58	1.42	1.17	1.00	1.00	1.00
Adrenals	4.80	3.87	2.40	1.53	1.13	1.00
Bl. Wall	4.80	3.87	2.40	1.53	1.13	1.00
Bone Surf.	1.00	1.00	0.95	0.95	1.00	1.00
Brain	4.80	3.87	2.40	1.53	1.13	1.00
Breast	4.80	3.87	2.40	1.53	1.13	1.00
S Wall	4.80	3.87	2.40	1.53	1.13	1.00
SI Wall	4.80	3.87	2.40	1.53	1.13	1.00
ULI Wall	4.87	3.87	2.40	1.60	1.13	1.00
LLI Wall	4.69	3.75	2.31	1.50	1.06	1.00
Kidneys	3.68	3.03	2.11	1.45	1.12	1.00
Liver	1.88	1.83	1.42	1.15	0.98	1.00
Lungs	9.47	6.32	3.26	2.11	1.47	1.00
Ovaries	1.00	1.00	1.03	1.03	1.10	1.00
Pancreas	4.80	3.87	2.40	1.53	1.13	1.00
R. Marrow	2.45	2.00	1.45	1.09	1.00	1.00
Skin	4.80	3.87	2.40	1.53	1.13	1.00
Spleen	4.80	3.87	2.40	1.53	1.13	1.00
Testes	1.55	1.45	1.31	1.10	1.10	1.00
Thymus	4.80	3.87	2.40	1.53	1.13	1.00
Thyroid	4.80	3.87	2.40	1.53	1.13	1.00
Uterus	4.80	3.87	2.40	1.53	1.13	1.00

[a] Cristy et al. (1986).

Table T–27S. External Dose-Rate Conversion Factors for ^{238}U[a]

U-238 4.468E9 y

	Submersion (Gy-m3/Bq-y)	Immersion (Gy-m3/Bq-y)	Ground Plane (Gy-m2/Bq-y)
Effective	1.39E-10	3.46E-13	1.75E-11
Adrenals	5.78E-11	1.41E-13	3.14E-12
Bl Wall	5.62E-11	1.36E-13	1.47E-12
Brain	5.51E-11	1.33E-13	1.63E-12
Breast	4.19E-10	1.06E-12	8.03E-11
Heart	4.95E-11	1.20E-13	1.57E-12
S Wall	5.38E-11	1.30E-13	1.95E-12
SI Wall	4.38E-11	1.06E-13	1.16E-12
ULI Wall	5.19E-11	1.25E-13	1.36E-12
LLI Wall	4.79E-11	1.21E-13	2.14E-12
Kidneys	5.92E-11	1.43E-13	1.58E-12
Liver	5.59E-11	1.35E-13	1.53E-12
Lungs	6.78E-11	1.65E-13	3.27E-12
Marrow	1.15E-10	2.78E-13	4.14E-12
R Marrow	3.81E-11	9.27E-14	1.50E-12
Ovaries	4.86E-11	1.18E-13	2.06E-12
Pancreas	4.03E-11	9.78E-14	2.04E-12
B Surf	1.22E-10	2.97E-13	5.65E-12
Spleen	5.22E-11	1.26E-13	1.91E-12
Testes	1.45E-10	3.57E-13	1.50E-11
Thymus	7.43E-11	1.80E-13	1.95E-12
Thyroid	1.02E-10	2.46E-13	4.24E-12
Uterus	4.32E-11	1.05E-13	1.14E-12
Skin	6.78E-10	1.69E-12	1.43E-10

[a] USDOE (1988).

Table T–28S. External Dose-Rate Conversion Factors for ^{235}U[a]

U-235 7.038E8 y

	Submersion (Gy-m3/Bq-y)	Immersion (Gy-m3/Bq-y)	Ground Plane (Gy-m2/Bq-y)
Effective	2.07E-07	4.62E-10	4.59E-09
Adrenals	1.71E-07	3.81E-10	3.76E-09
Bl Wall	1.56E-07	3.49E-10	3.46E-09
Brain	1.67E-07	3.73E-10	3.68E-09
Breast	2.58E-07	5.76E-10	5.95E-09
Heart	1.53E-07	3.41E-10	3.38E-09
S Wall	1.54E-07	3.43E-10	3.41E-09
SI Wall	1.35E-07	3.00E-10	2.97E-09
ULI Wall	1.62E-07	3.62E-10	3.59E-09
LLI Wall	1.51E-07	3.38E-10	3.32E-09
Kidneys	1.60E-07	3.57E-10	3.51E-09
Liver	1.56E-07	3.49E-10	3.43E-09
Lungs	1.71E-07	3.81E-10	3.76E-09
Marrow	2.47E-07	5.51E-10	5.46E-09
R Marrow	1.64E-07	3.65E-10	3.59E-09
Ovaries	1.35E-07	3.03E-10	3.00E-09
Pancreas	1.31E-07	2.92E-10	2.89E-09
B Surf	2.53E-07	5.65E-10	5.59E-09
Spleen	1.55E-07	3.46E-10	3.43E-09
Testes	2.36E-07	5.27E-10	5.24E-09
Thymus	1.81E-07	4.03E-10	4.00E-09
Thyroid	2.30E-07	5.14E-10	5.08E-09
Uterus	1.38E-07	3.05E-10	3.03E-09
Skin	2.64E-07	5.81E-10	6.14E-09

[a] USDOE (1988).

Table T-29S. External Dose-Rate Conversion Factors for ^{234}U[a]

U-234 2.445E5 y

	Submersion (Gy-m3/Bq-y)	Immersion (Gy-m3/Bq-y)	Ground Plane (Gy-m2/Bq-y)
Effective	2.05E-10	5.00E-13	2.18E-11
Adrenals	9.97E-11	2.37E-13	4.49E-12
Bl Wall	9.51E-11	2.25E-13	2.49E-12
Brain	9.30E-11	2.19E-13	2.62E-12
Breast	5.54E-10	1.38E-12	9.70E-11
Heart	8.49E-11	2.00E-13	2.51E-12
S Wall	9.11E-11	2.16E-13	3.00E-12
SI Wall	7.51E-11	1.77E-13	1.96E-12
ULI Wall	9.16E-11	2.16E-13	2.37E-12
LLI Wall	8.62E-11	2.04E-13	3.22E-12
Kidneys	1.01E-10	2.40E-13	2.70E-12
Liver	9.35E-11	2.21E-13	2.52E-12
Lungs	1.11E-10	2.65E-13	4.70E-12
Marrow	1.81E-10	4.32E-13	6.43E-12
R Marrow	7.46E-11	1.75E-13	2.47E-12
Ovaries	8.19E-11	1.95E-13	3.08E-12
Pancreas	7.14E-11	1.69E-13	3.00E-12
B Surf	1.92E-10	4.57E-13	7.97E-12
Spleen	8.95E-11	2.12E-13	2.95E-12
Testes	2.19E-10	5.32E-13	1.91E-11
Thymus	1.21E-10	2.86E-13	3.19E-12
Thyroid	1.64E-10	3.92E-13	6.24E-12
Uterus	7.41E-11	1.75E-13	1.90E-12
Skin	8.84E-10	2.16E-12	1.72E-10

[a] USDOE (1988).

Table T-30S. External Dose-Rate Conversion Factors for ^{234}Th[a]

Th-234 24.10 d

	Submersion (Gy-m3/Bq-y)	Immersion (Gy-m3/Bq-y)	Ground Plane (Gy-m2/Bq-y)
Effective	1.04E-08	2.44E-11	2.69E-10
Adrenals	7.27E-09	1.71E-11	1.79E-10
Bl Wall	7.41E-09	1.74E-11	1.81E-10
Brain	7.49E-09	1.76E-11	1.83E-10
Breast	1.48E-08	3.49E-11	4.41E-10
Heart	6.78E-09	1.60E-11	1.66E-10
S Wall	7.03E-09	1.65E-11	1.72E-10
SI Wall	5.97E-09	1.41E-11	1.46E-10
ULI Wall	7.32E-09	1.72E-11	1.79E-10
LLI Wall	6.54E-09	1.53E-11	1.60E-10
Kidneys	7.62E-09	1.79E-11	1.86E-10
Liver	7.32E-09	1.72E-11	1.79E-10
Lungs	8.14E-09	1.91E-11	2.00E-10
Marrow	1.39E-08	3.27E-11	3.41E-10
R Marrow	5.70E-09	1.34E-11	1.39E-10
Ovaries	6.14E-09	1.44E-11	1.51E-10
Pancreas	5.30E-09	1.24E-11	1.30E-10
B Surf	1.43E-08	3.35E-11	3.54E-10
Spleen	6.92E-09	1.63E-11	1.70E-10
Testes	1.22E-08	2.89E-11	3.14E-10
Thymus	9.41E-09	2.21E-11	2.30E-10
Thyroid	1.21E-08	2.84E-11	2.97E-10
Uterus	6.03E-09	1.42E-11	1.47E-10
Skin	2.38E-08	4.30E-11	4.78E-10

[a] USDOE (1988).

Table T–31S. External Dose-Rate Conversion Factors for ^{232}Th[a]

Th-232 1.4405E10 y

	Submersion (Gy-m3/Bq-y)	Immersion (Gy-m3/Bq-y)	Ground Plane (Gy-m2/Bq-y)
Effective	2.50E-10	6.03E-13	1.79E-11
Adrenals	1.41E-10	3.53E-13	4.86E-12
Bl Wall	1.44E-10	3.43E-13	3.76E-12
Brain	1.40E-10	3.32E-13	3.76E-12
Breast	5.41E-10	1.34E-12	7.35E-11
Heart	1.27E-10	3.00E-13	3.46E-12
S Wall	1.35E-10	3.19E-13	3.86E-12
SI Wall	1.14E-10	2.69E-13	2.95E-12
ULI Wall	1.37E-10	3.24E-13	3.54E-12
LLI Wall	1.25E-10	2.97E-13	3.81E-12
Kidneys	1.52E-10	3.62E-13	4.00E-12
Liver	1.42E-10	3.38E-13	3.73E-12
Lungs	1.61E-10	3.84E-13	5.30E-12
Marrow	2.70E-10	6.49E-13	8.08E-12
R Marrow	1.06E-10	2.50E-13	3.05E-12
Ovaries	1.20E-10	2.84E-13	3.68E-12
Pancreas	1.01E-10	2.40E-13	3.32E-12
B Surf	2.81E-10	6.76E-13	9.19E-12
Spleen	1.32E-10	3.14E-13	3.78E-12
Testes	2.78E-10	6.73E-13	1.58E-11
Thymus	1.85E-10	4.41E-13	4.86E-12
Thyroid	2.41E-10	5.76E-13	7.38E-12
Uterus	1.12E-10	2.66E-13	2.92E-12
Skin	7.89E-10	1.90E-12	1.31E-10

[a] USDOE (1988).

Table T–32S. External Dose-Rate Conversion Factors for ^{230}Th[a]

Th-230 7.7E4 y

	Submersion (Gy-m3/Bq-y)	Immersion (Gy-m3/Bq-y)	Ground Plane (Gy-m2/Bq-y)
Effective	5.24E-10	1.24E-12	2.44E-11
Adrenals	3.43E-10	8.03E-13	9.54E-12
Bl Wall	3.46E-10	8.14E-13	8.46E-12
Brain	3.49E-10	8.16E-13	8.62E-12
Breast	9.14E-10	2.20E-12	8.24E-11
Heart	3.14E-10	7.35E-13	7.84E-12
S Wall	3.27E-10	7.68E-13	8.35E-12
SI Wall	2.81E-10	6.57E-13	6.84E-12
ULI Wall	3.35E-10	7.86E-13	8.16E-12
LLI Wall	3.05E-10	7.16E-13	8.03E-12
Kidneys	3.59E-10	8.43E-13	8.78E-12
Liver	3.43E-10	8.05E-13	8.43E-12
Lungs	3.81E-10	8.97E-13	1.04E-11
Marrow	6.32E-10	1.49E-12	1.65E-11
R Marrow	2.76E-10	6.41E-13	6.97E-12
Ovaries	2.89E-10	6.78E-13	7.62E-12
Pancreas	2.51E-10	5.86E-13	6.81E-12
B Surf	6.51E-10	1.54E-12	1.78E-11
Spleen	3.22E-10	7.57E-13	8.24E-12
Testes	6.00E-10	1.42E-12	2.34E-11
Thymus	4.38E-10	1.03E-12	1.07E-11
Thyroid	5.59E-10	1.32E-12	1.48E-11
Uterus	2.81E-10	6.59E-13	6.86E-12
Skin	1.09E-09	2.66E-12	1.39E-10

[a] USDOE (1988).

Table T–33S. External Dose-Rate Conversion Factors for ^{228}Th[a]

Th-228 1.9132 y

	Submersion (Gy-m3/Bq-y)	Immersion (Gy-m3/Bq-y)	Ground Plane (Gy-m2/Bq-y)
Effective	2.65E-09	6.08E-12	7.43E-11
Adrenals	2.00E-09	4.57E-12	4.73E-11
Bl Wall	1.92E-09	4.41E-12	4.43E-11
Brain	2.01E-09	4.59E-12	4.65E-11
Breast	3.70E-09	8.57E-12	1.54E-10
Heart	1.83E-09	4.19E-12	4.21E-11
S Wall	1.86E-09	4.27E-12	4.32E-11
SI Wall	1.62E-09	3.68E-12	3.73E-11
ULI Wall	1.95E-09	4.46E-12	4.51E-11
LLI Wall	1.78E-09	4.08E-12	4.16E-11
Kidneys	1.97E-09	4.49E-12	4.54E-11
Liver	1.92E-09	4.38E-12	4.43E-11
Lungs	2.11E-09	4.81E-12	5.00E-11
Marrow	3.32E-09	7.59E-12	7.78E-11
R Marrow	1.76E-09	4.00E-12	4.05E-11
Ovaries	1.64E-09	3.76E-12	3.84E-11
Pancreas	1.50E-09	3.43E-12	3.54E-11
B Surf	3.41E-09	7.81E-12	8.11E-11
Spleen	1.86E-09	4.24E-12	4.32E-11
Testes	3.05E-09	7.00E-12	8.03E-11
Thymus	2.33E-09	5.32E-12	5.38E-11
Thyroid	2.97E-09	6.81E-12	7.00E-11
Uterus	1.64E-09	3.73E-12	3.78E-11
Skin	4.14E-09	9.16E-12	2.16E-10

[a] USDOE (1988).

Table T–34S. External Dose-Rate Conversion Factors for ^{239}Pu[a]

Pu-239 23,131 y

	Submersion (Gy-m3/Bq-y)	Immersion (Gy-m3/Bq-y)	Ground Plane (Gy-m2/Bq-y)
Effective	1.10E-10	2.62E-13	1.02E-11
Adrenals	6.30E-11	1.45E-13	2.41E-12
Bl Wall	5.54E-11	1.26E-13	1.25E-12
Brain	5.92E-11	1.35E-13	1.46E-12
Breast	2.70E-11	6.65E-13	4.38E-11
Heart	5.49E-11	1.25E-13	1.42E-12
S Wall	5.59E-11	1.28E-13	1.63E-12
SI Wall	4.68E-11	1.07E-13	1.08E-12
ULI Wall	5.84E-11	1.33E-13	1.32E-12
LLI Wall	5.49E-11	1.26E-13	1.76E-12
Kidneys	5.62E-11	1.29E-13	1.31E-12
Liver	5.54E-11	1.26E-13	1.31E-12
Lungs	6.54E-11	1.51E-13	2.42E-12
Marrow	1.03E-10	2.36E-13	3.24E-12
R Marrow	5.27E-11	1.21E-13	1.51E-12
Ovaries	4.97E-11	1.14E-13	1.62E-12
Pancreas	4.68E-11	1.08E-13	1.66E-12
B Surf	1.08E-11	2.49E-13	3.97E-12
Spleen	5.62E-11	1.29E-13	1.63E-12
Testes	1.17E-10	2.76E-13	9.35E-12
Thymus	6.73E-11	1.54E-13	1.53E-12
Thyroid	9.16E-11	2.11E-13	3.14E-12
Uterus	4.76E-11	1.09E-13	1.08E-12
Skin	3.92E-10	9.18E-13	7.57E-11

[a] USDOE (1988).

Table T–35S. External Dose-Rate Conversion Factors for ^{237}Np[a]

Np-237	2.14E6 y		
	Submersion (Gy-m3/Bq-y)	Immersion (Gy-m3/Bq-y)	Ground Plane (Gy-m2/Bq-y)
Effective	3.08E-08	7.16E-11	8.68E-10
Adrenals	2.19E-08	5.08E-11	5.43E-10
Bl Wall	2.17E-08	5.03E-11	5.30E-10
Brain	2.21E-08	5.11E-11	5.27E-10
Breast	4.49E-08	1.05E-10	1.66E-09
Heart	2.02E-08	4.68E-11	4.84E-10
S Wall	2.07E-08	4.81E-11	5.05E-10
SI Wall	1.77E-08	4.11E-11	4.24E-10
ULI Wall	2.19E-08	5.08E-11	5.32E-10
LLI Wall	1.96E-08	4.54E-11	4.78E-10
Kidneys	2.26E-08	5.27E-11	5.70E-10
Liver	2.14E-08	4.95E-11	5.19E-10
Lungs	2.38E-08	5.54E-11	5.92E-10
Marrow	3.95E-08	9.14E-11	9.70E-10
R Marrow	1.81E-08	4.19E-11	4.35E-10
Ovaries	1.82E-08	4.22E-11	4.49E-10
Pancreas	1.62E-08	3.76E-11	3.97E-10
B Surf	4.05E-08	9.41E-11	1.01E-09
Spleen	2.06E-08	4.78E-11	5.00E-10
Testes	3.62E-08	8.43E-11	1.00E-09
Thymus	2.68E-08	6.22E-11	6.54E-10
Thyroid	3.49E-08	8.11E-11	8.78E-10
Uterus	1.78E-08	4.14E-11	4.24E-10
Skin	4.57E-08	1.05E-11	2.04E-09

[a] USDOE (1988).

Table T–36S. External Dose-Rate Conversion Factors for ^{241}Am[a]

Am-241	432.2 y		
	Submersion (Gy-m3/Bq-y)	Immersion (Gy-m3/Bq-y)	Ground Plane (Gy-m2/Bq-y)
Effective	2.52E-08	6.19E-11	7.95E-10
Adrenals	1.51E-08	3.70E-11	4.41E-10
Bl Wall	1.73E-08	4.24E-11	4.95E-10
Brain	1.58E-08	3.86E-11	4.51E-10
Breast	3.97E-08	9.76E-11	1.50E-09
Heart	1.40E-08	3.43E-11	4.03E-10
S Wall	1.54E-08	3.76E-11	4.43E-10
SI Wall	1.30E-08	3.19E-11	3.70E-10
ULI Wall	1.54E-08	3.78E-11	4.41E-10
LLI Wall	1.36E-08	3.32E-11	3.92E-10
Kidneys	1.87E-08	4.57E-11	5.35E-10
Liver	1.68E-08	4.14E-11	4.81E-10
Lungs	1.87E-08	4.57E-11	5.43E-10
Marrow	3.55E-08	8.22E-11	9.68E-10
R Marrow	1.01E-08	2.47E-11	2.92E-10
Ovaries	1.37E-08	3.35E-11	3.95E-10
Pancreas	1.05E-08	2.56E-11	3.05E-10
B Surf	3.43E-08	8.43E-11	9.97E-10
Spleen	1.48E-08	3.62E-11	4.24E-10
Testes	3.11E-08	7.62E-11	9.57E-10
Thymus	2.31E-08	5.65E-11	6.57E-10
Thyroid	2.97E-08	7.27E-11	8.57E-10
Uterus	1.26E-08	3.08E-11	3.59E-10
Skin	3.81E-08	9.35E-11	1.73E-09

[a] USDOE (1988).

Table T–37S. External Dose-Rate Conversion Factors (Gy y^{-1}) in Air above Ground for Uniform Slab Sources between the Ground Surface and Different Depths in Soil[a]

	Emitted photon energy (MeV)												
	0.010	0.015	0.020	0.030	0.040	0.050	0.060	0.080	0.100	0.150	0.200	0.300	0.400
Depth (cm)													
0.5	1.46E-8	5.52E-7	1.79E-6	3.42E-6	3.83E-6	4.13E-6	4.73E-6	6.65E-6	9.60E-6	1.68E-5	2.40E-5	3.97E-5	5.37E-5
1		5.54E-7	1.92E-6	4.64E-6	6.03E-6	7.04E-6	8.44E-6	1.25E-5	1.84E-5	3.28E-5	4.69E-5	7.81E-5	1.06E-4
2			1.93E-6	5.20E-6	7.87E-6	1.02E-5	1.30E-5	2.05E-5	3.12E-5	5.72E-5	8.19E-5	1.38E-4	1.87E-4
3				5.28E-6	8.51E-6	1.17E-5	1.56E-5	2.59E-5	4.03E-5	7.56E-5	1.08E-4	1.85E-4	2.52E-4
4				5.29E-6	8.77E-6	1.25E-5	1.73E-5	2.96E-5	4.71E-5	9.00E-5	1.29E-4	2.24E-4	3.05E-4
5					8.87E-6	1.30E-5	1.83E-5	3.24E-5	5.22E-5	1.01E-4	1.46E-4	2.55E-4	3.49E-4
7.5					8.93E-6	1.34E-5	1.96E-5	3.64E-5	6.05E-5	1.21E-4	1.76E-4	3.15E-4	4.33E-4
10					8.94E-6	1.35E-5	2.01E-5	3.83E-5	6.49E-5	1.34E-4	1.95E-4	3.54E-4	4.91E-4
15						1.36E-5	2.03E-5	3.97E-5	6.86E-5	1.45E-4	2.14E-4	4.00E-4	5.61E-4
20								4.00E-5	6.97E-5	1.50E-4	2.21E-4	4.21E-4	5.96E-4
25								4.01E-5	7.01E-5	1.52E-4	2.24E-4	4.32E-4	6.15E-4
30									7.02E-5	1.52E-4	2.26E-4	4.37E-4	6.24E-4
40										1.53E-4	2.26E-4	4.41E-4	6.32E-4
50											2.27E-4	4.42E-4	6.34E-4
60													6.35E-4

	Emitted photon energy (MeV)										
	0.500	0.600	0.800	1.000	1.500	2.000	3.000	4.000	5.000	6.000	8.000	10.000
Depth (cm)												
0.5	6.66E-5	7.89E-5	1.02E-4	1.22E-4	1.66E-4	2.05E-4	2.72E-4	3.32E-4	3.89E-4	4.24E-4	5.48E-4	6.53E-4
1	1.31E-4	1.55E-4	2.00E-4	2.39E-4	3.26E-4	4.03E-4	5.36E-4	6.55E-4	7.68E-4	8.74E-4	1.08E-3	1.29E-3
2	2.32E-4	2.75E-4	3.55E-4	4.25E-4	5.80E-4	7.19E-4	9.59E-4	1.17E-3	1.38E-3	1.57E-3	1.95E-3	2.32E-3
3	3.13E-4	3.71E-4	4.79E-4	5.73E-4	7.85E-4	9.74E-4	1.30E-3	1.60E-3	1.88E-3	2.14E-3	2.66E-3	3.17E-3
4	3.79E-4	4.50E-4	5.82E-4	6.98E-4	9.58E-4	1.19E-3	1.60E-3	1.96E-3	2.31E-3	2.63E-3	3.27E-3	3.90E-3
5	4.35E-4	5.17E-4	6.70E-4	8.05E-4	1.11E-3	1.38E-3	1.86E-3	2.28E-3	2.69E-3	3.07E-3	3.81E-3	4.54E-3
7.5	5.43E-4	6.47E-4	8.43E-4	1.02E-3	1.41E-3	1.77E-3	2.39E-3	2.95E-3	3.47E-3	3.97E-3	4.94E-3	5.90E-3
10	6.18E-4	7.40E-4	9.70E-4	1.17E-3	1.64E-3	2.06E-3	2.81E-3	3.48E-3	4.10E-3	4.70E-3	5.85E-3	6.98E-3
15	7.12E-4	8.58E-4	1.14E-3	1.39E-3	1.96E-3	2.49E-3	3.42E-3	4.27E-3	5.05E-3	5.80E-3	7.24E-3	8.65E-3
20	7.62E-4	9.23E-4	1.23E-3	1.51E-3	2.16E-3	2.77E-3	3.85E-3	4.83E-3	5.73E-3	6.60E-3	8.26E-3	9.88E-3
25	7.89E-4	9.60E-4	1.29E-3	1.59E-3	2.30E-3	2.97E-3	4.16E-3	5.24E-3	6.24E-3	7.20E-3	9.03E-3	1.08E-2
30	8.04E-4	9.81E-4	1.32E-3	1.64E-3	2.39E-3	3.10E-3	4.38E-3	5.55E-3	6.63E-3	7.66E-3	9.63E-3	1.15E-2
40	8.17E-4	1.00E-3	1.36E-3	1.69E-3	2.50E-3	3.27E-3	4.67E-3	5.96E-3	7.15E-3	8.30E-3	1.05E-2	1.26E-2
50	8.21E-4	1.01E-3	1.37E-3	1.72E-3	2.54E-3	3.35E-3	4.83E-3	6.20E-3	7.47E-3	8.70E-3	1.10E-2	1.32E-2
60	8.23E-4		1.38E-3	1.72E-3	2.57E-3	3.39E-3	4.93E-3	6.35E-3	7.67E-3	8.95E-3	1.14E-2	1.37E-2
80				1.73E-3	2.58E-3	3.43E-3	5.01E-3	6.50E-3	7.88E-3	9.23E-3	1.18E-2	1.42E-2
100					2.59E-3	3.44E-3	5.04E-3	6.55E-3	7.97E-3	9.34E-3	1.19E-2	1.44E-2
120							5.05E-3	6.57E-3	8.00E-3	9.40E-3	1.20E-2	1.45E-2
140								6.58E-3	8.02E-3	9.42E-3	1.21E-2	1.46E-2
160								6.59E-3		9.43E-3		
180										9.44E-3		

[a] Kocher and Sjoreen (1985).

Table T–38S. Radiation Doses to Embryo/Fetus per μCi of ^{238}U Introduced into Maternal Transfer Compartment (Blood)[a]

Days of gestation at introduction	Dose (rad) to embryo/fetus during indicated gestation periods (days)									
	0–30	31–60	61–90	91–120	121–150	151–180	181–210	211–240	241–270	0–270
0	*	*	*	*	*	*	*	*	*	*
31		1.23E-3	2.01E-5	4.59E-6	1.04E-6	4.38E-7	2.36E-7	1.51E-7	1.08E-7	1.26E-3
61			3.75E-3	6.86E-4	1.64E-4	6.83E-5	3.70E-5	2.37E-5	1.69E-5	4.75E-3
91				5.49E-3	1.32E-3	5.49E-4	2.98E-4	1.90E-4	1.36E-4	7.98E-3
121					7.06E-3	2.83E-3	1.55E-3	9.91E-4	7.08E-4	1.31E-2
151						8.30E-3	4.45E-3	2.86E-3	2.04E-3	1.77E-2
181							1.22E-2	7.76E-3	5.54E-3	2.55E-2
211								1.30E-2	9.23E-3	2.22E-2
241									2.07E-2	2.07E-2

[a] USNRC (1992).

Table T–39S. Radiation Doses to Embryo/Fetus per μCi of ^{235}U Introduced into Maternal Transfer Compartment (Blood)[a]

Days of gestation at introduction	Dose (rad) to embryo/fetus during indicated gestation periods (days)									
	0–30	31–60	61–90	91–120	121–150	151–180	181–210	211–240	241–270	0–270
0	*	*	*	*	*	*	*	*	*	*
31		1.29E-3	2.11E-5	4.84E-6	1.09E-6	4.60E-7	2.48E-7	1.59E-7	1.13E-7	1.32E-3
61			3.93E-3	7.19E-4	1.73E-4	7.18E-5	3.88E-5	2.49E-5	1.77E-5	4.98E-3
91				5.75E-3	1.39E-3	5.78E-4	3.12E-4	2.00E-4	1.43E-4	8.37E-3
121					7.40E-3	2.97E-3	1.62E-3	1.04E-3	7.41E-4	1.38E-2
151						8.70E-3	4.67E-3	3.00E-3	2.14E-3	1.85E-2
181							1.28E-2	8.12E-3	5.82E-3	2.67E-2
211								1.36E-2	9.69E-3	2.33E-2
241									2.17E-2	2.17E-2

[a] USNRC (1992).

Table T–40S. Radiation Doses to Embryo/Fetus per μCi of ^{234}U Introduced into Maternal Transfer Compartment (Blood)[a]

Days of gestation at introduction	Dose (rad) to embryo/fetus during indicated gestation periods (days)									
	0–30	31–60	61–90	91–120	121–150	151–180	181–210	211–240	241–270	0–270
0	*	*	*	*	*	*	*	*	*	*
31		1.40E-3	2.30E-5	5.26E-6	1.18E-6	5.00E-7	2.70E-7	1.73E-7	1.23E-7	1.43E-3
61			4.27E-3	7.82E-4	1.87E-4	7.79E-5	4.22E-5	2.70E-5	1.93E-5	5.41E-3
91				6.25E-3	1.51E-3	6.28E-4	3.39E-4	2.17E-4	1.55E-4	9.10E-3
121					8.05E-3	3.23E-3	1.77E-3	1.13E-3	8.07E-4	1.50E-2
151						9.46E-3	5.07E-3	3.26E-3	2.32E-3	2.01E-2
181							1.40E-2	8.88E-3	6.34E-3	2.92E-2
211								1.48E-2	1.05E-2	2.53E-2
241									2.36E-2	2.36E-2

[a] USNRC (1992).

Table T–41S. Radiation Doses to Embryo/Fetus per μCi of ^{239}Pu Introduced into Maternal Transfer Compartment (Blood)[a]

Days of gestation at introduction	Dose (rad) to embryo/fetus during indicated gestation periods (days)									
	0-30	31-60	61-90	91-120	121-150	151-180	181-210	211-240	241-270	0-270
0	*	*	*	*	*	*	*	*	*	*
31		2.52E-3	4.12E-5	9.40E-6	2.12E-6	8.97E-7	4.83E-7	3.10E-7	2.21E-7	2.57E-3
61			7.68E-3	1.40E-3	3.36E-4	1.40E-4	7.56E-5	4.85E-5	3.46E-5	9.71E-3
91				1.12E-2	2.71E-3	1.12E-3	6.07E-4	3.90E-4	2.78E-4	1.63E-2
121					1.45E-2	5.80E-3	3.17E-3	2.02E-3	1.44E-3	2.69E-2
151						1.70E-2	9.09E-3	5.85E-3	4.17E-3	3.61E-2
181							2.50E-2	1.59E-2	1.13E-2	5.22E-2
211								2.66E-2	1.88E-2	4.54E-2
241									4.23E-2	4.23E-2

[a] USNRC (1992).

Table T–42S. Dose Equivalent Factors for Embryo/Fetus per Unit Thorium Isotope in Maternal Blood[a]

Isotope	Dose factor (rem μCi^{-1})	GI uptake fraction f_1
Th-228	44.0	2×10^{-4}
Th-230	12.6	2×10^{-4}
Th-232	22.6	2×10^{-4}
Th-234	0.233	2×10^{-4}

[a] USNRC (1992).

APPENDIX U

FMPC DOMAIN DEMOGRAPHICS

INTRODUCTION

The topic discussed in this appendix involves the estimation of the size of the populations that live or lived around the Feeds Material Production Center (FMPC) near Ross, Ohio from 1950 to 1990. The information presented below describes the evolution of a model that would represent the best estimate of the number and location of individuals that resided within 8 kilometers (5 miles) of the FMPC over four decades. Four models are proposed, each based on different sources of data, as shown below:

- Model 1 estimates based on data presented in the 1989 FMPC Annual Environmental Monitoring Report.
- Model 2 estimates based on US Census Ohio Township data.
- Model 3 estimates based on US Census block data and census block maps.
- Model 4 estimates based on USGS topographical maps.

BACKGROUND

The domain of the Fernald Dosimetry Reconstruction Project (FDRP) study is defined as the area of a circle with an 8 km radius from the center of the FMPC (RAC, 1990). The domain is presented in Figure U–1 as a grid divided into the 16 compass sectors of a windrose with each compass sector partitioned into cells of 1 km from the center of the plant. The figure shows that the study domain includes areas of both Hamilton and Butler Counties, Ohio. Approximately 7% of this area is populated with farm houses, small communities and the small town of Ross, Ohio.

There are four townships within Butler and Hamilton Counties whose boundaries are within the FMPC domain. These townships include Ross and Morgan Townships in Butler County and Crosby and Colerain Townships within Hamilton County.

Morgan Township includes the WNW compass sector through the NNW compass section (see Figure U–1). The Ross Township, which includes the town of Ross, Ohio, is located within the compass sectors N to ENE. The Colerain township is located in compass sectors E to S, beginning at the 5th kilometer and extending through the 8th kilometer. The natural boundary between Colerain and Crosby Townships is the Great Miami River (see Figure U–1). Part of the Crosby Township is located in the compass sectors E to S beginning at the 1st kilometer and extending through the 4th kilometer. The rest of Crosby Township includes compass sectors SSW through W.

Butler County townships (Ross and Morgan) are each divided into 36 one square mile sections (BCEO, 1992). Approximately 18 sections or 50% of Ross Township sections lie within the FMPC domain while approximately 12 (33%) of the Morgan Township sections lie within the FMPC domain. In Hamilton County (HCRP, 1992) 100% of the Crosby Township

and approximately 36% (16 of 44.5 square miles) of the Colerain Township lie within the FMPC domain.

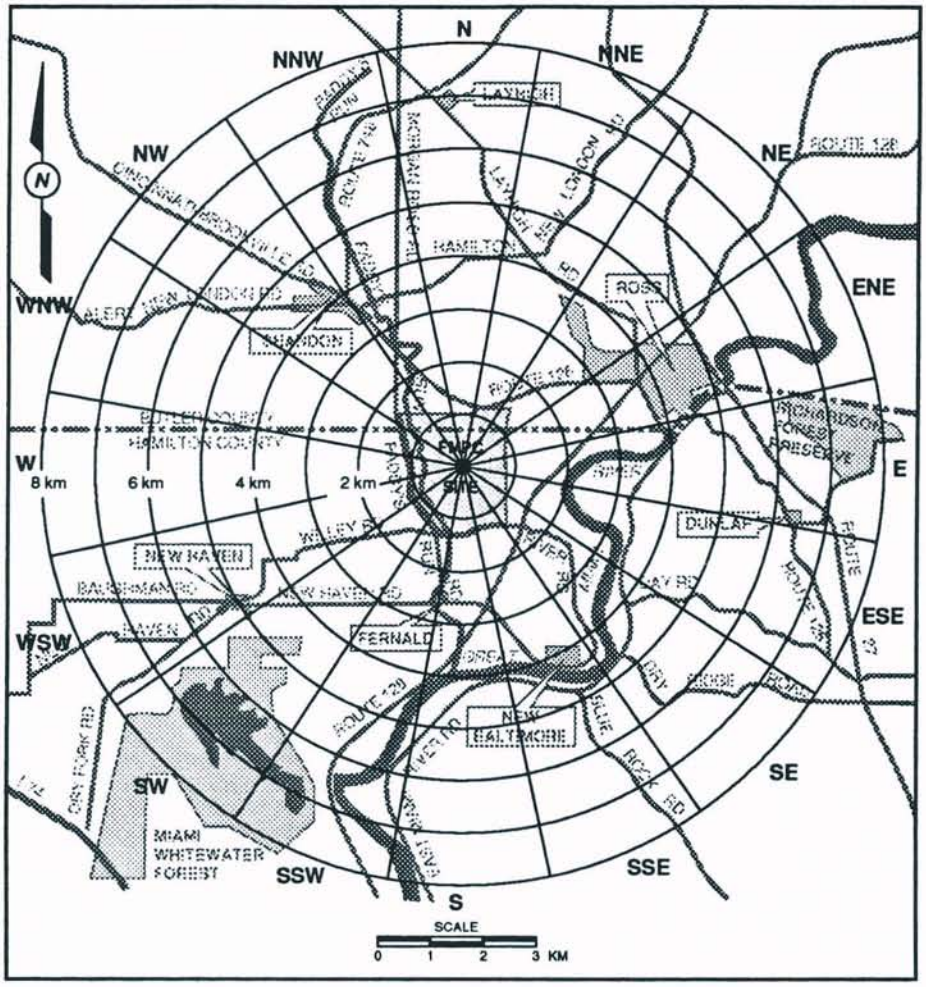

Figure U–1. The polar grid centered at the FMPC site, each marked with a direction toward which the wind blows. The circles are at 1 km intervals from the center of the site.

METHODS

To estimate the change in population in the FMPC domain over 4 decades (1950-1990) it was assumed that the population within the FMPC domain was representative of the Ohio townships surrounding the domain and that the populations within the townships grew exponentially, i.e. the population grew at a rate that was proportional to the number present at time t. A growth rate coefficient was calculated using census township data (U.S. Census, 1952, 1961, 1971, 1982, 1991) and the exponential equation:

$$p_2 = p_1 e^{r(t2-t1)} \qquad \text{(U–1)}$$

solving for r, where p_1 = initial populations at time t1, and p_2 = the population at time t2. The growth rate coefficients for each township and decade are shown in Table U- 1A. The growth rate coefficients assumed that the percentage of each township within the FMPC domain grew at the same rate as the whole township.

Table U-1A. Decade Growth Rate Coefficient Based on US Census Decade Population Estimates

Township	Growth Rate Coefficient	Decade Interval
Ross	0.052	1950–1960
	0.013	1960–1970
	0.039	1970–1990
	0.032	1980–1990
Colerain	0.13	1950–1960
	0.057	1960–1970
	0.010	1970–1980
	0.004	1980–1990
Crosby	0.036	1950–1960
	0.018	1960–1970
	0.035	1970–1980
	0.007	1980–1990
Morgan	0.036	1950–1960
	0.019	1960–1970
	0.044	1970–1980
	0.020	1980–1990

Tables U–2 through U–5 show that population estimates derived from Models 1, 2, 3, and 4 respectively. Each table list the 16 compass windrose sectors in the left column while distance from the center of the FMPC for each windrose cell is shown across the top of each table. The population estimates for each 1 kilometer cell within each township are shown in columns 1 through 8. The total population estimate for each township within the FMPC domain is listed to the left of the township name in each table.

MODELS

Model 1 (Table U–2) was developed from data in the 1989 FMPC Annual Environmental Monitoring Report (AEMR) (FMPC 1989). These data were prepared by the Geographic Data Systems Section of the Computing and Telecommunications Division at Oak Ridge National Laboratory (ORNL) in Oak Ridge, Tennessee.

The ORNL data are presented as a grid divided into the 16 compass sectors of a windrose with each compass sector partitioned into cells ranging from 1.6 to 16 kilometers from the center of the plant. The population data within the first 8 km, which represents individuals living within the FMPC domain were interpolated to estimated the population living within a windrose grid with a radius of 8 km and cells 1 km wide. Population estimates within each cell of the FMPC domain grid during the years 1950 to 1980 were calculated from the negative of the growth rate coefficients of the 1989 population data, using equation U–1 , and solving for p_2, the estimated change in population, where p_1 is equal to the 1989 population estimate.

To verify and/or improve the population estimates obtained from Model 1, a second model was suggested. The second model was based on 1990 U.S. Census township data (U.S. Census 1952, 1961, 1971, 1982, 1991). The assumption of this model was that the population in each township was evenly distributed. The crude population numbers used in the calculations were based on the fraction of each township within the FMPC domain and the township population. Estimates for each cell were based on the size and location of the cell relative to highways and communities. The results of Model 2 are given in Table 3.

The estimates obtained from Model 2 seemed reasonable for Ross, Morgan, and Crosby townships when compared to Model 1. However, the estimates for the Colerain township (> 20,000) were unreasonable since Colerain township includes portions of greater Cincinnati, Ohio and the region of the FMPC domain occupying the Colerain township is sparsely populated. Therefore a third model was considered.

The third model was developed from the use Census block data and census block maps(USCBM, 1992). The 1990 census block maps were overlaid with the FMPC domain grid. Estimates to each 1 kilometer cell within each windrose were assigned by scanning the area covered by the census block and inferring the fraction of a block population would be in each 1 kilometer cell. Applying the negative growth coefficient estimates to the 1 kilometer estimate, we extrapolated back in time to estimate the population distribution from 1990 to 1950. Since 1990 is the only census year for which the Census Bureau had data available at the block level for the entire U.S.(rural as well as metropolitan areas) the assumption was made that the 1990 census blocks for Hamilton and Butler counties would be representative of census blocks for previous decades. The population estimates for Model 3 for the FMPC domain are shown in Table U–4.

Model 3 estimates for the region of the four townships within the FMPC domain approached the estimates of Model 1 and seemed a reasonably good model. However, there was a large discrepancy between Model 2 and Model 3 domain population estimates. This discrepancy resulted from the assumption of Model 2, i.e. an even distribution of the census tract population throughout each township. Model 3 represented and improvement in the accuracy of the location of the domain population based on census block map data, however, it resulted in zero's in many cells. The question then arose as to how accurate are Model 3 population estimates relative to the area inhabited by individuals within the FMPC domain.

To resolve this problem a fourth model was proposed by investigating the use of USGS topographical maps (USGS, 1950, 1979–1981). that are published every 30 years. USGS maps, in addition to showing how the terrain is formed, show the location of highways, towns, and an estimate of structures located along transportation routes as well as in heavily populated areas. The structures on the USGS maps not only represent residences

but also small businesses, farm structures, and manufacturing buildings.

The USGS maps printed in 1979–1981 show both the structures seen in 1950 and 1979–1981 (Maps printed in 1979–1981 will be considered 1980 maps). By overlaying the topographical map with the FMPC grid (16 compass windrose sectors divided into 1 kilometer cells), the number of structures within each 1 kilometer cell of the windrose were counted, first for 1950 and then for 1980 to give structure estimates per cell for the 1950 and 1980 decades.

Based on the 1990 U.S. Census block data (USCBM, 1992), the housing occupancy for the FMPC domain is 2.87 (range 1 to 5). However, assuming 15% of the domain to be occupied by business and manufacturing industries, a 2.5 multiplier (conservative estimate of structure occupancy) was chosen to estimate the population based on structures in Ross, Morgan and Colerain townships. The occupancy rate for the Crosby township (2 per household) was calculated from census block data since approximately 100 % of the Crosby township was within the FMPC domain. The estimated population for each 1 kilometer sector of the 16 compass windrose for 1950 and 1980 was: # structures/cell X household occupancy. The results of the model 4 are shown below in Table U–5.

Using the two decade estimates obtained from USGS maps (1950 and 1980) a growth rate coefficient was calculated using equation U-1 for each cell within the domain windrose (Table 1-B). These growth rate estimates were used to interpolate population cell estimates for 1960 and 1970 decades. The estimates for the 1990 decade assumed that the growth rate coefficients generated for the time between 1950 and 1980 would be maintained for the next decade.

MODEL COMPARISON

Figure U–2 below gives the overall FMPC domain estimate comparison at the decade level. This comparison provides a measure of the uncertainty of the estimated numbers of individuals living within the FMPC domain during the years 1950 to 1990 calculated by four different modeling assumptions. Figure U–2 shows the population trends of the FMPC domain based on our four models. The figure shows clearly that Model 2, based on US Census township data, overestimates the domain population for 1960 through 1990. The assumption of this model that the population is distributed evenly throughout the townships, contributes to this unreasonable overestimation.

Using US Census data to calculate the growth rate coefficients for the townships over four decades did not reveal the true nature of the actual growth of the area of the Colerain township within the FMPC domain. Colerain township, which includes a large part of the city of Cincinnati, grew from a 1950 population of 7473 (US Census, 1950) to 50791 (US Census, 1970) in 1970, a seven fold increase. Using the growth rate coefficient calculated for the Colerain township from this exploding population (0.13, 1950-1960; 0.06, 1960-1970) to back calculate Colerain domain estimates from 1990 US Census data resulted in estimating few individuals living within the area of the FMPC domain occupied by the Colerain township in 1950; 457, 348 (Models 1 and 3, Tables U–2E, U–4E).

However, by using 1950 USGS Maps (Model 4) to estimate the 1950 Colerain domain population, we estimated that approximately 2,140 individuals live in the section of the FMPC domain within the Colerain township in 1950. This number grew to approximately

3,102 individuals in 1980 (USGS, 1980), a 1.5 fold increase that resulted in a smaller growth rate coefficient for the Colerain township within the FMPC domain, 0.002(low) to 0.043(high), (Table U–1B; E 5km–8km through S 5km–8km).

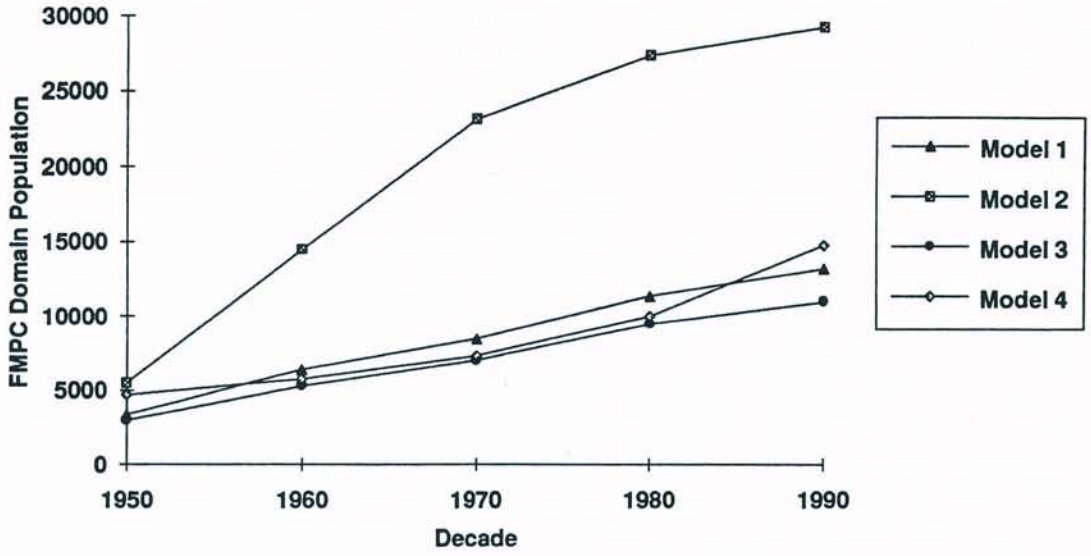

Figure U–2. Population estimates in the 8-km FMPC domain for Models 1, 2, 3, and 4 from 1950 through 1990.

Figure U–3 shows that the total FMPC domain population estimates based on Models 1, 3 and 4 are in good agreement. However, the primary advantage of Model 4 is that population size is estimated for each cell of the FMPC domain windrose, based on detailed locations of structures for two decades (1950 and 1980). For an example (see Tables U–4E and U–5E) estimates at 4 kilometers South East of the Feeds Materials Processing Plant for 1950, based on extrapolation from 1990 US Census block data and using township growth rate coefficients, predicted a cell with a population size of 22. However, 1950 USGS maps at the same location showed 77 structures with an estimated population size of 144, a 6.5 fold increase (Table U–5E).

Overall, when the FMPC 1950 domain cell population estimates from Model 3 (predicted from census data) and 1950 Model 4 domain cell population estimates (observed from USGS maps) were compared, the cell predicted/observed (P/O) ratios ranged from 0.40 to 7.96. The lesson learned here is that the past locations of populations cannot be predicted from the present locations. It may also be said that the future location of individuals living in the FMPC domain cannot be predicted from the past. Incorporating individual FMPC domain cell growth rate coefficients based on 1950 and 1980 USGS maps also provided a method of improving the accuracy in estimating where individuals settled within the FMPC domain over 40 years.

Model 4 provides a conservative domain population estimate that may be the result of the household occupancy multiplier. Model 4 was chosen as best representing the FMPC domain demographics for the four decades (1950-1990) under study by the Radiological

Assessments Corporation because of the resident location information within each FMPC domain cell provided by USGS maps (USGS, 1950-1980).

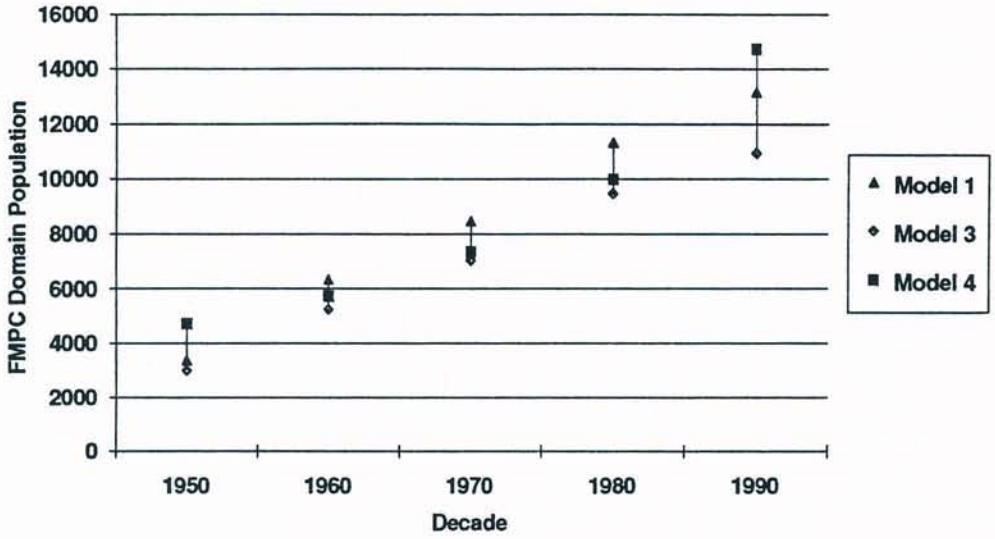

Figure U–3. Population estimates in the 8-km FMPC domain for Models 1, 3 and 4 from 1950 through 1990.

AGE AND SEX DISTRIBUTION

The age and sex distributions for the 1990 FMPC domain (Table U–6) were calculated from 1990 US Census block data (USCBM, 1992). The age distributions were set at infant to 9 years, 10 to 20 years of age, and 21 years and older to allow age stratification in an epidemiological study.

Sex distribution estimates for 1960-1980 FMPC domain were calculated from 1960-1980 US Census township data (U.S. Census, 1962, 1971, 1982), assuming that the male/female ratio in the townships were representative of the domain. Age distributions were not available on the township level. Therefore, the 1960-1980 age distributions were estimated from Butler and Hamilton county census data assuming that the percentage of individuals 0-9, 10-20 and >20 years of age at the county level were representative of the domain. Age and sex distribution estimates for the 1950 FMPC domain were estimated from 1950 U.S. census data which was reported at the county level.

CONCLUSIONS

The results of this exercise provide estimates of the number of individuals that may have been exposed to environmental releases from the FMPC between 1952 and 1988. The data also provide a decade level age and sex distribution which together with the population estimates will provide information for population dose estimates and for determining the

potential success of executing an epidemiological study.

REFERENCES

RAC (Radiological Assessments Corporation), 22 October 1990. Work Plan for the Fernald Dose Reconstruction Project, Task 4: Environmental Pathway Analysis, October 22, 1990

BCEO (Butler County Engineer's Office and Operational Facility, Hamilton, Ohio) 1992.

HCRP (Hamilton County Regional Planning Commission, Cincinnati, Ohio) personal communication, 1992.

U.S. Census (Census of the Population: 1950, Volume II. Characteristics of the Population, Part 35, Ohio. US Department of Commerce, Bureau of the Census, Washington), 1952.

U.S. Census (Census of the Population: 1960, Volume 1. Characteristics of the Population, Part 37, Ohio. US Department of Commerce, Bureau of the Census, Washington), 1961.

U.S. Census (Census of the Population: 1970, Volume 1. General Population Characteristics, Part 37, Ohio. US Department of Commerce, Bureau of the Census, Washington), 1971.

U.S. Census (Census of the Population: 1980, Volume 1. General Population Characteristics, Part 37, Ohio. US Department of Commerce, Bureau of the Census, Washington), 1982.

U.S. Census (Census of the Population: 1990, Volume 1. General Population Characteristics, Part 37, Ohio. US Department of Commerce, Bureau of the Census), 1991.

FMPC (Feed Materials Production Center, October 1989) Annual Environmental Monitoring Report, FMPC-2200, Special UC-707), page A–26, Table–25, Cincinnati, OH.

USCBM (US Census Block Maps: Detroit Regional Census Center. US Department of Commerce, Bureau of the Census, Southfield, Michigan), 1992.

USCBM (US Census Block Maps: Ohio, Kentucky, Indiana Regional Council of Governments, Cincinnati, Ohio), 1992.

USGS (US Geological Survey topographical maps 1979-1981. US Geological Survey, Denver, Colorado).

Table U–1B. Individual Cell Growth Rate Coefficient Based on 1950 and 1980 USGS Maps

	Distance in km							
	0–1	1–2	2–3	3–4	4–5	5–6	6–7	7–8
N	0.000	0.034	0.000	0.031	0.021	0.020	0.037	0.022
NNE	0.000	0.018	0.003	0.029	0.058	0.055	0.069	0.003
NE	0.000	0.014	0.075	0.058	0.033	0.023	0.023	0.019
ENE	0.000	0.040	0.057	0.039	0.046	0.019	0.023	0.000
E	0.000	0.015	–0.031	0.041	0.002	0.025	0.002	0.043
ESE	0.000	0.003	0.003	0.024	0.028	0.017	0.006	0.007
SE	0.000	0.034	0.043	0.014	0.014	0.022	0.008	0.019
SSE	0.000	0.049	0.003	0.012	0.009	0.012	0.003	0.008
S	0.000	0.035	0.039	0.019	0.006	0.056	0.004	0.012
SSW	0.000	0.029	0.054	0.083	0.021	0.007	–0.001	0.102
SW	0.000	0.026	0.019	0.015	0.095	0.038	0.066	0.059
WSW	0.000	0.000	0.003	0.003	0.008	0.033	0.028	0.051
W	0.000	0.000	–0.004	0.024	0.036	0.092	0.070	0.089
WNW	0.000	0.039	0.002	0.006	0.000	–0.004	–0.010	0.014
NW	0.000	0.055	0.010	–0.002	0.057	0.032	0.006	0.028
NNW	0.000	0.043	0.043	0.037	0.079	0.056	0.102	0.077

Table U–2. Model 1 Extension of 1989 FMPC 1989 Data

Table U–2A. Model 1 1990 Domain Population Estimates

	Distance in km									
	0–1	1–2	2–3	3–4	4–5	5–6	6–7	7–8	Township	
N	4	19	40	47	52	66	74	78		
NNE	3	16	36	40	46	68	140	188		
NE	5	55	128	86	76	80	151	198		
ENE	10	33	66	1370	1357	3	19	29	4583	Ross
E	15	25	38	67	70	57	110	147		
ESE	10	23	42	77	94	128	161	182		
SE	9	20	43	62	73	96	110	120		
SSE	5	22	41	52	76	160	285	369		
S	6	20	43	57	96	240	328	387	3289	Colerain
SSW	6	22	48	87	113	181	205	221		
SW	6	24	53	82	87	80	81	81		
WSW	11	27	53	81	98	135	165	185		
W	6	23	49	77	94	134	155	168	3515	Crosby
WNW	5	19	41	59	71	101	120	133		
NW	8	20	39	57	68	96	121	136		
NNW	11	22	40	59	74	116	165	197	1778	Morgan
Total									13165	

Table U–2B. Model 1 1980 Domain Population Estimates (FMPC 1989)

	Distance in km									
	0–1	1–2	2–3	3–4	4–5	5–6	6–7	7–8	Township	
N	3	14	29	34	38	48	54	57		
NNE	2	12	26	29	33	49	102	137		
NE	4	40	93	62	55	58	110	144		
ENE	7	24	48	995	985	2	14	21	3328	Ross
E	14	23	35	62	70	57	110	146		
ESE	9	21	39	72	94	128	160	181		
SE	8	19	40	58	73	96	110	120		
SSE	5	20	38	48	76	159	284	368		
S	6	19	40	53	96	239	327	386	3278	Colerain
SSW	6	20	45	81	105	168	191	206		
SW	6	22	49	76	81	74	75	75		
WSW	10	25	49	75	91	126	154	172		
W	6	21	46	72	87	125	144	156	3271	Crosby
WNW	4	16	34	48	58	83	98	109		
NW	7	16	32	47	56	79	99	112		
NNW	9	18	33	48	61	95	135	162	1459	Morgan
TOTAL									11335	

Table U–2C. Model 1 1970 Domain Population Estimates (FMPC, 1989)

	Distance in km									
	0–1	1–2	2–3	3–4	4–5	5–6	6–7	7–8	Township	
N	2	9	20	23	26	32	36	38		
NNE	1	8	18	20	23	33	69	92		
NE	2	27	63	42	37	39	74	97		
ENE	5	16	32	674	667	1	9	12	2253	Ross
E	10	16	25	44	63	51	99	133		
ESE	7	15	28	50	85	115	145	164		
SE	6	13	28	41	66	87	99	108		
SSE	3	14	27	34	69	144	257	333		
S	4	13	28	37	87	216	296	349	2966	Colerain
SSW	4	14	31	57	74	119	134	145		
SW	4	16	35	54	57	52	53	53		
WSW	7	18	35	53	64	89	108	121		
W	4	15	32	50	62	88	102	110	2305	Crosby
WNW	3	10	22	31	38	53	63	70		
NW	4	11	21	30	36	51	64	72		
NNW	6	12	21	31	39	61	87	104	939	Morgan
TOTAL									8463	

Table U–2D. Model 1 1960 Domain Population Estimates (FMPC 1989)

	Distance in km									
	0–1	1–2	2–3	3–4	4–5	5–6	6–7	7–8	Township	
N	2	8	17	20	22	28	32	34		
NNE	1	7	16	17	20	29	60	81		
NE	2	24	55	37	33	35	65	85		
ENE	4	14	28	591	586	1	8	13	1979	Ross
E	8	14	21	37	36	29	56	75		
ESE	5	13	23	42	48	65	82	93		
SE	5	11	24	34	37	49	56	61		
SSE	3	12	22	28	39	82	145	188		
S	3	11	24	31	49	122	167	197	1677	Colerain
SSW	3	12	26	48	62	99	112	121		
SW	3	13	29	45	48	44	44	44		
WSW	6	15	29	44	54	74	90	101		
W	3	13	27	42	51	73	85	92	1925	Crosby
WNW	2	8	18	26	31	44	52	58		
NW	3	9	17	25	30	42	53	59		
NNW	5	10	17	26	32	51	72	86	777	Morgan
TOTAL									6358	

Table U–2E. Model 1 1950 Domain Population Estimates (FMPC 1989)

	Distance in km									
	0–1	1–2	2–3	3–4	4–5	5–6	6–7	7–8	Township	
N	1	5	10	12	13	17	19	20		
NNE	1	4	9	10	12	17	36	48		
NE	1	14	33	22	20	21	39	51		
ENE	3	8	17	352	348	1	5	7	1176	Ross
E	6	10	15	26	10	8	15	20		
ESE	4	9	16	29	13	18	22	25		
SE	3	8	16	24	10	13	15	17		
SSE	2	8	16	20	11	22	40	51		
S	2	8	16	22	13	33	46	54	457	Colerain
SSW	2	8	18	33	43	69	78	84		
SW	2	9	20	31	33	31	31	31		
WSW	4	10	20	31	37	52	63	71		
W	2	9	19	29	36	51	59	64	1343	Crosby
WNW	2	6	12	18	22	31	37	41		
NW	2	6	12	17	21	29	37	41		
NNW	3	7	12	18	23	35	50	60	400	Morgan
TOTAL									3376	

Table U–3. Model 2 Estimates from 1990 Census Township Data

Table U–3A. Model 2 1990 Domain Population Estimates

	Distance in km									
	0–1	1–2	2–3	3–4	4–5	5–6	6–7	7–8	Township	
N	4	19	40	47	52	68	74	78		
NNE	3	16	36	40	46	69	140	188		
NE	5	55	128	1042	152	134	187	198		
ENE	10	33	66	1042	148	245	187	7	4748	Ross
E	12	18	27	46	386	336	660	838		
ESE	7	16	30	54	510	720	870	950		
SE	4	14	30	43	385	1176	1610	1370		
SSE	6	15	29	36	406	1226	1675	1683		
S	3	14	30	40	200	1786	1796	1625	20208	Colerain
SSW	2	8	17	33	68	241	137	143		
SW	20	9	18	28	378	63	56	56		
WSW	4	9	18	46	63	95	97	98		
W	4	16	34	53	65	189	53	58	2653	Crosby
WNW	6	28	57	84	100	84	84	36		
NW	11	28	56	81	54	72	84	94		
NNW	16	32	57	84	570	78	121	147	1151	Morgan
TOTAL									29169	

Table U–3B. Model 2 1980 Domain Population Estimates (Census Township)

	Distance in km									
	0–1	1–2	2–3	3–4	4–5	5–6	6–7	7–8	Township	
N	3	14	29	34	38	49	54	57		
NNE	2	12	26	29	33	50	102	137		
NE	4	40	93	757	110	97	136	144		
ENE	7	24	48	757	107	178	136	142	3348	Ross
E	11	17	25	43	385	335	658	835		
ESE	7	15	28	50	508	717	867	947		
SE	4	13	28	40	384	1172	1604	1365		
SSE	6	14	27	33	405	1222	1669	1677		
S	3	13	28	37	199	1780	1790	1619	20137	Colerain
SSW	2	7	16	31	63	224	127	133		
SW	19	8	17	26	352	59	52	52		
WSW	4	8	17	43	59	88	90	91		
W	4	15	32	49	60	176	49	54	2649	Crosby
WNW	5	23	47	69	82	69	69	30		
NW	9	23	46	66	44	59	69	77		
NNW	13	26	47	69	47	64	99	121	1272	Morgan
TOTAL									27326	

Table U–3C. Model 2 1970 Domain Population Estimates (Census Township)

	Distance in km								
	0–1	1–2	2–3	3–4	4–5	5–6	6–7	7–8	Township
N	2	9	20	23	26	33	36	38	
NNE	1	8	18	20	23	34	69	92	
NE	2	27	63	512	75	66	92	97	
ENE	5	16	32	512	73	120	92	96	2334 Ross
E	8	12	18	30	348	303	595	756	
ESE	5	10	20	35	460	649	784	857	
SE	3	9	20	28	347	1060	1452	1235	
SSE	4	10	19	24	366	1105	1510	1518	
S	2	9	20	26	180	1610	1619	1465	18221 Colerain
SW	1	5	11	22	45	158	90	94	
SW	13	6	12	18	248	41	37	37	
WSW	3	6	12	30	41	62	64	64	
W	3	10	22	35	43	124	35	38	1740 Crosby
WNW	3	15	30	44	53	44	44	19	
NW	6	15	30	43	29	38	44	50	
NNW	8	17	30	44	30	41	64	78	819 Morgan
TOTAL									23115

Table U–3D. Model 2 1960 Domain Population Estimates (Census Township)

	Distance in km								
	0–1	1–2	2–3	3–4	4–5	5–6	6–7	7–8	Township
N	2	8	17	20	22	29	32	34	
NNE	1	7	16	17	20	30	60	81	
NE	2	24	55	450	66	58	81	85	
ENE	4	14	28	450	64	106	81	85	2050 Ross
E	7	10	15	25	197	171	337	427	
ESE	4	9	16	30	260	367	444	484	
SE	2	8	16	24	196	600	821	699	
SSE	3	8	16	20	207	625	854	858	
S	2	8	16	22	102	911	916	829	10304 Colerain
SSW	1	4	9	18	37	132	75	78	
SW	11	5	10	15	207	35	31	31	
WSW	2	5	10	25	35	52	53	54	
W	2	9	16	29	36	104	29	32	1453 Crosby
WNW	3	12	25	37	44	37	37	16	
NW	5	12	24	35	24	31	37	41	
NNW	7	14	25	37	25	34	53	32	678 Morgan
TOTAL									14485

Table U–3E. Model 2 1950 Domain Population Estimates (Census Township)

	Distance in km									
	0–1	1–2	2–3	3–4	4–5	5–6	6–7	7–8	Township	
N	1	5	10	12	13	17	19	20		
NNE	1	4	9	10	12	18	36	48		
NE	1	14	33	267	39	34	48	51		
ENE	3	8	17	267	38	63	48	50	1219	Ross
E	5	7	10	18	54	47	92	116		
ESE	3	6	11	21	71	100	121	132		
SE	2	5	11	16	54	163	224	190		
SSE	2	6	11	14	56	170	233	234		
S	1	5	11	15	28	248	250	226	2808	Colerain
SSW	1	3	6	13	26	92	52	55		
SW	8	3	7	11	144	24	21	21		
WSW	2	3	7	18	24	36	37	37		
W	2	6	13	20	25	72	20	22	1014	Crosby
WNW	2	9	17	26	30	26	26	11		
NW	3	9	17	25	16	22	26	29		
NNW	5	10	17	26	17	24	37	45	473	Morgan
TOTAL									5514	

Table U–4. Model 3 Population Estimates from Census Block Data

Table U–4A. Model 3 1990 Domain Population Estimates

	Distance in km									
	0–1	1–2	2–3	3–4	4–5	5–6	6–7	7–8	Township	
N	0	4	0	204	0	58	8	86		
NNE	0	0	0	0	0	86	0	254		
NE	0	0	0	80	154	70	70	1		
ENE	0	26	284	706	1024	2	0	0	3117	Ross
E	0	27	17	64	120	241	290	220		
ESE	0	0	0	25	30	135	171	150		
SE	0	40	50	57	18	198	19	74		
SSE	0	9	91	242	9	95	531	281		
S	0	5	40	40	0	0	0	5	2587	Colerain
SSW	0	30	12	30	40	40	169	8		
SW	0	15	29	12	58	143	50	87		
WSW	13	15	0	0	168	246	388	63		
W	0	37	0	13	15	196	58	120	2762	Crosby
WNW	0	138	42	37	37	130	35	34		
NW	4	53	116	71	71	83	48	200		
NNW	4	19	77	77	77	388	303	147	2191	Morgan
TOTAL									10932	

Table U–4B. Model 3 1980 Domain Population Estimates (Census Blocks)

	Distance in km									
	0–1	1–2	2–3	3–4	4–5	5–6	6–7	7–8	Township	
N	0	3	0	148	0	42	6	62		
NNE	0	0	0	0	0	62	0	184		
NE	0	0	0	58	112	51	51	1		
ENE	0	19	206	513	744	1	0	0	2263	Ross
E	0	25	16	60	116	233	280	212		
ESE	0	0	0	23	39	130	165	145		
SE	0	37	47	53	17	191	18	71		
SSE	0	8	85	225	9	92	513	271		
S	0	5	37	37	0	0	0	5	2489	Colerain
SSW	0	28	11	28	37	37	157	7		
SW	0	14	27	11	54	133	47	81		
WSW	12	14	0	0	156	229	361	59		
W	0	34	0	12	14	182	54	112	2570	Crosby
WNW	0	113	34	30	30	107	29	28		
NW	3	43	95	58	58	68	39	164		
NNW	3	16	63	63	63	318	249	121	1797	Morgan
TOTAL									9465	

Table U–4C. Model 3 1970 Domain Population Estimates (Census Blocks)

	Distance in km									
	0–1	1–2	2–3	3–4	4–5	5–6	6–7	7–8	Township	
N	0	2	0	100	0	29	4	42		
NNE	0	0	0	0	0	42	0	125		
NE	0	0	0	39	76	34	34	0		
ENE	0	13	140	347	503	1	0	0	1532	Ross
E	0	18	11	42	26	211	253	192		
ESE	0	0	0	16	26	118	149	131		
SE	0	26	33	37	16	173	17	65		
SSE	0	6	60	159	8	83	464	246		
S	0	3	26	26	0	0	0	4	2260	Colerain
SSW	0	20	8	20	26	26	111	5		
SW	0	10	19	8	38	94	33	57		
WSW	9	10	0	0	110	161	254	41		
W	0	24	0	9	10	129	38	79	1811	Crosby
WNW	0	73	22	20	20	69	18	18		
NW	2	28	61	38	38	44	25	106		
NNW	2	10	41	41	41	205	160	78	1158	Morgan
TOTAL									7014	

Table U–4D. Model 3 1960 Domain Population Estimates (Census Blocks)

	Distance in km									
	0–1	1–2	2–3	3–4	4–5	5–6	6–7	7–8	Township	
N	0	2	0	88	0	25	3	37		
NNE	0	0	0	0	0	37	0	110		
NE	0	0	0	35	66	30	30	0		
ENE	0	11	123	305	442	1	0	0	1346	Ross
E	0	15	9	35	59	119	143	109		
ESE	0	0	0	14	15	67	84	74		
SE	0	22	27	31	9	98	9	37		
SSE	0	5	50	133	4	47	262	139		
S	0	3	22	22	0	0	0	2	1278	Colerain
SSW	0	16	7	16	22	22	93	4		
SW	0	8	16	7	32	78	27	48		
WSW	7	8	0	0	92	135	213	35		
W	0	20	0	7	8	107	32	66	1513	Crosby
WNW	0	60	18	16	16	57	15	15		
NW	2	23	51	31	31	36	21	87		
NNW	2	8	34	34	34	170	132	64	957	Morgan
TOTAL									5286	

Table U–4E. Model 3 1950 Domain Population Estimates (Census Blocks)

	Distance in km									
	0–1	1–2	2–3	3–4	4–5	5–6	6–7	7–8	Township	
N	0	1	0	52	0	15	2	22		
NNE	0	0	0	0	0	22	0	65		
NE	0	0	0	21	40	18	18	0		
ENE	0	7	73	181	263	1	0	0	800	Ross
E	0	10	6	24	16	32	39	30		
ESE	0	0	0	10	4	18	23	20		
SE	0	15	19	22	3	27	3	10		
SSE	0	3	35	92	1	13	72	38		
S	0	2	15	15	0	0	0	1	348	Colerain
SSW	0	11	5	11	15	15	65	3		
SW	0	6	11	5	22	55	19	33		
WSW	5	6	0	0	64	94	148	24		
W	0	14	0	5	6	75	22	46	1055	Crosby
WNW	0	42	13	11	11	40	11	10		
NW	1	16	35	22	22	25	15	61		
NNW	1	6	23	23	23	118	92	45	668	Morgan
TOTAL									2988	

Table U–5. Model 4 Population Estimates from 1950–1980 USGS Maps

Table U–5A. Model 4 1990 Domain Popultion Estimate

	Distance in km									
	0–1	1–2	2–3	3–4	4–5	5–6	6–7	7–8	Township	
N	0	31	5	95	47	51	199	178		
NNE	0	26	52	64	80	90	80	44		
NE	0	86	402	206	11	50	25	61		
ENE	0	15	172	1275	1084	109	38	8	4586	Ross
E	0	18	10	41	24	201	128	110		
ESE	0	5	7	71	132	146	179	208		
SE	0	12	45	196	173	168	374	332		
SSE	0	14	9	155	227	164	146	277		
S	0	16	59	56	19	187	153	243	3592	Colerain
SSW	0	33	35	111	116	26	77	947		
SW	0	23	35	67	363	159	203	223		
WSW	0	3	5	12	172	165	85	200		
W	0	0	7	17	36	81	240	378	4401	Crosby
WNW	0	12	8	19	35	43	39	137		
NW	0	23	11	148	124	117	32	93		
NNW	0	28	28	33	176	167	444	437	2153	Morgan
TOTAL									14742	

Table U–5B. Model 4 1980 Domain Population Estimates (1980 USGS MAP)

	Distance in km									
	0–1	1–2	2–3	3–4	4–5	5–6	6–7	7–8	Township	
N	0	22	5	70	38	42	137	145		
NNE	0	22	50	48	45	52	40	43		
NE	0	75	190	115	8	40	20	50		
ENE	0	10	98	861	682	90	30	8	3036	Ross
E	0	16	13	27	24	157	125	72		
ESE	0	4	7	55	100	123	168	193		
SE	0	9	29	180	150	135	345	272		
SSE	0	9	9	136	207	145	142	257		
vS	0	11	40	47	18	107	147	215	3102	Colerain
SSW	0	25	20	48	94	25	77	341		
SW	0	18	29	57	140	108	105	123		
WSW	0	3	4	11	158	119	64	121		
W	0	0	7	13	25	32	119	154	2536	Crosby
WNW	0	8	8	18	35	45	43	120		
NW	0	13	10	150	70	85	30	70		
NNW	0	18	18	23	80	95	160	202	1301	Morgan
TOTAL									9975	

Table U–5C. Model 4 1970 Domain Population Estimates (1950–1980 USGS)

	Distance in km									
	0–1	1–2	2–3	3–4	4–5	5–6	6–7	7–8	Township	
N	0	16	5	52	31	34	95	118		
NNE	0	18	48	36	25	30	20	40		
NE	0	66	90	64	6	32	16	41		
ENE	0	7	56	581	429	74	24	8	2058	Ross
E	0	14	18	18	24	123	122	47		
ESE	0	4	7	43	75	103	158	179		
SE	0	6	19	166	130	108	318	223		
SSE	0	5	9	120	189	128	138	238		
S	0	8	27	39	17	61	141	190	2714	Colerain
SSW	0	18	12	21	76	23	78	123		
SW	0	14	24	49	54	74	54	68		
WSW	0	0	4	11	146	85	49	73		
W	0	2	7	10	17	13	59	63	1649	Crosby
WNW	0	5	8	17	35	47	47	105		
NW	0	8	9	152	39	62	28	53		
NNW	0	12	12	16	36	54	58	93	896	Morgan
TOTAL									7326	

Table U–5D. Model 4 1960 Domain Population Estimates (1950–1980 USGS)

	Distance in km									
	0–1	1–2	2–3	3–4	4–5	5–6	6–7	7–8	Township	
N	0	22	5	38	25	28	65	96		
NNE	0	15	47	27	14	17	10	38		
NE	0	57	42	36	4	25	13	34		
ENE	0	4	32	392	270	61	19	8	1432	Ross
E	0	12	24	12	23	96	120	31		
ESE	0	4	7	34	57	87	149	167		
SE	0	4	12	152	113	87	293	183		
SSE	0	3	8	106	173	113	134	221		
S	0	6	18	32	16	35	135	168	2399	Colerain
SSW	0	14	7	9	62	21	78	44		
SW	0	10	20	42	21	50	28	38		
WSW	0	0	4	11	135	61	37	44		
W	0	2	8	8	12	5	29	26	1204	Crosby
WNW	0	4	8	16	35	48	52	92		
NW	0	4	8	155	22	45	27	40		
NNW	0	8	8	11	17	31	21	43	693	Morgan
TOTAL									5728	

Table U–5E. Model 4 1950 Domain Population Estimates (1950 USGS MAP)

	Distance in km									
	0–1	1–2	2–3	3–4	4–5	5–6	6–7	7–8	Township	
N	0	8	5	28	20	23	45	78		
NNE	0	13	45	20	8	10	5	38		
NE	0	50	20	20	3	20	10	28		
ENE	0	3	18	265	170	50	15	8	1026	Ross
E	0	10	33	8	23	75	117	20		
ESE	0	4	6	26	43	73	140	155		
SE	0	3	8	140	98	70	270	150		
SSE	0	2	8	94	158	100	130	205		
S	0	4	12	26	15	20	130	148	2140	Colerain
SSW	0	10	4	4	50	20	78	16		
SW	0	8	16	36	8	34	14	21		
WSW	0	0	4	10	124	44	28	26		
W	0	2	8	6	8	2	14	10	951	Crosby
WNW	0	3	8	15	35	50	58	80		
NW	0	3	8	158	13	33	25	30		
NNW	0	5	5	8	8	18	8	20	585	Morgan
TOTAL									4702	

Table U–6. Fernald Dose Reconstruction Project Age and Sex Distribution: 1950–1990

Township	Year	% Sex Distribution		% Age Distribution		
		Male	Female	<10	10–20	>20
Ross	1990	50.2	49.8	15.5	18.5	66.0
	1980	50.1	49.9	18.3	19.6	63.1
	1970	50.4	49.6	18.5	24.5	57.0
	1960	51.6	48.4	23.4	19.3	57.3
	1950	49.5	50.5	19.7	17.4	62.9
Colerain	1990	51.4	48.6	14.1	18.6	67.2
	1980	49.3	50.7	14.7	19.2	66.1
	1970	49.5	50.4	18.6	21.2	60.2
	1960	50.0	50.0	22.2	16.2	61.6
	1950	47.8	52.2	17.5	13.8	68.6
Morgan	1990	52.0	48.0	7.9	18.4	63.7
	1980	51.3	48.7	9.1	20.1	60.8
	1970	50.2	49.8	8.5	24.5	57.0
	1960	50.7	49.3	3.4	19.3	57.3
	1950	49.5	50.5	9.7	17.4	62.9
Crosby	1990	49.3	50.7	18.4	18.9	62.7
	1980	49.5	50.5	4.7	19.2	66.1
	1970	49.9	50.1	8.6	21.2	60.2
	1960	51.9	49.1	2.2	16.2	61.6
	1950	47.8	52.2	7.5	13.8	68.6

APPENDIX V

EPISODIC EVENTS

INTRODUCTION

For the purposes of the Fernald Dosimetry Reconstruction Project, episodic events are confined to those short-term events that result in releases which warrant special dose assessment procedures. The criteria and rationale for the definition of episodic releases are discussed in Appendix K of the Task 2/3 report (Voillequé et al. 1991). To summarize here, for a release to be considered episodic, it must increase the composite uranium release rate by a factor of at least 10 for a period of less than 10 days.

Episodic releases can not be defined until the baseline source term for each year of FMPC operations is defined. Thus, at this time, the total number of releases that will be considered episodic is unknown. During the 1960–1962 period, there was one release, from the Pilot Plant in November 1960, which qualifies for special assessment procedures. The methodology for treatment of this release is discussed here as an example of the treatment of an episodic release. However, it is expected that each episodic release will be handed differently depending on the types of data available.

DESCRIPTION OF THE NOVEMBER 1960 EPISODIC RELEASE AND BASIS FOR PREVIOUS RELEASE ESTIMATES

The following description of the potential episodic release is taken from the report of the investigation board (Starkey et al. 1960). During the period of November 8 through November 25, 1960, the stack sampler operated by the NLO Health and Safety Division indicated an estimated 1600 pound (730 kg) loss of slightly enriched (0.947%) uranium from dust collector G20–20 in the Pilot Plant. The cause of the loss was found to be holes in the dust collector bags, presumably from HF acid in combination with excessive moisture. The chemical form of the release was UF_4. The December 1 inventory substantiated a large loss (1849 pounds), but a special inventory taken on December 18 resulted in an indicated gain of 1303 pounds, for a net loss of 546 pounds of uranium for the period November 1 through December 18, 1960 (Table V–1).

The G20-20 dust collector serviced the entire enriched UF_6 to UF_4 operation, and prior to this time was one of the most reliable and efficient collectors in the Project. Monthly stack losses of uranium prior to this time had been less than 100 pounds per month since 1956 (Starkey et al. 1960). In the subsequent 11 months after the release, the monthly stack losses through G20–20 were less than 60 pounds per month, except for June 1961, when defective bags allowed a monthly release of 106 pounds (Cuthbert 1961).

Sapirie (1961), from the Oak Ridge Operations Office of the AEC, presented additional findings and conclusions about the November 1960 release from the Fernald Pilot Plant.

Table V–1. Summary of Previous Estimates of Uranium Losses through the Pilot Plant Dust Collector G20-20 between November 1 and December 18, 1960

Time Period	Estimated U Release (lbs)	Basis for Release Estimate	Reference
Nov 8 – 25	(1611)	Stack sampler	Starkey et al. 1960
Nov 1 – Dec 18	(546)	Special inventory[a]	Starkey et al. 1960
Nov 1 – Dec 1	(1849)	Book physical inventory difference	Starkey et al. 1960
Dec 1 – Dec 11	1100	Unofficial inventory	Starkey et al. 1960
Dec 1 – Dec 18	1300	Special inventory[b]	Starkey et al. 1960
Oct 17 – Nov 25	(1504)	Not given	Adams (1985)
Nov 1 – Dec 1	(1505)	Not given	Cuthbert (1961)

[a] 1303 minus 1849, or a loss of 546 pounds.
[b] Involves use of standard procedures and observation by Accountability Department representatives.

He emphasized the uncertainty involved in the measurement of stack losses and referred to three indirect checks of the release estimate, "none of which corroborated the stack loss measurement". These indirect checks were:

1. visual inspection and radiation monitoring of the roof, gutters, and surrounding ground
2. uranium material balance inventories
3. results from the FMPC environmental air monitoring system.

At this time, the original corroborating records for the visual inspection and radiation monitoring have not been located. Monthly reports from the IH&R department for November and December 1960 made no reference to such surveys. A search for another possible source, ground contamination reports, similarly did not provide any information on these measurements.

The second indirect check, material balance inventories, is performed monthly to prepare the accountability reports. Sapirie (1961) acknowledged that the book physical inventory difference (BPID) can be very uncertain for any given month, while over extended periods the BPID is relatively small. According to Sapirie, the November 1960 accountability report showed a monthly BPID loss of 344 pounds and a net measured loss of 1504 pounds. The net measured loss included an alleged stack loss of 1611 pounds. In December 1960 the BPID showed a *gain* of 1535 pounds, which was not conclusive evidence that the November stack loss was overstated, but did cast doubt on the validity of the measurement of the alleged November stack loss (Sapirie 1961). Sapirie (1961)

concluded that "the uncertainties involved in determining stack losses are so great as to preclude making an accurate estimate of the true loss, if any."

The third indirect check is discussed in the following section on supplemental environmental measurements.

SUPPLEMENTAL ENVIRONMENTAL MEASUREMENTS

Historical measurements of uranium in the surrounding ambient air and deposited onto gummed film were used to verify whether or not an episodic release occurred in late November 1960.

Air

The original air monitoring data for this time period were located and are presented in Appendix L of this report. Sapirie (1961) concluded that the air monitoring data do not support a large release. However, this conclusion was based only on the quarterly data and statements presented in the Fourth Quarter 1960 Environmental Monitoring report. Our examination of the original analytical data sheets revealed that perimeter air measurements were not taken for most of November and all of December 1960. The last record of air monitoring in 1960 was that of the samples taken from the NE and SE perimeter stations during November 6–8, 1960. The concentrations of uranium in air for those samples were in fact the highest observed for the entire year. Sampling was not resumed until January 11, 1961. Because of this data gap during the period in question, we conclude that the air monitoring data can not be used to dismiss the possibility of a significant episodic release during November 1960.

Gummed Film

Sapirie's review of indirect checks for this potential release did not include the gummed film monitoring data. During 1960–1962, daily measurements of fallout of uranium were made using a gummed film monitoring location just north of the Health and Safety Building. The gummed film is used to estimate the amount of uranium which deposits onto ground surfaces over a given time period. The measurement location was about 360 m east of the Pilot Plant. Figure V–1 shows the results of daily deposition measurements at this location between 1 October and 19 December 1960. The data show that there were substantial increases in deposition on 17 and 19 November and some increase on the 20th. Unfortunately, the result for 18 November has not been located. The time of day that samples were exchanged is not presently known.

Separate weekly measurements of uranium fallout were also made at the same location (Figure V–2). The results are plotted on the day that the sample was collected. The sample collected on 21 November is about 6 times greater than the estimated average deposition during the other eleven weeks shown in the plot.

In summary, the gummed film data clearly show that a substantially elevated deposition of uranium occurred during the same period identified by the effluent sampling results.

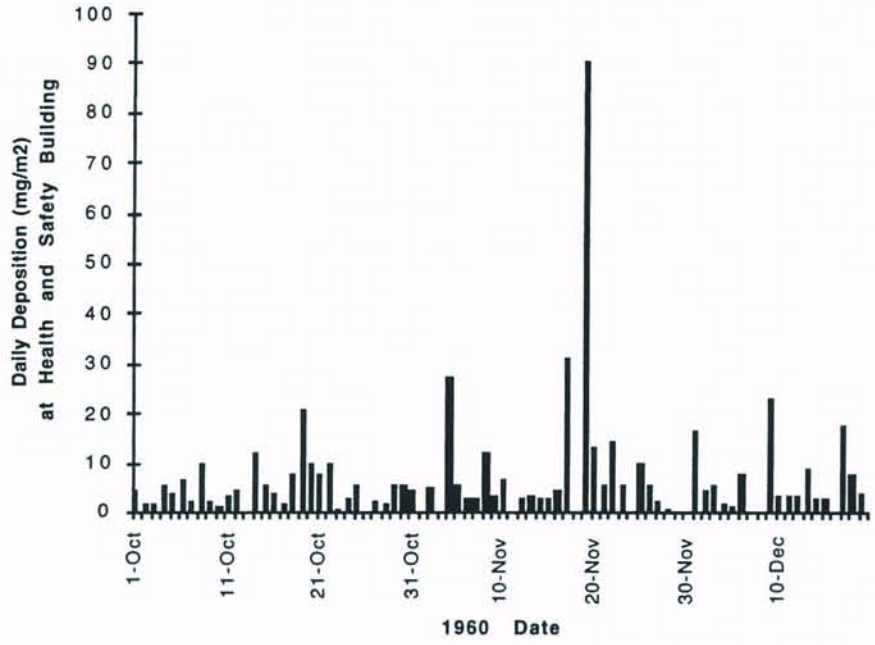

Figure V–1. Daily deposition measurements of uranium fallout at gummed film monitoring location north of the Health and Safety Building.

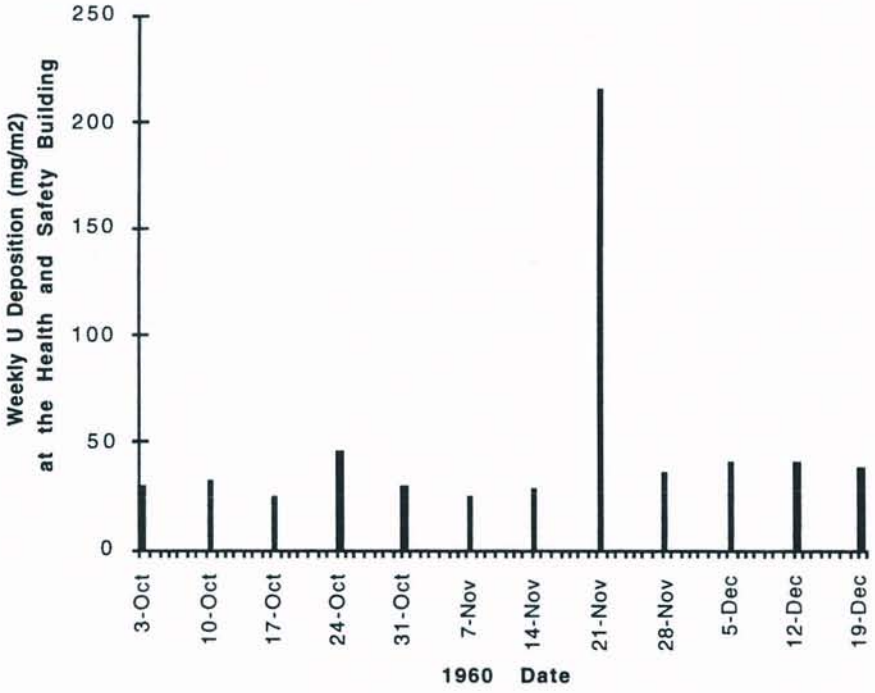

Figure V–2. Weekly deposition measurements of uranium fallout at gummed film monitoring location north of the Health and Safety Building.

ESTIMATE OF RELEASE MAGNITUDE AND RATE USED FOR THE DOSE RECONSTRUCTION PROJECT

Magnitude of the Release

Our estimate of the amount of uranium released is based upon the effluent measurements that were reported at the time. The material balance inventories, which yielded quite variable release estimates, were used to downplay the event. The investigation, however, did not discredit the effluent sampling data.

The methods used to estimate sampling biases due to anisokinetic sampling and deposition and impaction in the sampling line were described previously (Voillequé et al., 1991). When the filter bags were known to have failed, as in this case, the measured inlet particle size distribution was used in the calculations of sampling bias. The particles at the inlet to a dust collector are larger than those normally discharged, and the potential bias of a sample of that aerosol is correspondingly greater. Application of the results of the sampling bias calculations leads to an estimated release of about 2400 kg.

Timing of the Release

Starkey et al. (1960) provide a chronological listing of events relating to the release, including inspections of both the dust collector and the stack sampler, which were used to evaluate the probable timing of the release. We conclude that about 40% of the total release occurred between either November 12 or 14 and November 16, when the obviously damaged bag was tied off. The remaining 60% of the release occurred between November 16 and November 20, when all bags in this dust collector were replaced.

The first observation of elevated uranium deposition to gummed film does not coincide with the estimated start of the release, based on the effluent sampling measurement. First arrival at the monitoring location depends upon the wind direction during the release period. This remains to be investigated, as does the exact time of sample exchange.

Release Rate

The estimated release rates during the periods when the release occurred are 300 or 500 kg d^{-1} for the first 5 or 3 days, including 16 November, and about 200 kg d^{-1} during the last three days of the event. These release rates are much greater than the median release from the remainder of the FMPC facilities, which was about 22 kg d^{-1} during the month of November 1960.

APPROACH TO EVALUATING DISPERSION OF THE RELEASE AND OFFSITE CONSEQUENCES

Appendix E makes clear the difficulty of estimating meteorological regimes (wind speed, wind direction, stability) for specific periods in the past. It is nonetheless essential

that we explore what options there are for examining ranges of possibilities for meteorology during episodic events and assigning probabilities to them.

For the event in question, the period from November 12 or 14 through November 20, 1960, is 7 to 9 days. We propose the following procedure.

For each of the Novembers during 1986–1991, we would select a period of perhaps two weeks in mid-month, and we would examine hourly data from the Cincinnati record for wind speed, wind direction, and stability. Let us refer to each such triple as a "point." With each Cincinnati point, we associate the simultaneous point from the FMPC record. Where gaps occur in the FMPC data, we have no associated pair of points.

The numbers of each point must be put into the discrete intervals we have used in connection with the joint frequency tables. For example, we will use six wind speed intervals, and we will select the midpoint as a representative. If the lowest interval is 0 to 2 m s^{-1}, a wind speed of 1.7 m s^{-1} would be mapped to 1 m s^{-1}, the midpoint of the interval. Similarly, we would use six stabilities and 16 directions.

We combine all equal Cincinnati points and tabulate each one with its FMPC counterparts. In general, each Cincinnati point may be expected to be associated with multiple FMPC points, but there could be cases with only one.

Once such a tabulation of corresponding points is done, we consider the period of the actual release. For each hour during the period, a point may be derived from the Cincinnati data for November 1960. If that point is in the tabulation, there are one or more corresponding points for the FMPC. To each of these FMPC points is assigned a probability based on its frequency of occurrence. (For example, if for a given Cincinnati point there were five corresponding FMPC points and all five were different, each would have the probability 1/5 = 0.2.) Corresponding to each point from the Cincinnati data, then, there is a probability distribution over the possible points from the FMPC record (of course, many of the possible FMPC points may have probability zero).

One way of proceeding is by a Monte Carlo method. We set up simulations to step hour by hour through the period of the release. For each hour, we determine the actual Cincinnati point, sample from the corresponding distribution of FMPC points, and compute concentrations at receptor points according to the dispersion pattern determined by the selected sample point. For each receptor location, it would be useful to estimate the cumulative air concentration, i.e., to add the concentrations for each hour during the simulation. At the end of one simulation, we record the cumulative concentrations at the various receptors and repeat the simulation with new sampling. After all simulations were complete, for each receptor location we would have a distribution of cumulative air concentration, from which a distribution of inhalation dose, for example, could be derived.

It is not obvious how one gets around the problem of missing points. That is, if we turn up a point from the November 1960 Cincinnati record that has no match in the period that we sampled during 1986–1991, how do we proceed? If the problem is significant, one might reason that the sampling from the recent period was inadequate and extend it, e.g., to the whole of each November during the period. Otherwise, for a small number of occurrences, one might substitute points from the sampled period that were as "close" as possible to the November 1960 point.

Such a procedure appeals to the intuition, but its implementation is laborious and its dependence on the tenuous correspondence between the FMPC and Cincinnati data must

be emphasized. These and possibly other problems must be dealt with to the extent possible as they arise.

REFERENCES

Adams, W.J. 3 January 1985. "Major dust loss incidents." Letter to M.R. Theisen, DOE-OR. NLO, Inc., Cincinnati, OH.

Cuthbert, G.L. 12 December 1961. "Unusual incident." Internal memo to J. H. Noyes. National Lead Company of Ohio, Cincinnati, OH.

Starkey, R.H., J.O. Davis, P.N. McCreery, W.C. Hill and O.J. Turmelle. 22 December 1960. *Report of Investigation. Uranium Loss in the FMPC Pilot Plant between November 8 and November 25, 1960.* National Lead Company of Ohio, Cincinnati, OH.

Sapirie, S.R. 8 June 1961. "Uranium loss in the FMPC pilot plant between November 8 and 25, 1960". Memo to G.F. Quinn. U.S. Atomic Energy Commission, Oak Ridge Operations Office, Oak Ridge, TN.

Voillequé, P.G.; K.R. Meyer; D.W. Schmidt; G.G. Killough; R.E. Moore; V.I. Ichimura; S.K. Rope; B. Shleien; J.E. Till. December 1991. *The Fernald Dosimetry Reconstruction Project: Tasks 2 and Radionuclide Source Terms and Uncertainties — 1960–1962.* RAC Report No. CDC–2. Draft interim report for comment.